LBNL-42718

- Proceedings -

DYNAMICS OF FLUIDS IN FRACTURED ROCKS

CONCEPTS AND RECENT ADVANCES

In Honor of
Paul A. Witherspoon's 80th Birthday

February 10-12, 1999

BERKELEY LAB

LBNL-42718
Copy 1
REFERENCE COPY
Does Not
Circulate
Bldg. 50 Library - Ref.
Lawrence Berkeley National Laboratory

DISCLAIMER

This document was prepared as an account of work sponsored by the United States Government. While this document is believed to contain correct information, neither the United States Government nor any agency thereof, nor the Regents of the University of California, nor any of their employees, makes any warranty, express or implied, or assumes any legal responsibility for the accuracy, completeness, or usefulness of any information, apparatus, product, or process disclosed, or represents that its use would not infringe privately owned rights. Reference herein to any specific commercial product, process, or service by its trade name, trademark, manufacturer, or otherwise, does not necessarily constitute or imply its endorsement, recommendation, or favoring by the United States Government or any agency thereof, or the Regents of the University of California. The views and opinions of authors expressed herein do not necessarily state or reflect those of the United States Government or any agency thereof or the Regents of the University of California.

LBNL-42718

Proceedings of the International Symposium on
DYNAMICS OF FLUIDS IN FRACTURED ROCKS
Concepts and Recent Advances

In Honor of Paul A. Witherspoon's 80th Birthday

February 10–12, 1999

Edited by

Boris Faybishenko

Earth Sciences Division
Ernest Orlando Lawrence Berkeley National Laboratory
University of California
Berkeley, California 94720
U.S.A.

Ernest Orlando Lawrence Berkeley National Laboratory is administered for the U.S. Department of Energy by the University of California under Contract No. DE-AC03-76SF00098.

Foreword

This publication contains extended abstracts of papers presented at the International Symposium "Dynamics of Fluids in Fractured Rocks: Concepts and Recent Advances" held at Ernest Orlando Lawrence Berkeley National Laboratory on February 10–12, 1999.

This Symposium is organized in Honor of the 80th Birthday of Paul A. Witherspoon, who initiated some of the early investigations on flow and transport in fractured rocks at the University of California, Berkeley, and at Lawrence Berkeley National Laboratory. He is a key figure in the development of basic concepts, modeling, and field measurements of fluid flow and contaminant transport in fractured rock systems.

The technical problems of assessing fluid flow, radionuclide transport, site characterization, modeling, and performance assessment in fractured rocks remain the most challenging aspects of subsurface flow and transport investigations. An understanding of these important aspects of hydrogeology is needed to assess disposal of nuclear wastes, development of geothermal resources, production of oil and gas resources, and remediation of contaminated sites.

These Proceedings of more than 100 papers* from 12 countries discuss recent scientific and practical developments and the status of our understanding of fluid flow and radionuclide transport in fractured rocks. The main topics of the papers are:

- Theoretical studies of fluid flow in fractured rocks
- Multi-phase flow and reactive chemical transport in fractured rocks
- Fracture/matrix interactions
- Hydrogeological and transport testing
- Fracture flow models
- Vadose zone studies
- Isotopic studies of flow in fractured systems
- Fractures in geothermal systems
- Remediation and colloid transport in fractured systems
- Nuclear waste disposal in fractured rocks

We expect that the Symposium Proceedings will provide valuable information for different aspects of investigation of fractured rocks, and will be used by many governmental agencies, universities, research organizations, and private companies in solving a variety of fundamental scientific and practical problems in the earth sciences.

We appreciate the support for the Symposium provided by the U.S. Department of Energy (Oakland Operations Office, Office of Environmental Management, Office of Science and Technology, Subsurface Contaminants Focus Area, Office of Civilian Radioactive Waste Management), Lawrence Berkeley National Laboratory, Idaho National Engineering and Environmental Laboratory, U.S. Nuclear Regulatory

---

* Some articles within this collection were prepared using U.S. government funding. As such, the government retains a nonexclusive, royalty free, worldwide license to use those articles for internal government purposes. Questions regarding individual articles should be directed to the respective author(s).

Commission, U.S. Geological Survey, and American Institute of Hydrology. We also thank Julie McCullough and Nina Lucido for production of these Proceedings, Maria Fink for design of the cover, and Roy Kaltschmidt for the photograph of Paul Witherspoon.

Sally Benson
Boris Faybishenko

Symposium Steering Committee

Sally Benson, Chair (Lawrence Berkeley National Laboratory, Berkeley, CA)

Gudmundur Bodvarsson (Lawrence Berkeley National Laboratory, Berkeley, CA)

John Bredehoeft (The Hydrodynamics Group, Inc., CA)

Boris Faybishenko (Lawrence Berkeley National Laboratory, Berkeley, CA)

John Gale (St. Johns Memorial University, Newfoundland, Canada)

Iraj Javandel (Lawrence Berkeley National Laboratory, Berkeley, CA)

Jane Long (University of Nevada, Reno, NV)

Marcelo Lippmann (Lawrence Berkeley National Laboratory, Berkeley, CA)

Frank Morrison (University of California, Berkeley, CA)

Shlomo Neuman (University of Arizona, Tucson, AZ)

Thomas Nicholson (U.S. Nuclear Regulatory Commission, Washington, DC)

John Nimmo (U.S. Geological Survey, Menlo Park, CA)

Co-Sponsoring Organizations

U.S. Department of Energy, Oakland Operations Office

U.S. Department of Energy, Office of Environmental Management, Office of Science and Technology, Subsurface Contaminants Focus Area

U.S. Department of Energy, Director, Office of Civilian Radioactive Waste Management

Ernest Orlando Lawrence Berkeley National Laboratory

Idaho National Engineering and Environmental Laboratory

U.S. Nuclear Regulatory Commission

U.S. Geological Survey

Production Staff

Julie McCullough, Technical Editor; Nina Lucido, Production Assistant; Maria Fink, Designer; Roy Kaltschmidt, Photographer (Lawrence Berkeley National Laboratory, Berkeley, CA)

Table of Contents

Foreword iii

Symposium Steering Committee and Co-Sponsoring Organizations v

Investigations at Berkeley on Fracture Flow — From the Parallel Plate Model to Chaotic Systems
P. A. Witherspoon 1

SESSION 1: Theoretical Studies of Flow in Fractured Rocks **5**

A New Free Boundary Problem for Unsteady Flows in Porous and Fissured-Porous Rocks
G. I. Barenblatt and J. L. Vasquez 7

On Dynamic Permeability
G. Sposito 9

Fluid Flow in Rock Fractures: Cubic Law, Lubrication Equation, and Stokes Equation
R. Zimmerman and I. W. Yeo 13

On Non-Newtonian Flow in Spatially Variable Fractures
V. Di Federico 17

Predicting Hydrology of Fractured Rock Masses from Geology: Techniques, Successes and Failures from Recent Case Histories
P. R. La Pointe 20

SESSION 2: Multi-Phase Flow and Reactive Contaminant Transport in Fractured Rocks **23**

Multi-Phase Flow in Fractured Rocks - Lessons Learned from Mathematical Models
K. Pruess 25

Two-Phase Flow in a Variable Aperture Fracture: Laboratory Validation of a Two Dimensional Numerical Model
S. E. Anderson and N. R. Thomson 30

Influence of Fracture Network and Rock Matrix Properties on DNAPL Migration in Fractured Rock
E. A. Sudicky 35

Multicomponent Reactive Transport in Fractured Porous Media: Methods and Applications
P. C. Lichtner 36

Experimental and Mathematical Simulations of Gas Bubble and Water Flow Through Rock Fractures
K. Kostakis, J. P. Harrison, and S. M. Heath 40

SESSION 3: Fracture-Matrix Interactions **45**

The Fracture-Matrix Interaction
Y. Yortsos 47

Fracture-Matrix Flow: Quantification and Visualization Using X-Ray Computer Tomography
A. S. Grader, M. Balzarini, F. Radaelli, G. Capasso, and A. Pellegrino 48

Modeling Matrix Diffusion in Fractured Media: From Single Fracture Scale to Block Scale
C. Grenier, A. Genty, E. Mouche, and E. Tevissen 52

Multiple Rates of Mass Transfer Between Fractures and Matrix
L. Meigs, S. McKenna, and R. Haggerty 56

Using the Boundary Layer Concept for Modelling Chemical Transport in a Fracture-Matrix System
R. Wallach 58

SESSION 4: Hydrogeological and Transport Testing **61**

Development of Hydraulic Tests in Fractured Rocks
P. Hsieh 63

Evaluating Fracture Network Geometry from Hydraulic Data at Underground Test Facilities
T. W. Doe 65

Effects of Fracture Geometry and Flow Regime on Single and Two-Phase Flow Transmissivities
J. Gale 69

The Evolution of Fracture Topography and Flow Path Geometry Under Normal and Shear Stresses and Their Role in Hydromechanical Behavior
S. Gentier, D. Hopkins, J. Riss, and E. Lamontagne 71

Water Flow and Solute Transport in Porous Fractured Chalk
R. Nativ, E. Adar, O. Dahan, N. Weisbrod, B. Berkowitz, and D. Ronen 76

Modeling Signal Propagation and Well Response in Porous and Fractured Rock Aquifers
C. T. Simmons, D. H. H. Wye, and P. G. Cook 79

SESSION 5: Fracture Flow Models **85**

Discrete Fractures-Continuum Mixed Models: A Summary of Experiences in Test Interpretation and Model Predictions
J. Carrera and L. Martinez 87

Stochastic Continuum Modelling of Groundwater Flow Within the Swedish Performance Assessment Program
B. Gylling and D. Walker 89

Stochastic Analysis of Transport and Retention in a Multiple Fracture Pathway
S. Painter, V. Cvetkovich, and J.- O. Selroos 92

Connectivity of Fracture Networks with Power-Law Length Distributions
C. Renshaw 96

SESSION 6: Vadose Zone Studies **101**

Recent Developments and Unresolved Problems in Vadose Zone Hydrology and Contaminant Transport
W. Jury and Z. Wang 103

Type-Curve, Inverse and Geostatistical Analyses of Pneumatic Injection Tests in Unsaturated Fractured Tuffs at the Apache Leap Research Site Near Superior, Arizona
W. A. Illman, D. L. Thompson, V. V. Vesselinov, G. Chen, and S. P. Neuman 105

Accounting for Fractures and Other Macropores in Predictions of Unsaturated Hydraulic Conductivity
J. Nimmo 110

A Radionuclide Transport Model for the Unsaturated Zone at Yucca Mountain
B. A. Robinson, H. S. Viswanathan, A. V. Wolfsberg, and C. W. Gable 114

Fast Flow in Unsaturated Rock Fractures
T. Tokunaga and J. Wan 118

Role of Fractures at Different Scales in Underground Heater Experiments
Y. W. Tsang and B. Freifeld 120

SESSION 7: Isotopic Studies of Flow in Fractured Systems 125

Isotopic Effects in Dual-Porosity Fluid-Rock Systems
D. DePaolo 127

Measuring Groundwater Flow in Fractured Rocks With Environmental Isotopes, Clare Valley, South Australia
P. G. Cook, A. J. Love, and C. T. Simmons 130

Isotope Hydrology of Regional Flow Systems, Southern Nevada
J. B. Paces and Z. L. Peterman 134

Use of Chlorine-36 and Chloride Data to Evaluate Fracture Flow and Transport Models at Yucca Mountain
A. V. Wolfsberg, J. T. Fabryka-Martin, K. S. Campbell, S. S. Levy, and P. H. Tseng 139

SESSION 8: Fractures in Geothermal Systems 143

Pressure Transient Tests in a Fractured Geothermal Reservoir: Oguni Geothermal Field, Northern Kyushu, Japan
S. K. Garg and S. Nakanishi 145

In-Situ Stress and Fracture Permeability Along the Stillwater Fault Zone, Dixie Valley, Nevada
S. Hickman, C. A. Barton, M. D. Zoback, C. F. Williams, R. Morin, and R. Benoit .. 148

Characterization of Geothermal Reservoirs Using Inverse Modeling
S. Finsterle, K. Pruess, and A. Battistelli 152

How Should Permeability within the Oceanic Crust Be Represented in Numerical Models of Coupled Flows?
A. T. Fisher 155

Coupled 3-D Simulations of Forced Fluid Flow through Fractured, Hot Rock
T. Kohl and L. Rybach 160

SESSION 9: Remediation and Colloid Transport in Fractured Systems 163

Basic Research Strategies for Resolving Remediation Needs in Contaminated Fractured Subsurface Media
P. M. Jardine, T. M. Mehlhorn, I. L. Larsen, S. C. Brooks, J. P. Gwo, G. V. Wilson, and W. E. Sanford 165

Critical Biogeochemical Parameters Used for In-Situ Bioremediation of Solvents in Fractured Rock
T. Hazen 169

Fracture Clogging by the Deposition of Colloidal Particles
J. H. Kessler and J. R. Hunt 172

Field Verification of TCE Matrix Diffusion in a Fractured Sandstone and Implications for Natural Attenuation and Remediation
B. L. Parker and S. N. Sterling 175

SESSION 10: Nuclear Waste Disposal in Fractured Rocks 179

Geological Disposal of Nuclear Waste — Progress Made and Lessons Learned
B. Bodvarsson 181

Effective-Porosity and Dual-Porosity Approaches to Solute Transport in Fractured Tuff of the Saturated Zone at Yucca Mountain: Implications for Repository Performance Assessment
B. W. Arnold, H. Zhang, and A. M. Parsons 184

Numerical Studies of Effects of an Excavation Damage Zone and Discrete Fractures on ^{129}I Transport from a Used Nuclear Fuel Waste Disposal Repository in Low-Permeability Rock
T. Chan, M. R. Jensen, N. W. Scheier, and F. W. Stanchell 189

Calculation of Discrete Fracture Flow Paths in Dual-Continuum Models
C. Ho and M. L. Wilson 194

A Conceptual Model of the Temporal and Spatial Distribution of Net Infiltration and Recharge in Fractured Rock, Yucca Mountain, Nevada
A. L. Flint, L. E. Flint, J. A. Hevesi, and D. B. Hudson 198

SESSION P1: Alternative Models for Flow in Fractured Rocks 201

Hydraulic Properties of Fracture Networks Following a Power-Law Length Distribution
J.-R. de Dreuzy, P. Davy, and O. Bour 203

Evidence of Chaotic Behavior in Flow through Fractured Rocks, and How We Might Use Chaos Theory in Fractured Rock Hydrogeology
B. Faybishenko 207

On the Significance of Rock Wettability in Oil Recovery Processes
E. Isaacs, A. Babchin, and J.-Y. Yuan 213

Review of Recent Models of Transport in Fractured Rock; Their Approaches, Objectives and Methods
A. Nir 216

Describing Coupled Transport Processes in and through Fractured Rock Systems
W. Rose, A. Babchin, and J.-Y. Yuan 219

Scale-Dependent Darcy Flows in Fractured Media
D. M. Tartakovsky and C. L. Winter 224

SESSION P2: Coupled Processes in Fractured Rocks 227

Coupled Chemical Transport and Fluid Flow During Alcohol Flooding for DNAPL Remediation
R. W. Falta, E. Roeder, C. Lee, S. Brame, H. Schweninger, J. Coates, T. Ladaa, J. Myers, J. Martin, J. Pace, and D. Micolet 229

Results of Thermal Loading Studies Using the Unsaturated Zone Model of Yucca Mountain
C. B. Haukwa, Y.- S. Wu, and G. S. Bodvarsson 231

Coupled Hydromechanical Studies of Deep Injection Disposal of Solid Waste
J. Rutqvist and C.-F. Tsang 232

Numerical Modeling of Coupled Thermo-Hydro-Chemical Processes for the *In-situ* Thermal Tests at Yucca Mountain, Nevada
E. Sonnenthal, N. Spycher, J. Apps, and A. Simmons 234

SESSION P3: Fracture-Matrix Interactions and Reactive Chemical Processes 239

Calculation of Fracture Matrix Interaction for Unsaturated, Low-Permeability Welded Tuff
J. Fairley 241

Correlation of Mineral and Porosity Distribution at the Sub-Millimeter Scale, and Its Implications for Reactive Transport Simulations
W. Glassley, A. Simmons, and G. Lamble 244

Study of Diffusion Processes in Simple Fracture Systems
G. Li and C.-F.Tsang 247

The Influence of Different Fracture-Types in Chalk on Groundwater Salinization Processes
Y. Livshitz, A. Issar, and A. Yakirevich 251

Infiltration of Hyperalkaline Groundwater along Discrete Fractures at Maqarin, Jordan
C. Steefel and P.C. Lichtner 255

SESSION P4: Hydrogeological Field and Laboratory Testing and Measurements **259**

Hydrogeological Aspects of Siting Monitoring Wells in a Fractured Chalk Aquitard
E. Adar and R. Nativ 261

An Optimization Procedure for Borehole Emplacement in Fractured Media
D. Billaux and F. Guerin 264

An Unsaturated Zone Transport Field Test in Fractured Tuff
G. Y. Bussod and H. J. Turin 269

A Summary of Fracture Characterization Study at Raymond Field Site
K. Karasaki 272

Vaporizing Flow in Hot Fractures: Observations from Laboratory Experiments
T. Kneafsey and K. Pruess 277

Estimation of Capillary Pressure and Relative Permeability Curves in a Single, Rough-Walled Fracture Using Parameter Estimation Techniques
J. S. Konzuk and B. H. Kueper 280

Large Volume Slug Tests in a Fractured-Porous Medium With a Deformable Fracture
K. T. Lewallen and H. F. Wang 284

Seismic Imaging of Fractured Rock
E. L. Majer, T. M. Daley, J. E. Peterson, R. Gritto, M. Feighner, and T. V. McEvelly 288

Hydraulic Fractures in Shallow Soils as an Analog to Applications in Rock
L. Murdoch 293

The Cubic Law and Effects of Stress
L. R. Myer 294

Control of Fluid Injection into a Fractured Rock
T. Patzek and D. Silin 296

Observations of Water Movement in Variably Saturated Fractured Basalt and Its Possible Implications on Predictive Modeling
R. K. Podgorney and T. R. Wood 300

Calculating Fracture Temperatures from Wellbore Measurements
R. C. Schroeder 305

Laboratory Experiments on Solute Transport in Unsaturated Fractures
G. Su, J. Geller, K. Pruess, and J. Hunt 308

Hydraulic Characterization of Fractures and Faults in Sandstone
W. L. Taylor, R. Myers, A. Aydin, and D. D. Pollard 311

Evaluation of Seepage into a Mined Opening Constructed in Unsaturated Fractured Rock
R. Trautz, P. J. Cook, and J.S.Y. Wang 312

Quantifying Sorption of Colloids at Gas-Water Interfaces: Implications for Colloid Transport in Unsaturated Subsurface Media
J. Wan, T. Tokunaga, R. Stover, K. Olson, and J. Yang 316

Evidence of Scale-Dependent Dispersivity in Fractured Sedimentary Rocks, Newark Basin, NJ
C. Welty, G. Carleton, and H. T. Buxton 320

Automated Control and Measurement in a Fracture Junction Study
J. S. Wise, J. L. Wilson, R. Reedy, and C. Li 324

SESSION P5: Modeling Approaches for Flow and Chemical Transport in Fractured Rocks **327**

Prediction of Fracture Slip and Associated Permeability Changes in a Geologic Repository for Nuclear Waste.
P. A. Berge, S. C. Blair, and H. F. Wang 329

Predicting Large Scale Effective Hydraulic Conductivity from Local Measurements: A Percolation Approach
J. Guimerà and M. Ortuño 333

Numerical Investigation of the Asymptotic Behavior of Unsteady Groundwater Flows with Capillary Absorption and Forced Drainage
E. Ingerman and S. Shvets 337

Modeling Mass Transport through Fractured Media Using the Statistical Continuum Method in Two and Three Dimensions
B. Parney and L. Smith 341

Geometrical and Transport Properties of Disordered Fracture Networks: Analytical Results
A. Rodrigues and E. Medina 344

Homogenization of Contaminant Transport in Fractured Porous Media
P. Royer and C. Serres 348

Macroscopic Modelling of Gas Flow through a Fractured Porous Medium
P. Royer and J. L. Auriault 354

Simulation of Strata-Bound Tight Gas Reservoirs: Discrete Irregular Stochastic Fracture Networks and Network Drainage, Including Dynamic Matrix Recharge
M. W. Sams and M. McKoy 360

Multicontinuum Description of Flow and Transport in the Composite Heterogeneous Media
M. Shvidler and K. Karasaki 363

A Discrete-Fracture Boundary Integral Approach to Simulating Coupled Energy and Moisture Transport in a Fractured Porous Medium
S. Stothoff, G. Ofoegbu, and R. Green 365

A Model of Biofilm Growth in a Flowing Fracture
B. Travis 369

Estimates of Frequency-Dependent Compressibility From a Quasistatic Double-Porosity Model
H. F. Wang, J. G. Berryman, and P. A. Berge 371

On the Effective Continuum Model for Simulating Flow and Transport in Fractured Rocks
Y.- S. Wu 375

SGILD Modeling and Inversion for Single Phase Flow
G. Xie, J. Li, and P. A. Witherspoon 380

Reactive Chemical Transport in Fractured Rock: Supergene Copper Enrichment
T. Xu, K. Pruess, and G. Brimhall 385

Stochastic Analysis of Groundwater Flow in Fractured Porous Media: A Double Permeability Approach
D. Zhang and A. Sun 390

Lanczos Algorithm for the Simulation of Groundwater Flow in Fractured Porous Media Using Dual Porosity Approach
K. Zhang, A. D. Woodbury, and W. S. Dunbar 392

The Reduced Degree of Freedom Procedures for Solving Coupled-Field Problems
G. A. Zyvoloski and P.- H. Tseng 396

Investigations at Berkeley on Fracture Flow — From the Parallel Plate Model to Chaotic Systems

Paul A. Witherspoon

Earth Sciences Division, Lawrence Berkeley National Laboratory, and
Department of Material Sciences and Mineral Engineering
University of California, Berkeley

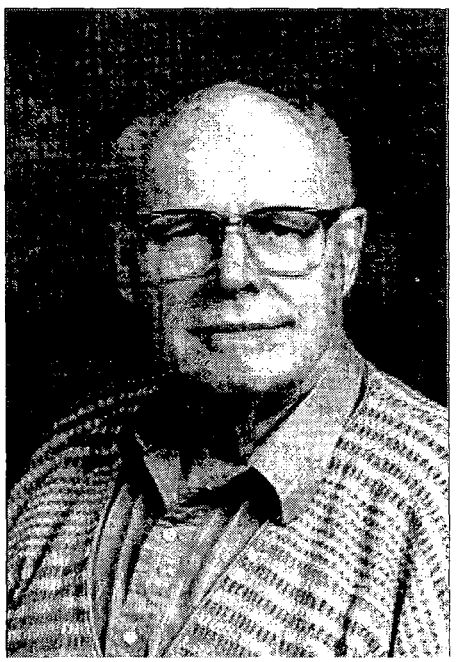

This is a review of the research effort that has been carried out over the past 35 years at the University of California and at the Lawrence Berkeley National Laboratory on the behavior of fractured rocks when subjected to perturbations of various kinds. In a review of this kind, where the range of investigations that has been carried out is quite large, only the highlights of the results of this work can be presented. This research effort has been focussed primarily on the flow of fluids through fractured rocks, but other aspects that involve the effects of thermal and mechanical perturbations have also been investigated. Initially, the work involved the analysis of steady state flow in orthogonal networks of rigid fractures. The development of a finite element code led to modeling investigations of two-dimensional networks of rigid fractures of arbitrary geometry. The analysis of pumping tests where fractures are intersected by the withdrawal well was developed using type curves, and in a related problem, a method was developed for extracting heat from hot dry rock using vertical fractures that are intercepted by inclined boreholes. The realization that fractures can deform as the stress acting across the fracture changes led to the development of a code to handle coupled stress and flow analysis in fractured rocks, and this code was used in the analysis of relevant engineering problems. To develop a better understanding of coupled stress-flow behavior, laboratory investigations on fractured rocks were carried out using granite cores with diameters ranging from 15 cm to 95 cm. A method was developed for the analysis of transient flow in tight fractures (1 μm to 10 μm). The mechanical and hydraulic properties of fractured rocks were examined with regard to the role they play in induced seismicity.

The initiation of the Stripa project in 1977, in an abandoned iron-ore mine in central Sweden, opened up a major program of investigations from the standpoint of radioactive waste isolation in fractured rocks. The fracture hydrology at the Stripa site was investigated by: mapping

discontinuities exposed on walls of underground excavations and surface outcrops; measurements on core samples; optical surveys of the walls of boreholes; and the analysis of results of hydraulic tests conducted in boreholes and tunnels. An innovative method of conducting a large-scale permeability measurement was carried out in a 5 m x 5 m x 33 m long drift. A thermomechanical program of investigations was implemented using: (a) two full-scale heater tests in which the near-field response of the rock mass was studied under simulated short-term and long-term conditions; and (b) an intermediate term time-scaled experiment covering the major part of the heatup period of the thermal pulse and interaction between adjacent heaters. In conjunction with the work at Stripa, several investigations were carried out on the hydromechanics of flow in a single fracture. The validity of the cubic law for laminar flow through open fractures of parallel planar plates was found to hold using rough fractures where the surfaces are in contact and the aperture is being decreased under stress.

Another approach to flow in fractures was introduced by the development of a model that can generate the porous media equivalent for networks of discontinuous fractures. This approach was also used in generating a conceptual model of the principal fracture zones at the Site Characterization and Validation Site of the International Stripa Project that was carried out from 1986 to 1992. An extension of this model was used in investigations of mechanical transport in fracture networks. An analytical model for fracture-dominated reservoirs was developed to analyze well test data where flow in the inner region around the withdrawal well is assumed to be linear and in the outer region, the flow is assumed to be radial. An analysis of fracture roughness and its effect on flow in a single fracture lead to another series of investigations. Transparent replicas of fracture surfaces were used in laboratory investigations where two-phase gas-liquid flows could be observed. Hydromechanical studies were made of the relationship in single fractures between normal stiffness, contact area, and the geometric distribution of asperities. The three-dimensional boundary element method was used in a stiffness-permeability analysis of a rough surfaced fracture. Investigations of seismic wave propagation in fractured rocks have led to methods of fracture detection that utilize the distinctive seismic signatures of such discontinuities.

The Yucca Mountain Site Characterization Project, which was started by DOE in 1983 for the purpose of locating an underground repository for commercial radioactive waste, is another major project that involves flow in fractured rocks. This project is located in southwestern Nevada, where there is a thick sequence of volcanic tuffs (~1000 m). The potential horizon for the repository is in the Topopah Spring Tuff (TSt), which is in the vadose zone some 325 m below the surface. A major effort has been the development of the Unsaturated Zone Site-Scale Flow Model. This model is being used in studies of: infiltration, matrix properties, fracture properties, pneumatic data, in-situ measurements, percolation flux, flow into drifts, fracture/matrix components, and flow patterns below the repository. To investigate the effects on fractured tuff of a thermal perturbation, a single heater test has been carried out underground in the TSt, and a drift scale heater test, of much larger dimensions, is currently under way.

One of the most recent developments in fracture hydrology has evolved from the results of lithological studies and infiltration tests in the basalt flows at the Box Canyon Site near the Idaho National Engineering and Environmental Laboratory in Idaho. The heterogeneous nature of the

fracture networks that result from the uneven cooling conditions that prevail within the basalt, as it solidifies from the liquid state, produces a chaotic system of flow channels. The result is a hierarchy of flow systems where the conditions that control the flow at one scale are not applicable to flow conditions at another scale. A detailed investigation of this chaotic flow behavior in fractured rock is currently under way.

Session 1:
THEORETICAL STUDIES OF FLOW IN FRACTURED ROCKS

A new free boundary problem for unsteady flows in porous and fissurized-porous rocks

G. I. BARENBLATT[1] AND J. L. VASQUEZ[2]

[1]Department of Mathematics
University of California, Berkeley
and
Lawrence Berkeley National Laboratory
1 Cyclotron Road
Berkeley, California 94720–3840

[2]Departamento de Matemáticas
Universidad Autonoma de Madrid
28049 Madrid, Spain

In the first part of the lecture, the model of flooding followed by a natural outflow through the endwall of the stratum will be considered. Horizontal porous stratum under the usual conditions of gently sloping fluid height profile $h(x,t)$ is assumed so that the governing equation is the classical Boussinesq equation

$$\partial_t h = \kappa \frac{\partial^2(h^2)}{\partial x^2}, \qquad \kappa = \frac{k\rho g}{2m\mu}, \quad 0 \le x < \infty \tag{1}$$

Here ρ is the fluid density, μ the viscosity of the fluid, k the permeability of the stratum, m its porosity, x the space coordinate, and t the time.

The explicit dipole solution is a generic intermediate asymptotic solution for this problem, and it gives a natural upper boundary for the outflow.

In the second part of the lecture the model of forced drainage performed to increase outflow will be considered. Forced drainage leads to a new kind of free boundary problem for the classical Boussinesq equation where the flux $q(t)$ and height $h = 0$ is prescribed on

the new free boundary $x = x_0(t)$, the end of the drainage tube. The qualitative behavior of the problem is described using self-similar solutions.

The following problems of control related to the problem under consideration seem to be of special interest. Control is performed via the outflow function $q(t)$: the fluid discharge at the moving boundary $x_0(t)$. Examples of possible control problems may be:

1. What conditions should be imposed on the control function $q(t)$ such that zero fluid level is supported at boundary $x = 0$?

2. What are the conditions on $q(t)$ for no return of the drainage boundary?

3. What are the conditions for the ground water dome to be trapped between some fixed boundaries?

In the third part of the lecture, the modifications introduced in the above models by capillary retention of a part of the fluid will be considered. Finally, the possible modifications in the above models due to influence of natural fissurization of the stratum will be discussed.

ON DYNAMIC PERMEABILITY

Garrison Sposito

Civil and Environmental Engineering

631 Davis Hall #1710

University of California

Berkeley, CA 94720-1710

e-mail: gsposito@nature.berkeley.edu

A cornerstone of nonequilibrium statistical mechanics is provided in the fluctuation-dissipation theorem (1), which is a very general relationship between the linear response of a physical system to an external perturbation and the thermal fluctuations in the system that occur spontaneously while it is in a state of equilibrium. In the case of fluid movement through a porous medium, which is a dissipative response to an applied gradient of chemical potential [the "driving force" for any mass transfer (2)], the fluctuation-dissipation theorem takes the form (3):

$$\mathbf{q}(\mathbf{x},t) = -(\rho k_B T)^{-1} \int_{-\infty}^{t} \int_{V'(\mathbf{x})} < \mathbf{j}(\mathbf{x},t)\, \mathbf{j}(\mathbf{x}',t') > \cdot \vec{\nabla}'\mu \; d^3x' dt' \qquad [1]$$

where $\mathbf{q}(\mathbf{x},t)$ is specific discharge, ρ is the fluid mass density, $\mu(\mathbf{x},t)$ is its chemical potential, and $\mathbf{j}(\mathbf{x},t)$ is its fluctuating mass-flux density vector at a point $\mathbf{x}$ in the porous medium (i.e., $\mathbf{j}(\mathbf{x},t)$ is the volume-averaged total linear momentum of all the fluid molecules in an element of porous medium with centroid at $\mathbf{x}$). The integral prefactor in [1] also contains the Boltzmann constant k_B and the absolute temperature T. The space integral is over a volume element $V'(\mathbf{x})$ with centroid at the point $\mathbf{x}$, in the usual continuum-hypothesis sense (4).

The dyadic enclosed by angular brackets in [1] is termed a "current-current space-time correlation function" (5, 6). It describes the average relaxation of the fluid in response to spontaneous local fluctuations in the velocities of its constituent molecules that are caused by

their random thermal motions. At some initial time $t' = t = 0$, these fluctuations simply reflect the average kinetic energy of the fluid molecules, and the space integral of the first scalar invariant of the current-current correlation function is proportional to the average thermal energy of the molecules (7):

$$\int_V \int_{V'} \langle \mathbf{j}(\mathbf{x},0) \cdot \mathbf{j}(\mathbf{x}',0) \rangle \, d^3x \, d^3x' = 3Mk_BT \qquad [2]$$

where M is the total mass of fluid enclosed within the volume of integration. At times $t' < t$, the current-current correlation function will decay in a roughly exponential manner while the equilibrium velocity fluctuations die out in the fluid (7). Equation [1] connects these decaying fluctuations with the dissipative fluid movement induced by an applied gradient in chemical potential. Hu and Cushman (8) have rediscovered this general result in a recent study of a nonlocal $(\mathbf{x} \neq \mathbf{x}')$, retarded $(t \neq t')$ form of the Darcy law for water movement in porous media.

Clarity in exposition is served if the porous medium is now assumed isotropic and homogeneous, and if advantage is taken of the time-stationarity of equilibrium correlation functions (6), such that [1] becomes:

$$Q_m(t) = -(\rho V k_B T) \int_0^\infty \int_{V'} \int_V \langle j_m(\mathbf{x},0) \, j_m(\mathbf{x}',\tau) \rangle \nabla'_m \mu(\mathbf{x}', t-\tau) \, d^3x \, d^3x' \, d\tau \qquad [3]$$

where

$$Q_m(t) \equiv \frac{1}{V} \int q_m(\mathbf{x},t) \, d^3x \qquad (m = 1,\ 2,\ 3) \qquad [4]$$

is the mth coordinate of the volume-averaged specific discharge vector. A further simplification is made by defining the normalized correlation function,

$$C_m(\mathbf{x}-\mathbf{x}',\tau) \equiv \frac{\langle j_m(\mathbf{x},0) j_m(\mathbf{x}',\tau) \rangle}{Mk_BT} \qquad [5]$$

such that [3] takes the form:

$$Q_m(t) = -\theta \int_0^\infty \int_{V'} \int_V C_m(\mathbf{x}-\mathbf{x}',\tau)\, \nabla'_m \mu(\mathbf{x}', t+\tau)\, d^3x\, d^3x'\, d\tau \qquad [6]$$

where $\theta \equiv M/\rho V$ is the (uniform) volumetric fluid content of the porous medium. Equation [6] is a generalized Darcy law relating specific discharge to the applied gradient of chemical potential.

Under a time-periodic, uniform applied pressure gradient with frequency ω,

$$\vec{\nabla}\mu = \mathrm{Re}\left\{\rho^{-1}\vec{\nabla}P \exp(i\omega t)\right\} \qquad [7]$$

and [6] reduces to the expression:

$$Q_m(t) = -(\theta/\rho)\mathrm{Re}\left\{\int_0^\infty e^{-i\omega\tau} \int_{V'} \int_V C_m(\mathbf{x}-\mathbf{x}',\tau)\, d^3x'\, d^3x\, d\tau\right\} \nabla_m P \cos(\omega t) \qquad [8]$$

where $\vec{\nabla}P$ is a uniform, constant pressure gradient. Comparison of [8] with the Darcy law (9) shows that the dynamic permeability is now defined by:

$$k_{mm}(\theta,\omega) = \theta\nu\, \mathrm{Re}\left\{\lim_{q\downarrow 0} \int_0^\infty e^{-i\omega\tau}\, C_m(q,\tau)\, d\tau\right\} \qquad (\omega > 0) \qquad [9]$$

where ν is kinematic viscosity and

$$C_m(q,\tau) = \int_{V'} \int_V \exp\left[i\mathbf{q}\cdot(\mathbf{x}-\mathbf{x}')\right] C_m(\mathbf{x}-\mathbf{x}',\tau)\, d^3x'\, d^3x \qquad [10]$$

is a Fourier transform. Equation [9] shows that the dynamic permeability is determined by the long-wavelength limit of the Laplace transform of $C_m(q,\tau)$. The static permeability is the zero-frequency limit of the right side of [9], in which case the time integral is simply the decay time constant τ_{qm} for $C_m(q,\tau)$ (7). In the case of water in an unsaturated soil, this time constant varies from 1 ps to 1 μs, depending on the value of the water content θ (7).

Calculation of $k_{mm}(\theta,\omega)$ for finite frequencies ($\omega > 0$) requires a physical model of the correlation function, $C_m(q,\tau)$. Some models for pure fluids are discussed by Boon and Yip (6). Sposito (7) has developed a model for fluids in porous media, based on the coupling of

fluctuations in the volumetric content of the fluid with fluctuations in its mass-flux density vector, leading to the permeability equation:

$$k_{mm}(\theta,\omega) = \theta v \lim_{q \downarrow 0} \frac{\omega^2/\tau_{qm}}{\left[\omega^2 - \omega_0^2(q)\right]^2 + \left(\omega/\tau_{qm}\right)^2} \qquad (\omega > 0) \qquad [11]$$

where

$$\omega_0^2(q) \underset{q \downarrow 0}{\sim} \theta g \left(\frac{\partial \psi}{\partial \theta}\right) q^2 \qquad [12]$$

with ψ being the pressure head and g the gravitational acceleration, and τ_{qm} is a time constant characterizing the decay of $C_m(q,\tau)$. The frequency in [12] describes fluid content fluctuations and depends on the relation between the pressure head and fluid content. It can be investigated by incoherent neutron scattering measurements (9). When $\omega = \omega_o(q)$, $k_{mm}(\theta,\omega)$ has a resonance whose sharpness (full width at half-maximum) is inversely proportional to the magnitude of τ_{qm}.

References

1. Kubo, R.; M. Toda; N. Hashitsume (1991) *Statistical Physics II* (Springer, New York).
2. Sposito, G. (1981) *The Thermodynamics of Soil Solutions* (Oxford Univ. Press, New York).
3. Sposito, G. (1978) *Water Resour. Res.* **14**:479-484.
4. Baveye, P.; G. Sposito (1984) *Water Resour. Res.* **20**:521-530.
5. Kadanoff, L.P.; P.C. Martin (1963) *Ann. Phys.* **24**:419-469.
6. Boon, J.-P.; Yip, S. (1980) *Molecular Hydrodynamics* (McGraw-Hill, New York).
7. Sposito, G. (1980) *Soil Sci. Soc. Am. J.* **44**:1159 – 1168.
8. Hu, X.; Cushman, J.H. (1994) *Stoch. Hydrol. Hydraul.* **8**:109-116.
9. Bear, J. (1988) *Dynamics of Fluids in Porous Media* (Dover, New York).
10. Sposito, G. (1982) *Mol. Phys.* **47**:1377-1389.

Fluid Flow in Rock Fractures: Cubic Law, Lubrication Equation and Stokes Equation

Robert W. Zimmerman[1] *and In-Wook Yeo*[2]

[1]Imperial College of Science, Technology and Medicine
London SW7 2BP, U.K.; r.zimmerman@ic.ac.uk

[2]Golder Associates UK
Nottingham NG12 4DG, U.K.; iyeo@golder.com

Introduction

Single-phase flow through a rough-walled rock fracture is the most basic problem in fractured-rock hydrology, and is the starting point for studies of more complex issues, such as two-phase flow, flow through fracture networks, hydromechanical coupling effects, *etc.* Nevertheless, this problem is not yet thoroughly understood, in that there is no agreement as to the conditions under which the Navier-Stokes equations can be replaced by simpler and more tractable governing equations such as the Stokes or lubrication equations. In this paper we will review the equations that govern single-phase fluid flow through a rough-walled rock fracture, and investigate the conditions under which the various levels of simplification are possible. Important practical implications of these mathematical considerations include the facts that (1) applicability of the Stokes equations implies a linear relationship between pressure drop and flowrate, *i.e.,* Darcy's law, and (2) presently, whereas the lubrication equation can be solved numerically for realistic fracture profiles, the Navier-Stokes and Stokes equations cannot.

From the Navier-Stokes Equations to the Stokes Equations

Fundamentally, flow through a rock fracture is governed by the Navier-Stokes (N-S) equations, a set of three coupled nonlinear PDEs which, in steady-state, can be written as

$$\rho(\mathbf{u}\cdot\nabla)\mathbf{u} = -\nabla P + \mu\nabla^2\mathbf{u}, \tag{1}$$

where ρ is the density, $\mathbf{u}$ is the velocity vector, μ is the viscosity, and P is a reduced pressure defined by $P = p + \rho g z$. The first term in (1) is the advective acceleration, the second term is the pressure gradient, and the third term represents viscous forces. To simplify the discussion, we will usually consider a fracture whose aperture varies in only one direction, the x-direction, which we take to be the direction of flow; the direction perpendicular to the fracture plane is z (Fig. 1a). The N-S equations must be supplemented by the equation for conservation of mass, $\nabla\cdot\mathbf{u} = 0$.

The starting point for all discussion of this problem is the special case of a fracture bounded by smooth, parallel walls separated by a distance h; this is in fact the only case that can be solved exactly. The velocity vector is given by (Zimmerman and Bodvarsson, 1996)

$$u_x = -(1/2\mu)(dP/dx)[z^2 - (h/2)^2], \quad u_z = 0. \tag{2}$$

This velocity profile can be integrated from $z = -h/2$ to $z = h/2$ to find the flowrate in the form

$$Q = w\int u(z)dz = -(1/12\mu)(dP/dx)wh^3, \tag{3}$$

where w is the length within the fracture, perpendicular to the flow direction. This result is usually written in terms of a transmissivity, T, defined by $Q = -(T/\mu)(dP/dx)$, in which case (3) gives the "cubic law" (Witherspoon *et al.,* 1980):

$$T = wh^3/12\,. \tag{4}$$

Unfortunately, the full N-S equations are too difficult to solve, either analytically or numerically, for real, rough-walled fractures. This is also true for idealised cases such as a fracture bounded by sinusoidal or sawtooth-shaped walls. Therefore, resort is usually made to various approximations that reduce the N-S equations to a more tractable form. The first level of

simplification is to discard the acceleration terms in the Navier-Stokes equations, which yields the steady-state Stokes equations, which are a coupled set of three *linear* PDEs:

$$\nabla P = \mu \nabla^2 \mathbf{u}. \tag{5}$$

This linearization is possible if the advective acceleration terms are small compared to the viscous terms. However, it is not easy to accurately estimate the size of the various terms without actually finding the detailed solution to the problem, so it is difficult to arrive at sufficient *a priori* conditions for the N-S equations to be replaced by the Stokes equations.

The simplest order-of-magnitude analysis is as follows. First, note that for the case of flow between two smooth, parallel plates, the velocity vector lies in the x-direction, whereas the velocity gradient lies in the z-direction, and so the advective acceleration terms, $\rho(\mathbf{u}\cdot\nabla)\mathbf{u}$, vanish identically. In the general case of variable aperture, there will be a non-zero z-component of the velocity, and both velocity components will vary in the x-direction, as well as in the z-direction. In component form, the Navier-Stokes equations (for 2-D, steady-state flow) can be written as

$$\rho\left(u_x \frac{\partial u_x}{\partial x} + u_z \frac{\partial u_x}{\partial z}\right) = -\frac{\partial P}{\partial x} + \mu\left(\frac{\partial^2 u_x}{\partial x^2} + \frac{\partial^2 u_x}{\partial z^2}\right), \tag{6}$$

$$\rho\left(u_x \frac{\partial u_z}{\partial x} + u_z \frac{\partial u_z}{\partial z}\right) = -\frac{\partial P}{\partial z} + \mu\left(\frac{\partial^2 u_z}{\partial x^2} + \frac{\partial^2 u_z}{\partial z^2}\right). \tag{7}$$

It seems reasonable to assume that the momentum-balance in the x-direction, *i.e.,* along the direction of flow, is in some sense the more important of these two equations. If we let U_x and U_z be characteristic velocities in the x- and z-directions, λ be the characteristic length scale in the x-direction, and $\langle h\rangle$ be the mean aperture, then we can estimate the size of the terms as follows

$$mag\left[\rho u_x \frac{\partial u_x}{\partial x}\right] \approx \frac{\rho U_x^2}{\lambda}, \quad mag\left[\rho u_z \frac{\partial u_x}{\partial z}\right] \approx \frac{\rho U_x U_z}{\langle h\rangle}; \tag{8}$$

$$mag\left[\mu \frac{\partial^2 u_x}{\partial x^2}\right] \approx \frac{\mu U_x}{\lambda^2}, \quad mag\left[\mu \frac{\partial^2 u_x}{\partial z^2}\right] \approx \frac{\mu U_x}{\langle h\rangle^2}. \tag{9}$$

Both inertial terms in (8) are zero for the parallel-plate case, so it is difficult to judge which of the two terms will be largest; both must therefore be considered. The relative magnitudes of the viscous terms in (9) depend on the ratio of aperture to wavelength, $\langle h\rangle/\lambda$. But small wavelengths always correspond to small values of roughness (Brown and Scholz, 1985), and small-scale roughness at a high spatial frequency is known to be irrelevant for laminar flow. So, it seems that we need only consider $\lambda > h$, in which case the second term in (9) is the dominant one. Therefore, for the inertial terms to be negligible, we must have

$$\frac{\rho U_x^2}{\lambda} << \frac{\mu U_x}{\langle h\rangle^2}, \quad \text{and} \quad \frac{\rho U_x U_z}{\langle h\rangle} << \frac{\mu U_x}{\langle h\rangle^2}, \tag{10}$$

which is equivalent to the two conditions

$$\frac{\rho U_x \langle h\rangle}{\mu} \cdot \frac{\langle h\rangle}{\lambda} << 1, \quad \text{and} \quad \frac{\rho U_z \langle h\rangle}{\mu} << 1. \tag{11}$$

An obvious choice for U_x is the mean velocity in the x-direction. Although the *mean* value of u_z must be zero, proper choice of a "characteristic velocity" in the z-direction is not as clear. If we consider the simple case of a sawtooth-type fracture profile (Fig. 1b), it seems that we can say

$$\frac{U_z}{U_x} \approx \frac{h_{\max} - h_{\min}}{\lambda} \approx \frac{\langle h\rangle}{\lambda}, \tag{12}$$

in which case we see that both conditions in (11) reduce to

$$\frac{\rho U_x \langle h \rangle}{\mu} \cdot \frac{\langle h \rangle}{\lambda} = Re \frac{\langle h \rangle}{\lambda} << 1, \tag{13}$$

where Re is the Reynolds number.

This is as far as one can go with order-of-magnitude analysis. We now compare condition (13) with the criterion that can be found using the second-order perturbation solution derived by Hasegawa and Izuchi (1983) for flow through a semi-sinusoidal channel (Fig. 1c):

$$T = \frac{w\langle h^{-3} \rangle^{-1}}{12} \left[1 - \frac{3\pi^2 (1-\delta^2)\delta^4}{5(1+\delta^2/2)} \left(1 + \frac{13}{8085} Re^2 \right) \varepsilon^2 \right], \tag{14}$$

where $\varepsilon = \langle h \rangle / \lambda$. The term in front of the brackets reduces to the cubic law when the channel is smooth. The term that varies with Reynolds number depends on both the normalized magnitude of the roughness, δ, and the smoothness parameter, ε. The δ-dependent term varies from 0 to 0.662, and so is on the order of 1. If we arbitrarily say that the inertial effects are non-negligible if they account for 10% of the total transmissivity, then the condition for neglecting inertia is

$$\frac{13}{8085} Re^2 \varepsilon^2 < 0.1, \quad \text{or,} \quad \varepsilon Re < 8. \tag{15}$$

This result is in rough agreement with the experimental findings of Iwai (1976) for flow through a tension fracture in granite. If we assume a value of ε on the order of 0.2, which seems reasonable, then (15) predicts that inertial effects will decrease the transmissivity by about 10% when the Reynolds number is about 40, in good agreement with the results in Fig. 4.36 of Iwai (1976).

From the Stokes Equations to the Lubrication Equation

Although they are linear, the Stokes equations are still very difficult to solve, and do not yet seem to have been solved for *any* realistic fracture geometry, either analytically or numerically. The next level of simplification often used in an attempt to arrive at a tractable governing equation is to replace the Stokes equations with the Reynolds lubrication equation (Brown, 1987). We start with the two Stokes equations for our "one-dimensional" fracture, which from (6) and (7) are

$$\frac{\partial P}{\partial x} = \mu \left(\frac{\partial^2 u_x}{\partial x^2} + \frac{\partial^2 u_x}{\partial z^2} \right), \qquad \frac{\partial P}{\partial z} = \mu \left(\frac{\partial^2 u_z}{\partial x^2} + \frac{\partial^2 u_z}{\partial z^2} \right). \tag{16}$$

All terms in (16b), which represents the momentum balance in the direction perpendicular to the fracture plane, are very small, so we neglect this equation. Using the estimates of the magnitudes of the two viscous terms in (16a) that were given in (9), we see that $\partial^2 u_x / \partial x^2$ will be smaller than $\partial^2 u_x / \partial z^2$, by a factor of about ten, if

$$\varepsilon^2 = \langle h \rangle^2 / \lambda^2 < 0.1, \quad \text{or} \quad \varepsilon = \langle h \rangle / \lambda < 0.3. \tag{17}$$

It is noteworthy that this condition does not depend on the variance of the fracture aperture; indeed, large aperture variations are acceptable, as long as they occur gradually.

If condition (17) is satisfied, the governing equations reduce to (in the more general case of a fracture whose aperture varies in both the x and y directions)

$$\frac{\partial P}{\partial x} = \mu \frac{\partial^2 u_x}{\partial z^2}, \qquad \frac{\partial P}{\partial y} = \mu \frac{\partial^2 u_y}{\partial z^2}. \tag{18}$$

These equations lead to an in-plane velocity vector that is parabolic in z, but which is directed parallel to the local pressure gradient. If this parabolic velocity profile is substituted into the conservation of mass equation, and integrated in the z-direction, we arrive at the Reynolds lubrication equation (Zimmerman and Bodvarsson, 1996):

$$\frac{\partial}{\partial x} \left(h^3 \frac{\partial P}{\partial x} \right) + \frac{\partial}{\partial y} \left(h^3 \frac{\partial P}{\partial y} \right) = 0, \tag{19}$$

which can be interpreted as a local version of the cubic law. The Reynolds equation can be solved by finite-difference or finite-element techniques for actual fracture aperture distributions. These solutions allow the estimation of transmissivity in terms of the statistics of the aperture distribution.

However, it is not clear that replacement of the Stokes equations by the lubrication equation is justifiable for real fractures, since there is often substantial roughness at wavelengths smaller than that required by (16). Furthermore, several researchers have recently compared Stokes and Reynolds simulations on simulated fracture aperture distributions (*i.e.,* Mourzenko *et al.*, 1995; Brown *et al.*, 1995), and concluded that the Reynolds approximation does not apply. Yeo (1998) measured apertures and transmissivities of a sandstone fracture, and found that the Reynolds equation overestimated the flow by a factor of 40-100%, despite the fact that the fracture was not particularly rough. One would assume that a Stokes simulation using the measured aperture profiles would yield the correct transmissivity, but this has yet to be verified.

Conclusions

The conditions under which the Navier-Stokes equations can be replaced by the Stokes equations seem to be fairly well-understood, and are consistent with experimental data. However, it is not clear that the Stokes equations can be replaced by the lubrication equation. Resolution of this issue will require Stokes simulations using real aperture profile data.

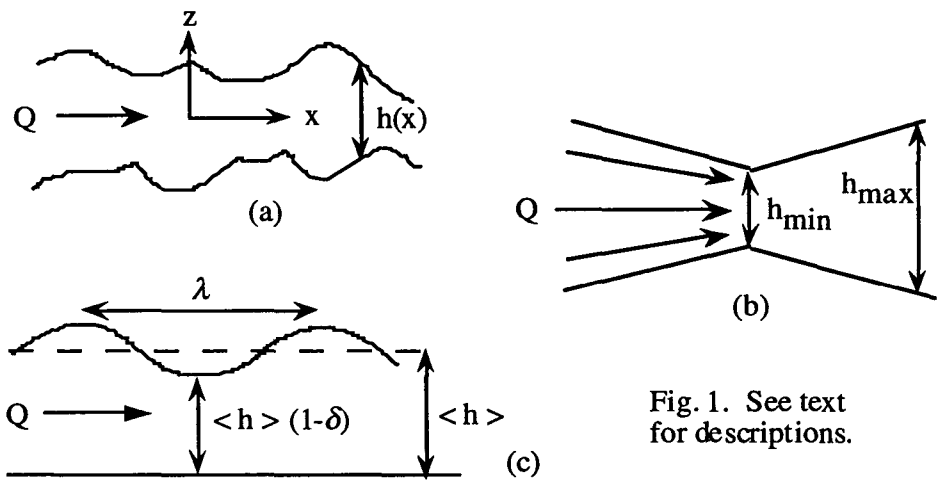

Fig. 1. See text for descriptions.

References

Brown, S. R., Fluid flow through rock joints: the effect of surface roughness, *J. Geophys. Res.*, vol. 92, pp. 1337-47, 1987.

Brown, S. R. and Scholz, C. H., Broad bandwidth study of the topography of natural surfaces, *J. Geophys. Res.*, vol. 90, pp. 12575-82, 1985.

Brown, S. R., Stockman, H. W., and Reeves, S. J., Applicability of the Reynolds equation for modeling fluid flow between rough surfaces, *Geo. Res. Letts.*, vol. 22, pp. 2537-40, 1995.

Hasegawa, E. and Izuchi, H., On the steady flow through a channel consisting of an uneven wall and a plane wall, *Bull. Jap. Soc. Mech. Eng.*, vol. 26, pp. 514-20, 1983.

Iwai, K., *FundamentalStudies of Fluid Flow through a Single Fracture,* Ph.D. diss., University of California, Berkeley, 1976.

Mourzenko, V. V., Thovert, J. F., and Adler, P. M., Permeability of a single fracture - validity of the Reynolds equation, *J. Phys. II*, vol. 5. pp. 465-82, 1995.

Witherspoon, P. A., Wang, J. S. Y., Iwai, K., and Gale, J. E., Validity of cubic law for fluid flow in a deformable rock fracture, *Water Resour. Res.*, vol. 16, pp. 1016-24, 1980.

Yeo, I. W., *Anisotropic Hydraulic Properties of a Rock Fracture under Normal and Shear Loading*, Ph.D. diss., Imperial College, London, 1998.

Zimmerman, R. W. and Bodvarsson, G. S., Hydraulic conductivity of rock fractures, *Transp. Porous Media*, vol. 23, pp. 1-30, 1996.

On Non-Newtonian Flow in Spatially Variable Fractures

Vittorio Di Federico

D.I.S.T.A.R.T. - Idraulica, Università di Bologna, Viale Risorgimento 2, Bologna 40136, ITALY e-mail: vittorio.difederico@mail.ing.unibo.it

Non-Newtonian fluid flow in porous and fractured media is of interest to hydrologists, geophysicists, and mining engineers. A large body of literature exists on non-Newtonian fluid flow in ordinary porous media (Savins, 1969, Barenblatt *et al.*, 1990). Several studies are specifically concerned with evaluation of an equivalent permeability, adopting different constitutive equations and porous medium models (Kutilek, 1972). In contrast to this, non-Newtonian fluid flow in fractured media has received little attention in the past, though it can be relevant, for example, in enhanced oil recovery operations, where often a power-law fluid of pseudo-plastic behaviour (water thickened with polymer additive) is used to minimize instability effects (James, 1984). Modeling these phenomena requires an understanding of non-Newtonian flow at the single fracture scale.

Laboratory and field investigations (Bear et al., 1993) evidenced a strong degree of variability in fracture aperture; the main goal of this study is to provide an estimation of the effects of this variability on the flow of a non-Newtonian fluid; much of the material that follows has been reported earlier by Di Federico (1997, 1998).

To model aperture variability in a single fracture, we follow two approaches: in the first one, the aperture is taken to vary as a two-dimensional, spatially homogeneous and correlated random field with a lognormal aperture density distribution of assigned mean $\langle b \rangle$ and variance σ^2 (Moreno at al., 1998; Silliman, 1989; Gelhar, 1993); in the second one, an idealized sinusoidal aperture variation (Zimmerman et al., 1991) of assigned mean aperture $\langle b \rangle$, amplitude of wall oscillations relative to mean aperture δ, and wavelength of aperture oscillations λ is examined.

To describe the fluid rheology, the power-law model (Bird *et al.*, 1960) of consistency index m and flow behaviour index n is used ($n < 1$ represents pseudoplastic fluids, $n > 1$ represents dilatant fluids).

An equivalent aperture for non-Newtonian fluid flow is then defined as the parallel plate aperture which would permit a given volumetric flux under an assigned pressure gradient, thereby generalizing the concept of hydraulic aperture used for Newtonian flow (Tsang, 1992). To derive an equivalent aperture for flow in a fracture with an isotropic aperture variation, we first consider one-dimensional flow in two limiting cases (Figure 1): in the first, flow is transverse to aperture variation; in the second, flow is parallel to aperture variation. In both cases, we derive analytical expressions for the fracture equivalent aperture by discretizing the fracture into elements of equal aperture and assuming that the resistances due to each aperture element are, respectively, in parallel and in series. In doing so, we assume that the shear between neighbouring channels and the drag against the connecting walls may be neglected. Further, in the random field case, the ergodicity assumption is invoked, i.e., the fracture dimensions are

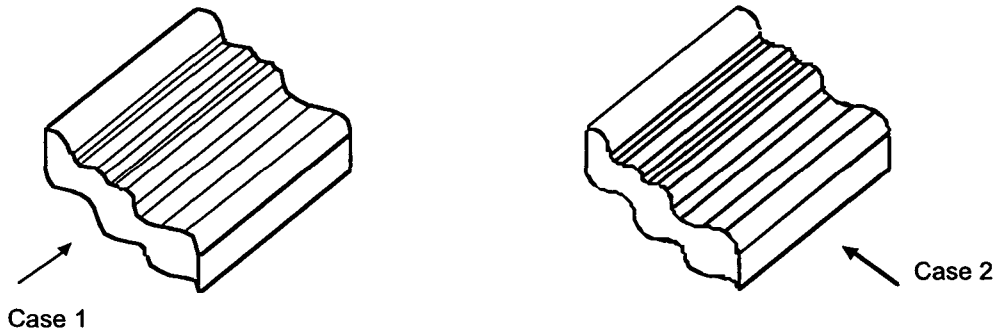

Figure 1

assumed to be much larger than the integral scale of the aperture autocovariance function; in the deterministic profile case, the sinusoidal profile is assumed to be hydraulically "smooth" enough for a lubrication-type approximation to hold.

For flow parallel to the aperture variation ("series" arrangement), the equivalent aperture is smaller than the mean, and their ratio decreases with increasing log-aperture variability, more so for a dilatant fluid ($n > 1$) than for a pseudoplastic one ($n < 1$); this is so because the volumetric rate is controlled mainly by the small apertures along the channel.

Flow in an isotropic aperture field is then addressed: while it is readily recognized that the actual flow field is highly complex, it can be argued that the equivalent apertures for "parallel" and "series" arrangements constitute respectively the upper and lower limits for the equivalent aperture in the two-dimensional case. The fracture is then envisaged as a random mixture of elements in which the fluid flows either transversal or parallel to aperture variation: an estimate of the equivalent aperture is derived as the geometric mean of the equivalent apertures for the two end cases.

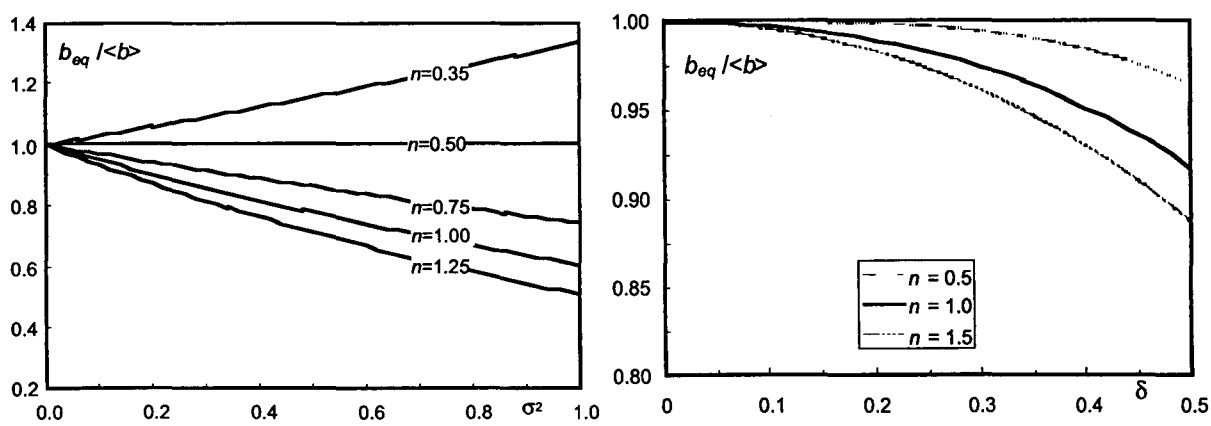

Figure 2

Results for stochastic (Figure 2a) and deterministic (Figure 2b) aperture variation are in agreement for $n > 0.50$: in this case, the equivalent aperture is less than the mean, and their ratio decreases as aperture variability (σ^2 or δ) increases, in agreement with results for a Newtonian

fluid obtained by several authors and reported by Zimmerman *et al.* (1991). This becomes more evident for a dilatant fluid ($n > 1$) than for a pseudoplastic one ($n < 1$). For very shear-thinning fluids with $n < 0.50$, results for stochastic and deterministic aperture variation differ. For a deterministic aperture variation, the equivalent aperture is less than the mean, and decreases as aperture variability increases, in agreement with the previous trend. For a stochastic aperture variation, the equivalent aperture is greater than the mean, and their ratio increases as aperture variability increases (for $n = 0.50$ it remains equal to one irrespective of aperture variability): in this case, the tendency of channels in parallel to increase permeability prevails upon the tendency of channels in series to reduce it.

For Newtonian flow ($n = 1$), all our expressions reduce to those derived by Silliman (1989) and Zimmerman et al. (1991), respectively for stochastic and deterministic aperture variation.

Our result, despite model simplifications, provide insight into non-Newtonian effects on flow in a variable aperture fracture; a more complete description of the real behavior should involve a comparison with experimental data.

References

Barenblatt, G. I., Entov, V. M., and Ryzhik, V. M.: 1990, *Theory of fluid flows through natural rocks*, Kluwer Academic Publishers, Dordrecht.

Bear, J., Tsang, C.-F., and deMarsily, G.: 1993, *Flow and Contaminant Transport in Fractured Rock*, Academic Press, San Diego, California.

Bird, R. B., Stewart, W. E., and Lightfoot, E. N.: 1960, *Transport Phenomena*, J. Wiley, New York.

Di Federico, V.: 1997, Estimates of equivalent aperture for Non-Newtonian flow in a rough-walled fracture, *Int. J. Rock Mech. Min. Sci. & Geomech. Abstr.*, **34**(7), 1133-1137.

Di Federico, V.: 1998, Non-Newtonian flow in a variable aperture fracture, *Transport in Porous Media*, **30**(1), 75-86.

Gelhar, L.W.: 1993, *Stochastic Subsurface Hydrology*, Prentice Hall, Englewood Cliffs.

Kutilek, M.: 1972, Non-Darcian flow of water in soils, Laminar region, in *Fundamentals of transport phenomena in porous media*, Developments in Soil Science 2, IAHR, Elsevier, Amsterdam, 327-340.

James, D. F.: 1984, Non-Newtonian effects in porous media flow, *Proc. IX Intnl. Congress on Rheology*, Mexico, 279-283.

Moreno, L., Tsang, Y. W., Tsang, C. F., Hale, F. V., and Neretnieks, I.: 1988, Flow and tracer transport in a single fracture: a stochastic model and its relation to some field observations, *Water Resour. Res.* **24**(12), 2033-2048.

Savins, J. G.: 1969, Non-Newtonian flow through poros media, *Ind. Eng. Chem.* **6**(10), 18-47.

Silliman, S. E.: 1989, An interpretation of the difference between aperture estimates derived from hydraulic and tracer tests in a single fracture, *Water Resour. Res.* **25**(10), 2275-2283.

Tsang, Y. W.: 1992, Usage of "equivalent apertures" for rock fractures as derived from hydraulic and tracer tests, *Water Resour. Res.* **28**(5), 1451-1455.

Zimmerman, R. W., Kumar, S., and Bodvarsson, G. S.: 1991, Lubrication theory analysis of the permeability of rough-walled fractures, *Int. J. Rock Mech. Min. Sci. & Geomech. Abstr.* **28**(4), 325-331.

Predicting Hydrology of Fractured Rock Masses from Geology: Techniques, Successes and Failures from Recent Case Histories

Paul R. La Pointe
Golder Associates Inc.
4104 148th Ave. NE
Redmond, WA 98052
plapointe@golder.com

Fractures are geological features that connect together to transport fluids through rock over long distances. The rate of movement, the volume of flow and the ability to transport mass through this system of interconnected fractures governs such diverse activities as petroleum reservoir development, safe disposal of nuclear waste, delineation of water supply or establishment of well head protection plans, recovery from geothermal reservoir, the efficiency of solution mining, the construction of underground openings and the remediation of contaminated rock.

It is common for engineers and hydrologists to rely upon hydrological testing of various types in order to carry out the previously mentioned activities. However, well tests are often expensive or logistically infeasible. For example, the number and the spatial reach of wells drilled from an offshore oil platform is very much restricted with respect to the reservoir. This may lead to the situation where direct hydrological test results are very sparse for the volume of rock under consideration, which is a problem, since hydrological heterogeneity is often quite high, so that a few tests may not provide an accurate description of the hydrologic properties of the remainder. There have been two generic approaches devised to extrapolate tests results to untested volumes of rock: statistical (geostatistics, stochastic inversion, fractals, etc.) and geological.

The statistical techniques utilize very little geology, except to delineate large-scale statistically homogeneous regions. The interpolation or extrapolation is carried out within each of these large-scale domains independent of the geology inside. The interpolation is a function of the spatial statistical model that the measurements appear to conform to, or an inversion that matches known well test results, but is constrained elsewhere to statistical parameters only. Such purely statistical simulation of hydrological properties such as permeability for numerical models has not proven successful for many fractured rock engineering projects, since the interpolation/inversion methods treat the rock as a stochastic continuum. Fracture-dominated flow in rock masses often significantly departs from this continuum assumption.

Geological techniques make the bold presumption that geology has *something* to do with hydrology, and that by understanding the geological characteristics that are associated with hydrological variability, it is possible or useful to assign values of permeability or some such property at unmeasured regions based upon the geological characteristics.

They have found increasing importance since they can be used to geologically condition discrete fracture models, such as are becoming increasingly useful in the fields of petroleum reservoir engineering and nuclear waste management. Such models are much more accurate than statistical models when the conductive fracture network does not respond as a continuum at the scale of interest, which turns out to be *most* scales of interest.

The geological approach is very appealing, since it is much more flexible in handling hydrological variability due to variability in underlying geology than any statistical model. However, the attempt to relate flow in fractured rock masses to underlying geology has proven less successful than might be expected. This paper illustrates several projects undertaken by the author and his colleagues using several different approaches in different geological settings. Among the parameters considered were host rock type; fracture aperture, planarity, roughness; filling types and thicknesses; alteration type, thickness and degree; weathering degree; proximity to large structural features such as faults; depth; mechanical layering contrasts; and grain size. Hydrological parameters include those pertaining to individual fractures, such as whether it is dry, moist, dripping or flowing, or its measured transmissivity; and to well tests of various types.

The techniques described include the application of several different types of neural nets, in particular, Kohonen self-organizing nets, Back-propagation (BP) nets of different architectures, probabilistic neural nets (PNN) and Generalized Regression neural nets (GRNN); conventional contingency table analysis; and linear discriminant analysis.

These studies show that certain geological features are characteristic of fractures that play a role in fluid movement on a regional basis, as opposed to fractures that play only a minor role. While some characteristics are site-specific, certain factors like size, planarity and orientation often are significant. Some parameters like aperture, are very complex; while open fractures are often more prone to be part of the regional flow system, closed fractures or fractures with very small geometrical aperture are as likely to be part of the flow system as not. In other words, being open is a positive factor, but being closed is not a negative factor; it is just a neutral factor. Making the connection between conductive fractures and well test results can be even more problematic.

This paper will briefly compare and contrast the various methods that can be used to relate geological parameters to hydrological parameters. Next, results from several case studies will be presented, illustrating the success or lack thereof in relating the geological parameters to the hydrological ones, along with observations as to why the linkage was successful or not. Finally, the paper will conclude with recommendations for future lines of research into improving the predictability of hydrological variability from the underlying mappable geology.

Session 2:
MULTI-PHASE FLOW AND REACTIVE CONTAMINANT TRANSPORT IN FRACTURED ROCKS

Multiphase Flow in Fractured Rocks - Lessons Learned from Mathematical Models

Karsten Pruess

Earth Sciences Division, Lawrence Berkeley National Laboratory
University of California, Berkeley, CA 94720

Introduction

Fractured rock formations encompass an enormous variety of hydrogeologic properties. For the recovery of resources such as oil, gas, and geothermal energy from fractured reservoirs we are primarily interested in systems with well-connected fracture networks of high permeability, and with good matrix permeability and porosity. For purposes of underground waste disposal, we generally prefer media with the opposite characteristics, i.e., sparse and poorly connected fractures, and low matrix permeability. Multiphase flow processes of interest in fractured media include two-phase flows of water and gas, water and NAPL (non-aqueous phase liquid), and water and steam, and three-phase flow of oil, water, and gas. Water seepage through the vadose zone is a special kind of multiphase flow process which is an essential component of the hydrologic cycle, and which may often be described in approximate fashion by considering the gas phase as a passive bystander. Multiphase flows may be further complicated by strongly coupled heat transfer effects, as e.g. in geothermal production and injection operations, in thermally enhanced recovery of oil and of volatile organic contaminants, and in the geologic disposal of heat-generating high-level nuclear wastes.

Depending on the nature of the fractured flow system under study, and the engineering or geoscientific interest and purpose in dealing with the system, different approaches will be employed for characterization and modeling. In this article we limit ourselves to methods that are based on the sound principles and well-established continuum field theories of classical theoretical physics, in which conservation of the active system components (water, air, chemical constituents, heat) is expressed by means of integral or partial differential equations (PDEs) for space-and-time varying fields of phase saturations, pressures, temperatures, solute concentrations, etc. Mass and heat fluxes are expressed through phenomenological relationships between intensive variables that drive flow, such as multiphase extensions of Darcy's law for phase fluxes, Fick's law for mass diffusion, Scheidegger's hydrodynamic dispersion, and Fourier's law for heat conduction. Alternative approaches such as lattice gas automata and chaos theory have shown promise for describing multiphase flows in fractures, but are outside the scope of this article.

Volume-Averaged Continuum Approaches

The study of fractured multiphase flow systems began in the context of oil and gas recovery. The groundbreaking concept on which most later work was based is the "double-porosity" method (DPM), formulated by Barenblatt et al. in 1960, and introduced into the U.S. petroleum literature by Warren and Root (1963). The basic idea is to associate with each "point" in a fractured reservoir domain not just one but two sets of hydrogeologic parameters and thermodynamic state variables. The fractures are viewed as a porous continuum which carries the global flow in the reservoir, and is characterized by customary porous medium-type parameters (absolute and relative permeability, porosity, and compressibility). The matrix blocks provide storage and exchange fluid with the fractures locally. This "interporosity flow" is assumed to be "quasi-steady," occuring at rates that are proportional to the difference in fluid pressures. A schematic illustration of the double-porosity method is given in Fig. 1. The early double-porosity work emphasized single phase flow and closed-form analytical solutions, while later developments used numerical simulation to study processes such as waterflooding of fractured petroleum reservoirs, where water injected into the fracture system is imbibed into matrix blocks by capillary

force, expelling oil (Kazemi et al., 1976, 1989; Thomas et al., 1983). Extensions of the double-porosity concept include the "dual permeability model" (abbreviated "DKM"), where global flow may occur in both fracture and matrix continua, and the method of "multiple interacting continua" (MINC; Pruess and Narasimhan, 1985), which partitions matrix blocks into several continua based on the distance of matrix material from the fractures. The MINC approach can resolve gradients driving interporosity flow under conditions where the perturbations in the fracture system invade the matrix blocks only slowly.

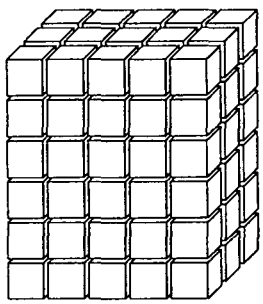

Figure 1. Schematic of the double-porosity concept (DPM; after Warren and Root, 1963). Global flow occurs exclusively through a network of interconnected fractures, which may interact with embedded matrix blocks of low permeability locally.

Absolute and Relative Permeability

Modeling of multiphase flow behavior with DPM, DKM, or MINC approaches requires specification of absolute and relative permeabilities for the fracture continuum. From the mid-60s to the mid-80s the prevailing view in the petroleum literature was that, for fractures, relative permeabilities of wetting and non-wetting phases should sum to 1 regardless of saturation, $k_{rw} + k_{rn} \approx 1$. Often the even more sweeping assumption was made that relative permeabilities should be equal to the respective phase saturations, $k_{rw} \approx S_w$, $k_{rn} \approx S_n$. These notions about fracture relative permeabilities can be traced back to laboratory experiments by Romm (1966), who used artificial assemblies of parallel plate fractures lined with different materials. Experimental and theoretical work during the last ten years has cast considerable doubt that simplistic notions of "fracture relative permeabilities" are applicable to realistic, rough-walled natural fractures, although the issue remains far from settled at the present time.

Considerable efforts have been made to determine permeability characteristics of individual fractures and of fracture networks in two and three dimensions, for both single-phase and multiphase conditions. The single-phase work has clarified the interplay between geometric characteristics of the fracture network (spacing, length, orientation) and permeability, and the approach to porous medium-like behavior for well-connected networks. The multiphase studies have considered the relative permeability of individual fractures, or fracture networks, to two phases flowing simultaneously. It was found that interference between phases is strong, causing the sum of wetting and non-wetting phase relative permeabilities to be small at intermediate saturations (Pruess and Tsang, 1990). This was confirmed in laboratory experiments (Persoff and Pruess, 1995), and is consistent with insights gained from percolation theory for the connectivity of two-dimensional lattices.

The practical implications of these findings are less clear. For field-scale flow processes it is conceivable that wetting phase may flow in the "small" fractures, and non-wetting phase in the "large" fractures, with minimal phase interference. In other words, the problem of two-phase flow in individual fractures may not be relevant to multiphase flow behavior in a field-scale fracture network.

High-Resolution Finite Differences

In thick unsaturated zones in fractured rocks of (semi-)arid regions, water seepage may proceed through highly localized preferential pathways. Then much of the fracture volume does not participate in flow, and large-scale volume averages may be completely meaningless. Continuum

concepts may still be applicable for these systems, however, if applied on the actual scale where the flow processes occur. A key concept that has provided much useful insight into multiphase flow behavior is the view of fractures as "two-dimensional heterogeneous porous media." Fractures are discretized into subregions of order 0.1 m, and the customary continuum concepts of absolute and relative permeability, and capillary pressure are applied (Pruess, 1998). Justification for this is provided by laboratory experiments which have shown that, for "slow" flows in "small" fractures, continuum concepts are indeed applicable on a scale of order 0.1 m (Persoff and Pruess, 1995). An areally extensive fracture is modeled as consisting of spatially-correlated subregions with different permeability and capillary pressure characteristics (Fig. 2).

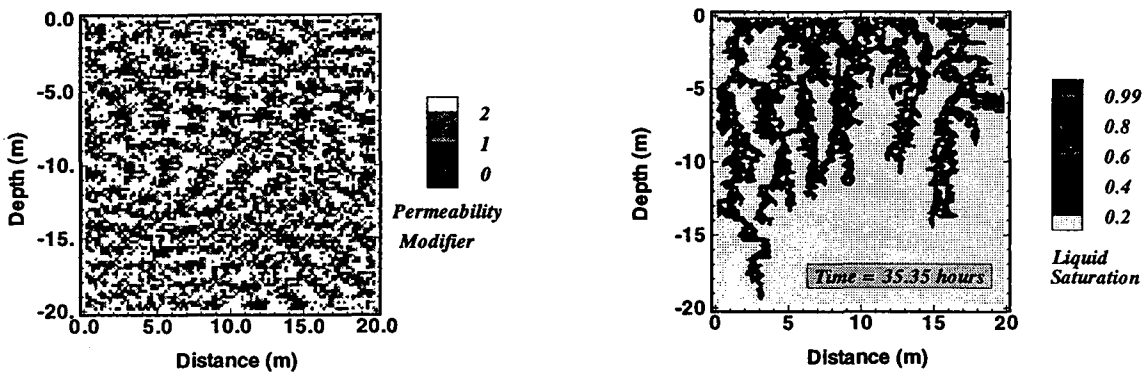

Figure 2. Stochastic permeability field (left) and seepage pattern (right) at the time of breakthrough at a depth of -19.5 m for water injection at a constant rate of 10^{-3} kg/s over the entire top of the fracture.

Simulation studies of water seepage in synthetic fractures with highly-resolved heterogeneity have produced useful insights into hydrogeologic mechanisms in thick unsaturated zones in fractured rock. Fracture flow was found to proceed not in smooth sheets, but in dendritic patterns along localized preferential paths, giving rise to such features as ponding and bypassing. As long as fluxes are small compared to saturated hydraulic conductivity, unsaturated seepage may be dominated by flow funneling into localized pathways, due to sub-horizontal barriers that may be formed by asperity contacts or fracture terminations. Flow funneling effects and localized seepage flux will increase with increasing length of sub-horizontal barriers, while average vertical fracture permeability, as could be measured by monitoring the propagation of gas pressure disturbances, would decrease. Thus we have the remarkable situation that unsaturated seepage can actually proceed faster in media with lower average permeability (Pruess, 1998). This seemingly paradoxical result emphasizes aspects that are unique to unsaturated flow in fractured media, and suggests that "average permeability" may not be a meaningful parameter for this process.

Water Injection into Vapor-Dominated Geothermal Reservoirs

Extensive steam production from the fractured vapor-dominated geothermal reservoirs at Larderello, Italy, and The Geysers, California, has caused a decline of reservoir pressures and well flow rates, and has led to an underutilization of installed electric generating capacity. Injection of water is the primary means by which dwindling fluid reserves can be replenished, and field life and energy recovery be enhanced. When cold water is injected into hot fractures, heat transfer from the rocks to the fluid occurs slowly (conductively), giving rise to very broad zones with gradual changes in fluid temperatures and saturations. In sub-vertical fractures injection plumes evolve through a complex interplay of heat transfer, boiling and condensation phenomena, gravity effects, and two-phase flow. Because vapor has much lower density than liquid water it has larger kinematic viscosity and acts as the more viscous fluid. Very considerable vapor pressure gradients may be generated during vaporization, which may be comparable in magnitude to gravitational body force on the liquid, providing a mechanism for lateral flow of liquid, with associated potential for early breakthrough at neighboring production wells.

Nuclear Waste Disposal

Mathematical models have been extensivley used in the investigations of Yucca Mountain as a potential site for a high-level nuclear waste repository. Numerical simulations of flow and transport at Yucca Mountain have generally emphasized large-scale spatial averages, and have employed fracture continuum approaches, such as DPM, DKM, MINC, and single effective continuum models (ECM). High-resolution models with explicit discretization of fractures have also been used to study basic mechanisms of fluid and heat flow in this unusual hydrogeologic environment. Large-scale volume-averaged models have been very successful at describing the propagation of barometric or artificial (man made) pressure pulses, and for describing temperature evolution during heater tests. Gratifying as this success is it is not unexpected, because gas flow and heat conduction, being described by parabolic partial differential equations, are subject to strong internal averaging mechanisms. Water seepage in fracture networks at rates far below saturated hydraulic conductivity, however, is described by a hyperbolic PDE. In this case internal averaging mechanisms are essentially absent, and volume averages are not enforced through physical processes in the flow system, but are formal constructs of the analyst. Predictions of water seepage from volume-averaged continuum models must therefore be interpreted with a great deal of caution.

Recent observations of environmental tracers in the Exploratory Studies Facility at Yucca Mountain have provided direct evidence that water can flow through unsaturated fractured rocks over vertical distances of several hundred meters at velocities of order 10 m/yr or more. As remarked by Cook (1991), it is difficult to understand "how fractures could remain sufficiently saturated to act as fast paths in the face of high matrix suction [of order $P_m \approx -3$ bar]." Matrix imbibition indeed would be a very strong process if water were flowing down fractures in the form of area-filling sheets. However, recent mathematical modeling has demonstrated and quantified several mechanisms that could drastically diminish water imbibition into the rock matrix, including (1) funneling of flow into localized preferential pathways, which reduces the wetted area where imbition occurs, (2) episodic nature of infiltration, which reduces the time available for removing water from the fractures, and (3) mineral coatings on fracture walls, which reduce imbibition fluxes.

Emplacement of heat-generating high-level nuclear wastes in thick unsaturated zones of fractured tuff at Yucca Mountain would give rise to complex multi-phase fluid flow and heat transfer processes. Numerical simulations for idealized systems have predicted that over time the rock in the vicinity of the heat sources will dry out. This observation has led some workers to propose a repository concept called "extended dry," in which high thermal loading would be used to effectively protect waste packages from being contacted by liquid water. However, critics have pointed out that liquid water can migrate considerable distances through fractured rock that is at above-boiling temperatures and be only partially vaporized (Pruess, 1997). An added concern is that large repository heat loads would increase rates of vaporization and condensate formation, promoting non-equilibrium matrix-fracture flow effects that could conceivably even enhance localized and intermittent water flow near the waste packages (Pruess and Tsang, 1994).

Concluding Remarks

Fractured flow systems exhibit a tremendous diversity of fracture and rock matrix properties, and flow and transport processes. Different approaches have been developed for flow modeling on a range of space and time scales. Early work on fractured flow systems emphasized applications to oil and gas reservoirs and large-scale volume averaged approaches. More recently there is increasing interest in applications related to waste disposal, and to environmental protection and remediation, which typically involve higher spatial resolution of small-scale processes. Much useful insight into multiphase flow behavior and mechanisms in fractured formations has been gained through the study of idealized systems. Examples include oil recovery from fractured reservoirs through water- and steam-flooding, injection of cold water into fractured geothermal reservoirs, and water seepage in unsaturated rock fractures. Applications to site-specific predictive

modeling have been more difficult to achieve, as they raise difficult issues of characterization and model calibration, and applicability of conceptualizations for processes operating on different space and time scales. A general problem with modeling of flow in fractured media arises from the geometric complexity of individual fractures and fracture networks. Fracture geometry on different scales is a very natural starting point for flow and transport modeling, but geometric features that are crucial for flow behavior, such as fracture connectivity, are very difficult to determine in the field.

Acknowledgement

The author appreciates careful reviews by Yushu Wu and Boris Faybishenko. This work was supported, in part, by the Assistant Secretary for Energy Efficiency and Renewable Energy, Geothermal Division, and by the Director, Office of Energy Research, Office of Health and Environmental Sciences, Biological and Environmental Research Program, of the U.S. Department of Energy under Contract No. DE-AC03-76SF00098.

References

Barenblatt, G.E., I.P. Zheltov and I.N. Kochina. Basic Concepts in the Theory of Seepage of Homogeneous Liquids in Fissured Rocks, *J. Appl. Math* , 24 (5), 1286-1303, 1960.

Cook, N.G.W., I. Javandel, J.S.Y. Wang, H.A. Wollenberg, C.L. Carnahan, K.H. Lee. A Review of Rainer Mesa Tunnel and Borehole Data and Their Possible Implications to Yucca Mountain Study Plans. Lawrence Berkeley Laboratory Report LBL-32068, December 1991.

Kazemi, M., L.S. Merrill Jr., K.L. Porterfield and P.R. Zeman. Numerical Simulation of Water-Oil Flow in Naturally Fractured Reservoirs, *Soc. Pet. Eng. J.*, 317-326, December 1976.

Kazemi, H. and J.R. Gilman. Multiphase Flow in Fractured Petroleum Reservoirs, Proceedings, Advanced Workshop on Heat and Mass Transport in Fractured Rocks, Laboratorio Nacional de Engenharia Civil (LNEC), Lisbon, Portugal, June 1989.

Persoff, P. and K. Pruess. Two-Phase Flow Visualization and Relative Permeability Measurement in Natural Rough-Walled Rock Fractures, *Water Resour. Res.*, Vol. 31, No. 5, pp. 1175-1186, May 1995.

Pruess, K. On Vaporizing Water Flow in Hot Sub-Vertical Rock Fractures, *Transport in Porous Media*, Vol. 28, pp. 335 - 372, 1997.

Pruess, K. On Water Seepage and Fast Preferential Flow in Heterogeneous, Unsaturated Rock Fractures. *J. Contam. Hydr.*, Vol. 30, No. 3-4, pp. 333 - 362, 1998.

Pruess, K. and T.N. Narasimhan. A Practical Method for Modeling Fluid and Heat Flow in Fractured Porous Media, *Soc. Pet. Eng. J.*, 25 (1), 14-26, February 1985.

Pruess, K., and Y.W. Tsang. On Two-Phase Relative Permeability and Capillary Pressure of Rough-Walled Rock Fractures, *Water Resour. Res.*, Vol. 26, No. 9, pp. 1915-1926, September 1990.

Pruess, K. and Y. Tsang. Thermal Modeling for a Potential High-Level Nuclear Waste Repository at Yucca Mountain, Nevada. Lawrence Berkeley Laboratory Report LBL-35381, March 1994.

Romm, E. S. *Fluid Flow in Fractured Rocks*, Nedra Publishing House, Moscow, 1966 (translated by W. R. Blake, Bartlesville, OK, 1972).

Thomas, L.K., T.N. Dixon and R.G. Pierson. Fractured Reservoir Simulation, *Soc. Pet. Eng. J.*, 42-54, February 1983.

Warren, J.E. and P.J. Root. The Behavior of Naturally Fractured Reservoirs, *Soc. Pet. Eng. J., Transactions, AIME, 228*, 245-255, September 1963.

Two-Phase Flow in a Variable Aperture Fracture: Laboratory Validation of a Two Dimensional Numerical Model

S.E. Anderson and N.R. Thomson
Department of Civil Engineering, University of Waterloo, Waterloo, Ontario, Canada

Introduction

Over the past few decades, dense non-aqueous phase liquids (DNAPLs) have been identified as an important class of groundwater contaminants due their low aqueous solubilities and even lower drinking water standards; together these properties enable a relatively small volume of a DNAPL to contaminate a large volume of groundwater. In addition, the relatively high densities and often low viscosities of DNAPLs allow them to migrate over considerable distances, both vertically and laterally in the subsurface.

Many sites at which DNAPLs are released into the subsurface are located above fractured geologic deposits (e.g., Smithville Waste Storage Facility, Smithville, Ontario; Bear Creek Burial Grounds, Bear Creek, Tennessee). It is critical to understand the behavior of DNAPLs in these environments because fractured rock aquifers are a common source of drinking water, and fractures can act as significant contaminant pathways in fractured aquitards. The remediation of fractured-porous media systems contaminated by DNAPL compounds is exceptionally difficult because complex fracture networks make it nearly impossible to predict the DNAPL distribution. Furthermore, existing remediation technologies are relatively ineffective in highly heterogeneous media, such as fractured rock [Mackay and Cherry, 1989].

The purpose of this paper is to present some of our current findings dealing with the comparison between results from a numerical model which simulates two phase flow in a variable aperture fracture, and observations from laboratory experiments. A transparent polymer resin was used to fabricate a cast of a natural rough-walled limestone fracture. The transparent nature of the synthetic fracture plane allowed for the measurement of aperture distribution using a co-ordinate measurement machine (Mitutoyo), and for the visualization of DNAPL flow and distribution. The aperture distribution of the laboratory fracture was used in the numerical model, thus permitting a meaningful comparison between the numerical simulations and the experimental observations.

Numerical Model

The model, which simulates two dimensional, two phase, transient flow in a single variable aperture fracture, is referred to as FRAC22. The model was based upon mass conservation in a parallel plate fracture, and uses a finite volume discretization technique [Murphy and Thomson, 1993]. Simulation results from FRAC22 demonstrate several dynamic processes for two phase flow in a variable aperture fracture, including [Murphy and Thomson, 1993]:

1. the hindrance of non-wetting fluids from entering larger aperture regions due to intervening smaller aperture regions;
2. the pinching off of a non-wetting fluid due to a decrease in capillary pressure upon encountering a larger aperture region;
3. the density driven migration of a denser fluid opposite to the flow direction of a lighter fluid; and
4. the migration of isolated globules due to pressure gradients in the surrounding fluid.

Laboratory Experiments

The process by which the synthetic fracture plane was constructed is illustrated in Figure 1. The method, adapted from Gentier *et al.* [1989], involves first using silicone to cast a negative of both fracture walls. The silicone negatives are employed to form a positive of each fracture wall using a transparent polymer resin. The transparent fracture walls are then mated to create a synthetic fracture plane.

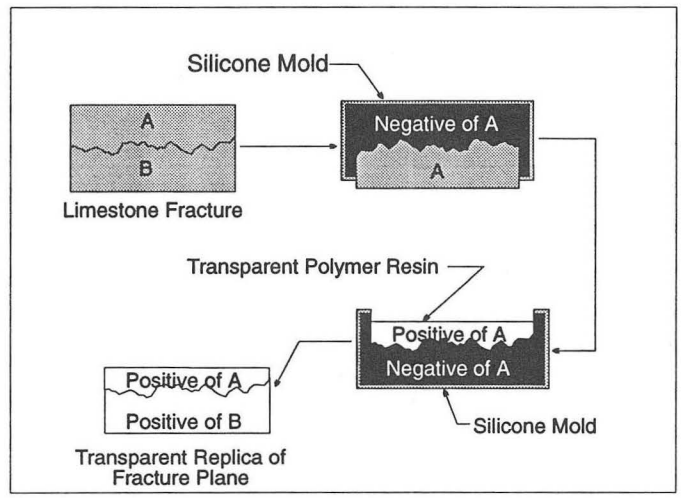

Figure 1: Construction of a Synthetic Fracture Plane

The synthetic fracture plane constructed for these experiments is approximately 24.5 cm long by 14.7 cm wide. It has a mass balance aperture of approximately 900 μm, a cubic law aperture of approximately 140 μm, and a frictional loss aperture of approximately 65 μm, as defined by Tsang [1992].

The aperture distribution was obtained using a co-ordinate measurement machine; the stylus measured the x, y and z co-ordinates every 2 mm on both limestone fracture faces. The co-ordinate mappings were then mated to obtain the aperture distribution.

The experimental methodology involved emplacing a DNAPL in the fracture plane under a fixed capillary pressure and observing the resulting DNAPL flow and distribution. Once a steady-state flow field was reached, the DNAPL source was removed and a water flush was conducted in an attempt to mobilize the entrapped DNAPL.

Figures 2 through 5 illustrate the results of a DNAPL emplacement experiment conducted in this synthetic fracture plane; the lighter color represents the DNAPL and the darker color represents the water. In this particular experiment, the DNAPL was emplaced under a capillary pressure of 1 cm of water.

Figure 2 illustrates the mechanism by which a smaller aperture region can obstruct the non-wetting fluid, thus preventing it from entering larger aperture regions beyond the tighter aperture regions. The pinching-off effect is illustrated in Figure 3. The DNAPL reached the end of the fracture plane, causing a decrease in capillary pressure; the resulting capillary pressure was no longer large enough to support the invasion of the non-wetting fluid in several smaller aperture regions. Figure 4 illustrates the downstream migration of a DNAPL globule, due to an increase in capillary pressure.

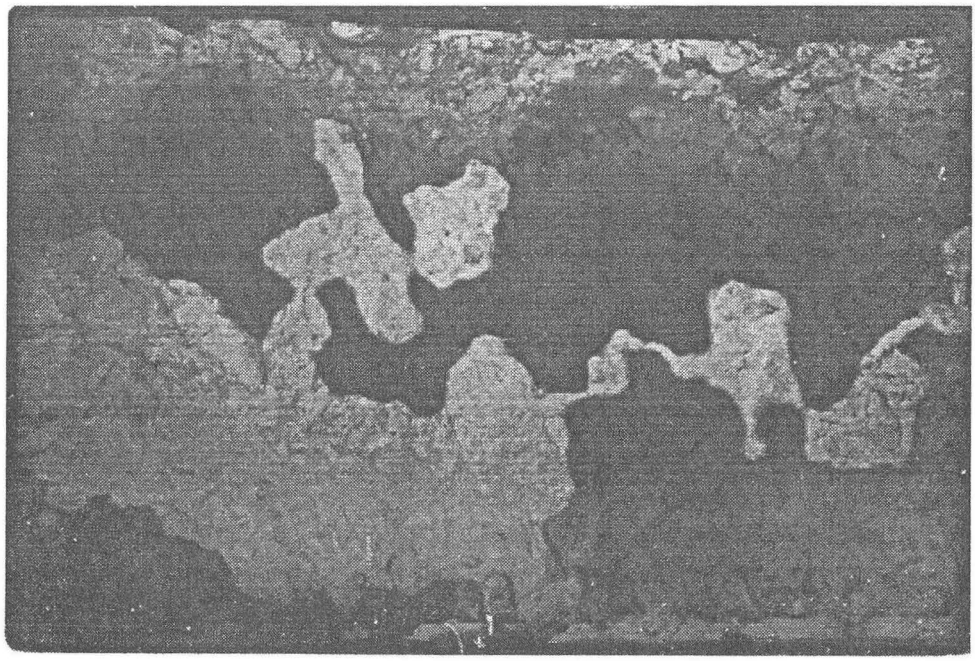

Figure 2: Synthetic Fracture Plane, Obstruction of DNAPL Movement
(2 minutes and 30 seconds after the start of DNAPL emplacement)

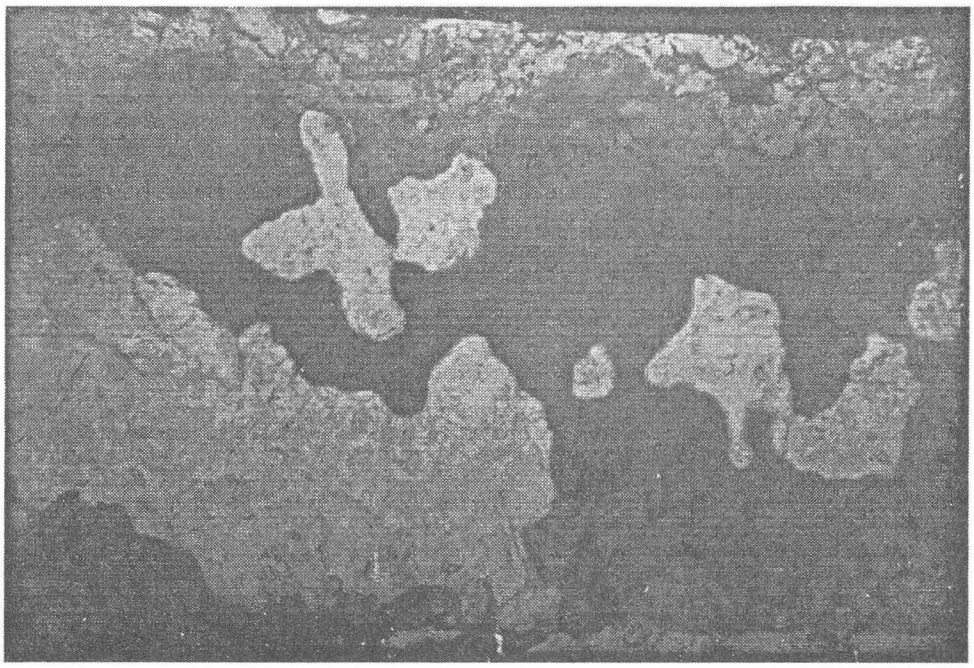

Figure 3: Synthetic Fracture Plane, Pinching-Off Effect
(2 minutes and 35 seconds after the start of DNAPL emplacement)

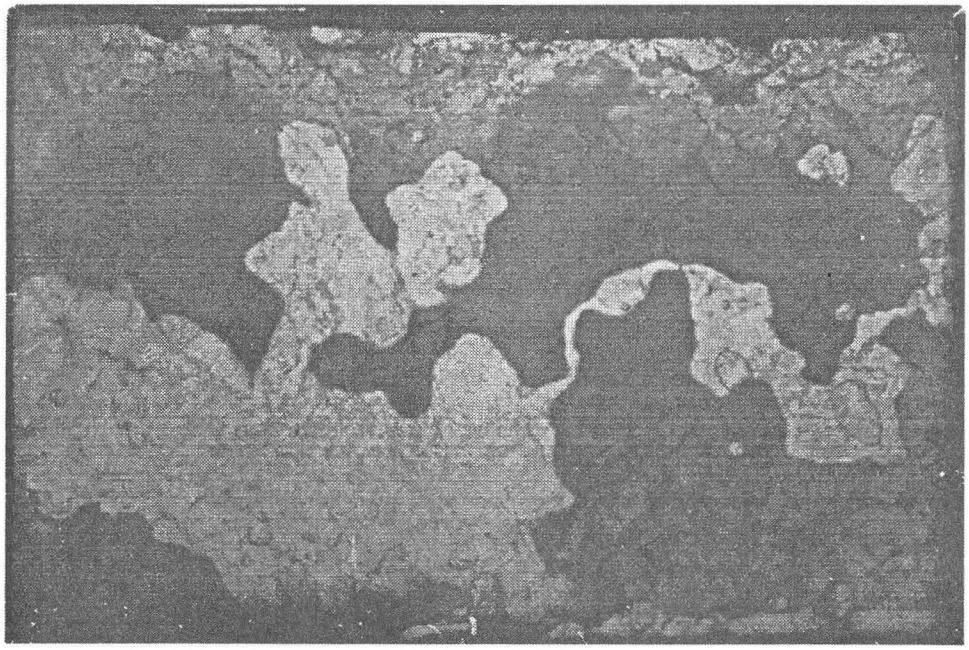

Figure 4: Synthetic Fracture Plane, DNAPL Migration
(3 minutes and 10 seconds after the start of DNAPL emplacement)

Summary

The laboratory experiments conducted to date have demonstrated two phase flow phenomena similar to those simulated by the FRAC22 model. The results of these laboratory experiments will be presented, and the validity of the model will be assessed.

The potential verification of this model suggests that it is feasible to mathematically model two phase flow in a variable aperture fracture. This provides a further step towards competently characterizing DNAPL spills in fractured rock and assessing the applicability of potential remediation strategies.

References

Gentier, S., D. Billaux and L. van Vliet, Laboratory testing of the voids of a fracture. *Int. J. Rock Mech. Rock Eng.*, 22:149-157, 1989.

Mackay, D.M. and J.A. Cherry, Groundwater contamination: pump-and-treat remediation. *Environ. Sci., Technol.*, 23(6):630-636, 1989.

Murphy, J.R. and N.R. Thomson, Two-phase flow in a variable aperture fracture. *Water Resour. Res.*, 24(12):2033-2048, 1993.

Tsang, Y.W., Usage of "equivalent apertures" for rock fractures as derived from hydraulic and tracer tests. *Water Resour. Res.*, 28(5): 1451-1455, 1992.

Influence of Fracture Network and Rock Matrix Properties on DNAPL Migration in Fractured Rock

E.A. Sudicky
Department of Earth Sciences
University of Waterloo
Waterloo, Ontario, Canada N2L 3G1

Cases of DNAPL contamination of carbonate bedrock are common throughout North America and the world. Typically, a DNAPL enters the rock mass via fractures, joints, and bedding planes that maybe present within the rock, and which may be enlarged by dissolution of carbonate minerals. While the permeability of the fracture network is commonly many orders of magnitude higher than the matrix permeability, the fracture network typically accounts for little of the bulk porosity of the rock. Thus, a small volume of DNAPL can occupy a large volume of the rock if the DNAPL is restricted to the fracture network due to the presence of a tight rock matrix with a high DNAPL entry pressure. Available capillary pressure curves for carbonate rocks of various depositional and diagenetic environments indicate that porosity and permeability are poor indicators of DNAPL entry pressure due to the complex pore geometry created by the myriad of physical and chemical processes affecting carbonate minerals, and that the range in values of entry pressures for the matrix can be large. Thus, considerable uncertainty exists in such data for the matrix, in addition to that typically related to the physical properties of the fracture network (e.g., fracture aperture, spacing, interconnectivity). Computations performed with CompFlow, a 3D numerical model capable of simulating multiphase flow, multicomponent transport, and interphase component partitioning (e.g., DNAPL dissolution, vaporization) in discretely fractured porous media, will be presented that show the sensitivity of the overall extent of the DNAPL contaminated zone within fractured rock to the capillary pressure saturation relationships of the rock matrix, and to the geometry and physical properties of the fracture network.

A case study is also presented in which CompFlow is applied to a problem involved PCB migration in fractured dolomite at an intensively studied field site located at Smithvile, Ontario. In addition to highlighting the degree of prediction uncertainty due to uncertainty associated with the properties of the fractured rock strata at the Smithville site, the case study is also used to discuss implications with respect to the effectiveness of alternative strategies for in situ DNAPL source removal and aqueous-phase plume containment. The results emphasize the importance of obtaining measurements of the DNAPL entry pressure, porosity, and permeability of the rock matrix, in addition to the need for collecting detailed field data on the properties of the fracture network when dealing with problems of DNAPL migration and remediation in fractured geologic media.

Multicomponent Reactive Transport in Fractured Porous Media: Methods and Applications

Peter C. Lichtner
Earth and Environmental Sciences Division
Los Alamos National Laboratory
MS-FC305, Los Alamos, NM 87545

INTRODUCTION

Incorporating fractured porous media in models of reactive flow and transport is important for describing natural systems. First, fractured media are ubiquitous in natural systems. Fracture dominated flow systems are involved in weathering, contaminant migration and ore deposition, to mention but a few. Second, fractured media are bimodal in the distribution of physical and chemical properties with generally distinct values for fracture and matrix. As a result, single continuum models are generally unable to capture the unique features of a fractured system.

Reactive transport models have been applied to numerous geochemical systems involving complex chemical interactions [see Lichtner (1996) for a general overview and references therein; Lichtner, 1998]. These systems include oxidation-reduction processes, leaching of copper ore, migration of a hyperalkaline plume and its neutralization by the surrounding host rock, and many others. Characteristic of geochemical systems involving mineral precipitation and dissolution reactions is the formation of a quasi-stationary state. The system's time-evolution may be represented as a sequence of stationary states separated by transient time periods (Lichtner, 1985; Lichtner, 1988), enabling calculations of complex multicomponent systems to be carried out over geologic time spans. This contribution provides an overview of methods based on a continuum approach for incorporating chemical reactions in models describing transport through fractured porous media. Several examples are presented to illustrate the different approaches.

MODELS FOR REACTIVE TRANSPORT IN FRACTURED MEDIA

A number of different conceptual frameworks have been used to represent fractured porous media. They include the equivalent continuum model, discrete fracture model, variations of the dual continuum model, and the representation of fractures as regions of high permeability in heterogeneous media.

Equivalent Continuum Model

Perhaps the simplest approach is to use a single continuum model to represent the fracture network ignoring completely the rock matrix. Alternatively, a composite medium obtained by suitably averaging fracture and matrix properties results in an equivalent continuum representation of a fractured porous medium. Concentrations of dissolved constituents, solids and mineral reaction rates are identical in the fracture and matrix.

Equilibrium of capillary pressure between fracture and matrix results in different levels of liquid saturations in fractures and rock matrix, however, this distinction is more an artifact of the model and should not be taken too seriously. The ECM predicts flow through fractures only when the matrix itself is near full saturation—a severe limitation of the model. The ECM cannot hope to capture the bimodal distribution of system properties that is often characteristic of fractured media and more complex models are needed.

Explicit Fracture Model

An alternative approach is to treat fractures explicitly, taking into account coupling with the rock matrix through a mass transfer term. This approach, referred to as the explicit fracture model (EFM), applies to a single fracture or an infinite number of equally spaced fractures. The approach becomes rapidly unwieldy for more than a few finite number of fractures.

Recently, Steefel and Lichtner (1999a,b) demonstrated a unique relation between mineral alteration along a fracture and that perpendicular to the fracture in the rock matrix. They found that a wedge-shaped front geometry was produced with slope

$$\frac{dx}{dz} = -\frac{\lambda_m}{\lambda_f} = -\left(\frac{\phi_m D_m}{v_f \delta} + \frac{\lambda_m}{\lambda_f^0}\right)$$

with z the fracture coordinate and x the perpendicular distance into the matrix. The slope is characterized by the sum of the two dimensionless groups: $\phi_m D_m / v_f \delta$ and λ_m / λ_f^0, where ϕ_m and D_m denote the matrix porosity and diffusivity, v_f the fracture velocity, δ the half-fracture aperture, and $\lambda_{m,f}$ equilibration lengths in the fracture and matrix, respectively. A surprising result of this analysis is that in spite of the high flow velocity in the fracture, the fracture behaves as a diffusion dominated system because of the strong interaction with the matrix. The results suggest that field observations of matrix alteration perpendicular to the fracture may be used to predict mineralization along the fracture itself. This result depends on communication between the fracture and matrix that could be significantly impeded by the presence of impermeable fracture coatings, for example.

Dual Continuum Models

The dual continuum model (DCM) represents a fractured porous medium as two interacting continua with one continuum corresponding to the fracture network and the other the matrix. A coupling term provides mass transfer between the two continua. The DCM enables separate values of the field variables to be assigned to fracture and matrix continua. Several new parameters are required to represent the average matrix block size and fracture aperture, or equivalently fracture volume, associated with a representative elemental volume (REV) of bulk medium. From these geometric quantities the interfacial

surface area between fracture and matrix can be computed. The DCM reduces to the ECM in the limit of infinite coupling between the fracture network and matrix. In this limit fracture and matrix concentrations become equal.

Because of the extreme limitation of one matrix node for every fracture node, with the DCM one can never hope to capture the detailed mineral alteration patterns obtained from the EFM [FEHM provides an option for two matrix nodes (Zyvoloski et al., 1997)]. In particular, the mineral alteration pattern computed for the matrix could not be expected to conform to the fracture continuum alteration pattern as obtained in the EFM.

This leads to an alternative approach embodied in the so-called MINC (Multiple Interacting Continua) approach (Pruess and Narisimhan, 1982). The term MINC is somewhat of a misnomer in that it refers to discretizing the matrix into concentrically nested blocks, the outer most block in direct contact with the fracture continuum. Thus if the matrix is considered as a single continuum in which provision is made for gradients in various field variables such as pressure, temperature, saturation, concentration etc., the MINC approach is in actuality another form of the DCM, rather than involving "multiple" continua.

The primary distinction between MINC and DCM is that in the conventional DCM the matrix continuum is connected, whereas in the MINC approach the matrix is disconnected with each matrix block surrounded by fractures. Thus in the MINC approach different matrix blocks can only communicate with one another through fractures. Which model is to be preferred depends on the extent of fracturing. The DCM is more appropriate for a more densely fractured rock, and the MINC approach is applicable to more widely spaced fractures in which gradients in the matrix become important.

Hierarchical Continuum Models

Finally, a hierarchical approach may be needed to account for "fast" reactions taking place at the microscale. "Fast" heterogeneous reactions have often in the past been represented by local equilibrium. However, in fact, such reactions may be much more complicated than surface controlled kinetic reactions because they may result in local concentration gradients and hence become sensitive to pore and fracture geometry. An important unanswered question is how to scale such processes to the macroscale where the continuum formulation is valid.

CONCLUSION

Numerical models describing reactive transport in porous media have advanced considerably over the past decade. Thanks primarily to ever faster computers, partial differential equations representing multicomponent geochemical systems involving literally hundreds of reacting species may be solved routinely in more than one spatial dimension. It can be expected that computer power will increase dramatically over the next decade as software is developed for massively parallel computing architectures. In

addition, advances in software techniques, such as the MINC implementation developed by Seth and Hanano (1995), will be essential.

Nevertheless, many conceptual difficulties remain in providing a quantitative description of reactive flow and transport in fractured porous media. Especially difficult is characterizing the reactive surface area of minerals in the field. The DCM and MINC approaches introduce additional parameters, matrix block size and fracture aperture, which represent averages over distributions and which are difficult to measure and characterize. It is questionable whether the DCM has sufficient flexibility to properly account for mineral alteration in the rock matrix. In such cases the MINC approach appears more robust.

REFERENCES

Lichtner P.C. (1985) Continuum model for simultaneous chemical reactions and mass transport in hydrothermal systems. Geochimica et Cosmochimica Acta, 49:779-800.

Lichtner, P.C. (1988) The quasi-stationary state approximation to coupled mass transport and fluid-rock interaction in a porous media. Geochimica et Cosmochimica Acta, 52:143--165.

Lichtner, P.C. (1998) Modeling reactive flow and transport in natural systems, Eds. G. Ottonello and L. Marini. Environmental Geochemistry, Pacini Editore, Pisa, Italy, 5-72.

Lichtner, P.C. (1999) FloTran User's Manual. In preparation.

Lichtner, P.C., Steefel, C.I., and Oelkers, E.H. (Eds.) (1996) Reactive transport in porous media. Reviews in Mineralogy, 34, 438 pp.

Pruess, K. and Narisimhan, T.N. (1982) A practical method for modeling fluid and heat flow in fractured porous media. Paper SPE-10509, Proc. Sixth SPE-Symposium on Reservoir Simulation, New Orleans, LA.

Seth, M.S., and Hanano, M. (1995) An efficient solution procedure for multiple interacting continua flow. Proc. of World Geothermal Congress. Florence, Italy. p. 1625.

Steefel, C.I. and Lichtner, P.C. (1999a) Multicomponent Reactive Transport in Discrete Fractures: I. Controls on Reaction Front Geometries, J. Hydrology, in press.

Steefel, C.I. and Lichtner, P.C. (1999b) Multicomponent Reactive Transport in Discrete Fractures: II. Infiltration of Hyperalkaline Groundwater at Maqarin, Jordan, a Natural Analogue Site, J. Hydrology, in press.

Zyvoloski, G.A., Robinson, B.A., Dash, Z.V., and Trease, L.L. (1997) Summary of the models and methods for the FEHM application---A finite-element heat- and mass-transfer code, LA-13307-MS, Los Alamos National Laboratory.

Experimental and Mathematical Simulations of Gas Bubble and Water Flow Through Rock Fractures

by K.Kostakis,[1] J.P.Harrison,[1] and S.M. Heath[2]

[1]Rock Mechanics Research Group
Department of Earth Resources Engineering
Imperial College of Science, Technology and Medicine
Prince Consort Road, London SW7 2BP, UK
Tel: +44 (0)171 594 7350, Fax: +44 (0)171 594 7444
Email: e.kostakis@ic.ac.uk

[2]BG Technology, Loughborough, UK

This paper describes numerical and experimental investigations on the formation and movement of gas bubbles in a single, water-filled natural rock fracture. The aim has been to study and model the process of gas escape, in terms of migration of bubbles through a rock fracture, which will provide the basis for the safe design of underground caverns for natural gas storage. The outcome is a new mathematical formulation and numerical solution for gas formation and movement, accompanied by detailed experimental work on the same phenomena.

A detailed overview of the work previously reported in the literature on the subject of underground storage of gas has shown that it is crucial to understand and model the process of gas formation and flow through water-filled fractures in order to be able to minimise gas migration to the ground surface.

A critical review of previous work on flow in restricted media has revealed the lack of theoretical models and experimental data on the subject. Factors related to two–phase flow itself, combined with the particularity of the fracture geometry, contribute to a complex problem. On the strength of the review reported here, the further study of two–phase flow in fractures both theoretically and experimentally has been undertaken.

A new experimental set-up (Figure 1) that can simulate gas and water flow in a fracture has been utilised. It consists of the transparent casts of the two parts of a natural fracture (Figure 2), inside which flow of gas and water can be introduced and observed. Preliminary experiments with the experimental set-up showed that a simple fluid dynamics approach cannot be directly applied in fractures; the type of flow occurring under the expected storage conditions was identified as discrete gas bubble and water counter-current flow.

A study of the principles of the dynamics of two–phase flow has led to the identification of the equations and the parameters that describe and control the processes of gas bubble formation at a fracture mouth and subsequent bubble migration through the fracture. A mathematical model is presented, which has been developed by the authors and is based on the particularities of the flow and the problem domain. The procedure that is used here for estimating the size of the newly-formed bubble is based on the knowledge of the value of the various forces that act on the point

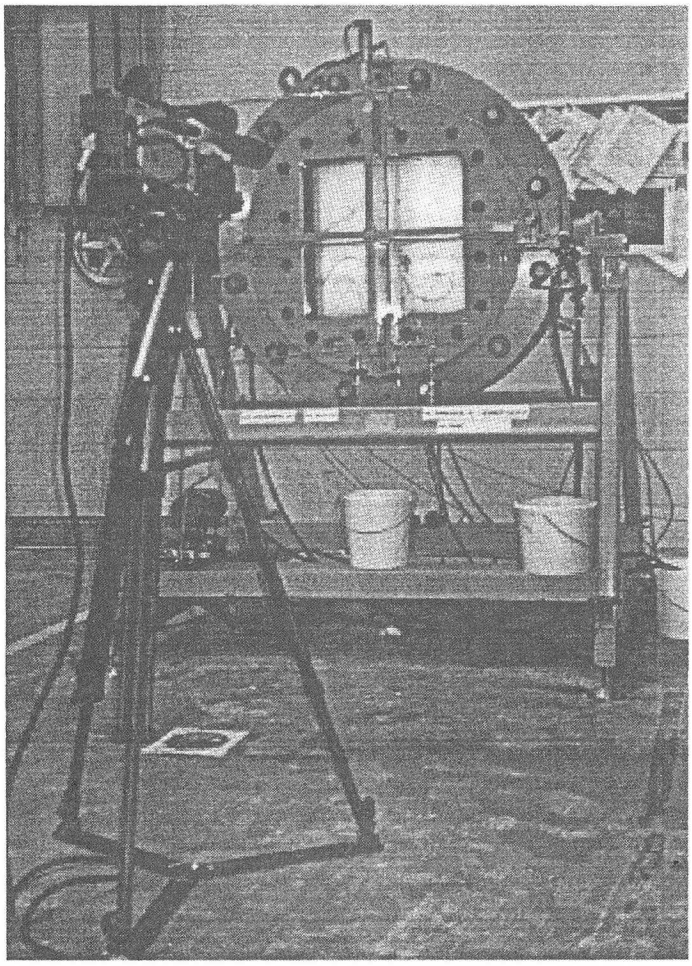

Figure 1: The experimental rig utilised for gas and water flow experiments.

of bubble formation and the distribution of fracture apertures at the fracture mouth. The forces that act on the bubble at formation can be estimated from the properties of the two fluids and the boundary pressures at the fracture mouth. An assumption that the gas bubble will enter the fracture at the point of maximum aperture has been made, and the aperture value is used in the computation of the wall force that acts on the bubble. This assumption is supported by previous experimental observations by Kumar and Kuloor (1970) and current experimental work undertaken by the authors.

The complexity of the equations that describe flow and the flow domain itself suggests the introduction of a numerical approach to their solution. A numerical procedure has been developed here, based on the identified set of differential equations cast into finite difference form and supported by the preliminary experimental observations. The numerical procedure followed by the newly developed computer program is given schematically in Figure 3.

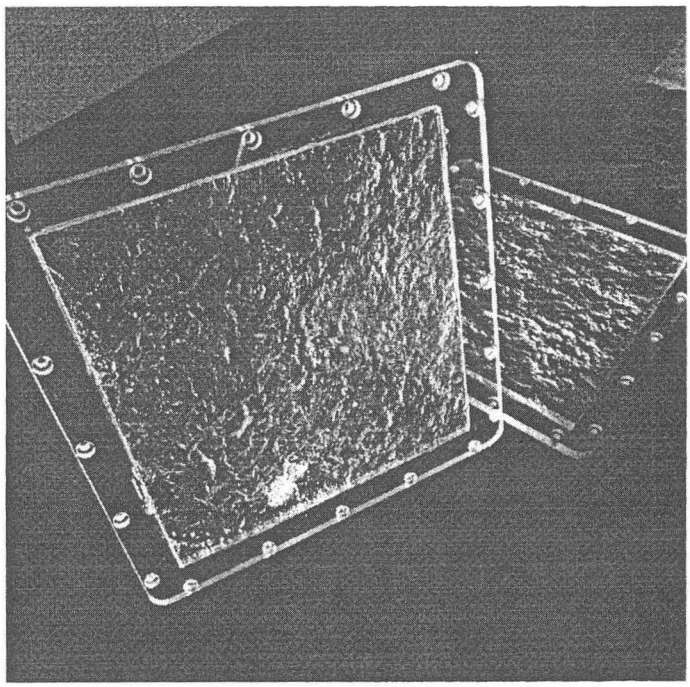

Figure 2: The two transparent casts of a natural fracture.

This validation process for the case of real fractures follows the first stage of validation of the mathematical model, where use has been made of previous experimental data and an analytical solution in the simplified case of flow between smooth, parallel plates.

Experimental and numerical work has indicated that the fracture aperture and its distribution govern flow to a great extent. As a result, a series of aperture characterisation experiments has accompanied the flow tests. The "Silicon Rubber technique" is a variation of the casting techniques as used by Gentier *et al.* (1989) and Hakami (1995).

Further research on the area of gas bubble formation and flow in fractures will include extension of the numerical work to a network of interconnected fractures and a more detailed examination of gas bubble dynamics and bubble interaction phenomena.

References

Gentier, S., Billaux, D. and van Vliet, L. (1989): Technical note: Laboratory testing of the voids of a fracture, *Rock Mech Rock Engng, Vol.22, p.149-157.*

Hakami, E. (1995): Aperture Distribution of Rock Fractures, *Ph.D. Thesis, Division of Engineering Geology, Dept. of Civil and Environmental Engineering, Royal Institute of Technology, Stockholm, Sweden.*

Kumar, R. & Kuloor, N.R. (1970): *Advances in Chemical Engineering, Vol. 8, p. 256-368.*

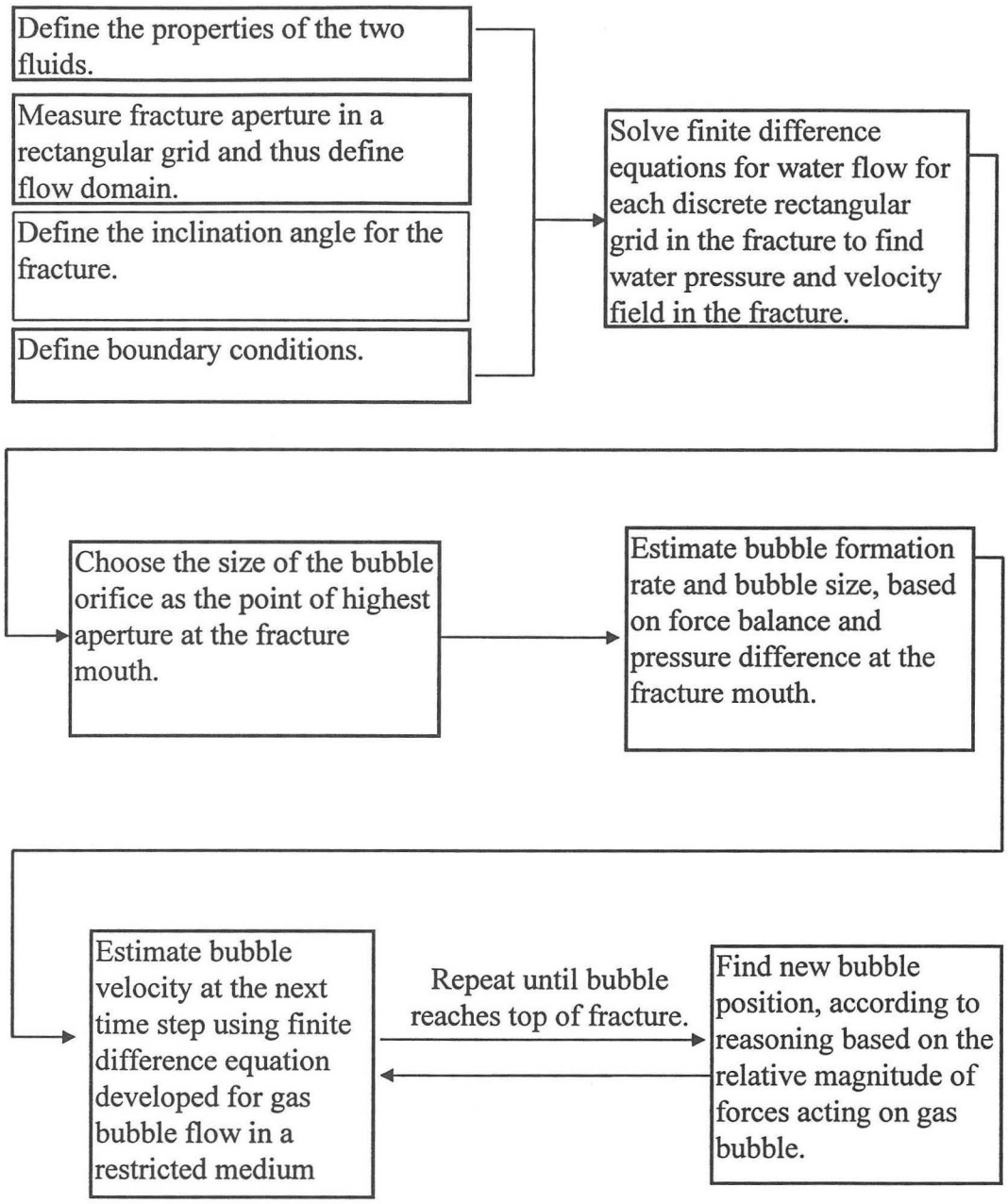

Figure 3: Solution procedure for the numerical scheme developed by the authors.

Session 3:
FRACTURE-MATRIX INTERACTIONS

The Fracture-Matrix Interaction

Yannis C. Yortsos
University of Southern California
Los Angeles, CA
yortsos@uclid.usc.edu

In flow and displacement in fractured rocks, the interaction between fracture and matrix dictates decisively the overall performance of the flow or displacement process. When capillary forces are important in the process, such as in drainage or imbibition, the fracture-matrix interface acts as capillary discontinuity boundary. In such processes, the partition of the two phases is expected to depend on the patterns of displacement in the fracture and on whether certain thresholds in flow rate (capillary number) have been exceeded. For the transport of momentum, heat or mass, the corresponding partition rate depends on the magnitude of the Peclet number, which is also rate-dependent.

In this paper, we review the state of the art in the way the fracture-matrix interaction has been treated in the literature so far. We consider two different levels, one involving the interaction at a single-matrix block and another in which many matrix blocks are involved. For the first case, we focus on how phenomena in the fracture affect and are being affected by the matrix. The second case involves the averaging of the fracture-matrix interaction over a multitude of matrix blocks of various sizes. Our main emphasis is on immiscible flow.

For the single matrix block-fracture interaction, we present findings from micromodel experiments for drainage, imbibition and steam injection. We discuss the importance of the fracture-matrix interface as a capillary discontinuity surface and the existence of capillary number thresholds. Of particular interest is the case of steam injection, where the condensation of steam contributes to the process of both drainage and imbibition characteristics. We then discuss how the presence of a matrix block affects the two-dimensional (or quasi two-dimensional) displacement patterns in the fracture. A brief discussion of other transport processes is also given.

For the case of multiple matrix blocks, we review the volume-averaging approaches used with particular emphasis on the dual permeability model and the modeling of the interaction using a reduction factor. We probe the origin of the latter.

Fracture-Matrix Flow: Quantification and Visualization Using X-ray Computer Tomography.

A.S. Grader, The Pennsylvania State University, USA; M. Balzarini, ENI/AGIP, ITALY
F. Radaelli, ENI/AGIP, ITALY; G. Capasso, Politecnico di Torino, ITALY
A. Pellegrino, ENI/AGIP, ITALY

The presence of fractures in a reservoir has a great impact on fluid flow patterns and on our ability to recover hydrocarbons. Fractures may have a positive impact on production. For example, in tight formations, the fracture system provides access to the hydrocarbons stored in the matrix. In low productivity wells, hydraulically induced fractures provide the necessary contact between the wells and the reservoir to allow economical production. In some cases, fractures can have a negative effect on production operations. They provide bypassing paths, especially in production-injection systems. Injected fluid preferentially flows through the fractures leaving behind valuable hydrocarbons that may become inaccessible. The understanding of the interaction between fractures and the rest of the reservoir is of critical importance to the design of efficient recovery schemes. In this paper we present a preliminary study exploring the impact of an artificially induced fracture on fluid flow patterns in a layered core sample using x-ray CT imaging.

The CT imager is a fourth generation scanner. The images presented here were acquired at 130 kV and 100 mA setting with a slice thickness of 2 mm. The in-plane pixel resolution is 0.5 mm. The water phase used in the experiment was doped with KI to provide a high CT registration. The oil used was not doped, and had a low CT registration.

The sandstone rock sample was a layered berea with a length of 60 cm and a diameter of 5.3 cm. The sample was fractured by compressing the rock in the diameter direction and, hence, creating a tensile fracture along the rock. The specimen was fractured inits central part whereas the extremes were kept unbroken. The inlet end was not fractured and the outlet end was fractured all the way to the end but not broken. The plane of the fracture is almost perpendicular to the layers, as shown in Figure 1a. The rock sample was placed in a modified tri-axial aluminum core holder with a confining pressure of about 30 Atm.

Figure 1 shows three images taken 27 cm from the inlet end of the core. Image **a** is a dry scan, showing vertical layers and the horizontal fracture. Note that the layers with low CT numbers have low density, andhave high porosity and high permeability. Image **b** is a water-saturated image. Image **c** is a porosity map at the same position. Note that the dark layers in the first two images are now light colored layers representing high porosity. Also, the fracture appears with a white color. The layer porosities are between 15% and 22%. The five rectangular regions shown in Image **c** are used to calculate the relationship between the porosity in the fracture and fracture width.

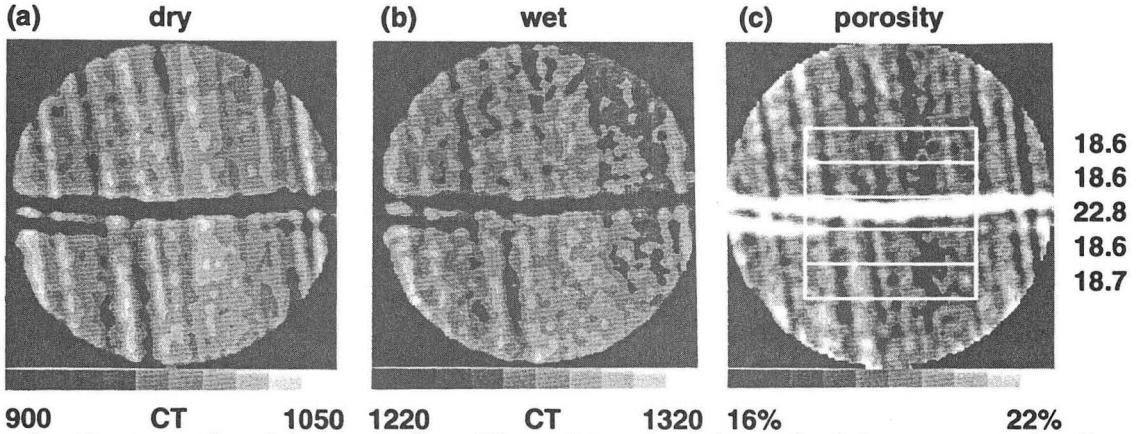

Figure 1: Cross-sectional images taken 27 cm from the inlet end of the core. **a**: dry. **b**: water saturated. **c**: porosity.

Each rectangle in Figure 1c has an area of 5 mm by 25 mm (or 10 pixels by 50 pixels). The average porosity of the rectangles are shown to the right of image c. The four regions not including the central one have an identical porosity. We assume that the center region had the same porosity before inducing the fracture. The same rectangular areas were applied to all images of the core. Two vertical reconstructions are shown in Figure 2. The upper reconstruction is a pixel-by-pixel projected average, generating an array of 58 pixels by 50 pixels. The reconstruction shows that the fracture is not a perfect line, but migrates inthe central area of the core. In order to develop a relationship between the porosity in the fracture and the width of the fracture we calculate the average porosity of each rectangle, leading to an array of 58 by 5, shown in the lower reconstruction in Figure 2. Since the core is quite homogeneous in areas that do not include the fracture, we can create a correlation for each image along the core detailing the porosity-width relationship shown in Figure 3. Effective fracture widths as a function of position along the core for various porosity values are shown in Figure 4. The fracture width is the largest at the center of the core. Also, the computed width of the fracture is about 0.2 mm when it porosity is 100% (no fill material).

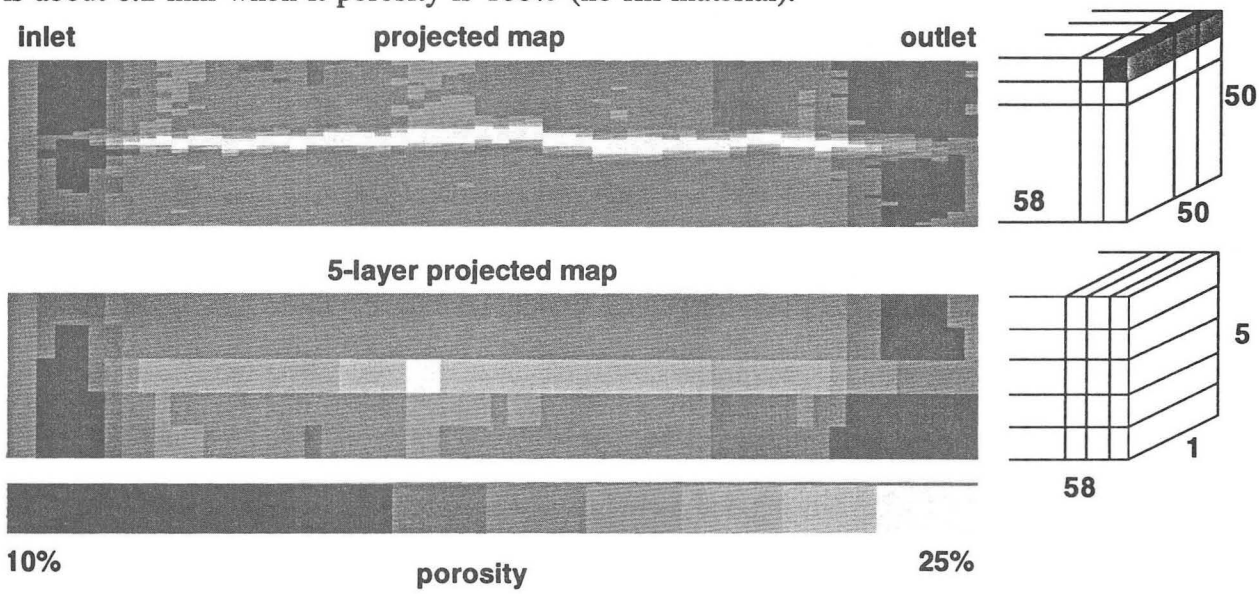

Figure 2: Projected vertical reconstructions of the central region of the core with the fracture.

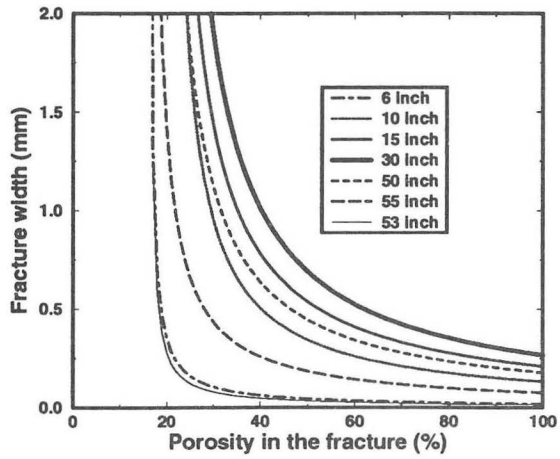

Figure 3: Width vs. porosity in the fracture.

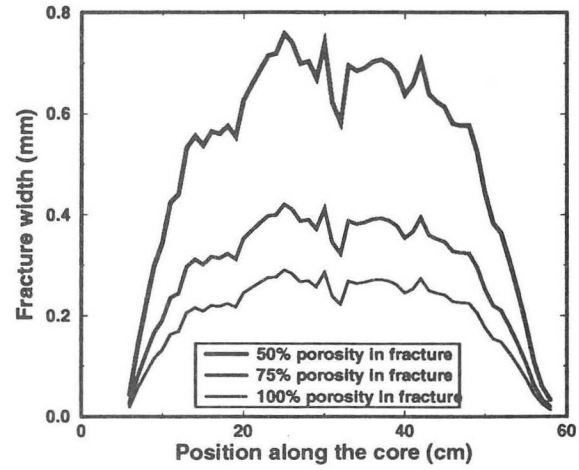

Figure 4: Fracture width along the core.

After the core sample was saturated with water a light mineral oil was injected and its distribution tracked using the x-ray imager. The total pore volume of the rock sample was 230 cc, and the overall porosity was 17.5%. After injecting 5 cc of oil (0.22 PV) the sample was scanned. Figure 5 shows the distribution of the oil phase in the fracture before oil breakthrough. This is a projected horizontal reconstruction that includes the fracture. Since the fracture did not extend all the way to the inlet end of the core, oil flow at the inlet is dominated by the layers shown as the dark and light alternating strips at the left of the figure. Once oil invasion reaches the fractured region, the flow converges to the fracture and displaces the water out of the fracture. The oil advances in the fracture sections adjacent to high permeability layers faster than opposite the low permeability layers. This can be seen at the leading edge of the oil in the fracture at the right of the figure. This observation illuminates the question: do the fracture permeability, width and porosity depend on the layers adjoining the fracture? This is a key question that determines the interaction between the fracture and the matrix during displacement and recovery processes.

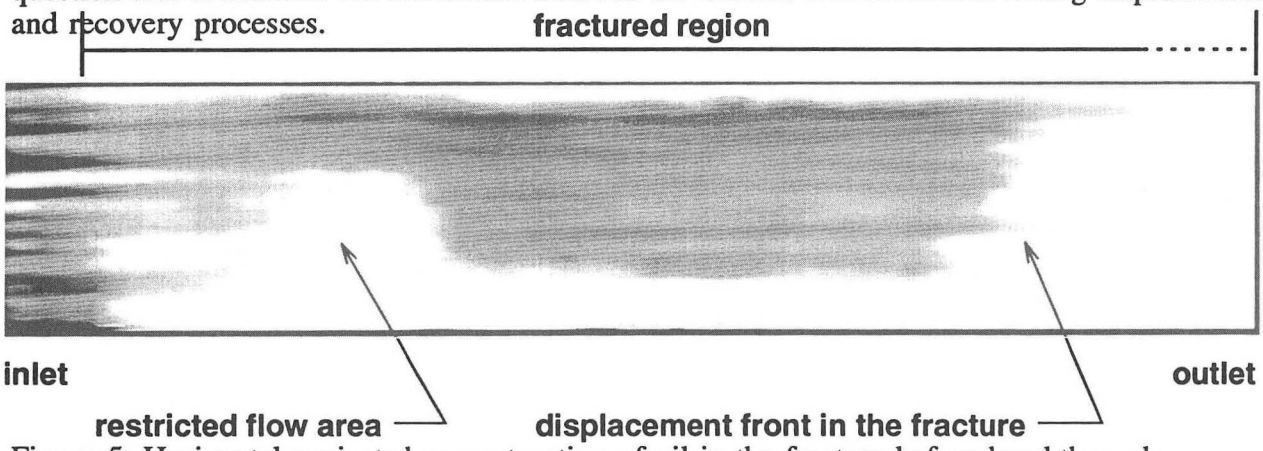

Figure 5: Horizontal projected reconstruction of oil in the fracture before breakthrough.

Oil injection was resumed and the scanner was positioned 1 cm from the outlet end of the core, collecting images during the breakthrough period. The fracture is evident all the way to the end of the core but is not open as much as in the central regions of the core, as shown in Figure 4. Hence, as oil arrives at the outlet, it is forced to displace water from the matrix. Figure 6 shows three images taken at the end of the core at three different times. The invasion of the oil phase into the layered matrix is denoted by the dark portions on the images. In the early image, **a**, the oils is only evident in the fracture, and is concentrated opposite the high permeability layers. In the second image, **b**, the fracture appears full of oil, and the oil has started to displace the water from the high permeability layers. In the third image, **c** one of the high permeability layers is almost fully displaced. The displacement in the layers is also affected by gravity, since the oil is lighter than the water. The dark streaks extend further in the upward direction than in the downward direction.

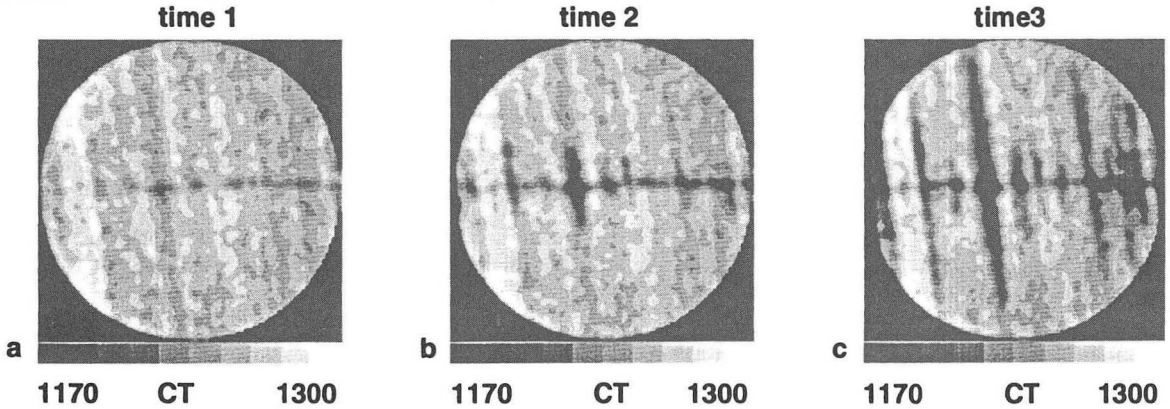

Figure 6: Oil displacing water at the outled end of the core.

Following breakthrough of oil, injection was continued, and the core was imaged five times at different PVI values: 0.035, 0.043 0.056, 1.0, and 10.0. Figure 7 presents profiles at these PVI values. Since this was a preliminary experiment, the CT profiles were not converted to saturation profiles. However, these profiles serve the purpose of describing the displacement process. The upper dark solid line is the profile just before oil injection, where the core is saturated with water. The thin line denotes the profile after injecting 0.035 PV. This curve shows that oil has accumulated at the injection end, mainly in the high permeability layers. Then the oil converges to the fracture and flows mainly in the fracture, denoted by the small gap between the 100% water curve and the 0.035 PVI curve. The third profile was collected after 0.043 PV were injected denoted by the dotted line. The two curves (the one for 0.35 and 0.43 PVI) are practically identical in the injection side of the core. The oil has now fully filled the fracture and started to accumulate in the outlet end as denoted by the difference between the dotted curve and the 100% solid curve. As the oil displacement extends, the water is displaced from the inlet end and the outlet end and high water saturation is left in the middle of the core. The displacement of water from the middle of the core is slow and is controlled by the presence of the high permeability fracture. As shown in Figure 6c, the water is displaced from the high permeability layers first and only them from the low permeability layers. The presence of the fracture controls a displacement order in the system. The CT values at the inlet end are declining even after 10 PVI, denoting that water is still being displaced (typical Buckely-Leverett process). After injecting 10 pore volumes of oil, the average oil saturation in the core was 46%. The presence of the fracture increases the time required to bring the core to residual water saturation, and prepare it for primary and secondary recovery processes.

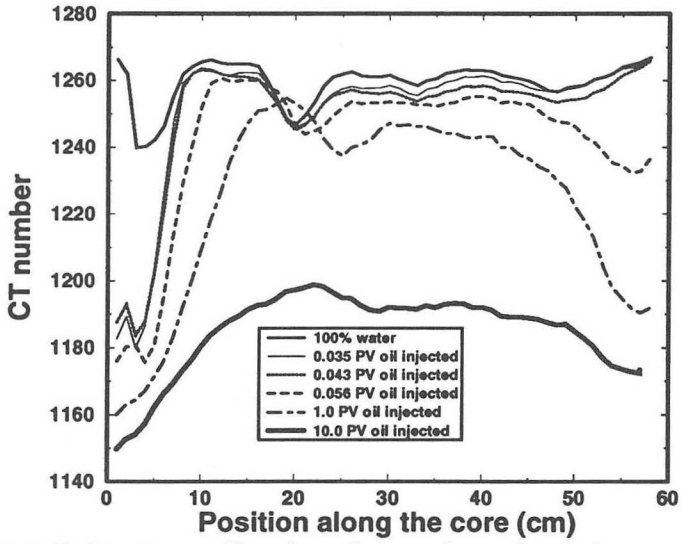

Figure 7: Average profiles along the core for various values of pore volumes of oil injection.

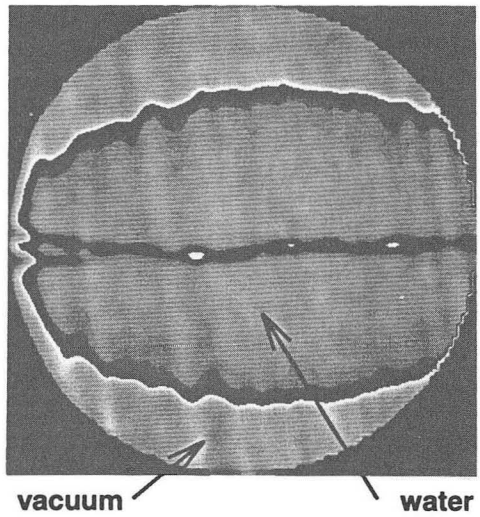

Figure 8: Image of water invading an evacuated core sample.

A most important issue in layered systems is the communication between layers. Figure 8 shows a single image in the middle of the core during invasion of water under vacuum, the first fluid introduced into the core. The water invaded portion is in the middle of the core, and the upper and lower parts still do not contain liquid water. Each region has its own color scheme. The border of the water is a dampened wave. We can also make the observation that the water invades the low permeability layers (light colored layers) ahead of the high permeability layers (dark colored layers). If the layers were not connected, we would get significant differentiation in the advance of the water in the layers. The damped wavy form of the interface indicates that there is communication between the layers. Monitoring this stage of the experiment is unique to x-ray imaging, and provides insight into flow patterns in the rock samples. However, it is a little explored process. The central fracture plays a key role in the vacuum saturation process, which in field applications resembles high viscosity ratio injection scenarios.

Modeling matrix diffusion in fractured media : from single fracture scale to block scale

C. Grenier[1], A. Genty[2], E. Mouche[2], E. Tevissen[3]*

[1] *GIST, 855, av. Roger Salengro, 92370 Chaville, France.*
christophe.grenier@gist.fr
[2] *CEA, C. E. Saclay, DMT/SEMT, 91190 Gif-sur-Yvette, France.*
manu@semt2.smts.cea.fr
[3] *ANDRA, Parc de la Croix Blanche, 1-7 rue Jean Monnet, 92298 Châtenay-Malabry, France*
etienne.tevissen@andra.fr
[*] *Now at IPSN/SERGD, CEA, 60-68 av. Gén. Leclerc, 92265 Fontenay-aux-Roses, France.*
genty@berlin.far.cea.fr

One of the major issues in assessing the performance of a deep repository in crystalline geologic media concerns the ability of the rock matrix to delay the transport of radionuclides. As a matter of fact, transport in the matrix is generally much slower than in fractures, matrix porosity is much greater than fracture porosity and, for a given species retardation coefficient is much greater in the matrix than on fracture walls. Consequently, in order to assess, by numerical modeling, the impact of matrix diffusion on solute transport in fractured media, a modeling program was initiated a few years ago at the CEA, the French Atomic Energy Commission, for ANDRA, the French Agency for Radioactive Waste Management. This program aims at modeling radionuclide transport at different scales, from single fracture scale up to fractured block scale, in order to make out which the mechanisms and parameters are relevant for a safety assessment modeling and which modeling approach to adopt, discrete fracture network or continuous approach (double continua). More precisely, the issues which have been addressed up to now are, at single fracture scale, the definition/identification of specific surface area in a single fracture, the influence of fracture aperture variability, the role of stagnant water zones; at block scale, the influence of matrix diffusion coefficient on breakthrough curves at the outlets of the block, the validity of a double continuum approach. Moreover part of this work has served for the calibration of experiments performed by TRUE (Tracer Retention Understanding Experiment) within the Äspö Task Force [1]. This paper summarizes the main results obtained up to now.

First of all it should be emphasized that there is a large contrast in flow and transport parameters, when passing from the fracture to the matrix blocks. The numerical tool, or numerical formulation, should be mass conservative. Among all the different numerical formulations it is acknowledged that the mixed hybrid finite element formulation, used in the petroleum engineering field, respects this criterion [2]. The flux and mass balance equations are solved simultaneously in each element. This formulation, applied to the transport of concentration fields, has been implemented in the finite element code CASTEM2000. CASTEM2000 is a general computational tool for mechanics and fluid mechanics applications developed at the CEA [3,4].

At single fracture scale, the influence of fracture aperture variability on transport of a non sorbing solute in a single fracture is studied [5]. Expressions for the effective specific surface

area, or flow wetted surface area, are proposed. All the known transport mechanisms are taken into account : advection and dispersion in a channel, matrix diffusion and molecular diffusion in the stagnant water zones. In a first step, constant fracture aperture is considered according to figure 1a : channel and stagnant water zones. It is found that matrix diffusion is multidimensional and that stagnant water is a major pathway for the diffusive mass transfer into the rock matrix. In a second step, the impact of aperture variability on transport in the channel and in stagnant water zones is studied by means of Monte-Carlo simulations. The flow corresponds to tracer tests conditions. The best expressions for the effective specific surface area are found to be the inverse of the arithmetic mean aperture for the channel and the inverse of the geometric mean aperture for the stagnant water zones. These expressions, providing a good fit for the mean of the breakthrough curves, could be used in a site scale performance assessment model. But the impact of fracture aperture variability is found to be very important on breakthrough curves as shown on figure 1b ($\sigma_{\ln\beta} = 0.5$) requesting the modeling of higher order moments.

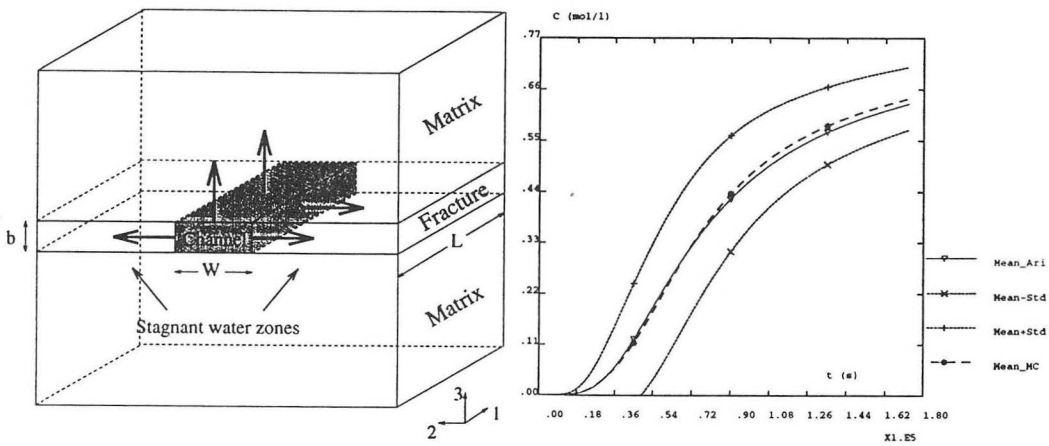

(a) System geometry

(b) Breakthrough curves: mean, standard deviation and fit

FIG. 1 – *Single fracture: channel with stagnant water zones*

At the block scale (hectometric), transport of concentration fields is studied for flow conditions typical of in situ natural flows. A 3D fracture/matrix sugar box geometry is considered. The block size is 125m and is composed of 5^3 matrix blocks. The fracture network is represented on figure 2a. Fracture zones are altered zones of width 0.1 m and porosity $\omega_F = 0.1$. Fracture transmissivity is equal to $T_F = 10^{-8}$ m^2/s, the head gradient is 5. 10^{-4} and the pore velocity is U_{FP} = 5. 10^{-10} m/s. The values of the longitudinal and transverse dispersivities in the fracture are respectively 4 m and 0.4 m (so that concentration is constant across the fracture width) and the pore diffusion coefficient is 10^{-10} m^2/s. Sources are placed in the middle of the block and breakthrough curves are measured at the block boundaries corresponding to major hectometric fractures with high flow rate. The uncertainties in the characterization of transport parameters has led to a series of calculation for three sets of matrix transport parameters: $\omega_M = 10^{-3}$ and D_{MP} = 10^{-11} m^2/s, $\omega_M = 5.10^{-3}$ and D_{MP} =2.10^{-11} m^2/s, $\omega_M = 10^{-2}$ and D_{MP} = 10^{-10} m^2/s. The fracture width is represented by a single mesh and the fracture wall is meshed regularly with

$\Delta x = 2.5\,m$. The domain is discretized by 13824 meshes. The time step is such that the Courant number in the fracture is one and the matrix discretization along the axis normal to the fracture wall is such that the Fourier number is one. There is complete mixing at the fracture intersections.
It is shown [6] that, the transport regime varies strongly over this span of diffusion coefficient values requiring further characterization of the transport parameters of the matrix blocks. As can be seen on figure 2b, for low values of the matrix diffusion coefficient, the transport is predominant in the fractures, and matrix blocs act as storage areas introducing a classical delay in the breakthrough curves. For large values of the matrix diffusion coefficient, the transport is essentially diffusive, the arrival peak is delayed and its level strongly reduced.

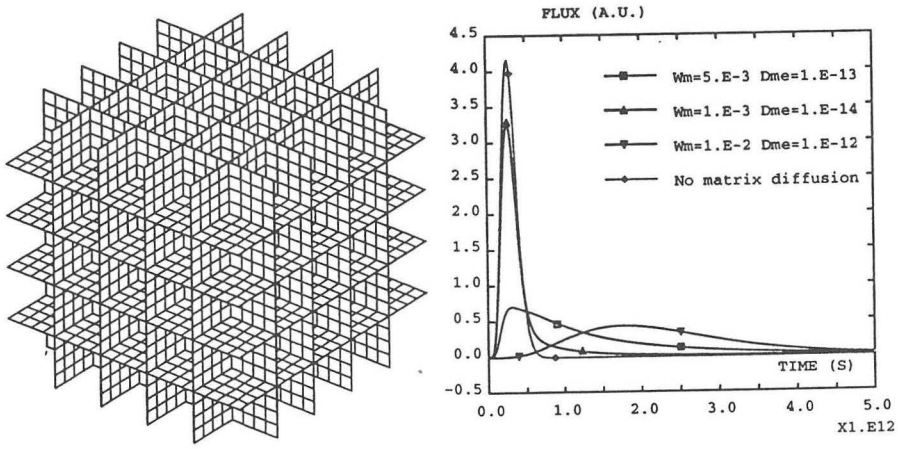

(a) System geometry: fractures network

(b) Breakthrough curves for different values of matrix diffusion coefficient

FIG. 2 – *3D fractured block geometry*

Concentration fields obtained for $D_{ME} = \omega_M D_{MP} = 10^{-12}$ and 10^{-14} m^2/s are provided respectively on figure 3a and 3b for a similar 2D geometry. Mass is released from the fracture intersection close to the upper right corner of the middle matrix bloc.

Sensitivity analysis fulfilled on the 3D geometry as well as on a similar 2D geometry, including different discretization strategies, show that the level of discretization adopted is sufficient for low and high values of matrix diffusion coefficient values. For the intermediate values, discretization should be refined for the 3D geometry, but such a level of discretization couldn't be reached due to storage memory limits.

An alternative approach to the simulation of concentration transport is given by continuous approaches like the so called double continua : continua are associated to fractures and matrix blocks. Coupling terms take into account the transfer of concentration from one continuum to the other and transport equations are resolved for each equivalent medium. A review of these methods is provided in [7]. A major prerequisite is the definition of a representative elementary volume for the fractured medium. In addition, it should be small enough compared to the dimension of the domain studied. The approach is here tested on the 2D geometry taking into account an equivalent 1D matrix diffusion geometry or a 2D block like geometry. Calibration of the transport parameters (advection velocity, dispersivity coefficient and diffusion

coefficient for all equivalent media, characteristic sizes of the matrix medium) is made by fitting breakthrough curves obtained by direct simulation of concentration transport on the actual 2D geometry.

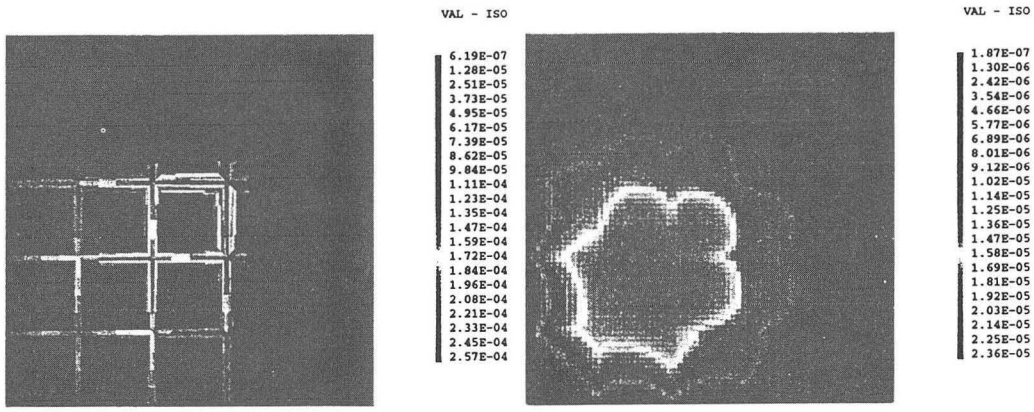

(a) Concentration field: low matrix diffusion, $t = 2.5\,10^{11}\,s$

(b) Concentration field: high matrix diffusion, $t = 2.5\,10^{12}\,s$

FIG. 3 – *2D fractured block gometry*

Références

[1] Grenier C., Treille E., Mouche E.. Etudes effectuées dans le cadre de l'exercice international Äspö Hard Rock Laboratory Task Force.. *To be published in SKB International Cooperation Report 98, published in Progress Report HRL-98-01.*

[2] Chavent G., Jaffre J., Mathematical models and finite elements for reservoir simulation; Single phase, Multiphase and Multicomponents flows through porous media, *Studies in Mathematics and its applications*, Vol. 17, North-Holland, 1986.

[3] Dabbene F., Mixed Hybrid Finite elements for Transport of Pollutants by Underground Water, *Proc. of the 10th Int. Conf. on Finite Elements in Fluids*, Tucson USA, 1998.

[4] CASTEM2000 User's Manual, English Version, CEA, 1997

[5] Grenier C., Mouche E., Tevissen E., Influence of variable fracture aperture on transport of non sorbing solutes in a fracture : a numerical investigation. *Proc. of the MIGRATION'97 Conf.*, Sendai, Japan, 1997. To be published in Journal of Contaminant Hydrology, 1998.

[6] Genty A., Grenier C., Mouche E., Tevissen E. Influence of matrix diffusion on solute transport in a three dimensions fracture network. *Proceedings of CMWR'98 in Crete (Greece).*

[7] Pinder G. F., Huyakorn P. S., Sudicky E. A.. Simulation of flow and transport in fractured porous media. In *Flow and contaminant transport in fractured rocks, Ed. J. Bear, C.-F. Tsang, G. de Marsily. Academic Press, 1993*

Multiple Rates of Mass Transfer Between Fractures and Matrix

Lucy Meigs and Sean McKenna
Geohydrology Department, Sandia National Laboratories, P.O. Box 5800, MS 0735
Albuquerque, NM 87185-0735. e-mail:lcmeigs@sandia.gov

Roy Haggerty
Department of Geosciences, 104 Wilkinson Hall, Oregon State University,
Corvallis, OR 97331-5506. e-mail: haggertr@ucs.orst.edu

Solute transport in fractured media is complex and is frequently modeled with a double-porosity model that allows for transfer of mass between well-connected high- permeability pathways and lower permeability matrix. Conventional models of mass transfer employ only a single rate coefficient to model a single time-scale of mass transfer. If the time and spatial scale of an experiment being modeled and any predictions based on those models are the same, the conventional single-rate model may be adequate. However in natural porous media, a single-rate model may be a poor conceptualization of the media. The use of a model with a single rate of mass transfer implies that the system can be adequately represented with a single rate of diffusion or sorption. In any natural porous media there will be multiple scales of mass transfer. There are many causes for the multiple time scales of mass transfer in heterogeneous porous media including: 1) variations in spacing of fractures or other advective pathways resulting in different lengths of diffusion pathways; 2) heterogeneity in the low permeability "immobile" portion of the media such as the distribution and variability of pore throat diameters resulting in a range of diffusion rates, and 3) variations in the sorptive capacity of the media resulting from variations in mineralogic compositions of the pore walls (e.g. uneven distribution of iron oxide coatings) to variations in surface area for sorption. Natural porous media are heterogeneous and there will always be variations in diffusion and sorption rates within the medium. Whether mass-transfer can adequately be conceptualized and modeled as a single rate depends on the application.

A growing body of evidence appears to indicate that multiple rates of mass transfer are required to adequately conceptualize transport in many media. A literature search was recently conducted to compile rate coefficients estimated from laboratory and field data. The duration of the experiment, which is an approximate surrogate for exposure time, was compared to the estimated first-order rate coefficient. Data from one hundred experiments shows the general trend that the longer the duration of an experiment, the slower the estimated rate of mass transfer. This result could be explained by assuming that all the experiments which range in time from minutes to years were fortuitously designed to cover the right time scale. A more realistic explanation is that a longer duration experiment in the same porous medium is likely to be sensitive to slower mass transfer, while a shorter duration of the experiment is likely to be sensitive to faster mass transfer. In a long duration experiment, the fast mass transfer will appear instantaneous and will likely be explained by a retardation factor or a larger advective porosity. In short duration experiments, the slow mass transfer rates may be slow enough that their effect is not seen in the

data. If a distribution of mass transfer rates is assumed, it should be possible to explain data from both long and short experiments with the same conceptual model.

Additional evidence for the existence of multiple rates of mass transfer comes from the examination of the late-time slope of tracer test breakthrough curves. The late-time data of single-well injection-withdrawal tests are especially well suited to the examination of mass-transfer because it is less sensitive to the effects of heterogeneity. The late-time data of two-well convergent-flow tests with pulse injection (rather than recirculation) can also potentially provide significant mass transfer information. Log-log plots of concentration versus time often reveal late-time slopes that are approximately constant. Examples from the literature show slopes ranging from as shallow as -0.85 to significantly steeper than -1.5. This is in contrast to conventional double-porosity models that produce a late-time slope of -1.5 for a period of time followed by a rapid transition to infinite slope as the matrix blocks begin to saturate. A constant late-time slope, other than -1.5, between approximately -0.5 and -3 can potentially provide information about the form of the distribution of rate coefficients.

Constant late-time slopes of data were analyzed in terms of the consequences for experimental interpretation and solute transport. Sustained slopes less steep than -3 indicate an infinite mean matrix (immobile zone) residence time. Since all breakthrough curves have a maximum observation time, we show that for breakthrough curve slopes less steep than -3, the minimum estimate of mean matrix residence time is the time-scale of the experiment. Very shallow slopes, less steep than -2, are indicative of increasingly long residence times in zones of increasingly large matrix capacity. Although slopes less steep than -2 must be unsustainable after a pulse injection, they may be sustained over the duration of observation. In all cases of breakthrough curve slopes less steep than -3, estimates of the mean matrix residence time will be strongly influenced by the time-scale of the experiment.

One medium that provides an excellent example of multiple rates of mass transfer is the Culebra dolomite in southeastern New Mexico. The Culebra dolomite is an extensively fractured dolomite with significant matrix heterogeneity. Porosity variations include fractures of various sizes, vugs, and porosity within both well-indurated crystalline dolomite and poorly cemented "silty" dolomite. A series of field convergent-flow tracer tests has been conducted to examine transport processes. The data from single-well injection-withdrawal tests have constant late-time slopes between -2.1 and -2.8. The data can not be adequately explained with a conventional single-rate double-porosity model. A model with multiple rates of diffusion provides an excellent fit to the data. A multirate diffusion model also provides a good explanation of data from multiwell tests. Laboratory diffusion experiments provide additional strong evidence for the importance of multiple rates of diffusion within the Culebra. For these experiments, x-ray absorption imaging was used to provide both visualization of the diffusion process and quantitative data on spatial variations in diffusion rates.

Sandia is a multiprogram laboratory operated by Sandia Corporation, a Lockheed Martin Company, for the United States Department of Energy under Contract DE-ACO4-94AL85000.

Using the Boundary Layer Concept for Modelling Chemical Transport in a Fracture-Matrix System

Rony Wallach
Department of Soil and Water Sciences
Faculty of Agricultural, Food and Environmental Sciences
The Hebrew University of Jerusalem, Israel

Many experimental observations have shown that preferential flow and transport is taking place in fractures, fissures, and cracks that are commonly found under most field conditions. In most cases, the volume of water within the preferential paths is much lower than the volume of the stagnant fluid, but a notable part of the displacing solution may be moving within the well-defined preferential paths ahead of the main flow.

The common approach to simulate the transport through fractured rocks is to use a dual porosity model. This approach is based on the assumption that naturally fractured reservoirs behave as two porous structures, fractures and surrounding matrix, rather than one. The dual porosity models have also been used to describe flow and transport in structured porous media where the intra-aggregates porosity of aggregated soil and the dead-end pores in the structured-soils are considered as the low-conductivity matrix while the inter-aggregate porosity are the paths where preferential flow takes place. The advection within the regions with the relatively low hydraulic conductivity is usually assumed zero, therefore, these domains act as sink/source components and the dual-porosity, dual-velocity model becomes a mobile-immobile model.

Several rate-limited mechanisms are involved in the solute-transfer process between the mobile and immobile solutes: (1) advective-dispersive transport from bulk solution to the boundary layer at the interface between the mobile and immobile porosities; (2) external mass transfer in the boundary layer (film diffusion); and (3) pore diffusion within the immobile region. If adsorption to the solid phase takes place, the appropriate equations should be added explicitly. Any or all of these three components may be rate-limiting steps and their relative contribution to the non-ideal breakthrough curves (BTCs) is not fully determined. Two different concepts have been used to describe the solute exchange between the fractures (mobile) and the surrounding matrix (immobile). The first is an instantaneous equilibration between fracture and matrix concentrations at their interface. The second is a rate limited exchange that is proportional to the difference between the laterally averaged concentrations in both fracture and matrix. The first approach is widely used by hydrogeologists and the second by soil physicists who deal with aggregated soils where the mobile solution is flowing within the macropores; the boundary layer (film) is the water surrounding the aggregates, and the immobile region is the aggregate solution. The last concept is known as the mobile-immobile model (MIM). The difference between the two concepts is embedded in the relative time scales of the affecting mechanisms.

The exact nature of the immobile pore system could vary significantly for various systems. Stagnant water could be found in aggregates, surrounding solid phase particles, or in "dead-end" pores or a matrix surrounding cracks or fractures. Different diffusion length scales are involved in these different cases, where the length scale of the intra-aggregate diffusion is a few

millimeters or less, while the length scale of diffusion into a matrix between well-defined fractures could be ten centimeters and more. The current study focuses on the dynamics of solute exchange between a single crack surrounded by a matrix with diffusion length scales of a few centimeters and more in the immobile solute. The effect of the detailed lateral chemical distribution within the matrix on the breakthrough curve at the crack outlet is analyzed as well.

The system setup is made of a single discrete fracture imbedded in an infinite porous rock matrix. The contaminant transport takes place in the fracture while the solution in the matrix is assumed stagnant. A boundary layer is formed along the interface between the crack and the matrix through which the solute concentration varies from its value in the flowing solution to its value in the matrix at the interface. This boundary layer is assumed to have a constant thickness for the steady flow conditions. The chemical transfer between the flowing and the stagnant solutes is a rate limited first-order process controlled by diffusion through the stagnant thin fluid film. Both mobile and stagnant fluid concentrations vary with time and depth. The flow and dissolved chemical concentrations normal to the flow direction are essentially uniform in the crack except for the boundary layer. The concentration in the matrix is not assumed to be spatially uniform, as is usually assumed in the mobile-immobile model. The lateral flux of dissolved chemicals in the matrix is by diffusion due to local concentration gradients and calculated by the diffusion equation. Due to distinctive time scales, differences between concentration variation in the vertical direction, by convection in the crack and by diffusion in the matrix, the chemical vertical fluxes in the matrix are neglected. The effect of both molecular diffusion and velocity-dependent dispersion on the concentration distribution within the crack is assumed to be minor. Thus, the dissolved chemical transport in the crack is assumed to be a sharp front convective process and is modeled by the kinematic-wave approach. An approximate analytical solution has been developed by applying the Laplace transform with respect to time. The model output has been successfully compared with measured data for 30-cm-long granitic drill cores (20-cm diameter) with a natural fissure that runs parallel to its axis and with 55-cm long undisturbed columns from pedal soil horizons with well-developed vertically oriented pores. The physical meaning of the fitted parameters is discussed.

The relative role of the two rate-limited processes, namely film transfer and diffusion in the stagnant matrix solute on the overall chemical exchange and BTC shape is analyzed by the non-dimensional version of the mass balance equations. The displacement duration has been divided into two stages. Soon after its initiation, the chemical transfer through the stagnant film controls the chemical exchange between the crack and matrix. The duration of this stage depends on different properties of the system. Subsequently, the matrix-diffusion controls the chemical exchange between the two domains and the model can then be simplified by replacing the rate-limited transfer by a local equilibrium. However, for cases in which the current study is dealing, the preferential flow is very fast and the rate-limited transfer through the stagnant film dominates the BTC shape. Using the local equilibrium at the crack-matrix interface underestimates the crack concentration during short and intermediate times after first breakthrough. The deviation between the two concepts depends on the system dimensions and flow rate in the crack.

Session 4:
HYDROGEOLOGICAL AND TRANSPORT TESTING

Development of Hydraulic Tests in Fractured Rocks

Paul A. Hsieh
U.S. Geological Survey, 345 Middlefield Road, MS-496, Menlo Park CA 94025
pahsieh@usgs.gov

During the past 40 years, significant developments have advanced the application of hydraulic tests for investigating fluid flow through fractured media. During this period, Dr. Paul Witherspoon and co-workers have lead many of these advances. Thus, it is a fitting tribute to Dr. Witherspoon to review the development of hydraulic tests and to look ahead to upcoming challenges.

The large collection of analytical solutions developed in the ground water, petroleum, and related field represents a major accomplishment. These solutions guide the interpretation of hydraulic test by using type curves (plots of drawdown versus time) to diagnose flow geometry (linear, radial, spherical), anisotropy, mechanism of fluid storage (fractures versus porous rock blocks), borehole conditions (skin, wellbore storage, borehole intercepting a highly transmissive fracture), presence of confining layers, and boundaries. Novel techniques have also extended the ability to determine hydraulic properties of low permeability rocks. Research to evaluate the tightness of caprocks for underground storage of natural gas lead to the theory of pumping tests in multiple aquifer- aquitard systems. The 1977 Invitational Well Testing Symposium at Berkeley saw the introduction of the pressure pulse test (also known as the pressurized slug test) to investigate transient flow in tight fractures. At the Stripa research mine in Sweden, the Ventilation Shaft Experiment represented a unique largest-scale hydraulic test (by design) in which a horizontal mine shaft, sealed at its entrance, served as the pumped well, ventilation of humidity from the mine shaft served as the pumping mechanism, and packer-isolated intervals in boreholes drilled radially away from the shaft served as monitoring points for hydraulic head response. This landmark experiment set the basic design for subsequent experiments of fluid flow and solute transport conducted in mine shafts.

With the advances in hydraulic tests also came the need to apply these methods to increasingly more difficult problems, which could involve complex geologic structures, multiphase flow, chemical and biological reactions, and predictions of long term migration of contaminants from waste storage or disposal facilities. In many cases, application of hydraulic testing on its own is insufficient. Rather, hydraulic tests should be considered as one component within a larger, multidisciplinary "tool box" that includes geophysical investigations, geologic studies, tracer tests, geochemical methods (including environmental tracers and ground water age dating), and computer modeling. Effective integration of different investigation techniques is a major challenge for the future. Two areas of potential future advances are discussed below: use of numerical models to analyze hydraulic tests, and combining hydraulic tests with geophysical tomography.

A central problem in field investigations of fluid flow in fractured rocks is how to characterize a medium that is highly heterogeneous. For example, hydraulic conductivity of crystalline rocks can vary by several orders of magnitude over distances of several meters. Fractured rocks often

contain zones of highly transmissive fractures nested within a network of less permeable fractures. Determining the locations and properties of these zones is a major challenge in the application of hydraulic tests. With a few exceptions, however, analytical solutions are developed on the assumption that the rock is homogeneous. This assumption imposes significant limitations on analyzing test data from heterogeneous systems. For example, consider a field setting in which a pumped well, a nearby observation well, and a distant observation well are all located along a straight line. An irregularly shaped, high permeability zone connects the pumped well with the distant observation well, but not with the nearby observation well. During pumping, greater drawdown is observed at the distant observation well than at the nearby observation well. This type of test response cannot be readily interpreted by analytical solutions based on the homogeneous assumption. By contrast, the response can be readily simulated with a conventional ground-water model by assigning different hydraulic conductivity values to different model sub- regions. At a sophisticated level, the use of numerical models to analyze hydraulic tests is equivalent to model building and model calibration, possibly using inverse methods. However, between a full-scale modeling effort on the one hand, and a traditional type-curve analysis on the there hand, there lies a broad range of opportunities to develop innovative computer software that enables the well test analyst to effectively use computer models in an visual and interactive manner to investigate the effects of various types or styles of heterogeneity. The development of such software could significantly enhance the analysis of hydraulic test data that were previously considered "not amenable to analysis."

Recent advances in geophysical tomography also provide important opportunities to combine geophysics with hydraulic testing. Under favorable conditions, cross-well tomography using seismic or electromagnetic waves can be used to map the distribution of wave velocity and attenuation in the vertical section between two boreholes separated by tens of meters. Because wave velocity and attenuation are affected by rock properties and the presence of fractures and fluids, tomography can be effectively used to delineate zones of contrasting hydraulic properties. This information is essential when constructing a numerical model for hydraulic test analysis. For example, at the fractured rock research site near Mirror Lake in New Hampshire, results of tomography and hydraulic tests provided mutually supporting evidence pointing to the presence of clusters of connected, highly transmissive fractures in the shallow bedrock. Methods to simultaneously analyze geophysical, hydraulic, and tracer tests are currently an area of active research. Results from this research will provide a formal procedure to better extract information from multiple methods of field investigation.

In conclusion, although the field of hydraulic testing has seen important developments in the past 40 years, significant challenges remain in integrating a broad range of techniques into a multidisciplinary approach to fractured rocks investigations. Future advances will likely require close collaboration among hydrologists, geologists, geophysicists, and geochemists.

Evaluating Fracture Network Geometry from Hydraulic Data at Underground Test Facilities

Thomas W. Doe, Golder Associates Inc.
4104 148th Ave. NE, Redmond, WA 98052, USA
Email: tdoe@golder.com

Introduction

This paper reviews how underground test facilities have been used to develop methods for determining the hydraulic structure and geometry of fracture networks. The paper describes the application of these approaches for recognizing and characterizing a compartmentalized flow system in the granitic rocks of the Kamaishi Mine in Japan.

Background

Research in underground test facilities has been a major driver for developing conceptual models of flow in fractured rocks over the past twenty years. Promoting the use of underground facilities for hydrogeologic research has been one of Paul Witherspoon's significant contributions to the field. The Stripa Project, for which Paul Witherspoon and John Gale initiated the hydrogeologic studies in 1977, was one of the first of these efforts. Underlying the Stripa Project was a conceptual model developed by David Snow, which held that continuum-equivalent, anisotropic hydraulic properties of fracture networks could be derived from a combination of geologic, geometric, and hydraulic data. The subsequent fifteen years of work at Stripa showed that larger scale structures, particularly fracture zones, provided a basis for the analysis of complex fracture networks, and set the stage for further discoveries at other sites, such as the compartmentalization phenomena described below.

The Stripa Project (both the initial Swedish-US cooperative effort and the subsequent OECD program) stimulated the development of discrete fracture network approaches at Lawrence Berkeley Laboratory, AEA-Harwell (UK), and Golder Associates. Discrete fracture network models area based on a premise that geologically definable features (such as individual fractures and fracture zones) control fluid flow in fractured rocks. Knowledge of the geometries of these features then forms the basis for constructing conceptual and numerical models. A major challenge to the discrete fracture approach has been the need to distinguish geologic geometry from hydraulic geometry, as typically only a small portion of geologically identifiable features are hydraulically significant.

This paper reviews some approaches for defining the hydraulic geometry of fracture networks with an application to the underground test facilities, particularly the Kamaishi Mine in Japan. The basic approaches include (1) flow logging, (2) pressure and flow

transient analysis for geometry properties, and (3) integration of pressure interference observations to develop models of hydraulic geometry.

Flow Logging

Flow logging methods have undergone major development since the inception of the Stripa Project. The standard approaches of twenty years ago used fixed-interval length packer tests as the basic characterization tool. Such tests are very useful for determining the frequency and transmissivity distributions of conductive features. However, the resolution of individual conductors may require a short packer spacing. Under such conditions, a significant portion of testing time may be wasted on intervals that contain no conductive features. Flow logging using heat-pulse methods or fluid conductivity approaches provides a rapid and efficient means of identifying the conductive features in boreholes. Although the analysis of such test data usually requires an assumption of steady flow, the data nonetheless provide useful initial estimates of feature transmissivity.

Interpretation of Hydraulic Geometry from Boundary Effects and Dimension in Well Tests

Flow logging identifies the locations of hydraulically significant features in boreholes. Once identified, these features become targets for more detailed pressure or flow transient testing. Traditionally hydraulic testing has been viewed primarily as a means for obtaining hydraulic property data using assumptions of radial cylindrical flow to or from a source well in a planar conducting feature. Partly due to the efforts of the Stripa Project, hydraulic testing now can be viewed as a means of identifying the hydraulic geometry of conducting features, as well. Indeed, the correct identification of a geometric model for a well test is prerequisite for proper interpretation of hydraulic properties. Geometric information comes from both boundary effects and dimensional effects.

In theory, well tests in single fractures or features should produce boundary effects in well tests, if the features are finite in extent. A finite fracture or fracture network will exhibit the depletion characteristics of no-flow boundaries, while the intersection with a high-conductivity feature away from the source well will produce the steady flow response of a constant pressure boundary. In field data, such effects are seldom seen. A review of well tests in fractured rock from Stripa and from the Kamaishi project in Japan does not show constant-pressure boundary effects. Finite boundary effects appear rarely, and volumetric calculations from Kamaishi suggest that the volume represents a network rather than single fracture.

Nonetheless, transient tests do provide geometric information, but mainly in the form of dimensional responses, both from source wells and from observation wells. Dimension, which is a confusing term applied to several different concepts in well testing, refers here

to a measure of how the conducting properties change with distance from a source well. Dimension is determined by a combination of area and conductivity changes. If one assumes constant hydraulic properties in a conducting feature, then the dimension, n, is an exponent describing area change with distance, where area is proportional to distance to the power $n-1$.

For the radial cylindrical flow, which is the most common dimension assumed in well testing, area grows linearly with distance, that is, to the $2-1=1$ power of distance. Considering the other integer dimensions, linear flow occurs in any geometry where the area changes to the $1-1=0$ power of distance, and spherical flow involves area increasing with the $3-1=2^{nd}$ power of distance. Fractional dimension approaches to well test analysis were first developed in the hydrologic literature by Barker (1988) and in the reservoir engineering literature by Chang and Yortsos (1988). Fractional dimensions arise when the flow area changes to a non-integer power of distance. The dimension of a well test is readily inferred from the log-log plots of pressure drawdown, inverse flow (for constant pressure tests), and from their derivatives. In pressure or inverse flow derivative plots, late time behavior follows a straight line in logarithmic plots with a slope of $1-n/2$.

Such behavior may appear if the conductive features are spatially distributed according to power-law or fractal geometries (Chang and Yortsos, 1988). Numerical simulations of fracture networks (Doe and Wallmann, 1995) have shown that the intensity of conducting fractures also can affect the well test dimension. For example, a space-filling fracture network within a planar feature, such as a fracture zone or carbonate aquifer, will produce the familiar exponential integral or Theis responses associated with radial cylindrical, dimension-2 systems. Decreasing the fracture intensity, even using non-fractal, Poissonian spatial models, also decreases the apparent dimension of the well test, as some pathways lose continuity over the planar region. The dimensional response is an important tool for assessing network geometries and space-filling properties of networks. It has a strong influence on predictions of oil reservoir performance, as the dimension of the conducting fracture network will influence long term cumulative production.

Applications to the Kamaishi Mine and the Compartment Model of Hydraulic Structure

Flow logging and dimension analysis have been applied to a block scale experiment at the Kamaishi test site in Japan. This site, which is hosted by granodiorite and diorite, has been investigated for a ten year period from 1988 to 1998. The main area of hydrologic investigation has been an area on the 550-m level (above sea level) of the mine in an area approximately 330 meters below ground surface.

The work at Kamaishi initially began with an assumption that the rock mass behaved as an anisotropic continuum. However, anomalously low pore pressures in some portions

of the rock mass, and distinctly non-continuous pressure interference responses from well tests supported the development of a compartment model of the flow field.

The compartment model was developed over the past five years of investigating an approximately 100-m square area knows as the Task 3-2 experiment (Uchida et al, 1997). The drilling program to investigate the site was a major part of the experiment. Our procedure involved careful monitoring of flow and pressure during drilling, flow logging each hole, and then emplacement of piezometer systems with up to ten packers each to isolate the major conductors. Analyses of the flows and interference responses during drilling showed that the block contained at least five compartments, a compartment being a fracture network which is conductive internally, but poorly connected to other compartments. Distinctive pore pressures can indcate compartments. Low pressure compartments have preferential connection to the mine. Compartments that are preferentially connected to the surface have higher pressures, approaching equivalent heads of 200-m relative to the 550-level, or about 2/3 of the hydrostatic pressure for that depth.

The compartments in the Task 3-2 block have a range of apparent sizes. They are clearly fracture networks rather than single fractures, as the compartments may have very irregular boundaries. The importance of isolating conducting features cannot be over-emphasized, as any short-circuiting of flow through the boreholes may destroy the possibility of recognizing the hydraulic structure. The source of the compartment structure is under investigation. Some alternate hypotheses include (1) clustering of fracture due to fractal spatial distributions, (2) faulting or shearing which has displaced conductors and created clay gouges, or (3) geochemical processes which locally fill the fracture porosity and block flow paths.

Dimensional analyses of well tests from Kamaishi show that the apparent dimension can vary considerably among observation zones in any given test. Monitoring intervals that are part of a common conductor generally have behaviors similar to the source well. Conducting intervals that have indirect connection to the source well have different, generally lower dimension behaviors.

Conclusion

The Kamaishi experiments once again demonstrate the importance of underground test facilities for developing and testing conceptual models of fracture flow. As with other facilities, such as Stripa, the research at Kamaishi has provided new insights into the hydraulic structure of fracture networks. This understanding has been the result of simple, but detailed measurements that have been conducted over a sufficient time period to develop and test alternate conceptual models.

Effects of Fracture Geometry and Flow Regime on Single and Two-Phase Flow Transmissivities

John E. Gale, Department of Earth Sciences, Memorial University of Nfld, St. John's, NF, Canada

The basic processes controlling fluid flow and transport through discrete fractures have been the subject of considerable research and debate over the past 40 years. The roots of this debate have their origin in the derivations of the flux and velocity equations, based on shear stress considerations, for open non-contacting parallel plate models and the validation of these theoretical models by experimental work on idealized smooth walled models. Extension of this experimental work to rough, no-contacting, fracture surfaces provided additional, friction factor-Reynolds Number, constitutive models for a range of relative roughness and flow regimes.

Much of the recent debate has centered on whether these parallel plate or cubic model based equations can be applied to rough natural fractures that are subject to a range of normal and shear stresses. Recognizing the coupled nature of flow in fractures with the stresses acting on the fracture plane, a number of workers have attempted to fit various empirical coupled stress-flow models to the measured changes in flowrate as a function of normal and or shear stress. While curve fitting to a data trend is a well established investigative technique, the validity of the published models can generally be related to the uniqueness and number of the index parameters on which each model is based. It is clear that once the fracture walls are in contact, under the applied stress, the concept of relative roughness in its current form does not apply. Very few or none of the published models are able to predict the changes in flux and fluid velocity with changes in stress and account for the well documented hysteresis effect between increasing and decreasing stress paths.

In order to increase our understanding of the basic processes governing both flux and velocity in discrete fractures, a series of single and two-phase flow experiments and tracer experiments, on several 200 mm by 300 mm sized samples, at different levels of normal and shear stresses, followed by resin impregnation of the fracture pore space, have been conducted. A photomicroscope approach has been used to map the distribution of the fracture pore space and the contact areas every 70 micrometers along a series of perpendicular profiles that are spaced approximately every 10 mm. These data represent a detailed sampling of the fracture pore space that existed during the final single phase and two-phase flow and tracer tests. The apertures and contact areas over the entire fracture planes have been described using both univariate statistics and geostatistics. The spatial structure of the pore space has been characterized using variograms and mapped using ordinary kriging.

The frequency histograms for the measured apertures were used to generate the hydraulic conductivities for a simple flow and transport numerical model, on both a 1.5 mm and on a 5 mm scale, with the hydraulic properties of the individual cells in the model being assigned randomly. The contact areas were then superimposed randomly, as no-flow cells, on the aperture field. When the experimental boundary conditions were applied to this numerical model, that was

generated using the univariate statistics, the computed flowrates did not agree with the measured flowrates. By contrast, when the hydraulic conductivities for each of the 1.5 mm by 1.5 mm cells in the model were generated by kriging both the aperture and the contact area data, the computed flowrates were within a few percent of the measured flowrates. The 1.5 mm by 1.5 mm data were also used to determine the role of both the small and large apertures in reducing the fracture transmissivities when degassing occurs in the fracture plane. When an attempt was made to scale up the model by kriging the aperture and contact area data at the 5 mm by 5 mm scale, the computed and measured flowrates did not agree.

Obviously, the basic cubic law, when corrected for roughness, applies in the open fracture pore space. However, when the pore space is averaged over a number of pores and contact areas such as occurs on the 5 mm scale for these fractures, the equivalent aperture that results does not give representative values for either the flux or the fluid velocity. This same problem is inherent in most of the existing curve fitting coupled stress-flow models. The essential problem is how to scale or average the aperture and contact area measurements at the appropriate fracture pore scale to the scale needed for realistic modeling of flow and transport in discrete fractures. A simple boot-strapping approach as been used to demonstrate the corrections needed to maintain a match between the computed and measured flowrates as the numerical model cell size is increased.

The Evolution of Fracture Topography and Flow Path Geometry under Normal and Shear Stresses and Their Role in Hydromechanical Behavior

S. Gentier,[1] D. Hopkins,[2] J. Riss,[3] and E. Lamontagne[4]

[1]BRGM, B.P. 6009, 45060 Orléans cedex 2, France (s.gentier@brgm.fr)
[2]LBNL, 1 Cyclotron Road, Berkekey, CA 94720, USA (DLHopkins@lbl.gov
[3]Université Bordeaux 1, Avenue des Facultés, 33405 Talence cedex, France
[4]UQAC, Boulevard de l'université, Chicoutimi, G7H2B1Québec, Canada

1 INTRODUCTION

Changes in either the normal or shear stresses acting on a fracture induce notable changes in the flow paths that can substantially change the hydraulic behavior of the fracture. The modifications of the paths can be observed using specially designed instrumentation during laboratory experiments, and can be understood by simultaneous analysis of the morphology of the fracture along with the results of traditional hydromechanical tests. The aim of the work presented here is to synthesize the approaches and techniques developed to date that help us understand the evolution of flow paths in natural fractures under stress.

2 HYDROMECHANICAL BEHAVIOR UNDER NORMAL STRESS

Under normal stresses the hydromechanical behavior of a fracture can be summarized as indicated in Figure 1. The intrinsic transmissivity of the fracture decreases rapidly at first with increasing normal stress, for stresses at the lower end of the range, then decreases less rapidly until a critical stress is reached at which point the intrinsic transmissivity tends to become stable. Simultaneously the closure of the fracture decreases, then stabilizes, This relatively well known behavior can be observed by analyzing both the number and location of the outlets around the fractured sample at various stress levels. The results of such a study, used in parallel with an analysis of the morphology of the sides of the fracture, clearly shows the relationship between the topography of the fracture walls and the void space and the flow paths (Gentier 1987). To

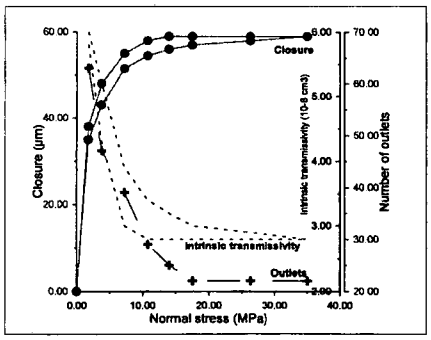

Figure 1 : Evolution of the intrinsic permeability during a transmissivity, closure hydraulic test. and number of outlets as a function of normal stress.

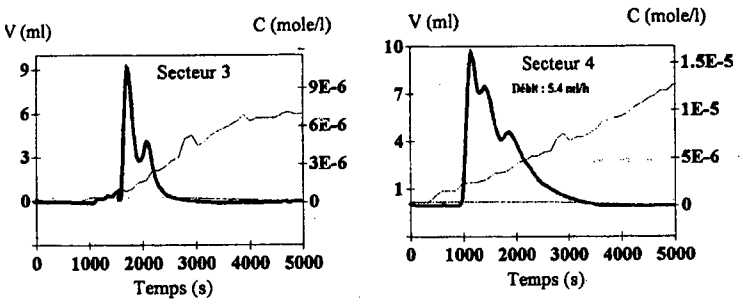

Figure 2 :Tracer recovery curve in two sectors of a fracture

increase the knowledge of the flow paths in a fracture, tracer tests have been performed during hydraulic tests highlighting clearly channeling in the fracture. All these results have led to think the flow paths in terms of channels and this all the more so since the normal stress applied on the fracture is high.

As the results described succinctly above indicate, the morphology of the void space like the result of the combination of the topography of each side of the fracture and of the matching of the two sides, controls the evolution of the flow paths. So the modeling developed to date is based on a map of the fracture apertures deduced from a cast of the fracture (Gentier et al., 1989).

Having such a map which corresponds to zero normal stress, it is possible to introduce it in a finite element flow code and get estimation of the flow rate and the pressure at each point of the fracture (Figure 3).

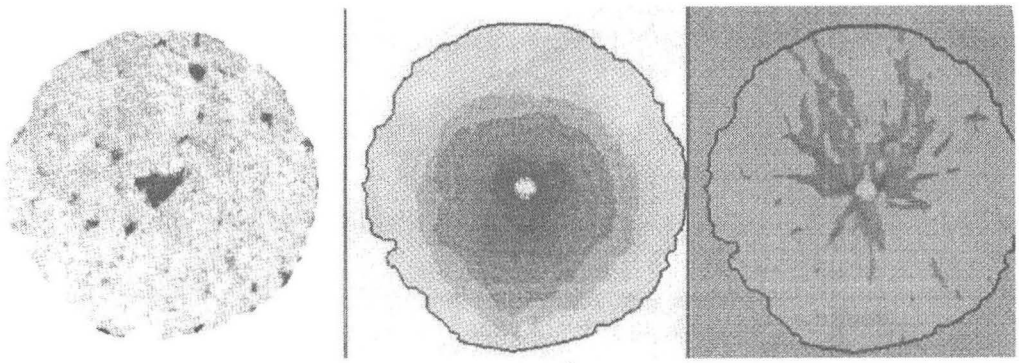

a b c

Figure 3 : pressure (b), flow rate (c) calculated from the aperture map (a).

Another solution developed before consisted to determine the possible channel network using various algorithms of mathematical morphology and to solve the flow in it (Billaux and Gentier, 1989).

In fact if we are able to calculate relatively easily the flow when the geometry of the voids is available the main problem is to determine accurately how the geometry of the voids evolves when the stress applied on the fracture changes. The initial approach to modeling, which is the simplest one, is based on the assumption that under a normal load, there is uniform closure across the fracture meaning that any two points on opposite sides come together by the same amount. This can be modeled by specifying successive thresholds corresponding to the progressive average closure of the fracture with increasing normal load (Fig. 4b). This approach is not very realistic particularly when contact areas become numerous. The second approach is based on a mechanical model that accounts for deformation of the fracture surfaces, asperity deformation, and mechanical interaction between contacting asperities (Hopkins, 1990). From the gray-level image of the fracture cast, the model can be used to calculate changes in aperture with increasing normal load. The gray-level image is transformed into a regular grid of elements and the average

aperture over each element is calculated (Gentier & Hopkins 1997). The result, expressed as (x,y,force) is shown Figure 4c. Comparing the images that result from application of the two methods helps in understanding the mechanical behavior of the fracture. The mechanical model indicates that deformation of the fracture surfaces results in less contact area than is predicted by the first model. It is also important to note that unlike the first approach, the mechanical model

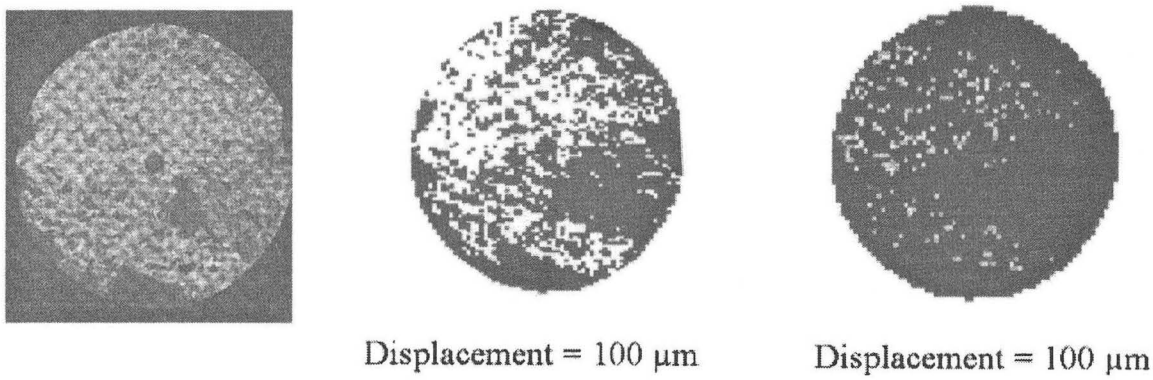

a b c

Figure 4 : Gray level image of the fracture cast (a), and contact areas obtain with the simple model (b) and .with the mechanical model (c) for a given closure.

predicts changes in void geometry with increasing normal stress that result from the roughness of the fracture surfaces. These results have important implications for fluid flow through the fracture.

3 HYDROMECHANICAL BEHAVIOR UNDER SHEARING

A classical shear machine has been adapted to perform hydromechanical tests under shearing. To be able to reproduce shear tests always on the same geometry all the tests are carried out on replicas. The conducted flow is radial divergent injection and fluid is recovered in eight sectors located at the periphery of the joint. In those studies (Gentier et al., 1997), experiments were performed for three directions of shearing for a normal stress held constant at 7 MPa.

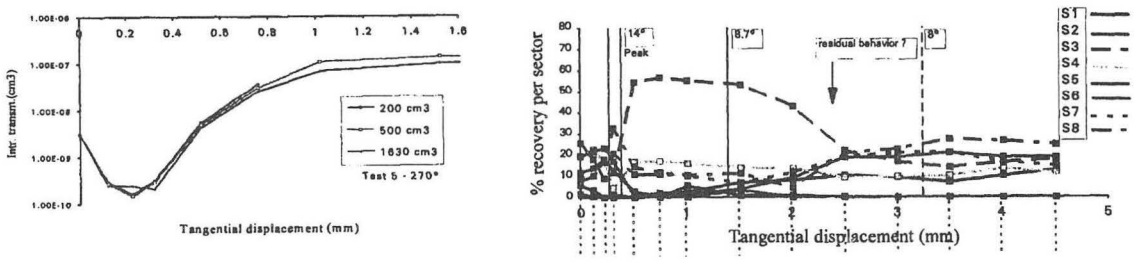

a b

Figure 5 : Evolution of global transmissivity as a function of tangential displacement (a) and recovery per sector associated to the various phase of the mechanical behavior (b).

Evolution of global intrinsic transmissivity as a function of tangential displacement is illustrated Figure 5a. For this fracture, the shear direction does not seem to play an important role in determining the magnitude of the intrinsic transmissivity corresponding to each phase; it seems to be more closely related to the tangential displacement corresponding to variations in transmissivity.

Figure 5b illustrates the percentage of recovery per each. The details of the results are complex but general overall behavior can be postulated and each change in the recovery pattern can be associated with a phase of the mechanical behavior (initial closure, dilatancy, softening phase, residual behavior).

The flow paths in a fracture submitted to a shear stress cannot be understood without a clear image of the evolution of the damage areas associated to the shear. In order, an analysis of the damage zones has been undertaken (Riss et al. 1997). The characterization of damage zones occurring during shear tests with various normal stresses, shear directions and tangential displacements, is based on the acquisition of gray-level images of the joint surfaces, followed by segmentation which allows identification of the damage zones and generation of binary images (Fig. 6a). The damage areas are identified in such a way that the damage contours can be superposed on a topography map of the corresponding joint wall (Fig. 6b). The surface is

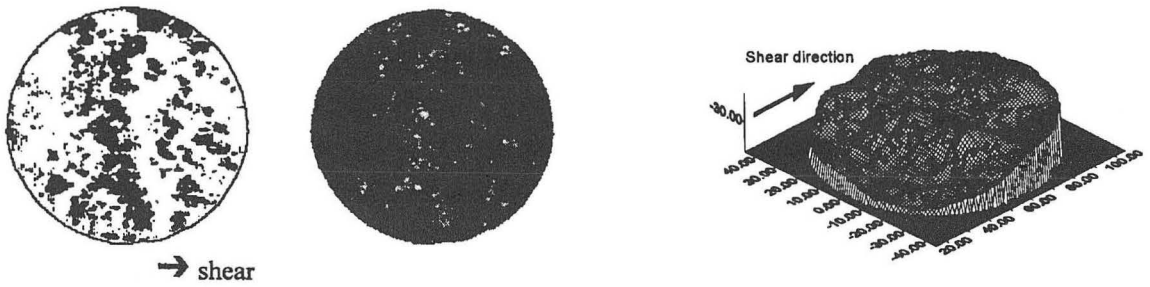

a b

Figure 6 : Binary image corresponding to damage areas (a) and location of the damage areas on the reconstructed topography of the fracture side (b).

reconstructed by kriging. For this direction of shearing, damage areas are created in a direction globally perpendicular to the shear direction and this arrangement becomes more and more pronounced as the normal stress is increased.

Developments on the prediction of the damage areas for a given initial topography of the fracture side is in progress (Riss et al., 1998). This analysis will be completed by casting of the fracture void under shear stress which is in progress too.

REFERENCES

Billaux, D. & S. Gentier 1990. Nurnerical and laboratory studies of flow in a fracture. In N. Barton and 0. Stephansson (eds.), *Proc. International Symposium on Rock Joints, Loen, Norway.* Balkema, Rotterdam, 369-373.

Gentier, S., E. Lamontagne, G. Archambault & J. Riss 1997. Anisotropy of flow in a fracture undergoing shear and its relationship to the direction of shearing and injection pressure. *Int. J,Rock Mech. & Min. Sci.,* 34:3-4, Paper No. 258.

Gentier, S. & D. L. Hopkins 1997. Mapping fracture aperture as a function of normal stress using a combination of casting, image analysis and modeling techniques. *Int. J. Rock Mech. & Min. Sci., 34:3-4,* Paper No. 132.

Gentier, S., D. Billaux & L. Van Vliet 1989. Laboratory testing of the voids of a fracture. technical Note. *Rock Mechanics and Rock Engineering,* 22, 149-15 7.

Gentier, S. 1987. Morphologie et comportement hydromécanique d'une fracture naturelle dans un granite sous contrainte normale - Approche expérimentale et théorique. Document BRGM n°167, 637p.

Hopkins, D. L., N. G. Cook & L. R. Myer 1990. Normal joint stiffness as a function of spatial geometry and surface roughness. In N. Barton and 0. Stephansson (eds.), *Proc. International Symposium on Rock Joints, Loen, Norway.* Balkema, Rotterdam, 203-2 1 0.

Riss, J., S. Gentier, G. Archambault & R. Flamand 1997. Sheared rock joints : Dependence of damage zones on morphological anisotropy. *Int. J Rock Mech. & Min. Sci.,* 34:3-4, Paper No 94.

Riss, J., S. Gentier, D. Hopkins 1998. Sheared behavior of rock joints : prediction of damaged areas.???

Water Flow and Solute Transport In Porous Fractured Chalk

Ronit Nativ,[1] Eilon Adar,[2] Ofer Dahan,[1] Noam Weisbrod,[1] Brian Berkowitz,[3] and Daniel Ronen[4]

[1]The Hebrew University of Jerusalem, Soil & Water Sciences, Rehovot 76100 Israel; nativr@agri.huji,ac.il; [2]Ben Gurion University of the Negev, Blaustein Institute for Desert Research, Sde Boker 84990 Israel; [3]Weizmann Inst. of Science, Department of Environmental Sciences and Energy Research, Rehovot 76100 Israel; [4] The Hydrological Service of Israel, Research Department PO Box 6381 Jerusalem 91063 Israel

The unique features of flow and transport in the chalk aquitard in the Negev desert were first documented on a regional scale by the monitoring of 23 wells which penetrate the chalk across the central and northern Negev. We suggested that water and solutes shortcut through the low-permeability matrix of the vadose chalk via fractures and joints, escaping much of the land surface exposure to evapotranspiration. This conclusion was based on observed seasonal fluctuations of water level in these wells and the chemical and isotopic composition of their groundwater (Fig. 1).

This inferred mechanism of groundwater recharge and contamination was confirmed using tracer concentrations in the vadose chalk. Tritium, oxygen-18, deuterium, chloride and bromide profiles representing water flux, evaporation and transport rates were obtained from chalk samples collected from four coreholes crossing the entire vadose chalk (Fig. 2). On the basis of these observations, we suggested that only a small portion of the rainwater percolates downward through the chalk matrix, while a large percentage of percolating water moves through preferential pathways in fractures intersecting the 20- to 60-m thick vadose zone.

The abundant fracture coating and filling materials can modify or even block and inactivate the flow paths in the fractures intersecting the chalk. Because the hydraulic aperture is a crucial parameter for evaluating fluxes through fractures, the need to study temporal and spatial variations of the preferential flow paths along a single fracture became clear. Consequently, a new system for direct measurement of flow and transport through a single fracture in the field was developed (Fig. 3). Flow and tracer experiments using this system along a pronounced >5-m-long fracture intersecting a vadose chalk outcrop revealed the flow to be restricted to small fracture segments along the fracture plane. These segments are generally associated with dissolution channels formed at the intersection of two fractures. Observations from our experimental area suggest that as little as 20% of the fracture void account for over 80% of the fracture flow. Long experiments (up to 5 days) did not result in a steady-state flow, suggesting temporal variations in the effective fracture void controlling the deep percolation through the fractures in the vadose chalk.

A possible reason for this instability is particle shearing from the relatively soft fracture surfaces and the disintegration of fracture filling materials. The temporal topographical variations in natural (coated and uncoated) fractured chalk surfaces were measured by laser scanning following wetting and drying cycles in the laboratory. The results suggested that under conditions of variable water content, the aperture, roughness and flow channels of fractures in chalk are transient properties (Fig. 4). These observations challenge the general assumption that the geometry of the fracture surfaces, although spatially variable, is constant over time.

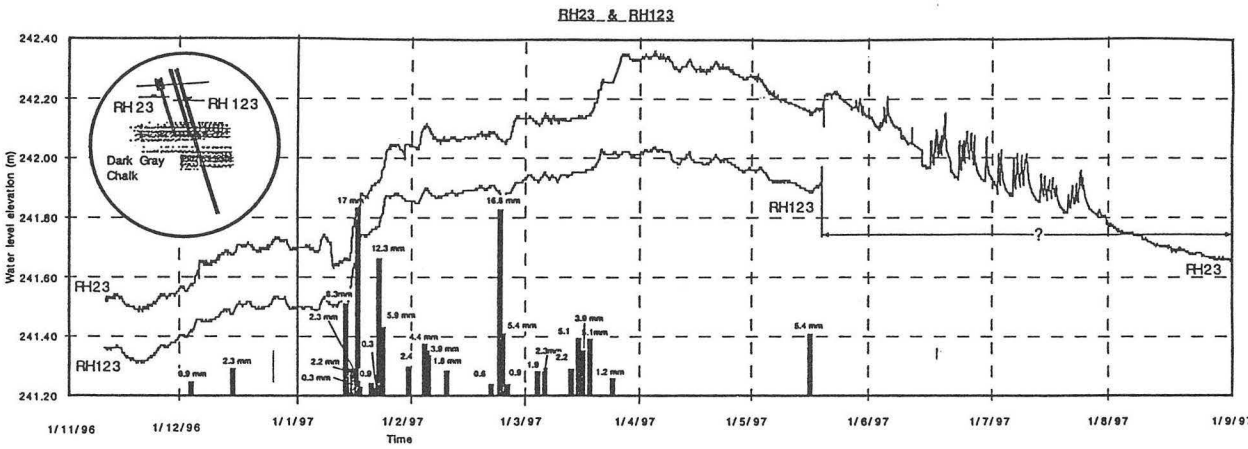

Figure 1: Continuous water level data from coreholes RH-23 and RH-123. Rectangles represent daily precipitation. Inset: Schematic configuration of the two slanted coreholes (lengths of 35 and 100 m, vertical depth of 33 and 94 m, respectively) and their completion. Note the seasonal and short-term water-level response to precipitation.

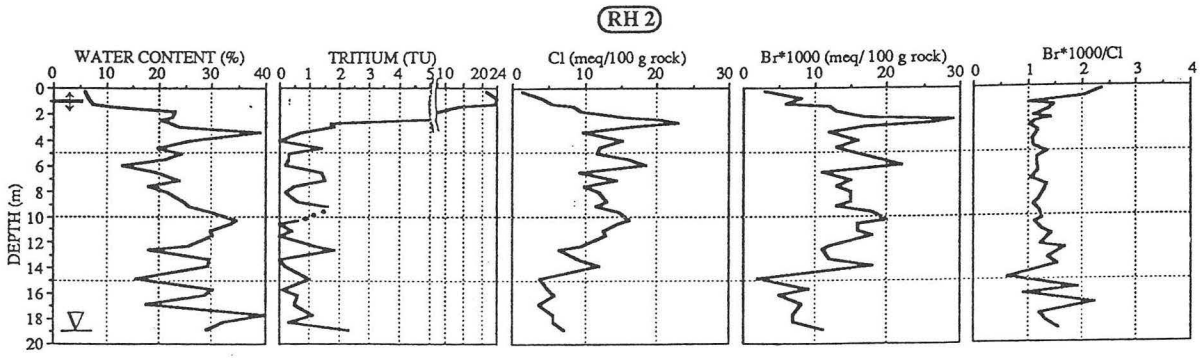

Figure 2: Chemical and isotopic profiles of the RH-2 borehole drilled throughout the entire vadose chalk. The contact between the chalk and the overlying sediments is marked by arrows. On the basis of these and similar profiles from three other boreholes in the study area it was concluded that the water percolating through the fractures penetrates the chalk matrix across the fracture walls, where it increases the tritium concentrations, depletes the stable isotopic composition (not shown here), and dilutes the salt concentrations.

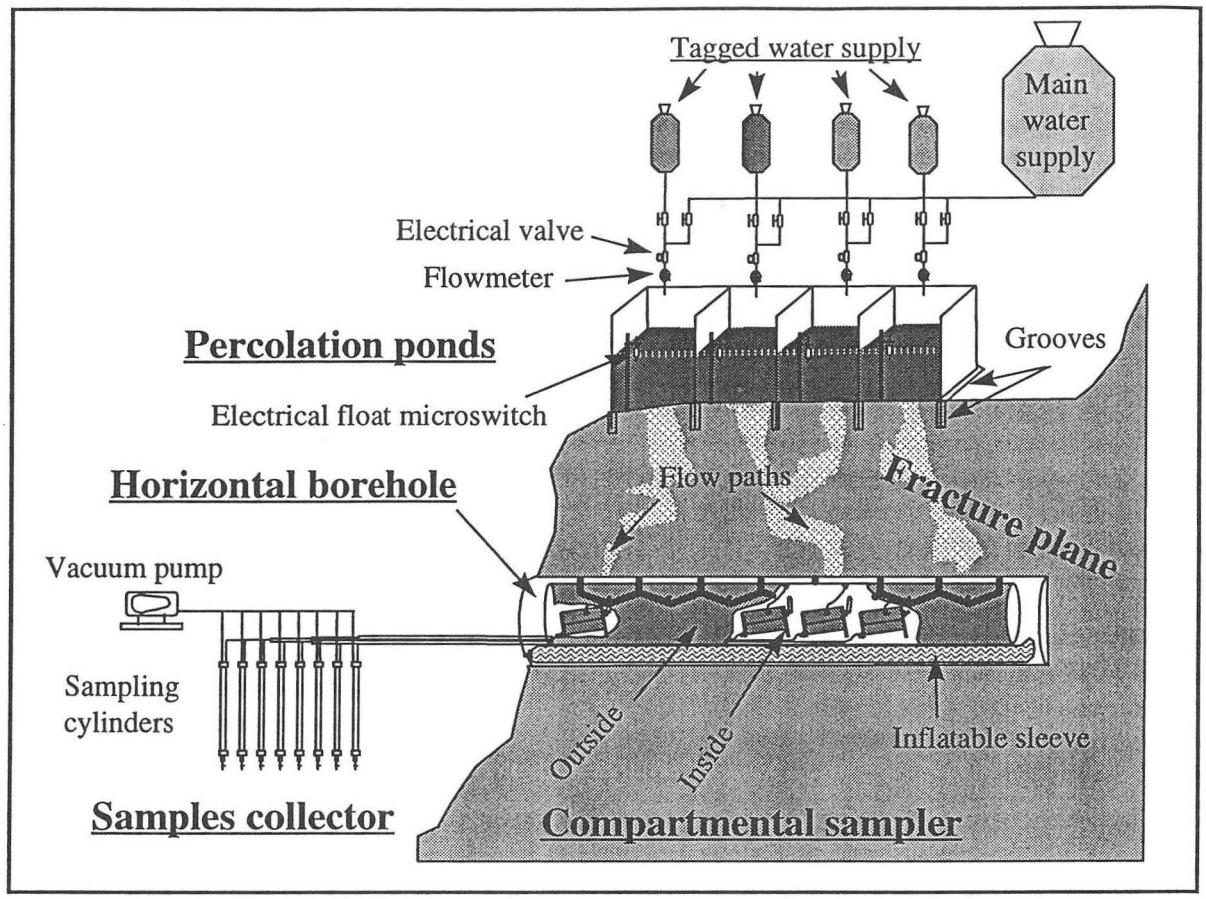

Figure 3: A schematic cross section of a measurement system designed to determine water fluxes and tracer migration rates in a field setup through a single natural fracture in the vadose zone. The system's components are: (1) a set of individually tagged percolation ponds, located above a chalk ledge crossed by a fracture; (2) a horizontal borehole cored into the same fracture at a depth below the ledge and the percolation ponds; (3) a compartmental sampler introduced into the borehole to collect the tagged water drained from the various ponds; and (4) a sample collector to retrieve the fluids stored in the compartmental sampler.

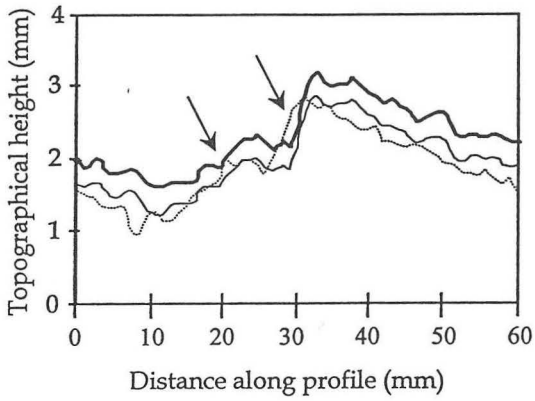

Figure 4: The topographical height of three profiles across a natural fracture surface of a chalk core. The fracture surface was measured using a high-resolution laser scanning system. The bold line depicts the topographical height of the original fracture surface. The solid and dashed lines were obtained from the very same cross section after submerging the core in tap water for 10 min and 14 hours, respectively. The observed variations in fracture-surface topography shown in this example and measured in 3000 scanned points on each side of the 60 x 50 mm core face suggest that under conditions of variable water content the aperture, roughness and flow channels of fractures in soft rocks are transient properties.

Modeling Signal Propagation and Well Response in Porous and Fractured Rock Aquifers

C. T. Simmons[1], D. Hee Hong Wye[1] and P. G. Cook[2]

[1]School of Earth Sciences, Flinders University of South Australia, GPO Box 2100, Adelaide, South Australia, Australia, 5001
(craig.simmons@es.flinders.edu.au / dhee@bow.intnet.mu)
[2]CSIRO Land and Water, PMB 2, Glen Osmond, South Australia, Australia, 5064
(peter.cook@adl.clw.csiro.au)

Introduction

Like any sedimentary porous aquifer, the hydraulic behaviour of fractured rock aquifers is constantly being driven by transient applied stresses which act as forcing functions. These may be imposed by tidal fluctuations, aquifer recharge and barometric fluctuations, to name just a few. The groundwater response to these stresses is usually recorded by piezometers or open wells installed at various points within an aquifer. It is often not clear how the recovered piezometric response in a groundwater system relates to the applied periodic stress on the aquifer and whether the act of measurement itself interferes with signal response. It still remains unclear as to what affect fractures may have on the hydraulic response, attenuation, frequency filtering and phase lag of signals relative to the source. In this paper, numerical simulations are carried out to examine some of these effects and to determine whether standard measurement methods themselves interfere with signal response.

Numerical Modeling

Using FRAC3DVS (Therrien et al., 1995), an aquifer, 500 m long in the x-direction and 50 m in both the y and z directions was considered. The details of the conceptual model are provided in Figure 1 and Table 1. The simulations were run for three years with 36 time steps each of one-month duration. In order to consider a square wave forcing function, a time variable head boundary was specified along the entire vertical face $x = 0$.
A square wave is used because in the frequency domain it is composed of an infinite number of odd-order harmonics which allow filtering effects to be studied. The head at $t = 0$ was set to 45 m and was switched back to 55 m at the end of sixth months. The square wave had a period of one year with amplitude of 10 m and an average value of 50 m. All other boundaries were assumed to be no-flow. The affect on signal attenuation caused by variations in hydraulic conductivity and matrix storativity were investigated by a sensitivity analysis on those parameters. A single vertical fracture was then inserted along the plane $x = 50$ m which intersected the entire model. Several simulations were also run with different fracture aperture widths ranging from 10^{-5} m to 10^{-1} m.

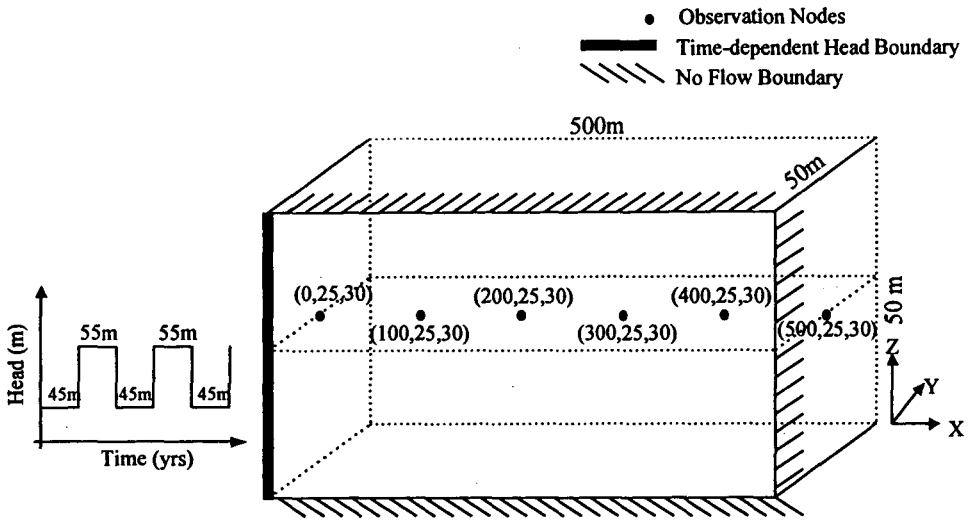

Figure 1. Conceptual model showing boundary conditions and observation nodes.

Parameter	Value
Fluid density	1000 kgm^{-3}
Fluid dynamic viscosity	3.15×10^4 kgm^{-1} yr^{-1}
Acceleration due to gravity	9.5796×10^{15} myr^{-1}
Discretisation in x direction	10 m, additional at $x = 49$ m & 51m
Discretisation in y direction	10 m, additional at $y = 25$ m
Discretisation in z direction	5 m
Isotropic hydraulic conductivity	20 myr^{-1}
Specific storage	0.005 m^{-1}
Porosity	0.025 (dimensionless)
Fracture Properties	
Storage coefficient	1 (dimensionless)
Fracture Location	$x = 50$ m
Aperture width	10^{-5}, 10^{-4}, 10^{-3}, 10^{-2} & 10^{-1} m

Table 1. Model parameters used in the analytical and numerical models.

Analytical Solution

Based upon Ferris' (1951) solution for a sinusoidal pulse travelling through an aquifer, the expression for the hydraulic head at (x, t) for the square wave considered here can be written as the summation of an infinite number of Ferris solutions to each odd-order sine term comprising the square wave function and is represented as follows:

$$h(x,t) = 50 - \left[\sum_{n=1}^{\infty(n=odd)} \frac{20}{n\pi} \exp\left(-x\sqrt{\frac{\pi n S}{T}} \right) \sin\left(2n\pi t - x\sqrt{\frac{\pi n S}{T}} \right) \right] \qquad (1)$$

where $h\ (x,t)$ is head relative to mean sea level at distance x (L) from the boundary and at time t (T); x is the distance from the fluctuating boundary; h_0 is the amplitude of sinusoidal fluctuations

(L); t is time (T); t_0 is the period of sinusoidal fluctuations (T); T is the transmissivity of aquifer (L^2/T); S is the storativity of the aquifer (dimensionless).

Results

Figure 2 shows a comparison between the analytical solution in Eqn (1) and that derived numerically for the porous case only. They are seen to be in excellent agreement.

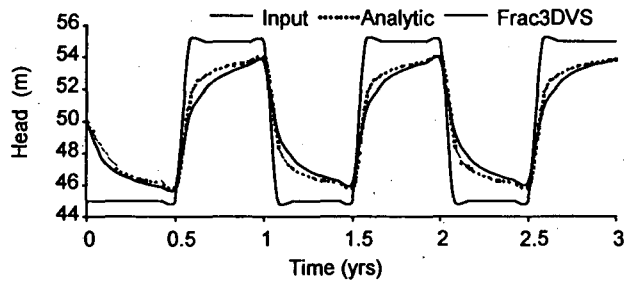

Figure 2. Response at x =100m to square periodic forcing, showing both numerical and analytical solutions.

Figure 3, a plot of signal amplitude As (normalised to forcing function amplitude Ao) against the sensitivity analysis parameter, shows that low hydraulic conductivity and high storativity enhance attenuation, whilst low storativity and high hydraulic conductivity promote signal transmission and reduce attenuation.

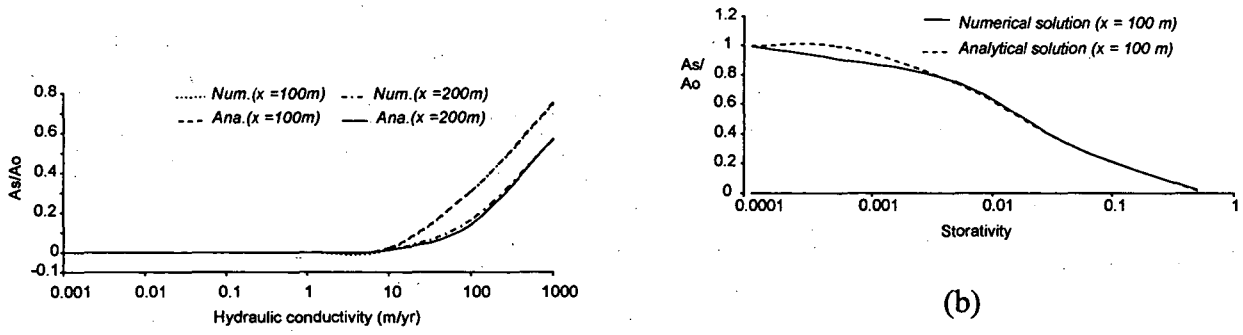

Figure 3. Sensitivity analysis: The effect of changing (a) hydraulic conductivity and (b) matrix storativity on recovered signals at observation nodes.

With a single vertical fracture located at x=50m and examining the response at x=100m, Figure 4 shows that the amplitude of the signal decreases linearly with increasing aperture width.

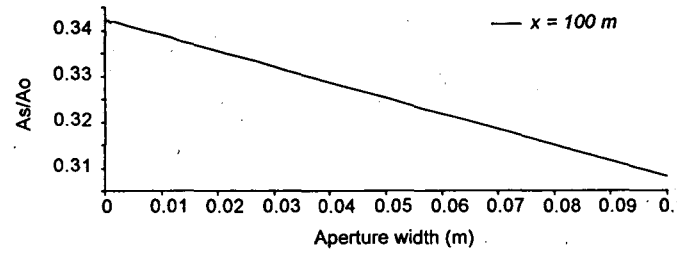

Figure 4. Normalised signal amplitude vs fracture aperture width.

To test the effect of the measurement process itself, the model was run with different values of storage coefficient without a well and the response was measured. A fully penetrating passive well was then introduced with the coordinates of the ends of the well being (100, 25, 0) and (100, 25, 50) respectively. Figures 5a and 5b show recovered signal amplitude with a well (normalised to what it would have been without one) as a function of well radius for different matrix storativities and different time periods of fluctuation respectively.

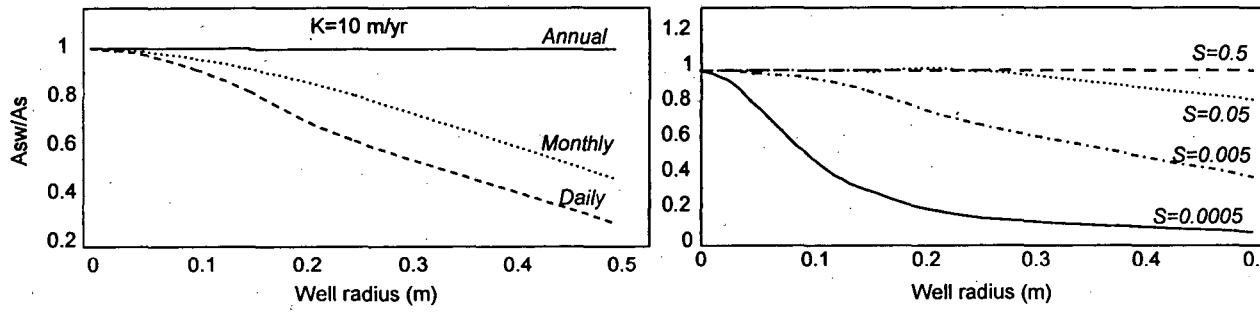

(a) (b)

Figure 5. Normalised signal amplitude as a function of well radius for (a) varying signal frequency and (b) varying matrix storativity.

Signal attenuation is particularly noticeable at lower matrix storativities and larger well radii. It is also evident that short daily fluctuations in applied stress to an aquifer are preferentially attenuated over longer monthly or annual ones, a result which is consistent with the analytical solution (Eqn. 1) and available field data. This has important implications for interpreting bore hydrographs in relation to recharge processes especially in low porosity environments such as those which are often encountered in hard fractured rock systems.

Conclusions

Signals propagating through an aquifer undergo attenuation and filtering. Attenuation is greatest in high storativity and low hydraulic conductivity systems. Higher frequency daily fluctuations are preferentially attenuated over lower frequency monthly or annual ones. A fracture creates a high storage environment and signal attenuation increases linearly with fracture aperture. Measurement methods such as open wells and piezometers create local high storage effects which may lead to attenuation of the signal. Attenuation caused by well storage effects is greatest for (i) lower matrix storativities, (ii) larger well radii, and (iii) signals of higher frequency or shorter time periods. This effect should not be ignored in low porosity

environments such as those typically encountered in hard fractured rock systems. The results of this work have important implications for the interpretation of piezometric and well responses in both porous and fractured rock aquifer systems and what these might infer about recharge processes or other hydraulic forcing functions.

References

Ferris, J.G., 1951. *Cyclic fluctuations of water level as a basis for determining aquifer transmissibility,* IAHS Publication No.33, p.148 - 155.

Therrien, R., Sudicky, E.A. and McLaren, R.G., 1995. *User's guide for NP 3.1: A preprocessor for FRAC3DVS 3.1,* Groundwater Simulations Group, 77 pp.

Session 5:
FRACTURE FLOW MODELS

Discrete Fractures-Continuum Mixed Models: A Summary of Experiences in Test Interpretation and Model Predictions

J. Carrera and L. Martinez

Department of Geotechnics and Applied GeoScience
School of Civil Engineering
Technical University of Catalonia
Barcelona, Spain

A number of conceptual models have been proposed for simulating groundwater flow and solute transport in fractured systems. They span the range from continuum porous equivalents to discrete channel networks. In each of them, heterogeneity can be handled deterministically or stochastically. In short, a large number of approaches are available to represent fractured media. Since the choice of appropriate conceptual models is largely based on experience, the diversity of approaches makes it hard for any method to emerge as best, because different conceptual models are difficult to compare. The objective of our presentation is to show the application of one particular conceptual framework to four cases, in the hope of building a case for this approach.

The model we have been using is termed mixed discrete fractures-continuum method, but it has also been called double permeability method. It consists of identifying the dominant fractures (i.e., those carrying most of the flow), which are modelled explicitly as two dimensional features embedded in a three dimensional continuum representing the remaining fracture network. The rationale behind the method is based on the observation that indeed most of the water often flows through one or two fractures, so that explicitly modelling them indeed helps in properly accounting for a large portion of the total water flow. The drawbacks of the method stem from the difficulties associated to (1) identifying the dominant fractures, (2) defining their extent and (3) building the grids to represent both the fractures and the continuum. Ways to overcome these difficulties are described through application of the method to four real cases.

The first case, which will be the one described in most detail, refers to extensive testing performed in granite at the Grimsel Test Site in Switzerland in the context of the Full Engineered Barrier Experiment (FEBEX). A large number of boreholes were available, so that they sufficed to geometrically describe the fracture network and quite accurately calibrate five long cross-hole tests with a single model. This model predicted steady-state heads and inflows into the test tunnel. The second case refers to the Chalk River Block (Canada), which was also extensively drilled, so that a rather good geometrical description was available. The model was calibrated against a long cross-hole test and successfully predicted the response to other tests performed in different fractures. The third case refers to hydraulic testing performed at El Berrocal (Spain), where long tracer tests could be predicted with a model calibrated against cross-hole hydraulic tests and short tracer tests. In this case, fracture geometry definition was aided by structural considerations. These were also very important in the fourth case, a large-

scale (about 2 km) model of El Cabril (Spain). A model calibrated against long records (5 years) of natural head fluctuations could be used to predict one month long hydraulic test and heads variations after construction of a waste disposal site.

The conclusion is that, in all four cases, the difficulties associated to the mixed discrete fracture-continuum approach could be overcome and that the resulting models have displayed some predictive capabilities. It must be acknowledged that a large amount of data was available in all cases, so that the validity of the method remains to be seen for situations in which data are scarce.

STOCHASTIC CONTINUUM MODELLING OF GROUNDWATER FLOW WITHIN THE SWEDISH PERFORMANCE ASSESSMENT PROGRAM

B. Gylling[1] and D. Walker[2]

[1)]Kemakta Konsult AB, Box 12655, 112 93 Stockholm, Sweden, e-mail: bjorn@kemakta.se

[2)]INTERA Duke Engineering & Services, 1650 University Blvd NE, Suite 300, Albuquerque, NM 87102, U.S.A., e-mail: ddwalker@dukeengineering.com

EXTENDED ABSTRACT

Groundwater flow simulations have been performed within the Swedish performance assessment program by using a stochastic continuum model. Two sites have been simulated with several variants to explore effects of scaling, stochastic anisotropy and spatial variability. The intent is to reveal how the tasks were handled within the studies and to raise questions on how to improve handling of some of the common difficulties in groundwater flow simulations.

Swedish Nuclear Fuel and Waste Management Company (SKB) is responsible for the safe handling and disposal of nuclear wastes in Sweden. This responsibility includes conducting studies into the siting of a deep repository for high-level nuclear waste. The Safety Report 1997 (SR 97) will present a comparative performance assessment (PA) of the overall long-term safety of a deep repository at three hypothetical sites in Sweden. The PA of each repository will include geosphere modelling to examine the possible transport of radionuclides from the emplaced waste packages through the host rock to the accessible environment. The site-scale groundwater modelling has been made using the code HYDRASTAR.

HYDRASTAR is a stochastic groundwater flow and transport modelling program developed by SKB as a quantitative tool for performance assessment (Norman, 1992). The current version uses the Turning Bands algorithm (Journel and Huijbregts, 1978) to generate realisations of the hydraulic conductivity field conditioned on the observed hydraulic conductivities. Trends in the data may be included implicitly through the use of ordinary kriging neighbourhoods or prescribed explicitly for specific regions. HYDRASTAR uses the governing equation for either time-dependent or steady state groundwater flow in three dimensions, assuming constant density. Transport in the resulting velocity field is modelled as pure advection using a particle-tracking

scheme. The process of geostatistical simulation of hydraulic conductivity, and particle tracking can be repeated in Monte Carlo fashion to develop probability distributions for the hydraulic conductivity field, and the travel paths and arrival times for advected contaminants. The code has been tested against well-known analytical and numerical solutions.

The base cases, representing the expected site conditions, used conductivities inferred from geostatistical models. Based on several field studies deterministic fracture zones were included. For each site, a single variogram model is inferred for the entire domain. The models of trends and spatial correlations are inferred using the iterative generalised least squares estimation (IGLSE) approach suggested by Neuman and Jacobsen (1984). Boundary conditions were obtained from larger regional models. The base cases are used as reference when comparing results for the several variants. In all cases, conductivity fields, particle path lines and exit locations were studied.

In the base case of one of the sites, a rather small variance in the conductivity field was used. A variant with larger variance was performed to study the impact. The effect was evident in visualisations of the conductivity fields, studies of particle path lines and exit locations. The median of the travel times decreased and the variance in the population increased. However, the differences were small since the presence of structures seems to control the flow paths and the increase in variance was not large enough to fully explore the effect.

Field data were obtained at a different scale to the model cell scale. By using a simple scaling rule based on empirical results the conductivity values were adjusted in the bases case and variant models. The effect was studied in a particular variant using a model with larger cells and up-scaled conductivity values. Scaling effects were also addressed in a case using a deterministic conductivity field. The base case and the deterministic run show similar travel times and flux at repository depth. Using a larger cell size in the grid decreased the travel times and increased the spread in the exit locations for the released particles. The results indicate that the scaling method worked but may be improved to yield better results.

Field data suggest that there may be an anisotropy in conductivity field at the sites. A stochastic covariance was used to simulate the effect of hydraulic anisotropy. Two sets of parameters in the geostatistical model were used to test the method. From the visualisations of the two anisotropy cases, a clear effect was observed in the conductivity fields. However, the travel times were not much different in the two cases. Difference in the particle path lines and exit locations were observed. A separate study was performed using a simplified model to compare the results with the theories by Gutjahr et al. (1978), Gelhar and Axness (1983) and Neuman and Depner (1988). In the model no structural data were included and a combination of Dirichlet and no-flow boundary conditions were used to create uniform flow in the grid. In this study, the variance in conductivity was varied.

REFERENCES

Gelhar L W, Axness C L, 1983. Three-dimensional stochastic analysis of macrodispersion in aquifers. Water Resources Research, Vol. 19:1.

Gutjahr, A L, Gelhar L W, Bakr A A, MacMillan J R, 1978. Stochastic analysis of spatial variability in subsurface flows. 2. Evaluation and application. Water Resources Research, Vol. 14:5.

Journel A G, Huijbregts Ch J, 1978. Mining Geostatistics, Academic Press.

Neuman S P, Jacobsen E A, 1984. Analysis of nonintrinsic spatial variability by residual kriging with application to regional groundwater levels. Math. Geol., Vol. 16:5.

Neuman S P, Depner J S, 1988. Use of variable-scale pressure test data to estimate the log hydraulic conductivity covariance and dispersivity of fractured granites near Oracle, Arizona. Journal of Hydrology, 102.

Norman S, 1992. HYDRASTAR - A code for stochastic simulation of groundwater flow. SKB Technical Report TR 92-12, Stockholm Sweden.

Stochastic Analysis of Transport and Retention in a Multiple Fracture Pathway

Scott Painter, Center for Nuclear Waste Regulatory Analyses, Southwest Research Institute, 6220 Culebra Rd, San Antonio TX 78238-5166; **Vladimir Cvetkovic**, Division of Water Resources Engineering, Department of Civil and Environmental Engineering, Royal Institute of Technology, Stockholm, Sweden; **Jan-Olof Selroos**, Swedish Nuclear Fuel and Waste Management Company, Stockholm, Sweden

Transport in the saturated zone of fractured, but otherwise low-permeability, rock occurs mainly by advection in water flowing through the interconnected fracture network. The microscopic processes matrix diffusion and sorption act together to retard, in a nonlinear fashion, the downstream movement of particles. These retention processes are significant in many applications, particularly those involving high-level nuclear waste repositories.

Transport in fractured rock is further complicated by uncertainty in the fracture attributes, as it is usually not possible to have direct observation of fracture attributes in the subsurface. In a typical application the best that could be hoped for is to know the joint probability distribution of fracture attributes such as aperture and length. This statistical uncertainty requires that radionuclide migration, and the related issue of waste repository performance assessment, be addressed in a probabilistic framework. In this paper, we develop such a framework taking into account advective transport through a series of connected fractures combined with matrix diffusion and sorption in the host rock. Our approach is of the discrete-fracture variety, but avoids the Monte Carlo fracture network simulation characteristic of that approach. Instead, we derive moments of the flux and related quantities analytically. This is made possible by a simplifying assumption, justified by field observations and previous network simulations, which allows us to replace complex interconnected fracture networks with an idealized migration pathway formed by n fractures connected in series.

Flowpath Model: Exact analysis of flow and transport in fracture networks requires consideration of the multiple routes that particles may take. This complication is why studies using discrete-fracture models rely on Monte Carlo simulation of the fracture networks. Such simulations using field-derived fracture attribute distributions reveal that a small number of transport pathways are often responsible for the majority of the mass flux [1]. Moreover, when the particle source is spatially localized, a single dominant transport pathway is often found. This result is also supported by field experiments on tracer transport [2].

Our main simplification is to ignore multiple routes through the fracture network and focus on a single flowpath formed by n quasi- two-dimensional fractures connected in series (Fig. 1). This approximation improves as the fracture density approaches the percolation threshold. Other factors improving the quality of this approximation include broad distribution of apertures and lengths, preferred spatial orientation and spatial clustering of fractures, incomplete mixing at fracture intersections, and spatial localization of the particle source.

In most application scenarios, solute particles are released into regions that are small compared to the physical width of a fracture. In the absence of strong dispersion internal to the fracture, particles will not spread out and sample the entire fracture surface, but will be transported along a streamtube determined by the two streamlines bounding the initial release. This is consistent with the flowpath model developed in [3] to model reactive transport in heterogeneous aquifers and used in [4] and [5] to model reactive transport in a single fracture. Our multiple-fracture variant consists of a rectangular contaminant-bearing streamtube with spatially varying aperture $b(x)$ and width $w(x)$, where x is the distance along the streamtube trajectory and $b(x) \ll w(x)$.

Water flows through this streamtube at a constant volumetric rate Q. Aperture variability internal to each fracture will cause the width to fluctuate around w_0, the size of the initial release. Fracture-to-fracture variability will also cause the local mean in the aperture to undergo stepwise changes as the streamtube passes from one fracture to the next. Here we neglect internal variability in fracture apertures relative to fracture-to-fracture variability. More general analysis including internal variability can be found in [6]. The flowpath then becomes a sequence of n segments. Each segment has a constant aperture b_i, a random length l_i, and the same width w_0. The apertures and lengths vary randomly from segment to segment. The goal is to relate the statistics for flux and related quantities at the output of the n-th fracture to the probability density function (pdf) for fracture apertures and length.

Retention Model: Downstream movement of particles is slowed by diffusion into an essentially immobile fluid in the rock pore space and by linear equilibrium sorption in the matrix. We neglect, for simplicity, sorption on the fracture surface and concentrate on diffusive effects. If diffusion in the rock matrix is one-dimensional without barriers and orthogonal to the fracture plane, the time-dependent flux of particles at the output of the n-th fracture due to a δ-function input at the beginning of the first fracture is [4,5]

$$r(t\,;\,\tau,\beta) = \frac{H(t-\tau)\kappa\beta}{2\sqrt{\pi}\,(t-\tau)^{3/2}}\exp\left[\frac{-\kappa^2\beta^2}{4(t-\tau)}\right]. \tag{1}$$

Here H is the unit step function, $\kappa = \theta\sqrt{DR_m}$, θ is the matrix porosity, $R_m = 1 + K_d^m$ is the retardation factor, K_d^m is the distribution coefficient for sorption in the matrix, and D is the coefficient of diffusion into the rock matrix.

The random variable τ is the residence or transit time for advection, and the new random variable, β controls the rate of diffusion and sorption:

$$\tau = \frac{1}{Q}\int_0^l w(x)b(x)\,dx = \sum_1^n \tau_i \approx \frac{1}{q}\sum_1^n l_i b_i \tag{2}$$

$$\beta = \frac{1}{Q}\int_0^l w(x)\,dx = \sum_1^n \beta_i \approx \frac{1}{q}\sum_1^n l_i$$

where $q = Q/w_0$ and $l = \sum_1^n l_i$ is the total length along the trajectory. The approximations apply within the context of our piecewise constant approximation to the flow path.

The time-of-arrival of a cumulative mass fraction φ is an important quantity in applications. Its value relative to the half-life for radionuclide decay is particularly important when considering migrating contaminants. It is calculated from (1) as $t_\varphi = \tau + \frac{\kappa^2}{4F^2}\beta^2$, where $F(\varphi)$ is the inverse complementary error function.

Stochastic Analysis: The flux and arrival time above are random quantities because of their dependence on the random variables β and τ, which depend in turn on random apertures and lengths. The stochastic analysis procedure [6,7] is to relate the joint pdf for τ,β for the pathway to the pdf for the individual fractures τ_1, β_1. This is in turn related to the pdf for individual apertures and lengths. For independent and identically distributed fractures, the pdf for the pathway $f_{\beta,\tau}(\beta,\tau)$ is related to that of individual fractures by an n-fold convolution, which is

easily calculated in the Fourier domain. Using the piecewise constant approximation to the flowpath, the pdf's for τ, β and aperture/length have a simple relationship [6,7]. These relationships can be used in a numerical calculation to obtain expected values of flux or arrival time at the output of the n-th fracture. Several examples are given in [6] and [7]. Here we concentrate on asymptotic results for the arrival time.

Asymptotic Results: The expected value of the cumulative arrival time can be related to moments of aperture/length without reference to the full pdf. The only requirement is that the aperture/length moments be finite. For example, neglecting terms of order $1/n$ relative to 1, we have

$$\frac{\langle t_\varphi \rangle}{\tau_d} = \frac{\langle l_1 b_1 \rangle}{\langle l_1 \rangle \langle b_1 \rangle} + \eta \tag{3}$$

where $\tau_d = \frac{n}{q}\langle l_1 \rangle \langle b_1 \rangle$ is the deterministic non-reacting travel time obtained by neglecting aperture/length variability and considering the multiple fracture pathway to be a single fracture with length $n\langle l_1 \rangle$ and aperture $\langle b_1 \rangle$. The angle brackets denote ensemble averages. Similar results have been developed for the variance in the arrival time. The dimensionless parameter

$$\eta = \frac{\eta_B}{4F^2} = \frac{\kappa^2 n \langle l_1 \rangle}{4F^2 q \langle b_1 \rangle} \tag{4}$$

quantifies the importance of mass exchange processes relative to advection for the multiple fracture pathway. Large values of η imply that the combined effect of diffusion and sorption dominate over advection, while the opposite is true for $\eta \ll 1$. Eqs. 3 and 4 show how the expected arrival time is enhanced over the deterministic non-reacting arrival time by retention processes, quantified through the dimensionless parameter η, and by length-aperture correlation, quantified by the first term on the right-hand side in Eq. 3. Positive correlation between length and aperture shifts the arrival time to later times.

The parameter η depends nonlinearly on φ through $F(\varphi)$. By varying φ and calculating the cumulative arrival time it is possible to map out the expected value for the entire breakthrough curve. This is shown in Fig. 2. The expected breakthrough curve depends only on three parameters: τ_d which serves to normalize time, the normalized moment in (3), and η_B which quantifies the relative importance of retention for the bulk of the plume.

Summary: In summary, we outline a stochastic model for transport and retention in a multiple fracture pathway and give examples of its application. This abstracted model is intended to complement more complex numerical calculation of radionuclide transport in saturated fractured rock. The model relates the expected value and variance for arrival time to the joint pdf of fracture aperture and length. The physical processes of advection, unlimited diffusion, and sorption are included in the initial examples, but the methodology can accommodate more general physical processes. For example, the method is currently being extended to treat the radionuclide decay chain, limited matrix diffusion, and spatial variability in sorption parameters.

Acknowledgments: This article documents work performed in part by the Center for Nuclear Waste Regulatory Analyses (CNWRA) under contract No. NRC-02-97-009. The report is an independent product and does not necessarily reflect the views or regulatory position of the NRC.

References

1. B. Dverstorp, J. Andersson, and W. Nordqvist, Water Resources Research, 28, 2327 (1992).
2. I. Neretnieks, in *Flow and Contaminant Transport in Fractured Rock,* edited by J. Bear, C.-F. Tsang, and G. de Marsily (Academic, San Diego, 1993).
3. G. Dagan and V. Cvetkovic, Proc. R. Soc. London, Ser. A. 452, 285 (1996).
4. V. Cvetkovic, J-O. Selroos and H. Cheng, Journal of Fluid Mechanics (in press).
5. J.-O. Selroos and V. Cvetkovic, SKB Technical Report 96-20, 1996.
6. S. Painter, V. Cvetkovic, and J.-O. Selroos (in preparation).
7. S. Painter, V. Cvetkovic, and J.-O. Selroos, Physical Review E, 57(6), 6917, 1998.

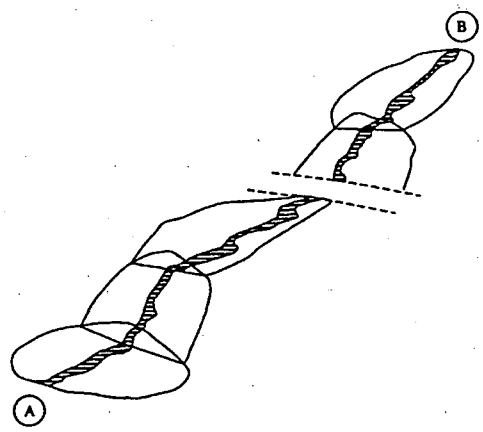

Figure 1: Transport pathway formed by multiple connected fractures in an otherwise impermeable medium. Fluid flowing at a constant volumetric flowrate through the fractures transports particles by advection. The particles also diffuse into the stagnant pore fluid in the surrounding rock. The fracture lengths and apertures are unobserved with joint probability density function that is assumed known.

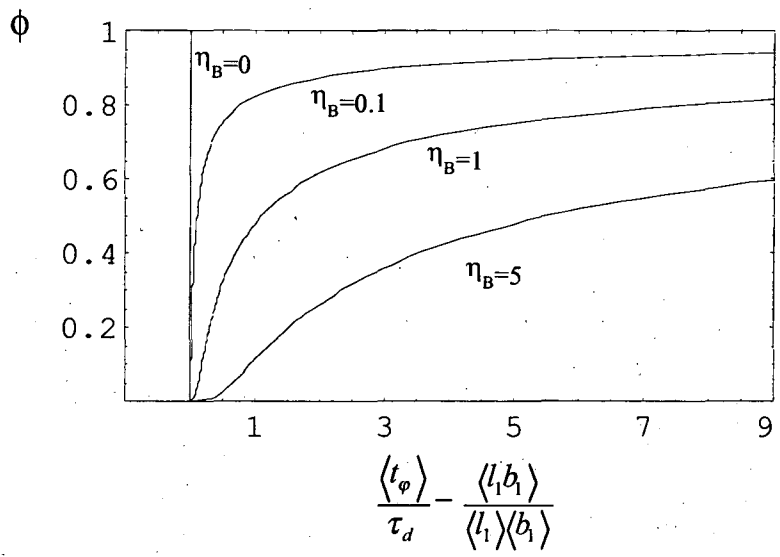

Figure 2: Expected value for the cumulative breakthrough curves for different values of the dimensionless retention parameter η_B

Connectivity of Fracture Networks with Power-Law Length Distributions

Carl E. Renshaw
Department of Earth Sciences, Dartmouth College, Hanover, NH 03755
carl.renshaw@dartmouth.edu

Introduction

Numerous conceptual models for the geometry of rock fractures have been proposed. However, except for systems with relatively few fractures, computational limitations require that the detailed geometry of these models be converted into an equivalent effective connectivity. Here connectivity is distinguished from permeability by the assumption of uniform fracture apertures. In contrast to the large number of geometric models, there exist relatively few closed-form predictive models for converting the conceptual geometry of a network into an equivalent connectivity. The model of Snow (1969), in which a fracture is represented by two infinite parallel plates, remains the most popular model despite its uncertain applicability to natural fracture systems. More recently a limited number of alternative models have been developed to account for the finite lengths of fractures. However, even for simple networks the connectivities predicted by these models are inconsistent.

For example, consider the simplistic, but oft used, representation of the complex geometry of natural fracture networks as a two dimensional bond percolation network. The effective connectivity of these networks predicted by various models, over the range of fracture densities commonly encountered in geologic formations (Renshaw 1997), are shown in Figure 1. Note the inconsistent predictions of these models even for these simplistic networks, with some models predicting connected networks ($K > 0$), and others not.

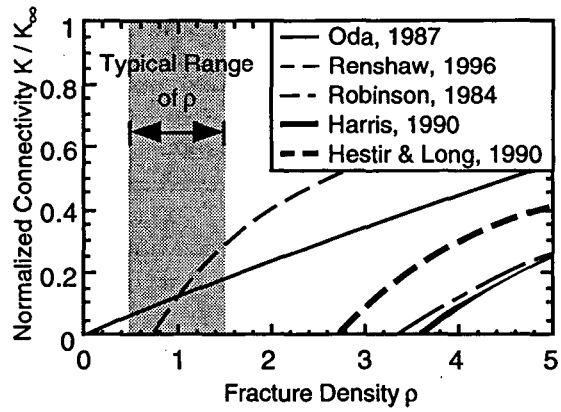

Figure 1. Curves show the effective connectivity of bond percolation networks predicted by various models. Shaded region indicates the range of fracture densities typically observed on surficial exposures. Connectivities are normalized by the connectivity predicted using the parallel plate model of Snow (1969).

Limitations of Existing Models

The discrepancies between the various connectivity models arise from differences in the assumed fracture length distribution. For example, the fracture connectivity model of Renshaw (1996) is based on an exponential fracture length distribution, while that of Robinson (1984) assumes constant length fractures. Since connectivity models are sensitive to fracture length distribution, it follows that the most appropriate connectivity model for fractured rock should be based on the fracture length distribution typically observed in rock.

Fracture length distributions obtained from outcrop-scale maps are often reasonably well described by a log-normal distribution. However, outcrop-scale maps under-represent both smaller and larger scale fractures. When data from several different scales of observation are combined, the distribution of fracture lengths often follows a power-law, or fractal, distribution.

The probability density function (pdf) for a power-law distribution of fracture lengths $n(l)$ can be written

$$n(l) = Cl^{-a} \tag{1}$$

where l is the fracture length, C is a constant, and a is the power-law exponent. It is easy to show that because observations indicate the fracture frequency decreases with increasing fracture length, and because the number of fractures must be finite, $1<a<3$.

Equation (1) is only valid over a given range of fracture lengths defined by the fracture length cutoffs. For example, the power-law pdf is unlikely to be valid at scales less than those of microcracks (often of the order 10^{-5} - 10^{-3} m) or at scales greater than that of the largest fracture, which may be of the order 10^{1}-10^{2} m or larger.

Within the range of fracture lengths for which equation (1) is valid, the value of the power-law exponent may not be constant. For example, it has been suggested that changes in the power-law exponent, known as scaling breaks, may occur across fundamental length scales that affect the growth of fractures, such as the grain size and the mechanical layer thickness in sedimentary rocks. However, here we assume that the power-law exponent is constant.

Typical values of a for geologic fracture networks can be estimated from published fracture trace maps (Figure 2). For all fracture trace maps considered the estimated value of the power-law length exponent falls within the range $1<a<3$, but the estimates are widely scattered within this range and there is no consistent dependence on scale of the trace map. The mean exponent value for all maps, shown by the solid line in Figure 2, is 1.8, with a standard deviation, shown by the dashed lines, of 0.4.

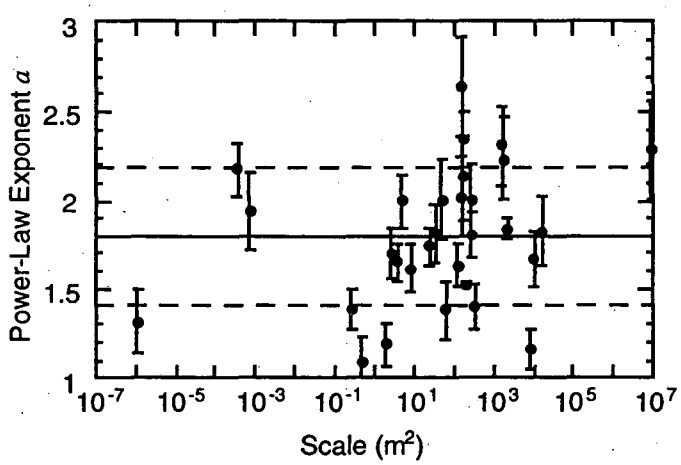

Figure 2. Values of the power-law exponent a estimated from published fracture trace maps versus scale of the map. Error bars indicate +/- one standard deviation of the estimate. Trace maps are the same as in Renshaw (1997).

Connectivity of Power-Law Networks

A number of investigators have developed fracture connectivity models based on percolation or equivalent medium theories. In these approaches, the connectivity of the network is typically given as a power-law function of the fracture intensity. Example results from these theories are shown in Figure 1. However, the percolation approach to network connectivity fails for fracture networks with power-law length distributions.

For example, note that all of the percolation based theories shown in Figure 1 can be expressed as a function of K_∞, which itself is a function of the mean fracture length l_o. For a power-law distribution of fracture lengths, l_o can be determined from the pdf as

$$l_o = \int_0^L lCl^{-a} = \frac{C}{2-a} l^{2-a}\Big|_0^L \tag{2}$$

where L is the largest fracture contained within the mapped area. Clearly, l_o can only be defined for $a < 2$. Thus in the absence of a well defined fracture length cutoff, K_∞ can not be defined for many of the networks shown in Figure 2.

An alternative normalization is motivated by the discussion of fractured rock permeability scaling in Renshaw (1998). In this work it is noted that the observed scaling of fractured rock permeability is similar to that of a single fracture crossing the entire system. Accordingly, the alternative normalizing connectivity K_* is given by the effective permeability of a single fracture spanning an L x L area,

$$K_* = \frac{t_f}{L} \tag{3}$$

where t_f is the transmissivity of the fracture, defined as

$$t_f = b^3 \frac{\rho g}{12\mu} \tag{4}$$

where b is the fracture aperture, g the gravitational constant, and ρ and μ the fluid density and viscosity, respectively (Renshaw 1995).

Given the normalizing connectivity, the connectivity of power-law networks can be defined as a function of the effective fracture spatial density

$$\rho_{eff} = \frac{1}{aL^2} \sum_{i=1}^{n} \left(\frac{l_i}{2} \right)^2 \tag{5}$$

where n is the number of fractures. Note that unlike the mean fracture length, the effective spatial density is defined for all a in the range $1<a<3$.

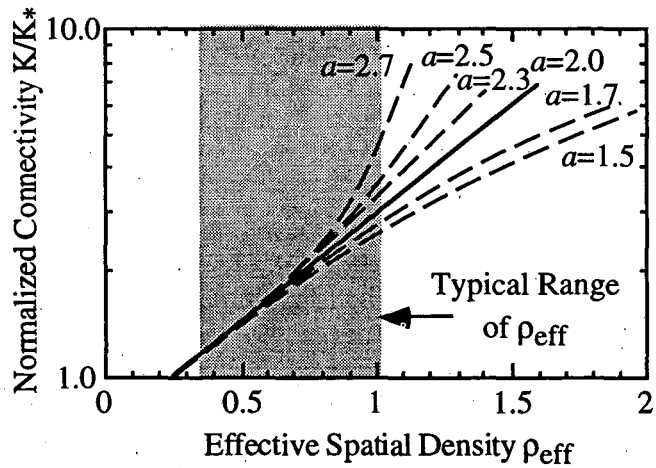

Figure 3. Normalized connectivity of isotropic fracture networks with power-law fracture length distributions and a function of the effective spatial density. Solid line indicates connectivity predicted by equation (7). Dashed lines indicates connectivities determined from numerical simulation of power-law networks.

We now propose that the change in connectivity of a network for a unit increase in effective spatial density is proportional to the connectivity. In other words, adding a given fracture to a network that is already well connected will have a greater impact on the network connectivity than adding the same fracture to a poorly connected network. More precisely,

$$\frac{d\left(K/K_*\right)}{d\rho_{eff}} = \beta K \tag{6}$$

where β is a constant that, for isotropic networks, only depends on the dimension of the fractures. Integrating, we have

$$\frac{K}{K_*} = C_1 e^{\beta\rho} \tag{7}$$

where C_1 is a constant.

Figure 3 shows the results from a series of numerical simulations of the connectivity of power-law networks as a function of the effective spatial density for various values of a. Also indicated by the shaded region is the typical range in ρ_{eff} observed on surficial outcrops. Within this range, equation (7) (solid line) provides a reasonable estimate of the connectivity for the range in a typically observed.

Summary

Existing models for the connectivity of fracture networks yield inconsistent results as each assumes a different distribution of fracture lengths. A new connectivity model is outlined here based upon the fracture length distribution most often observed in the field. Numerical simulations suggest that for effective spatial densities less than about one (which includes the typical range of effective spatial densities observed on outcrops), the new model provides a reasonable estimate of the connectivity of power-law networks for typical values of the power-law exponent.

References

Renshaw, C. E., 1995, On the relationship between mechanical and hydraulic apertures in rough-walled fractures, *J. Geophys. Res.* **100**, 24,629-24,636.

Renshaw, C. E., 1996, Influence of sub-critical fracture growth on the connectivity of fracture networks, *Water Resour. Res.* **32**, 1519-1530.

Renshaw, C. E., 1997, Mechanical controls on the spatial density of opening mode fracture networks, *Geology* **25**, 923-926.

Renshaw, C. E., 1998, Sample bias and the scaling of hydraulic conductivity in fractured rock, *Geophys. Res. Letts.* **25**, 121-124.

Robinson, P. C., 1984, Connectivity, flow and transport in network models of fractured media, Atomic Energy Research Authority, Harwell, United Kingdom.

Snow, D. T., 1969, Anisotropic permeability of fractured media, *Water Resour. Res.* **5**, 1273-1289.

Session 6:
VADOSE ZONE STUDIES

Recent Developments and Unresolved Problems in Vadose Zone Hydrology and Contaminant Transport.

William A. Jury and Zhi Wang
University of California, Riverside CA 92521
wajury@mail.ucr.edu

Flow and transport processes in the vadose zone differ from those in ground water in several important respects. The resistance offered by the matrix to the flow of water is a nonlinear function of the degree of saturation or the energy state of the water. Because of the transient processes occurring at the inlet boundary, flow and transport rarely, if ever, reach a steady state. Since temperature and air pressure changes can significantly influence the soil environment, representation of the flow and transport regime requires multiphase characterization. And, whereas in ground water, flow is generally parallel to stratification, in the vadose zone the usual direction of flow is perpendicular to the natural layering pattern of soil. In addition, spatial and temporal variability of important flow and transport properties is substantial, leading to extreme demands for data for both deterministic and stochastic modeling. As a result, theories for flow and transport processes in the vadose zone have not evolved as rapidly as those in ground water. At present, the Richards flow equation is used in virtually all simulations of water flow in the vadose zone, despite its limiting assumptions, and solute transport is represented by the advection dispersion equation, which suffers from similar drawbacks.

Field experiments of flow and transport have yielded little support for either of these equations, and frequently have revealed the existence of varying degrees of so-called preferential flow, wherein water moves at much higher than average rates through a small portion of the soil volume. Reasons for this occurrence are soil-dependent, but include: flow through structural voids, channeling caused by discrete obstacles within the soil matrix, and fluid instability, the latter arising from a host of causes. While once believed to occur exclusively in structured soils, preferential flow is now recognized as prevalent under a wide range of conditions in permeable, structureless soils as well as those containing cracks and crevices.

Improved understanding of preferential flow must await new developments in monitoring, and more experimental testing under natural conditions. At the moment, we do not have answers to a number of basic questions that limit our ability to manage or model this phenomenon. These questions include:

- What measurable soil properties are important in predicting the onset of preferential flow?
- What measurable soil properties are important in predicting the extent of preferential flow?
- How fast do water and dissolved chemicals move in a preferential flow channel?
- How can preferential flow be enhanced or reduced in a given environment?
- What is the role of water application method or surface water management in producing preferential flow?

- To what extent do sorption reactions occur during preferential flow, and how can they be characterized as a function of measurable soil properties?

The standard tools for monitoring water flow in soil are inadequate for addressing these questions. Monitoring of preferential flow has thus far been possible only using dyes, densely replicated soil coring, or analysis of tile-drain effluent. These tools either fail to characterize the speed of preferential flow, as is the case with dyes or coring, or provide no spatial resolution of the preferential flow event, as with tile-drain monitoring. To make any real progress in characterizing preferential flow, we need rapid response tensiometers and solution samplers that offer minimum disturbance of the soil, and some means of monitoring a substantial portion of the soil volume at a high degree of spatial resolution.

This talk will review the evidence for preferential flow obtained from several important field studies of vadose zone flow and transport, from which the following observations have been made: i) Preferential flow is a dominant feature of structured soils, particularly those with pronounced layering; ii) Preferential flow occurs to varying degrees in structureless soils, provided that the matrix conductivity is sufficient to support the large fluxes characteristic of preferential flow plumes; iii) Sorption of dissolved chemicals to stationary soil surfaces is greatly restricted in a preferential flow channel; iv) The depth of penetration of a preferential flow channel is limited by soil structure, soil layering and matrix conductivity, and could be considerable.

There are substantial obstacles to developing a practical model for flow and transport in a soil that manifests preferential flow to a significant degree. Deterministic modeling is impractical because of the enormous data requirements and lack of understanding of the causal connection between soil properties and extreme flow events. However, stochastic modeling is also impractical because a substantial soil volume could have only a few preferential flow channels within it, that nevertheless have a significant influence on mass transfer processes. The averaging volume for representing such a situation statistically may be so large as to be impractical. To the present time, theoretical investigations of preferential flow have largely been limited to characterizing the conditions for the onset of unstable flow. A number of laboratory studies have been conducted to investigate unstable flow, and they have largely supported the criteria developed through theoretical analysis. This talk will discuss the relation between the criteria derived from these studies and conditions found in flow through field soil, concluding that conditions for instability are often met during infiltration and redistribution events.

Some recommendations for future areas of study will also be made.

Type-Curve, Inverse and Geostatistical Analyses of Pneumatic Injection Tests in Unsaturated Fractured Tuffs at the Apache Leap Research Site Near Superior, Arizona

Walter A. Illman, Dick L. Thompson, Velimir V. Vesselinov,
Guoliang Chen and Shlomo P. Neuman

Department of Hydrology and Water Resources
The University of Arizona
Tucson, Arizona
e-mail: neuman@hwr.arizona.edu

Issues associated with the site characterization of fractured rock terrains, the analysis of fluid flow and contaminant transport in such terrains, and the efficient handling of contaminated sites are typically very difficult to resolve. A major source of this difficulty is the complex nature of the subsurface "plumbing systems" of pores and fractures through which flow and transport in rocks take place. There is at present no well-established field methodology to characterize the fluid flow and contaminant transport properties of unsaturated fractured rocks. In order to characterize the ability of such rocks to conduct water, and to transport dissolved or suspended contaminants, one would ideally want to observe these phenomena directly by conducting controlled field hydraulic injection and tracer experiments within the rock. In order to characterize the ability of unsaturated fractured rocks to conduct non-aqueous phase liquids such as chlorinated solvents, one would ideally want to observe the movement of such liquids under controlled conditions in the field. In practice, there are severe logistical obstacles to the injection of water into unsaturated geologic media, and logistical as well as regulatory obstacles to the injection of non-aqueous liquids. There also are important technical reasons why the injection of liquids, and dissolved or suspended tracers, into fractured rocks may not be the most feasible approach to site characterization when the rock is partially saturated with water. Many of these limitations can be overcome by conducting field tests with gases rather than with liquids, and with gaseous tracers instead of chemicals dissolved in water.

This paper focuses on single-hole and cross-hole pneumatic injection at the Apache Leap Research Site (ALRS) near Superior, Arizona. Over 270 single-hole tests have been conducted in six shallow vertical and inclined boreholes at the site by Guzman *et al.* (1996). These authors used steady state formulae to obtain permeability values for borehole test intervals of various lengths, based solely on late pressure data from each test. This paper describes more recent pressure and pressure-derivative type-curve analyses, as well as numerical inverse interpretations, of transient data from some of the single-hole tests. The transient analyses yield information about air permeability, air-filled porosity, skin factor, phenomenology and dimensionality of the flow regime on a nominal scale of 1 *m*.

Single-hole air injection tests provide information only about a small volume of rock in the close vicinity of the injection interval. Rock properties measured on such

small scales vary rapidly and erratically in space in a manner that renders the rock strongly and randomly heterogeneous. To determine the properties of the rock on larger scales ranging from meters to tens of meters, 44 cross-hole pneumatic interference tests have been conducted at the ALRS during the years 1995 – 1997. In most of these tests, air was injected at a constant mass flow rate into a relatively short borehole interval of length 1 - 2 *m* while monitoring a) air pressure and temperature in the injection interval; b) barometric pressure, air temperature and relative humidity at the surface; and c) air pressure and temperature in 13 short (0.5 - 2 m) and 24 longer (4 - 20 m) intervals within the injection and surrounding boreholes. Only one of these tests, labeled PP4, was fully analyzed to date. During this test, which the paper describes in detail, pressure responses were detected in 12 of the 13 short monitoring intervals and 20 of the 24 longer intervals. Of the 16 boreholes utilized in cross-hole testing, 6 had been previously subjected to single-hole testing. The results of single-hole tests (primarily spatial distribution of air permeabilities and local flow geometry) together with other site information (primarily core data and borehole televiewer images) served as useful guides in the design of cross-hole tests.

The earlier work of Guzman *et al.* (1994, 1996) and Guzman and Neuman (1996), together with the work described in this paper, suggest strongly that air injection tests yield properties of the fracture system, which are relevant to both unsaturated and saturated conditions. In particular, whereas the pneumatic permeability and air-filled porosity of fractures one determines from such tests tend to be somewhat lower than their intrinsic (fluid-independent) counterparts, the former nevertheless approach the latter as the applied pressure goes up. This is so because capillary forces tend to draw water from fractures into the porous (matrix) blocks of rock between the fractures, thereby leaving the latter saturated primarily with air. Water saturation in the matrix blocks is therefore typically much higher than that within the fractures, making it relatively difficult for air to flow through such blocks. It follows that, during a pneumatic injection test, the air moves primarily through fractures (most of which contain relatively little water) and the test therefore yields flow and transport parameters which closely reflect (though somewhat underestimate) the intrinsic properties of these largely air-filled fractures. The displacement of water by air under a constant rate of injection manifests itself in a rapid increase in pressure within the injection interval, followed by a gradual decrease. Two-phase flow of water and air additionally causes air permeabilities from single-hole pneumatic injection tests to exhibit a hysteretic variation with applied pressure.

In most single-hole pneumatic injection tests at the ALRS, pneumatic permeabilities increase systematically with applied pressure as air displaces water under two-phase flow. In a few single-hole tests, where the injection intervals are intersected by widely open fractures, air permeabilities decrease with applied pressure due to inertial effects. This pressure-dependence of air permeability suggests that it is advisable to conduct single-hole air injection tests at several applied flow rates and/or pressures. Pneumatic parameters derived from pressure data recorded in monitoring intervals during cross-hole tests appear to be much less sensitive to the rate of injection, suggesting that two-phase flow and inertial phenomena decay rapidly with distance from the injection interval. Enhanced permeability due to slip flow (the Klinkenberg effect) appears to be of little relevance to the interpretation of single-hole or cross-hole air injection tests at the ALRS.

The paper demonstrates that it is possible to interpret both single-hole and cross-hole pneumatic injection tests at the ALRS by means of analytically derived type-curves, and a numerical inverse model, which account only for single-phase airflow through the rock while treating water as if it was immobile. Type-curves are presented which represent linearized solutions to nonlinear partial differential equations that govern single-phase airflow in uniform, isotropic porous continua under three regimes: three-dimensional flow with spherical symmetry, two-dimensional flow with radial symmetry, and flow in a continuum with an embedded high-permeability planar feature (a major fracture). The method of linearization appears to have only a minor impact on test results obtained by means of these type-curves. The type-curves account for effects of compressible air storage and skin in the injection interval during single-hole tests, and in monitoring intervals during cross-hole tests. Type-curves of pressure derivative versus the logarithm of time are included to accentuate phenomena that might otherwise be missed (such as dual continuum), help diagnose the prevailing flow regime (distinguish between radial and spherical flow regimes), and aid in constraining the calculation of corresponding flow parameters.

The numerical inverse model simulates pneumatic tests at the ALRS on the computer using a three-dimensional finite volume code, FEHM (Zyvoloski *et al.*, 1988, 1996, 1997). It automatically estimates the pneumatic properties of the rock, as well as the effective storage volume of the injection borehole interval, by means of the inverse code PEST (Doherty *et al.*, 1994). The decision to use FEHM was based in part on its ability to simulate two-phase flow of air and water in dual porosity and/or permeability continua, and to account for discrete fractures. However, it was found possible to interpret pneumatic tests at the ALRS successfully without the need to activate any of these features of the code. The inverse model is able to represents pneumatic test conditions at the site more realistically than do type-curves by incorporating medium heterogeneity and the effects that vertical and inclined boreholes have on pressure propagation through the system. Yet the two methods of interpretation yield comparable results.

Steady state interpretations of single-hole pneumatic tests yield air permeability values for the rock in the immediate vicinity of the test interval. Transient type-curve analyses of such tests provide additional information about the phenomenology and dimensionality of the corresponding flow regime, skin factors and compressible air storage effects. Under radial flow, or in the absence of a significant borehole storage effect, transient type-curve analyses may also yield values of air-filled porosity. At the ALRS, air permeabilities obtained from steady state and transient type-curve interpretations of single-hole pneumatic injection tests, conducted in borehole intervals of 1-*m*, agree closely with each other but correlate poorly with fracture density data. Airflow around the vast majority of these relatively short test intervals appears to be three-dimensional; borehole storage due to air compressibility is pronounced; and skin effects are minimal. The combined effects of three-dimensional flow and borehole storage make it difficult to obtain reliable air-filled porosity values from these tests by means of type-curves, but do allow obtaining such values by means of the inverse model.

Flow in the vicinity of most 1-*m* single-hole pneumatic test intervals at the ALRS appears to be three-dimensional regardless of the number or orientation of fractures in the surrounding rock. This suggests that such flow is controlled by a single continuum,

representative of a three-dimensional network of interconnected fractures, rather than by discrete planar features. Indeed, most single-hole and cross-hole pneumatic test data at the ALRS have proven amenable to analysis by means of a single fracture-dominated continuum representation of the fractured-porous tuff at the site. Only in a small number of single-hole test intervals, known to be intersected by widely open fractures, have the latter dominated flow as evidenced by the development of an early half-slope on logarithmic plots of pressure versus time; unfortunately, the corresponding data do not fully conform to available type-curve models of fracture flow. Some pressure records conform to the radial flow model during early and intermediate times, but none do so unambiguously at late time.

Work at the ALRS clearly demonstrates that it is generally not possible to distinguish between the permeabilities of individual fractures, and the bulk permeability of the fractured rock in the immediate vicinity of a test interval, by means of pneumatic injection tests. Hence there is little justification for attempting to model flow through individual fractures at the site. The explicit modeling of discrete features appears to be justified only when one can distinguish clearly between layers, faults, fracture zones, or major individual fractures on scales not much smaller than the domain of interest.

Air permeabilities obtained from single-hole tests at the ALRS are poorly correlated with fracture densities. The same is known to be the case for hydraulic conductivities at many water-saturated fractured rock sites worldwide (Neuman, 1987). This provides support for Neuman's decade-old assertion that the permeability of fractured rocks cannot be reliably predicted from information about fracture geometry (density, trace lengths, orientations, apertures and their roughness) but must be determined directly by means of hydraulic and/or pneumatic tests.

Core and single-hole measurements, conducted over short segments of a borehole, provide information only about a small volume of rock in the immediate vicinity of each measurement interval. Available data from the ALRS indicate that rock properties, measured on such small scales, vary erratically in space in a manner which renders the rock randomly heterogeneous and pneumatically anisotropic. Local-scale air permeabilities from single-hole tests vary by orders of magnitude between test intervals across the site; their spatial variability is much more pronounced than their dependence on applied pressure. The paper demonstrates that it is possible to interpolate some of the core and single-hole measurements at the ALRS between boreholes by means of geostatistical methods, which view the corresponding variables as correlated random fields defined over a continuum. This is especially true about air permeability, porosity, fracture density, water content, and the van Genuchten water retention parameter α, for each of which there are enough site data to constitute a workable geostatistical sample. To differentiate between geostatistical models that appear to fit these data equally well, the paper uses formal model discrimination criteria based on maximum likelihood and the principle of parsimony (which places a premium on simplicity and penalizes models having an excessive number of parameters). Standard geostatistical analysis provides best (minimum variance) linear unbiased estimates of how each such quantity varies in three-dimensional space, together with information about the quality of these estimates.

The finding in this paper that core and single-hole test data are amenable to continuum geostatistical analysis supports the application of continuum flow and transport theories and models to unsaturated fractured porous tuffs at the ALRS on scales

of one meter or more. It implies that the data can be viewed as samples from a random field, or stochastic continuum, as proposed for fractured rocks by Neuman (1987) and affirmed more recently by Tsang *et al.* (1996). This is so despite the fact that the rock is fractured and therefore mechanically discontinuous.

Estimates of hydrogeologic variables, obtained by geostatistical methods such as kriging, are smooth relative to their random counterparts. The paper illustrates how one can generate less smooth and more realistic images of log air permeability, fracture density, log porosity, water content, and log α values in three dimensions that honor the available data, by means of a sequential Gaussian conditional simulation code due to Gómez-Hernández and Cassiraga (1994).

Cross-hole pneumatic injection test data from individual monitoring intervals at the ALRS have proven amenable to analysis by type-curve and numerical inverse models which treat the rock as a uniform and isotropic fractured porous continuum. Analyses of pressure data from individual monitoring intervals by the two methods gave comparable results concerning pneumatic connections between injection and monitoring intervals, corresponding directional air permeabilities, and air-filled porosities. All of these quantities were found to vary considerably from one monitoring interval to another in a given cross-hole test on scales ranging from a few meters to over 20 meters. Thus, even when the analysis treats the rock as if it was pneumatically uniform and isotropic, it ultimately yields information about the spatial and directional dependence of pneumatic permeability and connectivity across the site.

Some cross-hole pressure records reveal an inflection that is characteristic of dual continuum behavior. The prevailing interpretation of dual continua is that one represents the fracture network and the other embedded blocks of rock matrix. This paper advocates a broader view according to which multiple (including dual) continua may represent fractures on a multiplicity of scales, not necessarily fractures and matrix.

The pneumatic permeabilities of unsaturated fractured tuffs at the ALRS are revealed to vary strongly with location, direction and scale. In particular, the mean of pneumatic permeabilities increases, and their variance decreases, with distance between packers in a single-hole injection test, and with distance between injection and monitoring intervals in cross-hole injection tests. This scale effect is most probably due to the presence in the rock of various size fractures that are interconnected on a variety of scales.

Accounting for Fractures and Other Macropores in Predictions of Unsaturated Hydraulic Conductivity

John R. Nimmo,
USGS, Menlo Park, California 94025, jrnimmo@usgs.gov

In both soil and porous rock, fractures are a major type of macropore, frequently the dominant type. Thus there is much conceptual overlap in the problems of quantifying soil structure in relation to hydraulic properties and of characterizing the unsaturated flow of water through a fractured porous medium. There are several ways of treating these systems, for example as dual-porosity media.

Predicting unsaturated hydraulic conductivity (K) based on other properties of the medium is a common practice because K is difficult to measure, owing in large part to its extreme sensitivity to water content (theta). Capillary theory can mathematically link unsaturated K to more easily measured data, such as soil-water retention (the characteristic relation between water content and the matric pressure of the water held in the pores). Because of the drastic simplifications involved in this approach, the results usually have highly limited accuracy.

For soils with pronounced macropore structure, the model of Nimmo (1999) represents unsaturated K as an extension of a model for soil-water retention (Nimmo, 1997). These models use aggregate-size distributions as a quantitative indicator of structure in a way analogous to the use of this property by Gupta and Ewing (1992) and Rieu and Sposito (1991). The Nimmo (1999, 1997) models assume that all macropores, in effect, are fractures between aggregates. Modest additional development of these models allows application to fractured porous media in general. This presentation considers first a model of unsaturated hydraulic conductivity as a function of water content for structured soil, and second the adaptation of this model for fractured rock.

Model description and development

The dual-porosity concept allows one to treat structural pores differently from textural pores. For soil, the pore space is conceptually divided into texture space (within aggregates) and structure space (between aggregates). Five key assumptions relate this concept to unsaturated hydraulic properties. Assumption 1 defines structural effects: a hydraulic property represented as a mathematical function can be treated as a sum of two functions, one based on textural effects and one based on structural effects. Thus a textural retention curve added to a structural retention curve gives a complete retention curve as would be measured by ordinary methods.

Assumption 2 is that capillary theory can relate the water retention and hydraulic conductivity to pore sizes. Additionally, it is necessary to infer pore sizes from easily measured properties. In a soil it is convenient to use particle sizes for textural effects and aggregate sizes for structural effects. It is then necessary to model the relation between pore and particle (or aggregate) sizes. Assumption 3 is that the model of Arya and Paris (1981) is adequate for this purpose, usable directly for the textural components and with slight modification for the structural components. The central concept of the Arya-Paris model is that each particle size is associated with a pore size, larger pores with larger particles.

Assumption 4 is that a lognormal distribution can characterize aggregate sizes (Gardner, 1956). This allows the characterization of aggregate size by two parameters, the mean and the geometric standard deviation, both of which can then be used in formulating a model of hydraulic properties.

The representation of structural properties is improved by a modification of the Arya-Paris model because in natural media the pores between aggregates tend to be more uniform in aperture (and effectively less constricted at their openings) than the pores between particles within aggregates. Reasons for this include the fact that the malleability of aggregates lets them fit together better than solid grains, and that interaggregate pores such as cracks and wormholes are usually relatively long and narrow. Assumption 5 is that narrowness correlates with orderliness and hence with the uniformity of the pore-size distribution, in such a way that the lognormal standard deviation can serve as an index of variation of aggregate size distribution. This index of aggregate tightness is used as a factor directly incorporated into the model. It ranges from 0 for perfectly tight-fitting aggregates to 1 for looseness implying the character of randomly structured media. For water retention, the structure model based on these assumptions has the form of a cumulative lognormal distribution.

The extension to hydraulic conductivity relies on assumption 2, specifically that a capillary bundle model (e.g., Mualem, 1976) is adequate to predict unsaturated K from a pore-size distribution inferred from a measured retention curve. This sort of model considers laminar flow through the pores that are filled at a given unsaturated state, and integrates the conductance of filled pores to give K(theta). Assuming the two types of pore space are not coupled, but effectively allow flow through the structural space in parallel with flow through the textural space, two integrations are added to compute the K of the complete medium. This also permits the representation of the two spaces by different capillary models. Use of the Purcell (1949) model, with perfect continuity of pores, for the structural space and the Mualem (1976) model, with flow limited by pore connectedness, for the textural space, enhances the realism of the combined model. The model tested so far assumes that all pores, including fractures, have circular apertures, though adaptation can allow slits or other cross-sectional shapes for potentially more realistic geometry.

The application to fractured rock, rather than soil, differs both in the partitioning of the porosity into textural and structural portions, and in the use of particle-size distributions. For soils, the model takes the textural porosity to equal 0.3. Then the structural porosity equals the measured (total) porosity minus 0.3. For nongranular porous media such as fractured rock, this rule of thumb does not apply. The partitioning is better done along the lines of matrix porosity and fracture porosity, which have to be determined specifically for the medium of interest. It may be useful to define an index related to structural porosity based on crushed-rock size distribution. A bigger problem in the extension to fractured rock is that the particle-size distribution as required by the Arya-Paris model is not usually measurable. One alternative is to measure the water retention curve of the medium and use that information instead of the particle-size data.

Results and comparisons to data and other models

Model predictions have been compared to measured results for structurally disturbed and undisturbed silt loam soils. The measured data for each sample included retention curves, unsaturated K, and saturated K, in addition to particle- and aggregate-size distributions. The results show a steeper, better-fitting K(theta) curve than does a standard capillary-bundle model. The greater sensitivity of K to water content is as expected for a medium with significant macropore structure.

The model described here is overdetermined in that of three types of measurable input data -- the retention curve, the particle size distribution, and the aggregate size distribution -- only two are necessary. Different sorts of reliability and usefulness result from the different choices. One could, for example, use the retention curve plus one type of size data, to get K predictions in structured media that are better than the retention curve alone would produce. Another alternate use, without size-distribution data, would be to divide a measured retention curve into textural and structural components, and to model tailored textural and structural K contributions to obtain a combined prediction that may be suitable for fractured media.

Conclusions

The new model quantifies structure in terms of interaggregate pores, in effect a type of fracture, profiting from the use of additional data. For soils, aggregate-size data supplement the usual measured water retention for this purpose. The extension to K(theta) gives more realistic predictions for media with significant fractures or macropore structure.

References

Arya, L.M., and J.F. Paris. 1981. A physicoempirical model to predict the soil moisture characteristic from particle size distribution and bulk density data. Soil Sci. Soc. Am. J. 45:1023-1030.

Gardner, W.R. 1956. Representation of soil aggregate-size distribution by a logarithmic-normal distribution. Soil Sci. Soc. Am. Proc. 20:151-153.

Gupta, S.C., and R.P. Ewing. 1992. Modeling water retention characteristics and surface roughness of tilled soils. p. 379-388. In van Genuchten, Leij, and Lund (eds.) Indirect methods for estimating the hydraulic properties of unsaturated soils. Proc. Workshop. U.S. Salinity Lab. and Dep. Soil and Envir. Sci., U. Calif., Riverside.

Mualem, Y., 1976. A new model for predicting the hydraulic conductivity of unsaturated porous media. Water Resour. Res, 12:593-622.

Nimmo, J.R. 1997. Modeling structural influences on soil water retention. Soil Sci. Soc. Am. J. 61:712-719.

Nimmo, J.R. 1999. Predicting soil-water retention and hydraulic conductivity from textural and structural information. *In* van Genuchten, M.Th., and Leij, F., eds., Proceedings of the international workshop on hydraulic properties of unsaturated soils, Riverside, CA, October 22-24, 1997 [in press].

Purcell, W.R. 1949. Capillary pressures--their measurement using mercury and the calculation of permeability therefrom. Trans. Am. Inst. Min. Metall. Eng. 186:39-46.

Rieu M., and G. Sposito. 1991. Fractal Fragmentation, Soil Porosity, and Soil Water Properties: I. Theory. Soil Sci. Soc. Am. J. 55:1231-1238.

A Radionuclide Transport Model for the Unsaturated Zone at Yucca Mountain

B. A. Robinson, H. S. Viswanathan, A. V. Wolfsberg, and
C. W. Gable
Earth and Environmental Sciences Division
Los Alamos National Laboratory

The unsaturated zone at Yucca Mountain is one of the primary barriers to the migration of radionuclides from the potential repository to the accessible environment, and, as such, has received great attention in site-characterization activities. This report summarizes the transport model for the unsaturated zone at Yucca Mountain. The purpose of the modeling studies is to incorporate the latest hydrologic, mineralogic, and geochemical information into a set of numerical models to predict transport of radionuclides from the potential repository to the water table. Since these are predictions of repository performance after waste emplacement, the influence of repository waste heat and future climate changes must be accounted for.

The flow and transport simulations use data from the following sources:

- Hydrologic properties: Bodvarsson et al. (1997).
- Infiltration: Flint et al. (1997).
- Stratigraphy: Clayton et al. (1997).
- Mineralogy: Chipera et al. (1997).
- Radionuclide transport properties: Triay et al. (1997).

Using these data sources, two- and three-dimensional dual permeability flow and transport models were constructed using the FEHM computer code. Simulations of environmental isotopes and major-ion chemistry further constrain the model. The present study summarizes the findings of recent flow and transport simulations with respect to the transport of radionuclides: detailed analyses and discussion can be found in Robinson et al. (1997).

Results

Sensitivity to Hydrologic Property Values: Recent model calibration work presented in Bodvarsson et al. (1997) resulted in several hydrologic property sets that are consistent with the rock matrix saturation and capillary pressure data. These parameter sets were input to FEHM in a series of one-, two-, and three-dimensional simulations to examine the relative magnitude of flow through fractures and matrix predicted by the model, and to study the sensitivity of radionuclide transport in the unsaturated zone to hydrologic property values. Most of the parameter sets predict transport of 10% or less of the radionuclide inventory to the water table primarily through fractures, with the remainder percolating through the matrix rock.

Transport Parameter Sensitivity Studies: The portion of the radionuclide inventory traveling predominantly through fractures has predicted travel times as short as about 100

years. The peak in the distribution of residence times is on the order of a few thousand years in the absence of sorption (Figure 1), and represents a pathway in which both fracture and matrix transport are present. Actinides such as Np and U sorb preferentially to zeolites in the unsaturated zone. However, for these hydrologic property sets, zeolite matrix permeabilities are too low to transmit all of the infiltrating fluid, and the remainder travels through fractures. Therefore, sorption to zeolites has a relatively minor influence on radionuclide transport. However, when higher permeabilities are assumed for the zeolitic horizons, travel times increase and the proportion of radionuclides traveling through fractures decreases. One of the key uncertainties is therefore the permeability of the rocks underlying the potential repository as a function of zeolitic abundance.

Colloid-facilitated transport of strongly sorbing radionuclides such as Pu was also simulated. The key uncertain parameter influencing the importance of colloids is the partition coefficient for radionuclides onto mobile colloids. Unless Pu partitions almost exclusively onto mobile colloids at the expense of aqueous Pu, colloids will play a minimal role in the overall performance with respect to Pu. Measurements are currently being made to obtain values for this critical parameter.

Heterogeneous Property Simulations: Small scale variability of chemical and hydrologic properties can play an important role on the prediction of flow and transport in the unsaturated zone. The variation in chemical and hydrologic properties is strongly dependent on the mineral distribution. Due to the correlation between mineral distribution and hydrologic and chemical properties, the distribution of minerals such as zeolites can strongly influence the flow patterns of percolating fluids and the sorption of many radionuclides. Using the zeolite abundance measured at several boreholes and compiled in the site mineralogic model of Chipera et al. (1997), we carried out a conditional simulation of zeolitic abundance and investigated the relationship between percent alteration, permeability changes due to alteration, sorption due to alteration, and their overall effect on radionuclide transport. The key conclusion to the study is that Np retardation due to sorption predicted by a conditional simulation is much larger than the retardation predicted by the zeolite threshold method. The reason for larger retardation is a small but significant sorption coefficient Kd at locations with zeolite abundance less than 10%. At these locations, the Kd is low (less the 1 cc/g) but permeability is large enough for the flow to be matrix dominated. By contrast, the increased retardation is not due to high Kd values which occur at high zeolite abundance because very little flow travels through these low permeability regions.

Reactive Transport with Repository Heat: To predict Np migration after a repository breach, an understanding of the relevant hydrologic and geochemical processes is required. In addition to ambient flow conditions, the heat generated by the decaying radioactive waste will influence the transport of radionuclides such as Np. The geochemical processes that strongly affect Np migration include: solubility-limited release of Np from the near field environment, aqueous speciation of neptunium into non-sorbing carbonate/hydroxy complexes and the sorbing cation, sorption of neptunium onto the zeolitic tuffs via an ion exchange mechanism, and radioactive decay. We investigated the coupled effects of chemical interactions and heat on neptunium transport from the

potential repository to the water table. The simulations indicate that in the absence of irreversible changes in the hydrologic and transport properties, the heat pulse does not significantly affect the migration of neptunium, as the time scale of heat pulse propagation (of order 2000 to 10,000 years) is shorter than the time scales associated with neptunium release and migration (Figure 2). Water chemistry, particularly pH, calcium, and sodium concentration significantly affect the retardation of neptunium by the zeolitic rocks between the repository and the water table. Nonetheless, flow and transport under ambient conditions appears to be a reasonable abstraction that can be used for long-term performance predictions.

Acknowledgment

This work was supported by the Yucca Mountain Site Characterization Project Office as part of the Civilian Radioactive Waste Management Program. The Project is managed by the U. S. Department of Energy, Yucca Mountain Site Characterization Project. No new data are presented in this report.

References

Bodvarsson G.S., T.M. Bandurraga, and Y.S. Wu. The site-scale unsaturated zone model of Yucca Mountain, Nevada, for the Viability Assessment. Technical Report LBNL-40378, Lawrence Berkeley National Laboratory, 1997.

Chipera, S.J., K. Carter-Krogh, D.T. Vaniman, D.L. Bish, and J.W. Carey, Preliminary three-dimensional mineralogical model of Yucca Mountain, Nevada, Los Alamos National Laboratory YMP Milestone SP321AM4, 1997.

Clayton, R. W., W. P. Zelinski and C. A. Rautman, (CRWMS), ISM2.0: A 3-D geological framework and integrated site model of Yucca Mountain: Version ISM1.0, Doc ID B00000000-01717-5700-00004 Rev 0, MOL.19970122.0053, Civilian Radioactive Waste Management System Management and Operating Contractor, February 1997.

Flint, A.L, J. Hevesi, and L.E. Flint, Conceptual and numerical model of infiltration for the Yucca Mountain Area, Nevada, USGS WRIR MOL 19970409.0087, GS960908312211.003DOE Milestone, 3GUI623M., U.S. Geological Survey, (in preparation), 1996.

Robinson, B.A., H.S. Viswanathan, A.V. Wolfsberg, G.W. Gable, G. Bussod, The site-scale unsaturated zone transport model of Yucca Mountain, YMP Milestone SP25BM3, 1997.

Triay, I.R., et al., Summary report geochemistry/transport laboratory tests, Los Alamos National Laboratory YMP Milestone SP23QM3, 1997.

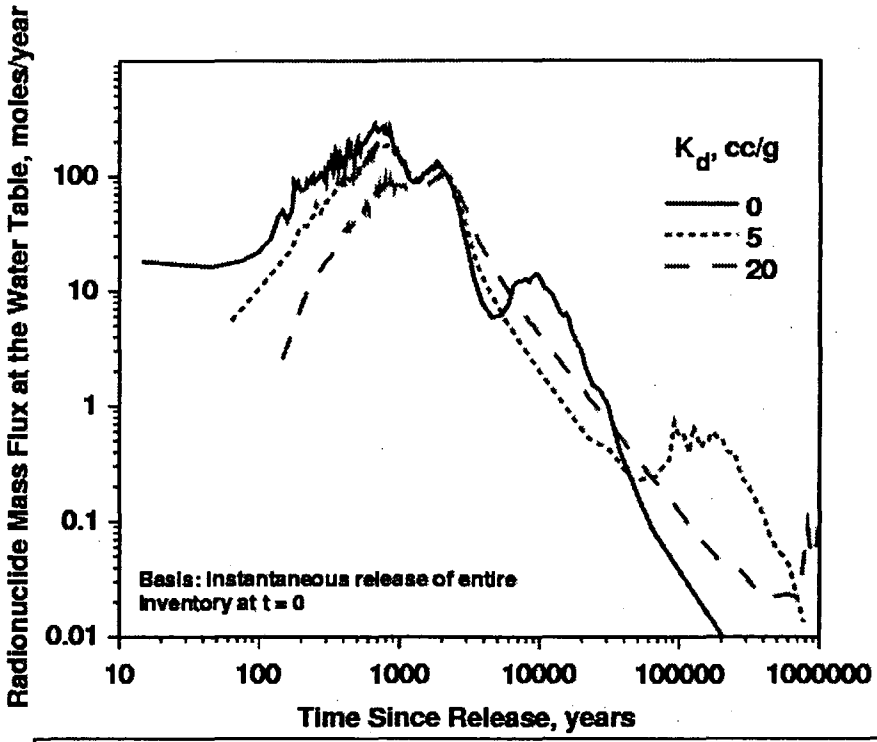

Figure 1. Breakthrough curves at the water table for an instantaneous release of radionuclides at time 0 for different sorption coefficients in the zeolitic rocks beneath the potential repository (no sorption elsewhere).

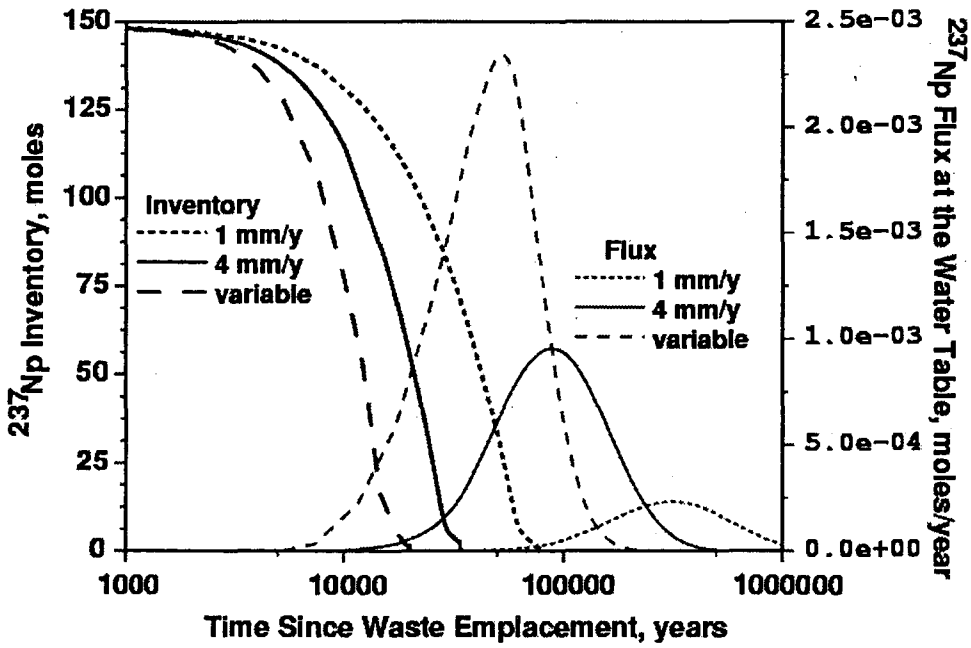

Figure 2. Predicted Np release curves (left axis) and water table breakthrough curves (right axis) for the full thermohydrologic and reactive transport model. Infiltration rates studied are 1 mm/y, 4 mm/y, and a spatially varying model that averages 4.8 mm/y, with a range from less that 0.5 mm/y to 18 mm/y.

Fast Flow in Unsaturated Rock Fractures

Tetsu K. Tokunaga and Jiamin Wan
Lawrence Berkeley National Laboratory
Berkeley, CA 94720

Although fractures in rock are well-recognized as pathways for fast flow, the mechanistic basis for unsaturated fast flow remains incompletely understood. Most conceptual models for fast flow require high saturations in fractures, despite the fact that this condition is not often observed in the vadose zone. Flow fingering and transient fracture flow during episodic infiltration events are recognized as gravity-driven fast flow mechanisms which occur along locally essentially saturated pathways. However, the possibility that fast flow could occur along unsaturated fracture (macropore) pathways has received much less consideration. The goal of this study is to develop and experimentally test conceptual models for fast flow in unsaturated rock fractures. Two previously unrecognized mechanisms which permit fast flow in unsaturated fractures are film flow and surface zone flow. This paper provides further results concerning film flow, and introduces the importance of surface zone fast flow along unsaturated fractures of low permeability rock.

A conceptual model for film flow in unsaturated fractures was recently presented, along with laboratory experiments illustrative of its general characteristics (Water Resour. Res. 33, 1287-1295, 1997). In this model, water film thickness can build up along fracture surfaces when matric potentials are high enough to sustain effectively saturated conditions in the underlying matrix. As matric potentials increase (approach zero) within this range, water films expand along fracture surfaces by first filling finer scale roughness features, and progressively filling coarser roughness features. It is important to recognize that water films on rough surfaces are comprised of both relatively thick "films" of capillarity-filled surface depressions and of true thin films along topographic ridges. Most of the water in films along unsaturated fractures is associated with filled depressions, and their connectivity largely determines film flow. The hydraulic properties necessary for characterizing steady-state film flow in unsaturated fractures of porous rock were identified as surface analogs to porous medium properties. These are the matric potential-dependent film transmissivity, the (non-hysteretic) film moisture characteristic function, and the average film velocity. The transmissivity of films increases with film thickness, and supports fast gravity-driven flow.

More recently we have conducted experiments into two other aspects of film flow; the influence of surface, and transient processes. Experiments on surfaces with well-defined topography were conducted to test the importance of surface roughness on film flow. These were conducted on ceramic blocks with simple, corrugated roughness features. Controlling influences of fracture surface channels and ridges were quantitatively demonstrated in these experiments. Another part of this study on film flow concerns transient processes in unsaturated fractures. The film hydraulic diffusivity has been identified and measured through steady-state and transient experiments.

In addition to film flow, the hydraulic characteristics of some vadose zone rocks exhibit fast flow along "fracture surface zone" pathways. Surface zone fast flow can occur when the surfacial regions of rock blocks (along fracture flow pathways) are more permeable than the bulk matrix. This condition can arise from permeability-enhancing alterations of physical (microfracturing) or chemical (precipitation-dissolution fracture coatings) origin, and will tend to be more significant when the bulk rock is low in permeability. Surface zone fast flow was tested qualitatively and quantitatively through two types of sorptivity (imbibition) experiments. Qualitative evidence for surface zone fast flow was obtained through experiments in which water flows parallel to the fracture, into both the surface zone and bulk rock simultaneously. More quantitative measurements of surface zone fast flow were obtained through imbibition normal to the fracture surface, with water first entering the surface zone, then the bulk rock. Experiments on a welded tuff revealed fracture surface zone pore water velocities about 900 times faster than that of the bulk rock. Experiments on a rhyolite showed about 30 times faster flow in the surface zone than in the bulk rock.

This study has introduced two mechanisms capable of explaining fast flow in unsaturated fractured rock, film flow, and surface zone flow. The validity of the proposed mechanisms was supported through multiple experimental tests. Future research will include aperture influences in order to obtain a more complete understanding of flow in partially saturated fractures.

Role of Fractures at Different Scales in Underground Heater Experiments

Y.W. Tsang (ytsang@lbl.gov) and B. Freifeld
Earth Sciences Division
Lawrence Berkeley National Laboratory

The impact of heat on flow and transport in a proposed high level nuclear waste repository is being addressed in underground heater experiments being conducted in the Exploratory Studies Facility at Yucca Mountain, Nevada. The Yucca Mountain Thermal Test Program includes the Single Heater Test (SHT) and the Drift Scale Test (DST), both residing in the non lithophysal, densely fractured, partially saturated welded tuff. The SHT involved a 5-m long, nominally 4-kW heating element, placed horizontally among 30 instrumental boreholes, which were drilled in directions both parallel and orthogonal to the heater. The experiment was in a rock block of approximately 13 m x 10 m x 13 m surrounded by drifts on three sides. All testing activities and analysis for the SHT have been concluded. The much larger-scale and longer-duration Drift Scale Test (DST) centers around a 47.5-m-long, 5-m-diameter heated drift, with close to 100 instrumented boreholes that span a rock block of 50 meters cubed. The heat load was distributed as 52 kW for the 9 canister heaters within the heated drift, and 135 kW among the 50 10-m long "wing" heaters placed in horizontal boreholes, extending from and uniformly spaced along the heated drift. The heating was initiated in the DST on December 3, 1997, for a planned heating period of four years. The extensive data that are becoming available from these *in situ* experiments provide a unique opportunity to improve our understanding of the coupled processes linking thermal, hydrological, mechanical, and chemical effects in the natural setting of the repository rocks. The thermal-hydrological conditions of both the SHT and DST were predicted with 3D numerical models. There was good agreement between modeling results and the extensive data set from the *in situ* tests, indicating that the fundamental basis of our understanding of the thermal-hydrological coupled processes in a multi-phase unsaturated system is sound.

In this paper, we take a narrow scope for our discussion and focus on air-permeability and gas-tracer migration measurements in the heater tests. In particular, results and insight gained from these field tests will be presented, with emphasis on how fractures control the flow and transport processes from sub-meter to tens of meters scale.

Interference air-injection tests were carried out for the SHT block in 31 boreholes prior to the activation of the heater. Under ambient conditions, the fractures and matrix are most likely to be in thermodynamic equilibrium, and because of the orders-of-magnitude difference in permeability and capillary suction between the matrix and fractures, most of the water is held in matrix pores. Thus the fractures are essentially free of flowing water at steady state. Therefore, the air-injection tests target the flow characteristics in the fractures, specifically, the fracture connectivity in the rock block and potential pathways for gas flow. Tests were done prior to the onset of heating. Inflatable packers were installed near the collar of each of the 31 boreholes in the SHT. A typical test consisted of injecting air in one borehole at constant mass flux, and

monitoring pressure responses in this and all other boreholes continually for about 20 to 30 minutes. Local permeability in the injection borehole was estimated from the steady-state pressure response (which typically occurred within minutes) to the air injection. Results show that the permeability values for 21 boreholes range from 5.0×10^{-15} m^2 to 5.2×10^{-12} m^2. These permeability values are averaged over the entire borehole, with length ranging from 2 to 11 meters.

However, since borehole videos indicate different degrees of fracturing in localized zones within each borehole, one would expect the permeability to vary from one localized zone to another within each borehole. This was confirmed by air-injection tests subsequently performed in 16 consecutive intervals of 0.69 m bracketed by a movable straddle packer string in a 12-m long borehole. The 16 intervals give estimated permeability values that range from less than 10^{-15} m^2 to 6.2×10^{-13} m^2. The permeability averaged over 11 m of the entire borehole is 5.1×10^{-14} m^2.

Interference pressure data show that in response to air injection in one borehole, there are cross-hole pressure responses in almost all of the other 30 monitoring boreholes. This indicates that on the scale of several meters, the fractures are well connected, and that the gas flow in the fractures resembles more that of flow through a heterogeneous continuum than flow through a discrete fracture network. In the latter case interference pressure responses would occur only in a limited number of monitoring zones. The interference data, corroborated by fracture maps on the drift walls of the SHT block and borehole video logs, also uncover a discrete, high-permeability fracture of about 4 meters in extent. In conclusion, based on the pre-heat characterization data on several meters scale, the fractures in the SHT block may be conceptualized as a heterogeneous continuum. The three-orders-of-magnitude difference in permeability values can be attributed to flow through fractures at a series of hierarchical scales, with microfractures accounting for the lower values, and larger fractures of a few meters in extent responsible for the higher values. The pre-heat characterization results were used as input to the construction of a numerical model to predict the performance of the SHT.

As the rock mass is heated during testing, water in the rock vaporizes, migrates, and condenses in the cooler rock away from the heat source. The zones of increased liquid saturation in the fractures can also be monitored by air-permeability tests. Two particular boreholes, designated as hydrology holes 16 and 18 in the SHT, were used to study this effect. They were each installed with a packer string consisting of four packers designed to sustain high temperatures. At different times throughout the heating and cooling phases of the SHT, constant-flowrate air-injection tests were carried out in different intervals isolated by the packers in these two boreholes. The data confirmed the predictions of 3D thermal-hydrological numerical simulations of the SHT; i.e., a reduction of air permeability values (by a factor of 2 to 4) were found only in those zones where numerical simulations predicted increased fracture saturation during the heating phase of the SHT. The permeability returned to their pre-heating values in the cooling phase of the SHT. In addition to the observed reduction of air permeability in these intervals in boreholes 16 and 18, an accumulation of water was observed in borehole 16. The water was sampled at four different instances during the heating phase of the SHT. Since borehole intervals represent a capillary

barrier, seepage into a borehole occurs only if the capillary barrier is overcome by presence of full saturation at the borehole wall. These locations of fully saturated rock at the borehole wall are more likely if there is a fast path for fluid transport. That water was found in borehole 16 and not in borehole 18 suggests that a fast path for vapor transport exists between the heater hole and the former, but not the latter.

Post-test pneumatic characterization, following the completion of the cooling phase of the SHT, allowed testing of the above hypothesis. With this in mind, air permeability tests were carried out in a multi-zone configuration for the heater borehole and boreholes 16 and 18. Specifically, injection was conducted in six consecutive intervals in the heater borehole, and pressure responses in the relevant intervals (where air permeability values have decreased during the heating phase) in boreholes 16 and 18 were analyzed to identify plausible fast path connections. Upon conclusion of air permeability tests, gas tracer tests were also conducted along these connected paths. Results show that the tracer transport from heater hole to borehole 16 was extremely rapid, with 100% tracer recovery occurring within 30 minutes of injection. On the other hand, the first arrival of tracer from the heater hole to borehole 18 took more than twice as long, and 100% tracer recovery took approximately 15 hours. The difference in transport times suggests that the path between the heater borehole and borehole 18 is far more indirect and tortuous than the path to borehole 16. These post-test characterization data therefore confirmed the hypothesis that there is a direct pneumatic connection (fracture) for vapor transport from the heater hole to borehole 16, and this local fracture is probably responsible for the seepage of water into borehole 16.

Experience in the SHT shows that pre-heating air-permeability characterization data were adequate to provide input for the numerical predictions of the general thermal-hydrological behavior. However, the detailed behavior in the SHT was impacted by site-specific features and local heterogeneities, which were not identified *a priori*. The presence of preferential pathways became apparent in the thermo-hydrologic data and associated modeling. Post-cooling hydrological characterization confirms the fast pathways suggested by those heating-phase results. The iterative approach between modeling and field testing in phases has proven to be immensely valuable for the SHT.

For the SHT, the relevant length scale for the thermal-hydrological processes are the radial extent of the drying and condensation zones, which are on the order of 2 to 3 meters. Hence the air-permeability tests were also carried out for those length scales. In the DST, the relevant length scale for the drying and condensation zones is commensurate with that of the wing heaters (~10m); hence, the air-permeability and gas-tracer tests conducted for the DST are on this larger length scale. Pre-heating characterization by air-injection tests were carried out in selective boreholes in the DST, for packed lengths of 6 to 20 meters. Estimated permeability for 148 measurements show that the permeability values range from 8.8×10^{-16} m^2 to 1.5×10^{-11} m^2. The geometric mean is on the order of 10^{-13} m^2. The interference data in the DST again indicate that fractures are numerous and well connected enough to be approximated as a continuum at the scale the measurements were made. Contrary to the interference pressure data in SHT where a high

permeability connection of 4-m length scale was observed in the pre-heating air injection tests, the DST pre-heating data show no special discrete high permeability feature at the (DST-relevant) scale of ~10m.

Again, in addition to pre-heating characterization, air-permeability tests are being conducted in 12 instrumented boreholes during the heating phase of the DST, in order to monitor the drying and condensation processes in the DST after the onset of heat. Each of the twelve 40-m long boreholes were installed with a string of four high-temperature packers to separate it into four borehole intervals. Each interval is equipped with an air-injection line and pressure sensor. The evolution of increased fracture liquid saturation zones in the DST were predicted by 3D thermal-hydrological modeling. Decrease in permeability in those intervals coinciding with model predictions has been observed in air injection data at 3 months, 6 months and 9 months after heating. Furthermore, in a small subset of these borehole intervals, seepage has occurred, and water has been sampled. We believe that as in the SHT case, local heterogeneity/fractures play the dominant role in causing water accumulation in certain borehole intervals in the condensation zone. This hypothesis is being investigated, by applying the iterative approach of modeling and testing that has proved so successful in the SHT.

Acknowledgment

We thank Chin-Fu Tsang and Dan Hawkes for review of this abstract. This work was supported by the Director, Office of Civilian Radioactive Waste Management, through a Memorandum Purchase Order EA9013MC5X between TRW Environmental Safety Systems, Inc. and E.O. Lawrence Berkeley National Laboratory through U.S. Department of Energy Contract No, DE-AC03-76SF00098.

Session 7:
ISOTOPIC STUDIES OF FLOW IN FRACTURED SYSTEMS

Isotopic Effects in Dual-Porosity Fluid-Rock Systems

Donald J. DePaolo

Earth Sciences Division, E.O. Lawrence Berkeley National Laboratory, and Dept. of Geology and Geophysics, U.C. Berkeley
Berkeley, CA

The thermal and chemical behavior of fractured rock systems depends to a substantial degree on the average spacing between fractures. Fluid moving through a system of fractures can interact thermally and chemically with the matrix blocks between them only by conduction (of heat) and diffusion of chemical constituents dissolved in the pore fluid or vapor phase. The spacing of fractures can be estimated from rock outcrops and core, but the spacing of the fractures actually carrying the bulk of the fluid is not usually known directly.

Isotopic ratios of certain pairs of elements can in theory be used to measure the effective matrix block size (or average fracture spacing) in some fractured rock systems. The sensitivity of isotopic ratios to block size stems from the differing solubilities of the elements, which can be expressed in terms of a rock/fluid concentration ratio ($K_{r/f}$), and differing fluid-phase ionic diffusivities. For example, $K_{r/f}$ for oxygen is about 0.8, whereas $K_{r/f}$ for Sr and C is typically about 100 to 1000. The degree to which the cores of matrix blocks are chemically isolated from the fracture fluid is less for high solubility elements (large $K_{r/f}$) than it is for low solubility elements.

The degree of isolation of matrix blocks can be determined from the diffusive reaction length (L_e), which depends on the fluid-rock reaction rate (=R) and the effective diffusivity for a dissolved element in matrix pore fluid. If this reaction length is smaller than the average block dimension (L_b), then the interiors of the blocks are not in equilibrium with the fracture fluid. The reaction length for element "i" that is applicable to the matrix blocks is given by:

$$L_{e,i} = \left(\frac{D_i \phi_m \rho_f}{R(1-\phi_m)\rho_s K_{r/f}} \right)^{1/2}$$

For two elements of differing solubility, the ratio of the reaction lengths is:

$$\frac{L_{e,i}}{L_{e,j}} = \left(\frac{D_i K_{r/f(j)}}{D_j K_{r/f(i)}} \right)^{1/2}$$

For Oxygen versus Strontium, for example, this ratio is about 100. If the average block size falls between $L_{e,Sr}$ and $L_{e,O}$, then the isotopic effects in the fracture fluids provide information on the matrix block size.

In cases where the reaction length is very large relative to the matrix block size, a steady-state system behaves chemically as if it had a single-porosity, and reaction effects on the fluid are determined mainly by the reaction rate, R, which describes the solution-precipitation rate averaged over the minerals in the rocks. The advective reaction length, which can be measured in the field, in this case is:

$$L_e(\text{single}) = \frac{v_f \phi \rho_f}{R(1-\phi)\rho_s K_{r/f}}$$

In general, the effective reaction rate as inferred from the effects of water-rock interaction on the fluid moving through the fractures in a dual porosity system can be shown (with some simplifying assumptions) to be:

$$R_{eff} = 8R\frac{L_e^2}{L_b^2}\sum_{n_{odd}}(1+n^2\pi^2\frac{L_e^2}{L_b^2})^{-1}$$

For $L_e < L_b$, then $R_{eff} \approx R\frac{L_e}{L_b}$. As long as the block dimension is larger than the reaction length, diffusion in the matrix blocks retards chemical and isotopic exchange between the rocks and the fluids by the factor L_e/L_b.

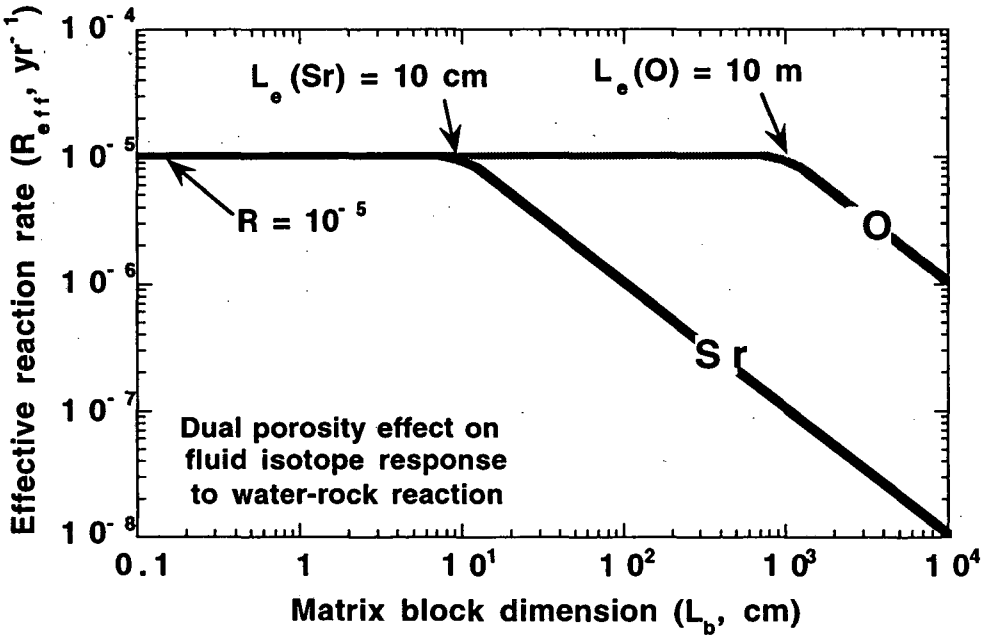

Figure 1: Calculated dual porosity effect for fluids moving in fractures and communicating with matrix blocks by fluid-phase diffusion. R is the solution-precipitation time constant in the matrix blocks, and R_{eff} is the apparent reaction time constant that is sensed by fluid moving in the fractures under steady state conditions.

It is normally assumed that fluid-rock systems behave as single porosity systems, or that dual-porosity effects are the same for all elements. If the model results above are applicable, then instead it may be possible to use isotopes of multiple elements to infer the effective structure of geothermal and groundwater systems. Other elements that have variable natural isotopic abundances and could be used include hydrogen, helium, boron, carbon, sulfur, lead, uranium, neodymium, thorium, and radon.

In non-steady systems, for example those with time-varying flow, the response time for re-establishment of a new steady state between the fracture fluids and the matrix blocks will also vary element by element. This effect could also be used to measure the effective matrix block size or porosity.

Measuring Groundwater Flow in Fractured Rocks with Environmental Isotopes, Clare Valley, South Australia

P. G. Cook[1], A. J. Love[2] and C.T. Simmons[3]

[1] CSIRO Land and Water, PMB2 Glen Osmond, SA 5064, Australia. (Peter.Cook@adl.clw.csiro.au); [2] Primary Industries and Resources, GPO Box 1671, Adelaide SA 5001, Australia. (alove@msgate.mesa.sa.gov.au); [3] Flinders University of South Australia, Bedford Park, SA 5042, Australia. (Craig.Simmons@es.flinders.edu.au)

Introduction

The Clare Valley, located approximately 100 km north of Adelaide, South Australia, consists of low-grade metamorphic, folded and faulted rocks of Protozoic age. The major lithologies are sandstone, shale, quartzite and dolomite. Mean annual rainfall is approximately 600 mm, and groundwater within the valley is used for irrigation of grape vines. Expansion of the wine industry is likely to cause increasing demand for groundwater, and has prompted a major investigation into the sustainability of the resource.

To date, hydraulic and applied tracer methods have been most widely used for characterising fracture flow systems at field scales. While they have received relatively less attention, environmental tracer methods have an inherent advantage in that they provide a natural integration over temporal and spatial scales. In the Clare Valley, a large research project is aimed at developing new methods for determining groundwater velocities and recharge rates. Previous work at the site has involved the use of dissolved ^{222}Rn concentrations to determine horizontal groundwater flow velocities (Cook et al., 1998). In this paper, we investigate the use of groundwater dating methods for determining vertical flow velocities and fracture characteristics.

Methods and Results

Nested piezometers have been installed at three sites, although data from only one of these is presented in this paper. At Pearce Road, the groundwater occurs within the Mintaro Shale. A 200 mm diameter bore was drilled to 99.5 m depth, and a 250 mm bore to 26.4 m depth. A nest of six 50 mm PVC piezometers were installed in the 250 mm bore, and three 50 mm piezometers in the 200 mm bore. (The bores are spaced only 5 m apart.) Piezometer screen lengths range from 0.5 to 5 m, being longer in the deeper piezometers. Gravel packs were used around the screens, which were separated using cement seals. The nest of nine piezometers allows groundwater samples to be collected from depths between 8.5 and 95 m below the land surface.

The position of the water table varies seasonally, from approximately 4 m depth in October - November to 8 m in July - August. The vertical head gradient is approximately 10^{-3}. The primary porosity has been measured to be 2% using helium porosimetry and mercury bulk

volume measurements. The horizontal hydraulic conductivity, determined from pumping tests, varies with depth, between 10^{-3} and 1 m^2 day^{-1}.

After purging three well volumes from the piezometers, samples were collected for ^3H, ^{36}Cl, CFC-12, ^{14}C and ^{13}C. All samples reported in this paper were collected between August 1996 and February 1998. Results are shown in Fig. 1. Carbon-13 activities range between -11.3 and -15.2 per mille, and are uncorrelated with ^{14}C. The data suggests that, as a first approximation, differences in ^{14}C activities can be ascribed to radioactive decay, and not to chemical reactions.

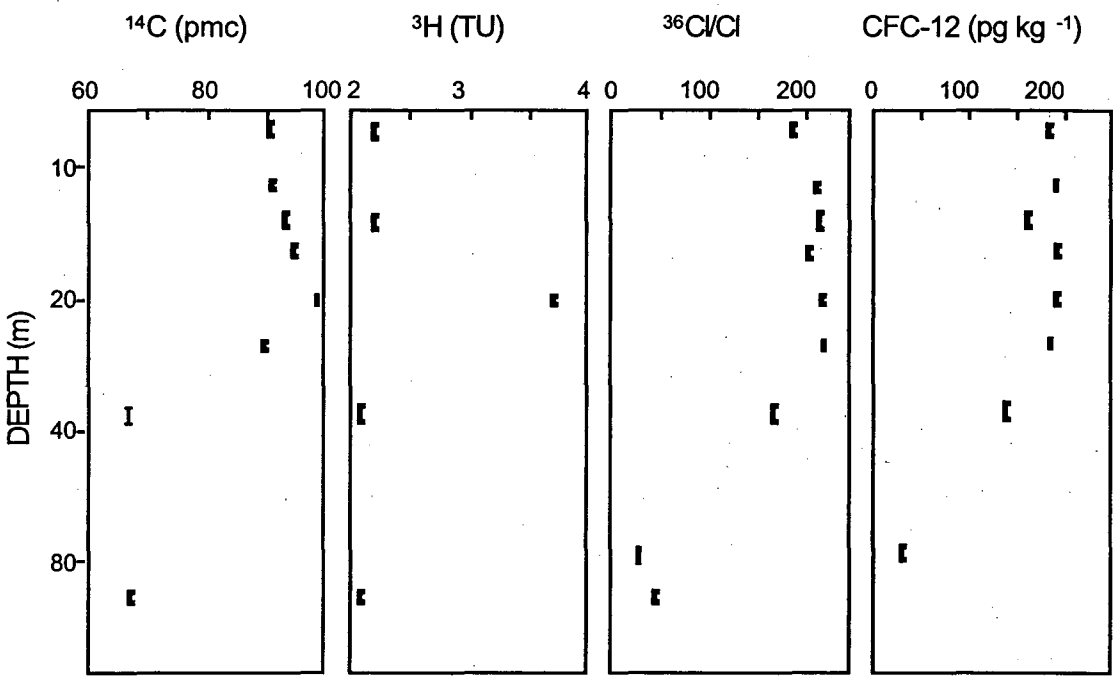

Figure 1. Environmental tracer concentrations measured in piezometers at Pearce Road.

Vertical Flow Velocities

Despite the large vertical variation in hydraulic conductivity, profiles of CFC-12, ^{36}Cl, ^3H and ^{14}C are remarkably smooth. The ^{14}C data suggests very young water (> 90 pmc) above 20 m, with much older water at greater depth. The presence of ^3H, bomb ^{36}Cl and CFC-12 at 95 m depth (the limit of sampling), indicates that the vertical fracture velocity (V_f) must be in excess of 3 m y^{-1}. CFC-12 age gradients can be used to determine minimum vertical water velocities as a function of depth. Between 8 and 20 m, the decrease in apparent CFC-12 age is less than 2 years, giving V_f 3 6 m y^{-1}. Between 20 and 36 m depth, CFC-12 ages increase by 6 years (from 12 to 18 years), giving V_f 3 2.7 m y^{-1}. For a vertical flow velocity of $V_f > 3$ m y^{-1} to occur with a vertical hydraulic head gradient of 10^{-3}, would require a fracture aperture of more than 10 μm.

Neretnieks (1981) has shown that apparent ^{14}C ages within fissured rocks are related to ages of water within the fractures by:

$$\frac{t_a}{t_w} = 1 + \frac{\theta(2A-1)}{b}\left(\frac{D}{\lambda}\right)^{0.5}$$

where t_a is the apparent ^{14}C age, t_w is the age of the water in the fracture, θ is the matrix porosity, 2b is the fracture aperture, D is the diffusion coefficient within the matrix, λ is the decay constant, and $0.5 \leq A \leq 1$ is a function of the fracture spacing (2B), λ and D. As 2B gets large, A ♦ 1. Since $t_a/t_w = V_f/V_t$, where V_t is the apparent tracer velocity, we can use the ^{14}C age gradient to obtain information concerning V_f.

The ^{14}C age gradient between 20 m and 36 m depth is approximately 2500 y in 16 m. Using D = 10^{-4} m^2 y^{-1}, $\lambda = 1.21 \times 10^{-4}$ y^{-1}, $\theta = 0.02$, 2b = 50 μm, we get $V_f \leq 728$ V_t. Equality occurs for 2B / 5 m. This gives $V_f \leq 4.7$ m y^{-1}. The estimated fracture velocity will increase if the fracture aperture is less than 50 μm. Using a lower limit for 2b of approximately 10 μm, gives $V_f \leq 23$ m y^{-1}.

We can also write: V_t 3 $V_{EPM} = R/\theta$, where V_{EPM} is the aerially averaged vertical water velocity, and R is the corresponding water flux. Equality occurs for complete exchange between fracture and matrix. Substituting gives $V_{EPM} \leq 6.5$ mm y^{-1}, and $R \leq 0.15$ mm y^{-1}. R is the recharge rate to the deeper flow system (below 20 m). Recharge to the shallow system would be much greater. Using $V_f/V_{EPM} = \theta B/b$, gives B/b ∪ 35000. Since 2b > 10 μm, this gives 2B > 0.35 m.

Groundwater Mixing

The above analysis has assumed that the measured concentrations are those in the fractures. However, large discrepancies between apparent groundwater ages estimated using CFC-12 and ^{14}C have not been able to be reproduced using fracture flow simulations. In fact, it is likely that pumped water samples represent a mixture between fracture and matrix water. Figure 2 depicts a simple, two end-member mixing model between young water with an age of 10 years, and an old water component (CFC-free) with an age of 20,000 years. Although the solution is not unique, the data is consistent with the samples being a mixture of young water derived from the fractures and older water derived from the matrix. The older ^{14}C ages at depth are consistent with a greater proportion of matrix water in the pumped samples. If this is the case, then the age gradients used in the above analysis, and resulting estimates of flow velocities, would need to be adjusted accordingly. Further work is underway to better determine the sources of water obtained by pumping fractured rock aquifers.

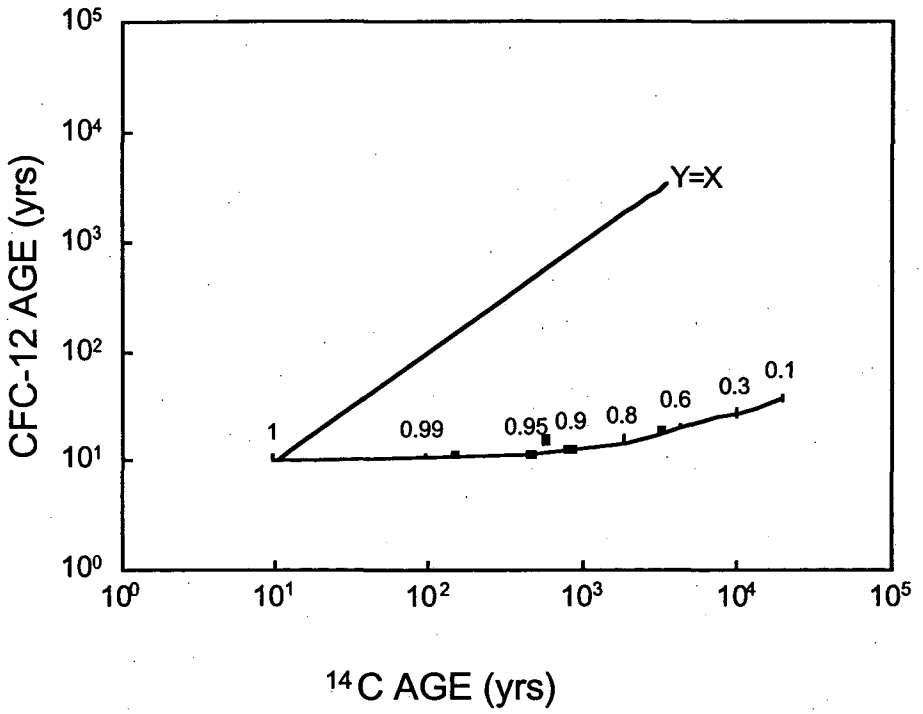

Figure 2. ^{14}C versus CFC-12 ages, compared with results of a two end-member mixing model, with 10 year and 20,000 year old end-members. Numerals indicate relative proportions of the young water component.

References

Cook, P.G., Love, A.J. and Dighton, J.C. (1998) Inferring groundwater flow in fractured rock from dissolved radon. Ground Water, submitted.

Neretnieks, I. (1981) Age dating of groundwater in fissured rock: influence of water volume in macropores. Water Resour. Res., 17(2):421-422.

Isotope Hydrology of Ground-Water Flow Systems, Southern Nevada

James B. Paces and Zell E. Peterman
U.S. Geological Survey
MS 963, Box 25046 Denver Federal Center
Denver CO 80225

Yucca Mountain in southern Nevada is being evaluated for the construction of a potential nuclear waste repository 100 to 200 meters above the water table in a thick unsaturated zone. Because release of radionuclides to the environment could occur through dissolution and transport of the waste by ground water, a comprehensive understanding of the hydrology at and downgradient of the site area is necessary. Dilution of a potential contaminant plume emanating from the repository will depend on the effectiveness of natural mixing in the upper part of the saturated zone. A low ground-water-flow velocity would allow decay of radionuclides in the plume prior to release to the accessible environment. An accurate representation of ground-water-flow paths and travel times in the saturated zone is important for estimating where the contaminant plume may discharge or be intercepted by boreholes in the future. Hydrogeochemical and isotopic data currently are being used by the U.S. Geological Survey (USGS), in cooperation with the Department of Energy under Interagency Agreement DE-AI08-97NV12033, to help constrain these hydrologic issues.

Distinctive isotopic and hydrogeochemical ground-water domains occur beneath Crater Flat, Yucca Mountain, Fortymile Wash, Jackass Flats, and the Amargosa Valley (Figure 1), although the location and nature of the boundaries between these areas are not well defined by existing data. Variations in the isotopic compositions of oxygen ($\delta^{18}O$) and hydrogen ($\delta^{2}H$) in ground water are related to temperature and climate conditions at the recharge areas (Clark and Fritz, 1997; Gat and Gonfiantini, 1981). Within a given ground-water system, spatial variations in these isotopes may identify ground water recharged at different times in the past under different climatic conditions. Ground water in the Yucca Mountain and Amargosa Valley domains is enriched in isotopically lighter oxygen and hydrogen isotopes (more negative $\delta^{18}O$ and $\delta^{2}H$ values, respectively) indicating recharge under colder climatic conditions such as in the late Pleistocene (Claassen, 1985; Benson and Klieforth, 1989; White and Chuma, 1987; Ingraham and others, 1991). In contrast, ground water beneath Fortymile Wash is enriched in the heavier isotopes of oxygen and hydrogen (more positive values of $\delta^{18}O$ and $\delta^{2}H$, respectively) (Benson and Klieforth, 1989) indicating recharge under warmer climatic conditions comparable to the present-day climate.

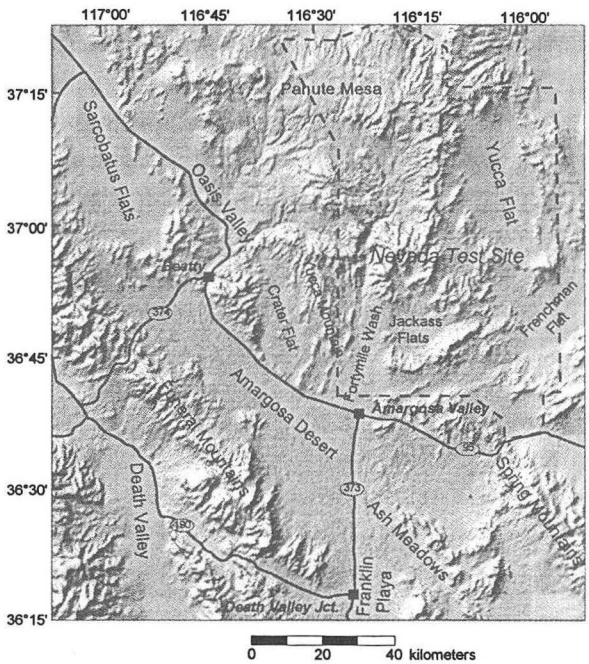

Figure 1.--Shaded Relief Map of the Yucca Mountain region.

Various hydrochemical modeling methods have been devised to try to correct ^{14}C ages for the effects of dissolution of dead carbon (inorganic carbon greater than 50,000 years no longer containing ^{14}C) incorporated at recharge and along flow paths (Clark and Fritz, 1997); but the adjusted ages are commonly ambiguous and unverifiable. If ground water can be sampled along flow paths in a volcanic-rock aquifer where the possibility of incorporation of dead carbon from the aquifer is minimal, the differences among ^{14}C ages can be used to calculate flow velocities without adjusting them for incorporation of dead carbon. Groundwater samples from UE-29a#2 in the upper reaches of Fortymile Wash have yielded uncorrected ^{14}C ages of 3,800 and 4,100 years, but the presence of measurable tritium (half life of 12.4 years) indicates that much of the water has been recharged within the last 50 years or so (Benson and Klieforth, 1989). The percentage of modern carbon [(^{14}C/total C)sample x 100 / (^{14}C/total C)modern standard] in ground-water samples from the shallow aquifer hosted in volcanic rocks or alluvium derived from these rocks decreases southward from UE-29a#2 along Fortymile Wash into the Amargosa Valley (Claassen, 1985) resulting in an apparent increase in ground-water age from north to south. Ground water from supply wells at intermediate positions along Fortymile Wash have unadjusted radiocarbon ages of 9,100 and 9,900 years whereas uncorrected radiocarbon ages of 10,000 to 14,000 are common in ground water beneath Amargosa Valley (Claassen, 1985, Figure 14). These data indicate a flow velocity along Fortymile Wash of approximately 4 meters per year, but this estimate does not consider lateral recharge from the Yucca Mountain domain and local recharge through the alluvium in Fortymile Wash. Shallow ground water in volcanic rocks beneath Yucca Mountain has unadjusted ^{14}C ages between 12,000 and 18,500 years (Claassen, 1985, Figure 14; Benson and Kleiforth, 1989, Table 1a) and contains less ^{14}C relative to ground water from volcanic rock units at the same latitude in Fortymile Wash. In contrast to ground water from the central Amargosa Valley, ground water discharging at Ash Meadows has unadjusted ^{14}C ages of greater than 30,000 years (Claassen, 1985) resulting from incorporation of dead carbon along flow paths in the Paleozoic carbonates (Thomas and others, 1996).

In a volcanic-rock aquifer, stable isotopes of carbon (^{12}C and ^{13}C) should be conservative from the values inherited at recharge areas and can be used to distinguish different ground-water domains and leakage between aquifers. At Yucca Mountain, differences in $\delta^{13}C$ between ground water in the volcanic aquifer and water in the regional carbonate aquifer have been used to identify the leakage from the latter into the former (Stuckless and others, 1991).

Chlorine-36, with a half life of 301,000 years, has been measured in ground water throughout the region (Rose and others, 1997). However, its value as a geochronometer is limited because of substantial past variations in the atmospheric production rate of chlorine-36 (Plummer and others, 1997) and the possibility of incorporation of older chlorine deposited in valley fill alluvium under arid conditions. Ratios of chlorine-36 to total chloride in ground water at Yucca Mountain are approximately 500×10^{-15} (June Fabryka-Martin and others, 1997, Table 4-17) which indicates recharge during the Holocene or latest Pleistocene based on past cosmogenic production (Plummer and others, 1997). Limited analyses for ground water in the regional carbonate aquifer show lower ratios of approximately 420×10^{-15} (Rose and others, 1997).

In contrast with the stable isotopes of oxygen and hydrogen, the isotopic compositions of strontium ($\delta^{87}Sr$) and uranium ($^{234}U/^{238}U$) in ground water are not conservative from the values inherited at recharge areas and can be modified by water/rock interactions along flow paths

within the aquifer. Ground water beneath Yucca Mountain has $\delta^{87}Sr$ values mainly between +1 and +3 per mil (Peterman and Stuckless, 1993; Peterman and Patterson, 1998), whereas samples from wells producing from the same volcanic units along Fortymile Wash typically have larger values between +3.0 and +3.5 per mil. These values may reflect recharge through the alluvium within Fortymile Wash where infiltrating water can acquire a $\delta^{87}Sr$ value of approximately +4.5 per mil from pedogenic calcite that is abundant in the alluvium (Marshall and others, 1993). South of Yucca Mountain, $\delta^{87}Sr$ increases to values as large as +11 per mil in the Amargosa Valley ground water. These large values probably reflect interaction of ground water with alluvium derived from Precambrian rocks in the northern Funeral Mountains or mixing with ground water with large $\delta^{87}Sr$ values flowing from the northwest along the axis of the valley. Ground water discharging from the regional carbonate aquifer at Ash Meadows mostly has $\delta^{87}Sr$ values between +4.4 and +5.0 per mil except for three southernmost springs with values as large as +14 per mil (Peterman and others, 1992; Peterman and Stuckless, 1992). Highly saline ground water at Franklin Lake Playa, a major ground-water discharge site near Death Valley Junction, has a narrow range of $\delta^{87}Sr$ values between +5 and +6 per mil in contrast with values for the potential upgradient water with $\delta^{87}Sr$ between +4.4 and +14 per mil (Peterman and Stuckless, 1993). The narrow $\delta^{87}Sr$ range in Franklin Lake Playa may indicate density-induced mixing of ground water in the playa driven by near-surface evaporation.

Variations of $^{234}U/^{238}U$ in regional ground-water samples relate to physiography, flow-path length, and aquifer types (Ludwig and others, 1993; Paces, Ludwig, and others, 1998). Oxidizing ground water in the upper part of the saturated zone incorporates ^{234}U from mineral surfaces within the aquifer preferentially to ^{238}U due to the effects of radioactive decay in the solid phases. The main mechanisms are preferential leaching of ^{234}U from radiation-damaged lattice sites, radiation-induced oxidation of ^{234}U leading to a more soluble uranyl ion, and alpha-recoil of ^{234}U off of crystal surfaces. The amount of excess ^{234}U relative to ^{238}U is controlled by rates of ^{234}U decay, water/rock ratios, flow-path length, and the amount of bulk-rock dissolution in the aquifer.

Recharge water dissolves uranium with characteristic $^{234}U/^{238}U$ ratios from soil-zone minerals. Calcrete and surface runoff in southern Nevada have $^{234}U/^{238}U$ activity ratios typically between about 1.4 and 1.8 (Paces and others, 1994). Ground water in carbonate-rock, alluvial, and Precambrian-rock aquifers from Oasis Valley, Amargosa Valley, Spring Mountains, and the easternmost Nevada Test Site have $^{234}U/^{238}U$ activity ratios between 1.5 and 4. In contrast, ground water from the volcanic-rock aquifers beneath Yucca Mountain and western Yucca Flat commonly has values greater than 4. The $^{234}U/^{238}U$ activity ratios in ground water from the volcanic-rock aquifer at Yucca Mountain are particularly large with values between 6 and 8.5. These larger $^{234}U/^{238}U$ ratios are in the same range as those for percolating water descending through fractures in the thick unsaturated zone as shown by analyses of secondary calcite and opal (Paces, Neymark, and others, 1998). Smaller $^{234}U/^{238}U$ ratios are characteristic of ground water in the volcanic-rock aquifer in the Fortymile Wash and Crater Flat areas, in the upland recharge area of Pahute Mesa north of Yucca Mountain, and in downgradient areas of Amargosa Valley. This regional variation in $^{234}U/^{238}U$ indicates 1) that local recharge to the saturated zone at Yucca Mountain may occur and 2) that flow out of this area is volumetrically small relative to that in the Fortymile Wash and Crater Flat domains, or that smaller volumes of saturated-zone

water beneath Yucca Mountain are mixed in the upper part of the saturated zone with greater volumes of ground water from upgradient domains having smaller $^{234}U/^{238}U$.

In summary, isotopic variability of ground water in the Yucca Mountain region allows definition of discrete domains in the flow system. Ground water in Fortymile Wash, Yucca Mountain, and Crater Flat has distinct isotopic compositions indicating that these domains have existed for thousands of years. Ground water in the upper reaches of Fortymile Wash contains more recent recharge and shows a pattern of increasing apparent ^{14}C ages and decreasing $\delta^{18}O$ and $\delta^{2}H$ compositions south towards Amargosa Valley. Values of $\delta^{18}O$, $\delta^{2}H$, and unadjusted ^{14}C ages indicate that ground water beneath Yucca Mountain has a greater component of older recharge relative to ground water at the same latitude in Fortymile Wash. Both $\delta^{87}Sr$ and $^{234}U/^{238}U$ isotopes indicate that ground water beneath Yucca Mountain is distinct from the Fortymile Wash domain. Collectively, the data indicate that water in the Fortymile Wash domain travels in a southerly direction at greater velocities and volumes relative to ground water beneath Yucca Mountain. Mixing in the upper part of the saturated zone may be sufficient to erase the distinctive $^{234}U/^{238}U$ values of the Yucca Mountain domain by the time water flow reaches Amargosa Valley.

References

Benson, Larry, and Klieforth, Harold, 1989, Stable isotopes in precipitation and ground water in the Yucca Mountain region, southern Nevada: Paleoclimatic implications *in* Peterson, D.H., ed., Aspects of Climate Variability in the Pacific and the Western Americas: Geophysical Monograph 55, p. 41-59.

Claassen, H.C., 1985, Sources and mechanisms of recharge for ground water in the west-central Amargosa Desert, Nevada—A geochemical interpretation: U.S. Geological Survey Professional Paper 712-F, 31 p.

Clark, Ian, and Fritz, Peter, 1997, Environmental isotopes in hydrogeology: New York, Lewis Publishers, 328 p.

Gat, J.R., and Gonfiantini, R., 1981, Stable isotope hydrology, deuterium and oxygen-18 in the water cycle: Austria, International Atomic Energy Agency, 337 p.

Fabryka-Martin, J.T., Flint, A.L., Sweetkind, D.S., Wolfsberg, A.V., Levy, S.S., Roimer, G.J.C., Roach, J.L., Wolfsberg, L.E., and Duff, M.C., 1997, Evaluation of flow and transportation models of yucca mountain, based on chlorine-36 studies for FY97: Los Alamos National Laboratory Report LA-CST-TIP-97-010, 243 p. plus 74 figures.

Ingraham, N.L., Lyles, B.F., Jacobson, R.L., and Hess, J.W., 1991, Stable isotopic study of precipitation and spring discharge in southern Nevada: Journal of Hydrology, p. 259-276.

Ludwig, K.R., Peterman, Z.E., Simmons, K.R., and Gutentag, E.D., 1993, $^{234}U/^{238}U$ ratios as ground water flow tracers, SW Nevada—SE California *in* Proceedings of the Fourth International Conference on High-Level Radioactive Waste Management,April 26-30, 1993: LaGrange Park, Illinois, American Nuclear Society, p. 1567-1572.

Marshall, B.D., Peterman, Z.E., and Stuckless, J.S., 1993, Strontium isotopic evidence for a higher water table at Yucca Mountain *in* Proceedings of the Fourth International Conference on High-Level Radioactive Waste Management, April 26-30, 1993: LaGrange Park, Illinois, American Nuclear Society, p. 1948-1952.

Paces, J.B., Ludwig, K.R., Peterman, Z.E., and Neymark, L.A., 1998, Anomalous ground-water $^{234}U/^{238}U$ beneath Yucca Mountain: Evidence of local recharge? *in* Proceedings of the Ninth International Conference on High-Level Radioactive Waste Management, May 11-14, 1998: LaGrange Park, Illinois, American Nuclear Society, p. 185-188.

Paces, J.B., Menges, C.M., Widmann, B.E., Wesling, J.R., Bush, C.A., Futa, Kiyoto, Millard, H.T., Maat, P.B., and Whitney, J.W., 1994, Preliminary U-series disequilibrium and thermoluminescence ages of surficial deposits and paleosols associated with Quaternary faults, eastern Yucca Mountain *in* Proceedings of the Fifth International Conference on High-Level Radioactive Waste Management, May 22-26, 1994: LaGrange Park, Illinois, American Nuclear Society, p. 2391-2401.

Paces, J.B., Neymark, L.A., Marshall, B.D., Whelan, J.F., and Peterman, Z.E., 1998, Inferences for Yucca Mountain unsaturated-zone hydrology from secondary minerals *in* Proceedings of the Ninth International Conference on High-Level Radioactive Waste Management, May 11-14, 1998: LaGrange Park, Illinois, American Nuclear Society, p. 36-39.

Peterman, Z.E., and Patterson, G.L., 1998, Isotopes aid in understanding the Yucca Mountain flow system *in* Proceedings of the Ninth International Conference on High-Level Radioactive Waste Management, May 11-14, 1998: LaGrange Park, Illinois, American Nuclear Society, p. 183-185.

Peterman, Z.E., and Stuckless, J.S., 1992, Application of strontium and other radiogenic tracer isotopes to paleohydrologic studies *in* Paleohydrogeological methods and their applications: Paris, Nuclear Energy Agency, p. 59-84.

Peterman, Z.E., and Stuckless, J.S., 1993, Isotopic evidence of complex ground-water flow at Yucca Mountain, Nevada, USA *in* Proceedings of the Fourth International Conference on High-Level Radioactive Waste Management, April 26-30, 1993: LaGrange Park, Illinois, American Nuclear Society, p. 1559-1566.

Peterman, Z.E., Stuckless, J.S., Mahan, S.A., Marshall, B.D., Gutentag, E.D., and Downey, J.S., 1992, Strontium isotope characterization of the Ash Meadows ground-water system, southern Nevada, USA *in* Water Rock Interaction: Rotterdam, Balkema, p. 825-829.

Plummer, M.A., Phillips, F.M., Fabryka-Martin, June, Turin, H.J., Wigand, P.E., and Sharma, Pankaj, 1997, Chlorine-36 in fossil rat urine: An archive of cosmogenic nuclide deposition during the past 40,000 years: Science, v. 277, p. 538-541.

Rose, T.P., Kenneally, J.M., Smith, D.K., Davisson, M.L., Hudson, G.B., and Rego, J.H., 1997, Chemical and isotopic data for groundwater in southern Nevada: Lawrence Livermore National Laboratory Report UCRL-ID-128000, 35 p.

Stuckless, J.S., Whelan, J.F., and Steinkampf, W.C., 1991, Isotopic discontinuities in ground water beneath Yucca Mountain, Nevada *in* Proceedings of the Second International Conference on High-Level Radioactive Waste Management, April 28-May 3, 1991: LaGrange Park, Illinois, American Nuclear Society, p. 1410-1415.

Thomas, J.M., Welch, A.H., and Dettinger, M.D., 1996, Geochemistry and isotope hydrology of representative aquifers in the Great Basin Region of Nevada, Utah, and adjacent states: U.S. Geological Survey Professional Paper 1409-C, 100 p.

White, A.F., and Chuma, N.J., 1987, Carbon and isotopic mass balance models of Oasis Valley—Fortymile Canyon groundwater basin, southern Nevada: Water Resources Research, v. 23, p. 571-582.

Use of Chlorine-36 and Chloride Data to Evaluate Fracture Flow and Transport Models at Yucca Mountain

A.V. Wolfsberg[1], J.T Fabryka-Martin[2], K.S. Campbell[1], S.S. Levy[1], P.H. Tseng[1]

1-Earth and Environmental Sciences Division
2-Chemical Science and Technology Division
Los Alamos National Laboratory
(MS-F649, Los Alamos, NM 87545, awolf@lanl.gov;)

Introduction

Development and testing of conceptual flow and transport models for hydrologic systems are strengthened when natural environmental tracers are incorporated into the process. Two such tracers are chlorine-36, a radioactive isotope (half-life of 301,000 years) produced in the atmosphere and carried underground with percolating groundwater, and stable chloride, deposited both with precipitation and dry, windblown fallout. A spatial distribution of subsurface chlorine-36 is obtained with over 250 samples from the Exploratory Studies Facility (ESF), an 8-km long tunnel constructed at Yucca Mountain for the study of relevant properties of the potential repository horizon. Chloride has been analyzed in over 35 samples from about 2km of the ESF. Whereas the primary use of the chlorine-36 data are to evaluate travel times from ground surface to the sample location, the chloride data are used to independently evaluate net infiltration estimates. Both data sets provide unique, complementary information integrating processes that occur through a complex geologic system consisting, from the surface moving downward, of welded, then nonwelded, and then welded volcanic tuff. The welded tuff tends to be characterized with low matrix permeabilities and porosities and ubiquitous fractures. The nonwelded tuffs have high matrix permeabilities and are poorly fractured.

These data are used in conjunction with one-, two-, and three-dimensional dual-permeability flow and transport simulations with the FEHM computer code (Zyvoloski et al., 1997). The coupled data and modeling analysis serves to evaluate infiltration rates, travel times through the various geologic layers, fracture/matrix interaction model parameters for different units, and predictive transport models for radionuclide migration away from the potential repository. One of the primary concerns highlighted with the modeling study is the significance of flow and transport processes in the PTn, the nonwelded tuff above the TSw welded tuff from which most ESF samples are collected. If flow and transport in the PTn occur predominantly in the matrix, then it is probably safe to assume that the PTn damps episodic infiltration events and that larger time steps can therefore be used in site-scale models. The brief summary that follows captures some of the highlights from detailed analyses by Fabryka-Martin et al. (1997,1998), and Robinson et al. (1997).

Data

Use of the chlorine-36 data to condition and evaluate flow and transport models requires assessment of the various potential contributions associated with any sample. Sample components representing four different age groups (travel times from the surface to the ESF), affect the measured $^{36}Cl/Cl$ ratio. These various sources are described in detail in the reports referenced above and are summarized below:

- Less than 50 years: Contributions of bomb-pulse ^{36}Cl with $^{36}Cl/Cl$ signals higher than background meteoric range due to fallout from atmospheric testing of nuclear weapons in the 1950s and 1960s.
- 50 to10,000 years: Contributions from the Holocene with constant present-day $^{36}Cl/Cl$ ratio.

- 10,000 to 100,000 years: Contributions from the end of the Pleistocene with higher than present-day $^{36}Cl/Cl$ ratios due to elevated signals during pluvial climates.
- Greater than 100,000 years: Age of water reflected by lower-than-background $^{36}Cl/Cl$ signals due to decay of chlorine-36.

Primary processes affecting travel times and, hence, sample ages are the percolation flux and the residence times of solutes in fracture and matrix material of the various units. Figure 1 shows a) the chlorine-36 data with distance in the ESF, b) the PTn thickness, c) measured and simulated chloride concentrations, and d) simulated travel times to the ESF. Based on the probability analysis of Fabryka-Martin et al. (1998), $^{36}Cl/Cl$ ratios above 1250 x 10^{-15} have high probability of being bomb-pulse signals and are mostly well correlated with faults. The $^{36}Cl/Cl$ data in Figure 1 are plotted on a log scale to spread out the lower part of the range for trend analysis. Excluding the samples with high probability of containing bomb-pulse, the background trend is reflected in the PTn thickness, with some samples in the south (further into the ESF) falling well below present-day background. The chloride data match the simulation well except in the south where indications are that actual infiltration rates are lower than those used in the model.

The conceptual model that these data support is that travel times in the north are greater due to thicker PTn, thus showing $^{36}Cl/Cl$ signals from over 10,000 years ago. In the south, the PTn is thinner so travel times are generally less than 10,000 years, except for samples which show obvious decay of the chlorine-36. Travel times to those locations are large due either to low percolation fluxes or unique local conditions conducive to matrix flow in the welded tuffs too.

The probability analysis involved fitting the histogram of $^{36}Cl/Cl$ ratios with a three-component mixture model, as shown in Figure 1e. One of the components clearly captures the ratios greater than 1250 x 10^{-15}. To fit the remaining samples, however, two different components are required. One of these background components has a mean of 450 x10^{-15}, about the present-day background. The other background component has a mean of about 700x10^{-15}, a value more representative of the Pleistocene. The distributions are well correlated with the physical system. The samples comprising the component with the present-day mean come predominantly from the southern ESF where the PTn is thinner. The samples associated with the component indicating ages greater than 10,000 years come from the ESF stations in the north, above which the PTn is thickest.

Model Simulations

The data and resulting conceptual model described above provide a verification test for numerical models. Previous modeling studies (Fabryka-Martin et al., 1997, Robinson et al., 1997) support the hypothesis that increased PTn fracture permeability in fault zones leads to arrivals of bomb-pulse ^{36}Cl at the ESF. Away from fault zones, simulated solute travel times to the ESF are sensitive to fracture-matrix interaction models, PTn thickness, the hydrologic parameters for the lithophysal subunits of the TSw, and the flow rate. Testing the effect of flow rate modification is relatively simple. Starting with the three-dimensional site-scale transport model using the infiltration rates of Flint et al. (1996), travel times from ground surface to the ESF and chloride concentrations are simulated. Then, the entire spatially variable infiltration map is scaled by a uniform factor and transport is simulated again. Figure 1d shows the mean simulated travel times for the base infiltration map and for a scaling factor of 1/3. Clearly, as the infiltration rate is reduced, travel times to the ESF increase. For the base-case infiltration map, simulated chloride concentrations match the measurements well except over the last two kilometers. Neither the I nor I/3 chlorine-36 simulations capture the trend of reduced travel

times as the PTn thins to the south, as suggested by the data. This is due to offsetting effects of infiltration rate and PTn thickness, as well as a model that simulates predominantly vertical flow. Local features such as the decayed ^{36}Cl signal near 6000m are reflected by the model results which show increased travel time there due to low local infiltration fluxes (which also accounts for the high simulated chloride porewater concentrations in Figure 1c). Near 2000m, however, the model predicts long travel times due to a very low local infiltration flux, but the measured data show no age-related decay. This apparent discrepancy indicates greater spatial damping of the variable local infiltration estimates than are captured in the model.

Modifying the site-scale model to capture a trend of longer travel times in the north with a Pleistocene geochemical component, and shorter travel times in the south with a Holocene geochemical component is a formidable project. Either the infiltration map needs to be modified to capture this trend or the hydrologic parameters require alteration. Possible directions include increasing the lateral flow in the PTn to increase the simulated residence time and/or reducing the amount of fracture flow simulated in the upper TSw units (lithophysal) to generate greater residence times in the matrix material. Such changes will have to be done in conjunction with the saturation matching part of the model calibration process. Although these modifications will not be easy, they will have significant implications for flow and transport in similar units below the potential repository through which radionuclides may migrate if released.

Acknowledgements
This work is supported by the Yucca Mountain Site Characterization Office as part of the Civilian Radioactive Waste Management Program. This project is managed by the U.S. Department of Energy, Yucca Mountain Site Characterization Project. No new data are presented in this report.

References

Fabryka-Martin, J.T., A.L. Flint, D.S. Sweetkind, A.V. Wolfsberg, S.S. Levy, G.J.C. Roemer, J.L. Roach, L.E. Wolfsberg, and M.C. Duff. "Evaluation of flow and transport models of Yucca Mountain, based on chlorine-36 studies for FY97," Los Alamos National Laboratory, Yucca Mountain Project Milestone Report SP2224M3, 1997.

Fabryka-Martin, J.T., A.V. Wolfsberg, S.S. Levy, K. Campbell, P. Tseng, J.L. Roach, L.E. Wolfsberg. "Evaluation of flow and transport models of Yucca Mountain, based on chlorine-36 studies for FY98," Los Alamos National Laboratory, Yucca Mountain Project Milestone Report SP33DDM4, 1998.

Flint, A.L., J.A. Hevesi, and L.E. Flint. "Conceptual and numerical model of infiltration for the Yucca Mountain Area, Nevada," U.S. Geol. Surv. Yucca Mountain Project Milestone Rep. 3GUI623M., 1996.

Robinson, B.A., A.V. Wolfsberg, H.S. Viswanathan, G.Y. Bussod, C.W. Gable, and A. Meijer. "The site-scale unsaturated zone transport model of Yucca Mountain," Los Alamos National Lab. Yucca Mountain Project Milestone SP25BM3, 1997.

Zyvoloski, G.A., B.A. Robinson, Z.V. Dash, and L.L. Trease. "Summary of the models and methods for the FEHM application-A finite-element heat- and mass-transfer code" Technical Report LA-13307-MS, Los Alamos National Laboratory, 1997

Session 8:
FRACTURES IN GEOTHERMAL SYSTEMS

Pressure Transient Tests in a Fractured Geothermal Reservoir: Oguni Geothermal Field, Northern Kyushu, Japan

Sabodh K. Garg
Maxwell Technologies, Inc., 8888 Balboa Avenue
San Diego, CA 92123, U.S.A.
garg@maxwell.com

Shigetaka Nakanishi
Electric Power Development Co.
15-1, Ginza 6-Chome, Chuo-ku
Tokyo, 104 Japan
den09222@epdc.co.jp

The Oguni and Sugawara Geothermal Fields together comprise the northwestern Hohi geothermal region, Kumamoto and Oita Prefectures, northern Kyushu, Japan (see Figure 1). An area of numerous hot springs and other thermal features, the Hohi geothermal region is located about 40 km southwest of the coastal resort of Beppu and approximately 20 km north of Mt. Aso, an active caldera. The subsurface stratigraphy in the Oguni geothermal field consists of a sequence of indurated sediments and volcanics overlying a granitic basement. The Hohi formation and the upper part of the Shishimuta formation (see Figure 2) constitute the principal geothermal aquifers. The feedzone pressures indicate that the northern Hohi region consists of two pressure zones, i.e., a high pressure zone in the area of boreholes GH-15, GH-19, GH-6, HH-2, N2-KW-3 and DY-2 in the southern part of the Oguni geothermal field, and a low pressure zone in the central and northern part of the area shown in Figure 1. At present, the reasons for the existence of two different pressure regions in close proximity to each other (within at most a few hundred meters) are poorly understood.

To delineate the permeability structure for the Oguni Geothermal Field, Electric Power Development Company (EPDC) performed numerous pressure transient tests. The available data set includes (1) cold fluid injection tests in single boreholes, (2) pressure drawdown and buildup tests in single boreholes, and (3) pressure interference tests involving multiple boreholes. This paper is restricted to analyses of the Oguni pressure interference test data from both slim holes and large-diameter wells.

In March 1991, EPDC installed downhole gauges of the capillary tube type in slim holes GH-3, GH-4, GH-5, N2-KW-1, N2-KW-2, and N2-KW-3. These six (6) slim holes were used as shutin observation boreholes during four separate production/injection tests carried out by EPDC from April 15, 1991 to April 27, 1992. With the exception of slim hole N2-KW-3, all the other

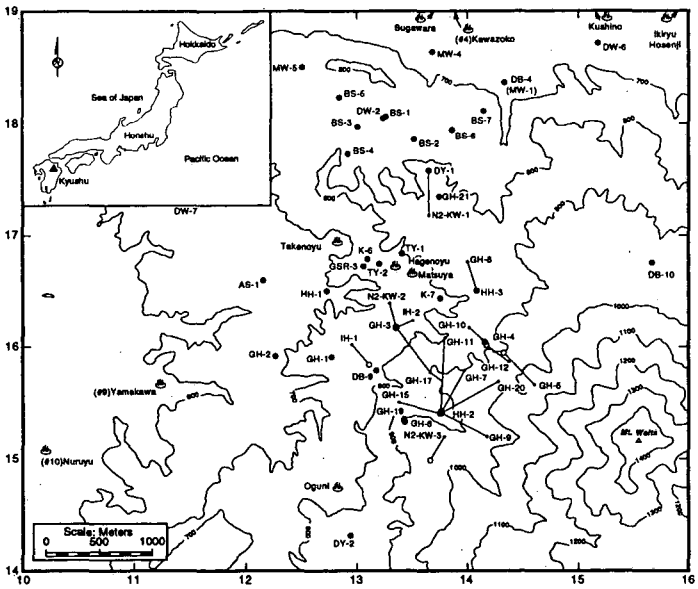

Figure 1. The Oguni and Sugawara geothermal fields, northwestern Hohi area, Kyushu, Japan. The Oguni geothermal field is delineated by the "GH" series wells; the "BS" series wells are drilled in the Sugawara geothermal field. The inset map of Japan shows the location of the Hohi area (solid triangle).

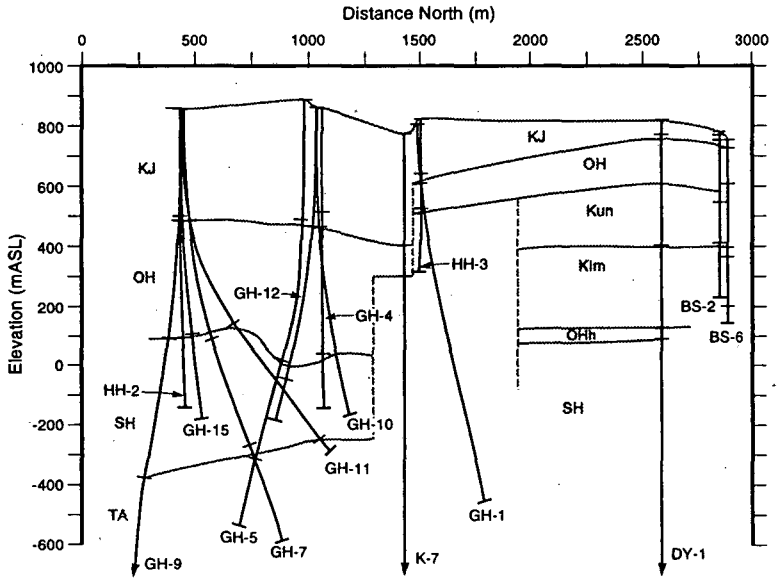

Figure 2. An east-west stratigraphic cross-section in the Oguni area. The following abbreviations are used for formation names: KJ (Kuju); Kun (Kusu/Nogami mudstone); OH (Hohi); Ohk (Hohi/Kotobakiyama lava; OHm (Hohi/Nambira lava); OHh (Hohi/Hatchobaru lava); SH (Shishimuta); TA (Taio).

observation boreholes lie in the low pressure zone. During test 1, low pressure well GH-20 was discharged for 12 days from April 15, 1991 to April 27, 1991. The separated liquid water was injected into slim hole IH-1 and high pressure well GH-15. Since fluid injected into IH-1 flowed into a shallow aquifer, pressures were not affected in the deeper aquifer(s) penetrated by other boreholes involved in the tests. Interference test 2 (June 5 to July 20, 1991) employed GH-11 as the production well and IH-1 and GH-15 as the injectors. For interference test 3 (September 5 to October 20, 1991), low pressure wells GH-12 (producer) and IH-2 (injector) were used as the active ones. Interference test 4 (December 13, 1991 to April 27, 1992) involved simultaneous discharge from boreholes GH-10, GH-11, GH-12 and GH-20, and injection into boreholes GH-17, IH-1, IH-2, GH-15 and GH-19. Because of the relatively simple borehole configuration employed during the first three interference tests, pressure data from these tests are especially useful for defining the reservoir permeability structure.

Analyses of the above-described pressure interference data indicate that the low pressure zone in the northern Hohi reservoir has a transmissivity of 100-250 darcy-meters. In contrast to the high transmissivity of the low pressure zone, the pressure interference data imply that the high pressure zone has only a modest transmissivity of 8-15 darcy-meters. The pressure interference data are consistent with the presence of one or more no-flux boundaries between the low- and high-pressure zones. In addition, a significant degree of permeability heterogeneity is indicated within both the low- and high-pressure parts of the northern Hohi geothermal reservoir.

In-Situ Stress and Fracture Permeability Along the Stillwater Fault Zone, Dixie Valley, Nevada

S. H. Hickman[1], C. A. Barton[2], M. D. Zoback[2], C. F. Williams[1], R. Morin[3] and R. Benoit[5]

[1]U.S. Geological Survey, 345 Middlefield Rd., Menlo Park, CA 94025 (hickman@usgs.gov)
[2]Dept. of Geophysics, Stanford University, Stanford, CA 94305
[3]U.S. Geological Survey, Box 25046, Denver Federal Center, Denver, CO 80225
[5]Oxbow Geothermal Corp., 5250 South Virginia St., Reno, NV 89502

Introduction

To help determine tectonic and geochemical controls on the hydrology of a fracture-dominated geothermal reservoir at Dixie Valley, NV, we are conducting an integrated study of fracturing, stress, hydrology and heat flow in geothermal wells drilled into and near the Stillwater fault zone (Figure 1). This fault is a major, active, range-bounding normal fault located in the western Basin and Range province, Nevada, and comprises the main reservoir for a ~62 MW geothermal electric power plant operated by Oxbow Geothermal Corporation. Although earthquakes have not ruptured this segment of the Stillwater fault in historic times, large (M = 6.8-7.7) earthquakes have occurred within the past 80 years along range-bounding faults ~20 km to the northeast and southwest of the Dixie Valley Geothermal Field (DVGF), and geologic evidence shows that the Stillwater fault abutting the DVGF experienced two or more faulting episodes (total offset ~9 m) during the past 12,000 years.

The principal goal of this study is to define the nature, distribution and hydraulic properties of fractures associated with the DVGF, and to characterize the manner in which these fractures, and hence the overall reservoir hydrology, are related to the local stress field. Toward this end, we have conducted an extensive open-hole logging program at Dixie Valley. This included borehole televiewer (BHTV) logging, temperature/pressure/spinner-flowmeter (TPS) logging, hydraulic fracturing stress measurements, and precision temperature logging in wells within the primary zone of geothermal production (transmissivities on the order of 1 m^2/min) and in wells within a few km of the producing zone that were relatively impermeable and, hence, not commercially viable (transmissivities of about 10^{-4} m^2/min). The measurements made in these wells make possible a systematic, comparative study of the effects of in situ stress on fracture permeability along producing and nonproducing segments of the Stillwater fault zone.

Results and Discussion

We have conducted measurements in a total of nine wells at Dixie Valley (Figure 1). With the exception of a 550-m-deep water well drilled ~1 km northeast of well 73B-7 (well 24W-5) and a 3.4-km-deep observation well drilled toward the center of Dixie Valley (62-21), all of these wells penetrate the Stillwater fault zone at depths of 2–3 km. Four of these wells (73B-7, 82A-7, 74-7 and 37-33) penetrated the highly permeable (i.e., producing) segment of the fault zone constituting the main geothermal reservoir. The other three wells (66-21, 45-14 and 76-28), which failed to encounter enough permeability to be viable production wells, penetrated segments of the Stillwater fault zone southwest and northeast of the main reservoir.

Producing Wells. BHTV logs from wells 73B-7 and 74-7 revealed extensive drilling-induced tensile fractures, the orientation of which indicates that the direction of the minimum horizontal principal stress, S_{hmin}, is S55°E ± 15°. As the Stillwater fault at this location dips S45°E at ~53°, it is thus nearly at the optimal orientation for normal faulting in the current stress field (Figure 2). Analysis of hydraulic fracturing tests from wells 73B-7, 82A-7 and 37-33 shows that the magnitude of S_{hmin} is very low relative to the calculated vertical stress, S_V, with S_{hmin}/S_V reaching values as low as 0.45–0.51 within a few hundred meters of the Stillwater fault zone (i.e., at depths of

2.4–2.7 km; see Figure 2). Coulomb failure analysis shows that S_{hmin}/S_V in these wells is close to that predicted for incipient normal faulting on the Stillwater and subparallel faults, using coefficients of friction of 0.6–1.0 and measurements of the in-situ fluid pressure prior to reservoir production (e.g., Figure 3a).

BHTV logs from wells 73B-7, 74-7 and 37-33 show pervasive macroscopic fractures with a wide range of orientations. TPS logs, both under static conditions and during injection, were used to identify fractures associated with fluid flow into or out of the boreholes. The orientations of these hydraulically conductive fractures are distinct from the overall fracture population, and—like the Stillwater fault itself—are near-optimally oriented for normal faulting in the measured stress field. TPS logs conducted in these wells at different injection rates indicate that geothermal production within the Stillwater fault zone is dominated by only a few fractures and that the transmissivities of these producing fractures are extremely high (~0.1–0.4 m^2/min). Using the measured stress orientations and magnitudes, we then calculated the shear and normal stress on each of the fractures observed in the BHTV logs and used the Coulomb failure criterion to determine whether or not these fractures are critically stressed for frictional failure (e.g., Figures 3a and b). Based upon laboratory measurements of the frictional strength of prefractured rock, we assumed that fractures with a ratio of shear to normal stress ≥ 0.6 are in a state of incipient frictional failure. This analysis suggests that the permeable fractures in these wells are critically stressed, active shear planes in the current north-northwest extensional stress regime at Dixie Valley.

Permeability reduction and the establishment of fault seals would be expected along this segment of the Stillwater fault, given the high reservoir temperatures (~220–250° C at 2.3–3.0 km); surface observations of hydrothermal alteration, mineralization and pressure-solution deformation within and adjacent to the fault zone; and thermal evidence for up-dip transport of silica-saturated fluids along the productive fault segment. In particular, the resultant silica precipitation might be expected to seal fractures within the Stillwater fault zone over geological time scales, thereby destroying the high overall fault-zone permeability. However, the observation that the permeability of fractures within and adjacent to the highly productive segment of the Stillwater fault zone is quite high and that these fractures are favorably aligned and critically stressed for normal faulting in the current stress field suggests that ongoing fault slip in response to high differential stresses (i.e., $S_V - S_{hmin}$) is sufficient to counteract the expected permeability reduction.

Non-Producing Wells. Similar data were collected in the relatively impermeable wells to the southwest of the DVGF (Figure 1). Unlike the wells adjacent to the productive fault segment, BHTV logs from wells 66-21 and 45-14 showed the development of stress-induced borehole breakouts. These breakouts show that the Stillwater fault is near-optimally oriented for frictional failure near well 66-21 but severely missoriented for failure at site 45-14 (Figure 2). Hydraulic fracturing tests conducted in these wells indicate that S_{hmin}/S_V adjacent to the non-producing segment of the Stillwater fault ranges from 0.55–0.64 at depths of 1.9–2.2 km, which is higher than the values of 0.45–0.51 observed immediately above the Stillwater fault zone in producing wells to the northeast. The observation that breakouts were present in these relatively impermeable wells, but absent in wells drilled into the productive main reservoir, indicates a significant increase in the magnitude of S_{Hmax} going from the producing to nonproducing segments of the fault. Theoretical analyses of the conditions necessary for breakout initiation indicate that the magnitude of S_{Hmax} in wells 66-21 and 45-14 is greater than S_V (Figure 2). This is in marked contrast to wells penetrating the permeable main reservoir, where S_{Hmax} is less than S_v.

BHTV logs conducted in wells 66-21 and 45-14 revealed extensive natural fracturing, with the dominant fracture set in each well being roughly parallel to the Stillwater fault. Analyses of TPS logs acquired in these wells under naturally flowing conditions and during injection indicate that hydraulically conductive fractures along the non-producing segment of the Stillwater fault have much lower permeabilities and are fewer in number than observed in the producing wells. Fluid pressures in wells 66-21 and 45-14 are artesian, in contrast to the subhdydrostatic pressures

encountered within the main geothermal reservoir. Coulomb failure analysis for well 66-21, taking account of these elevated fluid pressures and the appropriate rock densities, indicates that neither the hydraulically conductive fractures nor the nearby Stillwater fault zone are critically stressed for frictional failure (Figure 3c). Similar analysis for well 45-14 indicates that some—but not all—of the hydraulically conductive fractures in this well are critically stressed for frictional failure (Figure 3d). However, the combined effects of an increase in S_{Hmax} magnitudes relative to S_v (when compared to the producing fault segment) and the extreme misorientation of the Stillwater fault zone with respect to the principal stress directions near well 45-14 (Figure 2), leads to a decrease in the proximity of the Stillwater fault zone itself to Coulomb failure. This suggests that a necessary condition for high reservoir permeability is that both the local state of stress and the orientation of the Stillwater fault zone are such that the overall fault zone is critically stressed for frictional failure.

Analysis of precision temperature logs acquired in the non-producing wells provides additional information on coupled heat and fluid flow at the reservoir-scale. In well 62-21, 4 km southeast of the current producing limits of the DVGF, and 76-28, 2 km northeast of the DVGF (Figure 1), heat flow above the fault is close to the regional average of approximately 100 mW/m^2. In wells 66-21 and 45-14, located southwest of the main geothermal reservoir, the heat flow ranges from 130–140 mW/m^2. These results suggest that water flowing up the Stillwater fault zone in the vicinity of the non-productive wells 66-21 and 45-14 increases the measured heat flow by only 20–50% over the regional value, which is in contrast to measurements exceeding four times the regional value in the center of the producing reservoir (i.e., near well 73B-7). Simple two-dimensional analytical models for the thermal effects of water moving up the Stillwater fault yield estimated flow rates of 4–11 m^3/yr for each meter of fault length along the non-productive segment of the fault. This contrasts with estimated flow rates of 23–46 m^3/yr for each meter of fault along the highly permeable segment of the fault and no detectable flow up the fault 2 km northeast of the main reservoir (76-28) or 4 km southeast of the reservoir (62-21). The limited spatial extent of anomalous heat flow, particularly at 62-21, which is located approximately 6 km above the downdip extension of the fault, requires that enhanced permeability within the Stillwater fault is not only localized along strike but also limited to depths less than 3 to 4 km.

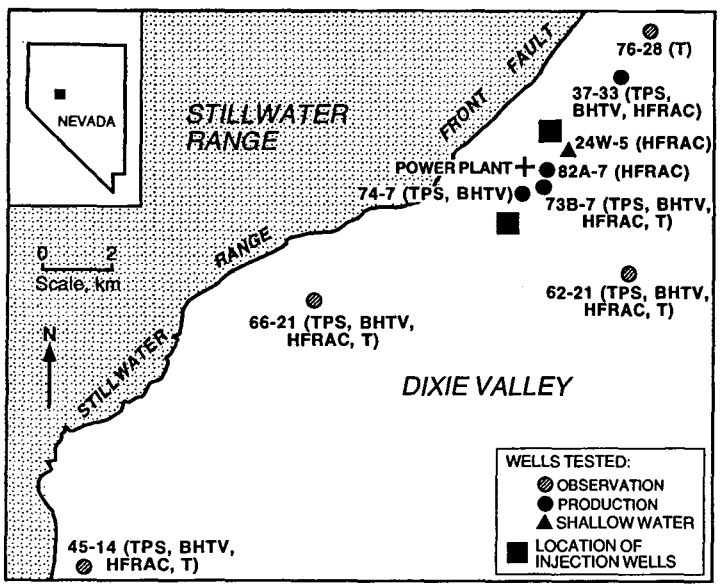

Figure 1. Geothermal wells in Dixie Valley, Nevada. Injection and production wells penetrate highly permeable portions of the southeast-dipping Stillwater fault zone, whereas observation wells fail to encounter sufficient permeability to be of commercial value. Measurements conducted in these wells are TPS: temperature/pressure/spinner log; BHTV: borehole televiewer log; HFRAC: hydraulic fracturing stress measurement, T: precision temperature log.

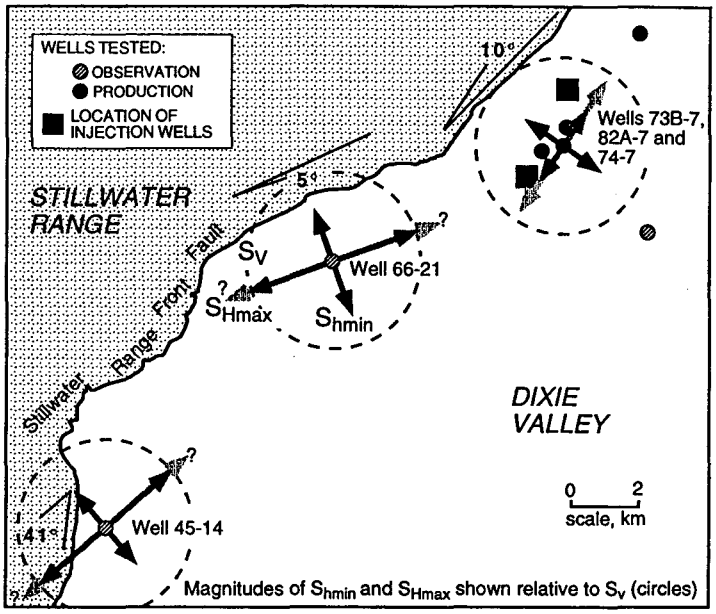

Figure 2. Orientations and relative magnitudes of the least horizontal principal stress, S_{hmin}, and the greatest horizontal principal stress, S_{Hmax}, for selected wells at Dixie Valley. The length of each arrow is proportional to the magnitude of the corresponding stress, normalized to the magnitude of the vertical stress S_V (dashed circle) appropriate for that well and test depth. Lower and upper bounds on S_{Hmax}, determined through analysis of conditions for breakout formation, are depicted as dark and light gray arrows, respectively. Stresses shown for wells 73B-7 and 82A-7 are average values from three measurements at 1.7 to 2.5 km depth. Also shown is the extent (in degrees) to which the Stillwater fault is locally deviated from the optimal orientation for normal faulting.

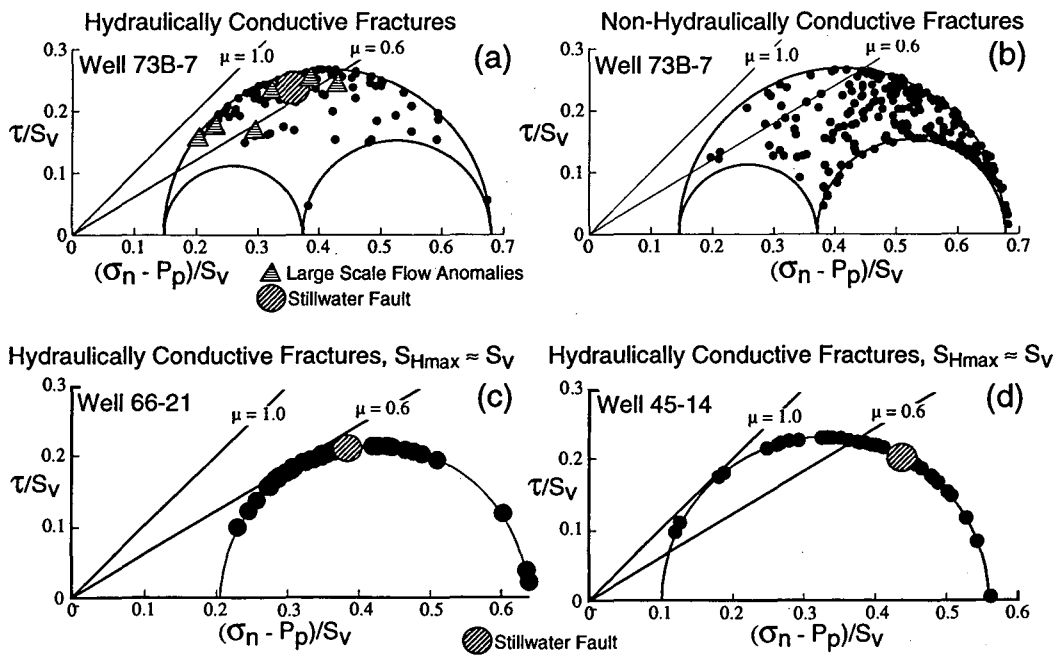

Figure 3. Shear stress versus effective normal stress, normalized to S_V, for (a) hydraulically conductive and (b) non-hydraulically conductive fractures in well 73B-7. Stresses on the Stillwater Fault adjacent to this well and on fractures primarily responsible for geothermal production (large scale flow anomalies) are also shown. Coulomb failure lines are drawn for coefficients of friction of 0.6 and 1.0. (c), (d) Same as Figure a, but for hydraulically conductive fractures encountered in non-producing wells 66-21 and 45-14, calculated assuming $S_{Hmax} = S_V$.

Characterization of Fractured Geothermal Reservoirs Using Inverse Modeling

S. Finsterle[1], K. Pruess[1], and A. Battistelli[2]

[1] Lawrence Berkeley National Laboratory, Earth Sciences Division, Berkeley, CA
[2] Aquater SpA, Lorenzo in Campo (PS), Italy

Flow of water, steam, gas, and heat in fractured geothermal reservoirs is strongly affected by the geometric and hydrological characteristics of the fracture network. The response to production and to reinjection of condensate is governed by the coupling between fluid flow in the fractures and heat transfer from the adjacent matrix blocks. Extraction of hot fluids and reinjection of cold water leads to vaporization and condensation effects near the production and injection wells, respectively. Furthermore, as a result of pressure and temperature declines during production of high-salinity geothermal fluids, precipitation of salt may occur, reducing fracture porosity and thus the overall permeability of the reservoir. On the other hand, injection of fresh water may dissolve solid salt and eventually reduce brine concentrations in the vicinity of the well. Changes in sodium chloride concentrations may therefore contain information about fluid flow in the fracture network, indicating potential connections between the injection well and the production well, which may eventually lead to unwanted thermal interference. Temperature data obtained in production and observation wells are not only affected by the hydrologic but also the thermal properties of the reservoir, which govern the conductive heat exchange from the matrix blocks to the flowing fluids in the fractures. The size and shape of the matrix blocks also determine the effectiveness with which thermal energy can be extracted from the reservoir.

Numerical modeling is an essential tool for the design and optimization of injection operations to sustain the energy recovery from partially depleted geothermal reservoirs. The reliability of such model predictions depends on the accuracy with which the coupled processes described above are accounted for. Furthermore, the salient features of the geothermal reservoir must be captured; an appropriate conceptual model must be developed, and geometric, thermal and hydrologic parameters must be determined.

Inverse modeling—automatic calibration of the numerical model against field data—is a means to obtain model-related parameters that can be considered optimal for the given conceptual model. However, the large number of parameters needed to fully describe coupled nonisothermal multiphase flow in fractured-porous media often leads to an ill-posed inverse problem, which is predisposed to yielding nonunique and unstable solutions. It is therefore crucial to carefully identify and maximize the information content of the data used for calibration, and to assess and minimize correlations among the parameters to be estimated.

We have developed inverse modeling capabilities for the TOUGH2 family of multiphase flow simulators (Pruess, 1991). With the ITOUGH2 code (Finsterle, 1997), any TOUGH2 input parameter can be estimated based on any type of data for which a corresponding TOUGH2 output is calculated. Parameter estimation is supplemented by an extensive residual and error analyses. In this study, we make use of the module EWASG (Battistelli et al., 1997), which accurately describes three-phase (liquid, solid, and gas) mixtures of three components (water, sodium

chloride, and a non-condensible gas). The dependence of brine density, enthalpy, viscosity, gas solubility and vapor pressure on salinity is taken into account. Precipitation and dissolution of salt is also included, with associated porosity and permeability changes. The method of "Multiple Interacting Continua" (MINC; Pruess and Narasimhan, 1982) is used to appropriately resolve the pressure and saturation gradients between the fractures and the matrix. The MINC concept is based on the notion that both the fractures and the matrix can be treated as interconnected continua, and that changes in matrix conditions will be controlled by the distance from the fractures. Note that in the MINC formulation, fracture spacing is simply an input parameter to the mesh generator producing the computational grid.

ITOUGH2/EWASG is used to simulate production from a hypothetical geothermal reservoir with high salinity and CO_2 as the non-condensible gas. Due to precipitation of salt near the well and the depletion of fluid reserves in the reservoir, the production of steam declines rapidly and almost ceases within a relatively short period of time. After five years of exploitation, condensate and wastewater is injected into three wells a few hundred meters from the production well. Figure1 shows the saturation distribution in the matrix and fracture continuum, respectively, five years after beginning of reinjection. Injection of cold water leads to a reduction of steam saturation in the immediate vicinity of the injection wells. Evaporation of injectate, however, increases the reservoir pressure, driving steam towards the production well, enhancing both the rate and enthalpy of the produced fluid. Furthermore, salt that precipitated due to the reduction in the pressure is redissolved by the fresh water, potentially increasing the permeability.

Time series of simulated temperatures, steam production rates, flowing enthalpies, and NaCl concentrations at the production well are considered to be the data available for calibration of the model. The parameters studied include fracture spacing, fracture absolute permeability, porosity, initial reservoir temperature, heat conductivity, and an exponent that describes the change in permeability as a function of porosity change due to salt dissolution and precipitation.

Sensitivity coefficients are calculated to identify the potential contribution of each of the observation types to the inverse problem at hand. Moreover, the uncertainty of the estimated parameters is evaluated, along with the correlation coefficients to detect the dependencies among the parameters. The ITOUGH2 analysis shows that the joint inversion of all data greatly improves the identifiability of key hydrologic and thermal properties. Adding concentration data to the analysis considerably reduces the correlation among some of the parameters, allowing for a more independent and more stable estimation of reservoir properties. Other characteristics such as fracture spacing remain difficult to determine because of their strong correlation with hydraulic and thermal parameters.

Inverse modeling is a powerful tool for the design of field tests, for the optimization of reinjection operations, and for the evaluation of prediction uncertainties from geothermal reservoir simulations. Combining the characterization efforts from a variety disciplines, and making use of all available data obtained during testing or production provides the basis for a better understanding of nonisothermal multiphase flow processes, for the development of an appropriate conceptual model, and for the estimation of the properties required to perform reliable model predictions.

This work was supported, in part, by the Assistant Secretary for Energy Efficiency and Renewable Energy, Office of Geothermal Technologies, of the U.S. Department of Energy, under Contract No. DE-AC03-76SF00098.

References

Battistelli, A., C. Calore and K. Pruess, The simulator TOUGH2/EWASG for modeling geothermal reservoirs with brines and a non-condensible gas, *Geothermics*, Vol. 26, No. 4, 437–464, 1997.

Finsterle, S., *ITOUGH2 Command Reference, Version 3.1*, Lawrence Berkeley National Laboratory Report LBNL-40041, Berkeley, Calif., 1997.

Pruess, K., *TOUGH2—A General Purpose Numerical Simulator for Multiphase Fluid and Heat Flow*, Lawrence Berkeley National Laboratory Report LBL-29400, Berkeley, Calif., 1991.

Pruess, K. and T. N. Narasimhan, T.N., On fluid reserves and the production of superheated steam from fractured vapor-dominated geothermal reservoirs, *J. Geophys. Res.*, 87 (B11), 9329–9339, 1982.

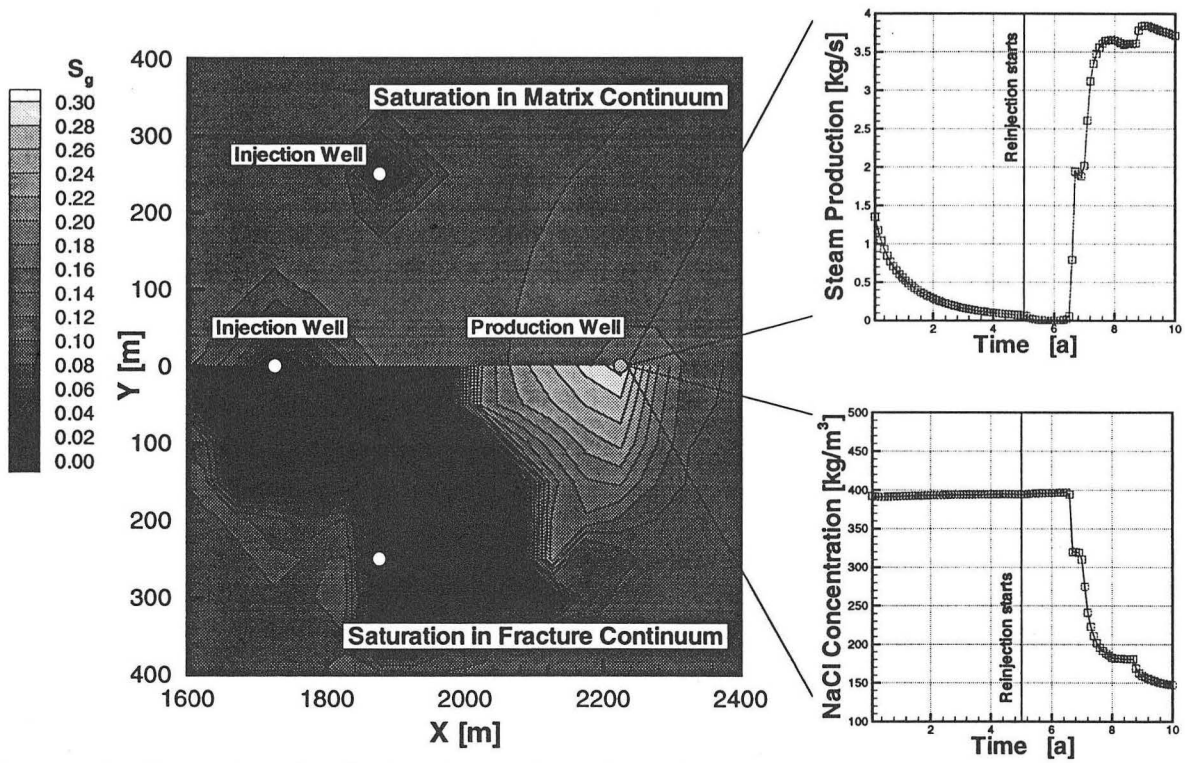

Figure 1. Saturation distribution in matrix (left, top) and fracture (left, bottom) continuum five years after reinjection of cold water into the geothermal reservoir. Steam production (right, top) and sodium chloride concentration in the production well (right, bottom) as a function of time. Simultaneous inversion of these data can be used to calibrate the numerical model.

How Should Permeability Within The Oceanic Crust Be Represented In Numerical Models Of Coupled Flows?

A. T. Fisher, Earth Sciences Department and Institute of Tectonics, University of California, Santa Cruz, 1156 High Street, Santa Cruz, CA, 95064, (831) 459-5598, (831) 459-3074 - fax, afisher@es.ucsc.edu

The oceanic crust is the largest fractured aquifer on Earth. Thermally-driven circulation of seawater through the oceanic crust profoundly influences the evolution of the crust and the oceans. While much effort has been focused over the past two decades on hot springs along the mid-ocean ridge axis, the global heat flow data set indicates that advective heat loss from the flanks is more than three times that at the axis [Stein and Stein, 1994]. Hydrothermal heat loss and fluid exchange between the crust and the oceans typically persist to an age of several tens of millions of years and thus affect more than one-third of the ocean floor [Sclater et al., 1980]. This flow also results in solute fluxes of several elements similar in magnitude to those of riverine and ridge-crest sources and contributes to extensive alteration within basaltic basement [Elderfield and Schultz, 1996; Alt et al., 1996]. Despite the importance of this process for cooling and alteration of the crust, and for chemical mass transport between the oceans and the crust, little is known about typical sites of discharge and recharge, the distribution of fluxes over a range of chemistries and temperatures, the pathways and length scale of lateral flow, or the depth extent of flow. Permeability is one of the most important, and least understood, of the primary hydrogeologic parameters influencing the flow of hydrothermal fluids on ridge flanks.

Ridge-flank flows have been simulated using numerical models and a representative elemental volume (REV) approach [e.g., Fehn et al., 1983; Fisher et al., 1990; Davis et al., 1996], but the depth and lateral extent of ridge-flank circulation, the distribution of permeability within the crust, and the influence of basement topography and tectonic fabric (fractures, faults, etc.) in guiding fluid, solute, and heat flow remain loosely constrained. For example, basement relief seems to enhance fluid circulation in the uppermost crust [Fisher et al., 1994; Wang et al., 1997], but its significance for deeper circulation remains unclear. Basement topographic highs also tend to be overpressured relative to an ambient hydrostatic water column [Fisher et al., 1997; Davis and Becker, 1998],, and the few well-studied examples of basement highs with relatively thin sediment are sites of ridge-flank discharge [Mottl et al., 1998].

The possibility that along-strike (ridge-parallel) faults host ridge-crest hydrothermal circulation is also recognized [Delaney et al., 1992], but the role of faults in guiding fluid flow within ridge flanks remains unclear, particularly if shallow, dominantly-horizontal permeability coupled with basement roughness can explain the large-scale distribution of many seafloor heat flow anomalies. In addition, it is not clear how best to represent fault zones in numerical models of oceanic crust. The most common approach is to consider faults as regions of elevated effective permeability [e.g., Fehn et al., 1983; Yang et al., 1996], but the potential importance of permeability anisotropy and fault gauge, to name two obvious complications, has not been evaluated.

Permeability in the oceanic crust has been directly quantified mainly with borehole methods originally developed for aquifers and in the oil field [e.g., Anderson and Zoback, 1982; Becker, 1996]. A related approach has involved measuring the rate at which ocean water is

drawn down into holes drilled into underpressured oceanic basement [Becker et al., 1983], or the rate at which hydrothermal water is driven from holes drilled into underpressured oceanic basement [Fisher et al, 1997]. A summary of apparent bulk permeabilities based on these approaches (Fig. 1) suggests several general observations. Bulk permeabilities in oceanic crust span seven orders of magnitude, from $\leq 10^{-17}$ m^2 at depths below 500 m into basement, to 10^{-10} m^2 within several 10-m-thick intervals, generally in the shallowest crust. The data from basaltic crust can be divided into two distinct sections, with relatively high bulk permeabilities ($\geq 10^{-14}$ m^2) extending to about 500 m into basement. There are no values greater than 10^{-13} m^2 that include intervals deeper than 100 m into basement, and intervals extending from 100 to 300 m into basement generally have bulk permeabilities of 10^{-14} to 10^{-13} m^2. While some of the depths at which bulk permeability appears to drop abruptly correlate with lithologic boundaries, these depths also reflect the extent of basement drilling and the thicknesses of the tested intervals.

Other approaches for estimating permeability in oceanic crust are much more idealized and indirect. For example, some scientists have attempted to use seafloor heat flow measurements to estimate the length-scale of hydrothermal circulation patterns [Williams et al., 1974; Anderson et al., 1977; Cathles, 1990]. Areas of high heat flow are interpreted to indicate upwelling circulation limbs within underlying permeable basement, while areas of locally low heat flow are interpreted to indicate downwelling fluid. By assuming some aspect ratio for circulation cells, and applying Rayleigh number stability criteria, scientists have estimated bulk permeability for the oceanic crust. Analytical and numerical models have similarly been used to "calibrate" the permeability in oceanic basement, but finding what bulk values are required to allow sufficient lateral flow to transport heat necessary to match seafloor heat flow patterns, or to drive flow at a chemically-necessary velocity.

Scientists working with ophiolites, pieces of oceanic crust that have been uplifted and emplaced on continents and islands, have mapped out fracture distributions and characteristics, and related these fracture distributions to effective permeability, generally using some form of a cubic law [e.g., Nehlig, 1994]. Similar approaches have been applied to boreholes drilled into the oceanic crust, with fracture patterns determined using borehole electrical or acoustic tools [Pezard et al., 1996]. The great challenge in applying these results to the oceanic crust is that fracture geometries (apertures, asperities, lateral continuity) are quite poorly known.

Compared to studies completed on land in mines and waste sites, experiments conducted on ophiolites and in-situ oceanic crust have been extremely crude. Borehole experiments have thus far comprised almost exclusively single-hole tests, and even within these single holes, intervals spanning tens or hundreds of meters have been tested at one time. Borehole pumping tests have typically lasted only a few minutes, with the exception of free-flow tests associated with overpressured or underpressured basement, which have lasted weeks to years.

While it may be possible to plan and execute a limited number of high-resolution, cross-hole tests in the oceanic crust, it is likely that over the next few decades, marine geologists will need to make due with a wealth of indirect geological, geochemical, and geophysical information to infer the character of oceanic crustal permeability. The value of these interpretations can be leveraged if marine geologists can learn lessons from terrestrial hydrologists who have studied fractured reservoirs on land. For example, are there ways that we can evaluate the possibility of one or more likely permeability distributions in the oceanic crust based on a limited number of fracture measurements? Are there self-consistent and testable ways of incorporating stochastic

representations of oceanic crustal permeability?

At the same time, there may be several advantages to terrestrial hydrogeologists in learning about fractured aquifers in the oceanic crust. Boundary conditions are well understood and easy to measure (hydrostatic as a function of seafloor depth and generally constant temperature at the seafloor, constant heat flow or constant temperature at depth) and the crustal stratigraphy is relatively simple compared to that in many terrestrial aquifers. We can measured thermal and chemical gradients within the upper oceanic crust relatively easily, and these are often fairly easy to interpret because the chemistry of the ocean has remained essentially constant over long periods of geological time.

References

Alt, J. C., D. A. H. Teagle, C. Laverne, D. A. Vanko, W. Bach, J. Honnorez, K. Becker, M. Ayadi, and P. A. Pezard, Ridge-flank alteration of upper oceanic crust in the Eastern Pacific: synthesis of results for volcanic rocks of Holes 504B and 896A, in *Proc. ODP, Sci. Res.*, vol. 148, edited by J. C. Alt, H. Kinoshita and L. Stokking, pp. 435-450, Ocean Drilling Program, College Station, TX, 1996.

Anderson, R. N., and M. D. Zoback, Permeability, underpressures and convection in the oceanic crust near the Costa Rica Rift, eastern equatorial Pacific, *J. Geophys. Res., 87*, 2860-2868, 1982.

Anderson, R., M. G. Langseth, and J. Sclater, The mechanisms of heat transfer through the floor of the Indian Ocean, *J. Geophys. Res., 82*, 3391-3409, 1977.

Becker, K., Permeability measurements in Hole 896A and implications for the lateral variability of upper crustal permeability at Sites 504 and 896, in *Proc. ODP, Sci. Res.*, vol. 148, edited by J. C. Alt, H. Kinoshita and L. Stokking, pp. 353-363, Ocean Drilling Program, College Station, TX, 1996.

Becker, K., M. G., Langseth, R. P. Von Herzen, and R. Anderson, Deep crustal geothermal measurements, Hole 504B, Costa Rica Rift, *J. Geophys. Res., 88*, 3447-3457, 1983

Cathles, L., Scales and effects of fluid flow in the upper crust, *Science, 248*, 323-329, 1990.

Davis E. and Becker, K. Borehole observatories record driving forces for hydrothermal circulation in young oceanic crust, *EOS*, Trans. AGU, 79, 369 and 377-378, 1998.

Davis, E. E., D. S. Chapman, and C. B. Forster, Observations concerning the vigor of hydrothermal circulation in young volcanic crust, *J. Geophys. Res., 101*, 2927-2942, 1996.

Delaney, J. R., V. Robigou, R. McDuff, and M. Tivey, Geology of a vigorous hydrothermal system on the Endeavor segment, Juan de Fuca Ridge, *J. Geophys. Res., 97*, 19,663-19,682, 1992.

Fehn, U., K. Green, R. P. Von Herzen, and L. Cathles, Numerical models for the hydrothermal field at the Galapagos Spreading Center, *J. Geophys. Res., 88*, 1033-1048, 1983.

Elderfield, H., and A. Schultz, Mid-ocean ridge hydrothermal fluxes and the chemical composition of the ocean, *Ann. Rev. Earth Planet. Sci., 24*, 191-224, 1996.

Fisher, A., Permeability within basaltic oceanic crust, Rev. Geophys., 36: 143-182, 1998.

Fisher, A. T., K. Becker, and T. N. Narasimhan, Off-axis hydrothermal circulation: parametric tests of a refined model of processes at Deep Sea Drilling Project/Ocean Drilling Program site 504, *J. Geophys. Res., 99*, 3097-3121, 1994.

Fisher, A. T., K. Becker, T. N. Narasimhan, M. G. Langseth, and M. J. Mottl, Passive, off-axis

convection on the southern flank of the Costa Rica Rift, *J. Geophys. Res., 95*, 9343-9370, 1990.

Fisher A. T., Becker, K., and Davis, E. E. The permeability of young oceanic crust east of the Juan de Fuca Ridge, as determined using borehole thermal measurements, *Geophys. Res. Lett.*, 24, 1311-1314, 1997.

Mottl M. J., Wheat C. G., Kadko D., Sansone F., Massoth G., Grehan A., Moyer C., Davis E. E., Baker E., Feely R., Lilley M., and Becker N. Warm springs discovered on 3.5 Ma crust, Baby Bare Outcrop, eastern flank of the Juan de Fuca Ridge. *Geology,* 26: 51-54, 1998.

Nehlig, P., Fracture and permeability analysis in magma-hydrothermal transition zones in the Samail ophiolite (Oman), *J. Geophys. Res., 99*, 589-601, 1994.

Pezard, P. A., M. Ayadi, A. Revil, G. Bronner, and R. Wilkens, Detailed structure of an oceanic normal fault: a multiscalar approach at DSDP/ODP Site 504, *Geophys. Res. Lett., 24*, 337-340, 1997.

Sclater, J. G., C. Jaupart, and D. Galson, The heat flow through oceanic and continental crust and the heat loss of the earth, *Rev. Geophys. Space Phys., 18*, 269-311, 1980.

Stein, C., and S. Stein, Constraints on hydrothermal heat flux through the oceanic lithosphere from global heat flow, *J. Geophys. Res., 99*, 3081-3095, 1994.

Wang, K., J. He, and E. E. Davis, Influence of basement topography on hydrothermal circulation in sediment-buried oceanic crust, *Earth. Planet. Sci. Lett., 146*, 151-164, 1997.

Williams, D. L., R. P. Von Herzen, J. G. Sclater, and R. N. Anderson, The Galapagos Spreading Centre, lithospheric cooling and hydrothermal circulation, *Geophys. J. R. astr. Soc., 38*, 587-608, 1974.

Yang, J., R. N. Edwards, J. W. Molson, and E. A. Sudicky, Three-dimensional numerical simulation of the hydrothermal system within TAG-like sulfide mounds, *Geophys. Res. Lett., 23*, 3475-3478, 1996.

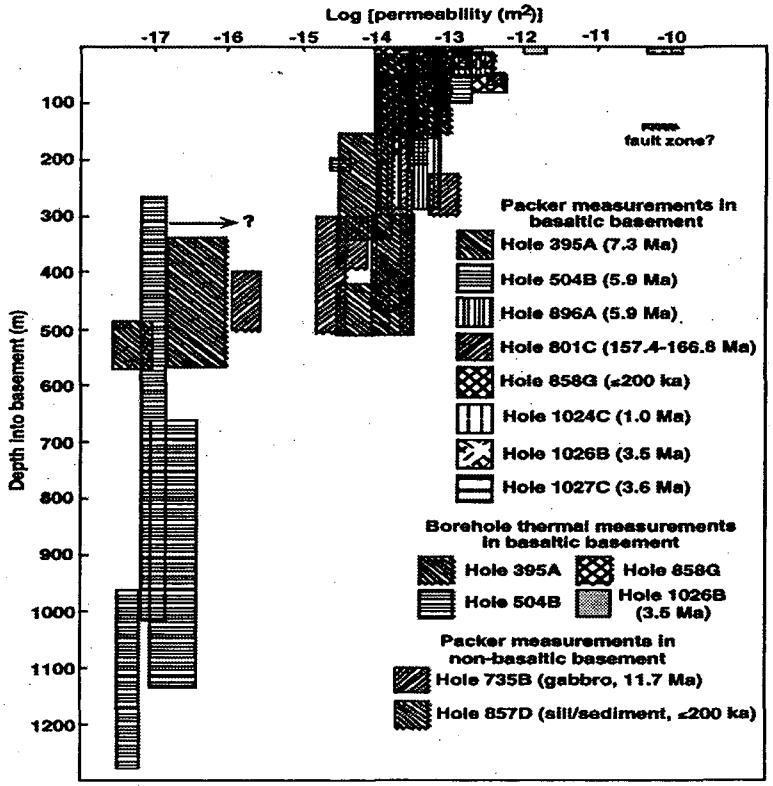

Figure 1. Bulk permeabilities within upper oceanic basement determined with a borehole packer and through analysis of borehole temperature logs measured over the last 30 years (modified from Fisher [1998], with additional data from Becker and Fisher [in prep]). See Fisher [1998] and references therein for a discussion of experimental methods and assumptions. Data from Holes 735B and 857D were collected in non-basaltic basement. The actual depths into "basement" for these measurements are not known, so the data are plotted relative to depth below seafloor (Hole 735B) and depth below the first sill (Hole 857D). The depth ranges for individual measurements indicate the borehole intervals over which the bulk permeability values are attributed. In some cases, these represent entire isolated intervals, while in other cases, the ranges are based on the differences between transmissivities calculated for overlapping intervals. The range of bulk permeabilities indicated by the width of the boxes reflects differences in values calculated for multiple tests and an estimate of experimental uncertainties. The arrow pointing to the right of the value calculated from an experiment in Hole 504B indicates that this test may have led to an underestimate of the bulk permeability over this thick depth interval because of uncertainties regarding system compressibilities [Becker, 1996].

Coupled 3-D Simulations of Forced Fluid Flow Through Fractured, Hot Rock

T. Kohl and L. Rybach
Institute of Geophysics, ETH, CH-8093 Zurich, Switzerland
E-mail: kohl@geo.phys.ethz.ch, Tel.: +41 1 633 3332, Fax: +41 1 633 1065

For securing future energy supply by renewable resources geothermal Hot-Dry-Rock (HDR) systems are of great interest. Hydraulic experiments are performed at several HDR test sites. The present lack of data and knowledge on flow behaviour and geometry, on the long term system performance and on operational experience highlights the importance of numerical simulations for comprehensive system analyses. In the framework of a co-operation with the European HDR Project at Soultz (France, see Figure 1), the finite element code FRACTure is used to simulate the coupled response of a fractured media to forced fluid flow. Three-dimensional full finite element solutions can be attributed to hydraulic, thermal and elastic processes. Several coupling mechanisms such as non-linear stress dependent joint aperture laws or linear elastic effects of temperature and pore pressure perturbations on the stress field developing in the bulk rock are treated and thermal transport by conduction and advection is included in the fracture and the matrix.

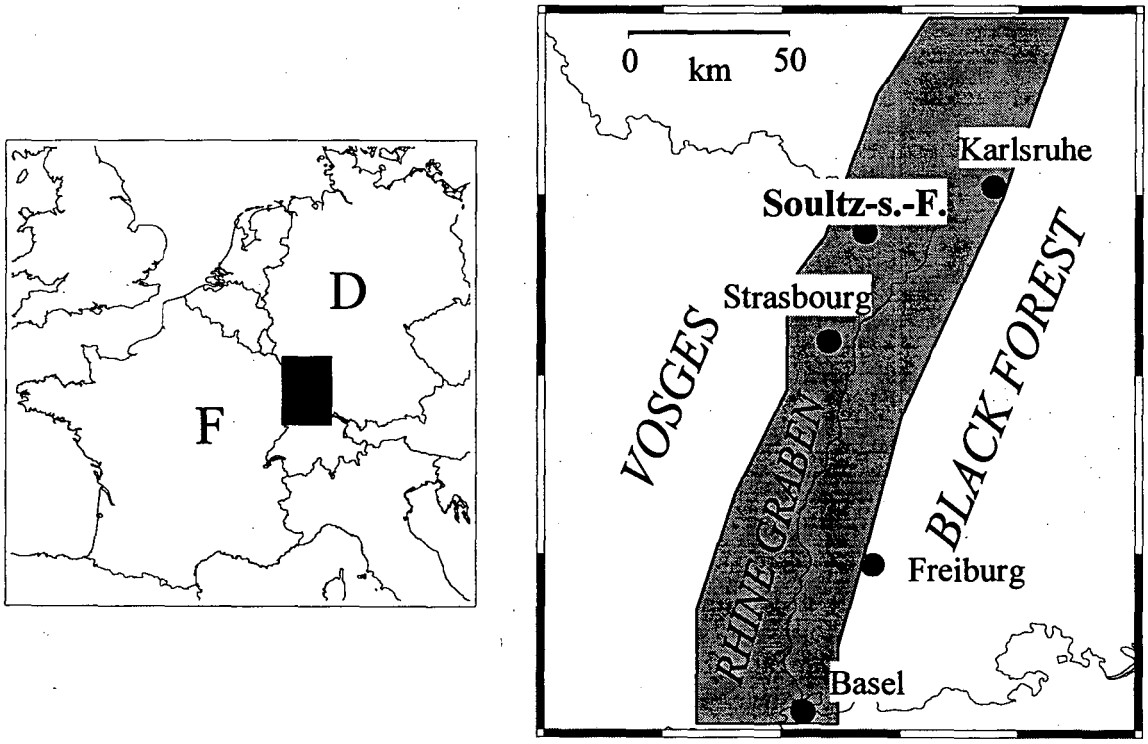

Figure 1: Location of the HDR test site Soultz-sous-Forêts in the Rhine Graben between the Vosges (France) and the Black Forest (Germany) mountains

At the HDR test site Soultz-sous-Forêts the hydraulic properties at the open hole sections of the GPK1 and GPK2 boreholes have been extensively investigated in the last 4 years by numerous multiple level flow rate injection or production experiments. They all show that downhole pressure response attains quasi steady state levels within a few days and that the duration of transient pressure changes depends strongly on flow rate. Earlier studies which quantified the short time (t<20 days) experiments have highlighted the importance of turbulent-like hydraulic behaviour in this reservoir and accurately fitted the pressure data by transient numerical simulations assuming non-Darcian flow in the fracture network (see the 95JUL01 injection experiments in Figure 2). Extensions of these simulations later on used

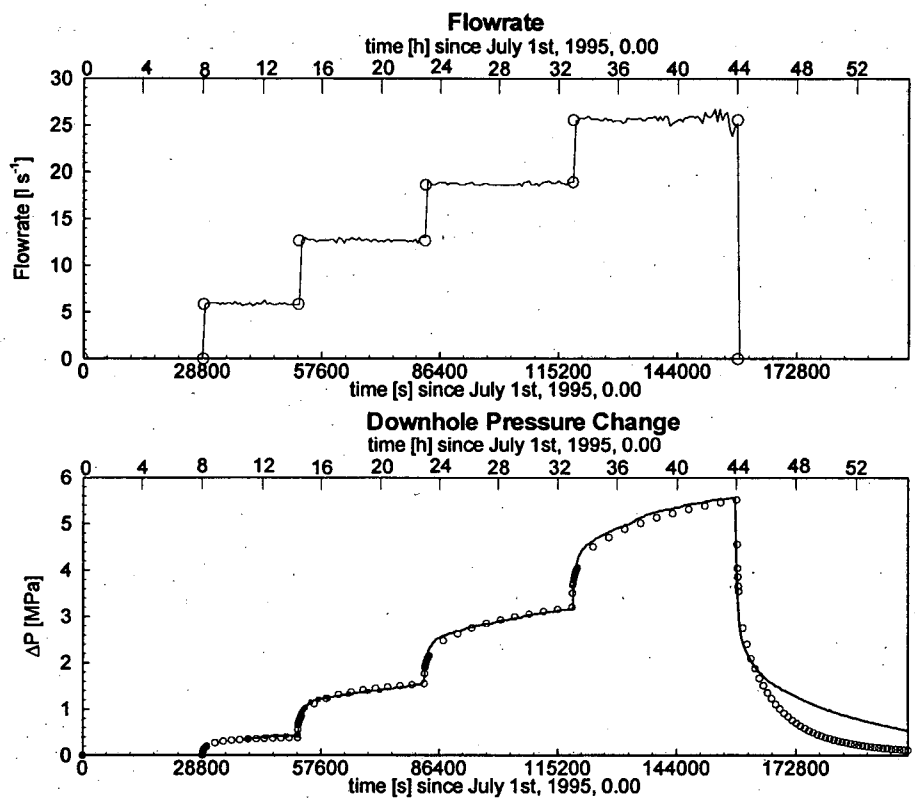

Figure 2: Flow rate (upper frame) and downhole differential pressure in the GPK2 borehole of the 95JUL01 injection test. Measurements are indicated by continuous lines and simulation results by open circles.

more sophisticated fracture geometries. Herein, particular attention to the influence of geometry and of far field fault systems was paid. By analysing the downhole pressure response and accounting for geological considerations alternative flow geometries were developed. These results allow to derive a conceptual model of the reservoir situation at Soultz. Further data from long term circulation experiments are however needed to elucidate the economical performance under operational conditions. Especially, the 4 month circulation test (Figure 3), performed between August and November 1997 shows clear indications of thermo-elastic coupling. Throughout the experiment the hydraulic impedance reduced continuously at the injection

borehole GPK1, due to the injection of cold fluid. In contrast, at the production hole, temperature increased continuously and hydraulic impedance increased accordingly. By FE simulations this experiment could be quantitatively interpreted and the importance of the thermo-elastic mechanisms in modifying system behaviour over time was highlighted.

It is thus demonstrated that numerical simulation of hydraulic data can yield a recognition of flow processes and of flow geometries and provides the necessary basis for more elaborated 3-D models. Such models allow to predict future HDR performance. This analysis is directed towards a general optimisation of HDR operation parameters and especially to explain data collected from the Soultz site.

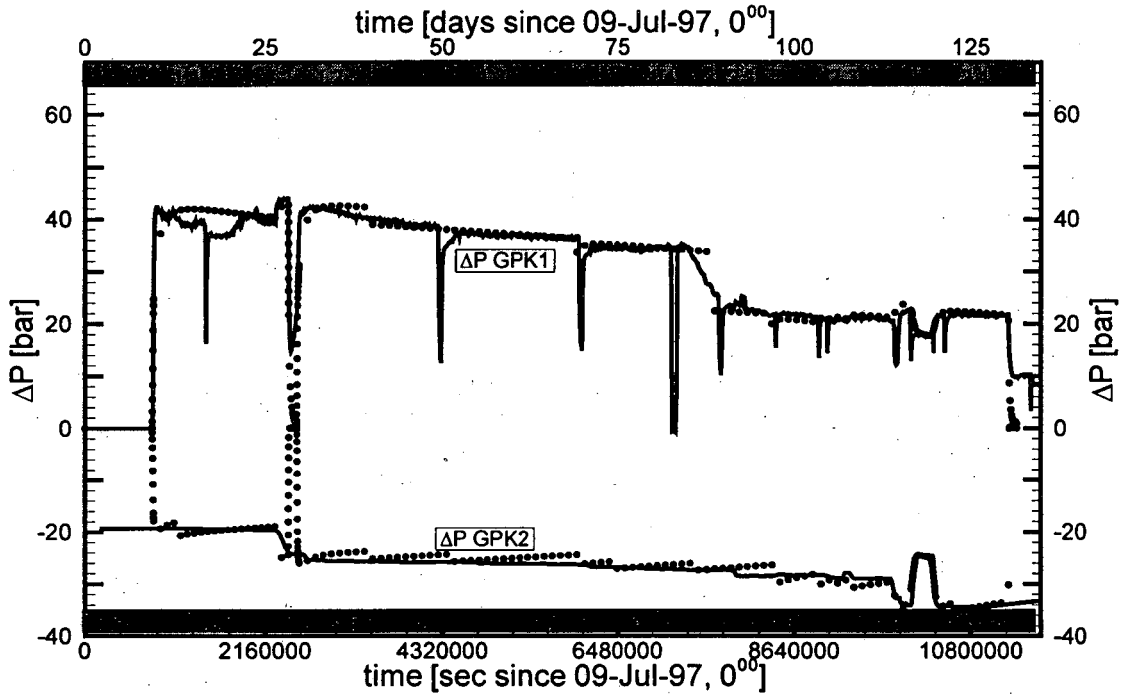

Figure 3: Segmental fit of the measured and simulated pressure histories of a 4 month circulation test. The upper row of factors indicates the ratio between measured and simulated injection (GPK1) and the lower factor row indicates the ratio between measured and simulated production (GPK2) differential pressure.

References:

Kohl, T., K. F. Evans, R. J. Hopkirk, and L. Rybach, 1995, Modelling of coupled hydraulic, thermal and mechanical processes in the simulation of Hot Dry Rock reservoir behaviour, in Fractured and Jointed Rock Masses, ed. L. R. Myer, et al., Lake Tahoe, California, 535-542, Balkema, Rotterdam.

Kohl T., R. Jung, R.J. Hopkirk & L. Rybach, 1996, Non-linear flow transients in fractured rock masses - The 1995 injection experiment in Soultz, Proc. 21st Workshop Geothermal Reservoir Engineering, Stanford Univ. CA, USA, 22-24 Jan. 1996, 21, pp.157-164

Kohl T., K.F. Evans, R.J. Hopkirk, R. Jung & L. Rybach, 1997, Observation and simulation of non-Darcian flow transients in fractured rock, Water Resources Research, 33(3), pp.407-418.

Session 9:
REMEDIATION AND COLLOID TRANSPORT IN FRACTURED SYSTEMS

Basic Research Strategies for Resolving Remediation Needs in Contaminated Fractured Subsurface Media

P.M. Jardine[1], T.M. Mehlhorn[1], I. L. Larsen[1], S.C. Brooks[1]
J.P. Gwo[2], Glenn V. Wilson[3], and W.E. Sanford[4]

[1]Environmental Sciences Div., Oak Ridge National Laboratory, Oak Ridge, TN (ipj@ornl.gov)
[2]Center for Computational Sciences, Oak Ridge National Laboratory, Oak Ridge, TN
[3]Southern Nevada Science Center, Desert Research Institute, Las Vegas, NV
[4]Department of Earth Resources, Colorado State University, Fort Collins, CO

A significant limitation in defining remediation needs at contaminated sites often results from poorly defined source terms. Monitoring activities often suggest that subsurface contaminant mobility from primary contaminant sources (e.g. subsurface pits and trenches) is complicated by preferential flow and significant contaminant diffusion into the matrix of the surrounding soil and bedrock. In many instances it is not known whether the primary contaminant sources are still active and perhaps worse yet, what the inevitable consequence may be of the secondary matrix sources. This presents a problem for environmental remediation since predictive simulations of transport phenomena using poorly defined source terms can be an inaccurate means of risk assessment.

These problems are common place at the Oak Ridge National Laboratory, in Oak Ridge, Tennessee, USA where the disposal of low-level radioactive waste has historically involved shallow land burial in unconfined pits and trenches. The subsurface media consists of fractured saprolite and shale bedrock which are conducive to rapid preferential flow coupled with significant matrix storage. This circumstance causes large hydraulic and geochemical gradients between the various flow regimes of the media and typically results in nonequilibrium conditions during solute transport. Our research over the past 10 y has sought to enhance the design and effectiveness of contaminant remedial strategies by providing an improved understanding of contaminant transport processes in highly structured, heterogeneous subsurface environments that are complicated by fracture flow and matrix diffusion.

Our approach involves integrated laboratory and field scale investigations that use a variety of techniques for assessing subsurface contaminant transport. At the laboratory scale, undisturbed columns are used in tracer transport experiments to assess the interaction of hydrology, geochemistry, and microbiology on the fate of nonreactive and reactive tracers. We use a number of techniques for assessing nonequilibrium processes, including (1) controlling flow path dynamics with manipulations of pore-water flux and soil-water tension, (2) isolating diffusion and slow geochemical processes with flow interruption, (3) using multiple tracers with different diffusion coefficients, and (4) using multiple tracers with grossly different sizes. When these techniques are combined, they become a powerful means of quantifying nonequilibrium processes in heterogeneous systems. The column scale results have provided new insights on the rates and mechanisms of dominant physical and geochemical processes controlling the fate and transport of contaminants in fractured media.

The information derived from the laboratory scale experiments is used to design and interpret field scale experiments conducted within both the unsaturated and saturated zones. Field facilities for understanding storm driven solute mobility in the unsaturated zone are equipped with isolated undisturbed soil blocks, buried line-sources for tracer release, and subsurface weirs (Fig. 1). The weirs are unique in that subsurface drainage can be collected and monitored from a 2.5 m deep by 16 m long trench that has been excavated across the outflow region of a subwatershed. The system is equipped with computer data acquisition allowing for the real-time monitoring of tracer fluxes during storm events. Besides the ability to capture subsurface drainage, the field facilities are equipped with solution samplers, tensiometers, and piezometers wells, with the latter used to assess perched water table dynamics during storms. The field sites also contain a 2 x 2 x 3m isolated, undisturbed soil block that is used for controlled tracer release studies at the pedon scale. The soil blocks are instrumented with a variety of solution samplers designed to monitor water and solutes from large, medium, and small pore size regions. Numerous long-term, storm-driven tracer studies have been conducted on these field facilities and our findings have provided insights into the rates and mechanisms of mass exchange between various pore regions of the media.

Field facilities have also been established in the saturated zone within fractured shale bedrock (Fig. 2). A transect of multilevel groundwater monitoring wells has been established along geologic strike within a fast flowing fracture regime and a slow flowing matrix regime. A sophisticated computer driven tracer injection system dispenses tracers into the fracture regime under natural gradient conditions. Two long-term, steady-state natural gradient experiments have been conducted using multiple nonreactive tracers (Br, He, Ne) and multiple reactive tracers (^{57}Co(II)EDTA, ^{51}Cr(III)EDTA, and ^{109}CdEDTA). The multiple tracer technique takes advantage of the difference in the molecular diffusion coefficient and geochemical reactivity between the tracers. Observed differences in the nonreactive tracer breakthrough curves were shown to be a function of their molecular diffusion coefficients. This confirmed that matrix diffusion was a significant process contributing to the overall physical nonequilibrium that controlled contaminant transport in the shale bedrock. The chelated radionuclides studies offer the added complexity of understanding how geochemical and microbial processes alter the fate and transport of contaminants in a physically heterogeneous system. The reactive tracers were significantly retarded relative to the nonreactive tracers and the mechanism of retardation was largely due to time-dependent sorption and mineral induced chelate dissociation reactions. The multiple tracer strategies not only improve our conceptual understanding of time-dependent contaminant migration in subsurface media, they also provide the necessary experimental constraints needed for accurate numerical quantification of the coupled nonequilibrium processes. Please see our web site for more information concerning these research activities (http://www.esd.ornl.gov/programs/ETPI/).

So how does our basic research strategies improve remedial options at contaminated sites? First, they provide an improved conceptual understanding of the geochemical and hydrological processes controlling contaminant migration from secondary sources. Second, they provide a direct measure of contaminant migration rates along fracture flow paths and into the soil and rock matrix. Such information is critical to contaminant fate and transport modeling and risk assessment modeling. Lastly, the basic research endeavors provide information that is necessary for improving our

decision-making strategies regarding the selection of effective remedial actions and the interpretation of monitoring results after remediation is complete.

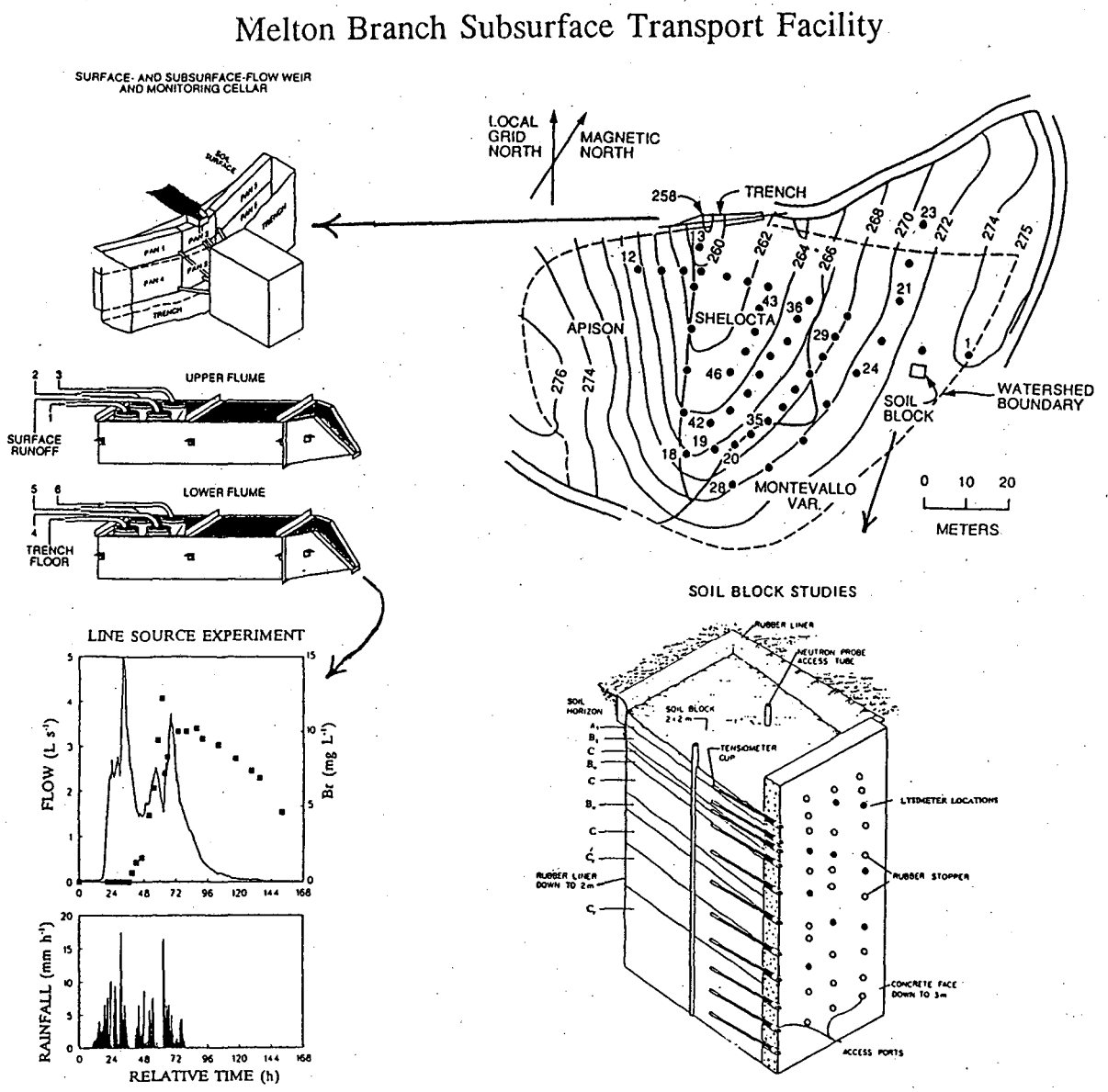

Figure 1: Subsurface transport facility for studying storm driven tracer transport in the unsaturated zone of a fractured weathered shale. Multiple pore region sampling capabilities are available at both the pedon and field scales. The unique subsurface weirs allow for the measurement of real-time subsurface tracers fluxes.

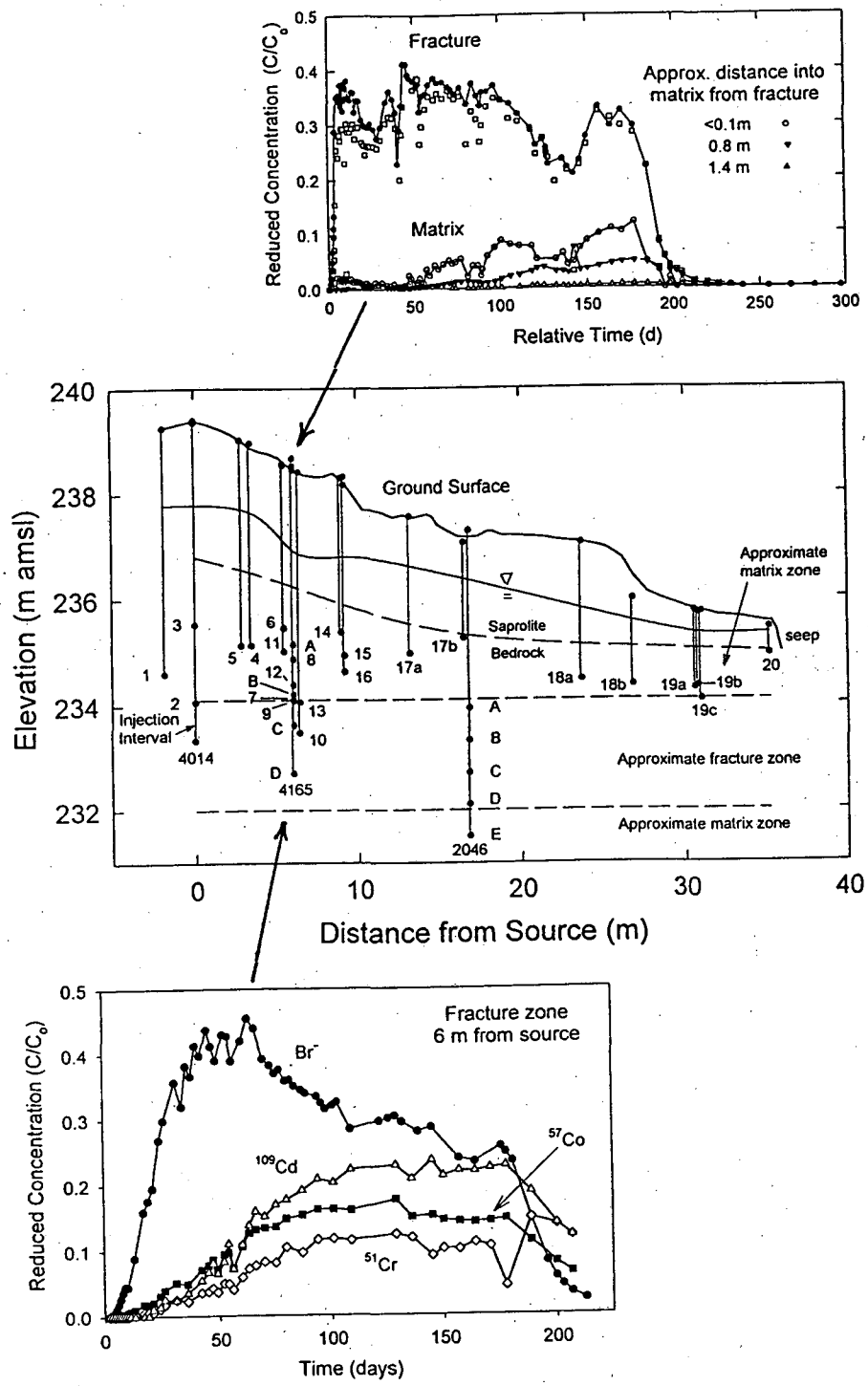

Figure 2: Cross-section of the experimental field facility located within a saturated shale bedrock, showing the location and sampling depth of the groundwater monitoring wells. Tracers are delivered into a fractured zone and can be monitored down gradient using multilevel sampling wells located within the fracture and matrix regimes.

Critical Biogeochemical Parameters Used for In Situ Bioremediation of Solvents in Fractured Rock

Terry C. Hazen
Earth Sciences Division
Lawrence Berkeley National Laboratory, Berkeley, CA 94720

Two full-scale demonstrations of in situ bioremediation via biosparging/bioventing illustrate the critical biogeochemical parameters for in situ bioremediation of solvents in fractured rock. Both sites were in Virginia, but differed significantly in contaminant composition. One site was dominated by non-chlorinated solvents at high concentrations, while the other site had only chlorinated alkenes. Both sites showed rapid responses to sparging and eventually required various other nutrient supplements to maintain high biodegradation rates of the chlorinated solvents.

Effective in-situ aerobic groundwater bioremediation depends upon the successful delivery of oxygen (and other amendments such as nutrients and methane) into the subsurface. While this process is relatively straightforward in granular overburden materials, it can be quite complex in fractured bedrock. Bedrock fractures serve as preferential pathways such that the resultant zone of influence is generally asymmetrical and often unpredictable. Full characterization of the depth, size, orientation, and degree of interconnection of bedrock fractures is prohibitive from a logistical and cost perspective. However, tracer tests and critical inorganic and organic measurements can provide a representative picture of crucial subsurface conditions.

Site 1. Contaminants of concern in bedrock groundwater included chlorinated solvents such as trichloroethylene (TCE); 1,1,1-trichloroethane (TCA); and their breakdown products, as well as acetone and isopropanol. Chemical and microbiological sampling verified that some degree of intrinsic (natural) anaerobic biodegradation was occurring. To optimize and accelerate contaminant breakdown, the natural subsurface conditions were converted to an aerobic state through the injection of air. Injection of gaseous-phase nutrients (triethyl phosphate and nitrous oxide) and methane were also included in the injection system to further stimulate the growth and biodegrading capabilities of native microbial populations.

Bedrock beneath the subject site consists of fractured shales and limestones of the Valley and Ridge physiographic province. The bedrock is overlain by thin, clay-rich overburden, with groundwater generally encountered at the overburden-bedrock interface. Outcrop fracture mapping, drilling and monitoring well installation, borehole geophysical surveys, pumping tests, and packer testing have been utilized to learn more about fracture size, orientation, and water-bearing properties of the subsurface.

In order to delineate the injection system zone of influence, a helium tracer test was conducted. This test produced observable effects in monitoring wells 25 feet or more away. Furthermore, monitored helium concentrations indicated the presence of preferential gaseous phase pathways within the fractured bedrock. This was confirmed by "short-circuiting" air flow observed in monitoring wells near the injection point.

Once air injection was initiated, it became apparent that the air zone of influence was not coextensive with the predicted helium zone, as evidenced by dissolved oxygen measurements in groundwater monitoring wells. This phenomenon may be the result of microbial utilization of oxygen which results in reductions of dissolved oxygen concentrations at the perimeter monitoring wells.

Variations in precipitation during the injection system operation resulted in varying backpressure in the injection well. This in turn limited the rate of air and nutrient injection, reducing the dimensions of the zone of influence during high water table conditions. Conversely, as the groundwater elevation dropped, injection could proceed at higher flow rates, expanding the zone of influence of the injection well. The injection system operation has been dynamically adjusted to correspond with changing subsurface conditions in the fractured bedrock groundwater regime. This enabled the successful conversion to aerobic conditions, with stimulation of native microbial populations, and accelerated contaminant degradation in the zone of influence.

The pilot system features sequential injection of air, gaseous-phase nutrients (nitrous oxide and triethyl phosphate), and methane to evaluate in-situ responses to aerobic microbial stimulation. Groundwater samples have been analyzed for VOCs (including breakdown products), microbial parameters (phospholipid fatty acids and methanotrophs by most probable number counts), nutrients, and groundwater quality parameters such as chlorides, methane, redox potential, and dissolved oxygen. Soil gas has been monitored for methane, carbon dioxide, and oxygen.

Groundwater VOC concentrations in the zone of influence, particularly for acetone, isopropanol, vinyl chloride, and cis-1,2-dichloroethylene, have decreased by one or more orders of magnitude following the air and nutrient injection campaigns. This data is consistent with increases in chlorides, nutrients, and dissolved oxygen, confirming that aerobic degradation processes have become dominant over the former anaerobic conditions.

This is largely attributed to increased microbial activity as evidenced by several orders of magnitude increases in observed biomass (based on phospholipid fatty acid, PLFA, measurements) in the four months since Interim Measure start-up. Further increases in microbial activity and VOC breakdown are expected to result from the methane injection phase that was initiated in July 1998.

Site 2. The site is in rural Virginia. Depth to groundwater is 8 to 10 ft (2.4 to 3 m), and average groundwater velocity is 1.2 cm/day. The formation consists of approximately 50 ft (15 m) of saprolitic overburden (hydraulic conductivity: $3 \bullet 10^{-4}$ cm/s) above bedrock. The maximum concentration of chlorinated VOCs —mainly tetrachloroethene (PCE) and TCE—is approximately 2000 µg/L; some hydrocarbon contamination is also present. The contamination is found throughout the saturated saprolite and the upper fractured bedrock. The areal extent of the plume is around 1 acre (0.4 hectare).

The in situ MTT evaluation was operated for 139 days. At the beginning of the test, bubbling and pressure buildup were detected in Well OW-1, possibly due to short-circuiting from the nearby injection well. To prevent stripping of TCE, this well was tightly capped for the rest of the test run.

Chloride was found at concentrations of 20 to 70 mg/L, precluding its use as a proxy for the degradation of approximately 2 mg/L of chlorinated ethenes. Nitrogen (nitrate-nitrite and total Kjeldahl) and phosphorus (orthophosphate and total phosphorus) were well below 1 mg/L, indicating that macronutrients would have to be added. Total organic carbon ranged from 1 to 10 mg/L, dissolved oxygen concentrations ranged from 0.1 to 2.8 mg/L, and pH ranged from 5.4 to 6.6. At the end of the evaluation, total Kjeldahl nitrogen was measured at 0.4 to 4 mg/L, whereas phosphorus (orthophosphate and total phosphorus) was mostly below the detection limit of 0.01 mg/L; the highest values were 0.11 mg/L, in Well MW-7. These low concentrations soon after the addition of the phosphate solution confirm that the subsurface environment is phosphorus-limited. Soil gas was also sampled and analyzed for methane and TCE. Background levels of methane were 2 to 5 ppmV, and no background TCE was detected (detection limit: 0.005 ppmV). On Day 21, and again on Day 48, methane concentrations of up to 4% by volume were found. We assume that disruptions in nutrient delivery limited carbon uptake, which allowed methane to build up in the subsurface. On Day 139, after four weeks of optimal operation, the methane levels had dropped to between 2 and 20 ppmV; 0.95 ppmV of TCE was measured in one vapor sampling well.

Trichloroethene (TCE) levels dropped from 2130 to 150 μg/L in the well initially exhibiting the highest concentration. The radius of influence of the air injection was approximately 30 ft (9 m). Methanotrophic bacteria increased over six orders of magnitude and eventually dominated the subsurface microbiota. The results indicate that, as long as nitrogen and phosphorus were reliably supplied, rapid (two to four weeks) growth of methanotrophs and associated oxidation of TCE followed. This pilot system was expanded to bioremediate the entire plume above bedrock; three additional injection wells were installed, along with observation wells, and a new TEP diffusion system was developed.

Conclusions. Fractured rock environments present some unusual obstacles to subsurface biostimulation. Careful control of injection pressure, increased screens, and increasing the number injection points can provide reasonable solutions. Helium tracer tests, respiration tests, pressure analysis over different injection conditions and measurements of microbial activity parameters, electron donors, electron receptors and daughter products help provide monitoring for controlling the bioremediation process in fractured rock.

Fracture Clogging by the Deposition of Colloidal Particles

John H. Kessler,
Electric Power Research Institute
3412 Hillview Ave
Palo Alto, CA 94304
Email: jkessler@paloalto.epri.com

James R. Hunt
Department of Civil and Environmental Engineering
University of California
Berkeley, CA 94720-1710
Email: hunt@ce.berkeley.edu

Colloid and particle transport in the subsurface has been recognized as an important process that requires quantitative understanding. The need arises from issues related to the long-term operation of geothermal and petroleum reservoirs and the safe disposal of toxic, hazardous, and nuclear waste in the subsurface. A number of literature reviews have summarized the possible importance of particle transport in porous media and the corresponding uncertainties that limit our understanding (McCarthy and Zachara, 1989; Ryan and Elimelech, 1996). The analysis of particle transport processes in porous and fractured media has almost exclusively been concerned with the initial deposition of single particles on clean mineral surfaces where the theories of particle transport and colloid stability could be applied. In contrast, the situations encountered in fractured rocks have flow paths with variable aperture widths and colloidal particles deposited on fracture surfaces. Similarly, the design and operation deep bed porous media filters for water treatment have had to address the coupling of particle deposition with fluid flow. The correct operation of such filters requires particle accumulation at much greater than monolayer coverage and such accumulation substantially alter the permeability.

Analysis of particle deposition within porous media filters has been empirically based and frequently utilizes site-specific pilot plant experimental data. Recent experimental work (Hunt et al., 1993; Boller and Kavanaugh, 1995; and Veerapaneni and Wiesner, 1997) has addressed the importance of the structure of the deposited material and how that deposited material causes a decrease in permeability of the medium. In general, these experimental studies are based on head loss and particle concentration measurements over relatively small (less than 10 cm) intervals along porous media filter columns. The permeability is observed to decrease by at least one order of magnitude when constant flow rates of at least 100 m/day are maintained. In these filtration applications, particle surfaces are altered by the addition of coagulants to promote aggregation and attachment, a situation not likely in the subsurface environment.

The literature on geothermal and petroleum reservoir engineering is very concerned about particle mobilization and permeability reduction by deposition and mineral precipitation although there is a disconnection between experimental data and theoretical models. For example, Bouddour et al. (1996) present a model for particle deposition and erosion that does not

couple deposition to fluid shear and assumes erosion is proportional to shear stress once shear stress exceeds a threshold. The model predictions are not compared with experimental observations.

Previously we examined colloid and dissolved contaminant transport through a single fracture when the walls of the fracture had a porous deposit (Kessler and Hunt, 1994). The presence of the deposited layer caused a dramatic increase in dissolved solute dispersion and a separation of colloidal contaminants from dissolved contaminants. That effort was based on earlier models from the chromatography literature, and an experimental study in the laboratory was undertaken to provide data on the dynamics of porous deposits in fractured media.

Experiments were conducted to provide data on long-term particle accumulation within a single fracture under controlled hydrodynamic conditions. An ideal fracture was constructed from two parallel plates of glass. The glass plates were 12.7 cm wide and 25.4 cm long with less than 0.0005 cm variability in thickness and planarity. The internal width of the fracture was 10.16 cm. The fracture spacing was set using Mylar™ gaskets. Micrometer measurements of the aperture width were 254±4 μm and measured head losses arrived at a fracture spacing of 257±1 μm using the cubic law for flow through a fracture. To maintain one-dimensional flow within the fracture, upstream and downstream channels across the entrance and exit of the fracture were added to provide uniform head and fluid composition. Flow was imposed either at a constant rate from a pump or with a constant head reservoir. Hydraulic gradients across the whole length of the fracture were determined from pressure transducer measurements.

All experiments utilized a suspension of montmorillonite clay. The montmorillonite was classified as SWy-1 from Crook County, Wyoming and was converted to the sodium form using a procedure described by Sposito et al. (1981). The experiments were conducted in a solution composed of 0.1 M NaCl, 0.1 M $CaCl_2$, and 1 g/L NaN_3 with a clay concentration of 500 mg/L. The high electrolyte and clay concentrations were adopted to promote particle deposition and minimize electrostatic repulsion between particles and glass surfaces. The sodium azide was necessary to minimize biological growth in the system during experiments that lasted up to 800 hours. The structure of the deposited clay and width of open channels were determined from photographs taken during deposition.

A series of experiments was conducted to investigate clay accumulation within the fracture and the release of that material under controlled hydrodynamic conditions. The intent is to understand how a fracture would fill with colloidal material and the characteristics of that deposited material in response to constant hydrodynamic forcing. At a fluid approach velocity of 0.22 cm/s the head loss across the fracture increased from 1.5 cm to 15 cm over an 800-hour period. The head loss during the experiment was not smooth and fluctuations corresponded to rearrangement of the deposited clay in the fracture. Photographs of the fracture showed that the clay deposit developed flow channels and these flow channels changed with time through erosion and reattachment of the clay aggregates. Dye studies revealed that some fluid was passing through the deposited clays although most of the flow was in the open channels. Head loss across the fracture was predictable based on the known flow rate and the measured open channel width. The hydrodynamic shear stress on the deposited solids reached a maximum value of about 5 dyne/cm^2 under constant flow rate conditions. This corresponds to the shear strength

of the deposited material in the fracture. By means of a mass balance on the clay solids, when 90% of the fracture was filled by a clay deposit, the volumetric clay concentration within the fracture was only 0.008 cm^3/cm^3. Such highly porous deposits are also observed during water filtration through porous media filters.

The experimental data has shown that long-term accumulation of clay aggregates is limited by the strength of the deposited solids. Considerable time is required to accumulate solids because of the need for deposition and erosion to select for stronger deposit structures that can resist the fluid shear. Under constant head conditions that are likely to be encountered in the field, the available fluid shear stress on the deposit would not be sufficient to maintain flow. These experimental and modeling results suggest that colloidal transport within fractured rocks will be self-limiting and result in the clogging and isolation of the contaminants associated with the colloidal material. The colloidal deposit could be resuspended if there where some physical or mechanical shock that exceeded the strength of the colloidal deposit.

References

Boller, M. A., and M. C. Kavanaugh (1995) Particle characteristics and headloss increase in granular media filtration, Water Research 29(4), 1139-1149.

Bouddour, A., J.-L. Auriault and M. Mhamdi-Alaoui (1996) Erosion and deposition of solid particles in porous media: homogenization analysis of a formation damage, Transport in Porous Media 25, 121-146.

Hunt, J. R., B.-C. Hwang, and L. M. McDowell-Boyer (1993), Solids accumulation during deep bed filtration, Environmental Science and Technology 27(6), 1099-1107.

Kessler, J. H., and J. R. Hunt (1994) Dissolved and colloidal contaminant transport in a partially clogged fracture, Water Resources Research 30(4), 1195-1206.

McCarthy, J. F., and J. M. Zachara (1989) Subsurface transport of contaminants, Environmental Science and Technology 23(5), 496-502.

Ryan, J. N., and M. Elimelech (1996) Colloid mobilization and transport in groundwater, Colloids and Surfaces A: Physicochemical and Engineering Aspects 107, 1-56.

Sposito, G., K. M. Holtzclaw, C. T. Johnson, and C. S. LeVesque-Madore (1981) Thermodynamics of sodium-copper exchange on Wyoming bentonite, Soil Science Society of American Journal 45(6), 1079-1084.

Veerapaneni, S., and M. R. Weisner (1997) Deposit morphology and head loss development in porous media, Environmental Science and Technology 31(10), 2738-2744.

Field Verification of TCE Matrix Diffusion in a Fractured Sandstone and Implications for Natural Attenuation and Remediation

Beth L. Parker and Sean N. Sterling
Department of Earth Sciences, University of Waterloo
200 University Avenue West, Waterloo, ON, Canada, N2L 3G1
blparker@sciborg.uwaterloo.ca.

Sedimentary rocks such as sandstones, siltstones, mudstones and shales are referred to as fractured porous media because of their appreciable primary porosity (intergranular porosity) in the matrix between fractures. The primary porosity of lithified sediments generally ranges from a few per cent up to 25%, several orders of magnitude greater than the secondary porosity due to the presence of fractures. Although the matrix has appreciable porosity, the permeability is governed by pore size, and these lithified sediments are referred to as dual permeability media given that the matrix generally has very low permeabilities compared to the fractures, which provide the main avenues for water and DNAPL flow, especially below the water table where the matrix pores are completely filled with water. This large difference between fracture and matrix porosities is an important feature of fractured sedimentary rocks and greatly influences the distribution of chlorinated solvent mass in these deposits in terms of DNAPL persistence as well as solute movement.

Groundwater samples collected from conventional monitoring wells represent a mixture of waters from various fractures, which can be biased in several ways. In some cases, one fracture with exceptionally high concentrations can cause an appearance of relatively high concentrations throughout the open interval in the borehole if this fracture has high hydraulic conductivity; or fractures with high hydraulic conductivity but low concentration levels can mask the presence of high concentration zones. There is no way to determine from monitoring well data alone whether the water samples from the well provide a representative average or a severely biased result. In addition, these groundwater samples are rarely in equilibrium with the pore water concentrations in the matrix and therefore, tell us nothing about the distribution of chemical mass between the relatively immobile pore water of the matrix as compared to the free-flowing water in the fractures. The contaminants such as trichloroethene (TCE) migrate into these low permeability yet porous matrix blocks between fractures by molecular diffusion, which is driven by the chemical's concentration gradient in the aqueous (groundwater) phase. The matrix blocks between the fractures serve as large reservoirs for contaminant mass allowing matrix diffusion alone to cause complete dissolution of immiscible-phase solvents initially present in fractures. Therefore, matrix diffusion diminishes concentrations within plumes, which is a form of natural attenuation.

To investigate this form of natural attenuation, the distribution of TCE in a sandstone matrix was determined by chemical analysis of rock core subsamples taken from two boreholes at an industrial site in southern California. Use of TCE over several decades has resulted in contamination in the underlying Cretaceous Age arkosic sandstone, which contains occasional

beds of siltstone and claystone. Estimated hydraulic conductivities of this formation range from 1.5×10^{-5} to 8.5×10^{-11} cm/s and matrix porosities range from 5 to 16% based on measurements on 11 core samples. The two corehole locations were selected where existing monitoring wells installed within the upper 100-ft of the formation yielded groundwater concentrations of TCE in excess of 10 mg/L. Continuous cores were collected from top of rock (at or near groundsurface) to a depth of 360 ft into rock. Using a field protocol developed specifically for this project, small subsamples (15-180 grams wet-weight) were taken from the core for immediate preservation in 120 ml glass VOA bottles containing a pre-weighted amount of high purity methanol. Three hundred and fifty-nine subsamples were collected and preserved in methanol in the field, of which 271 samples were analyzed. The vertical spacing between discrete-depth subsamples generally ranged between 5 and 10-ft, with 0.5 to 1-ft spacing near many apparent fractures identified during core inspection. The methanol-extract analysis provides total concentrations for TCE per unit-weight of water-saturated rock. These data for the two locations are presented in Figures 1 and 2. Calculations using parameter values for matrix porosity and sorption convert these concentrations to equivalent groundwater concentrations in the matrix pore water.

The rock core concentrations with depth shown in Figures 1 and 2 exhibit large contrasts in TCE distribution. At the location in Figure 1, which is closest to a historical TCE release location, the highest TCE concentrations occur in the vadose zone between 30 and 70-ft depths. At this location, the water typically fluctuates between 70 and 80ft below ground surface (bgs). Almost no TCE was found greater than 130-ft bgs. However, at the second location (Figure 2), no detectable concentrations were obtained in the vadose zone, but high concentrations are observed to a maximum depth of 250-ft bgs. The detection limit for rock core analyses, expressed as equivalent groundwater concentration, varies from sample to sample and ranges from 100-500 ug/L. The highest concentration measured in the matrix pore water was 40 mg/L using a representative retardation factor of 3.75 and matrix porosity of 12%. There is considerable variability in measured concentrations over short distance intervals, indicating the location of contaminant pathways. The profiles of TCE concentration vs. depth show thick zones of TCE at relatively high concentration. Therefore, because the matrix porosity is very large relative to the fracture porosity and because sorption occurs primarily in the matrix, it is apparent that nearly all of the TCE mass at the two locations exists in the rock matrix where groundwater flow has minimal influence. This TCE mass in the matrix serves as a reservoir causing long-term groundwater contamination.

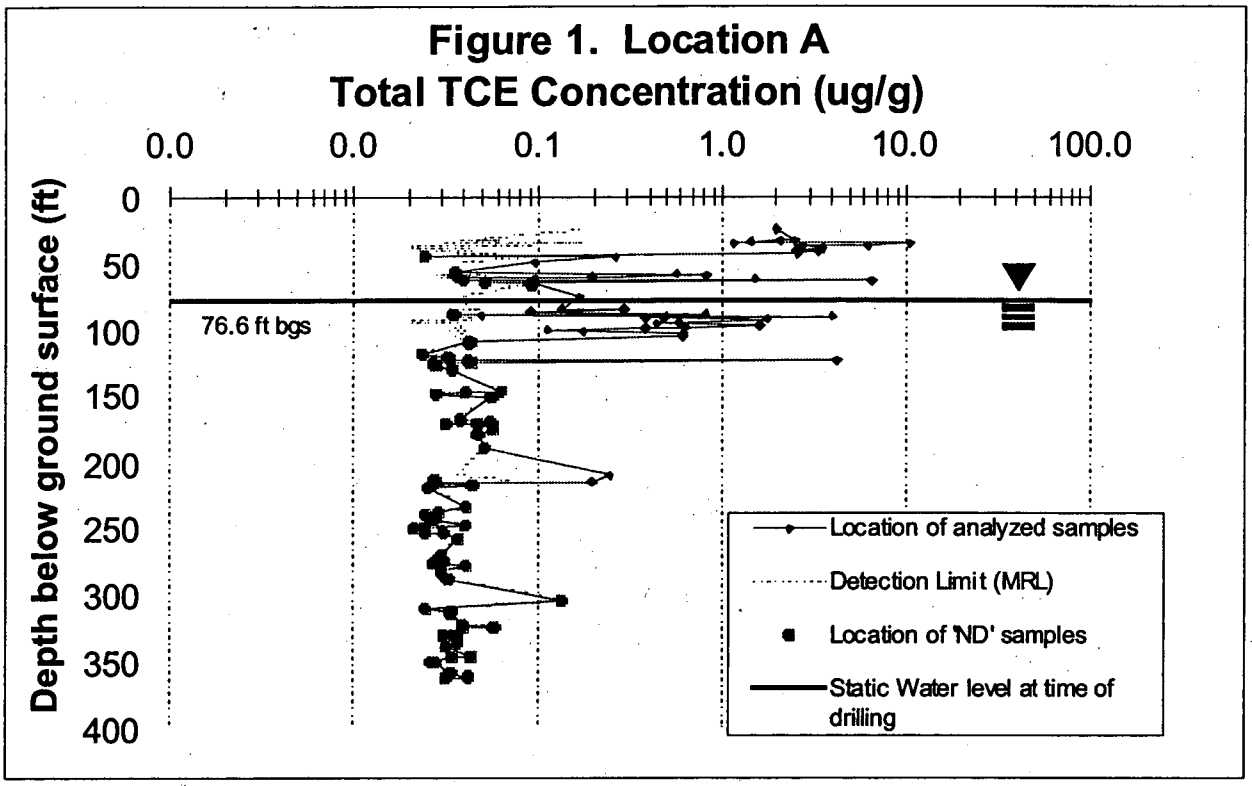
Figure 1. Location A
Total TCE Concentration (ug/g)
0.0
0.0
0.1
1.0
10.0
100.0
Depth below ground surface (ft)
0
50
100
150
200
250
300
350
400
76.6 ft bgs
Location of analyzed samples
Detection Limit (MRL)
Location of 'ND' samples
Static Water level at time of drilling

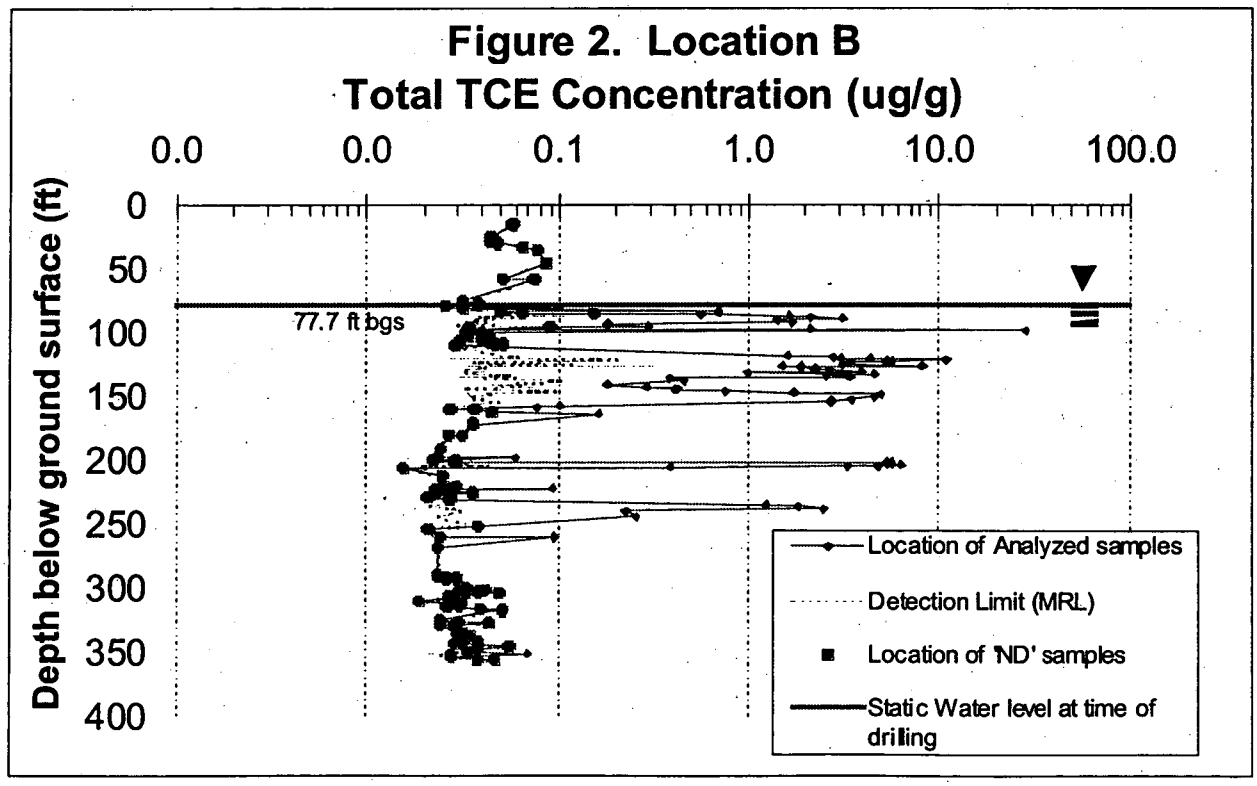
Figure 2. Location B
Total TCE Concentration (ug/g)
0.0
0.0
0.1
1.0
10.0
100.0
Depth below ground surface (ft)
0
50
100
150
200
250
300
350
400
77.7 ft bgs
Location of Analyzed samples
Detection Limit (MRL)
Location of 'ND' samples
Static Water level at time of drilling

Session 10:
NUCLEAR WASTE DISPOSAL IN FRACTURED ROCKS

Geologic Disposal of Nuclear Waste - Progress Made and Lessons Learned

Bo Bodvarsson
Lawrence Berkeley National Laboratory
Berkeley, California, 94720
GSBodvarsson@lbl.gov

Geologic disposal of high-level radioactive waste is the preferred means of permanent disposal. Many countries world wide are currently investigating and characterizing hypothetical and potential sites for disposal. The different geological media considered include granite, salt, volcanic tuffs, shales, clays, marl and basalts (Witherspoon, 1996). The United States is the only country that has selected a potential site for a repository, the Yucca Mountain site in Nevada. Studies are far along in evaluating the suitability of this unsaturated volcanic tuff site for permanent disposal of radioactive waste. Most other countries are currently performing regional screening investigations to locate favorable sites (e.g., Bulgaria, China, Hungary, Ukraine); and/or are conducting advanced underground testing at research sites (e.g., Belgium, Canada, Sweden, Switzerland, Spain, Japan).

Paul Witherspoon was a pioneer in advocating and developing underground testing strategies. He was the leader for the first large-scale underground testing facility at the Stripa Mine in Sweden, where an international collaboration effort, primarily funded by the United States, was carried out from 1977 to 1980. The testing program developed at Stripa consisted of many thermal, geophysical, and hydrological measurements, including extensive hydrological packer testing, large-scale drift seepage tests, conservative and reactive tracer tests, and an in-situ heater tests. The testing program provided the foundation for subsequent underground testing projects of fractured rocks such as those at Åspo, Sweden; NAGRA, Switzerland; and Yucca Mountain, USA. It is now acknowledged that underground testing is essential for any potential geologic site for the disposal of high-level radioactive waste.

The site characterization at Yucca Mountain (YM) has proceeded for over a decade, and is now nearing completion. In 1988, the Site Characterization Plan (SCP; DOE, 1988) for YM was completed. Since then, some of the many proposed tests have been carried out. However, as the SCP was extremely ambitious and comprehensive in scope, perhaps only about half of the planned testing activities have been carried out. As the project matured, some tests in the original SCP were deemed unnecessary, while other tests were added in order to reduce uncertainties in important hydrological, thermal, or geochemical parameters. It is of interest to note that most of the current in-situ tests in the Exploratory Studies Facility (ESF), which address key issues such as seepage into drifts, fracture/matrix interaction, lateral diversion, and fault flow (see Figure 1), were not explicitly a part of the suite of tests described in the SCP. On the other hand, other important ongoing large-scale tests, such as the in-situ transport test at Busted Butte (about 7 km from YM) and the drift-scale heater tests, were planned in the SCP.

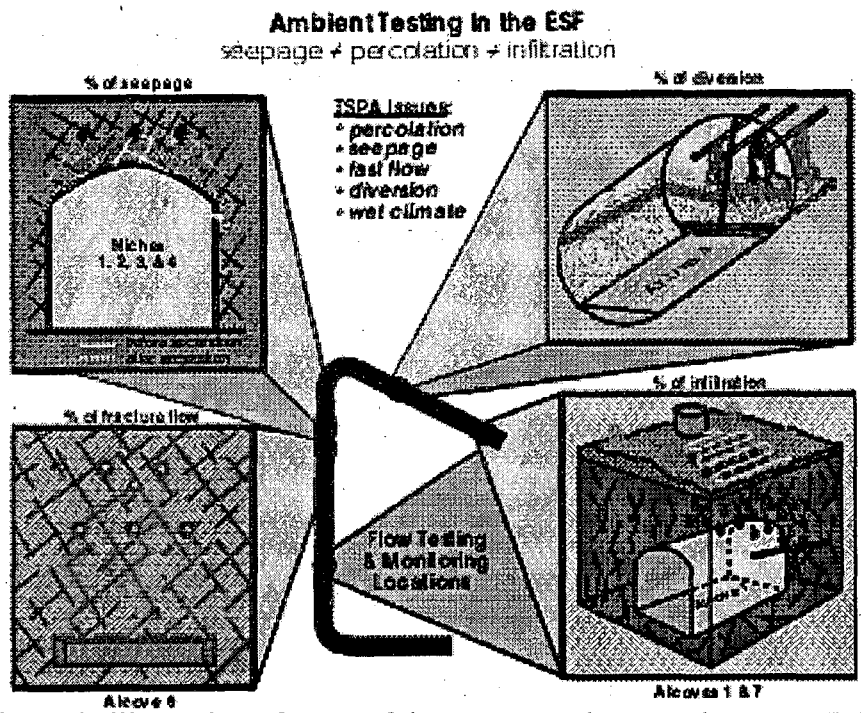

Figure 1. A schematic illustration of some of the current underground tests at YM, including seepage tests, fracture/matrix interaction tests, and lateral diversion tests.

Along with the site-characterization activities at Yucca Mountain, a series of numerical process models was developed during the last decade, including models for unsaturated flow (Bodvarsson et al, 1997) and transport (Robinson et al, 1997), saturated zone flow (Czarnecki et al, 1997) and transport (Zyvoloski et al, 1997) and coupled-processes (Hardin, 1998). Many of these models have become extremely detailed, complex, and sophisticated, involving hundreds of thousands of grid blocks. They also consider the most relevant processes, including multi-phase, multicomponent flow, and transport, nonisothermal conditions with multiple reactive chemical components and complexities associated with fracture/matrix interchanges. The calibration activities for some of these models have been emphasized for model reliability, and so are model predictions for experiments. Figure 2(a) shows examples of numerical gridding, including inclined faults, and Figure 2(b) shows simulation results of calcite dissolution/precipitation in response to water flow through the mountain from the UZ flow model.

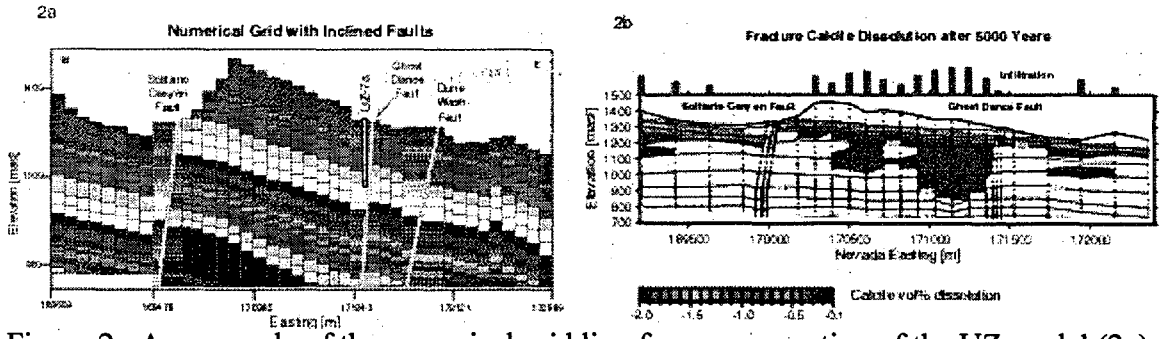

Figure 2. An example of the numerical gridding for a cross section of the UZ model (2a). Simulation results of calcite precepitation/dissolution (2b).

This paper provides an analysis of the evolution of field testing and modeling at YM in light of the evolution in the conceptual model, and the importance of various data and models to the performance assessment of the site. In addition, an evaluation is made of remaining issues, data uncertainties and model deficiencies. The detailed discussion of the work at Yucca Mountain illustrates the progress made in research related to nuclear waste disposal since the pioneer work performed at Stripa in the late 70's and early 80's. The approach of close integration between modeling and field measurements has been developed and advanced to solve the many complex and coupled interactions between the various processes.

References

Bodvarsson, G.S.; Bandurraga, T.M.; and Wu, Y.S. eds. 1997. *The Site Scale Unsaturated Zone Model of Yucca Mountain, for the Viability Assessment.* Lawrence Berkeley National Laboratory Report, LBNL-40376. Berkeley, California: Lawrence Berkeley National Laboratory.

Czarnecki, J.B.; Faunt, C.C.; Gable, C.W.; and Zyvoloski, G.A. 1997 (in prep.). *Hydrogeology and Preliminary Calibration of a Preliminary Three-Dimensional Finite-Element Ground-Water Flow Model of the Site Saturated Zone, Yucca Mountain, Nevada.* Milestone Report SP23NM3. Submitted for release as a U.S. Geological Survey Administrative Report. Denver, Colorado: U.S. Geological Survey.

DOE (U.S. Department of Energy) 1988. *Yucca Mountain Site Characterization Plan, Yucca Mountain Site, Nevada Research and Development Area, Nevada.* DOE/RW-0199. Washington, D.C.: U.S. Department of Energy, Office of Civilian Radioactivity Waste Management.

Robinson, B.A.; Wolfsberg, A.V.; Viswanathan, H.S.; Bussod, G.; Gable, C.W.; and Meijer, A. 1997. *The Site-Scale Unsaturated Zone Transport Model of Yucca Mountain.* Los Alamos, New Mexico: Los Alamos National Laboratory.

Hardin, E.L. 1998. *Near-Field/Altered Zone Models.* Livermore, California: Lawrence Livermore National Laboratory.

Witherspoon, P.A. ed. 1996. *Geological Problems in Radioactive Waste Isolation-Second Worldwide Review.* Lawrence Berkeley National Laboratory Report. LBNL-38915. Berkeley, California: Lawrence Berkeley National Laboratory.

Zyvoloski, G.A.; Robinson, B.A.; Birdsell, K.H.; Gable, C.W.; Czarnecki, J.; Bower, K.M.; Faunt, C. 1997. *Saturated Zone Radionuclide Transport Model.* Los Alamos, New Mexico: Los Alamos National Laboratory.

Effective-Porosity and Dual-Porosity Approaches to Solute Transport in Fractured Tuff of the Saturated Zone at Yucca Mountain: Implications for Repository Performance Assessment

by Bill W. Arnold[1], Hubao Zhang[2], and Alva M. Parsons[1]

Transport of solutes in fractured volcanic media of the saturated zone (SZ) at Yucca Mountain is governed by complex interactions among processes, including advection in fractures (and potentially in the matrix), dispersive processes, sorption, and diffusive transfer between groundwater in the fractures and in the matrix. These processes in the SZ influence repository performance by affecting the travel time of radionuclides to a location where they are likely to be pumped from a well and by changing their concentrations in groundwater. The flow pathway in the SZ traverses fractured tuffs and alluvium to reach the well. Characterization of contaminant transport in the fractured media requires simplified models of these processes in order to implement probabilistic analyses required for a Total System Performance Assessment (TSPA) that utilizes multiple realizations of the SZ system to capture the range in uncertainty and variability. For fractured media, two simplified models have been used in this study.

One possible simplified model uses the effective-porosity approach. In this approach, the medium is conceptualized as a single continuum, in which some fraction of the total matrix and fracture porosity is available for solute migration and storage during transport. This fraction available for solute transport is quantified by an effective porosity term. However, the volume of the medium accessible to the solute is, in reality, a complex function of fracture network geometry, diffusive properties of the matrix and solute, and history of the system. The effective porosity is thus a "lumped" parameter that incorporates uncertainty in underlying processes and results in an approximate solution for solute transport that implicitly accounts for matrix diffusion.

An alternative simplification is the dual-porosity model, in which the fractured media are conceptualized to consist of two continua. One continuum represents mobile groundwater (generally in the fractures) and the other continuum corresponds to immobile groundwater (generally in the matrix). This approach explicitly accounts for diffusion between fractures and matrix, but generally simplifies fracture network geometry due to the continuum assumption.

The objective of this study is to evaluate the potential inaccuracies of the effective-porosity approach relative to the dual-porosity approach, within the context of radionuclide transport calculations in the SZ for the TSPA for Viability Assessment (TSPA-VA) (DOE, in prep.). Simulations of radionuclide migration in the SZ were performed for the TSPA-VA using the effective-porosity approach in 1-D streamtubes from beneath the potential repository at Yucca Mountain to a distance of 20 km. Uncertainty and variability in SZ flow and transport were probabilistically assessed by stochastic variation of input parameters including effective porosity, longitudinal dispersivity, and flowpath length in alluvium. Flowpath length in the alluvium is

[1] Sandia National Laboratories, P.O. Box 5800, MS 0778, Albuquerque, NM 87185, e-mail: bwarnol@sandia.gov.
[2] Duke Engineering Services, Albuquerque, NM.

potentially significant to radionuclide transport in this system because of the larger values of effective porosity (and thus, slower pore velocities) for this unit relative to the fractured units. All simulations were performed using the FEHM computer code (Zyvoloski et al., 1995). The resulting concentration breakthrough curves for 100 Monte Carlo realizations of the SZ transport system are shown in Figure 1 and reflect significant differences in median travel times and apparent longitudinal dispersion.

Solute transport using the dual-porosity approach was simulated with FEHM for the TSPA-VA model domain using a 2-D numerical model. The conceptual model was transport through continuous parallel fractures in the volcanic units and porous flow in the alluvium as shown in Figure 2. The 2-D dual-porosity model domain extended from the center of a fracture to the middle of an adjacent matrix block, for various values of the fracture spacing. The specific discharge was held constant at 0.6 m/yr (as in the 1-D effective-porosity simulations). Thus, the groundwater flow rate and the fracture aperture were varied as functions of fracture spacing such that the groundwater velocity in the fracture remained constant with variation in fracture spacing. Significant groundwater flow occurred only in the fracture due to high permeability contrast between fracture and matrix in the model. A high-resolution, exponentially spaced grid consisting of 50 nodes in the transverse direction was employed to accurately simulate diffusive movement of solute in the matrix.

The results from the 2-D dual-porosity model simulations for varying values of fracture spacing in the fractured volcanic units are shown by the dashed curves in Figure 3. The solid curves show the concentration breakthrough curves from the effective-porosity model for various values of effective porosity for the volcanic units. The concentration breakthrough curve from the dual-porosity model with a fracture spacing (s) of 0.2 m is nearly the same as the breakthrough curve from the effective-porosity model with effective porosity equal to the matrix porosity for fractured volcanic units. The concentration breakthrough curve for a fracture spacing of 200 m is similar to the breakthrough curve for low values (less than 0.005) of effective porosity in the volcanic units. Note that the travel times in the concentration breakthrough curves for low values of effective porosity in Figure 3 are due almost exclusively to the higher value of porosity (0.25) assigned to the alluvium relative to the fractured units. Greater apparent dispersion and characteristic long tails on the concentration breakthrough curves result from fracture spacing in the range of approximately 1 m to 100 m.

Comparison of Figure 1 and Figure 3 indicates that the effective-porosity approach, as implemented in TSPA-VA analyses, has potentially significant differences from the dual-porosity approach, but these inaccuracies are generally conservative from the perspective of repository performance. Conservatism is defined here as computational results that underestimate radionuclide travel times or overestimate radionuclide concentrations relative to other computational methods. The shortest median travel times among the TSPA-VA realizations using the effective porosity approach shown in Figure 1 are shorter than the median travel times for the fastest breakthrough curves shown in Figure 3. This is because the effective porosity in the alluvium was stochastically varied to include lower values in the TSPA-VA analyses and was held constant at a higher value (0.25) in the simulations shown in Figure 3. The longest median travel times among the TSPA-VA realizations are shorter than the longest median travel times shown in Figure 3. This result is because none of the 100 TSPA-VA

realizations shown in Figure 1 simultaneously sampled values of effective porosity near the matrix porosity values for all four hydrogeologic units. The simulated concentrations using the 2-D dual-porosity model shown in Figure 3 are significantly lower for intermediate values of fracture spacing at later times (e.g., 8000 years) than the simulated concentrations from the effective-porosity approach. This result also indicates that the effective-porosity approach is conservative from the perspective of repository performance. Results from the 2-D dual-porosity model for intermediate values of fracture spacing indicate significantly greater spreading of the breakthrough curves (greater apparent dispersion) and earlier first arrival of solute than the effective-porosity approach as shown in Figure 3. The lower apparent dispersion from the effective-porosity approach is conservative in the context of TSPA calculations because longitudinal dispersion leads to attenuation of peak concentrations resulting from pulses of radionuclide mass at the source. The earlier first arrival of solute mass exhibited by the 2-D dual-porosity model indicates that the effective-porosity approach is potentially non-conservative. However, comparison of the first-arrival times shown for various fracture spacings in Figure 3 and the first-arrival times shown in Figure 1 indicates that the potential for early radionuclide arrival was represented in the TSPA-VA realizations.

The effective-porosity approach as implemented in the TSPA-VA analyses of SZ transport is conservative compared to the dual-porosity approach from the perspective of both radionuclide concentrations and generally for travel times. Future TSPA analyses of potential repository performance at Yucca Mountain may require more explicit modeling of matrix diffusion to move away from the apparent conservatism in the effective-porosity approach.

References:

DOE (U.S. Department of Energy). in prep. *Viability Assessment of a Repository at Yucca Mountain*. DOE/RW-xx-xxx, Vol 3. Las Vegas, Nevada: Civilian Radioactive Waste Management System, Management and Operating Contractor. MOL.19980729.0421 through MOL.19980729.0426.

Zyvoloski, G.A.; Robinson, B.A.; Dash, Z.V.; and Trease, L.L. 1995. *Models and Methods Summary for the FEHMN Application, Revision 1*. LA-UR-94-3787, 70 pp. Los Alamos, New Mexico: Los Alamos National Laboratory. TIC Catalog Number: 222337.

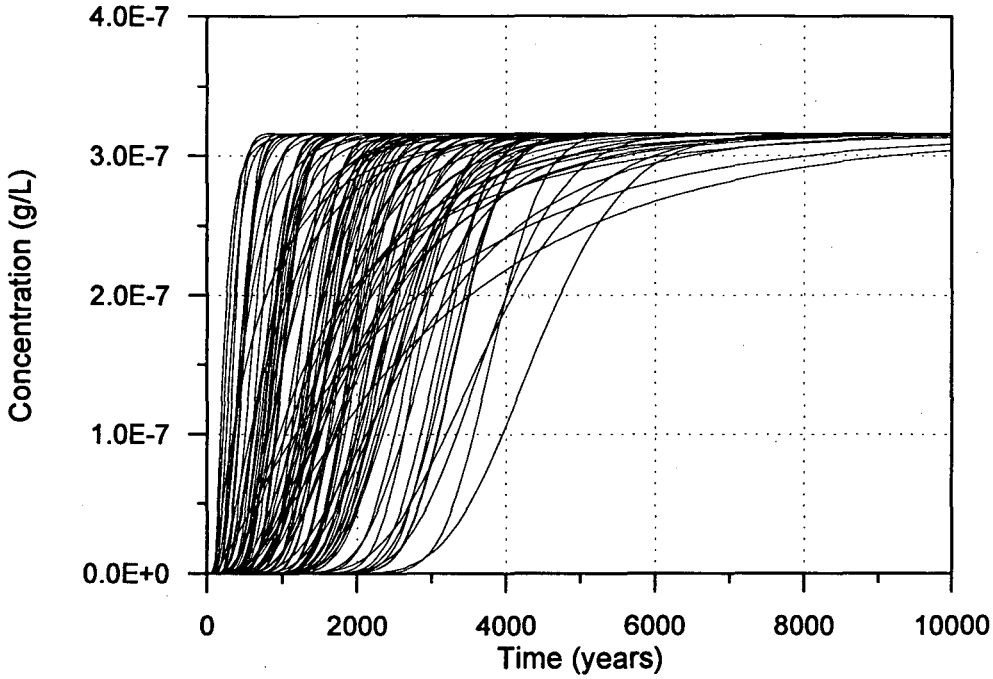

Figure 1. Simulated concentration breakthrough curves at a distance of 20 km from the potential repository using the 1-D effective-porosity transport model as implemented in TSPA-VA analyses. Results are shown for 100 realizations for a non-sorbing, non-decaying solute, with effective porosity and longitudinal dispersivity as stochastic parameters. A steady solute source of 1 g/yr was specified.

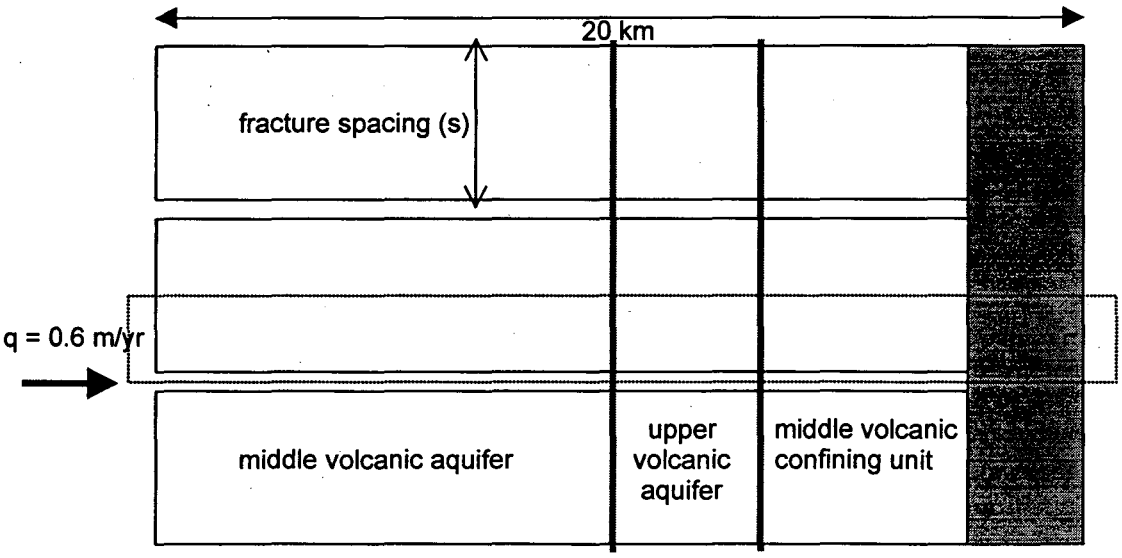

Figure 2. Schematic diagram showing the model of SZ dual-porosity transport in parallel fractures in tuff. The shaded area corresponds to non-fractured alluvial porous media. The 2-D model domain for the dual-porosity simulations is outlined by the dotted line. The specific discharge was a constant value of 0.6 m/yr in all simulations.

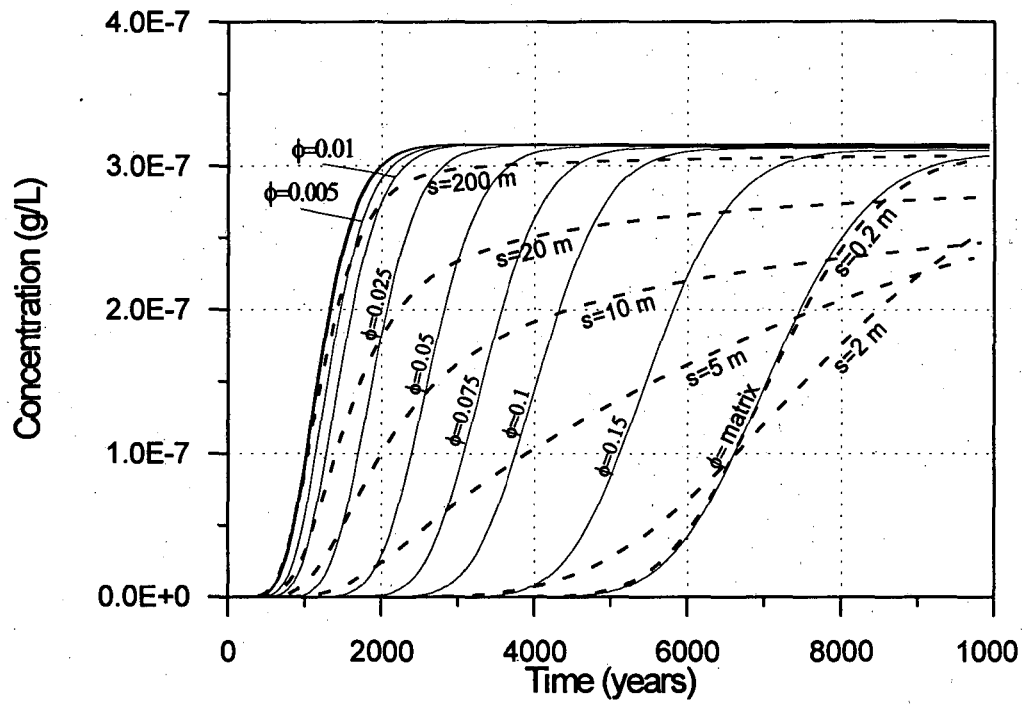

Figure 3. Simulated concentration breakthrough curves at a distance of 20 km from the potential repository using the 1-D effective porosity model and the 2-D dual-porosity model. The solid curves show the concentration breakthrough for various values of effective porosity (ϕ) for the volcanic units. The dashed curves show the concentration breakthrough for various values of fracture spacing (s) in the volcanic units. The porosity of the alluvium unit is constant (0.25) in all simulations.

Numerical Studies of Effects of an Excavation Damage Zone and Discrete Fractures on ^{129}I Transport From a Used Nuclear Fuel Waste Disposal Repository in Low-Permeability Rock

T. Chan,[1,3] M. R. Jensen,[2] N.W. Scheier,[1] and F.W. Stanchell[1]

[1]AECL Whiteshell Laboratories, Pinawa, Manitoba, Canada
[2]Ontario Hydro, Toronto, Ontario, Canada
[3]Correspondence address: c/o Ontario Hydro H16, 700 University Ave., Toronto, Ontario, Canada M5G 1X6 E-mail: CHANT@AECL.CA

The concept proposed by Atomic Energy of Canada (AECL) for disposal of Canada's nuclear fuel waste involves isolating the waste in corrosion-resistant containers emplaced in a sealed vault (repository) at a depth of 500 to 1000 m in plutonic rock of the Canadian Shield. The disposal vault would be a network of horizontal tunnels and disposal rooms excavated deep in the rock, with vertical shafts extending from the surface the tunnels. The waste containers would be placed either in the rooms (in-room emplacement) or in holes drilled from the rooms (in-floor borehole emplacement). Then the rooms, tunnels, and shafts would be filled and sealed with buffer, backfill, and possibly other vault seals. In the reference case study presented in the Environmental Impact Statement (EIS) the vault was assumed to be located at a nominal depth of 500 m in a conceptual geosphere with hydrogeological characteristics similar to those measured at the site of AECL's Underground Research Laboratory (URL) in the Whiteshell Research Area (WRA), southeastern Manitoba. Important features included a saturated, sparsely-fractured, very low-permeability granitic rock containing the waste emplacement areas of the vault with a number of major low-dip or near-vertical fracture zones that are much more permeable. A domestic water-supply well was assumed to exist and to draw water from a major low-dip fracture zone LD1 that transects the rock body in the vicinity of the vault. The shortest distance between the vault and fracture zone LD1 (the waste exclusion distance) was about 46 m.

Safety analysis indicated that the 46-m thick SFR, in which solute transport is dominated by molecular diffusion, would be the main barrier to radionuclide migration from the vault to the biosphere. A natural question to ask is whether excavation damage and discrete fractures would compromise the safety of the disposal system by acting as preferential pathways for radionuclide transport. This paper summarizes two finite-element studies conducted to investigate the effects of an excavation damage zone (EDZ) and one or two discrete fractures in the SFR surrounding the vault on groundwater mediated transport of ^{129}I - the radionuclide found by the safety analysis to be responsible for almost all the radiological dose at 10^4 a and 10^5 a after vault closure- to fracture zone LD1 and thence to the biosphere.

In Numerical Study No. 1 the simulations are performed using a combination of 3-D site-scale saturated groundwater flow models and corresponding 2-D solute transport models. All simulations are performed using AECL's MOTIF finite-element code which has special planar elements and line (pipe) elements for explicit representation of discrete fractures in 3-D or 2-D

models. Transport processes modelled included advection, dispersion, diffusion and radioactive decay. In particular, matrix diffusion and dispersion were simulated. The 3-D groundwater flow model, the central portion of which is illustrated, covers a volume of 10 km x 9 km x 1.5 km

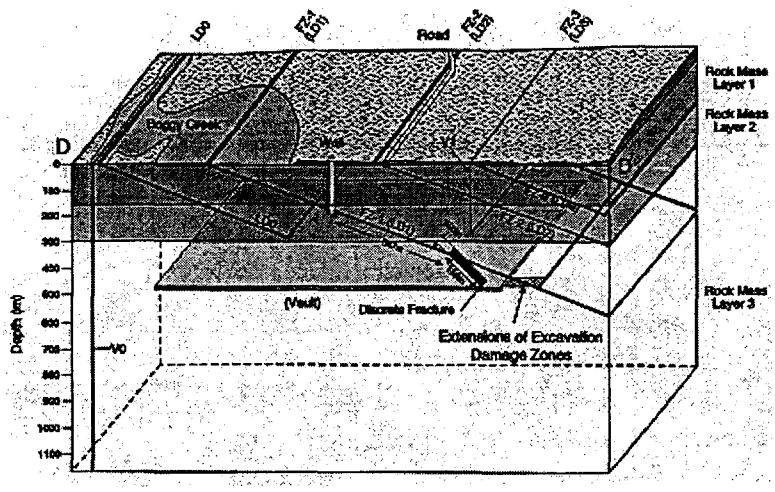

deep and is based on the EIS reference case. This model block is divided into approximately 35 400 3-D hexahedral elements and 10 planar quadrilateral elements. The background rock mass is idealized as three layers of equivalent porous media with permeability 10^{-15}, 10^{-17} and 10^{-19} m^2 and porosity 0.005, 0.004, and 0.003 for layers 1, 2 and 3, respectively. The major vertical and low-dip fracture zones are all 20-m thick with a permeability of 10^{-13} m^2 and a porosity of 0.01. The well is assumed to be pumping water at 200-m depth from LD1 at the steady rate of 1 330 m^3/a. The vault is represented as a 5-m high slab approximately 3 km^2 in area with hydraulic properties obtained by averaging backfill and SFR properties. The model also includes a 1-m thick EDZ that forms an envelope around the vault and a discrete fracture, or a narrow fracture zone modeled as a discrete fracture, that connects the vault to fracture zone LD1. The EDZ has a permeability of 10^{-18} m^2 above and 10^{-17} m^2 below the vault. The discrete fracture is about 158-m long, 100-m wide, dips at 45° and has an effective hydraulic aperture of 10 μm or, in the case where it represents a narrow fracture zone, has an aperture of 80 μm.

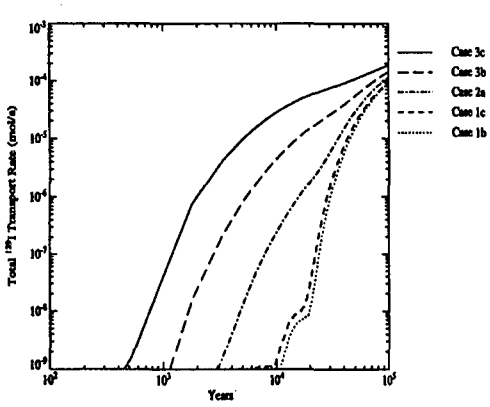

The 2-D solute transport model is located along vertical section D-D′ and covers an area approximately 2450-m long by 620-m deep bounded by fracture zones V0 and LD1. It is discretized into approximately 11 800 2-D quadrilateral elements and 20 line elements. The maximum element size is approximately 10 metres. Head values calculated by the 3-D flow model are projected onto 2-D section and used as the input flow field for the transport model. The rate of transport of ^{129}I into fracture zone LD1 and the associated approximate rate of radiation dose to the critical group of humans are

estimated as a function of time over a period of 10^5 years. Twelve different cases have been simulated. In some cases a 100-m wide strip of the EDZ is assumed to extend from the edge of the vault to fracture zone LD1.

The results of this numerical study indicate that (i) the presence of the discrete fracture (DF), its aperture and the distance of unfractured rock between the fracture and a waste container in the vault all affect the transport rate of ^{129}I very significantly (Cases 2a-10 μm DF, 3b and 3c- 80 μm DF vs. Cases 1b and 1c- no DF) ; (ii) The EDZ and the extension of the EDZ from the vault to fracture zone LD1 has only minor effects on ^{129}I transport (Cases 1b and 3b- no EDZ vs. Cases 1c and 3c- with EDZ) and (iii) the estimated dose rate to a member of the critical group is well below the *de minimis* regulatory limit of 50 μSv/a in all simulated cases at 10^4 years after closure and in most cases at 10^5 years after closure.

In Numerical Study No. 2 the geometry of the major fracture zones in the site-scale groundwater flow model is stylized but a 242 m x 90 m x 200 m (deep) block including three disposal rooms and its immediate environs is analyzed in detail by 3-D (room-scale) groundwater flow and solute transport models. As illustrated in the vertical section the site-scale model includes three connected major fracture zones and a domestic water-supply well pumping water from a fracture zone that was connected to the vault 50 m below by a pair of 200-m squared discrete fractures. The undamaged rock at vault level was assumed to be either SFR with 10^{-19} m^2 permeability and 0.003 porosity or moderately fractured rock (MFR) with 10^{-17} m^2 permeability and 10^{-4} porosity for the MFR case. In SFR the EDZ hydrualic properties ranged from a minimum-damage case of 10^{-18} m^2 permeability and 0.005 porosity to a maximum-damage, stress-relief notch of failed rock case - based on URL experience - of 10^{-13} m^2 permeability and 0.03 porosity. In MFR the EDZ permeability varies from a maximum-damage case of 10^{-15} m^2 to no damage. Discrete fracture aperture ranged from a median-value case of 25 μm to a pessimistic case of 80 μm. Well demand ranged from zero through a median-value of 1330 m^3/a to a maximum of 18 000 m^3/a. The site-scale model block is discretized using 21 619 3-D solid elements, 60 planar elements and 21 line elements. The line elements representing the disposal rooms have equivalent properties calculated from those of the backfill, buffer and the EDZ.

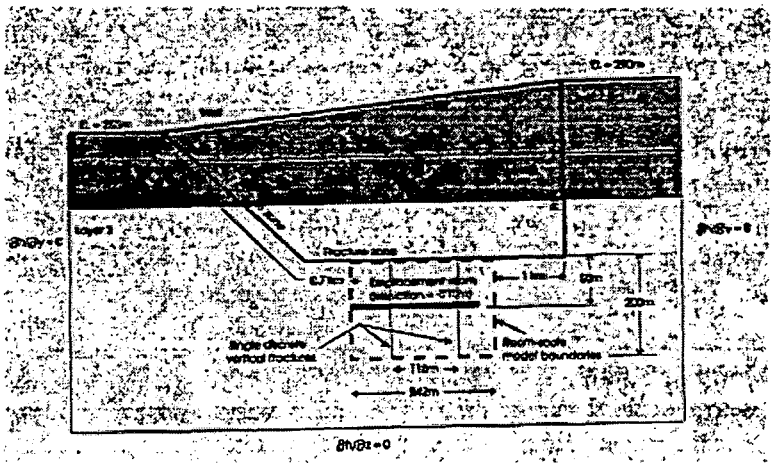

The flow field calculated by the site-scale flow model is used to determine the head boundary conditions for the room-scale flow model. In the transport model ^{129}I is assumed to be released from a pinhole defect in a container located 10 m from a discrete fracture. The room-scale model for in-room (IR) emplacement is divided into 56084 3-D (hexahedral or triangular prism) solid elements and 1046

(quadrilateral or triangular) planar elements. Element size ranges from about 0.04m to 50 m. For in-floor borehole (BH) emplacement the room-scale model is divided into 46565 3-D (hexahedral) solid elements and 958 (quadrilateral) planar elements. Element size ranges from about 0.06 m to 58 m. In both discretization schemes the mesh Peclet number ranges from 0.1 to 10. Great care has been exercised to match the finite-element mesh to the geometry of the rooms, the discrete fractures, the EDZ, the backfill, buffer and the container. Eighteen different cases are simulated to investigate the effects of the EDZ under various conditions of EDZ rock damage, the method of container emplacement (in room or in borehole), well pumping rate, discrete fracture properties, and buffer and backfill properties.

The results of Numerical Study No. 2 indicate that (i) although a highly permeable EDZ would lead to earlier release of ^{129}I to the fracture zone, at 10^4 years after vault closure the maximum-damage EDZ cases (e.g. BH-SFR4 and IR-SFR4) would lead to an ^{129}I release rate only about three times higher than the minimum-damage cases (e.g. BH-SFR5 and IR-SFR5); (ii) the annual radiation dose in an extremely pessimistic case with a maximum-damage EDZ, maximum-demand well (18, 000 m^3 per year), pessimistic discrete fractures (80 μm aperture) and pessimistic buffer and backfill properties was estimated to be approximately 0.12 μSv/a in SFR and 0.16 μSv/a in MFR, a factor of 400 or 300 below the *de minimis* regulatory limit of 50 μSv/a and (iii) transport of ^{129}I to the fracture zone occurs primarily through the discrete fracture 10 m downstream of the defective container, but an inspection of the evolution of concentration contours reveals that the radionuclide is also diffusing and dispersing from the EDZ and the discrete fracture into the rock and the backfill. Storage of the radionuclide in the pore water of the backfill and the rock is likely responsible for its slow migration. Consequently, assessment of the effects of the EDZ and discrete fractures on repository isolation performance based solely on calculation of groundwater flux by flow modelling or travel time calculation by particle tracking can be quite misleading

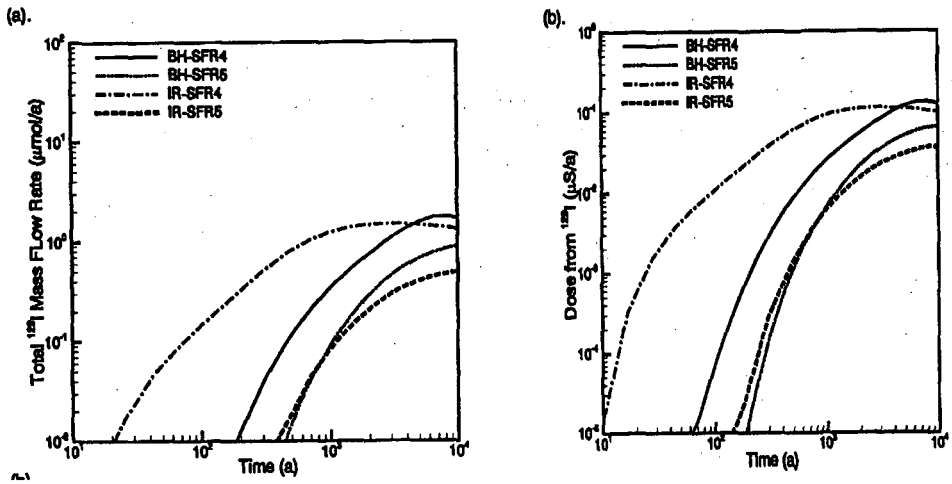

In both numerical studies matrix diffusion is found to significantly slow down radionuclide transport from the vault to the nearby major fracture zone LD1. In the most pessimistic case in Study No. 1 the average linear water velocity in the discrete fracture is found to vary between 1 and 7 m/a. This would indicate a groundwater travel time of 100 years or less from one end of the discrete fracture to the other. In the most pessimistic case in Study No. 2 the groundwater velocity is calculated to be about 20 m/a in the most severely damaged portion of the EDZ and about 100 m/a in the discrete fracture. This would imply a water travel time of about a year. In both cases, however, the ^{129}I mass flux is predicted by the transport models to be insignificant at the corresponding times. The transport models also show that the radionuclide that has diffused into the matrix would move towards fracture zone LD1. Thus transport models that assume that once the solute diffuses into the rock matrix it will remain there or can only diffuse back into the discrete fracture, may not be conservative.

CALCULATION OF DISCRETE FRACTURE FLOW PATHS IN DUAL-CONTINUUM MODELS†

Clifford K. Ho and Michael L. Wilson
Sandia National Laboratories
P.O. Box 5800
Albuquerque, NM 87185
ckho@sandia.gov, mlwilso@sandia.gov

ABSTRACT

Discrete fracture flow paths, referred to as "weeps," have been derived from dual-continuum models of fracture flow. The required parameters include the geometric fracture spacing, an assumed width of each weep, and a scaling factor that accounts for reduced flow between fracture and matrix elements in dual-continuum models. The formulation provides a convenient means to determine discrete weep spacing and flow rates that are mathematically consistent with the dual-continuum model. Specific applications and examples related to seepage into drifts are also discussed.

INTRODUCTION

Movement of water through fractures plays an important role in performance assessments of the potential high-level nuclear waste repository at Yucca Mountain, Nevada. The magnitude and frequency of water flowing though individual fractures impacts predictions of the near-field environment and waste-package corrosion. However, to date, few models of discrete fracture flow at Yucca Mountain exist. Current models of fracture flow at Yucca Mountain include dual-continuum models (dual-permeability or dual-porosity) that treat the fractures and matrix as separate continua. Simulated flow in dual-continuum models is typically interpreted as occurring uniformly through each computational grid of the model. Another interpretation, which is presented in this paper, is that the continuum-based flow can be mapped into discrete fracture flow paths, or weeps, for each grid block. This method is mathematically consistent with the dual-continuum model formulation, and it provides additional information about weep spacing that is required by near-field and waste-package modelers. The remainder of this paper presents a formulation to derive weep spacing, flow rate per weep, and seepage information from dual-continuum models for use in performance-assessment calculations.

THEORETICAL FORMULATION

Consider a grid block with dimensions L_1, L_2, and L_3 as shown in Figure 1. The objective is to derive a uniform weep spacing, a (m), in the grid block assuming a specified geometric fracture spacing, D (m), and a specified dimensionality of a uniform fracture set (1-D, 2-D, or 3-D). For simplicity, a one-dimensional fracture set is pictured in Figure 1, but the formulation can readily be extended to multiple dimensions. In a standard dual-continuum conceptual model, the total connection area, A_{DKM} (m^2), between fractures and matrix in a given primary grid block as shown in Figure 1 is assumed to be equal to the total surface area of all the fractures in the grid block:

† This paper has been published in the Proceedings of the Eighth International High-Level Radioactive Waste Management Conference, Las Vegas, Nevada, May 11-14, 1998, pp. 375-377. La Grange Park, Illinois: American Nuclear Society, Inc.; New York, New York: American Society of Civil Engineers.

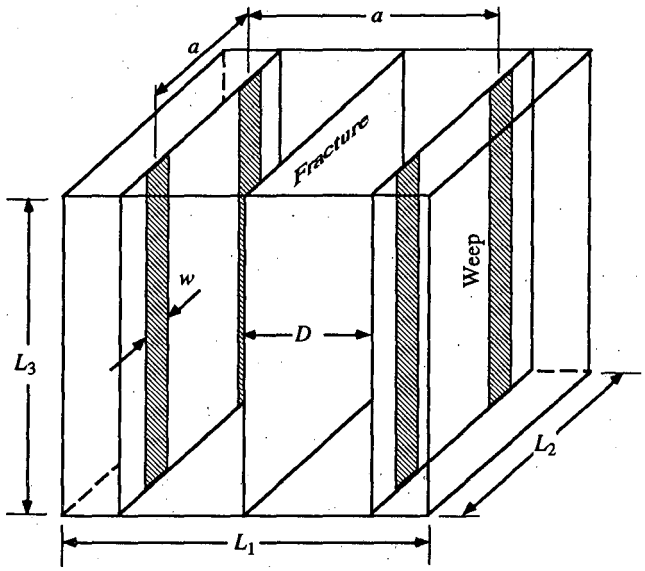

Figure 1. Conceptual model of available wetted area between fractures and matrix in a computational grid block.

$$A_{DKM} = \underbrace{(2\,L_2\,L_3)}_{\text{Fracture area per matrix block}} \overbrace{\left(\frac{L_1\,L_2\,L_3}{D\,L_2\,L_3}\right)}^{\text{Number of matrix blocks per grid block}} = \frac{2\,L_1\,L_2\,L_3}{D} \tag{1}$$

Equation 1 can be generalized for one-, two-, and three-dimensional uniform fracture sets if the right-hand side of Equation 1 is multiplied by n, where n is the dimensionality of the fracture set being considered (n = 1, 2, or 3 for one-, two-, or three-dimensional fracture sets, respectively):

$$A_{DKM} = \frac{2\,n\,L_1\,L_2\,L_3}{D} \tag{2}$$

For unsaturated flow, the actual wetted area between fractures and matrix is likely to be less than the total surface area of the fractures due to heterogeneities at various scales that channel liquid flow. Typical dual-continuum models assume ubiquitous "sheet" flow in all the fractures, but the discrete approach proposed here assumes that the flow occurs in discrete weeps of width w (m) and average uniform spacing a (Figure 1). The reduced wetted area between fractures and matrix, A_{weep} (m^2), can then be expressed as follows for a given grid block:

$$A_{weep} = \underbrace{(2\,w\,L_3)}_{\text{Area per weep}} \overbrace{\left(\frac{L_1\,L_2\,L_3}{a^2\,L_3}\right)}^{\text{Number of weep blocks per grid block}} = \frac{2\,w\,L_1\,L_2\,L_3}{a^2} \tag{3}$$

The reduced area can be accommodated in dual-continuum models through the use of a reduction factor (Ho 1995, Ho 1997), X_{fm}, defined as the ratio of the reduced weep area to the total geometric fracture area:

$$X_{fm} = \frac{A_{weep}}{A_{DKM}} \tag{4}$$

Assuming that X_{fm} is prescribed in the dual-continuum model (Ho 1997), Equations 2 and 3 can be plugged into Equation 4 to determine the weep spacing, a, as a function of geometric fracture spacing, D, weep width, w, reduction factor, X_{fm}, and fracture set dimensionality, n:

$$a = \sqrt{\frac{w\,D}{n\,X_{fm}}} \tag{5}$$

Equation 5 defines an equivalent discrete fracture spacing for flow (weep spacing) at any grid block in a dual-continuum model with a prescribed fracture-matrix reduction factor. The flow rate per weep, Q (m^3/s), can be readily obtained by multiplying the continuum percolation flux (m/s) by the area associated with each weep block (a^2).

It should be noted that the weep spacing defined in Equation 5 is an *average* spacing assuming uniformly spaced weeps. Because the actual weep spacing can be highly variable not only within a single fracture but also among multiple fractures, the average weep spacing can be a non-integer multiple of the geometric fracture spacing. In addition, X_{fm} in Equation 4 can be interpreted as the fracture saturation of the grid block depicted in Figure 1 if the fracture apertures are completely filled with water. However, the value of X_{fm} can be different from the actual fracture saturation simulated in the dual-continuum models if the fractures are only partially filled or if fracture coatings exist. For example, if X_{fm} is less than the simulated saturation, we can conceive that the fractures are nearly filled, but only one surface of the fracture is wetted. Fracture coatings may also prevent some of the weeps from contributing to the available wetted fracture-matrix surface area, causing X_{fm} to be much smaller than the liquid saturation. On the other hand, if X_{fm} is greater than the simulated saturation, we can conceive that film flow occurs on both fracture surfaces, which yields a large wetted fracture surface area (and hence, large X_{fm}) with only a small liquid saturation.

RESULTS AND DISCUSSION

The fracture-matrix reduction factor, X_{fm}, has been implemented in a dual-permeability model that is used to generate flow fields for performance-assessment calculations of the potential repository at Yucca Mountain (Bodvarsson et al. 1997). In the current base-case hydrologic property set, this factor is assumed to be a material-dependent constant and is determined via calibration studies (Bodvarsson et al. 1997). Alternative property sets include fracture-matrix reduction factors that are dependent on the hydrologic state of the grid block being considered (e.g., X_{fm} ~ relative permeability) (Ho 1997). Table 1 gives the weep spacing for several units in the vicinity of the potential repository at Yucca Mountain associated with the base-case hydrologic property set assuming a one-dimensional fracture set (n = 1). Two bounding weep widths of 0.01 m and 1 m are used. Note that the weep spacing can be significantly greater than the geometric fracture spacing when the fracture-matrix reduction factor is small and the weep width is large.

Table 1. Weep spacings for three stratigraphic units in the vicinity of the potential repository at Yucca Mountain using a reference hydrologic property set (Bodvarsson et al. 1997).

Unit	Geometric Fracture Spacing, D (m)	X_{fm}	Weep Spacing, a (m) $w = 0.01$ m	$w = 1$ m
tsw34	0.53	1.55×10^{-4}	5.8	58
tsw35	0.55	7.76×10^{-2}	0.27	2.7
tsw36	0.48	4.79×10^{-5}	10	100

The information in Table 1 can be used to complement drift-scale models of seepage. The weep spacings given in Table 1 can be used to estimate the amount of water that contacts waste packages assuming negligible capillary-barrier resistance to water flow at the drift surface. The fraction of waste packages contacted by weeps, P, can be estimated as the ratio of the cross-sectional area of a waste package to the area associated with a weep block (a^2). The amount of water contacting each waste package can then be estimated using the flow rate per weep, Q, and the number of weeps contacting a waste package (0 or 1 if $P < 1$; and P if $P > 1$).

ACKNOWLEDGMENTS

This work was supported by the Yucca Mountain Site Characterization Office as part of the Civilian Radioactive Waste Management Program, which is managed by the U.S. Department of Energy, Yucca Mountain Site Characterization Project. Sandia is a multiprogram laboratory operated by Sandia Corporation, a Lockheed Martin Company, for the United States Department of Energy under Contract DE-AC04-94AL85000.

REFERENCES

Ho, C.K., 1995. Assessing Alternative Conceptual Models of Fracture Flow, in Proceedings of the TOUGH Workshop '95, LBL-37200, SAND95-0324C, Lawrence Berkeley National Laboratory, Berkeley, CA, Mar. 20-22, pp. 323-330.

Ho, C.K., 1997. Models of Fracture-Matrix Interactions During Multiphase Heat and Mass Flow in Unsaturated Fractured Porous Media, SAND97-1198C, in Proceedings of the Sixth Symposium on Multiphase Transport in Porous Media, FED-Vol. 244, 1997 ASME International Mechanical Engineering Congress and Exposition, Dallas, TX, Nov. 16-21, pp. 401-412.

Bodvarsson, G.S., T.M. Bandurraga, and Y.S. Wu, eds. 1997. The Site-Scale Unsaturated Zone Model of Yucca Mountain, Nevada, for the Viability Assessment, LBNL-40376, Lawrence Berkeley National Laboratory, Berkeley, CA.

A Conceptual Model of the Temporal and Spatial Distribution of Net Infiltration and Recharge in Fractured Rock, Yucca Mountain, Nevada

By Alan L. Flint, Lorraine E. Flint,
Joseph A. Hevesi, and David B. Hudson,
U.S. Geological Survey

The understanding of the role of fractures in bedrock in unsaturated zone hydrology has increased dramatically in the last decade. Specifically, the study of Yucca Mountain, Nevada, by the U.S. Geological Survey in cooperation with the U.S. Department of Energy, as a potential high-level radioactive waste repository, has provided a great deal of field and laboratory data for the development of conceptual and numerical models of fluid flow in fractured rock. The conceptual model presented here is a summary of the efforts to characterize the surface infiltration that results in deep percolation into fractured bedrock based on ten years (1984-93) of field measurements of soil water content and soil water potential in the surface soil and rock and at the soil/bedrock interface. This conceptual model was incorporated into the development of a numerical model of infiltration that is used to distribute infiltration over the study area. In addition, a new method is presented to estimate recharge from modeled values of net infiltration over large areas using effective flow pathway porosity and the unsaturated zone thickness.

The current conceptual model identifies precipitation as the most significant environmental factor controlling net infiltration at Yucca Mountain. Precipitation averages 170 mm/yr over the study area but is temporally and spatially variable (Hevesi and others, 1991). The penetration depth of infiltration into the soil/bedrock profile fluctuates on a seasonal basis but is greatest in the winter due to lower evapotranspiration demands, higher amounts of precipitation, and slow snow melt.

The second most significant environmental factor controlling net infiltration is soil depth. When there is sufficient precipitation to produce net infiltration, the spatial distribution is generally defined by the spatial variability of soil depth. Field measurements indicate that when the soil/bedrock contact reaches near-saturated conditions, fracture flow is initiated in the bedrock, increasing the hydraulic conductivity by several orders of magnitude. Soils exceeding six meters in thickness virtually eliminate the infiltration of water to the soil/bedrock contact except in channels (Flint and Flint, 1995). Storage capacity in the soil profile is large enough that most water from precipitation is held in the root zone and removed by evapotranspiration processes. Soils that are less than six meters deep do not have enough storage capacity to store the volume of precipitation, and often allow near ponding conditions to occur at the soil/bedrock contact, particularly when the soil depth is less than 0.5 meters.

The third factor controlling net infiltration is bedrock permeability. At Yucca Mountain welded tuffs and nonfractured, nonwelded tuffs are the principal rock types present in surface exposures or directly under soils. The saturated hydraulic conductivity of the nonwelded tuff

matrix is higher than the welded tuff matrix (Flint, 1998). The fractures in the welded tuff increase the saturated hydraulic conductivity of those rocks but due to channeling and the presence of inactive as well as active fractures (Liu and others, 1998), the unsaturated bulk conductivity may be more similar to the unsaturated conductivity of the matrix of the nonwelded tuffs. The lower storage capacity of the fractured, welded tuffs allows moisture that has infiltrated to penetrate more deeply than in the nonwelded tuffs. Hydraulic properties of fractures depend on fracture aperture and whether or not the fractures are open or filled with calcium carbonate or siliceous materials, which is often the case at the ground surface where infiltration occurs. Calculations of fracture porosity, saturated hydraulic conductivity, and aperture (Kwicklis and others, in press) indicate that significant flux in fractures occurs only under saturated or near-saturated conditions. Fracture densities and matrix permeabilities vary greatly between the geologic units at Yucca Mountain.

Shallow infiltration processes at Yucca Mountain can be described on the basis of four infiltration zones that can be identified based on the manner in which volumetric water content changes with depth and time (Flint and Flint, 1995). The zones, which correlate with topographic position, are described as follows: (1) The ridgetop is flat to gently sloping, of higher elevation than the other zones, and has thin soils composed of both eolian deposits and soils developed in place from the weathering process. These soils often have higher clay content and higher water-holding capacity compared to soils on sideslopes and alluvial terraces. The ridgetops generally are located where the bedrock is moderately to densely welded and fractured. The presence of thin soil and fractured bedrock results in the deeper penetration of moisture following precipitation compared to other topographic positions. In some locations where runoff is channeled, large volumes of water can infiltrate. For the present-day arid climate, runoff generally is restricted to the upper headwater portions of drainages and to locations downstream of areas that have very thin soils underlain by relatively impermeable bedrock. (2) Sideslopes are steep, commonly have thin to no soil cover, and are usually developed in welded, fractured tuff. The steepness of the slopes creates conditions conducive to rapid runoff. The low storage capacity of the thin soil cover and the exposure of fractures at the surface may enable small volumes of water to infiltrate to greater depths, especially on slopes with north-facing exposures and therefore lower evapotranspiration demands. Shallow alluvium at the bases of the slopes can easily become saturated and initiate flow into the underlying fractures. (3) Alluvial terraces are flat, broad deposits of layered rock fragments and fine soil with a large storage capacity. Little runoff is generated on the terraces and the precipitation that falls there does not move beyond a meter or so in depth before evapotranspiration removes it. Consequently, this zone contributes the least to net infiltration in the drainage basin. (4) Active channels are similar to the terraces but are located in a position to collect and concentrate runoff which, although it occurs infrequently, can then penetrate deeply. Although local net infiltration can be high for some channel locations, under the current arid climate this mechanism is not considered to be a major contributor to the total volume of net infiltration at Yucca Mountain. This is because runoff is infrequent and because the channels are a very small percentage of the drainage basin area.

The conceptual model correlating infiltration zone with topographic setting was used in conjunction with detailed field and laboratory measurements of physical and hydrologic properties of the soil and rock to develop a numerical model of infiltration that provides estimates of the spatial and temporal variability of net infiltration at Yucca Mountain. The spatial distribution is based primarily on estimates of precipitation, maps of soil depth, geologic maps of surface bedrock, and the associated physical and hydraulic properties of each bedrock type. Sensitivity analyses made with the numerical model indicate that, as the climate becomes wetter, channel locations experience a greater relative increase in net infiltration compared to other infiltration zones, and the effect of bedrock permeability becomes increasingly more significant relative to the effect of soil thickness (as well as other factors affecting evapotranspiration) in controlling net infiltration.

References

Flint, L.E., and Flint, A.L., 1995, Shallow infiltration processes at Yucca Mountain-- Neutron logging data, 1984-93: U.S. Geological Survey Open-File Report 95-4035, 46 p.

Flint, L.E., 1998, Characterization of hydrogeologic units using matrix properties, Yucca Mountain, Nevada: U.S. Geological Survey Water-Resources Investigations Report 98-4243, 64 p.

Hevesi, J.A., Flint, A.L., and Istok, J.D., 1991, Precipitation estimation in mountainous terrain using multivariate geostatistics–II. Isohyetal maps: Journal of Applied Meteorology, v. 31, no. 7, p. 661-676.

Kwicklis, E.M., Thamir, F., Healy, R.W., and Hampson, D., 1998, Numerical simulation of water- and air-flow experiments in a block of variably saturated, fractured tuff: U.S. Geological Survey Water-Resources Investigations Report 97-4274.

Liu, H.H., Doughty, C., and Bodvarsson, G.S., 1998, An active fracture model for unsaturated flow and transport in fractured rocks: Water Resources Research, v. 34, no. 10, p. 2633-2646.

Session P1:
ALTERNATIVE MODELS FOR FLOW IN FRACTURED ROCKS

Hydraulic Properties of Fracture Networks Following a Power-Law Length Distribution.

Jean-Raynald de Dreuzy, Philippe Davy and Olivier Bour
Géosciences Rennes (UPR 4661) Campus de Beaulieu, 35042 Rennes Cédex
Jean-Raynald.Aupepin-de-Lamothe@univ-rennes1.fr, Philippe.Davy@univ-rennes1.fr, Olivier.Bour@univ-rennes1.fr

Field observations on fractured media have shown a broad and apparently non-limited distribution of fracture length, so that fractures are present at every scale. We study the theoretical consequences of this specific property of the fracture-size distribution on the bulk hydraulic properties of fractured media in various contexts of embedding dimension, orientation and aperture distributions. The lack of any characteristic length scale and representative elementary volume precludes the a priori use of homogenization methods. We choose to model the distribution of length by a power law, which turns out to be the sole distribution without characteristic scale apart from its lower and upper cut-off. $n(l)$ describing the number of fractures of length l in a bi-dimensional system, the power law has the following expression $n(l) \sim l^{a}$. For $a=1$, networks are mostly made of fractures of length equal to the upper cut-off, hence of infinite fractures compared to the system size (figure 1a). For $a=\infty$, networks are made of fractures of length equal to the lower cut-off, hence of infinitesimal fractures compared to the system size (figure 1c). Between these two extreme cases, networks are made of fractures of various length as for the example given by figure 1b for $a=2.5$.

We establish through the study of connectivity and permeability the domain of validity of these two endmost models. For $1<a<2$, networks can be considered as a superposition of main fractures (figure 1a), whereas for $3<a<\infty$, networks can be replaced by systems made of fracture of constant length. However there still remains a potentially geologically relevant zone, $2<a<3$, in which none of these two models can be applied. In this later zone, the large distribution of fracture length still introduces long-range spatial correlation in the system, but smaller fractures cannot be neglected. The range of relevant fracture size cannot be restricted to a unique value. In that case, the fractal dimension of the largest cluster which determines the spatial distribution of the connected network, and the fractal dimension of the backbone which determines the pathways for fluid flow, may be different than the ones expected from classical percolation theory. Consequently the transport properties of such systems will be in turn greatly modified.

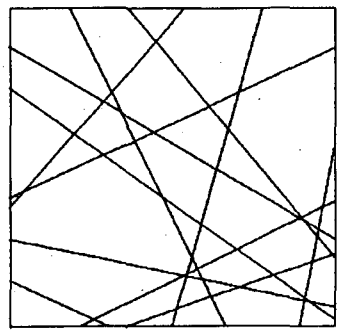

Figure 1a
a=1

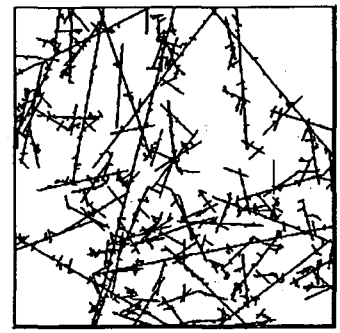

Figure 1b
a=2.5

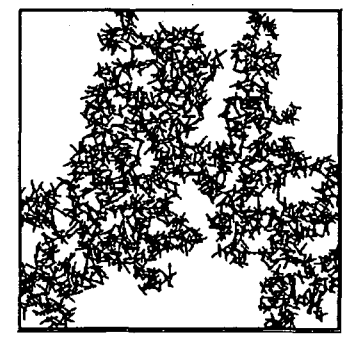

Figure 1c
a=∞

Network connectivity

Connectivity was described in two and three dimensions [*Bour and Davy*, 1997; *Bour and Davy*, 1998] in a generalized framework of percolation theory. Following this work, connectivity is determined by a unique parameter similar to the percolation parameter, which turns out to be the second moment of the fault length distribution. Different regimes of connectivity are identified depending on the power-law exponent a. For $a>3$, small faults rule the network connectivity, and classical laws of percolation theory apply according to the universal exponents. For $1<a<3$, both small and large faults control the connectivity in a ratio which depends on a. The percolation parameter, and thus the connectivity increases with scale, because of the increase of the probability of generating fractures of length of the system size order. In contrast with the classical percolation theory, the percolation threshold becomes a transition zone, whose width remains constant whatever the system size. This difference with the classical percolation theory is corroborated by the disappearance of the divergence of the correlation length at the percolation threshold; we thus expect different relationships between geometrical and hydraulic properties.

Network permeability

Figure 2 represents the flow computed on the network of figure 1b (assuming a constant aperture for all fractures) and highlights the hydraulic relevant sub-network. For a given set of the fracture-length distribution parameters, the distribution of permeability values is strongly scale dependent if $a<3$. In the vicinity of the percolation threshold, this distribution presents several relative peaks whose central values are proportional to the number of independent flow paths - i.e. the number of paths, which do not share any link. For example, two independent flow paths are identified in the simulation presented in figure 2. These flow paths are also statistically independent in the sense that the probability of occurrence of n flow paths, $P(n)$ is equal to $P(1)^n$. Above the percolation threshold, networks become homogeneous and can be progressively considered as "effective media", whose permeability linearly depends on the fracture density. The rate of convergence to the effective medium value is controlled by the parameter of percolation, which thus describes both the connectivity and the degree of

homogeneity. Scale analyses show a decrease of permeability below the percolation threshold, a slight increase above and an asymptotic value given by the effective media theory.

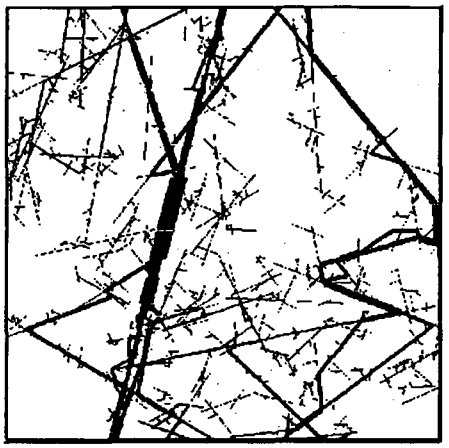

Figure 2. Flow computed on network 1b. The segment width is proportional to flow.

We extend the preceding study for networks having a fracture aperture distribution. As expected, increasing the width of the aperture distribution leads to a decrease of the number of significant producing flow paths, as well as an enhancement of the permeability variability. If length and aperture are not correlated, the average permeability decreases when increasing the standard deviation of the aperture distribution. This effect is particularly notable close to the percolation threshold. However, opposite trends are observed if we introduce a positive correlation between the length of a fracture and its aperture.

Well test simulations on the same kind of synthetic networks give more insights in the relevant hydraulic structure. The computation of transient flow uses a finite volume method implemented with a multistep scheme in time, well suited to the stiffness of the problem. This efficient method enables the simulation of long term pumping tests on large networks (Figure 3). The implicit scale analysis performed by well tests gives information on the existence of characteristic scales of correlation, that were not apparent in steady state. Besides the refinement of the simplified network structure, the classical analytical solutions of Théis and Barker [*Barker*, 1988] were compared with numerical simulations. With such comparisons we especially seek for the geometrical signification of the flow dimension and for the determination of the maximum information contained in well tests. We can hence define the type of network model that can be constrained by well test data. These results are used in a second step for the characterization of a site in Brittany, on which several well tests were performed. The observations of drawdown at evolving scale give an idea of the scaling of the parameters of the aquifer and of its degree of heterogeneity.

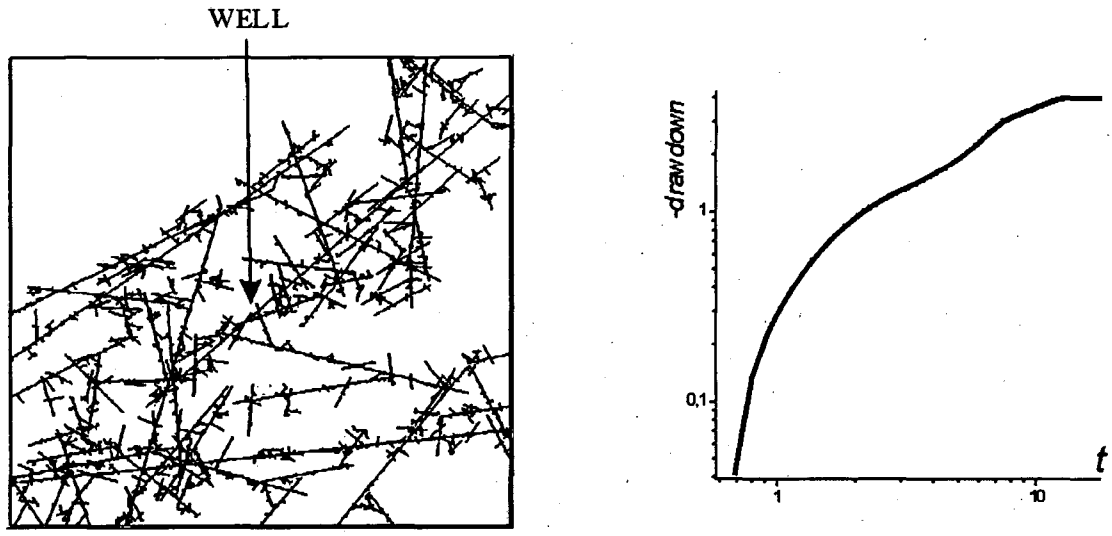

Figure 3. On the right side: network on which was performed the pumping test. On the left side: drawdown at the well

References

Barker, J.A., A Generalized Radial Flow Model For Hydraulic Test in Fractured Rock, Water Resources Research, 24 (10), 1796-1804, 1988.

Bour, O., and P. Davy, Connectivity of random fault networks following a power law fault length distribution, Water Resources Research, 33 (7), 1567-1583, 1997.

Bour, O., and P. Davy, On the connectivity of three dimensional fault networks, Water Resources Research, 34 (10), 2611-2622, 1998.

Evidence of Chaotic Behavior in Flow Through Fractured Rocks, and How We Might Use Chaos Theory in Fractured Rock Hydrogeology

Boris Faybishenko
E.O. Lawrence Berkeley National Laboratory, Berkeley, CA

Introduction. Field observations conducted in both porous and fractured media often show random-looking fluctuations in pressure, flow rate, and temperature. These fluctuations may not in fact be random, but rather a combination of deterministic-chaotic and random components. It is important to determine whether a system exhibits a chaotic behavior, because the long-term predictability of a chaotic system is limited. For such a system, one can determine only a range of possible predictions, rather than give a precise prediction. The purpose of this paper is to present evidence and sketch out some perspectives for using chaos theory to describe nonlinear flow processes in fractured media. A nonlinear dynamical analysis is conducted in the phase-space of the state variables affecting the system. This approach allows us to determine the role of chaotic and stochastic components affecting flow in fractured media.

The Vadose Zone is a Dissipative Physical System. The unsaturated soils and rocks of the vadose zone are a three-phase system: solid particles, liquid, and air. Air can be connected to the atmosphere, and it can be entrapped in water in the porous space. The phase-state variables affecting the state of the system are the water pressure, air pressure, moisture content, and water velocity. The relationships between these variables are nonlinear. Therefore, the phase-space volume varies with time, which is evidence of the chaotic behavior of the system.

Definition of Deterministic Chaos and Stochastic Chaos. In general, the term "deterministic chaos" is used to describe dynamical processes with random-looking data for which random processes are not a dominant part of the system (Schuster, 1989; Tsonic, 1992). The state of a dynamic system is characterized using a space of vectors $Y(t)$ with several dimensions, because several factors and processes affect the system. The trajectories of these vectors form an attractor describing the future states of the system. The attractor is a set of points in a phase-space towards which nearly all trajectories are converging. The attractor of a chaotic system is called a strange, or chaotic, attractor, for which:

(1) Adjacent trajectories diverge exponentially with time,
(2) The information on initial conditions cannot be recovered from later states of the system, because the system is sensitive to initial conditions, and
(3) The attractor characterizes the bounds within which the system behaves.

Chaotic flow behavior in heterogeneous media may result from a sensitive dependence of flow parameters upon the coupled effects of several nonlinear factors. Some of these factors are a nonlinear relationship between the flow rate, water content, pressure, and temperature; air entrapment; heterogeneity and roughness of fractures; clogging of the conductive fractures by sediments and biofilms; and kinetics of the matrix-fracture water exchange. Because of the effect of nonlinear processes, small changes in initial conditions

(spatial distribution of water content, pressure, and temperature) and boundary conditions (precipitation, ambient temperature and pressure, groundwater fluctuations, etc.) may lead to significant changes in predictions. When both deterministic-chaotic and stochastic processes play a significant role in the dynamics, the system can be called *stochastic chaotic*. The coupled effect of several nonlinear processes in unsaturated media is governed by nonlinear ordinary and partial differential equations, which may have bounded nonperiodic solutions. These equations may be either purely deterministic where no random quantities appear in the equations (Tsonic, 1992), and stochastic chaotic (Kapitaniak, 1988).

Evaluation of Diagnostic Features of Chaos. A basic idea in analysis of a nonlinear dynamical system is to use one-dimensional observations (i.e., scalar signals) to determine the structure of the dynamical source of these data (Abarbanel, 1996). The first step in this analysis is to reconstruct the phase-space, and then plot an attractor in the phase space. In order to plot the attractor, we have to determine, first, the correlation time, and, then, an embedding dimension of the attractor. The correlation time is the time between points when the relationship between the points almost vanishes. The embedding dimension is the dimension of the phase space needed to unfold the attractor of a nonlinear system from the observation of scalar signals.

For a dynamical system, which actually behaves in a space of vectors $Y(t)$ having several dimensions, the factors and processes affecting the system may often remain unknown to us. In order to identify the physics of the dynamical system, we have to use a *synthetic space* that is formally equivalent to the *physical state* of the system's original variables. For this purpose, we use coordinates made out of the independent time-delayed neighbors of the observed scalar variable. This process is called *Phase-Space Reconstruction*. The phase space reconstruction is accomplished using the present value of the variable $X(t)$ and the earlier value $X(t - n\tau)$, which are dynamically independent of $X(t)$, such as the vector $Y(t)$ given by:

$$Y(t) = [X(t), X(t-\tau), \ldots, X(t-n\tau)]$$

The critical point in the phase-space reconstruction is to determine an optimum correlation time, or delay time, τ. The correlation time of a nonlinear system is determined using the average mutual information function. This function provides the information learned about one observation from another observation on the average over all measurements. In other words, we determine the amount of information, in bits, learned about the point $P(t+n\tau)$, at the time $(t+n\tau)$, from the measurements of $P(t+(n-1)\tau)$ at the time $(t+(n-1)\tau)$. The first minimum of the average mutual information function versus τ is used to determine an optimum correlation time.

The dimension of the attractor is the number of phase space coordinates needed to unfold the attractor, i.e., to determine the number of coordinates when the orbits composing the attractor are no longer crossing one another in the phase space. The method of false nearest neighbors is used to determine the dimension of the attractor (Kennel et al., 1992). The attractor gives us a general idea about the long-term dynamics of the system.

In order to provide an understanding of the attractor and the role of both deterministic and chaotic components, we will use several simple examples of 2D attractors, which are the relationships between the value of the time-varying function at the time t and its value at the time $t + \tau$. Figure 1a shows that for the sine function, the attractor is an ellipse. For the sine

function with a small random component, the attractor is a set of points scattering around the ellipse (Figure 1b). For a random function, the attractor covers the whole phase-space (Figure 1c). For the deterministic chaotic system described by the well-known Lorenz equation, the attractor has a specific pattern (Figure 1d). It is intuitively apparent from this figure that the scatter of the points, which makes up the attractor, characterizes the contribution of random components. For more complex systems, the attractors have three or more dimensions, but we can plot only 3D attractors using the coordinates $P(t)$, $P(t+\tau)$, and $P(t+2\tau)$.

Some other diagnostic parameters needed to recognize a chaotic system in the otherwise random-looking time-series data are capacity (fractal) dimension, correlation dimension, Hurst exponent, and Lyapunov exponent (Tsonis, 1992). A comparison of these parameters reveals the relative contribution of deterministic-chaotic and random components.

Experimental Evidence for Chaotic Behavior. Some examples of dynamical systems that display nonlinear chaotic behavior for some system parameters are: avalanche fluctuations resulting from the perturbation of sandpiles of various sizes (Rosendahl et al., 1993), falling of water droplets (Cheng et al., 1989), river discharge, precipitation (Pasternak, 1996; Pelletier, 1996), and oxygen isotope concentrations (Nicolis and Prigogine, 1989). In laboratory studies of gravity-driven water seepage in coarse porous media, Prazak et al. (1992) observed irregular oscillations, which exhibited a pronounced "pulsing drop-to-drop" behavior. In their field infiltration tests, Podgorney et al. (1997) observed water dripping from a fracture, which was unstable and irregular in space and time even at a constant ponded-water level.

Janosi and Horvath (1989), in their laboratory and in numerical experiments of raindrops on a window pane determined that a critical coverage of the surface occurs regardless of the application rate of additional water to the surface, and this water is removed through streams. Geller et al. (1996) observed similar behavior in experiments conducted using a transparent replica of a natural rock fracture with a variable aperture. Geller et al. (1998) observed intermittent-type flow through capillary tubes inserted between glass plates (smooth, sand-blasted, and obscure). Calculation of several diagnostic parameters for the time variations of water pressure showed that a combination of both chaotic and stochastic components affected the flow regime.

Persoff and Pruess (1995), in their two-phase (air and water) flow experiments in natural rough-walled rock fractures, determined persistent instabilities of pressure fluctuations even under constant boundary conditions. They explained that these instabilities resulted from the interplay between capillary effects and pressure drop due to viscous flow. The diagnostic chaotic parameters for air pressure fluctuations confirmed that flow was affected by both chaotic and stochastic components. As an example, Figure 2a shows the time variation of the air pressure at the entrance to the fracture replica, and Figure 2b shows the attractor for these data.

Field hot-air-injection test in fractured basalt at the Box Canyon site, Idaho, revealed some evidence of chaotic behavior. Air (90°C) was injected into a rubble zone through an open interval in a borehole. Sporadic temperature fluctuations were observed only at depths of 10.3-11.3 m within the rubble zone. These fluctuations are believed to be a result of intermittent downward flow of colder air and liquid.

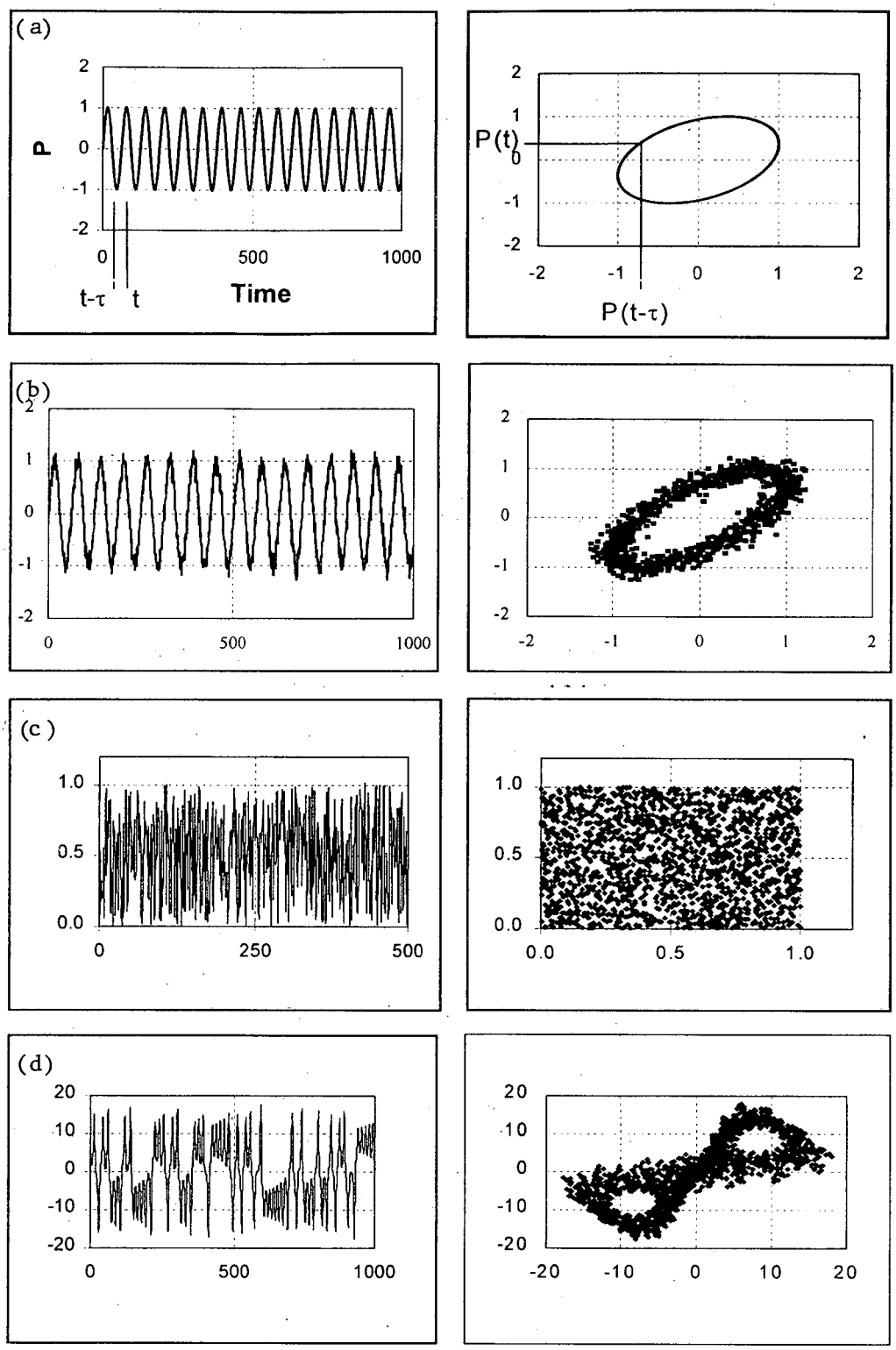

Figure 1. Examples of time-series functions (left) and corresponding 2D attractors (right) for (a) sine functions, (b) sine function with noise, (c) random function, and (d) chaotic function of the Lorenz equations.

Perspectives of Using Chaos Theory in Hydrogeology. A chaotic-dynamical model is one of the alternative phenomenological models to describe flow in fractured media. Nonlinear dynamical analysis can be used to distinguish between the deterministic-chaotic, stochastic-chaotic, and random models. The knowledge of chaotic processes is important for predicting water flow and solute transport. If we determine that flow can be described by chaotic equations, we can apply correct prediction models and determine the time frame within which we can give meaningful predictions. The optimum time of predictions can be determined using the Lyapunov exponent, which provides a measure of average rates of convergence and/or divergence of nearby trajectories in the phase space. If a dynamical system evolves in a chaotic manner, long-term predictability is not necessarily ruled out. For example, chaotic flows can provide for efficient fluid mixing, yielding dilution effects that are predictable. Once the attractor characterizing the system is determined, it can be used to determine the bounds within which the system parameters are expected to behave. It is also important to define regions of chaos within otherwise random fields. The dimension of the attractor can be used to determine the number of variables (or factors) affecting the physics of flow.

References

Abarbanel, H.D.I., *Analysis of Observed Chaotic Data*, 1996.

Cheng, Z., S. Redner, P. Meakin, and F. Family, 1989. Avalanche dynamics in a deposition model with "sliding," *Physical Review A*, vol. 40, no. 10, pp. 5922-5935.

Geller, J., G. Su and K. Pruess. Preliminary Studies of Water Seepage Through Partially Saturated Rough-Walled Fractures, Lawrence Berkeley Laboratory Report LBL-38810, Berkeley, CA, July 1996.

Geller, J.T., S. Borglin, and B. Faybishenko, Experimental study and evaluation of dripping water in fracture models, Abstract presented at the Chapman Conference on Fractal Scaling, Nonlinear Dynamics, and Chaos in Hydrologic Systems, 1998.

Janosi, I.M. and V.K. Horvath, 1989. Dynamics of water droplets on a window pane, *Physical Review A*, vol. 40, no. 9, pp. 5232-5237.

Kapitanyak, T., *Chaos in Systems with Noise*, World Scientific, Singapore, 1988.

Kennel, M.B., R. Brown, and H.D.I. Abarabanel, Determining embedding dimension for phase-space reconstruction using a geometrical construction, *Physical Review* A, Vol. 45(6), 3405-3411, 1992.

Nicolis, G., and I. Prigogine, *Exploring Complexity: An Introduction*, W.H. Freeman and Company, New York, NY, 1989.

Pasternak, G.B., Assessing claims for chaos in hydrologic records, *Hydrology Days*, 395-406, 1996

Pelletier, J.D., 1996. Power spectral analyses of climatological and hydrological time series: Identification of the Hurst phenomenon and application to drought hazard assessment, Hydrology Days, 407-422.

Persoff, P. and K. Pruess. Two-Phase Flow Visualization and Relative Permeability Measurement in Natural Rough-Walled Rock Fractures, *Water Resour. Res.*, *31*(5), 1175-1186, 1995.

Podgorney, R., T.R. Wood, and T. Stoops, Outcrop infiltration experiments, Data Summary Report, INEEL, 1997.

Rosendahl, J., M. Vekic, and J. Kelley, 1993. Persistent self-organization of sandpiles, Physical Review E, vol. 47, no. 2, pp. 1401-1447.

Prazak, J., M. Sir, F. Kubik, J. Tywoniak and C. Zarcone. Oscillation Phenomena in Gravity-Driven Drainage in Coarse Porous Media, *Water Resour. Res.*, *28*(7), 1849 - 1855, 1992.

Schuster, H.G., *Deterministic Chaos: An Introduction*, Weinhei, VCH, 1989.

Tsonic, A.A., *Chaos: From Theory to Applications*, Plenum Press, 1992.

Acknowledgment
Comments and discussions with Karsten Pruess, Garrison Sposito, Sally Benson, Christine Doughty, and Paul A. Witherspoon are very much appreciated. The Environmental Management Science Program of DOE funded the research.

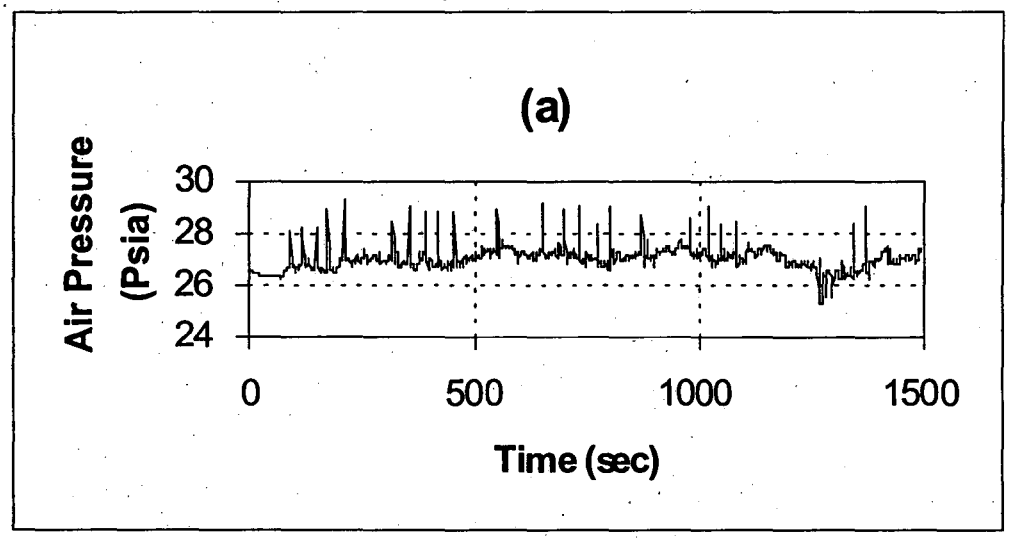

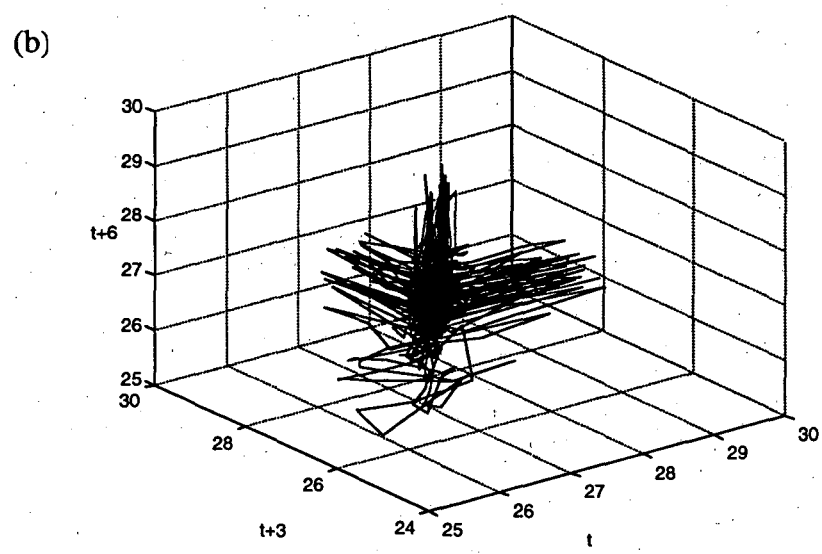

Figure 2. Time variations (a) and the attractor (b) of air pressure. In figure (b), time delay τ=3.

On the Significance of Rock Wettability in Oil Recovery Processes

Eddy Isaacs, Alexander Babchin and Jian-Yang Yuan

Alberta Research Council
250 Karl Clark Road
Edmonton, Alberta, Canada T6N-1E4

1. Abstract

The wettability of reservoir rock governs, to a large extent, the location, flow, and distribution of oil, gas and water. The importance of the rock wettability in oil recovery processes is well documented, but mechanisms are often poorly understood. In dual porosity systems, such as fractured rocks, it is believed that counter-current capillary imbibition is the major recovery mechanism. In this presentation we describe our work on practical methods for measuring the wetting preference. As well, we relate how the changes in the electric properties of the mineral/water and oil/water interfaces can be used as a predictive tool in characterizing wetting behavior. We provide a framework for relating productivity to wetting preference during the movement, flow and production of fluids in reservoir rock. Finally, we show how these concepts are used to numerically model and control wettability thereby improving productivity.

2. Introduction

In the fractured rock, the rate of oil recovery is controlled by imbibition of water into the porous matrix and counter-current drainage of oil into the fractures. The imbibition rate, in turn, depends on the wetting preference of the rock. For the simple 1-D case, we calculated the propagation velocity of the imbibing front, V_{front}, and derived the following equation:

$$V_{front} = \frac{dy_0}{dt} \approx \frac{KS_v S_o^* \gamma_{o/w} \cos\theta}{\phi \mu_o y_o}. \qquad (1)$$

K = absolute permeability
$\gamma_{o/w}$ = oil-water interfacial tension
ϕ = rock porosity
y_o = position of the front
S_v = specific surface area
θ = apparent contact angle
μ_o = oil viscosity
S_o^* = average oil saturation behind the front

The front velocity is seen to depend on the apparent contact angle, and thus on the physical chemistry of oil/brine/rock interactions. Equation (1) is a generalization of the Washburn Equation for the case of counter-current imbibition of water into the water-wet rock ($\theta < 90°$) saturated by viscous oil. At neutral wettability conditions $\theta = 90°$, no imbibition is possible. For oil-wet condition ($\theta > 90°$) the oil phase will resist water imbibition and external pressure is

required to drive the oil. In this oil-wet situation, oil is imbibed and water is drained when the mineral is partially water saturated and in contact with the oil. Note that Equation (1) is valid in the limit $\theta \to 0$. At $\theta = 0$, the stability of water wetting films covering mineral surfaces becomes an important issue.

Part of the problem in characterizing wettability is the lack of a method that is universally applicable. The laboratory methods that are generally used fall into two categories: those that directly (or indirectly) measure the contact angle of the mineral/oil/water contact line or those which determine residual saturations of water and oil in a core after the fluids have been introduced. Our approach to wettability is to consider that unless a three-phase contact line forms (the three phases usually considered are oil/water/mineral) contact angle arguments are invalid. In this approach, the stability of the wetting film is critical in establishing the wetting characteristics of the reservoir. For the most part this approach attempts to predict the conditions under which the water film is stable, indicating that the rock is completely water wet.

3. Interactions at the oil/water/mineral Interfaces

Most interfaces, both liquid-liquid and solid-liquid, are electrically charged owing to the dissociation of ionizable groups such as $-SO_3^-$, $-COOH$ and $-NH_4^+$ or by unequal adsorption of ions, such as surfactants, on the surface. These charges at interfaces are largely responsible for the interactions between surfaces. The interactions between oil and mineral (solid) surfaces separated by a water film can be described by the disjoining pressure, that is, the pressure which needs to be overcome for the oil to contact the mineral or sand surface and given by:

$$\pi(h) = F_A(h) + F_D(h) + F_H(h), \qquad (2)$$

where $\pi(h)$ is the disjoining and $F_A(h)$, $F_D(h)$ and $F_H(h)$ represent respectively the London-van der Waals force (generally attractive), the double layer force (generally repulsive) and the hydration force (which is short-range and repulsive). For the oil to contact the mineral surface through destabilizing the water film, the double layer force between the oil/water and the water/mineral surfaces must be overcome to allow the oil to approach and potentially contact the mineral surface. The double layer repulsive forces are uniquely a function of the water chemistry (pH and ionic content) and the charge characteristic of the oil/water and mineral/water interfaces.

The oil/water interfacial charge is related to the type of molecules naturally present in the oil that can adsorb at the oil/water interface. In some cases, these materials leave the oil/water interface and alter the charge characteristics of the mineral/water interface.

One of the better methods to characterize the magnitude and nature of interfacial charge is through the determination of electrophoretic mobility. At neutral and high pH the crude oil/water interfaces are electronegative. This is due mostly to the dissociation of chemical groups belonging to surfactants naturally present in the bitumen or oil; for example, carboxyl groups with $RCOOH \to RCOO^- + H^+$.

At low pH, largely because anionic surfactants are neutral, other charged chemical groups are activated exemplified by $RNH_2 + H^+ \rightarrow RNH_3^+$. This can render the oil/water interface electropositive providing for a greater tendency to oil wet mineral surfaces that maybe negatively charged at the water/solid interface.

The electric properties of the mineral-water interface can also be explained by the ionization of the surface groups. For example, the silica surface becomes positive ($-SiOH_2^+ \leftrightarrow -SiOH + H^+$) or negative ($-SiOH \leftrightarrow -SiO^- + H^+$) by altering the solution pH. Based on the electric properties at the oil/water and water/solid interface the disjoining pressure, π, can be calculated. In these calculations the hydration force, $F_H(h)$, can generally be neglected. In this case, the disjoining pressure can be represented by the quantity π_{max}, which is the maximum force that is calculated as a function of separation distance between the interfaces. If the hydration force were included the value of the disjoining pressure would be higher. The higher the value of π_{max}, the more the tendency to maintaining water-wet behavior.

Comparison of the disjoining pressure, π_{max}, for quartz and carbonate surfaces as a function of bulk pH and NaCl concentrations showed that carbonate surfaces have a greater tendency to be wetted by oil that quartz surfaces. These general trends provide guidance as to the wetting tendencies of various surfaces and were confirmed in experiments carried out at temperatures up to 200°C.

4. Application to Recovery Performance

To test the imbibition theory described by equation (1), we conducted waterflood experiments in cores using water-wet sand and having an oil-wet membrane at the production end. Significant improvement in oil recovery was observed when the flow of the water displacing fluid was stopped and started in a cyclical fashion. The enhanced recovery is due to imbibition of oil into the oil-wet membrane. This effect disappeared when the injection of water was continuous. In this case, the applied rate through the water phase was higher than the rate of imbibition and thereby suppressed the natural imbibition of oil into the oil-wet membrane. Based on this work we expect improvements in recovery in field processes where pressure drops are naturally low. Examples of field processes with relatively low pressure-drops include those using horizontal wells and having gravity drainage as the primary recovery mechanism. These expectations have been confirmed in scaled-model experiments and have been shown, using numerical simulation, to affect the reservoir and not just the near-wellbore.

Review Of Recent Models of Transport in Fractured Rock; Their Approaches, Objectives, and Methods

Aharon Nir
Department of Environmental Sciences and Energy Research
Weizmann Institue of Science. 76100 Rehovot, Israel
ciniraha@weizmann.weizmann. ac.il

Transport in fractured media is one of the important subjects of interest, reflected in the number of articles in hydrogeological journals and topical conferences for the last decade. The references are too abundant to quote in a brief review, therefore only a representative selection is included. The motivation for this review by an outsider is an attempt to identify the broad professional approaches, objectives and methods of this important activity.

The emphasis on transport in fractured rock may be regarded as an intrinsic part of (a) enhancement of basic understanding of the flow and transport in natural porous media (naturally inhomogeneous, homogeneous natural porous media being a conceptual artifact of singularity); and (b) an attempt to reduce the uncertainty in the transport related decisions with effects on human welfare and safety.

Fracture models were invoked fairly late in the last decades as a mechanically deterministic description of the preferential flow paths. There are still other attempts to model flow channeling within the existing approaches of stochastic analysis of groundwater systems (Anderson, 1997), hydraulic conductivities and dispersivities models in nonstationary systems and fractal flow models. These were found more acceptable at relatively larger scales, where fracture zones were included as stepwise increases in hydraulic conductivity in relation to the surrounding rock mass (Walker et al., 1977). Processes that may explain some of the experimental observations without the use of flow channeling are discussed by Tsang and Neuman (1977) and Tsang and Neretnieks (1997). In certain cases indicated by Neuman (1977), continuum stochastic flow and transport models, which account for medium heterogeneity, provide a better and more effective representation than previous discrete fracture network models.

One of the most direct representations of the relevance of the fracture models was demonstrated in the Stripa Mine Project in Sweden (Olsson, 1992; Long at al., 1992; Long et al., 1997). The fracture modeling approach in geological formations was extended using the assumptions of fractal geometry (Gringrod and Impey, 1993) and its application by the iterated function system in an inversion process (Doughty et al., 1994).

The fracture models serve in the applied aspect in support of the performance assessment and site characterization of the planned depositories of chemical-biological contaminant species and in location of spent nuclear fuel and high-level nuclear waste storage. While formal validation concept of the approval of these programs is not deemed feasible by present scientific methodology (Oreskes at al., 1994) their accepted objective is the reduction of uncertainties and the associated risks on the part of the decision level authorities. This process and the achievement of its objectives is subject of an ongoing discussion. The article by Freeze et al.

(1987) entitled " Some uncertainties about uncertainty" was used as a benchmark for an estimate of this process in the subsequent decade. The incorporation of the fracture flow and transport mechanism has contributed to a better understanding of the risks involved in these projects. However this increase in understanding indicated that many sources of uncertainty have not been removed and new ones are being identified (Chestnut and Faybishenko, 1997; Neuman, 1997; Vasco et al. 1997). The incorporation of geophysical techniques in aquifer characterization (Rubin et al., 1998) is expected to improve the modeling capabilities and reduce some of these uncertainties. The experimental results of Weisbroad et al. (1998) indicate temporal changes in fracture conductivities in unsaturated chalk formations. The absence of other projected experimental methods of significant promise to the evaluation of 3-D local contaminant transport in fractured media, e.g. positron emission tomography, is apparent.

The modeling methods of transport in fractured media may be subdivided into two broad categories: the "stand alone" method, and the integrated fracture-stochastic continuum method. The "stand alone" method concentrates on a conceptual fracture network, designed by stochastic simulation of its interconnection directions, lengths and aperture variability. It is usually limited to its "backbone" structure, disregarding non-conductive links. Relative simplicity of this presentation is achieved by restriction to saturated media, which neglects matrix flow, chemical species dependence on matrix interactions and capillary matrix effects in unsaturated conditions, as well as the double porosity diffusive effects of the discarded connections. The transport is simulated by particle tracking through the conductive structure, producing a probability distribution function of the transport, conditioned on the structural modeling assumptions. These are compared to the outputs of large scale tracer experiment in support of the exhibited features of the simulated transport. Examples of this approach are described by Moreno and Tsang (1994) and Margolin et al. (1998).

The alternative approach, while returning to the stochastic continuum model, integrates the features of fracture flow as long-range correlations of hydraulic conductivities, conditioned on site-specific data (Tsang et al., 1996). An integrated fracture network of fractal characteristics is applied in simulation of the Yucca Mountain site radionuclide transport, including retardation effects of the fracture and matrix surfaces (Mukhopadhyay and Cushman, 1997). The results of tracer transport experiments at varying distances are analyzed in terms of the relevance of the flow channeling models (Tsang and Neretnieks, 1997). A more comprehensive integration of the fracture flow in the varied processes and geological structures in the unsaturated zone site at the Yucca Mountain is described by Bodvarsson et al. (1997).

The lingering questions are: to what extent has this serious and dedicated effort enhanced our understanding of the nature of transport in complex porous media beyond the detailed behavior of our own models, our contribution to the decision process in important human endeavors and what should be the direction to further these goals.

References

DN- Dagan, G. and S.P. Neuman, (ed.), Subsurface Flow and Transport: A Stochastic Approach, Cambridge University Press, UNESCO 1997

FATM-Field Testing and Associated Modeling of Potential High-Level Nuclear Waste Geologic Disposal Sites, LBNL Workshop, Berkeley, 1997.

Anderson, M. P., Characterization of Geological Heterogeneity, DN, 23, 1997.
Bodvarsson, G. S. et al., A Site Scale Modeling Unsaturated Zone Processes at Yucca Mountain, Nevada, FATM, 1997.
Chestnut, D.A. and B. Faybishenko, Alternative Approaches for Modeling Unsaturated Flow and Transport in Fractured Rocks, FATM, 1997.
Doughty, C., J. C.S. Long, K. Hestir and S. M. Benson, Hydrologic characterization of heterogeneous geologic media with an inverse method based on iterated function systems. Water Resour. Res., *30*(6),1721, 1994.
Freeze, R. A., G. De Marsily, L. Smith, and J. Massmann, Some Uncertainties About Uncertainty, Proc. Conf. on Geostatistical, Sensitivity, and Uncertainty Methods for Ground-Water Flow and Radionuclide Transport Modeling, CONF-870971, Batelle Press, 1987.
Grindrod, P. and M.P. Impey, Channeling and Fickian Dispersion in Fractal Simulated Porous Media, Water Resour. Res., 29(12), 4077, 1993.
Long, J.C.S. et al., Prediction of flow and drawdown for the site chatacterization and validation site in the stripa mine, Technical Report 92-05, SKB, 1992.
Long, J.C.S. et al., Component characterization: an approach to fracture hydrology. DN, 179, 1997.
Margolin, G., B. Berkowitz and H. Scher, Structure, flow and generalized conductivity scaling in fracture networks, Water Resour. Res., 34(8), 2103, 1998.
Moreno, L. and C.-F. Tsang, Flow channeling in strongly heterogeneous porous media. A numerical study. Water Resour. Res. 30, 1421, 1994
Mukhopadhyay, S. and J.H. Cushman, Monte carlo simulation of radioactive contaminant transport in fractured geologic media: disorder and long range correlation , Mat. Res.Soc. Symp. Proc. Vol. 465, 1997.
Neuman, S.P., Stochastic approach to subsurface flow and transport: a view to the furture. DN, 231, 1997.
Olsson, O., (ed.) , Site Characterization and Validation- Final Report. Stripa Project Technical Report, 92-22, SKB, 1992.
Oreskes, N., K. Shrader-Frechette, and K. Beltitz, Verification, validation and confirmation of numerical models in the earth sciences.
Science, 263, 641, Feb. 4, 1994.
Rubin, Y. et al., Aquifer Characterization, Chap. 10 in Delleur, J. (ed.), Handbook of Groundwater Engineering. CRC Press, 1997.
Tsang, C.-F., and S.P. Neuman, Introduction and general comments on INTRAVAL. Phase 2, Working Group 2, Test cases. Paris, NEA/OECD, 1997
Tsang, Y.W., C.-F. Tsang, and F. H. Hale, Tracer transport in a stochastic continuum model of fractured media, Water Resour. Res., 32(10) , 1996.

Tsang, C.-F. and I. Neretnieks, Flow channeling in heterogenous fractured rocks. Rev. Geophys., 36(2), 275, 1997.
Vasco, D.W., A. Datta-Gupta and J.C.S. Long, Resolution and uncertainty in hydrologic characterization, Water Resour. Res., 33(3), 379, 1997.
Walker, D. et al., Three Dimensional Inverse Modelling of Multi-scale Hydraulic Test Data, FATM, 1997.
Weisbrod, N., R.Nativ, D. Ronen and E. Adar, On the variability of fracture surfaces in unsaturated chalk, Water Resour. Res., 34(8) , 1998.

Describing Coupled Transport Processes in and through Fractured Rock Systems

Walter Rose
Illini Technologists International
P O Box 2430/A, Champaign, IL 61825, USA
wdrose@prairienet.org

Alexander Babchin and Jian-Yang Yuan
Alberta Research Council
250 Karl Clark Road
Edmonton, Alberta, Canada T6N-1E4

In Philip and De Vries [1957], an analysis was given about what then was believed to be a sensible way to model non-isothermal liquid and associated vapor transport in under-saturated soil-like porous media. These pioneering authors, however, failed to take coupling phenomena into account even though the governing theory about the necessity for this had been already well-established (c.f. Onsager [1931] for paradigm cases that involve Soret and Dufour effects during thermo-diffusion processes; and by Yuster [1951] (and later gradually by Rose [1954] and many others) for those special cases where viscous coupling occurs across interfacial boundaries between contiguous pore level immiscible fluid phase streams. Surprisingly, this omission unfortunately seems to have persisted even up to the present day as illustrated by Baggio et al [1997]. Even so, it is to be implied here that the cited (40 years old) Philip and De Vries work is more or less a good starting place to arrive at an enhanced modeling of similar transport processes in complex permeable fractured rocks.

Here attention will be directed to the presumed characteristics of idealized representative fractured rock systems. This is done by applying the Onsager [1931] Reciprocity Relationships (ORR) that are descriptive of irreversible transport processes with coupling (cf. elaboration by Bear [1972] for porous media), in the form:

$$\mathbf{J}_i = \sum_j K_{ij}\mathbf{X}_j \; ; \; T\left(\frac{ds}{dt}\right) \equiv \sum_i \mathbf{J}_i \cdot \mathbf{X}_i > 0 \; ; \text{where if } i \neq j \text{ then } K_{ij} = K_{ji} . \qquad (1)$$

In Equations (1): $\mathbf{J}_i$ are the observable mass-energy fluxes; $\mathbf{X}_i$ are the observable conjugate energy gradient driving forces; K_{ij} are the "material response" coefficients of proportionality to be measured in the laboratory; ds/dt is the positive-definite entropy production rate, T is the absolute temperature; and the indices i and j designate respectively the conjugate forces and fluxes that apply to fluid flow, and/or to vapor diffusion, and/or to heat transfer processes under consideration. In a two-phase flow system, for example, i (and j) =1,2.

For transport processes where no coupling is involved, however, all cross coefficients in Equation (1), i.e., K_{ij} (where $i \neq j$), vanish. Furthermore, diagonal coefficients become classical mobility coefficients, for example, that appear in Darcy's Law in single-phase fluid flow. While

this simplistic description that historically been employed to describe the classical Philip and De Vries thermo-diffusion problem (cf. Baggio et al, loc.cit.), it is Equations (1) that some modern workers prefer since they are substantiated by the Theorems of Irreversible Thermodynamics, as shown by. Onsager [1931]).

Given the above background of ideas, speculations naturally can be undertaken about the application of Equations [1] to describe (i.e. model) coupled vapor diffusion, liquid flow, and heat transfer processes in fractured rocks. These include:

(i) The systems referred to in this paper are ones where permeable (or impermeable) fractures, and/or fault planes, and/or bedding stratifications can occur. These may be characterized by a variety of sizes, shapes, orientations, spatial network connectivity forms, and transport process conductivities.

(ii) In the in-situ subsurface systems of interest, each of the fracture/fault/bedding surfaces may serve as source-sink boundaries of adjacent sediments that themselves may (or may not) be porous and permeable. In the affirmative case, however, modeling based on dead-end dual porosity concepts clearly can be employed (cf. Rose et al, [1961]).

(iii) Given the extension reported here of the problem addressed by Philip and De Vries so long ago, and also in a similar way by Baggio et al [1997] more recently, it is to be noted that while vapor diffusion, liquid flow, and heat transfer occur in and through contiguous pore space paths, the possibility of heat transfer also occurring directly through the solid matrix phase (e.g. across the fluid-solid boundaries) also may have to be considered.

(iv) While in some cases the transport phenomena of interest will be located in connected fracture spaces, in others it can additionally be important to focus on transport in and out of surrounded un-fractured porous and permeable sediment blocks. As for this, apparently one can advantageously employ some of the modeling ideas of Payatakes and Valavanides [1998]. For example, these latter authors conclude from their network model studies that in the internally surrounded un-fractured matrix blocks, flow transport can be described as involving ganglia dynamics (GD) and/or drop traffic flow (DTF) and/or connected pathway flow (CPF). Direct observation of fluid flow combining films and train of droplets was performed recently by Faybishenko et al. [1997]. Theoretical consideration of a droplet train model by Babchin and Yuan [1997] has shown the significance of the capillary effects along with the importance of viscous effects which was traditionally considered as dominating factor in coupled two-phase fluid flow. Furthermore Babchin and Yuan [1997] showed that, under certain conditions, ORR are satisfied, predicting equal share of the capillary resistance to flow by each of the two phases.

(v) In those cases when transport events in the fractured rock system under study occur mostly in the spaces occupied by the fractures, CPF rather than GD and DTF modes of transport are all that will have to be considered. This is because low Capillary Numbers are needed to hold ganglia together and/or to cause emulsions to form and persist, i.e. as respectively needed to give rise to the GD and DTF modes of transport. In consequence, for example, it can be anticipated that future experimental data will show comparatively large values for the so-called interaction (viz.

cross) coefficients, K_{ij}(where $i \neq j$). Figure 1, for example, shows this to be the case according to analytical calculations for an idealized fracture geometry as reported in Rose [1998] and [1996]. And the approaches taken by Rose and Witherspoon [1956] and [1957], and more recently by Payatakes and Valavanides (loc.cit) and many others, present clues about how computerized network model analyses can be used to upscale pore-level understandings to have macroscopic meaning and utility.

(vi) For the more complicated cases where in the spaces bounded by the extensive fracture networks, one additionally will have to deal locally with transport in and out of the enclosed porous and permeable elements perhaps in GD and DTF modes. The essential thing to keep in mind, however, is the non-equilibrium character of the transport processes under study. That this will most likely be the rule is consistent with the notoriety of the fact that Onsager was the 1968 Nobel Prize Laureate in Chemistry for his remarkable (Onsager [1931]) achievements (cf. Rose [1969]).

(vii) To successfully apply ORR Dogma for the description of coupled transport processes that occur in fractured rocks will frequently prove to be a daunting task. To solve Equations [1] when undertaking simulations of subsurface events, is severely complicated by the need for coherent computing schemes, and also for reliable input information coming from coherent laboratory experiments and field observations. These essential requirements, for example, are identified in Rose [1988], [1990a], [1990b], [1991], [1995], [1996], [1997], and [1998 in press]. Even in such a complicated process as in steam assisted gravity drainage (SAGD) recovery of heavy oil, the coupled description of fluids flow (Babchin, Yuan and Nasr [1998]) provides more consistent model than traditional theory based on the relative permeability approach. It should be noted the senior author of this paper was the first who overstepped (Rose [1969]) the concept of relative permeability in petroleum engineering (Rose [1987]), in development of which he spent many decades.

REFERENCES

A. BABCHIN and J.-Y. YUAN (1997), "On the Capillary Coupling between Two Phases in a Droplet Train Model," *Transport in Porous Media,* v. 26, pp. 225-228.

A. BABCHIN, J.-Y. YUAN and T. NASR (1998), "Generalized Phase Mobilities in Gravity Drainage Processes," presented at the 49th Annual Technical Meeting of the Petroleum Society of CIM in Calgary, Alberta, June 8-10, 1998, paper #98-09.

P. BAGGIO, C. BONACINA and B. A. SCHREFLA (1997), "Some considerations on modeling heat and mass transfer in porous media," *Transport in Porous Media,* v.28, pp. 233-351.

J. BEAR (1972), *Dynamics of Fluids in Porous Media*, Elsevier.

B. FAYBISHENKO et al. (1997), "A Chaotic-Dynamical Conceptual Model to Describe Fluid Flow and Contaminant Transport in a Fractured Vadose Zone," Progress Report, Lawrence Berkeley National Laboratory Report, LBNL-41223.

L. ONSAGER (1931), *Physical Review,* v. 37, pp. 405-426, 2265-2279.

A. C. PAYATAKES and M. S. VALAVANIDES (in press, June 1998), "True-to-mechanism

macroscopic theory of steady-state two phase flow in porous media," *Proceedings of XII Conference on Computational Methods in Water Resources*, Crete.

J. R. PHILIP and D. A. DEVRIES (1957), "Moisture movement in porous materials under temperature gradient," *Transactions American Geophysical Union,* v. 38, pp. 222-233.

W. ROSE et al (1954-1999), Some various ORR representative papers, "*various journals*"

[i] **(1954)**, "An explanation of the Yuster Effect," *Journal of Petroleum Technology*, v. 4, pp 19-25, with **P. H. SCOTT**;

[ii] **(1956)**, "II. Trapping oil in a pore doublet," *Illinois State Geological Survey*, Circular 234, with **P. A. WITHERSPOON**;

[iii] **(1957)**, "III. Use of Network Models," *Ibid*, Circular 237;

[iv] **(1961)**, "Dead-end pore volume as distributed sources and sinks," *Journal of Physical Chemistry*, v. 58, pp 1440-1441, with **H. C. TUNG** and **C. NEWMAN**;

[v] **(1969)**, "Transport through interstitial paths of porous solids," *METU (Turkey) Journal of Pure & Applied Science*, v. 2, pp. 117-132;

[vi] **(1988)**, "Attaching new meanings to the Equations of Buckley & Leverett," *Journal of Petroleum Science and Engineering*, v. 1, pp. 222-238;

[vii] **(1990a)**, "Optimizing experimental design for coupled 2-phase flows," *Experimental Thermal & Fluid Science*, v. 3, pp. 613-622;

[viii] **(1990b)**, "Lagrangian simulation of coupled two phase flows," *Mathematical Geology*, v. 22, pp. 642-655,

[ix] **(1991)**, "Critical questions about the coupling hypothesis," *Journal of Petroleum Science and Engineering,* v. 5, pp. 299-307;

[x] **(1995)**, "Ideas about viscous coupling in anisotropic media," *Transport in Porous Media,* v.18. pp. 87-93;

[xi] **(1996)**, "Generalized description of multiphase flow through porous media," *Proceedings Society of Engineering Science,* 32nd Annual Technical Meeting in New Orleans, pp. 483-484;

[xii] **(1997)**, "An upgraded viscous coupling measurement methodology," *Transport in Porous Media*, v. 28, pp. 221-231;

[xiii] **(1998, in press)**, "Myths about later-day extensions of Darcy's Law," *International Non-Recoverable Energy Sources Congress*, <http://www.staff.uiuc.edu/~wdrose/DARCY.html> .

W. ROSE (1987), "Relative Permeability," *Petroleum Engineering Handbook,* Chapter 28, Society of Petroleum Engineers, Richardson, TX, USA.

S. T. YUSTER (1951), "Theoretical considerations of multiphase flow in idealized capillary systems," *Proceedings Third World Petroleum Congress*, Den Haag, v. II, pp. 437-445.

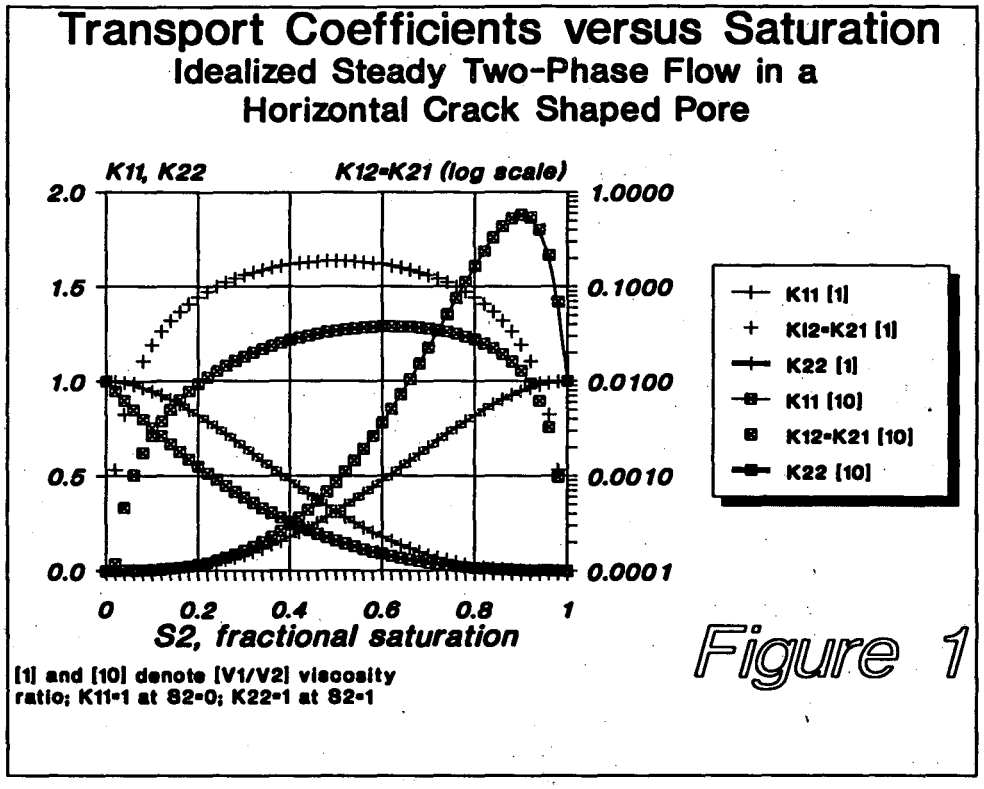

FIGURE 1. N.B. While the curves of Figure 1 are drawn to quantitatively describe viscous coupling in an idealized crack space, qualitatively they also could just as well describe Dufour or Soret effects in thermodiffusion systems, or also the non-colinearity of fluxes and forces during flow in 2-D anisotropically fractured media as shown by Rose [1996]. This is because of the universal way Equations (1) can be applied to generalized coupled transport systems.

Scale-Dependent Darcy Flows in Fractured Media

Daniel M. Tartakovsky and Larry Winter
Los Alamos National Laboratory

Darcy's Law has been used to predict groundwater flows across a very wide range of experimental scales; however, different scales generally require different parameterizations, even within the same site. This may be due to sampling across increasing levels of material heterogeneity as the volumes used to average parameters expand. The application of Darcy's Law is further complicated by our uncertain knowledge of the detailed structure of porous media. In fact, hydraulic conductivity and other parameters are usually observed at a relatively small number of locations in groundwater studies. It is by now standard practice to represent uncertainty in flow parameters by homogeneous stochastic processes. This is appropriate for porous media that result from a uniform process of geological formation. However, many porous media are statistically heterogeneous because their statistical properties vary with location. Recently, we have begun to explore probabilistic models in which heterogeneity is represented by location-dependent mixtures of disjoint homogeneous random fields.

In what follows we demonstrate these concepts by considering flow through a fractured porous matrix M with disjoint fractured zones F. We conceptualize these fractured inclusions as continua whose hydraulic conductivity K_f is different from hydraulic conductivity K_m of the ambient matrix. Naturally, the geometry of such inclusions cannot be known with certainty. A separate source of uncertainty is the high degree of spatial variation of K_m and K_f combined with lack of detailed information. In other words, in this view of fractured media uncertainty arises from two distinct sources: small scale within-block (matrix or fractured inclusions) variations and large scale across-block (matrix-inclusions) variations. In this framework, each homogeneous block corresponds to a diffferent ensemble of porous media. Thus, hydraulic conductivity fields are statistically heterogeneous when viewed across blocks, but are homogeneous within blocks. Solutions for ensemble mean hydraulic head $\langle h(\mathbf{x})\rangle$ require an expression of mean conductivity, $\langle K(\mathbf{x})\rangle$, that reflects heterogeneity at the larger, across-block scale. Across-block variation adds the spatial extent and arrangement of the blocks themselves as a new element of randomness in the analysis of the stochastic Darcy model. We show that the conductivity and head random fields can be averaged by dealing with each scale explicitly and more or less separately.

The essence of our approach (see also, *Winter and Tartakovsky*, 1998) is that the hydraulic conductivity and head fields can be averaged by using large-scale probabilities of across-block geometry to weight small-scale within-block probabilities. As a result, we can apply the convenient properties of small within-block variances σ_Y^2 of log conductivities Y_m and Y_f to perturbation expansions, while at the same time we allow statistical heterogeneity due to random variations in the large-scale geometry of blocks. Suppose the usual assumptions of stochastic hydrogeology hold: the statistics of the block structure of a porous medium are known, as are the distributions of conductivity within individual blocks. The result of averaging is a mixture of small-scale probability distributions that

leads to a straightforward expression for the critical parameter, $\langle K(\mathbf{x})\rangle$. Next assume, as usual, that σ_Y^2 is small within blocks. Then our approach also extends the range of perturbation analysis to highly heterogeneous domains that can be represented by mixtures of mildly heterogeneous blocks. We substitute the relatively tractable problem of determining the spatial distribution of disjoint blocks of homogeneous material for the difficult problem of dealing with large perturbation variances.

Across-block averaging provides a natural framework for assimilating the results of different methods of aquifer characterization. First, the method includes the kinds of spatially distributed material heterogeneities that are the result of most characterization studies; second, error models for characterization techniques can be explicitly included in models of random block boundaries; and third, the outputs of different characterizations can be combined using standard techniques like Bayesian updating since the multi-scale model is probabilistic. This is different from the ordinary approach in stochastic hydrology where observations of conductivity are lumped together without regard to material distribution and are then used to estimate statistics for an equivalent continuum. In most cases this results in estimates of $\langle K(\mathbf{x})\rangle$ that are very coarse and estimates of σ_Y^2 that are very large.

REFERENCES

1. Winter, C.L., and D.M. Tartakovsky, Scale-Dependent Statistics for Darcy Flows in Highly Heterogeneous Porous Media, *Geophysical Research Letters*, (under review) 1998.

Session P2:
COUPLED PROCESSES IN FRACTURED ROCKS

Coupled Chemical Transport and Fluid Flow During Alcohol Flooding for DNAPL Remediation

Ronald W. Falta, Eberhard Roeder, Cindy Lee, Scott Brame, Heather Schweninger, John Coates, Tarek Ladaa, Jim Myers, John Martin, Jennifer Pace, and Delphine Micolet

Departments of Geological Sciences and Environmental Engineering and Science, Clemson University, Clemson, South Carolina

Alcohol flooding appears to be a promising new technique for removing DNAPLs trapped below the water table in high permeability formations. An alcohol flood involves the injection and recovery of a mixture of alcohol, water, and selected additives. This cosolvent mixture achieves DNAPL removal through a combination of enhanced dissolution and separate phase mobilization, and the magnitude of these two mechanisms depends on the design of the alcohol flood.

Due to concerns about downward mobilization of DNAPL, most current surfactant and alcohol flooding approaches emphasize the enhanced dissolution mechanism. However, NAPL mobilization is a much more efficient way to remove the contaminants, provided that the issue of possible downward DNAPL migration can be addressed.

We are currently designing a field test of alcohol flooding for removing separate phase tetrachloroethylene (PCE) from an unconsolidated water table aquifer at Dover Air Force Base, Delaware. This experiment will be performed in a 5m by 3m by 15m deep test cell formed by sheet pile walls. The PCE will be introduced as a controlled release of approximately 100 liters, near the base of the unconfined aquifer, above a confining clay layer. Our goal in this test will be to mobilize the PCE (which has a density of more than 1.6 times that of water) as an LNAPL. This is theoretically possible because certain alcohols (with densities of about 0.8 times that of water) partition very strongly into separate phase PCE. This partitioning leads to swelling of the DNAPL phase until it is an LNAPL.

One difficulty in recovering DNAPLs by alcohol flooding is that the low density of the alcohol relative to water makes the cosolvent solution tend to override the resident pore water, leading to poor contact with the DNAPL. This issue can be addressed by adding a very dense solute such as sucrose or $CaCl_2$ to the cosolvent mixture. This dense solute does not partition significantly into the NAPL. With this formulation, it is possible to create an aqueous cosolvent flooding solution which is neutrally buoyant or denser than pure water, and which has the property of mobilizing separate phase PCE as an LNAPL. Examples of cosolvent formulations having these properties include tert-butanol, water, and sucrose; n-propanol, water and sucrose; isopropanol, water and sucrose; and isopropanol, water and $CaCl_2$. We are currently measuring the phase and transport properties of these and other mixtures, and have performed several 2-D

sandbox experiments as well as compositional multiphase flow numerical simulations of this displacement process.

The strong phase interactions between the cosolvent flooding solution and the NAPL phase leads to an extremely strong coupling between the chemical transport and the multiphase fluid flow. An alcohol flooding solution designed to mobilize a NAPL will have the property of reducing the NAPL-water interfacial tension (IFT) to zero at high concentrations. In other words, the alcohol can turn a two-phase NAPL water mixture into a single phase. Thus the NAPL aqueous solubility, residual saturation, relative permeability, and capillary pressure all are strong functions of the alcohol concentration.

The buoyancy effects in this type of flood are also very strong functions of the phase chemical compositions. Due to the partitioning of components between the aqueous and NAPL phases, the phase compositions and phase densities and viscosities depend on the nature of the multiphase fluid contact.

With our most recent formulations, we inject a cosolvent mixture (alcohol, water, dense additive) which is slightly denser than pure water. As this solution flows through the aquifer, it underrides the resident pore water, promoting good contact with the DNAPL which is typically found near the bottom of an aquifer. As the flooding solution contacts the DNAPL, the alcohol component strongly partitions out of the aqueous phase, into the NAPL phase. This partitioning reduces the NAPL density as discussed above, and the NAPL is mobilized as an LNAPL. However, the preferential alcohol partitioning also causes the formation of an alcohol depleted zone downstream of the swollen NAPL. This aqueous phase becomes somewhat more dense than water because it still contains large amounts of the dense additive. Unfortunately, this dense aqueous fluid can exert buoyancy forces which divert the more active solution (the solution with high alcohol concentrations) up and away from the desired treatment zone. This effect appears to be manageable though, and current numerical modeling and experimental work is focusing on the effective delivery of the swelling alcohol to the desired DNAPL treatment zone.

Results of Thermal Loading Using the Unsaturated Model of Yucca Mountain

Charles B. Haukwa, Yushu Wu and G.S. Bodvarsson
Earth Sciences Division
Ernest Orlando Lawrence Berkeley National Laboratory
1 Cyclotron Road
Berkeley, CA 94720

We present the results of Mountain scale thermal loading for the proposed repository at Yucca Mountain. The study investigates the response of Yucca Mountain to thermal loading under varied conditions of infiltration, thermal load, numerical grid discretization, boundary conditions, fracture-matrix interaction model as well as. The simulations are conducted using both the ECM and dual-k formulations with 1D, 2D and 3D numerical grids. The results provide range of flux, temperature and saturation both at repository and at the water table, and at selected locations. Completely dry conditions are predicted at several location within the repository. At the dry-out locations, temperatures in excess of 130 °C are predicted. Thermal load results in liquid flux several hundred times above ambient flux, particularly in the first 500 years of thermal load.

Application of the ROCMAS Code to Coupled Thermo-Hydro-Mechanical Problems

Jonny Rutqvist and Chin-Fu Tsang
Earth Sciences Division
Lawrence Berkeley National Laboratory
Berkeley, CA 947 05, USA

ROCMAS is a finite element program for transient analysis of coupled thermo-hydro-mechanical (THM) processes in fractured rocks. It has recently been expanded for analysis of the variably saturated media, for example, for analysis of resaturation and swelling of the clay buffer in a nuclear waste repository (Noorishad and Tsang, 1996). Some of the ROCMAS features are:

- 3D finite element model
- Discrete fractures embedded in continua
- Coupled temperature, fluid flow and mechanical deformations

Continua
- Elasto-plastic stress-strain for isotropic and ubiquitously fractured medium
- Darcy fluid flow and anisotropic permeability in a ubiquitously fractured media
- Variable saturation
- Water vapor flow
- Heat conduction and convection

Discrete fractures
- Non-linear aperture-normal stress relation
- Elasto-plastic dilating strain softening shear
- Parallel plate fluid flow
- Heat convection

Two recent application of the ROCMAS code are presented:

Application 1: In situ determination of fracture normal stiffness

In situ hydromechanical properties of fractures are determined by high-pressure injection testing in deep boreholes and coupled numerical modeling. The fracture normal stiffness is the most important parameter dictating the pressure flow response. To determine this parameter, the following procedure was applied to analyze the data for two granite sites and the injection test :

1) Pulse test (to determine the initial hydraulic aperture and flow dimension near the well bore)
2) Low pressure constant head injection test (to establish hydraulic properties and detect boundary effects away from the well bore)
3) Hydraulic jacking test (a step pressure injection test to back-calculate fracture normal stiffness,)

4) Pulse test (to detect changes in hydraulic aperture due previous jacking test)
The results of the above study is presented in Rutqvist *et al.*, (1997) and a method of using high pressure injection testing for determination of fracture storativity is presented in Rutqvist *et al.*, (1998).

Application 2: The Kamaishi THM experiment

The Kamaishi THM field experiment is designed to study resaturation of a deposition hole in fractured rocks with a heater surrounded by bentonite. The experiment is being conducted in a 5 by 7 meters alcove off an existing drift at a 250 meter depth. A test pit of 1.7 meter in diameter and 5 meters in depth has been drilled in the floor of the alcove. The problem has been divided into three subtasks:

Task1: Effects of excavation on water flow into the empty test pit.

Task2: Resaturation of Buffer only: The thermo-hydro-mechanical behavior, including dehydration, resaturation and swelling.

Task3: Resaturation of Buffer + rock interaction: A simultaneous modeling of resaturation with interaction of the rock and buffer.

The results of the modeling will be compared to actual field measurements .

REFERENCES

Noorishad J. and Tsang C-F. Coupled Thermohydroelasticity phenomena in variably saturated fractured porous rocks – Formulation and numerical solution. In *Coupled thermo-hydro-mechanical processes of fractured media* (Stephansson, Jing and Tsang, Eds), 93-134 Elsevier (1996).

Rutqvist J., Tsang. C.F, Ekman D. and Stephansson O. Evaluation of in situ hydromechanical properties of rock fractures at Laxemar in Sweden. Proceeding of the 1st Asian Rock Mechanical Symposium: ARMS '97, Seoul, Korea. A. A. Balkema publisher, 619-624 (1997).

Rutqvist J., Noorishad J., Stephansson O. and Tsang C.-F. Determination of fracture storativity in hard rocks using high pressure testing. *Water Resources Research* September Vol. 34 (10), 2551-2560 (1998).

Numerical Modeling Of Coupled Thermo-Hydro-Chemical Processes For the In-Situ Thermal Tests At Yucca Mountain, Nevada

Eric Sonnenthal, Nicolas Spycher, John Apps, and Ardyth Simmons
Earth Sciences Division
Lawrence Berkeley National Laboratory
Berkeley, CA 94720

1. INTRODUCTION

The long-term performance of the potential repository at Yucca Mountain will be affected by the coupling of thermal, hydrological and chemical processes (thermo-hydro-chemical, or THC) in the rock around the emplacement drifts. The net affect of the transport of heat, fluid, and vapor will be mineral dissolution and precipitation which may lead to permanent changes in porosity, permeability and unsaturated flow hydrologic properties. The purpose of this contribution is to describe an approach for modeling reaction-transport in unsaturated fractured porous media, with applications to the ongoing Drift Scale Heater Test (DST) and the completed Single Heater Test (SHT). A recurring theme in this work, no doubt also in others in this symposium, is the importance of the interaction of flow and transport between a fracture medium and the adjoining porous matrix. We note here that chemical equilibrium cannot be maintained in a system where mineral precipitation and dissolution are taking place at different rates in fractures and matrix, advective transport in fractures is faster than diffusive transport in the matrix, and the distribution and identities of minerals are initially very different in the two media.

The major driving forces for THC processes in the thermal tests and in the potential repository are the thermal heat load and (over long time periods) boundary conditions such as infiltration rate. For the time scales of the thermal tests the infiltration rate is negligible. The initial water and gas compositions, mineral distributions and compositions define the chemistry of the system. The development of a conceptual model and the strategy of incorporating the important THC processes for the thermal tests draws on numerous studies done on TH processes for the Single Heater and Drift Scale Tests (Birkholzer and Tsang, 1996, 1997), thermochemical processes (Glassley, 1997), and THC processes (Lichtner and Seth, 1996).

The previous studies and our current work show that several important considerations are required to account for the major THC processes that are likely to take place over the life of the potential repository. These include: (a) CO_2 transport in the gas phase and equilibration with the liquid phase; (b) dual permeability (or multiple interacting continua) so that the strong chemical, mineralogical, and hydrological differences between fractures and matrix can be captured; (c) multidimensional (2-D in this case, to account for gas phase convection and fluid flow in heterogeneous media); (d) kinetics of mineral-fluid reactions to account for slow reaction rates and rapid flow rates through fractures; and (e) consideration of aluminosilicate mineral reactions (e.g. feldspars, clays, sheet silicates, and zeolites) in addition to the silica phases and calcite.

2. GEOCHEMICAL AND MASS-TRANSFER CALCULATIONS

Simulations of the thermal tests were carried out with the TOUGHREACT code (Xu et al. 1998). TOUGHREACT was modified and enhanced for the Drift Scale and Single Heater Test model

simulations (Sonnenthal et al., 1998; Spycher et al., 1998) to simulate boiling conditions and interactions between fractures and matrix (diffusion and advection of aqueous and gaseous species across interfaces). The geochemical module incorporated in TOUGHREACT solves simultaneously a set of chemical mass-action and mass-balance equations to compute the extent of reaction and mass transfer between a set of given aqueous species, minerals, and gases at each grid block of the flow model. Equations for flow, transport, and chemical reactions are solved sequentially rather than in a coupled fashion for efficiency in computational time and memory.

The setup of mass-action and mass-balance equations in the geochemical module of TOUGHREACT is, in general, similar to the formulation implemented in other geochemical models (e.g., Reed, 1982), with additional provisions for mineral dissolution and precipitation under kinetic constraints and a volume-dependent formulation for gas equilibrium. The chemical system (minerals, secondary aqueous species, and gases) is described in terms of primary aqueous species (the independent variables). The system of nonlinear equations describing chemical mass-balance and mass-action is solved by a Newton-Raphson iterative procedure.

Kinetics of mineral precipitation and dissolution reactions are treated using a rate law that is dependent on the magnitude of the saturation index *(Q/K)* of each considered mineral (Aagaard and Helgeson, 1982) as follows:

$$r = \mathrm{sgn}[1 - Q/K]kS\left[1 - (Q/K)^m\right]^n \qquad (1)$$

where $$k = k_0 \exp\left[-E_a / R(1/T(K) - 1/298.15K)\right] \qquad (2)$$

where r is the mineral precipitation (negative) or dissolution (positive) rate, k, E_a, and S are the rate constant, activation energy, and reactive surface area, respectively, T is temperature, R the ideal gas constant, and *sgn[1-Q/K]* is the sign of the quantity *[1-Q/K]*. We assume that the exponents m and n equal one. The effects of pH and other aqueous species activities on reaction rates are not considered in the simulations presented here.

3. SIMULATIONS OF THE THERMAL TESTS

A few of the highlights of the THC modeling completed on the DST are illustrated here. In addition to water vapor, an important species in the gas phase is CO_2, which is released from the water phase during heating, and is also produced by calcite dissolution. DST simulations have shown a large halo of increased partial pressure of CO_2 extending into regions of near-ambient temperature (Figure 1) that has been corroborated by gas sample measurements (Conrad, 1998). The effect of the transport of CO_2 out of the boiling regions into areas of condensation is to shift the waters to a lower pH than that for the ambient waters (Figure 2). Strong differences between the water chemistry and reaction rates in fracture and matrix continua are prominant in the regions of water condensation and drainage. Recent analyses on elevated temperature waters that have collected in the hydrology boreholes, and those done previously for the SHT, are in general agreement with the decreased pH and salinity in condensate waters predicted by the modeling.

Within the high-temperature zone (> 90°C) of vapor condensation and condensate drainage the modeling predicts the greatest amounts of silica (predominantly cristobalite) and calcite dissolution.

In areas where the condensate waters are boiling and there is a drying-out trend, calcite and amorphous silica are predicted. The chemistry of waters collected in boreholes, and the model results also indicate that there are reactions between aluminosilicates (feldspars, zeolites, etc.) and the condensate waters, in addition to reaction with calcite and silica phases. The modeled precipitation of zeolites at high temperatures in the condensate zone is consistent with the observed paragenesis of zeolites during the early cooling and hydrothermal alteration of the tuffs.

Because the effective reaction rates for these more complex systems are more uncertain and depend on the effective reactive surface area of the mineral phases, some isotopic systems (e.g., $^{87}Sr/^{86}Sr$, carbon and oxygen isotopes) can provide independent controls on the actual rates of reaction. This is essential for long-term predictions of chemical alteration, changes in flow patterns below the repository, and the chemistry of waters that may seep into drifts.

References

Aagaard P. and Helgeson, H.C. 1982. Thermodynamic and Kinetic Constraints on Reaction Rates among Minerals and Aqueous Solutions, I. Theoretical Considerations. *Amer. J. Sci. 282,* 237-285.

Birkholzer, J.T. and Tsang, Y.W. 1997. *Pretest Analysis of the Thermal-Hydrological Conditions of the ESF Drift Scale Test.* Yucca Mountain Project Level 4 Milestone SP9322M4, Lawrence Berkeley National Laboratory.

Birkholzer, J.T. and Tsang, Y.W. 1996. *Forecast of Thermal-Hydrological Conditions and Air Injection Test Results of the Single Heater Test at Yucca Mountain.* Yucca Mountain Project Level 4 Milestone SP918M4; Report LBNL-39789, Lawrence Berkeley National Laboratory.

Conrad, M. 1998. "Isotope Analyses of Samples from the Drift Scale Test Hydrology Holes." In: *Second Quarter TDIF Submission (Hydrological, Radar and Microseismic),* Chapter 3. Yucca Mountain Project Level 4 Milestone Report SP2790M4, Lawrence Berkeley National Laboratory.

Glassley, W.E. 1997. *Thermochemical Analyses of the Drift-Scale Test: Mineralogical and Geochemical Characteristics.* Milestone SP9320M4, Lawrence Livermore National Laboratory.

Lichtner, P.C. and Seth, M. 1996. Multiphase-Multicomponent Nonisothermal Reactive Transport in Partially Saturated Porous Media. *In: Proceedings of the 1996 International Conference on Deep Geological Disposal of Radioactive Waste, 3,* 133-142.

Reed, M.H. 1982. Calculation of Multicomponent Chemical Equilibria and Reaction Processes in Systems Involving Minerals, Gases, and an Aqueous Phase. *Geochimica et Cosmochimica Acta, 46,* 513-548.

Sonnenthal, E.; Spycher, N.; Apps, J.; Simmons, A. 1998. *Thermo-Hydro-Chemical Predictive Analysis for the Drift-Scale Heater Test.* Yucca Mountain Project Level 4 Milestone SPY289M4, Lawrence Berkeley National Laboratory.

Spycher, N.; Sonnenthal, E.L.; and Apps, J. 1998. "Interpretive Analysis of the Thermo-Hydrological-Chemical Aspects of the Single Heater Test." *In:* Tsang, Y.W.; Apps, J.; Birkholzer, J.T.; Freifeld, B.; Hu, M.Q.; Peterson, J.; Sonnenthal, E.; and Spycher, N. *Single Heater Test Final TDIF Submittal and Final Report,* Chapter 4. Yucca Mountain Project, Level 4 Milestone SP1190M4 and SPY147M4, Lawrence Berkeley National Laboratory.

Xu, T.; Gerard, F.; Pruess, K.; and Brimhall G. 1998. Introducing Reactive Solute Transport to TOUGH2: Application to Supergene Copper Enrichment. *Proceeding of the TOUGH Workshop1998*, Lawrence Berkeley National Laboratory.

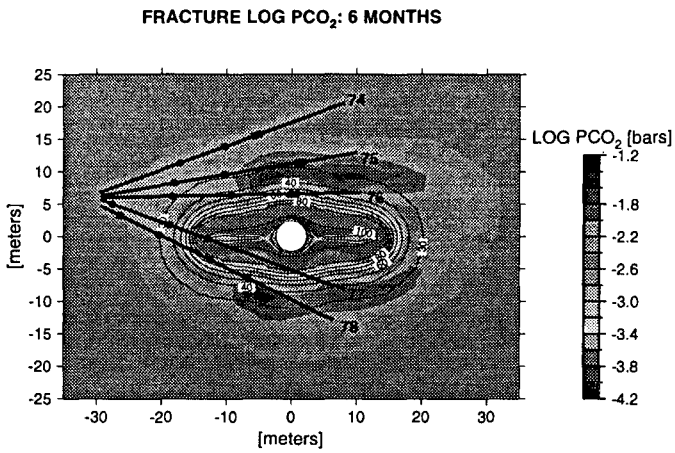

Figure 1. Partial pressure of CO_2 (log scale) in fractures predicted for the DST after six months of heating. Hydrology boreholes are depicted.

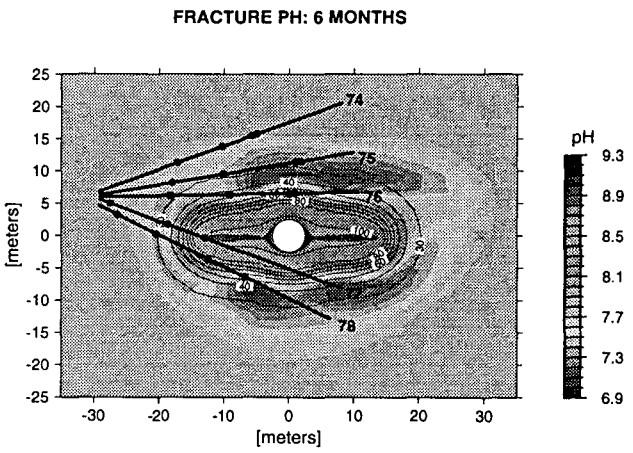

Figure 2. Fracture water pH predicted for the DST after six months of heating. Hydrology boreholes are depicted.

Session P3:
FRACTURE-MATRIX INTERACTIONS AND REACTIVE CHEMICAL PROCESSES

Calculation of Fracture/Matrix Interaction for Unsaturated, Low-Permeability Welded Tuff

J.P. Fairley
Earth Sciences Division
Lawrence Berkeley National Laboratory
Berkeley, CA

The quantity of interaction between fractures and matrix in an unsaturated, fractured porous medium has recently become an important issue, primarily due to its connection with the disposal of high-level radioactive waste. Numerical modeling by a number of investigators indicates that a significant reduction in the geometric area of interaction between fractures and matrix is important for accurately matching site conditions at Yucca Mountain, the proposed site of the nation's first high-level radioactive waste repository (Ho, 1996; Bandurraga and Bodvarsson, 1996). Reduced f/m interaction may translate to higher peak doses and faster travel times of transported radionuclides to the accessible environment. In addition, reduced f/m interaction decreases the site's ability to attenuate infiltration pulses and leads to a greater likelihood of water contacting the waste packages and causing premature canister failure.

To address some concerns about the magnitude of fracture/matrix (f/m) interaction, Lawrence Berkeley National Laboratory conducted, at the request of the Department of Energy, a series of field experiments in the fractured, welded tuffs that comprise Yucca Mountain. These experiments measured f/m interaction by mass-balance calculations between an injection borehole and a slot, positioned so as to collect any excess water injected over the amount imbibed by the matrix. The present paper discusses an analytical model that was used for design calculations, model predictions for the test, and the results of the test as interpreted by the model.

CONCEPTUAL MODEL AND MODEL QUANTIFICATION

Flow was assumed to take place from a single fracture that formed a continuous path between the injection borehole and the collection slot. Imbibition to the matrix was calculated using a closed-form, approximate analytical solution to the Richards' Equation for imbibition from a fracture under negative water potential derived by Fairley et al. (1997). The area of interaction was assumed to be proportional to the cumulative injection volume until breakthrough of flow into the collection slot. This breakthrough time was designated as t_0, and the wetted interaction area was assumed to remain constant after t_0. The model further assumed a constant saturation in the wetted portion of the fracture, and imbibition to be small compared to the injected volume.

The quantity of water imbibed to the matrix as a fraction of water injected, θ, was found to be:

$$\theta = \begin{cases} \dfrac{2\phi(S_w - S_i)}{3bS_f}\left[\dfrac{2\beta n k_r(\psi)}{n+1}\dfrac{\partial\psi}{\partial S}\right]_{S=S_w}^{\frac{1}{2}} t^{\frac{1}{2}} & 0 < t \le t_0 \\ \dfrac{2\phi(S_w - S_i)t_0}{bS_f}\left[\dfrac{2\beta n k_r(\psi)}{n+1}\dfrac{\partial\psi}{\partial S}\right]_{S=S_w}^{\frac{1}{2}} \dfrac{(t^{\frac{1}{2}} - \frac{2}{3}t_0^{\frac{1}{2}})}{t} & t > t_0 \end{cases} \quad (1$$

where t is the time since the onset of injection, ϕ is porosity, S is saturation, b is effective fracture aperture, β is wetting phase mobility, k_r is matrix relative permeability, n is a function of matrix initial and imposed saturations, and ψ is water potential. The subscripts f, i, and w refer to fracture, matrix initial, and matrix imposed (at the f/m interaction boundary) saturations, respectively.

In addition to calculating matrix imbibition, Eq. (1) allows a determination of maximum θ. Setting the derivative of θ with respect to t equal to zero and solving yields:

$$t_{max} = \frac{16}{9} t_0$$

This prediction implies the ideal length of time to run a test for minimum mass balance error.

RESULTS

A number of tests were performed in the f/m interaction field test. In order to avoid the complications of superposing results for multiple tests with inadequate matrix equilibration times, the analytical model is here compared to the results of the first test within a single fracture with permeability, as measured by air-injection testing, of 1.09×10^{-12} m^2.

Breakthrough at the collection slot for this test was observed at $t_0 = 300$ seconds after the onset of injection. Allowing for water stored in the fracture, θ appeared to begin decreasing at some time between t_0 and $2t_0$, ultimately stabilizing at a quasi-steady value after about $10t_0$. This behavior is in accordance with the model prediction of t_{max}, above. To t_0, the volume injected was approximately $4 \times 10^{-4} m^3$ (400ml), an average injection rate of about $1.3 \times 10^{-6} m^3/s$ (80ml/min). During the time following breakthrough, injection rates slowly climbed to stabilize at about 2.2×10^{-6} m^3/s (130ml/min). This rise in injection rate presumably resulted from an increase in relative permeability following dissolution and displacement of entrapped air in the fracture, a phenomena that violates the assumption of constant wetted area following breakthrough at the collection slot. In future tests, slower infiltration rates may alleviate this problem and help to reduce test uncertainty.

Pre-test design calculations were carried out using a variation of Eq. (1) that employed an explicit function for t_0:

$$t_0 = \frac{bh^2}{4R}$$

where h is the distance between the injection borehole and the collection slot. This formulation assumes a triangular shaped wetted area with a maximum width at the collection slot equal to one-half h. Enforcing the above area function on the imbibition calculations underestimated both breakthrough times and θ by about one order of magnitude (Fairley et al., 1997). The opposite effect arises in the application of Eq. (1): estimates of wetted interaction area and θ are both $O(10^2)$ greater than indicated by field observation.

CONCLUSIONS

A comparison of the results of Fairley et al. (1997) with Eq. (1) indicates that the most important assumption of the model proposed, that imbibition is small compared to injection volume, was violated in the f/m interaction field test. Two possible approaches may be used in the future to overcome this difficulty: Eq. (1) could be modified to include a term for loss to the matrix, and the resulting equation solved iteratively, or the non-linear mass-balance equation itself may be amenable to solution directly. These approaches are currently being investigated, and future analysis of f/m interaction tests will account for this aspect of testing. In spite of this difficulty, the model yielded valuable insight for test planning, including bounds on breakthrough times, and an estimate of the time of maximum fraction of water imbibed.

REFERENCES

Bandurraga, T.M., and Bodvarsson, G.S. 1997. Calibrating matrix and fracture properties using inverse modeling, In: G.S. Bodvarsson, T.M. Bandurraga, and Y.S. Wu, eds., The Site-Scale Unsaturated Zone Model of Yucca Mountain, Nevada, for the Viability Assessment, Chapter 6. Yucca Mountain Project Level 4 Milestone SP24UFM4. Report LBNL-40376. Berkeley, California.

Ho, C.K., 1997. Models of fracture-matrix interactions during multiphase transport in porous media, In: Proceedings of The Sixth Symposium on Multiphase Transport in Porous Media. 1997 ASME International Mechanical Engineering Congress and Exposition, November 16-24, Dallas, Texas.

Fairley, J.P., C. Doughty, and R. Salve, 1998. Discrete fracture modeling, In: Progress Report on Fracture Flow, Drift Seepage and Matrix Imbibition Tests in the Exploratory Studies Facility, Chapter 3. Yucca Mountain Project Level 4 Milestone, Berkeley, California.

Correlation of Mineral and Porosity Distribution at the Sub-millimeter Scale, And Its Implications For Reactive Transport Simulations

William E. Glassley, Lawrence Livermore National Laboratory, Livermore, CA
Ardyth Simmons, and Geraldine M. Lamble, Lawrence Berkeley National Laboratory, Berkeley, CA

Introduction

Reactive transport models that simulate processes in porous media have generally required abstracted representation of porosity, permeability and mineralogy. This has usually been accomplished by assuming that both permeability and mineralogy are homogeneously distributed within each cell of the computational mesh. This approach has been required because cell sizes scaled to the dimensions of mineralogical and porosity heterogeneity would result in meshes >> 10^9 cells, to represent most geological processes. In addition, the spatial distribution of mineralogical and porosity heterogeneity is often not adequately characterized to justify such a detailed representation. To evaluate the effects of these abstracted, homogeneous cell representations on the outcomes of reactive transport simulations, we have initiated an analytical study of mineral and porosity distribution in fractured tuffaceous rock, and used these measurements in reactive transport simulations. We have compared the results obtained using homogeneous cell representations of the rock with simulations using the discrete, realistic representation of mineral and porosity distribution.

Approach

A sample containing a fracture was selected from core CHE-2, borehole footage 128.9-129.6, from the Yucca Mountain Drift-Scale Heater Test (DST). The fracture was about 1 cm long and 40 microns wide, appeared to be filled with silica, and belonged to the first generation of fracture filling, associated with vapor-phase alteration. Samples were made into polished thin sections and optically examined. The dominant phenocrysts are sanidine and plagioclase, with lesser quartz and Fe-oxides. Accessory minerals include zircon and apatite. The bulk of the groundmass consists of the devitrification products sanidine, quartz, and cristobalite. Alteration textures are highly varied (including spherulitic textures, relict vitric textures, and granophyric crystallization) and spaced anywhere from less than 1 mm to several cm apart. Vapor phase crystallization includes quartz, quartz after tridymite, a zeolite (heulandite?) and alkali feldspar. Vapor-phase cavities range from 0.3 - 4.5 cm^2 in area. Fracture filling minerals in the DST samples are primarily silica phases, with minor occurrence of a zeolite.

Areas that exhibited characteristic mineralogical features were selected for detailed study using the focussed soft X-ray beam line at the Advanced Light Source (ALS), Lawrence Berkeley National Laboratory. Area scans that mapped element distributions were made over 1,000 by 1,000 micron regions, to map mineral distributions. Porosity distribution was determined by

using I as a tracer and mapping its concentration. The samples were prepared by swabbing with saturated potassium iodide, which imbibed into the rock pores. The solution was then allowed to evaporate, and the surfaces repolished, removing KI deposits from mineral surfaces but leaving them behind in the porosity.

The resulting mineral grain sizes and abundances were then used in reactive transport simulations. In one suite of runs, homogeneous mineral distributions were used throughout the flow domain. In another set ('discrete suite'), minerals were distributed through the domain, approximating their grain size and distribution pattern as observed in the rock, although total mineral abundance was the same as in the homogeneous case.

Results

Grain size in the groundmass varies considerably with texture, which correlates closely to the degree of devitrification of the groundmass. In devitrified areas where it is possible to estimate grain size by optical microscopy, the average cross-sectional area for quartz, cristobalite, tridymite, and sanidine falls into the range of 0.01 mm^2 (range is 0.004 - 0.4 mm^2). The vapor-phase, cavity lining zeolites and albite phenocrysts are an order of magnitude larger (0.16-7.2 mm^2). The Fe-Mn oxides are bimodally distributed in size; smaller grains are finely disseminated and correlated with areas of abundant cristobalite, whereas the larger grains are more widely distributed and correlate with areas of abundant quartz. Furthermore, the larger oxides appear under reflected light to be distinctly two-phase, consisting of hematite and ilmenite.

For the purpose of quantifying mineral domains on the ALS maps, we assumed that an element could proxy for a mineral, e.g., K was assumed to proxy for alkali feldspar, Si for silica polymorphs, Fe for hematite. The spacing between mineral domains is about the same for each element, on the order of 70 microns. The domains of feldspar and silica are an order of magnitude larger (thousands of microns) than those of the oxides (hundreds of microns). Across an area of 300 $microns^2$, the number of domains of any mineral ranges from 10-22, and their size distribution ranges from 50-5800 $microns^2$.

For the method of using I as a tracer for porosity to be viable, it is important to demonstrate that the location of I high intensity is not correlated with K, or Ca, nearby peaks in the spectrum which could occlude the I reading. Covariance plots demonstrate the lack of correlation.

Our DST samples did not include fractures of the second generation, i.e. those coated partially with silica, calcite, Fe-oxides, and clays, although these tectonic-related fractures are thought to be the primary ones that have experienced fluid flow, and they are abundant at larger scales than our sampled area. Both generation fractures may be partially void, and the first-generation fractures may terminate in open vapor-phase cavities. The second-generation fractures may be void for longer intervals (10s of cm), and are probably the main contributors to fracture porosity.

Our element map indicates that the silica-filled fracture is not a location of porosity, but that porosity is concentrated in the matrix of the sample. Hence, locations that are K-rich (alkali feldspar) and Si-rich (silica polymorph) regions possess the lowest porosities, as does the Si-rich vein. An hypothesis consistent with this observation is that the porosity is dominantly along

grain boundaries of the fine-grained, interstitial matrix material. Furthermore, pore space is smaller than 1 micron, the resolution of the beam.

Reactive transport numerical simulations were then conducted, as described above. The results show that differences between the amount of mineral dissolved along the flow path, the abundance of secondary minerals formed, and the distributions of the minerals varied by more than a factor of two between the homogeneous and discrete suites of runs. These differences result from the localized concentration of secondary mineral development at specific locations where the initial mineralogy favored the formation of certain phases in the discrete mineral distribution suite of simulations. Nontronite formation, for example, concentrated in those locations where magnetite was an original mineral phase, completely replacing the original mineral. However, its formation was also enhanced by the inhomogeneous distribution of solute components due to localized mineral reactions.

In addition to the distribution and abundance of secondary phases, the composition of fluids in the flow domain can be significantly different between the two representations. This effect results in complex compositional distribution patterns that strongly contrast with the smooth, linear variations observed for the homogeneous case.

Conclusions

Mineral distributions exhibit complex, heterogeneous patterns in the devitrified and welded tuffs. Using these distribution patterns in reactive transport simulations demonstrates that homogeneous cell models of mineral and fluid chemistry evolution can underestimate or overestimate mineral abundances and distribution by a significant degree. The results have significant implications for simulations that attempt to represent fluid compositional characteristics, as they may influence local environmental conditions. Estimates of the durability of materials sensitive to water composition may be affected by these uncertainties.

In addition, efforts to understand and simulate sorption of contaminants on mineral surfaces need accurate estimates of the available surface area. The results presented here indicate that such estimates may be strongly influenced by how the original mineral distribution is represented. If reactive transport plays a role in the stability of the relevant sorptive mineral phases, it would be appropriate to develop a strategy to determine the extent to which either homogeneous or discrete mineral representations influence the outcome of the simulations. Furthermore, as it is certain that the properties of individual rock units will differ significantly, the sensitivity of simulation results to the specific properties of individual lithologies needs to be established.

Efforts are underway to refine these simulation results, and to develop algorithms to allow representation of mineral heterogeneity, without the need to resort to discrete mineral representations, which would be computationally prohibitive. The impact of porosity variability correlated with mineral distributions is currently underway.

Study of Diffusion Processes in Simple Fracture Systems

Guomin Li and Chin-Fu Tsang

Earth Sciences Division
E.O. Lawrence Berkeley National Laboratory
Berkeley, CA94706
(e-mail: gmli@lbl.gov and cftsang@lbl.gov)

Potential radionuclide migration in fractured rock has called for many studies dealing with the different aspects of flow and transport in strongly heterogeneous porous medium. A Lagrangian type of simulation technique, which takes into account dispersion and diffusion, is a way to model solute transport in heterogeneous porous media. The Random Walk Method is one such technique. Simulations will be made by following particles moving through rock fracture in steps simulating advective and diffusion. Two studies are designed to study and understand the effects of the diffusion process on flow in simple fracture systems. The first study is made to explore the effects of "stagnant" pool on the particle movement in a single fracture. The second study is to investigate the mixing behavior at fracture junctions.

A Flow Channel in a Single Fracture

We assume that the singe fracture can be represented by a 2-D domain with dimension 120-mm length and 60-mm width covered by a finite difference grid comprising of 120×60 nodes. The permeability field is high permeability (0.001 m/d) along a flow channel in the 2-D plane embedded in a very low permeability (1.0E-33 m/d) background. Model 1 represents a 20-mm width flow channel through the domain. Model 2 is modified from Model 1 by adding a small pool of 20×20 square mm near the middle of the flow channel. Model 3 is modified from Model 2 by enlarging the pool to 40×30 square mm. The groundwater flow through this domain is calculated for constant piezometric head boundaries: the left-hand boundary is assumed to have pressure head of 1-mm and right-hand boundary 0-mm, with no-flow conditions imposed on the upper and lower boundaries.

We consider the diffusion effect on the tracer transport through the flow channel. We assume $\sqrt{2D_f t}$ as the diffusion length and t is the average time of particle moving through the domain. For a steady flow field, t is fixed, so that the diffusion length increases with the diffusion coefficient. These values of the diffusion length, 12.00-mm, 6.91-mm and 0.69-mm, are used in our simulations.

The Random Walk Method is based upon the process that the particles are transported under the influence of spatial fluid velocities and diffusion process. It is possible for some particles to go backward out the left-hand boundary or to go into the low permeability background field from one time step to the next one. We assume that the particle will disappear once it goes out the left-hand boundary, and also it will be reflected back into modeling domain if it goes out of flow channel and into the background low permeability field.

Given the flow model the velocities can be calculated at any position in the domain. All particles are initially at 20 mm from the left-hand high piezometric head boundary and those that arrive at the right-hand low piezometric head boundary are collected. A plot of the number of particles collected at the right-hand boundary at different arrival times constitutes the

breakthrough curves. In our presentation 20 particle traces were plotted to show the solute transport paths, but 1000 particles were used to plot the breakthrough curves.

Figure 1 shows the 20 particle traces in Model 3 for different diffusion lengths. It shows that under the influence of diffusion, many of the particles have moved into the pool. For high diffusion lengths some particles have moved into the deepest part of the pool.

The breakthrough curves, show that low diffusion lengths result in narrow and high peaks. Without the pool the particles should at arrive right-hand boundary at about the same time. For the same diffusion length, but with a larger pool size, the peak height of the breakthrough curve decreases and the tail of the curve increases. This study will attempt to characterize the behavior of breakthrough curves as a function of the flow velocity and the size of the "stagnant" pool.

Fracture Intersections

For this problem, we start by constructing a 2-D domain, 60-μm length and 60-μm width, covered by a finite difference grid of 60×60 nodes. Each grid block has the dimension of 1μm×1μm. The domain is cut by one vertical and one horizontal paths, representing two intersecting fractures 20-μm width, with a high permeability of 1.0 μm/d, surrounded by very low permeability background of 1.0E-36 μm/day. The groundwater flow through this domain is also calculated for constant piezometric head boundaries: the left-hand boundary and the bottom boundary are assumed to be at 1-μm, and the right-hand boundary and the top boundary are assumed at 0-μm.

The velocity distribution can be calculated at any position in the domain. All particles are put initially at 20μm from the left-hand high piezometric head boundary and those that arrive at the right-hand and the top low piezometric head boundary are collected.

Figure 2 shows 20 particle traces with the diffusion length of 1.55-μm. Note that the t used to calculate the diffusion length here is defined as the time to pass the 20-μm intersection region. All particles that go in the left-hand boundary will all go out of the top boundary if the diffusion length is very low, e. g., 0.05-μm. It means the diffusion term is too small to affect the particle movement in the flow field, and the particles just follow the streamlines. For large values of diffusion length with, some of the input particles jump into nearby streamlines, and then these particles move out of the right-hand boundary.

What percentage of particles can go through the right-hand boundary? It is clear that this is a function of the diffusion length. In these calculations both 1000 and 20000 particles were used to investigate the percentage of the incoming particles cross the streamlines and emerge through the right-hand boundary. Figure 3 shows the detailed results. When the diffusion length is very large, the streamlines become not important and there is "perfect mixing" at the intersection, then the percentage is near 50%, as would be expected.

The purpose of this preliminary work is to apply the Random Walk Method to investigate the mixing behavior at the fracture intersection to understand the transport of particles to different outflow fractures as a function of flow velocities and diffusion coefficient.

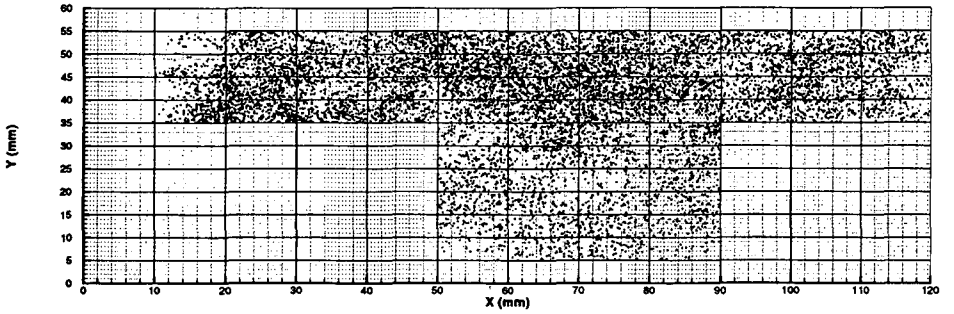

a)

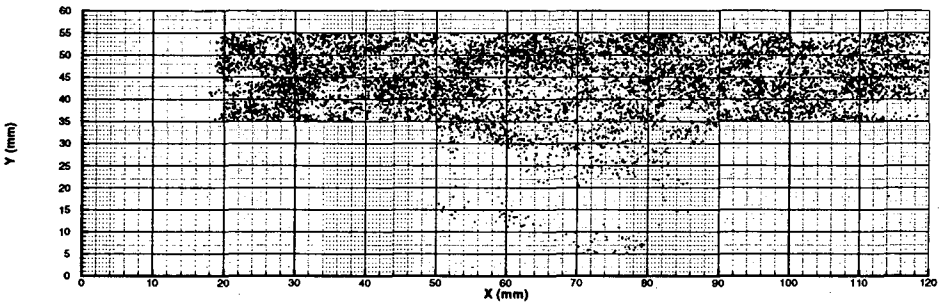

b)

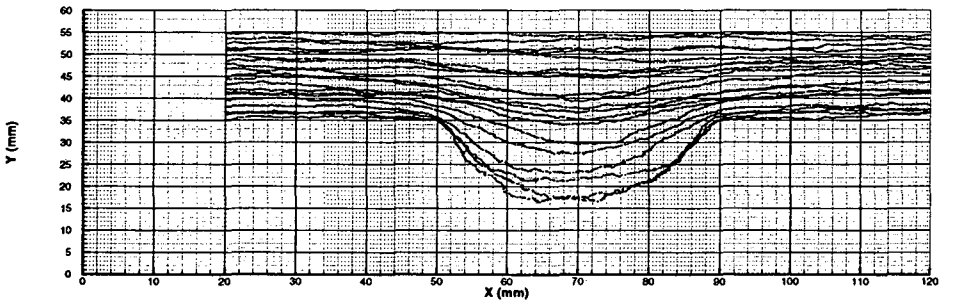

c)

Figure 1. Spatial particle trace in model 3 for different diffusion lengths: a) 12.0 mm, b) 6.91 mm and c) 0.69 mm.

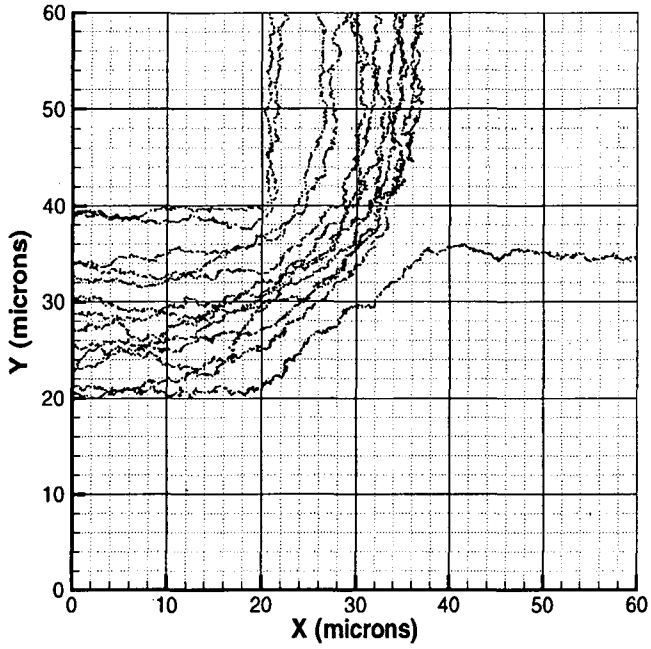

Figure 2. Spatial particle trace in cross-fracture model for diffusion length of 1.55-μm.

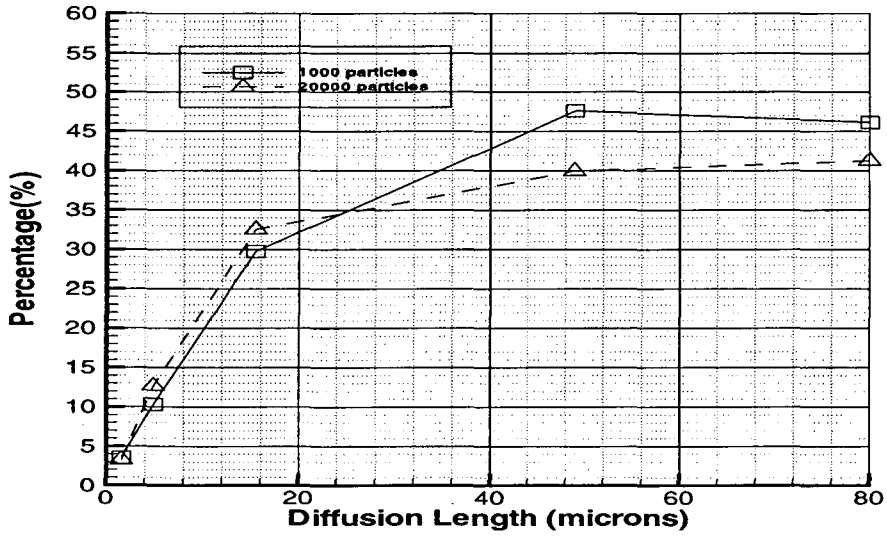

Figure 3. The percentage of the particles through out the right-hand boundary over the total particles is a function of diffusion length.

The influence of different fracture-types in chalk on groundwater salinization processes

Livshitz Y., Issar A., Yakirevich A.

Water Resources Research Center, J. Blaustein Institute for Desert Research
and Department of Geology and Environmental Sciences,
Ben-Gurion University of the Negev Sede-Boker, 84990, Israel.

The groundwater in the Eocene chalk aquitard in the Northwestern Negev Israel is characterized by brackish water (TDS of 600-10,000 mg/l). It is assumed that the main source of this salinity is ancient residual water trapped in the chalk pores. The groundwater flow is mostly controlled by fractures. Two main types of fractures are recognized in the chalks:
a) single-layer fractures with openings of several mm, that were developed as a result of stress that prevailed during the downwarp of a sedimentary basin; b) multi-layer fractures with openings up to 10 mm caused by tension formed during the Neogene uplift. Some fractures, mostly of the multi-layer group, are enlarged by karst processes.

Pumping tests indicate two major stages with respect to salinity. During the initial stage of pumping, water salinity increases sharply. Subsequently, as pumping continued, groundwater salinity decreases. At the final stage of pumping, salinity decreases significantly compared to the salinity values prior to pumping (Fig 1). Current studies of previous water levels and salinity data from several production wells reveals that decreasing water levels accompanied by decreasing groundwater salinity is a common phenomenon for this aquitard (Fig. 2). Transmissivity values and storage coefficient, determined from pumping tests, vary from 0.01 up to 100 m^2/day and $1*10^{-8}$ up to 0.5, respectively, whereas maximal trasmissivity is associated with minimal storage coefficient. It is important to note, however, that in most cases drawdown and recovery curves can be divided into two sections 1) an initial stage, characterized by low transmissivity and high storage coefficient; and 2) a final stage, characterized by high transmissivity and high storage coefficient. The above-mentioned findings associated with decreasing in water levels accompanied by decreasing groundwater salinity, and the occurrence of marine-like saline water in the chalk pores can be explained by the following conceptual model:

The flow and transport processes involve three media.

- Chalk porous medium. Due to high porosity (~40%) and with low connectivity, this medium is characterized by a very high storage coefficient and extremely low conductivity.
- Medium of fine fractures (fractures unaffected by karst development, mainly single-layer ones). Each fine fracture is characterized by low hydraulic conductivity and low specific storage. However, a large number of such fractures define low transmissivity and high storage coefficient.
- Medium of karstified fractures (fractures enlarged by karst development mainly along multi-layer fractures). Each karst-affected fracture is characterized by high hydraulic conductivity and high specific storage. However a relatively small number of karst-affected fractures (compared with fine fractures) cause the entire medium have karstified fractures to be of high transmissivity and low specific yield.

The salinization of groundwater can be explained as follows:

1 Ancient residual saline water (TDS up to 35 mg/l) originated in the Eocene or Miocene sea, is trapped in the chalk pores. This type of water does not participate in the groundwater flow process but still contributes salts by diffusion to the fine fractures.

2. Brackish-saline water occurs in the fine fractures. These fractures do not control the groundwater flow, but transport salt from the porous media to the karst fractures.
3 Recent fresh-brackish water occupies the karst fractures. Most of the groundwater flows through these fractures.

To test this conceptual model, the simulation of pumping test was carried out using synthetic, dual porosity medium {A} characterized by high transmissivity and low storage coefficient. The medium A consisted of two media: 1) a medium characterized by high transmissivity and low specific yield ({K} analogous to karstified fractures) and 2) a medium characterized by low transmissivity and high specific storage ({F} analogous to fine fractures). The goal of the modeling was to estimate quantities of water contributed from the fine fractures at different stages of pumping. Calculations where carried out by applying Theis solution to drawdown pumping test for medium A. The contribution of fine fractures was calculated by applying calculated drawdown and parameters from media F.

Calculations were carried out for A with transmissivity ranging from 10 up to 100 m^2/day and storage coefficient within the range of 0.001- 0.01, constant F transmissivity (0.1 m^2/day) and storage coefficient (0.5) with constant pumping rate of 45 m^3/day. Results show that the relative contribution of water from fine fractures decreases with drawdown (Fig 3).

Simulations of the pumping performed in the Moshe Revivim well (Fig. 1) were carried out using measured drawdown, pumping rate, synthetic fine fracture transmissivity of 0.1 m^2/day and synthetic storage coefficient of 0.5. Results show same trend for the calculated contribution of the water coming from fine fractures and the measured water salinity (Fig 4).

The simulation using synthetic parameters confirm the assumptions on which the conceptual model is based. The transport scheme during the pumping test can be as follows:

1 At the initial stage of the pumping, the first water to be pumped is the fresh water from karst fractures, around the vicinity of the well. Due to high transmissivity and low specific yield of these fractures this stage is very short (several seconds).
2 Subsequently, water from fine fractures and remote karstified fractures reach the pumping well. Contribution of the water coming from fine fractures is relatively high and it depends on the transmissivity ratio between karst and fine fractures, as well as the ratio of storage coefficients between karstified and fine fractures. The increase of fine fracture contribution causes an increase of water salinity. Due to high contribution of fine fractures to the groundwater system, this stage is characterized by low transmissivity, high storage coefficient and high water salinity.
3 Continuos drawdown involves remote karst fractures. The increasing contribution of water coming from karst fractures decreases the water salinity. At this stage of pumping most of the water comes from karstified fracture. The influence of fine fractures is negligible, therefore this stage is characterized by highest transmissivity, lowest specific yield, and lowest water salinity.

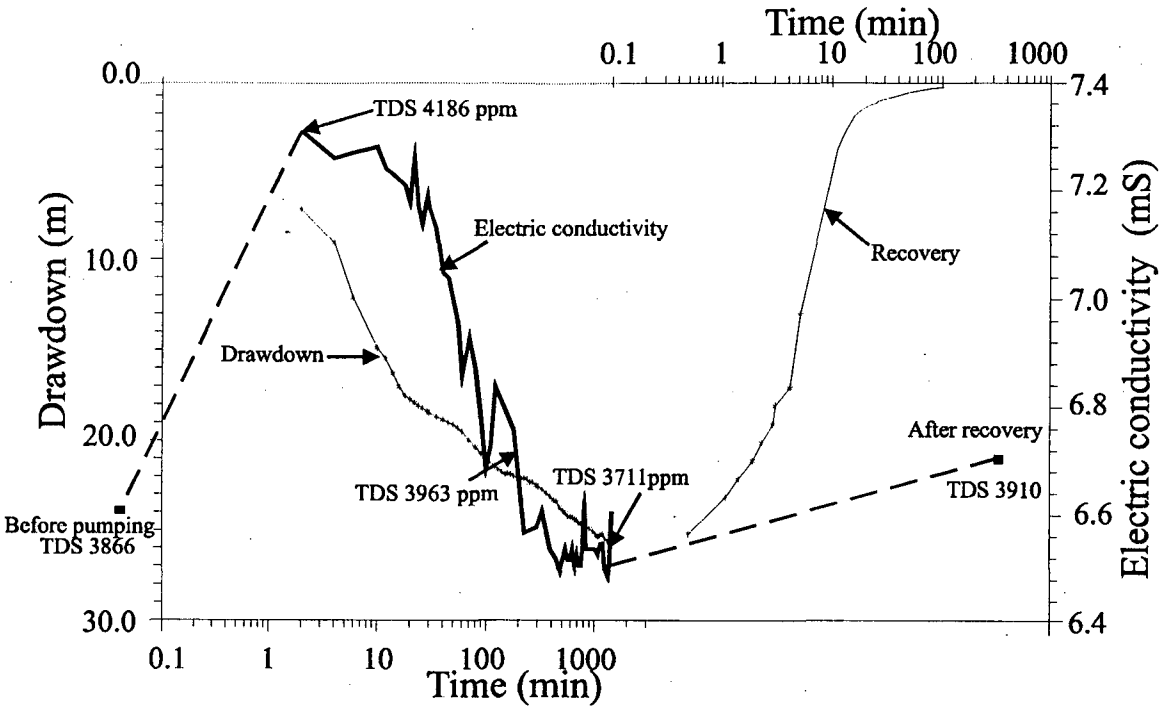

Fig. 1 Pumping test from Moshe Revivim well

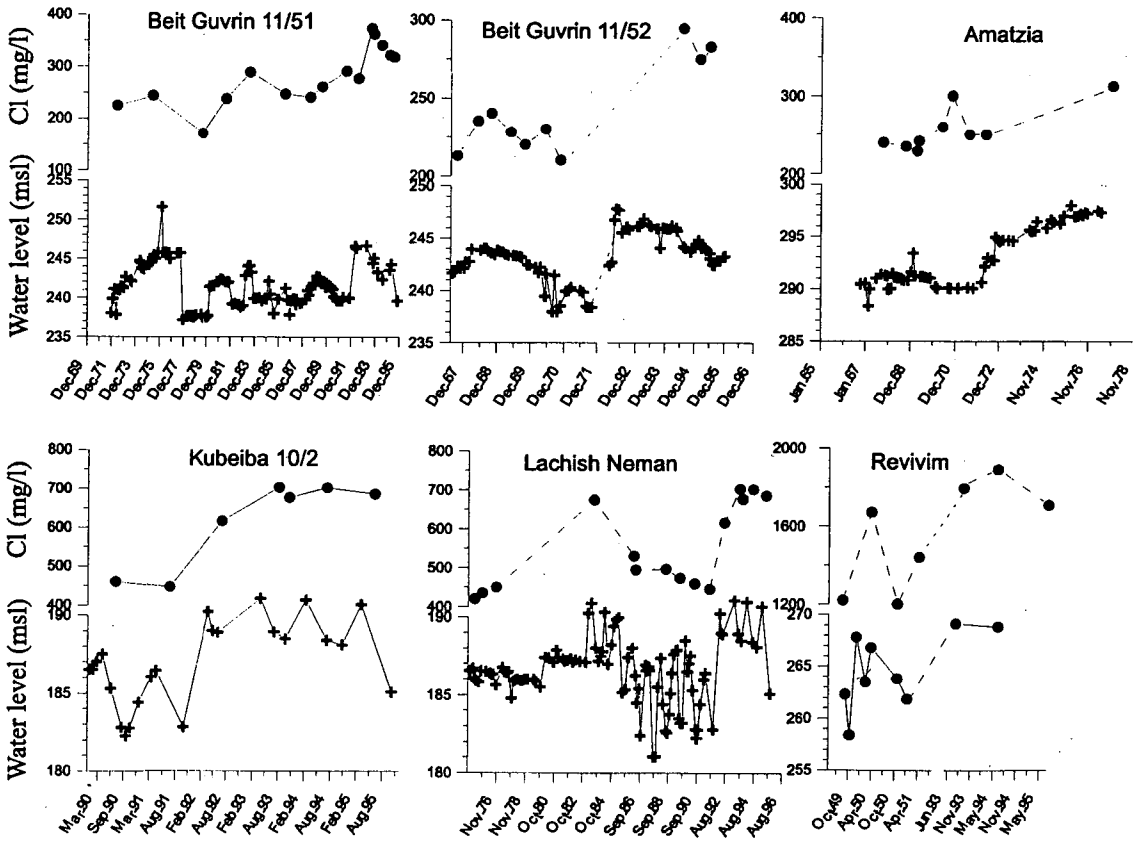

Fig.2 Water levels and salinity from several production
(Data from Hydrological service of Israel)

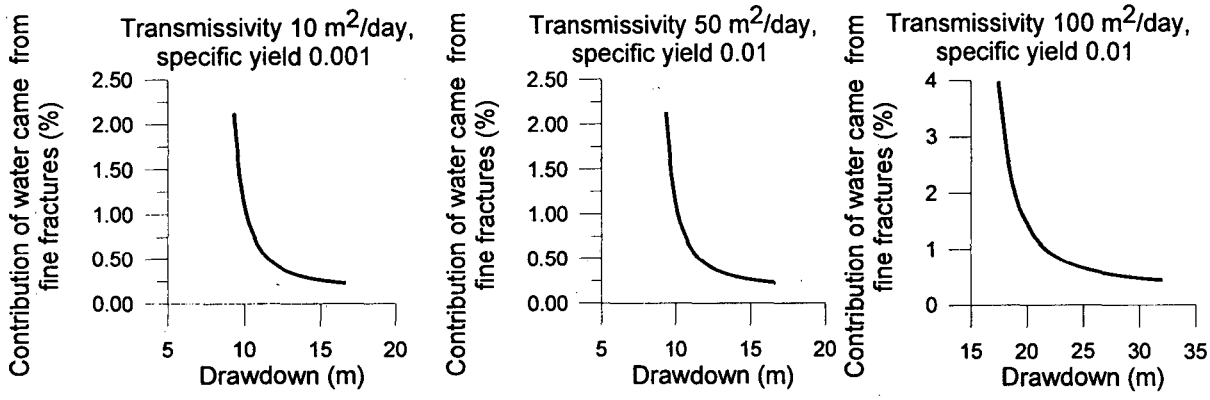

For all calculations we used fine fracture medium with transmissivity of 0.1 m^2/day, specific yield of 0.5 and pumping rate 45 m^3/day,

Fig 3. Quantities of water contributed from the fine fractures at different stages of pumping for different synthetic media

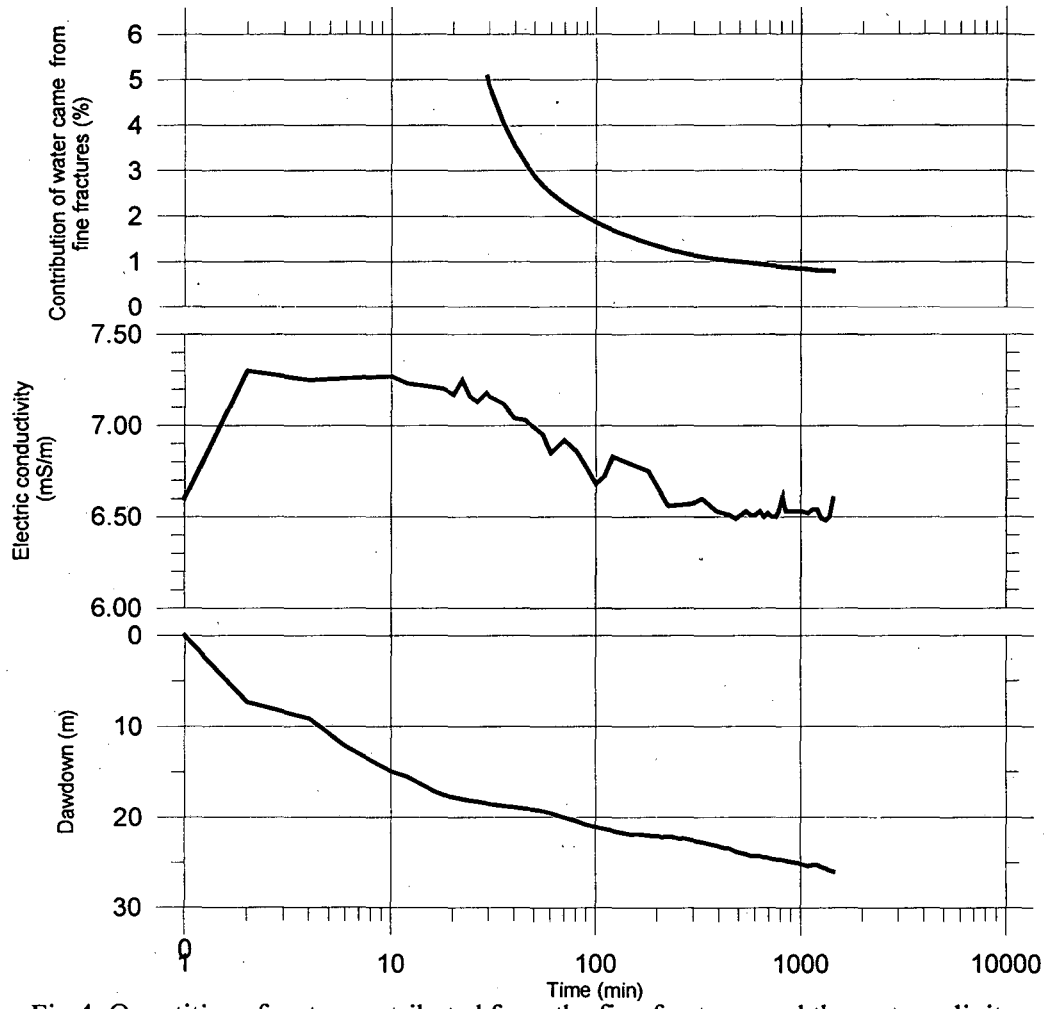

Fig 4. Quantities of water contributed from the fine fractures and the water salinity. Calculation for the pumping test from Moshe Revivim well.

Infiltration of Hyperalkaline Groundwater along Discrete Fractures at Maqarin, Jordan

Carl I. Steefel[1]
Peter C. Lichtner[2]

[1]Geosciences and Environmental Technologies Division, Lawrence Livermore National Laboratory, Livermore, CA 94550;
[2]Los Alamos National Laboratory, Los Alamos, NM 87545

Introduction

The intention of many nations to dispose of radioactive wastes in low-permeability formations has led to an increased interest in the behavior of contaminants in fractures. While a substantial body of work has been devoted to understanding the physics of flow and transport in discrete fractures, a much smaller amount of research has focused on the coupling of multicomponent chemical reactions and transport in such systems (Steefel and Lichtner, 1994; Novak, 1996; Steefel and Lichtner, 1998a and b). An understanding of multicomponent chemical effects in the vicinity of nuclear waste repositories is important because of their potential influence on both radionuclide retardation and the physical properties of the rock and matrix. Because nuclear waste repositories need to function over long periods of times (hundreds to tens of thousands of years), reaction-induced modifications of the physical and chemical properties of the near-field host rock may be important. A related issue in the design of a nuclear waste repository is how the materials used in its construction may affect performance. Much of the attention in this regard has focused on the use of large amounts of cement in repositories, since groundwater reacting with cement may attain very high pH values. The long time scales over which nuclear waste repositories must function has led to an interest in natural analogue sites where one or more of the processes or conditions expected at the repository site has been operating for substantial lengths of time. One such site which is being actively investigated is located at Maqarin, Jordan where the dissolution of naturally-occurring portlandite (the principal component of cement) has led to high pH groundwater infiltrating the local rock along fractures (Alexander et al., 1998). Here we use a numerical multicomponent reactive transport model to interpret the mineralogical alteration effects and the hydrogeochemistry along discrete fractures in the Eastern Springs area at Maqarin, Jordan.

Hyperalkaline Groundwater and Alteration at Maqarin, Jordan

At Maqarin, Jordan, hyperalkaline groundwater results from interaction with natural occurrences of portlandite [$Ca(OH)_2$] which formed initially as a result of in situ combustion of bituminous marls (Alexander et al., 1998). Maqarin is located in northern Jordan, close to the Syrian border (Figure 1) within a stratigraphic sequence of Cretaceous-Tertiary carbonate rocks overlain by Quaternary basalts and soils. Groundwater circulating through a zone of metamorphosed marl (or clay biomicrite) containing portlandite takes on a chemical composition very close to that found in cement porewater, i.e., a very high pH (12.1 to 13.5) and high Ca^{+2} contents (Smellie, 1998). In addition, much of the groundwater flow is through fractures, so the site represents an

excellent analogue of the kind of hydrologic and hydrogeochemical conditions expected in the near-field region of a cement-bearing nuclear waste repository.

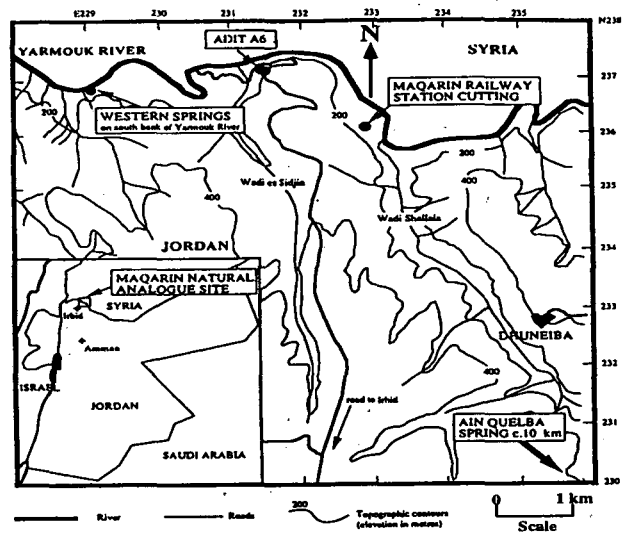

Figure 1: Location of the Maqarin natural analogue field site

Regional groundwater flow in the Maqarin area is generally westwards towards the Jordan River valley and northwest towards the Yarmouk River valley (Khoury et al., 1998). Several spring complexes occur in the area, including an Eastern Springs area and a Western Springs area (Fig. 1).

There is evidence that the $Ca(OH)_2$-rich hyperalkaline springs have been active for some time, since extensive alteration products are observed in fractures and rock matrix bordering fractures. Alteration in the Eastern Springs area is particularly well exposed in the A-6 adit (or tunnel) and has been examined in detail at two points, the M1 and M2 sampling sites where the principal host rock is a clay biomicrite (Figure 2). Wallrock bordering the fractures is leached of calcite, kaolinite, and silica, with porosity immediately adjacent to the fracture increased. Primary silicate and carbonate phases are replaced by fine-grained ettringite [$Ca_6Al_2(SO_4)_3(OH)_{12}.26\ H_2O$] and CSH (hydrated calcium-silicate) phases. Fracture mineralization at the M1 and M2 sites is dominated by an infilling of ettringite with lesser amounts of CSH-phases, which generally postdate the ettringite.

The focus of this study is on a set of approximately N40W-trending fractures exposed in the A-6 adit within the Eastern Springs area at Maqarin (Figure 2). Groundwater collected at the M1 and M2 sites shows pH values of 12.30 and 12.09 respectively (Smellie, 1998).

Contouring of the phreatic surface in the vicinity of the A-6 adit indicates a hydraulic gradient of about 0.1 toward the northwest (Khoury et al., 1998). According to the hydrologic data, the M2 site lies downgradient from the M1 site, suggesting the possibility that the decrease in pH observed between the M1 and M2 sites (about 100 meters along the fracture trace) may be due to water-rock interaction. Below, we use reactive transport modeling of discrete fractures to test this hypothesis.

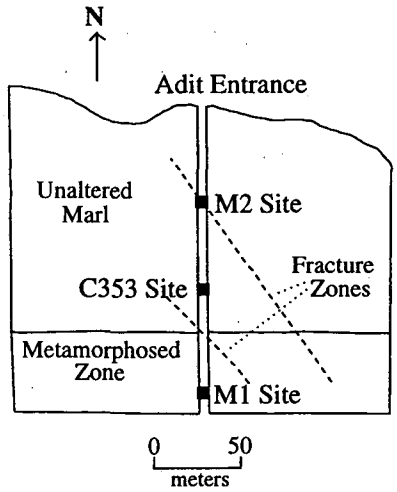

Figure 2: Map of the A-6 adit in the Eastern Springs area, Maqarin. Note location of M1 and M2 sites. Local hydraulic head contours are sub-perpendicular to principal fracture directions with a slope of the water table toward the northwest.

Modeling the A-6 Adit Fracture System

As discussed above, fracture sets exposed in the A-6 adit (Eastern Springs area) at Maqarin are oriented approximately N40W, sub-perpendicular to the local hydraulic head contours which slope toward the northwest. Assuming the flow system is at steady-state, the average rainfall of 458 mm/year can used as an approximation of the bulk Darcian flux through the metamorphosed section A-6 adit area at Maqarin. Combining this information with the hydraulic gradient gives a bulk hydraulic conductivity of about 10^{-7} m s^{-1}, in agreement with the results of pumping tests carried out in the area (Khoury et al., 1998). What is not known at this stage is the average fracture aperture(s) and fracture spacing, both of which will influence the velocity of groundwater in the fracture itself. One approach to calculating fracture apertures and flow velocities is to use an analytical expression derived by Steefel and Lichtner (1998a) for reaction front geometry in a discrete fracture system. The analytical model predicts that at quasi-steady state, reaction front contours will be linear with a slope given by $dx/dz = f\ D/vd$ where x is the coordinate perpendicular to the fracture into the rock matrix, z is the coordinate along the fracture, f is the rock matrix porosity, D is the effective diffusion coefficient in the rock matrix, v is the flow velocity in the fracture, and d is the fracture aperture half-width. Field investigations within the A-6 adit indicate the width of the alteration zone in the rock matrix adjacent to the fracture changes from about 4 mm at the M1 site to about 1 mm at the M2 site downstream. Although this information by itself only constrains the quantity vd, both quantities can be obtained by making use of the cubic law for fracture permeability along with the hydraulic head data (see Steefel and Lichtner, 1998b for details of the calculation). Using this approach, we calculate an average fracture aperture half-width of 0.1 mm and an average fracture flow velocity of 267 m day^{-1}. The high fracture flow velocities computed here are probably the result of the limitations in applying the cubic law for fracture permeability to real fractures.

The average fracture aperture and flow velocity calculated above made use of the change in alteration thickness as a function of distance along the fracture. We can also use the change in

water chemistry for actively conducting fractures to constrain these quantities. In this case we use the full numerical model for multicomponent reactive transport in discrete fractures described in Steefel and Lichtner (1998a). Matching of the pH data at the M1 and M2 sites gives a fracture aperture half-width of 0.11 mm (within 10% of the value calculated using the change in alteration thickness) and a fracture flow velocity of 341 m day^{-1} (Figure 3). It is noteworthy that the results obtained from the hydrogeochemistry of the active groundwater system are in close agreement with those obtained from the change in rock alteration thickness which reflect the paleo-flow system in the area.

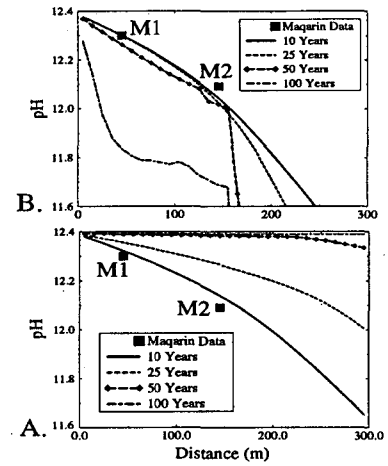

Figure 3: pH versus distance along the fracture. (a) Case where reactive surface area of secondary minerals in the rock matrix is equal to that in the fracture. (b) Case where reactive surface area of secondary minerals in the rock matrix is 10 times less than in fracture.

References

Alexander W.R., Smellie, J.A.T., Milodowski A.E., Clark I., Hyslop E., Khoury H., Linklater C.M., Mazurek M., Salameh E., and Waber H.N., 1998, Potential effects of hyperalkaline leachates on cementitious repository host rocks: an example from Maqarin, northern Jordan. Geol. Soc. Eng. Geol. Spec. Publ. (in prep.)

Khoury, H.W., Salameh, E., Mazurek, M., Alexander, W.R., 1998, Geology and hydrogeology of the Maqarin area. In: Smellie J.A.T. (ed.), 1998: Maqarin Natural Analogue Study: Phase III> SKB Technical Report TR 98-04, Stockholm, Sweden.

Novak, C.F., 1996, Development of the FMT chemical transport simulator: coupling aqueous density and mineral volume fraction to phase compositions. *J. Contam. Hydrol.* **21**: 297-310.

Smellie, J.A.T., 1998, Executive summary. In: Smellie J.A.T. (ed.), 1998: Maqarin Natural Analogue Study: Phase III> SKB Technical Report TR 98-04, Stockholm, Sweden.

Steefel, C.I. and Lichtner, P.C., 1994, Diffusion and reaction in a rock matrix bordering a hyperalkaline fluid-filled fracture. *Geochim. Cosmochim. Acta* **58**: 3995-3612.

Steefel, C.I. and Lichtner, P.C., 1998a, Multicomponent reactive transport in discrete fractures I: Controls on reaction front geometry. *J. Hydrol.* **209**: 186-199.

Steefel, C.I. and Lichtner, P.C., 1998b, Multicomponent reactive transport in discrete fractures II: Infiltration of hyperalkaline groundwater at Maqarin, Jordan, a natural analogue site. *J. Hydrol.* **209**: 200-224.

Session P4:
HYDROGEOLOGICAL FIELD AND LABORATORY TESTING AND MEASUREMENTS

Hydrogeological Aspects of Siting Monitoring Wells in a Fractured Chalk Aquitard

Eilon M. Adar[1] and Ronit Nativ[2]

[1]The J. Blaustein Institute for Desert Research -- Water Resources Center and Department of Geological and Environmental Sciences, Ben-Gurion University of the Negev, Sede Boker Campus 84990, Israel

[2]The Seagram Center for Soil and Water Sciences, Faculty of Agricultural, Food and Environmental Quality Sciences, The Hebrew University of Jerusalem, P.O. Box 12, Rehovot 76100, Israel

Percolation of a relatively small amount of pollutants into a fractured chalk aquitard may result in a relatively wide distribution of contaminants along preferential fractures. Low matrix permeability and a small volume of effective fractures enhance the range of spatial distribution of pollutants within the fractured flow domain while the saturated surrounding matrix maintains its original water quality for a much longer period of time. For practical monitoring purposes pollutants are mainly distributed along the fractures which serve as preferential thin conduits within an impermeable matrix domain.

Monitoring of contaminants within a fractured chalk aquitard requires a precise siting of boreholes so that they intersect the target fracture domain below the water table. Otherwise, water sampled out of the monitoring wells might represent primarily the saturated chalk matrix rather than the flow within the major conduits in the fractures.

Shallow groundwater in the fractured chalk aquitard near an industrial complex in the Northern Negev Desert, Israel has been contaminated over the past 25 years. The industrial complex overlies Eocene fractured chalk formations of high porosity (app. 40 %), but with very low matrix permeability (less than 1.5 mD). The transmissibility of the chalk matrix is so low that the chalk formation was assumed to act as a hydrological barrier. However, contrary to this past assumption, the chalk aquitard does not serve as a hydrological barrier, since recent tritium levels and industrial pollutants have been documented in the shallow groundwater, 20 to 30 m below the surface. Therefore, any migration of subsurface dissolved contaminants is dictated and controlled by the hydrological properties of the fracture system.

The regional hydraulic gradient is toward the northwest (azimuth 295°). However, seepage of highly contaminated groundwater was identified a few hundreds of meters down-gradient from the wastewater storage lagoons, but at an azimuth of 262° along through-going fractures. A few existing boreholes located less than 250 m apart, revealed large variations in groundwater pollution from almost clean water with only traces of pollutants to heavily polluted groundwater attributed to the specific nearby source of pollution. When pumped, groundwater in the relatively clean boreholes was barely replenished, and was assumed to be fed primarily by the surrounding matrix. Therefore, the latter boreholes could not properly represent the hydraulic

properties and the chemical composition of groundwater within the major conduits. This and other hydrological evidences suggest the rapid infiltration and percolation of contaminants via preferential flow routes in the aeration zone, and groundwater flow mainly in open fissures and fractures.

Monitoring the preferential flows in the study area required siting the monitoring boreholes into the predominant fracture systems leading pollutants from potential sources. Drilling operation is time consuming and too expensive to allow for random siting, in hope that some wells will eventually intersect the contaminated fractures.

Following are the steps representing the strategy taken to establish a monitoring system capable of intercepting the main conduits intersecting the aquitard and identifying the spatial distribution of contaminants in a fractured chalk formation.

- Potential sources of groundwater pollution were identified.
- Lineaments that might serve as conduits from potential sources of pollutants were traced from aerial photographs and later field-examined to sort out the large-extension, through-going, multi-layer fracture systems crossing the study area.
- A geological model was then established to allow the prediction of a fracture distribution system covered by soils and sediments.
- Monitoring boreholes were placed along the most predominant conduits intersecting potential sources of pollutants.
- Target fractures were exposed at each proposed drilling site and verified below the sediment cover using trenches within the massive chalk bedrock.
- Slanted boreholes were drilled at a distance from the fracture systems so that each borehole would intersect the targeted fracture plane below the water table.
- A hydrochemical mixing-cell model was applied to identify the connectivity and to quantify the relative contribution of each source of pollution to the major groundwater conduits.

Old aerial photos taken before the development of the site were processed to identify all lineaments in the study area. A detailed geological survey and modeling of the stress fields within the local chalk formations revealed detailed systematic joints that were classified into expanded (possibly very permeable) and compressed (relatively sealed) fracture systems with determined orientations. Each targeted fracture was specifically identified in a 25 m-long trench 4 - 5 m within the chalk formation. Most of the joints were found to be sub-vertical. Thirty five boreholes and coreholes placed along the predominant open joint system, down-gradient from potentially contaminating facilities, were therefore drilled at 22° from the normal, so as to intersect the joint system below groundwater level. Various levels of groundwater contamination were evidenced in all holes, suggesting that the aforementioned surveying and drilling protocols were appropriate for the siting and construction of observation holes in the fractured chalk aquitard. Stable isotopes, ions and several organic compounds were used in a mixing-cell

optimization model. Results elaborate on massive fluxes of contaminants along dominant conduits. They also illuminate the magnitude of connectivity among various fracture systems, diverting pollutants into secondary conduits off the main direction of the regional groundwater gradients.

An Optimization Procedure for Borehole Emplacement in Fractured Media

Daniel Billaux
Itasca Consultants S.A., 40 avenue Guy de Collongue, F 69130 Ecully, France

Frédéric Guérin
Dames & Moore, 87 Avenue F. Arago, F92022 Nanterre Cedex, France

Introduction

This work was commissioned by ANDRA in the framework of the study of a possible Underground Research Laboratory in granite in the Vienne area. The sinking of the planned access shaft will cause an hydrogeological perturbation of the volume it will cut. Following the effect of this perturbation by means of an appropriate array of monitoring boreholes will yield useful information about the properties of the hydrogeological system.

Laying the monitoring boreholes is an optimization problem. By formalizing (i.e. « translating into mathematical terms ») some aspects of the geological and hydrogeological reasonning, we develop a tractable borehole selection procedure, which includes both our incomplete knowledge of the site and the specific objectives assigned to the borehole or group of boreholes.

Note that we are interested here by the « large fractures » network, with scales of several hundred meters at least.

Rationale

We first note that site characterization is an iterative endeavour: we are not defining all boreholes *a priori*, but are working back and forth between field phases and interpretation / modelling stages. Also, in order to enable a rigorous process, the objective of the campaign must be precisely defined. The methodology we present here is oriented towards detecting the large flow paths. The basic principles can easily be used to develop a procedure aimed at other objectives.

We start from the following simple observations :

Borehole positions are severely constrained by technology, logistics, cost.

From a strictly geometrical viewpoint, the « quality » of a given borehole is higher if it has more connections with the network we are trying to explore. In fact, a given fracture intersected by a borehole is all the more interesting that it provides connections to other conducting elements which will be able to influence measurements in the borehole, and therefore be possibly detected.

It is mostly through interference tests that the large fractures network may be characterized. During such tests (for example the « pumping test » due to sinking the access shaft), measurements by the monitoring system will contain all the more information if they integrate the largest possible share of the disturbance.

Steps of the optimization process

We start from the set of all possible borehole arrangements, generate fracture networks integrating the known properties of the site, select several groups of boreholes based on geometrical rating, and then chose between these groups by modelling the hydraulic disturbance created by the access drift and computing what flow rates are detected.

Building the model

This consists of two operations : defining possible boreholes, then generating fracture networks. Possible boreholes are specified by the positions of the boring rigs, orientation (dip, dip direction) intervals, their length.

Fractures are considered as discs or polygons, with orientations and linear densities (i.e. numbers of fractures per meter of borehole) given by the existing borehole information. They are generated in a 3 km by 3 km by 1 km high box, centred on the planned position for the access drift. Disc centres have random positions (Poisson point process) in the generation volume. Two boreholes have already been drilled in this volume, and seven fractures were detected. The fracture generation process is conditioned on these known fractures.

Geometrical sort

We assign a mark to each borehole depending on its connections with the fracture network, and on its links through fractures with the access shaft and other boreholes.

A large number (50 to 200) of realizations of the fracture network is generated. For each realization and for each borehole, we compute the parameters illustrated in figure 1. The mean value of a parameter for all realizations is used to assign a mark between 0.5 and 1.2. The final mark of the borehole is the product of these various individual marks. The grading scale for each parameter is chosen to reflect as closely as possible the thinking of the geologist and hydrogeologist. For example, the hydraulic path towards the access shaft should be short enough to insure detection of the hydraulic perturbation.

The treatment is first performed in order to chose the first borehole in the first group. These grades only take into account the network properties and *a priori* chosen constraints. We name them « intrinsic marks ». We then recompute grades for all the boreholes, taking into account the presence of the first chosen borehole, and use these new grades to chose the second borehole. By repeating this procedure, we can chose all the boreholes in the first group.

In order to obtain the first borehole in a new group, we come back to the intrinsic marks, discarding boreholes already chosen as heads of a previous group. The following boreholes in the group are then chosen in the same manner as before.

Figure 1 Parameters used for the geometrical sort

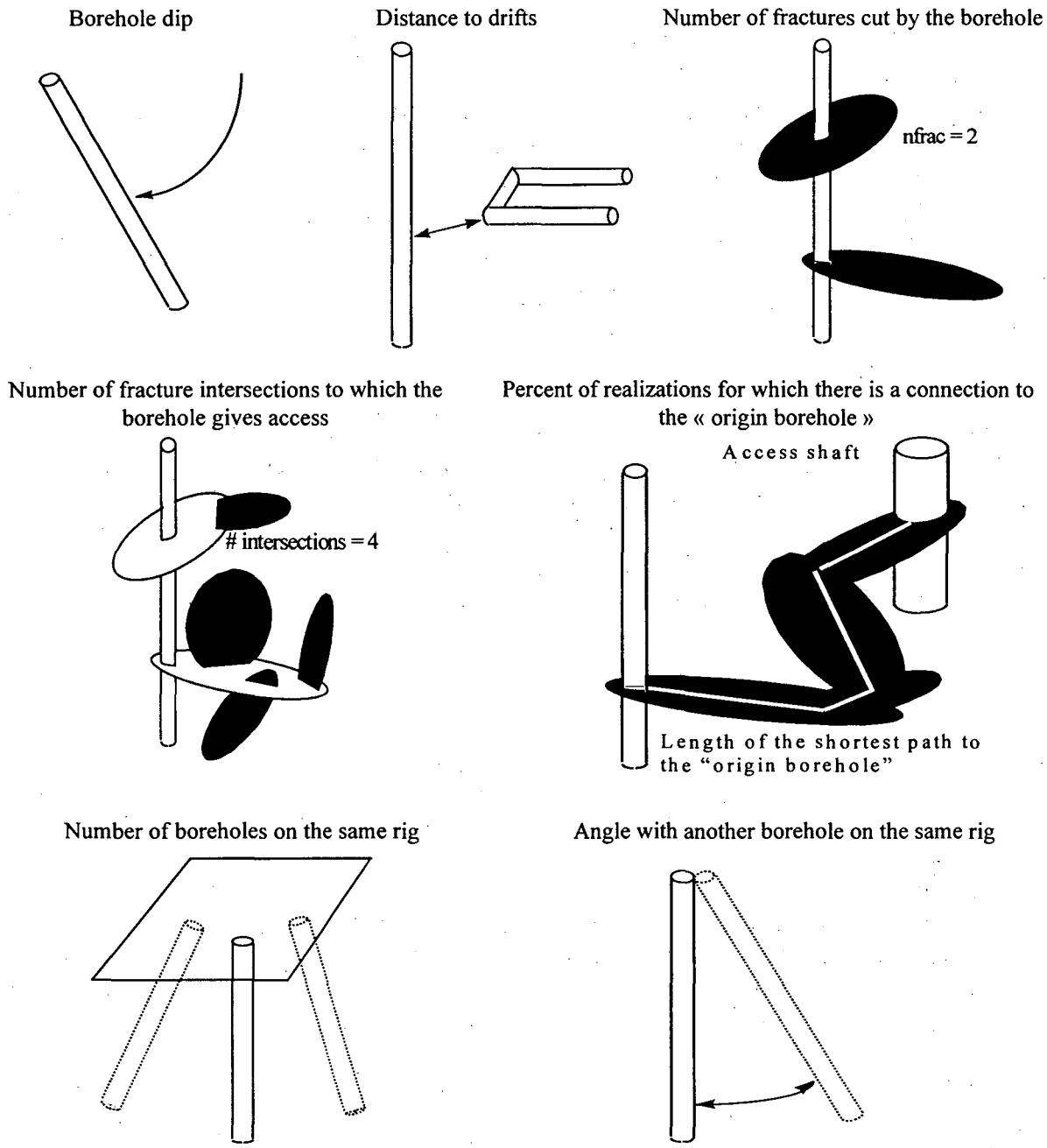

Hydrogeological sort

This final step discriminates between the groups of boreholes selected by the geometrical sort. For each realization of the network, the sinking of the shaft is simulated. For each selected

borehole, flowrates through its intersections with fractures are summed. The « best » group of boreholes is then the one detecting, on the average, the largest share of the flowrate pumped from the shaft.

Results and conclusion

To help visualize parameter behaviour, we interpolate the intrinsic mark for each borehole, using Schmidt diagrams (lower hemisphere) as a mapping support. One interpolation is done for each position of the rig. This interpolation is a krigeing based on a simple linear model. Figure 2 shows the five Schmidt diagrams corresponding to the five possible rig positions, and the arrangement of the diagrams on the figure roughly reproduces the relative positions of the five rigs. On these diagrams, each dot corresponds to one possible borehole orientation. The isolines represent the intrinsic mark. We also figure by crosses all the boreholes selected in at least one group.

Figure 2 Schmidt diagrams (lower hemisphere) of intrinsic marks normalized to 10, and boreholes selected (crosses). « Best » boreholes are outlined by stars.

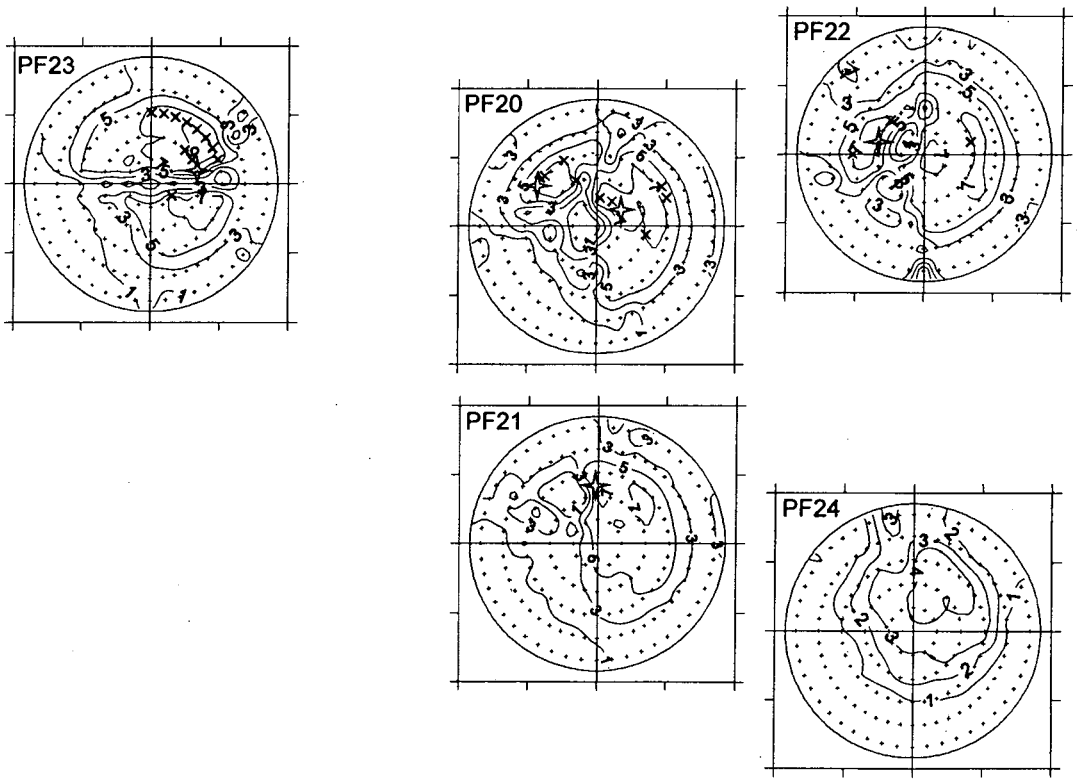

The main borehole directions are to the east and north, which is coherent with the main fracture dip directions to the west an south. However, the influence of relative positions of the rigs can also be seen : in PF22 the weight of the « path length » parameter forces selection of west-trending boreholes. The flow simulations yield for the groups of boreholes average total

flowrates detected (over 200 realizations) of 4 % to 10 % of the flowrate from the shaft. The « best » group from these simulations is outlined in figure 2.

The use of this method should obviously never be of the « black box » type. It is mainly a tool for understanding, by which the geologist and the engineer can check how the priorities they chose affect the choice of borehole positions. In radioactive waste disposal studies, the decision-making process can thus be formalized and made more tractable.

AN UNSATURATED ZONE TRANSPORT FIELD TEST IN FRACTURED TUFF

G. Y. Bussod[1] and H. Jake Turin[2]

[1]Earth and Environmental Sciences Division
[2]Chemical Science and Technology Division
Los Alamos National Laboratory,
MS F-649, Los Alamos, NM 87545, gbussod@lanl.gov

An underground transport test facility has been sited, designed, and constructed at Busted Butte, in Area 25 of the Nevada Test Site (NTS), approximately 160 km northwest of Las Vegas, Nevada, and 8 km southeast of the potential Yucca Mountain repository area. The site was chosen based on the presence of a readily accessible exposure of unsaturated rocks of the Topopah Springs/Calico Hills formations and the similarity of these units to those beneath the potential repository horizon.

The principal objectives of the test are to evaluate fundamental processes and uncertainties associated with flow and transport in the unsaturated zone site-scale models for Yucca Mountain. These include but are not restricted to:

(1) The effect of heterogeneities on flow and transport under unsaturated and partially saturated conditions in the Calico Hills. In particular, the test aims to address issues relevant to fracture/matrix interactions and permeability contrast boundaries.
(2) The migration behavior of colloids in fractured and unfractured Calico Hills rocks.
(3) The validation, through field testing, of laboratory sorption experiments in unsaturated Calico Hills rocks.
(4) The evaluation of the 3-D site-scale flow and transport process model (i.e., equivalent-continuum/dual-permeability/discrete-fracture-fault representations of flow and transport) used in performance assessment abstractions.
(5) The effect of scaling from lab scale to field scale and site scale.

The test involves the use of a mix of conservative and reactive tracers and polystyrene microspheres and is subdivided into test Phases 1, 2 and 3 (Figure 1). Phase 1 initiated April 2, 1998 is a scoping test which involves 6 injection and 2 collection boreholes each 2m in length and located in the hydrologic Calico Hills and in the Topopah Spring formation. Phase 2 initiated July 23, 1998, involves two horizontal planes each containing four subparallel 7.5-8.0 meter injection boreholes, and twelve 8.5-10.0 meter horizontal collection boreholes located at right angles to the injection boreholes in a large in-situ block 10m x 10m x 7m and. Phase 3 is under consideration at this time, and may include the use of radionuclide tracers. Electrical Resistance Tomography (ERT), Ground Penetrating Radar (GPR) and neutron logging are used to determine the saturation state of the block prior to and during testing.

Parallel laboratory tests of Busted Butte core samples are underway to characterize the hydrologic and transport properties of the lithologies. Critical evaluation and iterative improvement of the flow and transport conceptual and numerical models awaits the collection

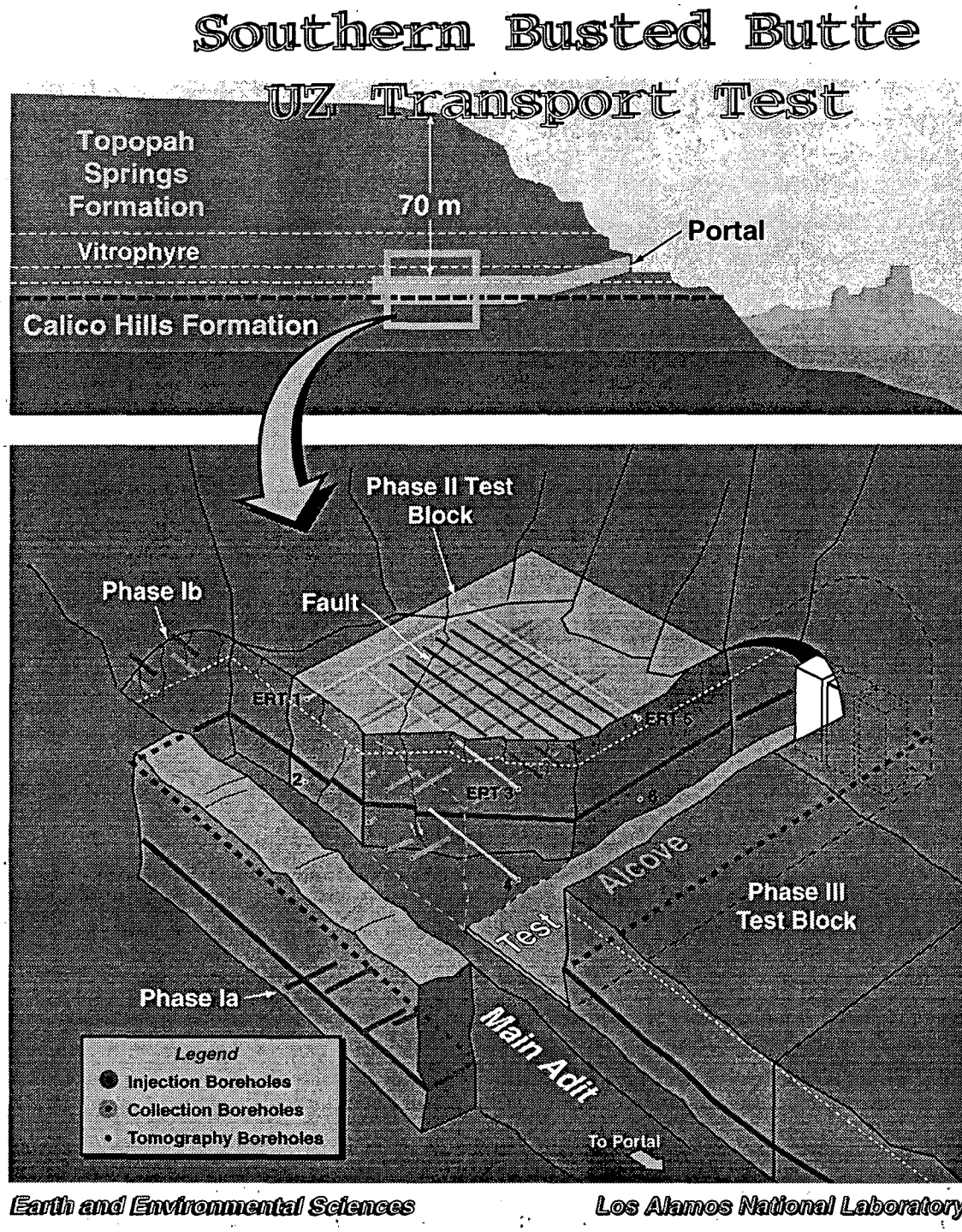

Figure 1. Schematic of the Busted Butte Phase-2 blocks. This schematic shows the relative locations of the different test phases and borehole locations.

of data, which is currently in progress. Although flow and transport field data collected to date are limited, observations of the available data collected so far, and the modeling of these data, lead to several key conclusions of relevance to performance assessment.

The modeling analyses for Phase 1A indicate that strong capillary forces in the rock matrix of the Tac unit are likely to modulate fracture flow from overlying units, thereby dampening pulses of infiltrating water and providing a large degree of contact between radionuclides and the rock matrix. Several modeling approaches, from deterministic to Monte Carlo to stochastic models, were used to simulate the Phase-1A experiments. All yielded similar qualitative results. From these results, we conclude tentatively that the deterministic modeling approach taken at the site scale may be adequate. The parameterizations used in performing these calculations must be evaluated after data from the UZTT are available.

Tracer "breakthrough " has been detected in collection borehole 6 for the 10-ml/hr injection-rate experiment in Phase 1B. As expected, fluorescein and bromide, both conservative tracers, showed similar breakthrough patterns. In both cases, first significant breakthrough was picked up on June 16, 1998, five weeks after injection commenced. No lithium breakthrough has been detected (through August 26, 1998) in Phase-1B pads; FBA and microsphere analyses are not yet complete. Complete data analysis awaits the completion of these chemical analyses. These observations from the Phase-1B experiment in the Topopah Springs formation (Tptpv2), suggest that, even when injection occurs immediately adjacent to a fracture, water appears to be imbibed quickly into the surrounding matrix. The transport times observed immediately below the injection point were on the order of 30 days, whereas pure fracture flow would have resulted in travel times of minutes to hours at this flow rate. Site-scale models must be evaluated in light of this observation. Models that predict significant fracture flow at percolation rates low enough for the matrix to transmit the flow may be inconsistent with the Phase-1B experiment.

Preliminary "blind" predictions of the behavior of the Phase-2 block have been made to test the current modeling concepts and tools available to the integrated site-scale model and their abstractions for performance assessment. Modeling results for fluorescein, indicate that we expect tracer breakthrough at several sampling locations within the first year of testing. For some sampling locations, tracer breakthrough is predicted for travel times of less than a month. Tracer breakthroughs could be even quicker than predicted if the ECM assumption does not hold. Fracture flow through the Topopah Springs formation (Tptpv2) could result in faster travel times. The fracture parameters for the van Genuchten model are not known to a high degree of accuracy. Sensitivity analyses on these parameters will be performed to determine how sensitive travel times are to these fracture parameters. Another caveat in these modeling results is the effect of physical heterogeneities within each layer. Small-scale heterogeneities could result in preferential flow paths, which results in faster flow paths in some parts of the block and slow flow paths in other parts of the block. In the future, Monte Carlo simulations and more elegant stochastic techniques will be employed to attempt to capture the uncertainty in the travel times.

So far these predictions use parameters from the available Yucca Mountain hydrologic and geochemical databases. To date no calibrations have been performed using information from Busted Butte. As more data become available from the UZTT, they will be incorporated into refined versions of the models employed in these preliminary predictions and documented.

A Summary of Fracture Characterization Study at Raymond Field Site

Kenzi Karasaki
Lawrence Berkeley National Laboratory
1 Cyclotron Rd. ,Berkeley, CA 94720

INTRODUCTION

Characterization and prediction of flow and transport in a fractured rock mass is extremely difficult. The main reason for this is because the geometry of the flow path in a fractured rock mass is often very complex and heterogeneous, and therefore, very difficult to define. Field testing can be problematic for various reasons. The geometry of the fractures intersecting boreholes greatly influences test parameters and interpretation results. In a network of fractures, there are typically no definable upper and lower boundaries and only a fraction of the interval length in a borehole is open to flow. Moreover, the REV may be much larger than the scale of the test, particularly for tracer tests. Assumptions regarding the flow geometry often have to be made a priori due to lack of information. The analysis of the test results in light of necessary assumptions is difficult and often leads to model parameters estimates yielding large uncertainty in predictions of flow and transport. To develop field testing techniques and analysis methods for characterizing flow and transport properties of fractured rocks, a dedicated field site was established near the town of Raymond, California. Various kinds of geophysical and hydrological tests were conducted at the site. This paper summarizes the studies carried out at the site.

RAYMOND FIELD SITE

The Raymond Field Site is located in the Sierra Nevada foothills, approximately 3.2 kilometers east of Raymond, California and 100 kilometers north of the city of Fresno. The site lies within the Knowles Granodiorite, which is light-gray, equi-granular and non-foliated. A cluster of nine boreholes have been drilled. Driller's logs indicate that relatively unweathered granite is located beneath less than 8m of soil and regolith. The wells are laid out in a reverse V pattern with increasing spacing between boreholes. Spacings of 7.5, 15, 30, and 60 meters from the central well were chosen to allow the study of directional and scale effects on the flow and transport parameters. The angle between the southwest and southeast leg is approximately 60 degrees. Two of the wells, SW2 and SE2, are reamed to 25cm in diameter with the remaining wells being 15cm. The wells are cased to approximately 10 meters and vary in depth between 75 and 100 meters. The water level is normally between 2 and 3 meters below the casing head.

GEOLOGIC STUDY

Detailed geologic and fracture map of exposed outcrops in the vicinity of the Raymond Field Site was constructed using the curved scan-line technique (Grossenbacher, et al., 1997). Zawislanski (1994) mapped fractures in the vicinity of the site with a particular focus on the distribution of pegmatite dikes. Attempts were made to correlate surface linearments to subsurface hydrology. Quantitative analysis of fracture interval at 10 surface outcrops and in 9 boreholes was conducted. Correlation study between grain size and macroscopic and microscopic fracture intervals and porosity has been performed and it was found that there is a significant correlation between the two.

An abandoned quarry approximately half a mile west of the site provides a vertical exposure of the granite for fracture mapping and fracture coring. Surface profiles of large fracture surfaces were also collected at the quarry. Some profiles extend over 4 meters, which is probably among the largest fracture surface profile ever taken. A method to digitize such data for statistical analysis was developed (Grossenbacher, et al. 1996). Tectono-fractographic technique (Bahat, et al., 1995) was then used to study the fracturing processes. The data are useful for modeling flow in fractures using actual data obtained at a much larger scale than a typical core. An innovative method of collecting fracture samples was developed to study in-situ aperture and tortuosity of fractures. In this method a resin is injected into the fracture opening and after hardening of the resin, a core is drilled out with an intact fracture. The core

is then cut diagonally to expose a fracture cross section, which can be digitized for analysis and a thin section have been used to analyze alteration near the fracture.

GEOPHYSICAL SURVEYS

Geophysical logs for the nine boreholes were taken including natural gamma, resistivity, acoustic televiewer (ATV), caliper, and deviation. Benito (1994) correlated fractures observed by an ATV with those observed at outcrops. Cohen (1995) and Cohen et al. (1996) evaluated various borehole characterization tools used at the site. Conventional television camera logs using fish-eye lens as well as high-resolution digital borehole color scanner (BSS) surveys were conducted in all nine boreholes. Thapa (1994) used the digital image of a fracture to calculate the fracture friction angle. Thapa (1997) also developed an algorithm for automatic fracture detection from the digital borehole image.

Two different types of intra-borehole flow surveys were also conducted in most boreholes. One was performed by using a heat-pulse flow meter. The other survey was conducted by first replacing the borehole fluid with de-ionized water and, subsequently, repeatedly running a conductivity probe down the borehole to monitor changes in the fluid conductivity under a pumping condition. The heat pulse flow survey was useful in quantifying the inflow and outflow rate distribution, while the fluid logging was particularly useful in pin-pointing inflow locations, i.e., the flowing fractures (Cohen, 1995). The latter was found to be even more effective when combined with the images obtained from the digital borehole scanner.

High resolution cross-hole seismic tomography surveys were conducted between ten pairs of boreholes. Results from the surveys conducted between the five wells closest to 0-0, (0-0, SE-1, SW-1, SE-2, and SW-2) were analyzed by simultaneously inverting the travel times and amplitudes (Vasco et al, 1996). Vasco et. al showed that there are two zones where both velocities and amplitudes are strongly attenuated: at a depth of 30m and 60m. The 30m depth coincides with the location of an anomaly identified by a ground penetrating cross-hole radar survey (Korkealaakso, 1993). The radar tomography survey was conducted between SW1 and SW3 between the depths of 15 and 45m. Results from the borehole fluid logging, cross-hole seismic tomography, and the radar tomography indicate that there is a major feature at a depth of approximately 30m. The seismic tomography and the fluid logging indicate that there is another feature at a depth of approximately 60m. Unfortunately the radar tomography was not conducted to this depth. It should be noted that all three surveys respond to different physical properties, i.e., the fluid logging method responds to the inflow locations in a borehole, the seismic method responds to a rock stiffness contrast, and the radar responds to the electromagnetic properties of the rock. The information obtained by the geophysical surveys was used to determine the types of hydraulic tests and the locations for setting packers. It is shown in the following sections that the features detected by the geophysical methods are indeed hydrologically significant.

PTST AND PUMP TESTS

Various kinds of hydraulic tests have been conducted. These include single well pump tests, falling head slug tests, pressure injection tests and several interference tests with various packer and pumping well configurations. Prematurely terminated slug tests (PTST) were also conducted in selected wells. In a PTST or systematic drillstem test, a slug test is shut in or terminated before it completes and subsequent pressure recovery is monitored. Some pump tests were conducted without packers to investigate the effect of short-circuiting by boreholes. In other pump tests the upper fracture zone in each well was isolated with packers. A minimum of two packers were used in each well with a total of 22 packers in 9 wells. A total of 29 transducers instrumented each packed-off zone.

The results from these tests indicate that flow is mainly confined in the two fracture zones and that there is a high degree of heterogeneity within the zones. Another observation is that the larger the time or the distance from the pumping well, the closer the pressure responses are in the upper and lower zone in a same well. This indicates that the features in the upper and lower zone identified by the geophysical logs are hydraulically connected with each other. Furthermore, a significant degree of heterogeneity within and among the wells was observed. Drawdowns in the SE wells are generally higher than in SW wells

indicating preferred high permeability in the south-east direction. Results from the tiltmeter surveys discussed in the later section also indicates a preferential flow in the direction of SE wells. Some log-log time drawdown curves exhibit non-Theis characteristics that may be caused by non-uniform and discontinuous fracture connectivity. Some of the data, however, may have been affected by the very existence of the boreholes, i.e., the storage capacity and "conductivity" of boreholes are comparable or greater than those of the rock. Therefore, observation wells may act like reservoirs and/or short circuit otherwise unconnected fractures.

HYDRAULIC IMAGING

Systematic injection tests were conducted in all nine wells. A straddle packer string with an interval length of 6.1m was used to isolate and inject water into the isolated interval. A typical duration of an injection test was, on the average, ten minutes. After each test, the packer string was lowered by approximately 6.1m. Segments of formation covered by the packers during a particular injection test were kept unobstructed during the next, so that the entire length of the well was tested. There were approximately 15 injection tests per well in all nine wells. While these injection tests were being conducted, the pressures in the remaining 31 intervals were simultaneously monitored. As a result, a total of some 4000 interference pressure transients were recorded. An analysis of the injection data provides an estimate of the near-wellbore transmissivity distribution along each well, while the interference data provide information about inter-well connectivity. Inversion algorithm such as simulated annealing can be used for analyzing transient cross-hole hydraulic test data (Mauldon, 1994; Nakao, 1998). However, the algorithm is computationally quite demanding.

To keep the computer time and size practical, and still take advantage of such a large amount of cross-hole information, the binary inversion method was developed (Karasaki, et al., 1995; Cook, 1996). In this method each set of interference transient pressure data was reduced down to a binary set: 1 (yes) if an observation zone responds to an injection, and 0 (no) otherwise. This method was later extended to incorporate the magnitude of pressure responses (Cook, 1996). In analyzing connections between wells, only the existence of a response has been investigated as a first step (binary inversion). The next step was to take into account the magnitudes of responses coupled with flow rates for injected intervals. These measures had to be normalized not only to distances between wells but to heights between zones since some of the wells are so close together. By visualizing connectivity with various cut-off values, one can selectively focus on features at different scales.

Each well had only three to four packed-off zones for observation, which doesn't lead to very high resolution when looking for possible connections. However, if the injected intervals (as many as twenty per well) are taken into account for pairs of wells, the resolution can be increased substantially. If (1) a given injection with a measurable flow creates a response in a packed-off zone in another well, and (2) this second well has an interval with flow somewhere in this zone when *it* is later injected, and (3) this later injection in turn registers a response in the original well in a zone containing the original injection, then a note is made that these two wells are hydraulically connected between their two injected intervals. Since the injected intervals are roughly 6.1m in length the method affords a 6.1m per connection.

The result from the binary inversion analysis shows an image of two horizontal features, one at a depth of approximately 30m and another at approximately 60m. As noted in the previous section, these features correspond to those identified by the geophysical surveys. Another interesting result is the lack of connection between the features.

TILTMETER SURVEY

During the pressure tests, an interesting phenomenon was observed. While water was being pumped or injected in one well, opposite pressure responses were observed in some intervals in the wells in distance. For example, the pressure in the bottom interval of SE4 increased initially while 0-0 was being pumped, and conversely, the pressure declined during the injection at 0-0. The phenomena was completely reversible and repeatable. The possibility of experimental error was ruled out. Cook (1996) postulated that this is due to the mechanical opening and closing of the fracture. To investigate such hydromechanical

properties of the fracture zone, we conducted tilt meter surveys. Nine high resolution tiltmeters were placed in shallow holes and two were directly placed on the ground surface. A total of three surveys were conducted. In the first two tests, well 0-0 was pumped at two different flow rates, and in the third test, water was injected in well 0-0. All three surveys showed consistent results. Vasco et. al (1996) inverted the tilts and the subsurface structure was revealed.

TRACER TESTS

Various tracers, including deuterium, fluorescein, lithium, bromide, iodide, fluoride, and polyurethane micro-spheres were used in a series of tracer tests. The first set of tests were radially convergent tests using the well pair 0-0 and SW-3, which are both 30m apart (Karasaki et al., 1994). Well 0-0 was first pumped at a constant rate of 11 litters/min for a few days prior to the tracer injection to establish a quasi-steady flow field. A three tracer mixture of deuterium, fluorescein, and micro-spheres was subsequently injected at the upper fracture zone in Well SW3. Two and a half hours later a mixture of bromide and fluoride was injected in the same zone. The first tracer arrival occurred at about 10 hours after the injection. Unfortunately, the micro spheres were not detected in the samples. The background concentration of fluoride was too high for the fluoride concentration result to be meaningful.

The breakthrough curves of fluorescein, bromide, and deuterium normalized to the injection concentration did not lie on top of each other, although all of these three tracers are presumably "conservative". It is not clear why this is the case, although fluorescein has been reported elsewhere to react with certain minerals in the rock and fluoresce more to give apparent increase in mass. Two possible scenarios are that there may be differences in the degree of reaction (or non-reaction) among the tracers and/or these chemicals may have different mixing characteristics. Other problems with the tests include: (1) The injection zone volume was too large and most of the injected tracer remained in the injection zone. (2) The tests were interrupted prematurely.

A second set of tracer tests was conducted with re-injection and re-circulation (Freifeld et al., 1995). They were essentially a weak dipole test where only a fraction of pumped water (approximately 5%) was re-injected back into the injection zone. The re-injection was designed to help the tracer to exit the injection zone and yet small enough not to disturb the predominantly radial convergent flow field. Care was taken to minimize the dead-zone volume in the injection interval. A separate re-circulation plumbing was devised to introduce the tracer without disturbing the flow field and to mix the tracer quickly and uniformly in the injection zone.

Two well pairs were tested: 0-0 and SE-1 which are 10m apart, and 0-0 and SE-3 which are 30m apart. In both tests the micro-spheres were detected at the pumping well. However, the recovery was minimal and the shape of the breakthrough curve was markedly different from that of other tracers. It was found that fluorescein concentration is affected by exposure to the sun-light and algae growth. The analysis results of the breakthrough curves do indicate that the best-fit dispersivity from the 30m test is larger than that from the 10m test. It was also shown that deuterium can be used successfully as a conservative tracer.

DISCUSSIONS

Information obtained by geophysical surveys and geologic observations is frequently used in designing the subsequent hydrologic investigations. This was indeed the case at the Raymond Field Site. We began our hydrologic tests with the packer configuration that made the best sense with then available information. As we conducted more tests, we learned more about the flow system. We progressively changed the packer configurations to tighten the packed-off zones or moved a zone entirely as new information was obtained. This was fine for the purpose of conducting a specific test. However, the fact that packer geometry was different for each test made it very difficult to compare test results to each other.

In light of the site characterization of a fractured rock mass, we question the value of irregular packer configuration based on the knowledge of the fracture system. In particular, it is of questionable value to try to characterize each individual fractures. The reasons are as follows. In the first place, it is usually impossible to individually pack-off every fracture in a borehole. Therefore, any observed data are already

an average behavior of the fractures influenced by the test geometry in an unknown way in time and space. The analysis of such data necessarily involve averaging by assuming a convenient geometry. Predictive tools (numerical model) require the use of averaged parameters at the scale of rasterization.

It would be very interesting to compare two opposing characterization approaches at the same field site. In one approach, efforts are made to collect and use information for designing and conducting hydrologic tests. The test results will be used to construct a model to predict future hydrologic behavior of the rock mass. In the other approach tests are designed and conducted systematically without regard to observed fracture geometry. The results will be used likewise to construct a predictive model. Comparisons will be made on the robustness of the models as well as the overall cost of characterization. We may find the results surprising.

REFERENCES

1. Bahat, D., K. Grossenbacher, and K. Karasaki, "Investigation of Exfoliation Joints in Sandstone and Granite by Tectonographic Techniques" LBL Report No. 36973, 1995.
2. Benito, P.H., Measurement of hydrogeologic fracture parameters at surface outcrops as a possible method for identifying high-yield fractures in a bedrock aquifer, Raymond, California. Honors thesis, Dept. Geology, Amherst College, Amherst MA, 1994.
3. Cohen, A., 1993. Hydrogeologic Characterization of a Fractured Granitic Rock Aquifer, Raymond, California, M.S. Thesis, University of California, Berkeley, LBL-34838.
4. Cohen, A.J.B., Hydrogeologic characterization of fractured rock formations; A guide for groundwater remediators. LBL-38142, October, 1995.
5. Cohen, A., Karasaki, K., Benson, S., Bodvarsson, G., Freifeld, Benito, P., Cook, C., Clyde, J., Grossenbacher, K., Peterson, J., Solbau, R., Thapa, B., Vasco, D., Zawislanski, P., Hydrogeologic Characterization of Fractured Rock Formations: A Guide for Groundwater Remediators, EPA Project Summary, EPA/600/S-96/001, May 1996.
6. Cook, P., Analysis of Interwell Hydraulic Connectivity in Fractured Granite, M.S. Thesis, University of California, Berkeley, 1996.
7. Freifeld, B., K. Karasaki, R. Solbau, and A. Cohen, "Reactive Transport Studies at the Raymond Field Site," in Proceedings, 6th International High Level Radioactive Waste Management Conference, Las Vegas, 1995.
8. Grossenbacher, K., D. Bahat, and K. Karasaki, "TRIANGULATOR: excel spreadsheets for converting relative bearings to XYZ coordinates, with applications to scaling photographs and orienting surfaces," Computers and Geosciences, vol. 22, no. 10, pp1053-1059, 1996.
9. Grossenbacher, K., K. Karasaki, and D. Bahat, "Curved Scanline Theory," Mathematical Geology, vol. 29, no. 5, 1997.
10. Karasaki, K., B. Freifeld, and C. Davison, LBL-34707, also in the Proceedings of 5th International High Level Radioactive Waste Management Conference, Las Vegas, 1994.
11. Karasaki, K., B. Freifeld, P. Cook, and A. Cohen, "Hydrologic Imaging of Fractured Rock." in Proceedings of XVIII International Symposium on the Scientific Basis for Nuclear Waste Management, Kyoto, Japan, 1994.
12. Korkealaakso, J., Okko, O. ja Hassinen, P., Borehole radar measurements at the Raymond test site. Rock Mechanics Symposium. Papers of the Engineering - Geological Survey of Finland, Espoo. 12p., 1993.
13. Mauldon, A., Some Statistical Methods Using Markov Random Fields for Spatially Dependent Media and Fracture Flow Systems. , Ph. D. Thesis, University of California, Berkeley, 1994.
14. Nakao, S., Najita, J., and Karasaki, K., Sensitivity Study on Hydraulic Well Testing Inversion Using Simulated Annealing, submitted to Groundwater, 1998.
15. Thapa, B., Analysis of In-Situ Rock Joint Strength Using Digital Borehole Scanner Images, Ph.D. Thesis, University of California, Berkeley, 1994.
16. Thapa, B., P. Hughett, and K. Karasaki, "Semi-Automatic Analysis of Rock Fracture Orientations from Borehole Wall Images," Geophysics, vol. 62, no. 1, pp129-137, 1997.
17. Vasco, D. W., Peterson, J. E., and Majer, E. L., A simultaneous inversion of seismic traveltimes and amplitudes for velocity and attenuation, Geophysics, 61, 1738-1757, 1996.
18. Vasco, D.W., Karasaki, K., and Myer, L., Inversion of surface tilt caused by fluid migration, v124, n1, Jour. of Geotechnical and Geoenvironmental Engineering, 1998.
19. Zawislanski, P., Surface Fracture Distribution at Raymond Field Site, Raymond, California, LBNL-42675, 1994.

Vaporizing Flow in Hot Fractures: Observations from Laboratory Experiments

Timothy J. Kneafsey (TJKneafsey@lbl.gov)
Karsten Pruess (K_Pruess@lbl.gov)
Earth Sciences Division
Lawrence Berkeley National Laboratory
Berkeley, CA, 94720

Understanding water seepage in hot fractured rock is important in a number of fields including geothermal energy recovery and nuclear waste disposal. Heat-generating high-level nuclear waste packages emplaced in the partially saturated fractured tuffs at the potential high-level nuclear waste repository at Yucca Mountain, Nevada, will cause significant impacts on moisture distribution and migration. Liquid water, which occupies anywhere from 30 to 100% of the porespace, will be vaporized as the temperature reaches the boiling temperature. Flowing primarily in fractures, the vapor will condense where it encounters cooler rock, generating mobile water. This water will flow under gravitational and capillary forces and may flow back to the vicinity of the emplaced waste where it may partially escape vaporization. Water flowing down (sub-) vertical fractures may migrate considerable distances through fractured rock that is at above-boiling temperatures; thus, flowing condensate may contact waste packages, and provide a pathway for the transport of water-soluble radionuclides downward to the saturated zone.

Thermally-driven flow processes induced by repository heat may be as important or even more important for repository performance than natural infiltration. For a nominal thermal loading of 57 kW/acre, vaporization may generate an average equivalent percolation flux from condensate of 23.1 mm/yr over 1,000 years, and 5.2 mm/yr over 10,000 years. These numbers are comparable to or larger than current estimates of net infiltration at Yucca Mountain. This condensate, which is generated in the immediate vicinity (meters) of the waste packages, will likely have a larger impact on waste package and repository performance than a similar amount of water introduced at the land surface.

Laboratory experiments have been conducted to visualize liquid flow in fracture models, transparent fracture replicas, rock-replica assemblies, saw-cut fractures made with Topopah Spring Tuff and glass, and a natural fracture in Topopah Spring Tuff. In these experiments, portions of the models were kept at above-boiling temperatures, while portions were kept at below-boiling temperatures. To facilitate many of these experiments, pentane, with a boiling temperature of 36.1°C was used as the working fluid instead of water. Video recording and spatially resolved thermal monitoring were used in experiments to (1) investigate seepage and boiling phenomena in fracture models and replicas, (2) investigate seepage into a heated natural fracture at different flow rates, (3) quantify liquid flow in refluxing heat pipes in glass fracture models, and (4) examine the effect of fracture angle on flow, and finger and film penetration into the boiling region.

In fracture models and replicas, liquid flow was observed to occur in continuous and intermittent rivulets, and films. Rapid evaporation events were seen frequently in the experiments. These events occur when liquid superheats and spontaneously boils, generating large volumes of vapor quickly, and causing pressure pulses. These rapid evaporation events could potentially disturb capillary barrier conditions at fracture/drift intersections at the potential repository, possibly causing drop snap-off or water spray out of fractures. Continuous rivulet flow was seen at high liquid flow rates, intermittent rivulets occurred when liquid was added by flow or condensation to capillary-held liquid islands causing the gravitational force to exceed the stabilizing capillary force, and film flow along the fracture-wall faces was predominant under low-flow or wide aperture conditions.

Water at three flowrates (~1.35 $ml \cdot hr^{-1} cm^{-1}$, ~0.68 $ml \cdot hr^{-1} cm^{-1}$, and ~0.34 $ml \cdot hr^{-1} cm^{-1}$) was introduced with three nonvolatile dyes into a heated natural fracture (~20 x 20 cm). The water penetrated the boiling region, with dye stains indicating that a wider finger was present at the highest flow rate used, and a narrower finger at the medium flow rate. In some locations, dye from the medium flow rate case was present outside the dye remaining from the high flow rate case, indicating flow-rate dependent flow paths. Flow did not penetrate deeply into the boiling region at the lowest flow rate used. Thermal gradients of several hundred degrees Centigrade per meter occurred in this experiment.

Liquid flow rates in glass fracture models were quantified by measuring heat flux from the models during refluxing, as well as in dry conditions. The heat transfer difference between these two cases was attributed to phase change (heat pipe), which was directly proportional to the liquid flow rate. Liquid flow rates were evaluated in two models that were similar except for aperture; one had a nominal 0.76 mm aperture and the other ranged from zero to several hundred microns. Contrary to what had been expected, a higher flow rate was observed in the smaller aperture fracture. This was explained by noting that in the wide aperture fracture, flow is restricted to films, whereas in the narrow fracture, flow occurs in thicker pendular or corner structures in addition to films.

Finger and film penetration into the boiling region was not well described by a simple model which accounts only for gravitational force. Reduction of the gravitational force by reducing the inclination of the fracture, while holding other parameters constant, was expected to reduce finger and film length, reduce the number of fingers, and increase finger width. In some cases, finger and film lengths exceeded the predicted lengths when the fracture inclination was reduced. These differences may be attributed to changes in fluid mechanics and aperture heterogeneity. Films on the hanging (top) wall penetrated deeper into the boiling zone than predicted, whereas the film on the foot (bottom) wall did not penetrate nearly as far. For the same liquid saturation, a film on one wall will carry twice the flow of equal films on two walls. Aperture heterogeneity affects the local saturation at a given capillary pressure, and thus is important in determining flow paths. At non-vertical angles, gravitational influence will cause liquid to be distributed differently in the aperture, affecting the flow path.

A simple physical model of sheet flow into a fracture exceeding the boiling temperature was developed, and measurements of finger penetration into the boiling region from several experiments were used in the simple model to estimate the rate of liquid flow. These liquid flow rates matched well with thermal techniques of quantifying liquid flow rates.

The laboratory experiments have revealed some surprising phenomena during vaporizing flows in hot rock fractures, which were neither expected nor easily explained on the basis of conventional continuum models for fluid flow and heat transfer. There is a strong interplay between heat transfer, gas and liquid flow processes, and phase change. Investigations are ongoing to determine behavior of non-isothermal flows in fractures on different space and time scales to bridge the gap to *in-situ* heater experiments at Yucca Mountain, and to gain an understanding of large-scale, long-term thermohydrologic effects in an actual nuclear waste repository.

This work was supported by the Director, Office of Civilian Radioactive Waste Management, U.S. Department of Energy, through the Memorandum Purchase Order EA9013MC5X between TRW Environmental Safety Systems, Inc. and the Ernest Orlando Lawrence Berkeley National Laboratory, under Contract No. DE-AC03-76SF00098. The technical review by Sumit Mukhopadhyay was greatly appreciated.

Estimation of Capillary Pressure and Relative Permeability Curves in a Single, Rough-Walled Fracture Using Parameter Estimation Techniques

J.S. Konzuk, and B.H. Kueper
Department of Civil Engineering, Queen's University, Kingston, Ontario, Canada, K7L 3N6
konzuk@civil.queensu.ca

Capillary pressure (P_c) and relative permeability (k_r) curves are useful in representing average microscopic multi-phase flow processes at the macroscopic scale. They are essential components of numerical models used in many areas of multi-phase research, including groundwater contamination by nonaqueous phase liquids (*e.g.*, DNAPLs), assessment of nuclear waste repositories, and petroleum reservoir engineering. Below, we describe a procedure using parameter estimation techniques to arrive at these macroscopic relationships from steady-state two-phase flow data for rough-walled fractures.

Data from laboratory experiments conducted by Chown (1994), utilizing two fractured limestone samples, were used for the parameter estimation. The hydraulic apertures of the two fractures were estimated at 372 μm, and 199 μm from single-phase flow data. The laboratory apparatus consisted of a pool of perchloroethylene (PCE) placed above the fracture and controlled by a constant-head tank, and a constant-head water tank that controlled the pressure of the water applied to the bottom of the fracture. The steady-state PCE flow rate at several increments of capillary pressure was measured during the tests.

The one-dimensional numerical model used to simulate the laboratory experiments included a choice of four different functions representing the capillary pressure and relative permeability curves. These functions included those developed by Brooks and Corey (1966) and van Genuchten (1980); a combination recommended by Mendoza (1992) for use in fractured media that consisted of the Brooks-Corey equation for the capillary pressure curve and a power law function describing the relative permeability curve; and a fourth described below that is a modification of the Brooks-Corey approach. The parameters that govern the shape of each of these functions were estimated using a method in which the best-fit parameter combination was found by calculating the magnitude of the least-squares residual difference (SSQ) between the simulated and experimental non-wetting steady-state flow rates at different combinations of the parameters. The combination of parameters tested were dictated by a grid that covered a range in each parameter. The grid spacing was refined until the parameter combination corresponding to the global minimum was adequately defined. This procedure was used in place of the more often utilized nonlinear least-squares steepest gradient methods because the use of only flow rates in the objective function led to an ill-posed optimization problem, caused by local minimums leading to non-unique parameter estimates, and low sensitivity to some parameters. The "response volume" approach described above was found to perform better in locating the global minimum, but was much more time consuming with respect to computing time. The effect of data error on the magnitude of the estimated parameters was evaluated through the use of a hypothetical simulation that closely approximated the laboratory setup with model error removed but data error incorporated. The global minimum was observed to occur at parameter values that were very close to the true values for only those parameters that the flow rates exhibited high sensitivity to. As the sensitivity of the flow rates to the parameter decreased, the quality of the

estimate of that parameter became poorer. The only parameter that this behavior significantly affected, however, was the wetting-phase residual saturation (S_r).

The relative performance of each function in representing the observed behavior was evaluated in several ways. These included comparing the magnitude of the minimum SSQ value for each function; the simulated and observed two-phase flow behavior - specifically with regards to the entry pressure of the fracture; and the observed and simulated flow rates. The van Genuchten function performed poorly in all regards. The minimum SSQ value was an order of magnitude above that of the Brooks-Corey SSQ, and several orders of magnitude above the others. This function was unable to reproduce the distinct entry pressure observed during the laboratory tests; this inadequacy is the major cause of the high SSQ value and poor fit to the observed flow rates. The Brooks-Corey function allows for a distinct entry pressure behavior, but was still unable to provide a good match to all of the observed flow rates or to the magnitude of the entry pressure estimated from the laboratory experiment, and a minimum SSQ value two or more orders of magnitude greater than the other two functions resulted. The third function, which used the Brooks-Corey equation for capillary pressure, was also able to reproduce the distinct entry pressure. The use of the power law functions to describe the relative permeability curves allowed for more flexibility in fitting these curves, but this led to non-uniqueness in the parameter fits. Every local minimum SSQ value, however, was several orders of magnitude less than the other functions and the fit to the observed flow rates was excellent. The corresponding local minimum capillary pressure and relative permeability curves varied significantly, with one major exception; the magnitude of the non-wetting relative permeabilities at residual wetting saturation [$k_{r,NW}(S_r)$] were all less than 0.3 (see Figure 1a). This is significantly different from the value of 1.0 predicted by both the van Genuchten and Brooks-Corey functions, but is similar to the behavior observed by Demond and Roberts (1993) and Lin *et al.* (1982) for organic liquid/water systems in porous media.

The fourth relationship tested was developed to remove the constraint imposed by the Brooks-Corey and van Genuchten functions that the non-wetting relative permeability at residual wetting-phase saturation must be 1.0, while at the same time somewhat constraining the relative permeability curves to the form of the capillary pressure curve, which allows for a unique solution of the parameters. The Brooks-Corey and van Genuchten functions are constrained to $k_{r,NW}(S_r) = 1.0$ because both use the assumption made by Burdine (1953) that the length of the non-wetting flow path in the presence of residual wetting phase will be the same as that with no wetting phase present [*i.e.*, tortuosity ratio (X_r) = 1.0]. We modified that constraint by setting X_r at S_r to some constant less than or equal to 1.0 (exact value unknown). The new relationship incorporating this assumption was derived following the method of Brooks and Corey (1966), with the following result:

$$P_C = P_d \cdot S_e^{-1/\lambda}$$

$$k_{r,W} = A^2(1-S_r)^2 S_e^{(2+3\lambda)/\lambda}$$

$$k_{r,NW} = B^2(1-S_r)^2(1-S_e)^2\left(1-S_e^{(2+\lambda)/\lambda}\right)$$

where A and B are some unknown constants that become fitting parameters. For an initially 100% wetting-phase saturated medium, A^2 can be assigned the value of $1/(1-S_r)^2$ because the tortuosity ratio is 1.0 at a wetting saturation of 1.0. Thus, the equation for $k_{r,W}$ reduces down to the original Brooks-Corey equation. The magnitude of the fitting parameter B is unclear, but is likely dependent upon the medium, the fluids used, the flow conditions and the magnitude of S_r. The results of

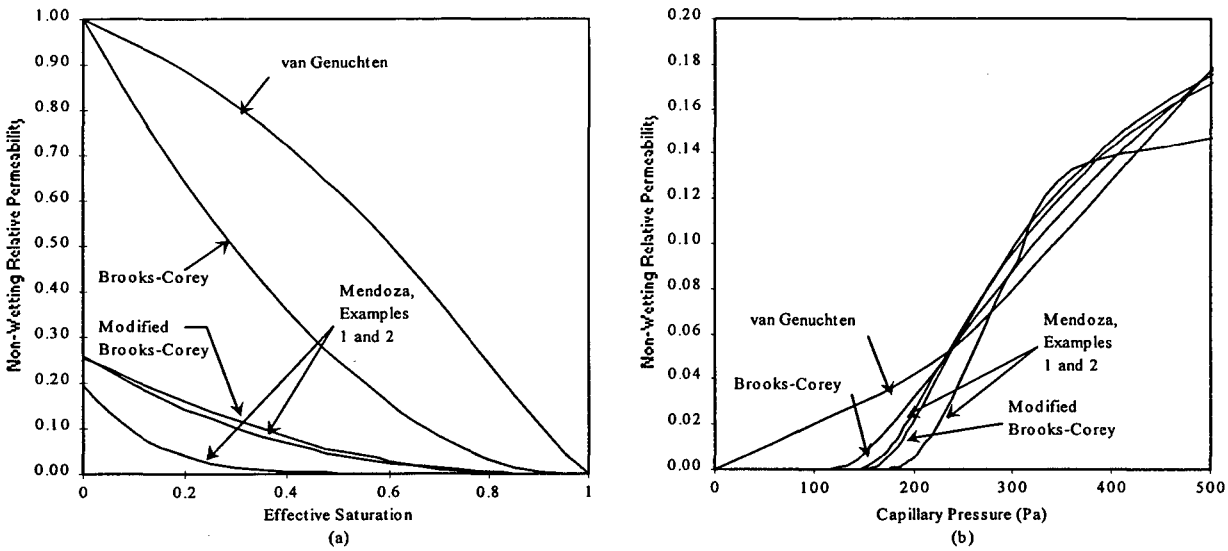

Figure 1: Best-fit relative permeabilities and capillary pressures.

Demond and Roberts (1993) and Lin *et al.* (1982) for liquid-liquid, capillary pressure dominated, porous media systems seems to indicate that B is somewhere in the neighborhood of $-0.59/(1-S_r)$ and $-0.63/(1-S_r)$. When Demond and Roberts (1993) increased their flow rates such that the flow behavior was likely no longer dominated by capillary forces, the magnitude of B increased to $-0.84/(1-S_r)$. For the air-water, fractured medium system tested by Persoff and Pruess (1995), the magnitude of B was approximately $-1/(1-S_r)$. However, it has been shown that in gas-liquid systems, flow behavior such as evaporation and condensation across the trapped gas phase occurs, along with frequent switching between gas and liquid occupancy in critical pores, air bubbles flowing within the water phase, and liquid occasionally breaching a gas-filled region (Persoff and Pruess, 1995; Melrose, 1965; Caudle *et al.*, 1951). These flow processes can be important mechanisms of liquid and vapor-phase transport and would act to increase the relative permeabilities of both phases such that they tend to 1.0 even in the presence of residual amounts of the other phase. Therefore, it seems that, based on the information we currently have about two-phase flow mechanisms, the magnitude of B can be expected to vary somewhere between 0 and $-1/(1-S_r)$, with the absolute value of B increasing as flow behavior that overcomes the trapping mechanisms becomes more prominent.

When this modified form of the Brooks-Corey function was fit to the experimental data, excellent fits to the laboratory behavior were obtained. The experimental flow rates were matched very well, along with the entry pressure of the fracture. The resulting SSQ values, while slightly higher than those of method three, were still orders of magnitude less than those of the Brooks-Corey and van Genuchten fits. Unique estimates of the best-fit parameter combination was obtained, with the magnitude of $k_{r,NW}(S_r)$ estimated at 0.25 for the larger fracture and 0.19 for the smaller fracture. These values are significantly less than the results of Demond and Roberts (1993) and Lin *et al.* (1982), who measured $k_{r,NW}(S_r)$ values of 0.40 and 0.35 respectively in porous media. This may be a result of fewer potential flow paths around a trapped blob of fluid available in a predominantly two-dimensional medium such as a fracture, in comparison to those of a three-dimensional, porous medium. The lack of potential flow paths would increase the tortuosity of the flow path of the fluid, which would result in a significant depression of the relative permeability.

When the relationship between the non-wetting relative permeability and capillary pressure was plotted for the four relationships (see Figure 1b), all the curves plotted reasonably close to each other, but with significant deviations observed for both the Brooks-Corey (minor) and van Genuchten (major) functions at lower capillary pressures. Using only flow rates in the least-squares objective functions provides a good fit to the link between the capillary pressures and corresponding relative permeabilities, but provides little information on the corresponding saturations. To obtain an adequate estimate of the saturation profile, prior information of the saturations must be included in the objective function. If the relative permeability curves had been estimated only from experimentally measured capillary pressure curves, as is often the practice for porous media systems, or equally had the objective function contained only capillary pressure and saturation data, then significantly worse fits to the non-wetting flow data than that obtained here would occur.

Brooks, R.H., and A.T. Corey, Properties of porous media affecting fluid flow, *J. Irrig. And Drain. Div., Proc. Of the Am. Soc. Of Civ. Eng.*, 92(IR2), 61-88, 1966.

Burdine, N.T., Relative permeability calculations from pore size distribution data, *Pet. Trans., AIME*, 198, 71-78, 1953.

Caudle, B.H., R.L. Slobod, and E.R. Brownscombe, Further development in the laboratory determination of relative permeability, *Pet. Trans., AIME*, 192, 145-150, 1951.

Chown, J.C., The influence of upward water flow on downward DNAPL migration through vertical rough-walled fractures, M.Sc. Thesis, Queen's Univ., Kingston, Canada, 1994.

Demond, A.H., and P.V. Roberts, Estimation of two-phase relative permeability relationships for organic liquid contaminants, *Water Resour. Res.*, 29(4), 1081-1090, 1993.

Lin, C., G.F. Pinder, and E.F. Wood, Water and trichloroethylene as immiscible fluids in porous media, *Rep. 83-WR-2*, 33 pp., Water Resour. Program, Dep. of Civ. Eng., Princeton Univ., Princeton, N.J., 1982, as quoted by A.H. Demond and P.V. Roberts, 1993 (above).

Melrose, J.C., Wettability as related to capillary action in porous media, paper SPE-1085 presented at SPE-AIChE Joint Symposium on Wetting and Capillarity in Fluid Displacement Processes, Kansas City, May 17-20, 259-271, 1965.

Mendoza, C.A., Capillary pressure and relative transmissivity relationships describing two-phase flow through rough-walled fractures in geologic material, Ph.D. dissertation, Univ. Of Waterloo, Waterloo, Canada, 1992.

Persoff, P., and K. Pruess, Two-phase flow visualization and relative permeability measurement in natural rough-walled rock fractures, *Water Resour. Res.*, 31(5), 1175-1186, 1995.

van Genuchten, M.Th., A closed form equation for predicting the hydraulic conductivity of unsaturated soils, *Soil Sci. Soc. Am. J.*, 44, 892-898, 1980.

LARGE VOLUME SLUG TESTS IN A FRACTURED-POROUS MEDIUM WITH A DEFORMABLE FRACTURE

Kyle T. Lewallen
Exxon Exploration Company
233 Benmar, Houston, TX 77070
kyle.t.lewallen@exxon.sprint.com

and

Herbert F. Wang
Dept. of Geology and Geophysics
University of Wisconsin - Madison
wang@geology.wisc.edu

INTRODUCTION

Fractured-porous rocks pose unique problems to the understanding of subsurface flow systems. Flow and storage parameters of the fracture as well as the matrix must be determined in order to describe completely flow and transport in a fractured-porous rock. For example, fluid injection or withdrawal by pumping changes the pressure in high-conductivity fractures relative to the matrix. The induced pressure differential will enhance cross-flow between the matrix and the fracture. In a deformable fracture, however, a pressure drop in the fracture also reduces the fracture aperture and, hence, its permeability. Conversely, a large volume slug test raises the pressure in the fracture sufficiently to increase the fracture aperture.

We develop a model in which radial flow from a well occurs in a layered matrix-fracture system where the fracture is deformable. Boulton and Streltsova (1977) obtained analytical results for this model assuming a compressible fracture with constant transmissibility. We extend the model by numerically analyzing the non-linear change in fracture transmissibility caused by changes in fracture aperture. The utility of this research is to explore the applicability of the deformable fracture model and its implications for flow parameter estimation and ultimate fluid recovery.

MATHEMATICAL MODEL

The mathematical model consists of one matrix block with thickness $2H_m$, porosity ϕ_m, and permeability k_m, and one horizontal fracture with aperture $2H_f$ and permeability k_f (Figure 1). It is assumed that the fracture permeability is large relative to the matrix ($k_f \gg k_m$), the matrix thickness is large compared to the fracture ($H_m \gg H_f$), and that the vertical normal stress, σ_T, is constant. The cylindrically symmetric model contains a well of finite radius.

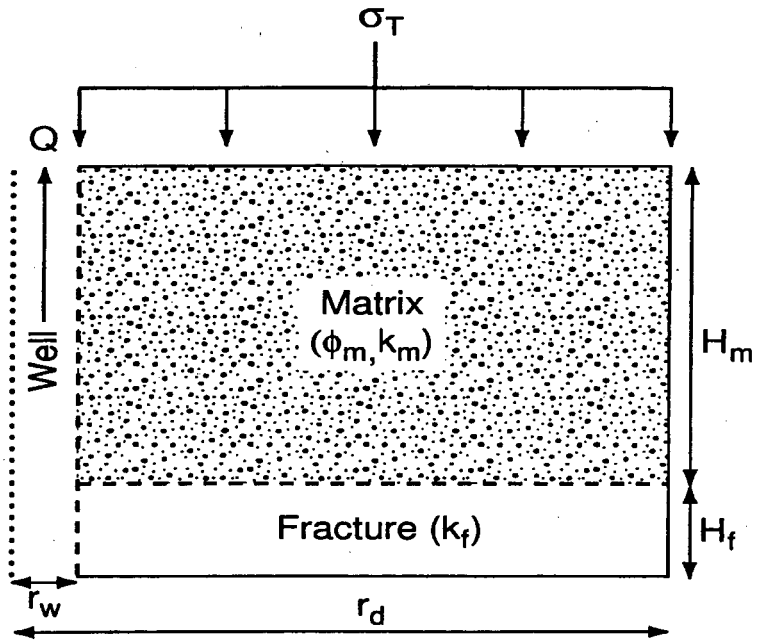

Figure 1. Schematic representation of the mathematical model of a fractured-porous medium assuming cylindrical symmetry. Solid lines represent no-flow boundaries and dashed lines are permeable boundaries.

Darcy's law and the conservation of fluid mass principle are used to obtain the following governing equations:

$$\frac{\partial}{\partial r}\left(\frac{H_f^{\,3}}{12\mu}\frac{\partial P_f}{\partial r}\right)+\frac{H_f^{\,3}}{12\mu r}\frac{\partial P}{\partial r}+R=\frac{S}{\rho_0 g}\frac{\partial P_f}{\partial t}$$

and

$$\frac{H_m k_m}{\mu}\frac{\partial^2 P_m}{\partial^2 r}+\frac{H_m k_m}{\mu r}\frac{\partial P}{\partial r}-R=\frac{S}{\rho_0 g}\frac{\partial P_m}{\partial t}$$

where the subscript f and m represent the fracture and matrix block, respectively, r is the radial flow direction, k is permeability, ρ_0 is fluid density for zero excess fluid pressure, μ is viscosity, P is pressure, R is the cross-flow term between the matrix and fracture, S is storage coefficient, g is acceleration of gravity, and t is time. The equations are written in terms of excess pressure or pressure above hydrostatic. The premise is that the aquifer is at sufficient depth and initial fluid pressure so that large changes in pressure are possible.

Laminar, single-phase flow in the fracture is defined using the cubic flow law to describe the fracture transmissibility, $T_f = H_f^3/(12\mu)$. Because of this cubic power relationship, the transmissibility is extremely sensitive to the fracture aperture. A small change in the aperture significantly changes its transmissibility.

Fracture deformability is implemented using the Walsh and Grosenbaugh (1979) model where the change in fracture aperture resulting from a change in effective stress given by

$$\frac{\delta H_f}{\delta \sigma_e} = -\frac{a}{\sigma_e}.$$

The coefficient, a, is the standard deviation of asperity height in the fracture and the effective stress, σ_e, is the total stress minus the pore fluid pressure. Fracture stiffness is related to the magnitude of the standard deviation of the asperity height. Fracture stiffness varies with the change in the fluid pressure in the fracture.

Matrix-to-fracture cross-flow is handles using the Warren and Root (1963) approximation, which specifies that cross-flow is proportional to the difference between the average pressure in the matrix block and the pressure in the fracture,

$$R = -C\frac{k_m}{\mu}A\left(\frac{P_f - \overline{P_m}}{H_m}\right),$$

where C is a constant which controls the magnitude of cross-flow, and A is the surface area of cross-flow. This approximation underestimates early flow. Deviations from the exact solution are insignificant at long time intervals and for small matrix blocks or closely spaced fractures.

RESULTS

The pressure response of a layered matrix-fracture system to the instantaneous change in fluid pressure at the well due to a large volume fluid injection is anomalous compared to a homogeneous, single-porosity aquifer. A three-stage pressure decline results when fractures are highly deformable (Figure 2). The opening of the fracture aperture increases the fracture transmissibility and causes an early and rapid pressure decline during stage one. An inflection in the decline curve develops when the fracture aperture begins to close. The fracture stiffness and

the contrast in transmissibility between the matrix and fracture control the magnitude and rate of fracture deformation during the second stage in the pressure decline. Stage three is the late time exponential decline of the combined fracture and matrix system. The applicability of the deformable fracture model will be investigated relative to a high head slug test at Yucca Mountain which shows a three-stage pressure decline.

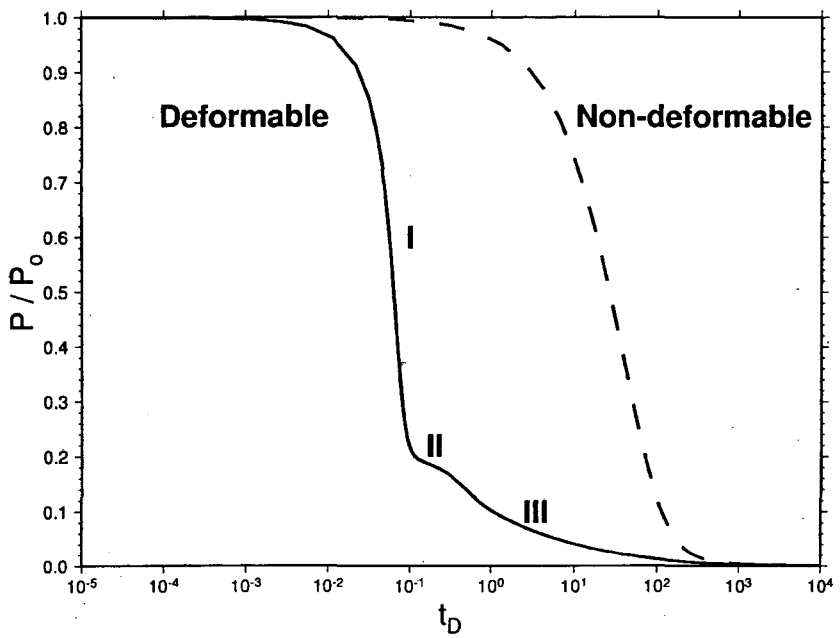

Figure 2. Comparison between the expected smooth decline in normalized pressure for an incompressible fracture and the three-stage decline behavior for a highly deformable fracture. $t_D = Tt/(Sr_w^2)$.

REFERENCES

Boulton, N.S. and Streltsova, T.S. (1977). Unsteady flow to a pumped well in a fissured water-bearing formation. *Journal of Hydrology*, **35**: 257 - 269.

Walsh, J.B. and Grosenbaugh, M.A. (1979). A new model for analyzing the effect of fractures on compressibility. *Journal of Geophysical Research*, **84**: 3532 - 3536.

Warren, J.E. and Root, P.J. (1963). The behavior of naturally fractured reservoirs. *Society of Petroleum Engineers Journal*, **3**: 245 - 255.

Seismic Imaging of Fractured Rock

E. L. Majer, T. M. Daley, J.E. Peterson, R. Gritto, M. Feighner and T.V. McEvilly
Lawerence Berkeley National Laboratory
1 Cyclotron Road
Berkeley, CA 94720

Introduction

Fractured rocks have presented a significant challenge when the objective has been an accurate location of the few connected permeable fractures controlling flow and transport properties over a relatively large volume. Over the last twenty years personnel at LBNL have been conducting research in using seismic imaging at a variety of scales to image characteristics of fractured rocks. Initially this work was driven by issues in geothermal energy research where the problem was to define regions of fractures that may contain enough permeability within a hot rock mass to be economically attractive. In this work both active and passive methods were used to infer the location and directions of fractures. Later applications for nuclear waste disposal in crystalline rock drove the research towards higher resolution and a need to know not only the location and directions of the fractures but also the density, spacing and aperture. The latter being in practice almost impossible to achieve at the present time. Although both geothermal and nuclear waste issues are still pressing, more recent applications for environmental remediation and fossil energy have driven the research towards even higher resolution. The objective of this work being to have as a complete a description of the most significant fractures controlling flow and transport as possible. Described here will be the evolution of our methods and a summary of our current research for developing methods at the field scale for characterizing fractured rock masses.

The primary focus of our work has been research in employing a controlled seismic source to image the subsurface. The scale of resolution of this work has varied from sub-meter to hundreds of meters. Initial work for geothermal exploration involved using surface vibrators and explosions to derive 2-d reflection sections over producing and potential geothermal regions. The first work was in Basin and Range geology to delineate fractures and faults that might be acting as conduits for geothermal fluids (Majer 1978). Similar work was done in the Imperial Valley of California (Majer and McEvilly, 1980) and in the Geysers (Denlinger and Kovach, 1980). This work as well as later work (Okaya and Thompson, 1985) in Dixie Valley Nevada had mixed results at best when the objective was to directly image the major faults or fractures responsible for geothermal energy fluids. Although good images were obtained in many areas adjacent to the productive geothermal regions, "washed out" images were more the rule rather than the exception within the area of interest. This was thought to be due to the complex nature of faulting and fracturing common to a productive geothermal reservoir, highly altered rocks and/or severe lateral variation in rock properties all resulting in scattered, attenuated or dispersed energy which was difficult to derive a coherent image from. A good example is shown in Figure 1. This is a reflection profile over Leach Hot Sprigs in Nevada, the image is degraded over the hot springs, but away from the hot springs the image is quite good, showing the normal faulting by offsets in the sedimentary layers. At this point in time 2-D reflection imaging was the state-of-

the-art (versus 3-D as is the case today), reflection imaging technology was focused on imaging the subsurface with P-wave energy by obtaining the best estimate of the velocity field and aligning the coherent reflections to estimate the spatial location of the layers and structure. It was obvious from the initial geothermal work that this approach would not be sufficient in a heterogeneous system as chaotic as a fractured media with multiple length scales. Although research has continued in the use of seismic reflection methods for fracture characterization, it has been driven by the petroleum and gas industry where the target depths are large, and other methods are not practical (borehole).

After surface methods we decided to pursue methods that would yield greater resolution and wider bandwidth. To do so required higher frequencies, which implied borehole access. In the early 1980's we embarked on a program of utilizing vertical seismic profiling (VSP) to image fracture and faults in the subsurface. The advantage being closer proximity to the targets, validation of results, and higher resolution. The disadvantage being often limited coverage due to limited boreholes in the area of interest. VSP also had the attraction of recording multiple component data, utilizing both shear wave and compressional wave data. In the late 1970's and early 1980's both equivalent and discrete media theories were being advanced to describe wave propagation in fractured media. On one side Crampin (Crampin, 1978, 1981, 1984a, 1984b, 1985) had advanced the theory that fractured media could be represented by an equivalent media of aligned cracks in order to explain field cases of observed seismic anisotropy. A related but separate theory held that the media could be represented by discrete fractures in a matrix, with each fracture having a separate effect related to the mechanical property (stiffness) of each fracture on the seismic wave (Myer et al 1985, Schoenberg (1980, 1983)). The theory differs from Crampin's theory in that at a fracture or an interface the displacement across the surface is not required to be continuous as a seismic wave passes, only the stress must remain continuous. This displacement discontinuity is taken to be linearly related to the stress through the stiffness of the discontinuity. The implication is that for very thin discontinuities, for example fractures, there can be significant effect upon the propagation of a wave. The theory is attractive from several points of view. Schoenberg shows that the ratio of the velocity of a seismic wave perpendicular and parallel to a set of stiffness discontinuities is a function of the spacing of the discontinuities as well as the stiffness. The subtle but important difference being that if the stiffness theory were correct one could in principle derive the actual properties of the fracture (location, density, aperture, filling) with seismic measurements. Several important series of experiments were carried out to test the fracture stiffness theory.

The first experiment was using VSP at The Geysers geothermal filed in northern California (Majer et al 1987). Ourselves as well as others had pointed out the phenomenon of shear wave splitting and the anisotropy effects of SH versus the SV waves in addition to P versus S wave anisotropy (Leary and Henyey, 1985). In order to test the applicability of multicomponent VSP surveys for fracture detection we had the opportunity to carry out a multi-offset VSP using compressional and shear-wave sources with a 3-component geophone in a geothermal well. It was desired to know what, if any, VSP techniques could be used to map the fracture content, dominant fracture orientation or fracture spacing. The results of this work being that there was a dual effect of shear-wave splitting and shear-wave Hodogram analyses of the rotated data clearly showed nonlinear polarization in the two different shear wave planes (H1 and H2) (see Figure 2). This was one of the first observations of shear wave delay indicating a shear wave anisotropy in

a fractured media. The data set collected at the Geyser's was limited and not sufficient to determine exact fracture density and orientation. However, this data does indicate, as Crampin and others have pointed out, the utility of using 3-component data for determining fracture content and orientation. Also, applying the theory developed by Schoenberg relating SV and SH velocity differences to fracture stiffness, additional information on average fracture spacing may also be obtained. The data presented clearly showed that fractures have a significant effect on the propagation of shear waves.

The Geysers VSP was followed by numerous muticomponent multi-offset VSPs in fractured media, aimed at using P and S-wave data to infer fracture orientation, density and spacing. Although VSP was an improvement over surface reflection methods, it was still limited to relatively low frequencies (few hundred hertz at best in most environments) which limited resolution. Again if the objective was to find and delineate the location of the fractures controlling flow and transport, it was obvious that higher resolution was needed. This then led us to the next step of using borehole to borehole methods. This had the advantage of avoiding surface effects that limited frequency content, thus offering higher resolution. The disadvantage being two or more boreholes are needed to perform the work. A major borehole experiment was carried out in a very controlled environment as part of detecting fractures for nuclear waste isolation. This experiment was carried out in an underground research facility in Switzerland over a period of three years (1987-1989). Two boreholes were drilled through a fracture zone. Cross borehole imaging was then carried out as the fracture before and during pressurization (inflation) of the fracture. The goal being to evaluate and develop high-resolution seismic imaging of fractured rock masses, as well as validate the fracture stiffness theories. This work was highly successful in demonstrating the ability of seismic methods at high frequency (kilohertz) for mapping fractures in rock (Majer et al, 1990). The purpose of the inflation tests was to determine the mechanical stiffness of the fracture (kakirite) intersected by the boreholes in order to evaluate the influence of changing fluid pressure in this fracture on seismic wave propagation and hydrologic behavior. The mechanical stiffness of the kakirite fracture was pertinent to interpretation of both the in-situ hydrologic and seismic experiments. Relative to the hydrologic measurements, storativity of a fracture is directly related to fracture stiffness. In addition, the fracture stiffness relates the applied stress to the changes in fracture aperture, which significantly affects the permeability of the fractures. With respect to the seismic measurements, the objective was to obtain an in-situ measurement of fracture stiffness that could be input into the theoretical model to predict the effect of the fracture on seismic wave propagation. If changes in fluid pressure were sufficient to change the fracture stiffness, then the effects of this change would be observed in seismic measurements made during the inflation tests. The results of this three-year project indicated that seismic measurements could yield information on the details of the fractures, given enough bandwidth. Such parameters as fracture stiffness, storativity and spacing were derived.

The next major effort was to scale these methods up from the 10's of meters used in the Swiss work to hundreds of meters needed for larger scale definition in applications such as nuclear waste, geothermal and fossil energy applications. Since the early 1990's the focus of work has been to develop and apply borehole seismic methods for fracture definition and characterization. The primary thrust to define the fractures that control flow and transport. This work is being carried out in a number of environments to gain a fundamental knowledge of scaling of seismic

wave propagation in fractured media This work is being carried out in a number of environments and at a variety of scales. As part of work in fossil energy we have been developing borehole seismic methods for characterizing naturally fractured gas reservoirs. This work has been in conjunction with Conoco, Inc., at their borehole test facility in Oklahoma. This work (Majer et al 1997) has shown that very small aperture fractures have a large effect on seismic wave propagation. In this work crosswell surveys were performed before and after an air injection that was designed to displace water from the fracture zone in order to increase the visibility of the fracture zone to seismic imaging and to confirm previous hydrologic tracer test data that indicated a preferred pathway. The results indicate that the air did follow a preferred pathway that was prediced by hydrologic modeling. In addition, single well seismic imaging also detected the fracture zone in a location consistent with the crosswell and hydrologic inversion results. A "target" fracture zone was identified by combining the results of the single well and crosswell seismic imaging for a drill back experiment. The drilling hit the target within one meter of the predicted location of the target fracture zone. The seismic anomaly appears to be caused by a discrete fracture on the order of less than a centimeter in width.

As a final example of fracture characterization using tomographic methods we show an case from the Yucca, Mt Nevada area. In this work it is necessary to know the location of significant faults and fracture zones, perched water and variation in lithology and rock to properly design and predict the performance of the potential repository. Previous surface geophysical work carried out from 1994 through 1996 (Majer et al, 1996) concluded that the mountain as a whole was difficult to characterize from the surface due to topography variation, surface noise, near-surface weathering and lithology, as well as a variety of other access issues. Therefore, by using borehole to borehole or at least by placing sensors in a borehole (in this case the "borehole" was a mined out drift) we believed that one could increase the resolution as well as ground truth the results by directly observing such properties as lithology, fracture and fault patterns and relate these properties to the seismic results. In order to meet a subset of the above needs a program to use seismic methods to image the potential repository horizon was initiated in December of 1997.These were crosshole, crossdrift, drift-to-borehole, and surface to drift tomographic seismic imaging tests. The general concept was to place receivers in the subsurface tunnel (ESF) at regular distances to record seismic energy from the surface and other drifts. The concept being to first image from the surface into the ESF, predict the geology in the cross drift area, use the mapping information in the crossdrift to calibrate the seismic results, then refine and improve the image by performing tunnel to tunnel imaging between the crossdrift and the ESF. Multiple source locations along lines on the surface and the crossdrift would mimic a cross-borehole geometry, thus providing data which one could process in a tomographic manner. Vibroseis sources were used on the surface for sources and two component (vertical and radial) geophones were cemented in place in the ESF at 15-meter intervals. Source intervals were 30 meters at the surface on a line 5 km long, the receiver line was approximately 3 km away in the ESF, parallel to the source line, about 3 km long. The tomography experiment proved to be a successful test. We demonstrated the potential of large scale, surface-to-tunnel, seismictomography at Yucca Mountain with numerical modeling and prototype experiments. We successfully installed 224 sensors in the ESF and deployed a large-scale acquisition system while mining operations were underway. We acquired a large volume of data in a short time window of mining shutdown, doing so on schedule. We developed novel techniques to maximize our imaging of the repository horizon. We applied these techniques and produced interpretable images of over 5 square

kilometers of the subsurface We have produced images of two major seismic properties, velocity and attenuation. The zero offset relative amplitude distribution revealed surprising results, in that the amplitudes are increased in regions of high fracture intensity. Having excluded a site amplification effect, one explanation may be that the horizontal fractures are guiding energy during propagation and constructively interfering to cause an increase in amplitude in a fracture zone rather than a decrease that one would expect through a highly fractured zone.

It is clear that there is still a great amount of research that needs to be done to find effective methods for seismic characterization of fractures that control fluid transport. The research has made advances over the last 20 years and future advances will come in higher resolution and a better understanding of the fundamentals of wave propagation in fractured media.

References

Crampin, S., 1978, Seismic-wave propagation through a cracked solid: polarization as a possible dilatancy diagnostic: .i "Geophys. J. Roy. Astron. Soc.," v. 53, pp. 467-496.

_____ 1981, A review of wave motion in anisotropic and cracked elastic-media: .i "Wave Motion," v. 3, pp. 343-391.

_____ 1984a, Effective anisotropic propagation through a cracked solid: .i In Crampin, S., Hipkin, R.G., and Chesnokov, E.M., eds., Proc. of the First Internat. Workshop on Seismic Anisotropy, .i "Geophys. J. Roy. Astron. Soc.," v. 76, pp. 135-145.

_____ 1984b, Anisotropy in exploration seismics: .i "First Break," v. 2, pp. 19-21.

_____ 1985, Evaluation of anisotropy by shear wave splitting: .i Geophysics, v. 50, no. 1, pp. 142-152.

Denlinger, R.P. and R.L. Kovach, 1980, Seismic-reflection investigations at Castle Rock Springs in The Geysers geothermal area: U.S. Geol. Survey .i "Prof. Paper # 1141," pp. 117-128.

Leary, P.C. and T.L. Henyey, 1985, Anisotropy and fracture zones about a geothermal well from P-wave velocity profiles: .i Geophysics, v. 50, no. 1, pp. 25-36.

Majer E.L.,1978, Seismological investigation in geothermal areas, Ph.D. Thesis, University of California at Berkeley, Berkeley, California, 225pp.

Majer, E.L. and T.V. McEvilly, 1978, Seismological investigations at The Geysers geothermal field: .i Geophysics, v. 44, no. 2, pp. 246-269.

Majer E.L., T.V. McEvilly, F. Eastwood, and L. Myer, 1988 Fracture Detection Using P- and S-wave VSP's at the Geysers Geothermal Field, v 53, no. 1, p 76-84.

Majer E.L., L.R. Myer, J.E. Peterson, Jr., K. Karasaki, J.C.S. Long, S.J. Martel, P. Blumling, and S. Vomvoris, 1990, Joint Seismic, Hydrogeological, and Geomechanical Investigations of a Fracture Zone in the Grimsel Rock Laboratory, Switzerland, LBL-27913, DOE report.

Majer, E.L., Feighner, M.A., Johnson, L., Daley, T., Karageorgi, E., Lee, K.H., Williams, K., McEvilly, T., Synthesis of Borehole and Surface Geophysical Studies at Yucca Mountain, Nevada and Vicinity, Volume 1: Surface Geophysics, Milestone Report OB05M, Lawrence Berkeley National Laboratory, August 30, 1996.

Majer E.L., R. Gritto, T. M. Daley, V. A. Korneev, M. A. Feighner, and J. E. Peterson, 1998, Full Scale Tomographic Seismic Imaging of the Potential Repository Horizon Milestone Report: SP3B2FM4, LBL report

Myer, L.R., D.L. Hopkins, and N.G.W. Cook, 1985, Effects of an interface in partial contact on attenuation of acoustic waves: .i Geophysics

Schoenberg, M., 1980, Elastic wave behavior across linear slip interfaces: .i "J. Acoust. Soc. Am.," v. 68, no. 5, pp. 1516-1521.

Schoenberg, M., 1983, Reflection of elastic waves from periodically stratified media with interfacial slip: .i "Geophys. Prosp.," v. 31, pp. 265-292.

Hydraulic Fractures in Shallow Soils as an Analog to Applications In Rock

Larry Murdoch
Geological Sciences Department, Clemson University

Hydraulic fractures are often created at significant depths in rock for a variety of applications ranging from the stimulation of oil wells to the disposal of wastes, and new applications related to environmental remediation are on the horizon. The performance of these applications depends on understanding and predicting the geometry of the fractures, although with a few exceptions, the geometry of hydraulic fractures in rock has only be inferred indirectly from geophysical evidence. Hydraulic fractures are readily created in fine-grained sediments within a few m of the ground surface, however, where they can be studied in detail using geophysical methods or by direct inspection in excavations. Fractures created under these shallow conditions may provide a useful analog to the less accessible conditions of deeply buried rock, provided that the relevant mechanical properties of the two settings are similar or can be scaled appropriately.

The growth of hydraulic fractures in rock is typically analyzed using linear elastic fracture mechanics, where the fracture propagates when the Mode I stress intensity at the crack tip reaches a critical value. Laboratory experiments using fine-grained soils over a range of water contents suggest that initiation and propagation of hydraulic fractures in soils can be explained using the critical stress intensity concept from linear elastic fracture mechanics. The state of stress is widely recognized as perhaps the major factor controlling the orientation of hydraulic fractures in rock: fractures are oriented normal to the least principal compressive stress. The horizontal compressive stress in rock exceeds the vertical stress in many regions at depths less than a few 100 m or so. But with increasing depth, the vertical stress increases faster than the horizontal stress, so their relative magnitudes cross over at depths of 300 to 500 m. Curiously, the state of stress in many fine-grained soils mimics that in rock, but at a reduced scale. Large horizontal compressive stresses occur at depths of a few m in many fine-grained soils, but the magnitudes of the stresses change with depth and they cross over at depths of 3 to 5 m. As a result, the orientation of hydraulic fractures in some fine-grained deposits changes from flat-lying at depths of a few m to steeply dipping (and upwardly propagating) at greater depths.

The analog between hydraulic fractures in these two settings provides at least two important opportunities for insight; the mechanics of emplacement, and environmental applications. Details of fluid flow and deformation within the tip of the fracture are critical to how fractures are analyzed, but this region is inaccessible at the field scale in rock. Evaluation of hydraulic fractures in soil suggests that the fracture opens ahead of the injected fluid and can cause pore fluid to enter the crack tip. Environmental applications have demonstrated that hydraulic fractures will increase the productivity of wells in silty clays, much like they increase the productivity of oil wells. However, recent applications have shown that hydraulic fractures in soils can be used to deliver reactive solids, such as zero-valent iron, potassium permanganate, zeolite, or biologically active materials, to form layers that destroy or immobilize contaminants in situ. Similar applications for hydraulic fractures filled with reactive material appear to hold a great potential for the remediation of contaminated rock.

The Cubic Law and Effects of Stress

L. R. Myer
Earth Sciences Division
Ernest Orlando Lawrence Berkeley National Laboratory
1 Cyclotron Road
Berkeley, CA 94720

The idea that a fracture can be modeled as two parallel plates separated by a constant distance, or aperture, has received wide recognition in hydrology. It is also well known that fracture surfaces are rough, so the separation, or aperture, between the surfaces will be areally variable including regions of contact where the aperture is essentially zero. If the details of the aperture distribution is known, it is possible, for single phase flow, to derive an average aperture. The details of the aperture distribution are rarely, if ever, known, so the concept of hydraulic aperture is frequently invoked, particularly in interpretation of measurements. Given an observed flow rate, the hydraulic aperture is the separation between two parallel plates necessary to carry the observed flux under the imposed head conditions.

If the distance between two plates is decreased, the flow will decrease in proportion to the cube of the change in aperture. When a fracture is subjected to a change in stress, deformation occurs in the plane of the fracture. The relationship of this deformation to the change in aperture between two plates or the change in hydraulic aperture has often been studied, but still remains largely unknown.

The simplest relationship is to assume that the average deformation normal to the plane of the fracture is equivalent, or at least proportional, to the change in hydraulic aperture. This concept was initially tested by Iwai (1976) in laboratory tests on mechanically induced tensile fractures in marble, granite and basalt. Iwai (1976) found that the proportionality between deformation and hydraulic aperture failed in two of three tests when the fracture aperture became small. He also observed a "residual" flow or a flow which could not be reduced by further fracture deformation. Similar observations have subsequently been made by many others.

Experiments like those of Pyrak-Nolte et al. (1987), combining mechanical and flow measurements with direct observations of fracture aperture distributions from casts, have provided insight into the relationship between fracture deformation and hydraulic aperture changes. As normal stress is increased, fracture contact area increases. However, it does so in a very heterogeneous fashion so that even at high stresses there can be large (areally extensive) voids. Reduction in flow occurs not only by reduction in aperture but also by formation of "critical necks" as the increasing contact area reduces the connectivity between void areas. Presence of disconnected void areas will lead to observation of continued mechanical deformation without an impact on flow. The "critical necks" tend to be more equidimensional in cross section than the areally extensive voids. As a result they will deform little as stress increases, leading to irreducible flow.

The conclusion is that the proportionality between the normal component of fracture deformation and hydraulic aperture is not constant. At very low stress levels deformation and hydraulic aperture change are nearly equivalent. As stress increases, the hydraulic aperture decreases at a faster rate than the fracture deformation.

Many questions remain unanswered regarding effects of stress and the relationship between fracture deformation and hydraulic aperture. Among these are: what is the stress range for which it is valid to assume that hydraulic aperture is constantly proportional to fracture deformation? what is effect of rock type? fracture infilling? tectonic motion? and what is the effect of imposed shear?

References:

Iwai, K., 1976. Fundamental studies of fluid flow through a single fracture, Ph.D. dissertation, University of California, Berkeley, California.

Pyrak-Nolte, L.J., Myer, L.R., Cook, N.G.W., Witherspoon, P.A., 1987. Hydraulic and mechanical properties of natural fractures in low permeability rock, Proceedings of 6th International Congress of Rock Mechanics, Montreal, Vol. I, pp. 225-232.

Control of fluid injection into a fractured rock.

T.W. Patzek
Lawrence Berkeley Laboratory
Earth Sciences Division
1 Cyclotron Road, MS 90-1116
and
University of California at Berkeley
Materials Science and Mineral Engineering
591 Evans Hall #1760
Berkeley, CA 94720
Email: Patzek@Patzek.berkeley.edu

D.B. Silin
Lawrence Berkeley Laboratory
Earth Sciences Division
1 Cyclotron Road, MS 90-1116
Email: DSilin@lbl.gov

In this presentation we develop a control model of fluid injection into a growing hydrofracture. The model is based on transient linear flow into a low permeability, soft rock. The purpose of the injection is displacement of oil towards producing wells. On the one hand, an injection policy that is too aggressive may lead to the creation of channels connecting the injector to a producer and irreversible reservoir damage. On the other hand, injection that is too low results in delayed oil displacement and economic losses. Hence it is important to inject at a reasonably high rate and, at the same time, to make correct decisions when the hydrofracture extends. We show that hydrofracture extensions are inevitable. The corrective actions should ensue within seconds; therefore a smart automatic controller is needed to adjust the current injection rate according to the instantaneous information about the injection rate and pressure. Such a controller is discussed here. The control objective is stabilization of the injection rate with regard to unexpected fracture extensions and other disturbances. The stabilizing controller is designed through modeling of the injection process and solving a linear-quadratic optimal control problem. The controller itself is a part of an integrated system of fieldwise injection and production analysis and control system, which is being developed.

First, we revisit Carter's model of hydrofracture growth during fluid injection [1]. Under similar assumptions we incorporate into the model derived in [1] variable injection pressure:

$$Q(t) = wA(t) + 2\frac{kk_r}{\mu\sqrt{\pi\alpha}}\int_0^t \frac{\left(p_{inj}(\tau) - p_i\right)A(\tau)}{\sqrt{t-\tau}}d\tau \tag{1}$$

Here α and p_i denote, respectively, the hydraulic diffusivity and the initial pressure in the formation outside the fracture, k denotes the absolute permeability of the rock and k_w is the relative permeability of the injected fluid, here water. The viscosity of the fluid is denoted by μ. As in [1] we assume that the fracture has constant width w.

Equation (1) relates the cumulative injection $Q(t)$ to the hydrofracture are $A(t)$ and the injection pressure $p_{inj}(t)$. The model (1) shows that the driving force of the flux of the fluid into the formation is the difference between the initial pressure and the injection pressure. However the injection is determined not only by the current instantaneous injection pressure and the area, but also by the whole history of injection. The term $\sqrt{t-\tau}$ in the denominator of (1) means that the influence of recent injection history is much more important than the earlier observations. The model (1) involves no hypothesis about the geometry of the hydrofracture. The hydrofracture itself is not an ideal geometric object. So when we put the area $A(t)$ and the width w, we mean effective area and width, respectively, rather than precise geometric measurements.

Instead of injection rate in [1] we use cumulative injection in (1). This allows us to avoid dealing with usually noisy injection rate measurements. Indeed, integration of the injection rate

$$Q(t) = \int_0^t q(\tau)d\tau \tag{2}$$

averages out the disturbances of the measurements.

The model (1) implies the square root of time rule usually used in petroleum reservoir modeling. Moreover, it leads to the conclusion that if the hydrofracture does not grow the cumulative injection grows as square root of time, and, consequently, the average injection rate must decay as one over square root of time. Therefore, keeping injection rate above a certain level inevitably leads to a hydrofracture extension. Depending on the formation properties and the aggressiveness of the injection policy such extensions can be moderate or fatal. Our estimates for several wells in the South Belridge diatomite oil field show that a hydrofracture extension should happen at least once in 100 days. Whenever an extension occurs, the injection pressure must be lowered promptly. Since manual observation is not feasible, a smart automatic controller is required.

In order to design such a controller we set the following optimal control problem:

Minimize

$$J[p_{inj}] = \frac{1}{2}\int_0^T w_q(t)\left(Q(t) - Q_*(t)\right)^2 dt + \frac{1}{2}\int_0^T w_p(t)\left(p_{inj}(t) - p_*(t)\right)^2 dt \tag{3}$$

subject to (1).

The weight functions w_p and w_q take on only positive values. They reflect the trade-off between the closeness of the actual cumulative injection $Q(t)$ to the target injection $Q_*(t)$, and the well-posedness of the optimization problem. The less the value of w_p is, the more functional (3) reflects the intention to follow the planned injection strategy

$Q_*(t)$. At the same time, if the value of w_p becomes too small, then the problem of minimization of the functional (3) becomes ill posed and unstable. Moreover, in the equation characterizing the optimal control, derived below, the function w_p is present in the denominator, which means that stability and solvability of this equation deteriorates as w_p approaches zero. However, if we consider specific modes of control, e.g. piecewise constant control, then w_p can be put equal to 0. The function $p_*(t)$ defines a reference value of the injection pressure. Theoretically it can be selected arbitrarily; however, practically it should give a rough estimate of the optimal injection pressure. We provide a simple recipe how this function can be selected.

The input parameters of the controller are the hydrofracture area $A(t)$, the history of measured actual injection $Q(t)$ and injection pressure $p_{inj}(t)$, and the target injection $Q_*(t)$. The output parameter is the injection pressure, which has to be applied via regulation of the valve at the wellhead. The optimal injection pressure $p_0(t)$ is obtained by solving the following system of integral equations:

$$Q_0(t) = wA(t) + 2\frac{kk_w}{\mu\sqrt{\pi\alpha}}\int_0^{\vartheta}\frac{(p_{inj}(\tau)-p_i)A(\tau)}{\sqrt{t-\tau}}d\tau + 2\frac{kk_w}{\mu\sqrt{\pi\alpha}}\int_{\vartheta}^{t}\frac{(p_0(\tau)-p_i)A(\tau)}{\sqrt{t-\tau}}d\tau; \quad (4)$$

$$p_0(t) = p_*(t) - 2\frac{kk_w}{\mu\sqrt{\pi\alpha}w_p(t)}A(t)\int_t^T\frac{w_q(\tau)}{\sqrt{\tau-t}}(Q_0(\tau)-Q_*(\tau))d\tau. \quad (5)$$

Here $Q_0(t)$ is the actual cumulative injection. We have developed a numerical procedure of solving (4) - (5) based on the method of conjugate gradients.

We design our controller on a sliding time interval $[\vartheta, T]$. This interval slides forward as the time goes on. There are several reasons for splitting the entire time interval. First, this way we retain the flexibility of the controller: unexpected events can be incorporated into the input of the controller and the control can be refreshed accordingly. Second, we avoid dealing with very large arrays of data and therefore reduce the dimension of the system (4) - (5). This allows us to obtain the solution in a short time and imitate feedback mode of control. It is impossible to design a genuine feedback control due to the convolution involved in (1). To summarize, the controller works on the following way: first we design control on the initial sliding interval $[\vartheta, T]$. If no fracture extension occurs on this interval, we design the control on the next interval, which overlaps the first one. If an extension occurs we terminate the current interval immediately and initiate a new sliding interval. This process is iterated as long as it is needed.

One of the input parameters of the controller is an effective hydrofracture area. Despite great progress in field measurement technology, such as surface and downhole tiltmeters, hydrofracture area measurements remain difficult and problematic. However,

the controller model can be reused to estimate the hydrofracture size. Indeed, if the injection pressure and cumulative injection data were available, they could be substituted into the equation (1), which then could be solved with respect to $A(t)$. Again, the parameter $A(t)$ may not be exactly equal to the geometric hydrofracture area. However, it is exactly what we need as the input to the controller. Moreover, the size of the hydrofracture comprises a major part of $A(t)$ and, therefore, sharp changes of $A(t)$ at least qualitatively reflect hydrofracture extensions. The historical records about the injection pressure and the cumulative injection, which are required for the inversion, should be maintained for controller input anyway. Moreover, oil companies normally gather these data to analyze their operations even when injection is performed with no controller. Thus, maintaining data necessary for the estimation of $A(t)$ requires no special effort.

References.

[1] G.C.Howard, C.R.Fast Drill. and Prod. Prac., API , 261 (1957).

Observations of Water Movement in Variably Saturated Fractured Basalt and its Possible Implications on Predictive Modeling

Robert K. Podgorney and Thomas R. Wood
Parsons Infrastructure and Technology Inc.,
Idaho National Engineering and Environmental Laboratory,
PO Box 1625/MS3954, 200 South Woodruff Avenue, Idaho Falls, ID, 83415,

Introduction

The motivation of this research is to obtain a better understanding about the processes governing flow in variably saturated fractured basalt. The objective of the investigation was to collect a data set to evaluate flow processes through discrete vertical and horizontal fractures and a basalt matrix on the meter scale (Podgorney et al., 1997). The field investigations were conducted at the Hell's Half Acre (HHA) site in Idaho.

Site Characterization

The research site consists of an overhanging basalt block (thickness approximagely 1m with a 2 x 3m areal extent) on the edge of a collapsed lava tube. The basalt at the site is moderately vesicular to dense. A single fracture is exposed on the land surface. The fracture bifurcates in the lower part of the block, resulting in two fracture traces on the underside. A horizontal fracture, which intersects the vertical fracture, is exposed on the face of the block, approximately 25 cm from the underside.

Site Instrumentation

A 40 by 80-cm infiltration gallery was emplaced over the surface expression of the fracture, in which a constant water level was maintained during the infiltration experiments. The site was instrumented to collect extensive data sets to describe both the temporal and spatial variations of the following parameters:

- Water head and the flow rate into the infiltration gallery,
- Temperature of rock, water, and air,
- Tensiometric pressure at 14 locations,
- Barometric pressure, and
- Outflow from the underside of the outcrop as water drip intervals (20 points) and water volumetric discharge (12 locations).

The area below the fracture is covered with a grid of 20 by 30-cm pans, which are used to collect the cumulative volume of water drips from the fracture. Each pan collected one or more drips and thus averaged the outflow rate from the drip points above it. The water was routed from the pans to bottles attached to loadcells to measure the outflow at high resolution. The outflow rates determined from the pans can be used to examine the temporal and spatial variations in the fracture discharge.

During infiltration experiments, the upper boundary condition was a constant water head in the infiltration gallery. The infiltration tests were run for up to 18 days. The drainage periods between infiltration tests were up to several weeks to allow for sufficient drying of the rock. Successive tests started when the water pressure in the basalt matrix was approximately –100 mBars.

Results of Observations

In order to give a general understanding about the flow processes, we will discuss the analysis of data obtained using the infiltration and volumetric outflow rates from a typical test. Figure 1 (a and b) shows typical plots of the time variation of infiltration and outflow at five pans located along the fracture. Figure 1a shows that immediately following flooding of the infiltration gallery, the infiltration rate increases as water saturates fractures and imbibes into the dry basalt. As water saturates the porous matrix, air is presumably pushed out into fractures, where it becomes entrapped in zones with small aperture. This leads to a decrease in the overall hydraulic conductivity and, consequently, a decrease in both the infiltration and outflow rates after 40 hours from the beginning of the test.

Figures 1a and 1b also show that after approximately 100 hours both the infiltration and outflow rates began to increase. The trend of the volumetric outflow rates for several locations have a steeper positive slope than the infiltration rate. This suggests that initially the rock matrix was not fully saturated and the saturation increases with time. This is supported by the tensiometric pressures, which continuously increased at the same time (Figure 1c). The increasing trend in the flow rates continued until the saturation reached a critical value, which triggered a rapid increase in both the infiltration and outflow rates. From this time on (~ 202 hours) the pattern of the infiltration rate is similar to that of the outflow rate. At this time, it is likely that a direct hydraulic connection between the infiltration gallery and these discharge locations was established. The tensiometric pressures were practically constant from 202 hours to the end of the test (Figure 1c). The different trends in the outflow rate for locations 8 and 12 (situated outside the footprint of the infiltration gallery) suggest that these locations are not in direct hydraulic connection with the infiltration gallery.

It is important to note that tensiometers cannot resolve high frequency fluctuations, like those observed for the flow rate. Also, the tensiometers could not detect a positive water pressure, which is likely to develop in the fracture as water flows under gravity. This is because the porous tip of the tensiometer averages the pressure over the volume of the tensiometer (Finsterle and Faybishenko, 1998).

Discussion and Conclusions

In an attempt to analyze the observations, it is convenient to divide the data set into 2 periods. As shown on Figure 1, Period 1 occurs from the start of the test until elapsed time is approximately 202 hours. During this time, our analysis suggests that: 1) rapid fracture saturation occurred just after the beginning of flooding (0 to ~25 elapsed hours) and 2) water was imbibed into the matrix (~25 to 202 elapsed hours). The flow rate increased with time, possibly, because entrapped air dissolved in moving water and was removed in both mobile and dissolved phases. The outflow rates increase faster in comparison with the infiltration rate because the overall

permeability of rock increased as its saturation increased. This process continued until the saturation reached a critical value, at which time a dramatic increase in both inflow and outflow rates was observed. The large increase in the infiltration rate at 202 elapsed hours marks the transition to Period 2, where high flow through the fracture and matrix is observed.

Montazer and Wilson (1984) discuss critical saturation levels in fractured rock vadose zones and suggest that matrix flow will dominate under low matrix potential situations. Only after matrix potential rises to the critical saturation will fracture flow begin in the system. Our observations suggest that during ponded infiltration the opposite is true: the fracture system dominates the flow system at the highest matrix potentials with the capillary forces in the matrix adjacent to the fracture acting to interfere or reduce the fracture's ability to transmit water. After a critical saturation is achieved in the matrix, its effects become negligible, and a true effective hydraulic conductivity of the fracture/matrix system is achieved. The time for this to occur may depend upon many site-specific factors, such as the matrix and fracture characteristic curves.

The trends in the infiltration rate during both Period 1 and Period 2 are similar. Both contain; 1) an initial maximum value followed by an exponential decline, 2) a period of nearly constant infiltration, and 3) a general increasing trend. An identical flow behavior was observed in soils in the presence of entrapped air (Faybishenko, 1995). However, the increase in the outflow rate at different locations along the fracture is quite different and is accompanied by significant spatial fluctuations. It can be seen that small variations in the minimum values of the flow rate during Period 1 may lead to a wide range of the rates during Period 2. It is important to remind the reader that these changes occurred under a constant boundary condition at the surface.

Several main features of the infiltration at HHA can be described using traditional methods to estimate flux through the vadose zone, based upon well studied mathematical models (e.g., Horton's Equation, Mezencev's Equation, Holtan's Equation, Green-Ampt Models, Richards Equation models, etc., see Ravi and Williams (1998) for a general review). These models generally predict that the infiltration rates will reach some steady state minimum value as time increases and can to used to describe the data collected at the HHA research site if each period of flow is considered separately. Williams et al. (1998), in a review of commonly used predictive vadose zone models, show this phenomena for several commonly applied numerical models. However, in fractured vadose zones, the complex interaction of multiple, inherently non-linear processes in both the fracture and the matrix can lead to instability that the current modeling approaches fail to predict. This instability is evidenced by the large increase in the infiltration and outflow rates at the boundary between Periods 1 and 2.

As shown on Figure 1a, the infiltration rate increased by nearly an order of magnitude from the minimum value observed during Period 1 to the maximum during Period 2. Failure to capture this behavior in a predictive model may lead to serious underestimates in contaminant transport predictions.

Acknowledgements

The authors would like to thank Boris Faybishenko of Lawrence Berkeley National Laboratory and Thomas Stoops of Idaho National Engineering and Environmental Lab for their helpful comments and suggestions. This work was funded by the Office of Environmental Management,

Environmental Management Science Program of the U.S Department of Energy under Contract No. DE-AC03-76SF00098.

References

Faybishenko, B.A., 1995, Hydraulic behavior in quasi-saturated soils in the presence of entrapped air: laboratory experiments, Water Resources Research, 31(10), pp. 2421-2435.

Finsterle, S. and B.A. Faybishenko, 1998, What does a tensiometer measure in fractured rock?, Lawrence Berkeley National Laboratory, LBNL-41454, 10 p.

Montazer, P. and W.E. Wilson, 1984, Conceptual hydrologic model of flow in the unsaturated zone, Yucca Mountain, Nevada, USGS Water-resources Investigation Report 84-4345, 55 p.

Podgorney, R.K., T.R. Wood, and T.M. Stoops, R.G. Taylor, and J.M. Hubbell, 1998, Basalt outcrop infiltration tests to evaluate chaotic behavior of unsaturated flow in fractured rock, Data summary report—1997 field season, unpublished internal report, Idaho National Engineering and Environmental Laboratory.

Ravi, V. and J.R. Williams, 1998, Estimation of infiltration rate in the vadose zone: compilation of simple mathematical models, volume I, EPA/600/R-97/128a

Williams, J.R., Y. Ouyang, and J-S. Chen, 1998, Estimation of infiltration rate in the vadose zone: application of selected mathematical models, volume II, EPA/600/R-97/128b

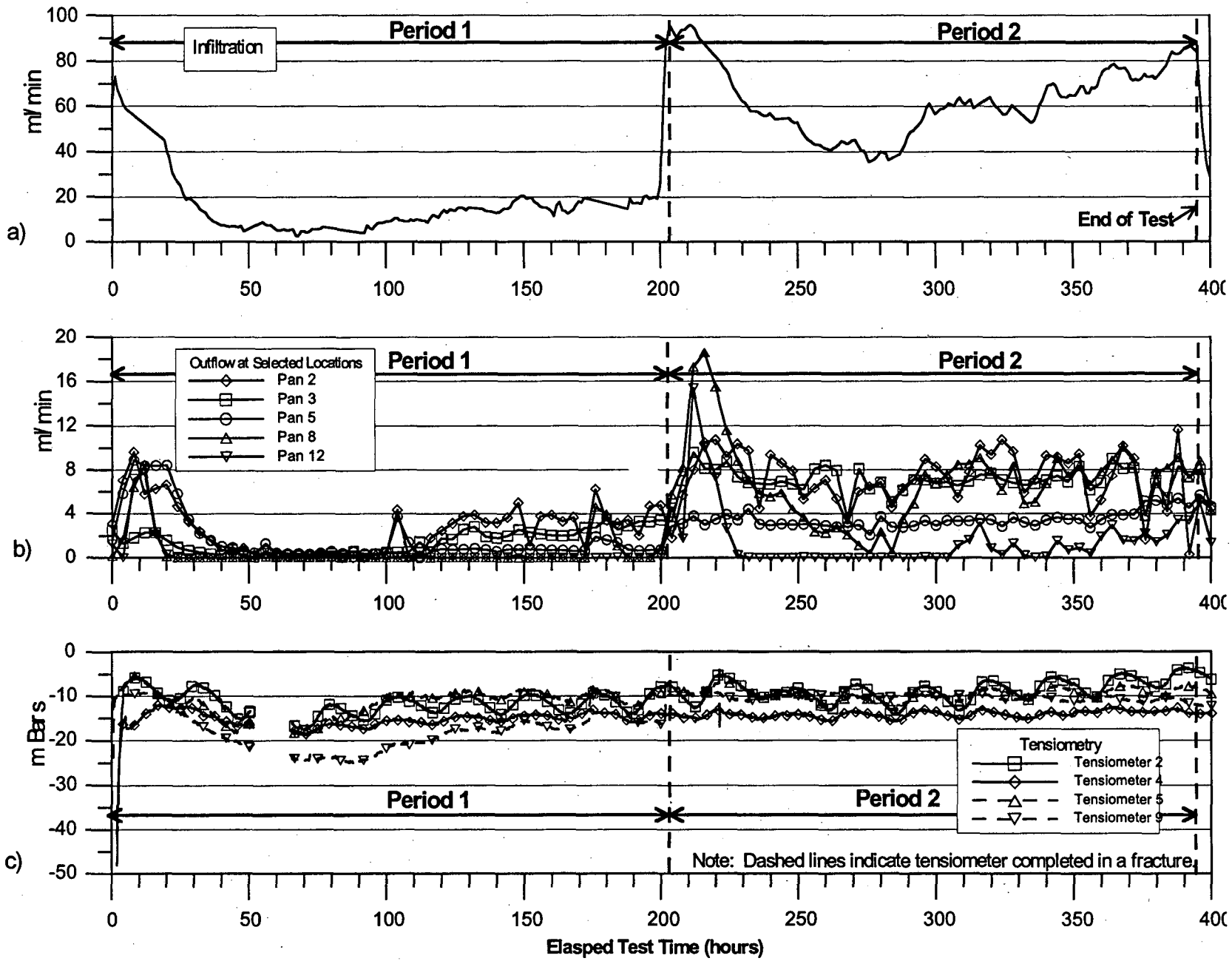

Figure 1. Time trend plots of a) infiltration, b) outflow, and c) tensiometry.

Calculating Fracture Temperatures from Wellbore Measurements

R. C. Schroeder

Berkeley Group Inc
245 Gravatt Dr. Berkeley, CA
rcsch@slip.net

This paper describes a method for calculating the temperatures in multiple fractures during well production. When more than one fracture is intercepted by a production well the flow up the wellbore is a mixture of the fluids from the individual fractures, and the wellbore temperature is dependent upon the individual fracture temperatures and fracture flow rates. It is important to know the individual fracture temperatures to assist in reservoir simulation of fractured reservoirs. This is especially true in the case of injection and production, where the injection temperature can be much lower than the undisturbed fractures and undisturbed reservoir-rock temperature.

Equipment is currently available to make routine (PTS) measurements of pressure, temperature, and spinner (relative velocity) in high temperature wellbores during production. These measurements provide data that describes the hydrodynamic and thermodynamic conditions of the wellbore fluid-mixture being produced from multiple fractures.

A simple mixture model has been incorporated into the wellbore simulator, WELF98, and simulations of a series of PTS measurements during injection and production is presented for the Hijiori geothermal site in Japan. The WELF98 mixing model, used at each feed point, is based on the following mass and energy conservation equations.

$$q = q_f + q_{wb} \qquad \text{Mass}$$

$$hq = h_f\, q_f + h_{wb}\, q_{wb} \qquad \text{Energy}$$

The subscript, f, refers to fluid entering the wellbore from a fracture. The subscript, wb, refers to the water flowing up the wellbore from below the fracture. The values without a subscript are the mixture quantities for the fluid above the fracture.

The mixing model allows the extraction of fracture temperatures from the measured data. The calculations can then provide a time-history of the cooling of the individual fracture temperatures during a measurement period after start-up.

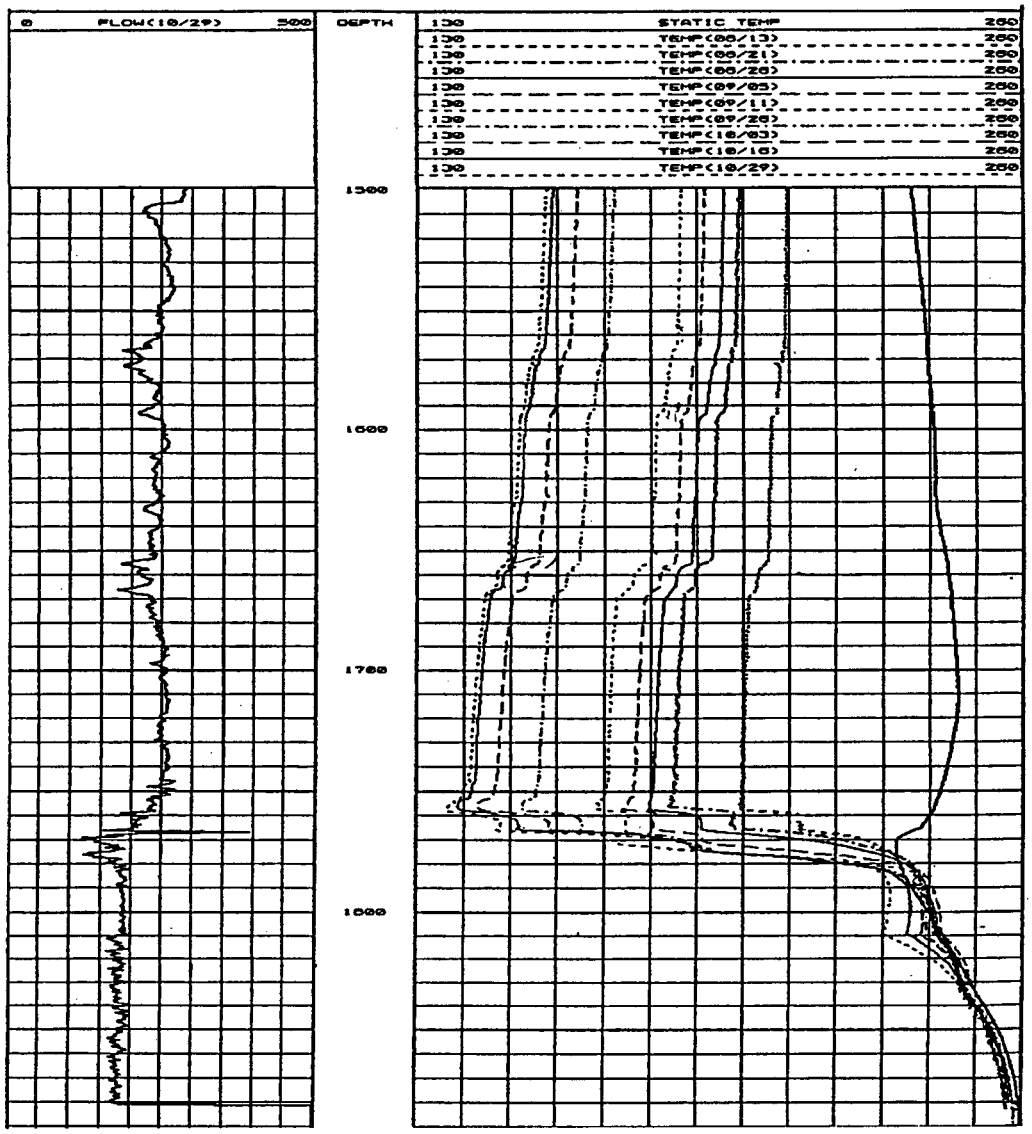

Figure 1. A series of temperature measurements and a single spinner measurement (at the left) for well HDR-2.

Figure 1 shows an example of a series of temperature measurements, and a single spinner measurement in the well HDR-2. The wellbore mixture temperature clearly shows the presence of numerous fractures in three separate zones.

The calculated fracture temperatures depend upon the measured temperatures and flow rates. The measurements provide several constraints that aid in accurate calculations. An extended discussion of these constraints and other, remaining sources of error is provided. A study of the sensitivity of the fracture-temperatures to errors in the measured data (and in the simulator's input data) is also provided. The study shows that the calculated fracture temperatures are weakly dependent upon the measured fracture flow rates and strongly dependent upon the measured mixture temperatures

The wellbore simulator WELF98 was used to simulate the data in figure 1, above. In figure 2, below, an example of the comparison between the measured and calculated data is shown.

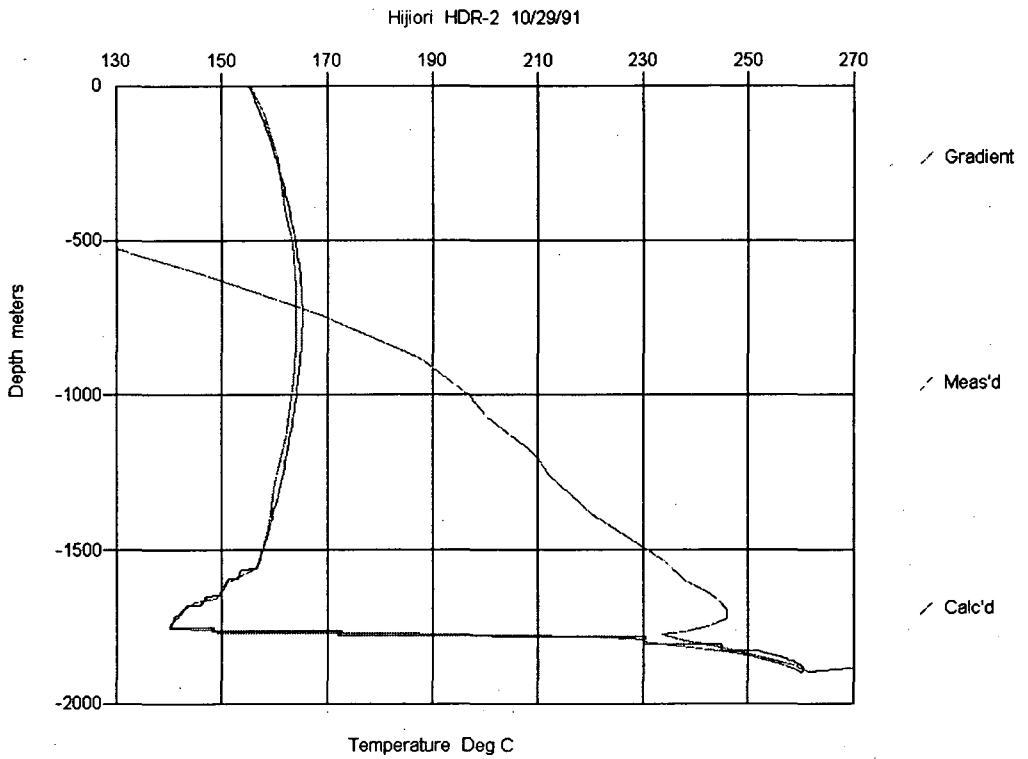

Figure 2. An example of a comparison between the calculated (red) and the measured (green) wellbore temperature data for one date in HDR-2. The static (undisturbed) reservoir temperature is shown in gray. Temperature is in °C, and depth is in meters.

Figure 2 shows that this well experienced severe cooling due to injection at a depth near 1780 meters. The calculated temperature in the coolest fracture in that zone (at 1765 m) was 106 °C while the minimum temperature of the wellbore mixture at about 1765 m was about 140 °C.

Another feature seen in Figure 2 is the large radial heat transfer. When the wellbore temperature is less than the far-field temperature (shown in gray) the wellbore heats up, and when the wellbore temperature is higher than the far-field temperature (near the wellhead) the radial heat transfer cools the wellbore. This effect is accentuated in this well due to a relatively low total flow rate and is an important factor in the calculations.

In the main body of this report the basic fracture structure that is being simulated and the injection and production well completions are described in detail. All aspects of the calculation method are covered in detail in the main body of the report. Additional figures and tables, of fracture temperatures that were outlined briefly above are presented.

Laboratory Experiments on Solute Transport in Unsaturated Fractures

Grace Su[1,2], Jil Geller[2], Karsten Pruess[2], and James Hunt[1]

[1] University of California at Berkeley, Department of Civil and Environmental Engineering, Berkeley, CA, 94720

[2] Lawrence Berkeley National Laboratory, Earth Sciences Division, Berkeley, CA, 94720

corresponding e-mail address: grace_su@lbl.gov

Introduction and Background

Fractures in the unsaturated zone can provide fast pathways for the transport of contaminants to the groundwater. Flow visualization experiments conducted in a transparent fracture replica showed that seeps in a heterogeneous, unsaturated fracture proceed along preferential channels consisting of wide, liquid-filled regions connected to rivulets or threads of liquid (Su et al., submitted to WRR). Even though constant inlet conditions were maintained, the flow of water generally proceeded in an intermittent manner where threads would typically break following a period of no observable changes in liquid distribution. The persistent occurrence of intermittent flow in our seepage experiments suggests that it is an important feature controlling flow through unsaturated fractures, which is not described by current analytical and numerical models.

The cyclic formation and snapping of liquid threads is due to the interplay of capillary and gravity forces and the geometry of the flow path. Intermittent flow occurred as liquid flowed through a sequence of apertures progressing from small to large to small over a certain range of flow rates for a particular angle of inclination. For a given flow rate, intermittent flow occurred more frequently as the relative strength of gravity increased

Intermittent flow may have significant implications on solute transport. Laboratory tracer tests are conducted in a transparent epoxy fracture replica to examine the importance of intermittent flow on solute transport in unsaturated fractures.

Laboratory Tracer Tests in a Fracture Replica

A transparent fracture replica of a granite rock was placed over an inclined light table to allow visualization of the flow path during the tracer test. Breakthrough curves of a chloride tracer through this fracture were obtained by measuring the conductance of water at the outlet of the fracture using gold wire electrodes. Calibration of the resistance as a function of tracer concentration verified that the conductance is linearly related to the tracer concentration. A solution of 0.5 g/L calcium chloride was used as the tracer and supplied to the fracture at a constant flux with a syringe pump. The location of the flow channel in the fracture during the experiment is shown in Figure 1 (a). Two series of tracer tests were made with inlet flow rates of 3 and 5 ml/hr at three angles of inclination ($\phi = 21°$, 46°, and 81°) measured from the horizontal for each flow rate. The angle was varied without disassembling the fracture. The flow through the fracture was allowed to equilibrate for approximately 24 hours after changing the angle of inclination.

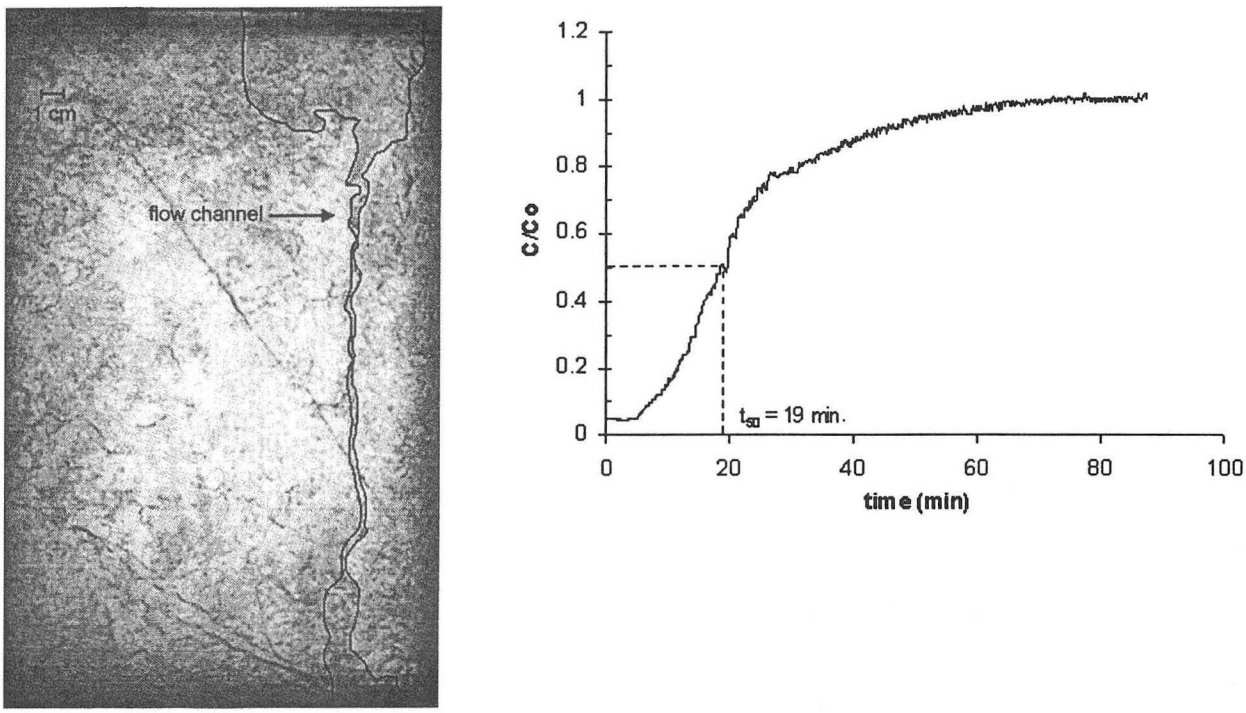

(b)

Figure 1: (a) Flow channel in epoxy fracture replica for Q = 5 ml/hr and $\phi = 81°$. (b) Corresponding breakthrough curve for Q = 5 ml/hr and $\phi = 81°$.

The breakthrough curve for an angle of inclination of 81° and flow rate of 5 ml/hr is presented in Figure 1 (b). The fluctuations in the breakthrough curve are due to intermittent flow events occurring in the flow channel. The mean travel time of the tracer (t_{50}) was obtained from the breakthrough curve corresponding to the time when the normalized effluent concentration reached 0.5. The average seepage velocities were obtained by dividing the mean travel times into the length of the fracture (32 cm) and are plotted in Figure 2 as a function of the relative strength of gravity (sin ϕ) for the two flow rates. The average velocity decreases at higher angles of inclination for a given flow rate, contrary to what is expected as the relative strength of gravity increases. The reason for this trend is the increase in the frequency of intermittent flow events as the angle of inclination increases. When the intermittent flow events are more frequent, the channel is disconnected more often, delaying the downstream movement of the solute and decreasing the average velocity.

The effective water velocities and dispersion coefficients were obtained by fitting the breakthrough curve to the one-dimensional advection-dispersion equation (ADE) for a homogeneous porous medium. Both effective parameters were adjusted to give the best fit of the ADE to the experimental data. The effective velocities are also included in Figure 2, but do not follow the trend of the average velocities as the relative strength of gravity changes. The effective dispersion coefficients generally increased as the velocity increased. The effective parameters may not have any physical meaning, however, since we are dealing with a heterogeneous medium, and the breakthrough curves are further complicated by intermittent flow.

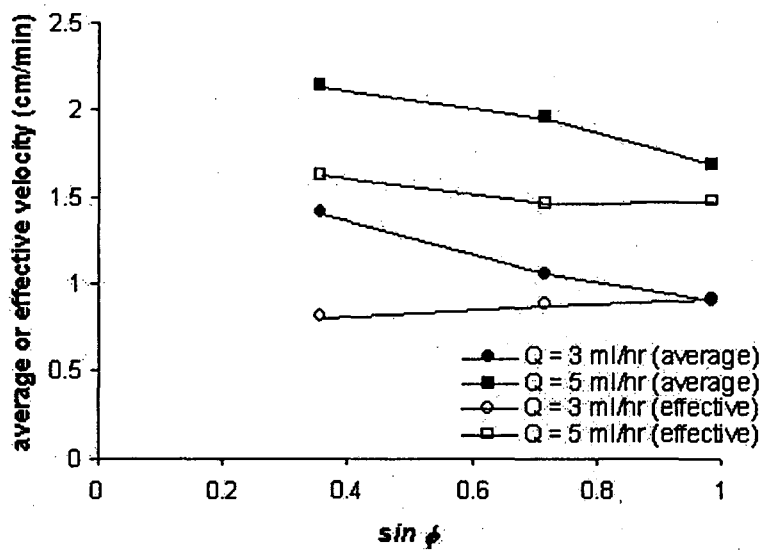

Figure 2: Average and effective velocities plotted as a function of angle of inclination. The filled symbols correspond to the average velocities, while the open ones are the effective ones.

Conclusions

The cyclic snapping and reforming of the flow channel, or intermittent flow, is a mechanism affecting flow in unsaturated fractures. Laboratory tracer tests were conducted to study the effect of intermittent flow on solute transport. Measurements of the average travel time and seepage velocity were obtained from the breakthrough curves. The average seepage velocity was larger as the flow rate increased for the same angle of inclination. For a given flow rate, the seepage velocity decreased at higher angles of inclination due to the increase in the frequency of intermittent flow events. The advection-dispersion equation fits well to the breakthrough curves, but the effective parameters obtained may not have any physical meaning due to the heterogeneous flow field and occurrence of intermittent flow. Intermittent flow affects the shape of breakthrough curves and should be considered in the interpretation of results from tracer tests.

References

Su, G., J. Geller, K. Pruess, and F. Wen, Experimental Studies of Liquid Seepage and Intermittent Flow in Unsaturated, Rough-Walled Fractures, submitted to *Water Resources Research.*

Acknowledgement

This work was supported by the Director, Office of Energy Research, Office of Health and Environmental Sciences, Biological and Environmental Research Program, of the U.S. Department of Energy under Contract No. DE-AC03-76SF00098.

Hydraulic Characterization of Fractures and Faults in Sandstone

W. Lansing Taylor, Rodrick Myers, Atilla Aydin, and David D. Pollard
Rock Fracture Project, Department of Geological & Environmental Sciences,
Stanford University, Stanford, CA 94305-2115

We have identified a mechanical process of fracturing and faulting in a porous sandstone (the Aztec Sandstone in the Valley of Fire, Nevada), where successive generations of fractures are formed by slip on pre-existing ones creating a hierarchical fracture network. This hierarchy continues at larger scale where faults and related new fractures are formed by shearing across individual fractures and fracture zones.

The initial structure components (fractures and fracture zones) are fast fluid flow paths. It is shown that connectivity due to a small amount of shearing is the most crucial element for this stage. The amount of fluid exchanged between fractures and the matrix compartments depends on the effective permeability of the fracture zones, which is controlled by the spatial distribution of the fractures within the zone, their individual hydraulic properties, and the matrix permeability.

Increasing shearing produces larger faults with fine grained fault rocks and the associated new fracture networks at the faults' peripheries. Permeability of fault rocks is quite low so that faults are aquitards perpendicular to their trends whereas the associated fracture networks result in an enhance permeability parallel to the faults. It is this dichotomy that characterizes reservoirs and aquifers in sandstone.

Evaluation of Seepage into a Mined Opening Constructed in Unsaturated Fractured Rock

Robert C. Trautz
Lawrence Berkeley National Laboratory, 1 Cyclotron Road, MS 90-1116,
Berkeley, California, 94720, rctrautz@lbl.gov

Paul J. Cook
Lawrence Berkeley National Laboratory, 1 Cyclotron Road, MS 90-1116,
Berkeley, California, 94720, pjcook@lbl.gov

Joseph S.Y. Wang
Lawrence Berkeley National Laboratory, 1 Cyclotron Road, MS 90-1116,
Berkeley, California, 94720, jswang@lbl.gov

A capillary barrier may form when an unsaturated hydrogeologic unit containing relatively fine pores or fractures overlies a unit consisting of relatively coarse pores. Coarse-pore soils typically drain at relatively large water potentials and, like any porous material, will not conduct appreciable amounts of water at or below their residual saturation. In contrast, a relatively fine-pore soil may still be able to conduct water at and below the same water potential. Since the fine-pore soil can still conduct water and the underlying coarse-pore soil cannot, a capillary barrier is created at the contact between the two layers under unsaturated conditions.

By analogy, the potential exists for a capillary barrier to form when a fine-grained unit, such as a highly fractured rock, overlies a large open space, such as an underground cavity. Conditions such as these exist at the proposed radioactive-waste repository located at Yucca Mountain, Nevada. If constructed, the monitored geologic repository will include 117 km of mined openings or waste emplacement drifts housing containers of radioactive waste (Daniel et al. 1998). In addition, the repository would be constructed approximately 200 meters (m) below the land surface and at least 100 m above the regional water table within the fine-grained Topopah Spring Tuff (Tpt), a densely welded, intensely fractured, devitrified ash-flow tuff (Buesch and Spengler 1998).

It is important to determine whether a capillary barrier will form above a waste emplacement drift because such a barrier can have a direct impact on waste isolation and repository performance. Water introduced at the land surface during a natural precipitation event, assuming it migrates to the repository level, may be excluded from seeping into the drift and instead may be diverted laterally around the opening if a capillary barrier forms. In contrast, if a capillary barrier does not form, then water may drip into the opening and come in contact with the waste package, potentially hastening canister corrosion and premature failure.

A series of tests was conducted in four specially constructed drifts, called niches, located in the Exploratory Study Facility (ESF). Each niche consists of an 8.2 to 9.0-m-long drift, or mined opening, constructed on the west side of the ESF main drift within the middle nonlithophysal zone of the Topopah Spring welded unit. Air-injection tests and liquid-release tests were

conducted at each site to characterize the flow of air and water through fractures and to quantify water seeping into an underground opening from an artificial localized liquid-release event.

Pre-Excavation Tests

Approximately 3,000 air-injection tests were conducted in boreholes at the four niche sites (referred to as Niches 3566, 3650, 3107 and 4788) prior to their excavation. The test results were used to determine the distribution of single-hole air permeabilities within the rock mass. These data were then used to select test intervals for subsequent liquid-release tests. A series of low-flow-rate, liquid-release tests were conducted in boreholes installed prior to the excavation of Niches 3566 and 3650 during early June and early August 1997, respectively. Pre-excavation liquid-release tests were also performed at Niches 3107 and 4788, starting in late April and late June 1998, respectively.

The liquid-release tests were conducted in the same boreholes as the air-injection tests, by pumping approximately 1 liter of water containing colored or fluorescent dyes into 0.305-m-long test intervals straddling both high and low air-permeability zones. Various colored and fluorescent tracers were used during the study to document the flow path traveled by the wetting front. The dye-spiked water was introduced into each test interval, with essentially no pressure buildup.

Niche Excavation Activities

The niches were excavated dry using a mechanical device called an Alpine Miner to observe and photograph the distribution of fractures and dye within the welded tuff. Dye was observed along individual fractures as well as along intersecting fractures to depths ranging from 0 to 2.6 m below the liquid-release points at the Niche 3566 and 3650 sites. Likewise, dye was observed at a maximum depth of 1.19 m below the release point at Niche 3107 and 1.79 m at Niche 4788. Flow of water through a relatively undisturbed fracture-matrix system was documented in this manner.

Two primary types of flow paths were observed in the field during the mining operation, including: (1) flow through individual or small groups of high-angle fractures; and (2) flow through several interconnected low- and high-angle fractures creating a fracture network

The mass of water injected into each interval was compared to the maximum depth of infiltration, lateral distance traveled by the wetting front, and ratio of depth to lateral distance (hereafter defined as the aspect ratio). As one would expect, there was a general trend for the wetting front to move deeper into the rock beneath the release location as the mass of water injected increased. Surprisingly, the data did not indicate that the wetting front moved deeper into the profile when water is introduced into high-angle fractures as opposed to fracture networks. This apparent anomaly may be an artifact of sampling and observation bias rather than that of fracture flow mechanics. Any near-vertical fractures that contribute to flow and that are oriented parallel to the mined face of the niche will not be observed as frequently as low-angle fractures. This is because the vertical fractures will be mined away during a single cut of the working face (typically 0.15 to 0.305 m per cut) before the dye can be observed and the depth of the wetting front mapped.

There was no direct correlation between the mass of water injected and the maximum observed lateral (horizontal direction from the injection point) distance traveled by the wetting front. However, the data showed that water spread laterally over larger distances in the interconnected network of fractures than in vertical fractures, as one would expect.

In general, the maximum distance that the wetting front traveled from the point of injection to the furthest point of observation increased with the mass of water injected. As was the case with depth of infiltration, the data did not show that the type of flow (i.e., network or vertical fracture flow) had any significant influence on the maximum travel distance. However, the ratio of depth to lateral distance traveled (aspect ratio) versus mass of water injected showed an important trend. Although the data were sparse, the aspect ratio is consistently higher for the near-vertical fracture flow data than for the fracture network data

Post-Excavation Seepage Tests

An extensive series of tests was performed at Niche 3650 to determine the amount of water that would seep into the cavity. The air-injection tests were repeated in three boreholes (UL, UM, and UR) that remained after Niche 3650 was excavated to determine the post-construction distribution of air permeabilities. A dramatic increase in air permeabilities was observed after the niche was constructed. The geometric mean air permeability of zones tested in borehole UM increased by nearly two orders of magnitude after the niche was excavated because of mining-induced damage to the surrounding formation. Furthermore, the air-permeability results obtained during this study are representative of fracture permeabilities, because the geometric mean permeability of the rock matrix is much lower: 4.1E-18 m^2 as reported by Flint (1998).

A series of short duration seepage tests were performed starting in mid November 1997, continuing for approximately 4 months, and ending in mid March 1998. The seepage tests were conducted after Niche 3650 was excavated, by pumping water into boreholes UL, UM, and UR located 0.65 meters above the niche. The tests were used to quantify the amount of water seeping into the drift from a localized source of water of known duration and intensity. In addition, the tests were used to establish the threshold rate of liquid release at which water would no longer seep into the mined opening.

Forty liquid-release tests were performed on 16 test intervals positioned above Niche 3650 to determine the *seepage threshold flux*, defined as the liquid-release flux at which water will no longer seep into the drift. Seepage threshold fluxes were determined for 10 test zones that seeped. The seepage data were used along with the air permeability values to demonstrate that water was excluded from entering the niche because of the capillary barrier. Direct field observation, indirect field evidence, and numerical models were also used to confirm that a capillary barrier was present.

The seepage threshold data were interpreted using an analytical solution formulated by Philip et al. (1989) describing the exclusion of water from a buried cylindrical cavity analogous to a niche. The resulting analysis produced realistic estimates of the quantity $2\alpha^{-1}$ defined as the sorptive length, a useful parameter that characterizes the capillary properties of the unsaturated medium. Values of $2\alpha^{-1}$ equal to 19.6 and 981 Pascals (Pa) were measured and believed to be representative of flow through two types of *in situ* fractures, including individual or small groups

of high-angle fractures and interconnected fracture networks, respectively. The sorptive number α was used along with wetting front arrival times to generate fracture-water characteristic curves (volumetric water content (θ) versus water potential (Ψ)) for several test zones. These curves indicate that the residual θ may be on the order of 0.1% and that the saturated θ (i.e., porosity) may be as high as 2.4% for the seepage flow paths tested. Preliminary numerical modeling results and laboratory measurements support the conclusion that the volumetric water contents reported in this paper probably represent fracture properties. Rock samples analyzed from the niche sites showed that dye-spiked water released into the fractures penetrated to a depth of only 6-7 millimeters into the adjacent rock matrix. This reveals the relatively minor influence the matrix had on transient fracture flow conditions observed during the liquid-release tests.

The results of this investigation and future study will be part of the input used in the design and construction of a monitored geologic repository.

References

Buesch, D.C. and Spengler, R.W. 1998. Character of the Middle Nonlithophysal Zone of the Topopah Spring Tuff at Yucca Mountain. In: Proceedings of the American Nuclear Society 8th International Conference on High-Level Radioactive Waste Management, Las Vegas, Nevada.

Daniel, R.S., G.M. Teraoka, D.G. McKenzie, S.J. Meyers, and J.R. Compton, 1998. Overview of the Current CRWMS Repository Design. In: Proceedings of the American Nuclear Society 8th International Conference on High-Level Radioactive Waste Management, Las Vegas, Nevada.

Flint, L.E. 1998. *Characterization of Hydrogeologic Units Using Matrix Properties, Yucca Mountain, Nevada.* Yucca Mountain Project Milestone 3GUP603M. U.S. Geol. Surv. Water Resour. Invest. Rep. 97-4243. Denver, Colorado: U.S. Geological Survey.

Philip, J.R., J.H. Knight, and R.T. Waechter, 1989. "Unsaturated Seepage and Subterranean Holes: Conspectus, and Exclusion Problem for Cylindrical Cavities." *Water Resour. Res., 25*(1), 16-28.

Quantifing Sorption of Colloids at Gas-Water Interfaces:Implications for Colloid Transport in Unsaturated Subsurface Environments

J. Wan, T.K. Tokunaga, R.C. Stover, J.Y. Yang, and K.S. Olson
Earth Sciences Division, Lawrence Berkeley National Laboratory,
Berkeley, California 94720

Introduction. Colloidal particles are found to favorably accumulate at air-water interfaces in many natural environments and engineered systems. Ocean and lake surfaces play important roles in transport and transformations of many physical, chemical, and biological entities. Enrichment of particle-associated heavy metals and organic compounds has been found at the surface of oceans and lakes (1-6). For instance, the concentrations of lead, iron, nickel, copper, fatty acids, hydrocarbons, and chlorinated hydrocarbons were found to be 1.5 to 50 times higher in the surface layer (approximately 150 μm thick) of Narragansett Bay relative to the bulk water, with most of the enrichment in the particulate and organic fractions (2). Clays, humic acids, and microorganisms have been found accumulated at air-water interfaces in unsaturated soils (7-10). Engineered systems such as floatation-based mineral separation methods also take advantage of particle partitioning at air-water interfaces (11). These examples suggest that colloidal partitioning at air-water interfaces can be significant in a wide variety of natural and engineered systems. For surface active molecules, changes in surface tension with changes in solution concentration determine their surface excesses through the Gibbs equation (11). However, for suspensions of particles, surface tension changes are often not measurable. There is no existing method for quantifying colloid sorption at the gas-water interfaces in our knowledge. In this study we developed a method to quantify particle surface excesses at air-water interfaces. In this paper colloid particle surface excesses are defined in a manner similar to that used for dissolved molecules. This quantity is the excess number of particles per unit interfacial area relative to that obtained by assuming that the bulk suspension concentration extends unchanged up to the air-water interface. Using this new method we measured partition coefficients of humic acid and clay colloids at the air-water interfaces as function of solution chemistry.

Theory and Method. A bubble column device was used for quantifying colloidal surface excesses. In the bubble column system, gas is bubbled through a vertical column containing the dilute aqueous suspension (or solution) of the colloids (or solute), with an open free surface at the top. The rising bubbles sorb and carry the surface-active species upwards, then release them back to the solution at the free surface where the bubbles burst. At steady-state, a concentration profile is established along the column length which reflects the balance between upward transport by partitioning onto rising bubbles and downward transport by eddy dispersion. By predetermining the column eddy dispersion coefficient for given conditions (column dimensions, air flow rate and bubble size) and measuring the steady-state concentration profile, the partitioning between bulk and surface regions can be determined. Lemlich (12-13) and Shah and Lemlich (14) introduced a non-foaming bubble fractionation technique to separate dissolved surface-active materials such as dyes from solutions. They provided a useful conceptual framework for evaluating the separation process. However, quantitative testing of the method was not demonstrated because the eddy dispersivity was not measured. In our work, all parameters were independently determined. We also improved the column design of Lemlich (12) by increasing the air-water interfacial area per unit volume of solution. This improved the sensitivity of the method and made it possible to generate measurable concentration gradients of less surface-active species such as clays, bacteria, and humic acids.

In a bubble fractionation column at steady-state, the local mass balance for a surface active compound requires that the upward and downward transport rates be equal. This condition is represented by

$$af\Gamma = AD\frac{dC}{dz} \quad , \tag{1}$$

where a is the surface area per bubble, f is the bubble generation rate, Γ is the surface excess, A is the column cross-sectional area, D is the column eddy dispersion coefficient, C is the concentration in solution (suspension), and z is the vertical coordinate (symbol definitions and dimensions are provided at the end of this article). For dilute solutions (suspensions) in which partitioning at the water-gas interface is linear with respect to concentration, the surface excess is given by

$$\Gamma = KC \quad . \tag{2}$$

For surface-active molecules, K is the linear adsorption isotherm coefficient. The magnitude of K represents the thickness of the bulk solution which contains the same mass of surface active substance as is associated with the interface. To test the bubble column model, experiments within the linear range of K for the surfactant SDBS were performed, as described later. In extending this approach to particulate systems, we define K as the particle partition coefficient, relating particle surface excesses to their bulk suspension concentrations. The extension of eq. 2 to linear partitioning of particles is intended to apply in dilute suspensions, when K is relatively constant. It is expected that in many natural systems the suspended colloid concentration will be sufficiently dilute such that the linear K approximation can be useful. The extension of this model to nonlinear colloid partitioning is outside the scope of this study. The solution to eqs. 1 and 2 is an exponential profile, and the steady-state ratio of the concentration at elevation z versus at the bottom of the column is

$$\frac{C(z)}{C_b} = \exp(Jz) \quad , \tag{3}$$

where

$$J = \frac{afK}{AD} \tag{4}$$

and C_b is the concentration at the bottom of the column at steady-state. The constraint of mass conservation within the column provides the relation between C_b and the initial (also average) concentration C_o. Integration of eq. 3 over the column height H, and equating this result with HC_o gives

$$C_b = \left[\frac{HJ}{\exp(HJ)-1}\right]C_o \, , \tag{5}$$

such that

$$\frac{C(z)}{C_o} = \left[\frac{HJ}{\exp(HJ)-1}\right]\exp(Jz) \quad . \tag{6}$$

Thus, measurement of the steady-state column profile of a solute or colloid permits determination of the separation parameter J. When A, a, f, and D have been independently determined, measurement of steady-state $C(z)$ permits determination of K. The accuracy with which K can be

determined with the bubble column method is largely limited by uncertainties in the rate of interfacial area generation (the product *af*).

Verification of the bubble column method. To verify the uniqueness of the bubble column results, adsorption isotherm constants obtained with the bubble column method can be compared with values obtained by surface tension (γ) measurements. For a dilute surfactant solution, combining the Gibbs adsorption equation

$$\Gamma = -\frac{C}{RT}\frac{d\gamma}{dC} \quad , \tag{7}$$

with eq. 2 gives

$$K = \frac{-1}{RT}\frac{d\gamma}{dC} \quad , \tag{8}$$

where R is the gas constant and T is the Kelvin temperature. Thus, whether or not surface excesses measured by bubble column and surface tension measurements are equivalent can be tested in simple surfactant solutions through comparing K values obtained using eq. 6, versus using eq. 8. The surface tension measurements of SDBS were conducted with a Wilhelmy plate tensiometer (Kruss) at 22.8 ±0.5 °C. Solutions containing up to 1.0×10^{-4} M SDBS (in 1.0 mM NaCl, at pH 5.7) were measured. This range of SDBS concentrations encompasses that used in the bubble column experiments. Combining the aforementioned slope of the SDBS surface tension-concentration function with eq. 8 yielded a K = 56 ±3 μm. This value of K was then compared with K = 56 ±13 μm resulted from the bubble column with eq. 6. The K values for SDBS from two different methods are in fair agreement. This agreement validated the bubble column technique as a method for determining partitioning of surface-active components at air-water interfaces.

Results and Discussion. Steady-state bubble column profiles were measured and modeled for soil humic acid (HA, 1S102H, International Humic Substances Society, St. Paul, MN), and kaolinite clay (KGA1b, well crystallized, Source Clay, Columbia, MO). The three humic acid (HA) solutions used in the bubble column contained 4, 10, and 20 mg l^{-1} HA respectively, in 5.0 mM Na_2SO_4 at pH 6.0. Kaolinite was tested at concentrations of 10^6, 10^7, and 10^8 particles ml^{-1}, in a solution of 1.0 mM NaCl and 0.5 mM $CaCl_2$ at pH 5.6 - 5.8. Kaolinite clay was used as supplied without any additional treatment. Both of these systems clearly exhibited concentration gradients, with preferential partitioning of humic acid and kaolinite at the air-water interface.

A best-fit K of 27 ± 6 μm for HA was obtained. We are not aware of any reports of surface tension-based measurements of HA surface excesses at such low concentrations. Given the extremely wide range of reported values of molecular weights for HA (19), it was not possible to report either bulk or surface concentrations on a number or molar basis. Nevertheless, our measured K permit determination of HA surface excesses in terms of mass per interfacial area.

The well-developed concentration gradients for kaolinite in the bubble column demonstrated that under the given solution chemistry, this clay partitions favorably at air-water interfaces, despite the lack of measurable changes in surface tension. Over a two order of magnitude range in concentrations, the clay suspensions gave a fairly linear partitioning relation, although the data show slightly higher separation efficiencies at lower concentrations. A K value of 39 ± 9 μm accounted for kaolinite partitioning over the tested range of suspension concentrations. When clay suspension concentrations are expressed in terms of mass per unit volume, surface excesses of clays are identified in terms of mass per interfacial area. Since experiments with kaolinite included quantification of suspension concentrations in terms of particle numbers per unit volume, it was possible to express surface excesses in terms of the number of colloids per

interfacial area. Surface excesses (Eq. 2) ranged from 80 to 4000 particles mm^{-2} (10^4 to 300 μm^2 per particle) for the three kaolinite suspension concentrations. The results indicate that the bubble column method gives reproducible measurements of colloids partitioning at air-water interfaces. The mechanisms responsible for colloid partitioning at the air-water interface are under inverstigation.

Vadose Zone Implications. With this new ability to measure colloid surface excesses, more quantitative analysis of a wide variety of environmental processes becomes possible. Implications of these types of measurements are especially relevant in the vadose zone because this portion of the environment can have high values of air-water interfacial area per unit bulk volume. surface-active colloids between bulk water and the air-water interface can become very significant. In partially water-saturated soil, the mass of colloidal material associated with air-water interfaces, N_Γ, relative to their mass in aqueous suspensions, N_s, can be estimated. From Eq. 2 it follows that

$$\frac{N_\Gamma}{N_s} = K\frac{A_s}{V_w} \quad , \tag{9}$$

where A_s/V_w is the air-water interfacial area per volume of soil water. The inverse of this ratio is the effective thickness of water films in partially-saturated soils (averaged over both true water films and pendular water around grain-grain contacts), typically ranging from nanometers up to about 100 μm. Given the K values ranging from 27 to 39 μm for humic acid and kaolinite, respectively, eq. 9 indicates that the amount of interface-associated colloids is of the same order as that in suspension in partially-saturated soils (under similar solution chemistries). This result indicates that colloid partitioning at air-water interfaces of partially-saturated porous media can be much more significant than previously recognized. It should be noted that eq. 9 does not apply when film thicknesses are less than or equal to characteristic colloid sizes. Under these conditions air-water interfaces are retracted onto hydrophilic colloids (15), and colloids are in contact with air-water interfaces regardless of their K values.

Acknowledgment
This work was carried out under U.S. Department of Energy Contract DE-AC03-76SF-00098. Funding was provided by DOE's Environmental Management Science Program.

References

1 Sutcliffe, W. H.; Baylor, Jr. E. R.; Menzel D. W. Deep-Sea Research **1963**, 10, 233-243.
2 Duce, R. A.; Quinn, J.; Olney, C.; Piotrowicz, S.; Ray, B.; Wade, T. Science **1972**, 14, 161-163.
3 MacIntyre, F. Sci. Am. **1974**, 230, 62-77.
4 Gershey, R. M.; Limnol. Oceanogr. **1983**, 28, 309-319.
5 Lewis, B. L.; Landing, W. M. Marine Chemistry **1992**, 40, 105-141.
6 Skop, R. A.; Viechnicki, J. T.; Brown, J. W. J. Geophy. Res. **1994**, 99, 16395-16402.
7 Chen, Y.; Schnitzer, M. Soil Sci. **1972**, 125, 7-15.
8 Wan, J. ; Wilson, J. L. Water Resour. Res. **1994**, 30, 11-23.
9 Wan, J. ; Wilson, J. L.; Kieft, T. L. Appl. Environ. Microbiol. **1994**, 60, 509-516.
10 Powelson, D. K.; Mills, A. L. Appl. Environ. Microbiol. **1996**, 62, 2593-2597.
11 Hiemenz, P.C. Principles of Colloid and Surface Chemistry, **1986**, Marcel Dekker Inc., New York.
12 Lemlich, R. A. I. Ch. E. J. **1966**, 12, 802-804.
13 Lemlich, R. in Recent Developments in Separation Science, Edited by Li, N. N. **1972**, The Chemical Rubber Co., Cleveland Ohio.
14 Shah, G.N.; Lemlich, R. Ind. Eng. Chem. Fundamentals **1970**, 9, 350-355.
15 Wan, J.; Tokunaga, T.K. Environ. Sci. Technol. **1997**, 31, 2413-2420.

Evidence of Scale-Dependent Dispersivity in Fractured Sedimentary Rocks, Newark Basin, New Jersey

Claire Welty, Drexel University, School of Environmental Science, Engineering, and Policy
Philadelphia, PA 19104, weltyc@drexel.edu
Glen Carleton and Herbert T. Buxton, U.S. Geological Survey Water Resources Division 810
Bear Tavern Road, Suite 206, West Trenton, NJ 08628, carleton@usgs.gov

The U.S. Geological Survey, in cooperation with the New Jersey Department of Environmental Protection, conducted field-scale aquifer and tracer tests in 1994-95 at a site in Hopewell Township, Mercer County, N.J., to determine hydraulic and transport properties of the fractured sedimentary rock. Prior to this study, which is described in detail in Carleton and others (in press), little quantitative information on the solute-transport properties of this aquifer was available. This extended abstract describes the field tests that were carried out at the site and the interpretation of the field data to determine the hydraulic-conductivity tensor, specific storage, effective porosity, and dispersivity at distances ranging from 30 to 183 m.

The site is in the Newark Basin, an elongate (210 by 55 kilometers), northeast-southwest-trending fault trough filled with late Triassic and early Jurassic fluvial and lacustrine sediments and igneous intrusions that is part of the Piedmont Physiographic Province (Olsen, 1980). The site is underlain by the Late Triassic Passaic Formation, an important aquifer in New Jersey and Pennsylvania that consists of red arkosic mudstones, siltstones, and fine-grained sandstones. Bedding planes strike approximately east-west and dip moderately to the north near the wells tested. The two dominant fracture sets are bedding-plane partings and east-west-striking structural fractures that dip steeply to the south.

A network of 13 wells (Vecchioli and others, 1969) and two additional pre-existing wells at the site, shown in figure 1, includes a central well (well 1); well 6, located 30.5 m downdip (north); wells 2 and 10, located 91.4 and 183 m, respectively, approximately along strike (west); and well 5, located 92.7 m downdip. The wells are constructed of 6 m of steel surface casing and are about 46 m deep, except for well 6, which was drilled to 61 m in order to penetrate the same bedding planes intersected by well 1. A full suite of geophysical logs--gamma, electric, electromagnetic conductance, caliper, fluid temperature and resistivity, video, acoustic borehole televiewer, and heat-pulse flowmeter--was collected in wells 1 - 13 (Morin and others, 1997) to determine the location and orientation of fractures and to construct lithologic sections that were used to correlate producing zones on the basis of geologic characteristics.

A 9-day aquifer pumping test was conducted in October 1994 by extracting water from well 1 at a rate of 108 L/min (liters per minute) (+/- 2 percent), and recording the hydraulic heads in the pumped well and the other 14 wells as a function of time. The drawdown curves in the strike and dip directions differ significantly, indicating that hydraulic conductivity at the site is anisotropic. The analytical method of Hsieh and Neuman (1985, case 4) and Hsieh and others (1985) was used to make preliminary calculations of aquifer hydraulic properties. The analysis yielded principal values of hydraulic conductivity of 6.4, 0.30, and 0.0043 m/d (meters per day), and a value of specific storage of 9.2×10^{-5} m^{-1}. The maximum principal direction of hydraulic conductivity was nearly aligned with strike, which was approximately parallel to land surface;

the minimum value was perpendicular to land surface (across the bedding planes). The analytical results were used as a guide for calibrating a three-dimensional numerical model, consisting of nine layers aligned with the bedding planes, to the measured heads. The best-fit values of hydraulic conductivity determined with the numerical model were 7, 3, and 4 x 10^{-5} m/d in the strike, dip, and normal-to-bedding-plane directions, respectively.

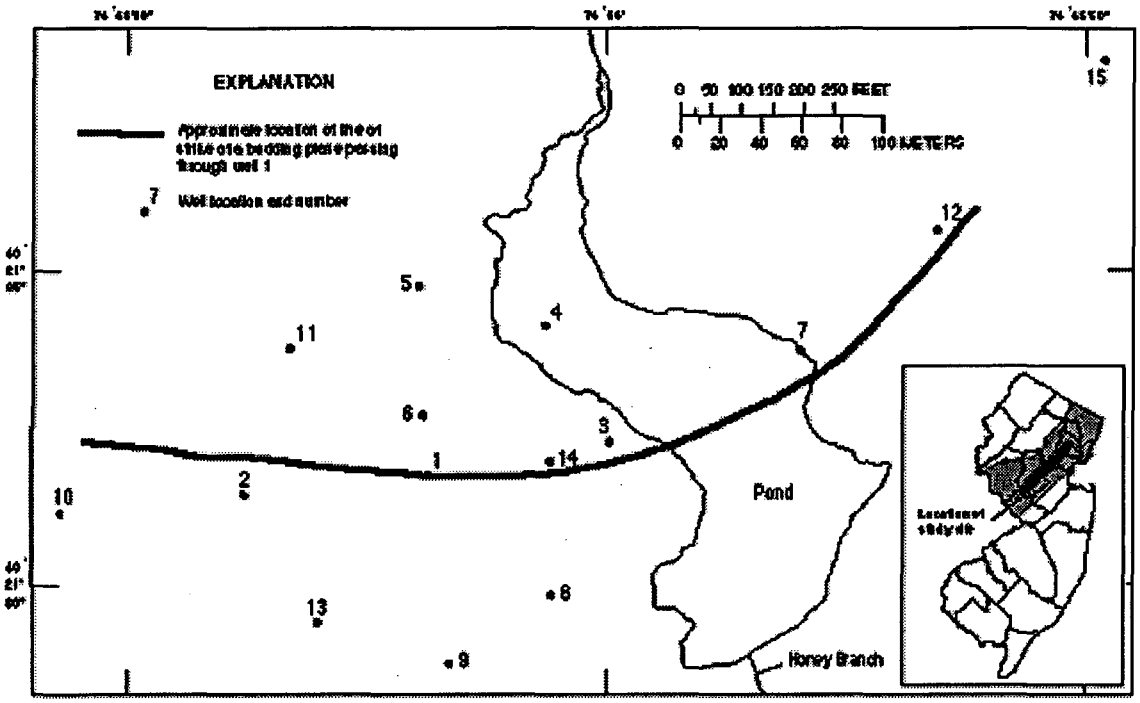

Figure 1. Location of wells and significant features in study area, Hopewell Township, N.J.

Three non-recirculating doublet tracer tests were conducted at well spacings of 30.5 m, 91.4 m, and 183 m in the 40-m-long open boreholes using pulse injections of bromide. Water was injected into well 6, 2, or 10 and withdrawn from well 1 at a flow rate of approximately 120 L/min for each test. Well 5 was used as a source of water for injection because it was believed to be sufficiently isolated hydraulically from the pumped well so as not to interfere with the hydraulic regime of the tracer tests. Water withdrawn from well 1 was discharged to the pond. Bromide concentrations were measured in water withdrawn from well 1.

The analytical solution of Welty and Gelhar (1994) for a doublet tracer test was applied to the rising limbs and peaks of plots of measured bromide concentrations as a function of time (breakthrough data) to obtain estimates of dispersivity and effective porosity. Calculated values of dispersivity for each test were as follows: 4.6 m for the well 6 to well 1 test (a scale of 30.5 m); 10.1 m for the well 2 to well 1 test (a scale of 91.4 m); and 12.8 m for the well 10 to well 1 test (a scale of 183 m). These dispersivity estimates are considered to be approximate because the analytical solution is based on the assumptions of constant dispersivity, homogeneous and isotropic media, and an infinite domain. Effective-porosity values obtained from the analyses ranged from 3.7 x 10^{-4} to 3.0 x 10^{-3}. Tracer mass recoveries were lower than expected; this result may be explained in part by the diversion of flow toward well 5 and along flow paths that were not simulated.

A two-dimensional, finite-element transport model was calibrated to the aquifer-test data and to the well 10 to well 1 (183-m scale) tracer test (bromide concentration as a function of time) data, to incorporate the effects of anisotropy and boundaries. The value of dispersivity obtained with the numerical model was identical to that obtained with the analytical model (12.8 m); the best-fit value of effective porosity was 1.2×10^{-3}.

Test results indicate that dispersivity increases with distance between the injection and three withdrawal wells at the site. Whether the value of dispersivity of 12.8 m could be considered a constant, asymptotic value, or whether the concept of Fickian transport is valid at this site can be ascertained only by conducting additional tracer tests at larger scales. The values of dispersivity observed in this study are greater than most of those reported for porous media at similar scales, but are typical of those reported for more heterogeneous fractured-rock environments (Gelhar and others, 1992).

On the basis of the shapes of the breakthrough curves, matrix diffusion does not appear to be an important process; however, this could result from the rapid transport typical of forced-gradient doublet tests. The influence of matrix diffusion could be determined by using natural-gradient tests that more realistically mimic natural flow conditions or tests in which multiple tracers with different molecular diffusion coefficients are used.

The study site offered a unique opportunity to conduct tracer tests at multiple scales at relatively low cost because the wells were already in place at the site. Available information on the dispersive properties of fractured-sedimentary-rock aquifers is scant (National Research Council, 1996); this study was a preliminary attempt to characterize this type of hydrogeologic environment in New Jersey. The results of this study indicate that continuum-based porous-medium models can be applied reasonably well to hydraulic and tracer tests in this type of fractured sedimentary rock.

Future work at this site could include (1) conducting tracer tests at larger scales to determine whether the concept of an asymptotic dispersivity is valid at any scale in this type of aquifer; (2) conducting tests to assess the importance of matrix diffusion; and (3) collecting and analyzing additional heat-pulse flowmeter data to determine whether approximate analytical expressions (see, for example, Gelhar, 1993) for predicting large-scale hydraulic conductivity and dispersivity on the basis of results of geostatistical analyses of fine-scale variations in hydraulic conductivity are valid for heterogeneous fractured-rock aquifers.

References

Carleton, G.B., Welty, Claire, and Buxton, H. T., in press, Design and analysis of tracer tests to determine effective porosity and dispersivity in fractured sedimentary rocks, Newark Basin, New Jersey; U.S. Geological Survey Water Resources Investigations Report 98-4126, 122 p.

Gelhar, L.W., 1993, Stochastic subsurface hydrology; Prentice-Hall, Englewood Cliffs, N.J., 390 p.

Gelhar, L.W., Welty, Claire, and Rehfeldt, K. R., 1992, A critical review of data on field-scale dispersion in aquifers; Water Resources Research, v. 28, no. 7, p. 1955-1974.

Hsieh, P., and Neuman, S.P., 1985, Field determination of a three-dimensional hydraulic conductivity tensor of anisotropic media. 1. Theory; Water Resources Research, v. 21, no. 11, p. 1655-1665.

Hsieh, P., Neuman, S.P., Stiles, G. K., and Simpson, E.S., 1985, Field determination of a three-dimensional hydraulic conductivity tensor of anisotropic media. 2. Methodology and application to fractured rocks; Water Resources Research, v. 21, no. 11, p. 1666-1676.

Morin, R.H., Carleton, G.B., and Poirier, Stephane, 1997, Fractured-aquifer hydrogeology from geophysical logs; the Passaic Formation, New Jersey; Groundwater, v. 35, no. 2, p. 328-338.

National Research Council, Committee on Fracture Characterization and Fluid Flow, 1996, Rock fractures and fluid flow--Contemporary understanding and applications; National Academy Press, Washington, D.C., 551 p.

Olsen, P.E., 1980, The latest Triassic and early Jurassic formations of the Newark Basin (eastern North America, Newark Supergroup)--Stratigraphy, structure, and correlation; New Jersey Academy of Science Bulletin, v. 25, p. 25-51.

Vecchioli, John, Carswell, L.D., and Kasaback, H.F., 1969, Occurrence and movement of ground water in the Brunswick Shale at a site near Trenton, N.J.; U.S. Geological Survey Professional Paper 650-B, p. B154-B157.

Welty, Claire, and Gelhar, L.W., 1994, Evaluation of longitudinal dispersivity from nonuniform flow tracer tests; Journal of Hydrology, v. 153, no. 1, p. 71-102.

Automated Control and Measurement in a Fracture Junction Study

J. Sidney Wise, New Mexico Institute of Mining and Technology (jswise@nmt.edu)
John L. Wilson, New Mexico Insitute of Mining and Technology (jwilson@nmt.edu)
Robert Reedy, Texas Bureau of Economic Geology
Chunhong Li, Sandia National Laboratories (cli@nwer.sandia.gov)

In order to predict the fate and transport of solutes in fractured rock systems, it is necessary to understand their mixing behavior at fracture junctions. In other words, a method is needed for predicting the concentrations of solutes leaving a fracture junction when the input concentrations, flow rates, and fracture geometry are known. For this reason, laboratory studies have been conducted to observe mixing behavior under varying flow conditions in a simplified physical model. The results of these experiments, in combination with lattice gas and lattice-Boltzmann modeling techniques, are used to determine empirical relationships for predicting solute transport.

Although the results of these studies will be found elsewhere, the focus of the present abstract is to describe the problems encountered in control and measurement and the methods developed to address them. The development of these technniques, which has resulted in a highly automated system, has proven to be as interesting as the resulting data. It is hoped that future work in fracture flow and transport will benefit from the lessons learned in approaching these issues.

The physical system modeled in this project is the intersection of four fractures. Water enters through two of the fractures and exits through the other two. If the inflow fractures are adjacent to each other, the situation is analogous to the intersection of two one-way streets. In all cases of interest here, the flow is laminar. For the sake of simplicity, the fractures meet at right angles and the fracture apertures (widths) are equal. In addition, the fracture walls are smooth and impermeable.

When a solute molecule enters the junction, it has the option of leaving through either of two fractures. In high Peclet number situations, where advective transport is more significant than diffusive transport, the solute will follow the path of the water. This is known as streamline routing, and it is a simple process to model and predict. In very low Peclet number situations, where diffusive transport dominates, the solute will migrate between streamtubes. If the flow rates are equal in the two outflow fractures, the solute will be equally likely to leave through either of them. This condition is known as complete mixing, and it is also fairly simple. Of interest here is the transition zone between these two states, where the influences of advection and diffusion are approximately equal. In this zone, mixing behavior is much more difficult to predict.

In order to observe the zones of transition and complete mixing, the experimental apparatus must produce flow conditions in which the Peclet number is near one. Since the Peclet number is defined as the ratio of advective to diffusive influence, this means that the advective term (average velocity * fracture aperture) must be approximately equal to the diffusion coefficient. For a typical diffusion coefficient of 2e-5 cm^2 / sec, both the fracture aperture and the velocity must be extremely small. The experiments utilize a fracture aperture of 0.5mm and a velocity in the neighborhood of four microns per second.

In order to achieve such a small velocity, the experiments were initially conducted using a pair of high-precision, low volume syringe pumps. One pump was connected to each inflow fracture. At the two outflow fractures, the flow rates were found by measuring the pressure drops across fixed lengths of tubing. Needle valves controlled the flow in the outlets. Since adjusting the valve on one outflow fracture affected the flow rates in both fractures, adjusting the outflow rates was a tedious process.

A variety of ideas for improvement came from experience with this apparatus. For subsequent work, the setup was redesigned and automated. In addition, allowance was made for visually observing and photographing the fracture junction using a microscope.

The pumps and needle valves were replaced with a single push-pull pump that uses four syringes. A single mechanism simultaneously pushes two syringes and pulls two others, ensuring

that the flow rates in all four fractures maintain a known and consistent relationship. The pump is small enough to fit inside a temperature-controlled box with the fracture model, making temperature control simpler and more reliable.

The pump is controlled by an external computer. Two valves for routing flow, along with a set of thermistors and pressure transducers, are also operated by the computer. Using this equipment, a control system was developed to operate the experiments and to monitor temperature and pressure. This control system automatically runs through a preplanned sequence of Peclet numbers. When necessary, it refills the pump from reservoirs contained within the temperature-controlled box.

Sampling of the outflow is accomplished by an inline detection system. Flow from each outflow fracture is routed through a multicell UV-visible spectrophotometer, then back to the pump. In addition to the flow-through cells, the spectrophotometer also holds several cells with fixed concentrations for calibration.

Analysis of the absorption spectra is a two step process. First, initial guesses at the tracer concentrations are made by integrating the spectrum over relevant wavelengths. Next, an optimization routine compares predicted absorption spectra to observed spectra. This routine determines the concentration values that most closely match the observed spectra.

The concentration data are then combined with temperature and flow rate data to determine the Peclet number at the time of each measurement. The mixing behavior as a function of Peclet number can then be determined.

Session P5:
MODELING APPROACHES FOR FLOW AND CHEMICAL TRANSPORT IN FRACTURED ROCKS

Prediction of Fracture Slip and Associated Permeability Changes in a Geologic Repository for Nuclear Waste.

P.A. Berge
Lawrence Livermore National Laboratory
PO Box 808, Livermore, CA 94551
berge1@llnl.gov

S.C. Blair
Lawrence Livermore National Laboratory
PO Box 808, Livermore, CA 94551
blair5@llnl.gov

H.F. Wang
University of Wisconsin
Madison, Wisconsin, 53706
wang@geology.wisc.edu

Deep geologic disposal is thought to be a safe method for permanent disposal of high-level nuclear waste now stored at surface sites throughout the country. Dr. Paul Witherspoon was one of the first to recognize the importance of finding and developing a suitable site for a repository and has been actively involved in the U. S. and other nuclear waste disposal programs for many years. His early work on fracture flow forms part of the basis for thermohydrologic modeling of repository performance, and many of his former students have made, and continue to make major contributions to the Yucca Mountain Site Characterization Project (YMP), which is currently investigating development of Yucca Mountain, Nevada as a viable repository site. Over the past few years Paul has directly influenced the nature and direction of the repository program by serving as chair of the YMP thermohydrologic peer review committee, and as a member of the YMP performance assessment peer review committee.

It is well known that the rock mass forming the potential repository horizon at Yucca Mountain is a fractured, densely welded, ash-flow tuff, and the *in situ* permeability of the rock mass is dominated by the fractures. In his role as external reviewer Paul has championed the inclusion of thermomechanical (TM) behavior of fractures in the thermohydrologic (TH) and performance assessment (PA) simulations of repository systems. In this paper we present the results of two numerical modeling studies we have performed to predict how TM behavior of fractures may change the permeability of the host rock in a nuclear waste repository.

We have examined two geometries and heating loads that are of interest to YMP. In these analyses, change in permeability is assumed to occur in regions where slip occurs on fractures. This is based on the work of Barton et al. (1997) who have recently presented convincing evidence that hydraulically conductive fractures in the Dixie Valley geothermal field are critically stressed potentially active normal faults, based on the Mohr–Coulomb frictional slip criterion. Their work is significant because it implies that the occurrence of slip on the critically stressed fractures causes increased permeability. Thus, Barton et al. have provided a method for introduction of T-M effects into T-H analysis through alteration of permeability.

For our modeling, we used 2-dimensional (2-D) and 3-dimensional (3-D) versions of the finite-difference code FLAC (Fast Lagrangian Analysis of Continua) (Itasca Consulting Group Inc. 1996; Itasca Consulting Group Inc. 1997) to compute changes in stress and displacement in an elastic model subjected to temperature changes over time. All simulations have weak coupling of TH to TM behavior, in the sense that a temperature field is calculated using the NUFT thermohydrological code (Nitao 1993). The temperature field is then used to calculate TM stress

and displacement fields. We then estimated how and where the stress changes could affect permeability by evaluating regions where fracture slip may occur.

2-D Analysis of Drift Scale Test.

The first analysis is for the Drift Scale Test, which was started December 3, 1997 in Alcove 5 of the Exploratory Studies Facility (ESF) at Yucca Mountain (Peters et al. 1998). This is a large scale test in which a series of canister and "wing" heaters are being used to heat a 60 m long drift and surrounding rock in order to form a planar boiling region approximately 30 m wide and 70 m long in the potential repository horizon at Yucca Mountain. We simulated the first four years of heating for a 2 dimensional cross-section of the DST (Wang et al. 1998).

In broad terms three fracture sets have been identified in the ESF: set #1 is a steeply dipping set of fractures striking EW, set #2 is a steeply dipping set of fractures striking NS, and set #3 is a subhorizontal set of fractures striking EW (Albin et al. 1997). The axis of the heated drift is oriented EW; hence set #1(EW) and set #3 (subhorizontal) have their strike perpendicular to the plane of this 2-D model. Thus, calculations of shear slip for vertical and horizontal fractures correspond to slip on fractures in set #1 and set #3, respectively.

To estimate regions of increased permeability for the DST we assume that permeability will double at any location where slip on fractures is predicted to occur (Wang et al. 1998). This assumption is based on combining the standard parallel plate relationship between flow in a fracture and the fracture aperture, with the fracture aperture distribution model of Brown (1995; 1997). We also assume that slip on one set of fractures does not interfere with slip on any other set, and that changes in permeability predicted for one set of fractures can be added linearly to changes in permeability predicted for the other sets. Thus, if a zone of enhanced permeability predicted for slip along a vertical set of fractures overlaps a zone of enhanced permeability predicted for a set of horizontal fractures, we predict a total permeability enhancement of 4 times for the overlapping region. This is a conservative estimate as work by Ouyang (Ouyang and Elsworth 1993), and others has shown that slip along a fracture may increase fracture permeability by more than an order of magnitude.

For the vertical fracture set our results show that the zone of enhanced permeability predicted to occur after one-half year of heating (i.e., heating to a temperature of ~100°C at the drift wall) consists of two large wedge-shaped regions, one above and the other below the plane of the wing heaters that are deployed in the test. These areas are illustrated in Figure 1 using the light shading, and are essentially symmetric about the horizontal wing heater plane. The scale of these regions is on the order of the separation of the heated drift and the observation drift, and the width is on the order of half the drift separation (i.e., 13.5 m).

Regions of changed permeability for horizontal fractures occur between the wing heater plane and the observation drift, and are centered at a distance about four meters above and below the plane of the wing heaters. Permeability is predicted to be enhanced by a minimum of 4 times in zones which occur where both fracture sets are expected to slip. These zones are also symmetric above and below the wing heater plane and comprise approximately one-fourth of the total area of permeability enhancement.

We also predict that zones of enhanced permeability will grow with time, while maintaining the same basic shape formed after 0.5 year of heating. Zones of enhanced permeability may recede outward from the heaters as heating continues. This is due to rotation of the stress field associated with the geometry of the heaters and the thermal gradients that are introduced by the heating. Comparison with stress plots shows that the permeability is enhanced in areas of high thermal gradients as is expected from the formulation, because such areas have high stress gradients.

3-D Analysis of Drifts with 50 yr. of Heating.

For the 3-D study (Berge et al. 1998), we simulated three drifts in a potential repository after 50 years of heating. These drifts were centered at a depth of 385 m in a model extending from 337 m depth to 431.8 m depth; because the problem is symmetrical, only 1.5 drifts are actually modeled, and the plane at X=0.0 is a symmetry plane. The model, which has 3240 zones, represents the drifts and two tuff units, geological units Tptpll (TH unit tsw36, TM unit TSw2) and Tptpmn (TH unit tsw35, TM unit Tsw2).

We began with the model at thermal and mechanical equilibrium and then ran FLAC3D (Itasca Consulting Group Inc. 1997) to compute stress and displacement changes resulting from temperature changes appropriate for 50 yr. of heating. The temperature field was computed using the NUFT code. The maximum temperature was about 420°K (147°C) in the center of a drift.

After 50 yr. of heating, the stress field rotated in the heater region so that the principal stress directions exhibited a lot of lateral heterogeneity between drifts and below the heaters. The asymmetrical temperature field with large temperature gradients above the heaters produced an asymmetrical stress field with large stress gradients above the heaters, and all the stresses have increased significantly up to 20 MPa, compared to the initial values near 5 to 10 MPa in compression before heating. The horizontal stresses increased to about 15 to 20 MPa in compression near the bottom of the model.

High shear stresses of about 5 MPa were found in the vertical plane midway between the drifts and the horizontal plane containing the drifts. Note that in a previous 2D simulation shear stresses in these directions were not computed because the shear stresses are found in planes perpendicular to the plane for the 2D model. The displacement had a magnitude of several cm in the middle of the model, increasing near the top. Most (5 to 7 cm) of the displacement was in the vertical direction. Horizontal displacements were 1 to 2 cm for most of the model.

Estimates of permeability changes were obtained by analyzing stresses, following a method we developed previously for 2-D models. The results show consistently that fracture set #2 is likely to exhibit slip due to thermal stresses, in many parts of the model, and fracture set #1 may have slip in regions just above the drifts, but fracture set #3 is unlikely to have any thermally induced slip. Therefore, we conclude that widespread permeability enhancement of about a factor of two is likely for fractures parallel to fracture set #2, the vertical fractures that strike north-south, for regions above the drifts. In some regions just above the drifts, permeability may increase by a factor of four if slip also occurs along the vertical fractures in set #1, the east-west fractures. Note that slip on fracture set #2 could not be modeled in the previous 2D FLAC modeling because these fractures lie in the plane of the 2D FLAC model rather than intersecting that plane.

References:

Albin, A.L., Singleton, W.L., Moyer, T.C., Lee, A.C., Lung, R.C., Eatman, G.L.W., and Barr, D.L. 1997. *Geology of the Main Drift—Station 28+00 to 55+00, Exploratory Studies Facility. Yucca Mountain Project, Yucca Mountain, Nevada.* Denver, Colorado: Bureau of Reclamation and U.S. Geological Survey. MOL.19970625.0096.

Barton, C.A., Hickman, S., Morin, R., Zoback, M.D., Finkbeiner, T., Sass, J., and Benoit, D. 1997. "Fracture permeability and its relationship to in-situ stress in the Dixie Valley, Nevada, Geothermal Reservoir." In proceedings from *Twenty-Second Workshop on Geothermal Reservoir Engineering.* Stanford University, Stanford, California: January 27–29, 1997. MOL.19980710.0823.

Berge, P.A., Wang, H.F., and Blair, S.C. 1998. *Estimated Bounds on Rock Permeability Changes from THM Processes.* UCRL-ID-131492; SPLL35M4; BA0000000-01717-5700-00005. Livermore, California: Lawrence Livermore National Laboratory.

Brown, S.R. 1995. "Simple mathematical model of a rough fracture." *J. Geophys. Res.* **100**:5941–5952. 222415.

Brown, S.R., and Bruhn, R.L. 1997. *Fluid Permeability of Deformable Fracture Networks.* SAND97-0159. Albuquerque, New Mexico: Sandia National Laboratories. MOL.19980514.0045.

Itasca Consulting Group Inc. 1996. *FLAC, Fast Lagrangian Analysis of Continua, Version 3.3, Vol. I–IV, User's Manuals.* Minneapolis, Minnesota: Itasca Consulting Group, Inc.

Itasca Consulting Group Inc. 1997. *FLAC^{3D}: Fast Lagrangian Analysis of Continua, Version 2.0, Vol. I-IV, User's Manuals.* Minneapolis, Minnesota: Itasca Consulting Group, Inc.

Nitao, J.J. 1993. "The NUFT Code for modeling nonisothermal, multiphase, multicomponent flow and transport in porous media." *EOS, Trans. Am. Geophys. Union, Fall Meeting Supplement* **74**(43):313–314. (Also UCRL-JC-114769-ABS, Lawrence Livermore National Laboratory, Livermore, California)

Ouyang, Z., and Elsworth, D. 1993. "Evaluation of groundwater flow into mined panels." *International Journal of Rock Mechanics and Mining Science & Geomechanics Abstracts* **30**(2):

Peters, M.T., Boyle, W.J., Datta, R.N., Elkins, N.Z., Yasek, R.N., Wagner, R.A., and Weaver, D.J. 1998. "The Drift Scale Heater Test at Yucca Mountain, Nevada." *Proceedings of the Eighth International Conference on High-Level Radioactive Waste Management Conference.* La Grange Park, Illinois: American Nuclear Society.

Wang, H.F., Blair, S.C., and Berge, P.A. 1998. "Estimating Changes in Rock Permeability Due to Thermal-Mechanical Effects." *Proceedings of the Eighth International Conference on High-Level Radioactive Waste Management Conference.* La Grange Park, Illinois: American Nuclear Society.

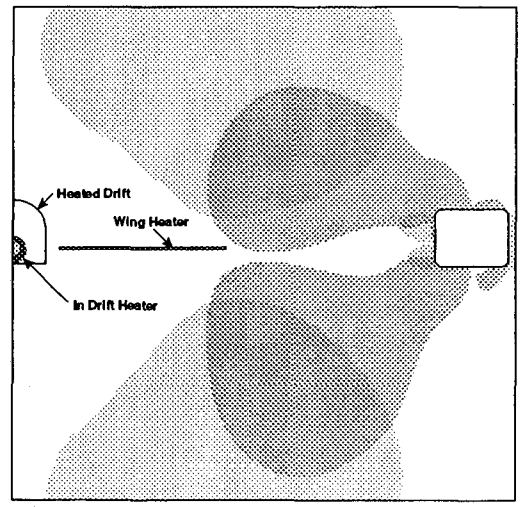

Figure 1. Zones of enhanced permeability after 0.5 years of heating in the Drift Scale Test. Drift wall is aproximately 100 °C.

PREDICTING LARGE SCALE EFFECTIVE HYDRAULIC CONDUCTIVITY FROM LOCAL MEASUREMENTS: A PERCOLATION APPROACH

Jordi Guimerà (1) and Miguel Ortuño (2)

(1) jguimera@quantisci.es

QuantiSci, S.L. PTV, 08190 Cerdanyola, Barcelona, Spain

(2) moo@fcu.um.es

Departamento de Física, Universidad de Murcia, 30071-Murcia, Spain

1. Introduction

Upscaling of hydraulic conductivity has been reported notably by Clauser [1992] among several authors (Kiraly,1975; Desbarats, 1987; Dagan, 1989; Neumann, 1990). Like electrical conductivity in disordered media, hydraulic conductivity tends to display a widespread range of local values in heterogeneous formations. The most commonly accepted ways to calculate effective values from local measurements depend on dimensionality. Matheron [1967] obtained that the effective conductivity falls between the arithmetic and the harmonic mean in one dimensional flow, while in 2D flow domains, the effective K is associated to the geometric mean (K_g). For statistically homogeneous 3D domains, Gutjahr et al. [1978] proposed to use the expression:

$$K_{eff} = K_g\ [1+ (1/2 - 1/n)\sigma^2] \qquad (1)$$

where σ^2 is the variance of ln-K. For large σ^2 values, Gelhar and Axness [1983] proposed to consider (1) as the first two terms of an exponential expansion. Then, instead of (1) they proposed to use:

$$K_{eff} = K_g \exp[\ (1/2 - 1/n)\sigma^2] \qquad (2)$$

A number of approaches to upscaling -defining block conductivities from point values- are available (see Sánchez-Vila et al., 1995, for a revision). Next we propose to use a percolation approach to assess the effective hydraulic conductivity of heterogeneous media. Applications of this approach are presented for field data from test sites and consequently discussed.

2. Model of site percolation for hydraulic conductivity

Let us assume a number of local measurements of hydraulic conductivity which display a large range of variability and correspond to a given length scale L. We also assume that these measurements are highly independent of each other; otherwise, a larger length scale should be considered so that correlations become negligible. We want a procedure to obtain the effective large scale conductivity from this set of local measurements.

Let us consider that our large scale sample can be divided into small blocks of a linear size L. These blocks expand over the whole sample and we assume that they are periodically arranged, so that they form a lattice. For example, in 2D we can consider squares arranged in a square lattice or hexagons in a triangle lattice. The flow will go through a path formed by high conductivity blocks, and K_{eff} will be determined by the less conductive block of this path. Percolation is the best tool to solve the difficult problem of finding this path. First, let us choose a value K' relatively high and let us consider the most conductive blocks, with $K>K'$, as occupied sites and try to see whether they constitute a site percolation path through the sample. Blocks with $K<K'$ are considered vacant. If the percentage of occupied blocks is small, they will not constitute a percolation path. The next step lowers K', and again considers as occupied sites the blocks with $K>K'$. We continue this procedure up to the moment that a percolation path across the sample is found. If our sample is very large, this will occur when the occupation probability is equal to the critical one (p_c) for site percolation of the corresponding lattice. Thus, the effective conductivity (K_{ef}) is implicitly given by the expression:

$$p_c = \int_{Kef}^{Kmax} p(K)\, dK \qquad (3)$$

where K_{max} is the maximum possible value of K (that can be equal to ∞) and $p(K)$ is the probability density of K. As the conductivity of the blocks not considered is usually much smaller than those of the blocks considered, due to the large distribution of K values, their contribution to the effective hydraulic conductivity is very small. The effective conductivity of the sample, will be dominated by the blocks of lowest K in the percolation path.

From the practical standpoint, it remains to assign a value to p_c, since it depends on the type of lattice considered. Real samples will be constituted by irregular blocks of irregular size. So, it is not clear which is the best lattice to be considered for each dimensionality. For 2D, we will assume $p_c = 0.5$, while slightly higher than 0.2 is assumed for 3D (see Sahimi, 1995 for further details).

According to this approach, the best estimate of the effective conductivity from a set of local measurements is to choose the value of the conductivity for which ~ 50% of the measurements, in 2D, and ~ 20% of the measurements, in 3D, are more conducting. This is the procedure that we will use in the next section

3. Application to field data

Figure 1 summarizes the results for the El Berrocal site (Guimerà et al., 1995). Dots in the smallest scale (0.1 m) represent the median of a set of measurements made in each borehole with a single packer spacing. Median values at each scale suggest that scale effects are indeed present. Besides, using equation (1), a log K_{eff} of -8.7 would have been obtained, smaller than those obtained by cross-hole tests at the site scale.The continuous line links values of K_g at each scale and the dotted line, values of K_{eff} obtained using equation 2. The dotted fringe in Figure 1 represents the log K_{eff} values obtained by the model based on percolation theory. It barely displays any trend across the four orders of magnitude over which the measurements extend. Furthermore, if the values of the scale of

meters were more representative, the effective value at all scales would remain invariant. Thus, predicting log K at large scale from local measurements is achieved rather accurately, less than half an order of magnitude of difference. The only remaining point is that concerning the effective value at the scale of meters. We attribute the anomalous result to the lack of more precise data.

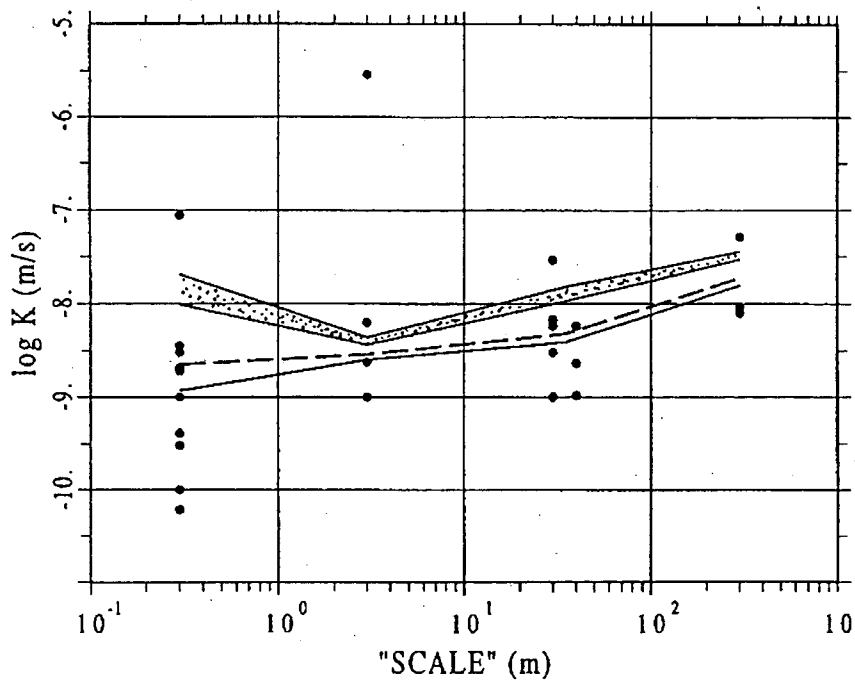

Figure 1. Values of hydraulic conductivity obtained at El Berrocal site. Values are considered to be representative of the order of magnitude to which they belong. The dotted fringe are the values of effective hydraulic conductivity obtained by the percolation model. The upper and lower bounds correspond to results of percolation thresholds = 0.2 and 0.3 respectively.

4. Conclusions

A site percolation model is presented to average local values of hydraulic conductivity either in 2D or 3D domains. The methodology is applicable to any set of K values that presents large variability - over several orders of magnitude - and when the measurements are not or roughly not correlated. The main application of the model is a new averaging method of values obtained at a given scale that is able to predict the effective value at a greater scale. It has been shown that the effective value obtained by using the results of pulse tests, considered to be representative of a scale of linear size of 0.1 m, fairly match the values obtained by regional models or regional estimates. For a proper application of this method, it is compulsory that measurements at local scale - single hole tests - account for all possible ranges of hydraulic conductivity values. It turned out that while distribution of hydraulic conductivity values suggested that scale effects were present at a given site, the effective value at each scale of measurement remains almost invariant, and size effects can be neglected.

Acknowledgements
El Berrocal project was funded by ENRESA. Part of the work performed by the first author was carried out in the Technical University of Catalonia at Barcelona (UPC).

References

Clauser, C., Permeability of crystalline rocks. *EOS*, May 26, 233-238, 1992.

Dagan, G., *Flow and transport in Porous Formations,* Springer-Verlag, Berlin, 1989.

Desbarats, A.J., Numerical estimation of effective permeability in sand-shale formations. *Water Resour. Res.*, 23(2)273-286, 1987.

Gelhar, L.W. and C.L. Axness, Three-dimensional stochastic analysis of macrodispersion in aquifers. *Water Resour. Res.*, 19(1), 161-180, 1983.

Guimerà, J., L. Vives and J. Carrera, A discussion of scale effects on hydraulic conductivity at a granitic site (El Berrocal, Spain), *Geophys. Res. Lett.* 22 (11) 1449-1452, 1995.

Gutjahr, A.L., L.W. Gelhar, A.A. Bakr and J.R. McMillan, Stochastic analysis of spatial variability in subsurface flow 2: Evaluation and application. *Water Resour. Res.,* 14(5) 953-959, 1978.

Kiraly, L., Rapport sur l'état actuel des connaisances dans le domaine des caractères physiques des roches karstiques. in Burgu and Dubertret (eds) Hydrogeology of karstic terrains: France, IAH Int. Contrib. to Hydrogeology, 2, 53-68, 1975.

Neuman, S.P., Universal scalling of hydraulic conductivities and dispersivities in geologic media, *Water Resour. Res., 26*(8), 1749-1758, 1990.

Sahimi, M., *Flow and transport in porous media and fractured rock,* VCH, Weinheim. 482 p., 1995.

Sánchez-Vila, X., J.P. Girardi and J. Carrera. A synthesis of approaches to upscaling of hydraulic conductivities. *Water Resour. Res.,* 31(4), 867-882, 1995.

Numerical Investigation of the Asymptotic Behavior of Unsteady Groundwater Flows with Capillary Absorption and Forced Drainage

Eugene A. Ingerman and Helen Shvets
Department of Mathematics and Lawrence Berkeley Laboratory
University of California at Berkeley
Berkeley, CA 94720-3840
Telephone: (510) 486-2142
E-mail: eugening@math.berkeley.edu shvets@math.berkeley.edu

We consider a model for a short, but intense, flooding followed by natural outflow through a wall in an aquifer. The aquifer consists of a long porous stratum bounded below by an impermeable bed and on one side by a vertical wall. The space coordinate x is directed along horizontal axis with $x = 0$ at the vertical wall. In the region $x < 0$ we have a water reservoir, so that water drains freely from the aquifer at the wall. We assume that the flow is homogenous in the y-direction and treat the problem as 2-dimensional. Initially, the stratum is assumed to be empty. At some time $t=-\tau<0$, the water level at the wall begins to rise, and water enters the porous medium. The height of the mound is denoted by $z = h(x, t)$. By the time $t=0$ water level at $x=0$ returns to normal and water mound with a certain height distribution $z = h(x, 0)$ appears in the stratum. We assume that the initial distribution is concentrated over the region $[0, \varepsilon]$ (compactly supported). We also assume, for the sake of simplicity, that $h(x,0)$ is concave down. At $x=0$ water can drain freely into the reservoir, so the boundary condition $h(0, t)=0$ is assumed (Fig.1). The position of the mound tip is denoted by $x_r(t)$ and it should be determined as a part of the problem.

In the absence of capillary retention, this model is described by the Boussinesq equation [1]:

$$\partial_t h = \kappa\, \partial^2_{xx} h^2 \qquad (1)$$

Here $\kappa = k\rho g/(2m\mu)$, k is the permeability of the medium, m--its porosity, ρ--the fluid density, μ--its dynamic viscosity, and g -- the gravitational acceleration. The following initial and boundary conditions supplement the equation:

$$h(x,0)=h_0(x) \qquad (2)$$
$$h(0,t)=0 \qquad (3)$$
$$h(x_r, t)=0;\ \partial_x h^2(x_r,t)=0 \text{ (free boundary condition);} \qquad (4)$$

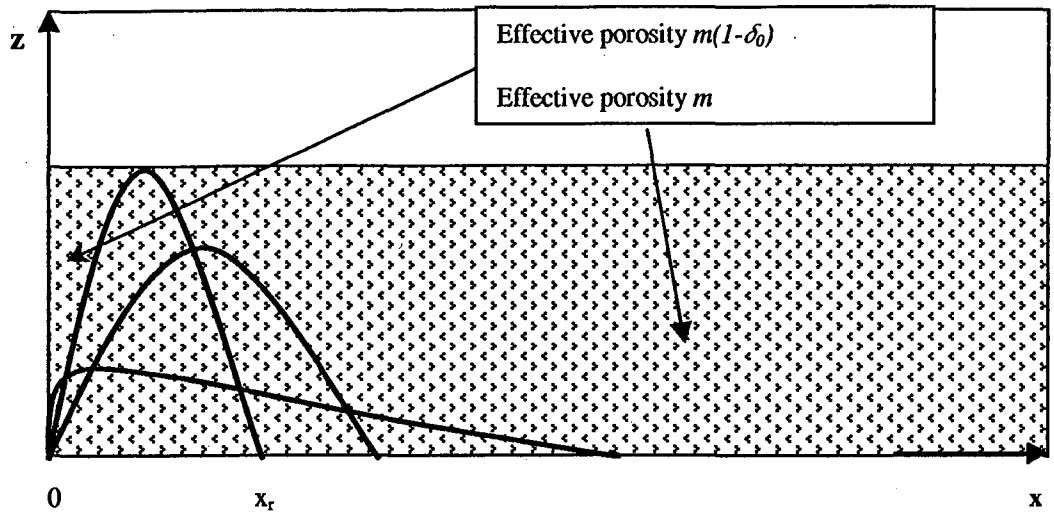

Figure 1.

To incorporate the effects of capillary retention, variable effective porosity is introduced. It is set equal to m, when water is entering a previously unfilled region ($\partial_t h > 0$), and $m(1-\delta)$, for regions that were previously filled with water ($\partial_t h < 0$). This modification leads to the generalized porous medium equation:

$$\partial_t h = \kappa\, \partial^2_{xx} h^2 \text{ ,where } \kappa = \begin{cases} \kappa_1 \text{ if } (\partial_t h > 0), \\ \kappa_2 \text{ if } (\partial_t h < 0); \end{cases} \tag{5}$$

For a rigorous analysis of this problem see [2]. In the case of $\kappa_1 = \kappa_2$, the dipole moment is conserved and on the basis of dimensional analysis a self-similar solution can be obtained, which has the form:

$$h(x, t) = (Q/\kappa t)^{1/2}\, \Phi(\xi), \quad \Phi(\xi) = \frac{\sqrt{5}}{3}\xi^{1/2}(1-\xi^{3/2}) \qquad \xi = x/x_r \tag{6}$$

Here Q is the conserved dipole moment:

$$Q = \int_0^\infty x h(x,t)\,dx = const \tag{7}$$

The solution above is a special exact solution, which corresponds to an idealized dipole initial condition. However, it is not merely a special solution, but is an intermediate asymptotics for a wide range of initial value problems.

In the case of retention, the dipole moment (7) is no longer conserved. This precludes the existence of a self-similar solution of the first kind (a solution which can be determined on the basis of dimensional analysis alone), which exists in the case of Boussinesq equation with boundary and initial conditions (2-4). It turns out that for $\kappa_1 \neq \kappa_2$, the initial width of the distribution cannot be excluded from the list of governing parameters, as it is done in the derivation of self-similar solution (6) (see [2]). However, a special self-

similar solution below, which is an asymptotics for a class of initial conditions that we consider, does exist for this problem. On the basis of dimensional analysis, we expect this solution to have the form:

$$h(x, t) = A\ t^{-\alpha} f(\xi; \kappa_1/\kappa_2),\ x_r=(B\ t^{\beta}),\quad \xi = x/x_r \tag{8}$$

With this in mind, we solve the problem (2-5) numerically for a range of values of (κ_1/κ_2). After scaling $\xi=x/x_r$, and $u(x,t)=h(x,t)/h_{max}(t)$ (where $h_{max}(t)= max_x\ h(x,t)$), we observe that after some initial time, the solutions for later times collapse into a single curve. This confirms the existence of a self-similar intermediate asymptotic solution. As a part of the solution we compute $x_r(t)$ and $h_{max}(t)$. Plotting $log\ (x_r(t))$ and $log\ h_{max}(t)$ against $log\ t$ (Fig 2.), we observe that the plots eventually become straight lines, i.e. $log\ x_r(t)=\beta \cdot log\ t + C_1$, and $log\ h_{max}(t)= \alpha\ log(t)+C_2$. From the plot (Fig.3) we determine the values for β and α.

If we substitute (8) into partial differential equation (5), we obtain an ordinary differential equation:

$$\alpha f+\beta f'\xi+\kappa(A/B^2)\,(f^2)''\,t^{1-\alpha-2\beta}= 0 \tag{9}$$

$$\kappa = \begin{cases} \kappa_1 \text{ if } \alpha f + \beta\xi f < 0 \\ \kappa_2 \text{ if } \alpha f + \beta\xi f > 0 \end{cases}$$

Where $1-\alpha-2\beta= 0$, because (9) cannot be time dependent. For the boundary conditions we have:

$$f(0)=0;\ f(1)=0;\ f'(1)= -\beta/(2\kappa_i);$$

Here, we set $A/B^2=1$, which is possible because we can scale f, and use the fact that $x_r=B\ t^{\beta}$, to set the boundary at $\xi=1$. We thus obtain a non-linear eigenvalue problem, which we proceed to solve numerically. This gives a dependence of β on κ_1/κ_2. As is evident from (Fig. 2), the values of β coincide remarkably well with the values obtained from the numerical solution to the partial differential equation. Thus, we have found an intermediate asymptotic solution for the dipole-type problem considered in the case of groundwater flow with capillary absorption.

Next, we extend the problem to include forced drainage. This model was first proposed in (2), where a rigorous analytical treatment can be found. We study the problem numerically, following an approach similar to the one presented above.

References:

1. J. Bear, *Dynamics of Fluids in Porous Media.* Dover, New York, 1972.
2. G.I. Barenblatt, J.L. Vazquez, *A new free boundary problem for unsteady flows in porous media,* Euro. Jnl of Applied Mathematics (1998), vol. 9, pp. 37-54.
3. G.I. Barenblatt, V.M. Entov, V.M. Ryzhik, *Theory of fluid flows through natural rocks,* first ed., Kluwer Academic Publishers, Dordrecht, 1990.

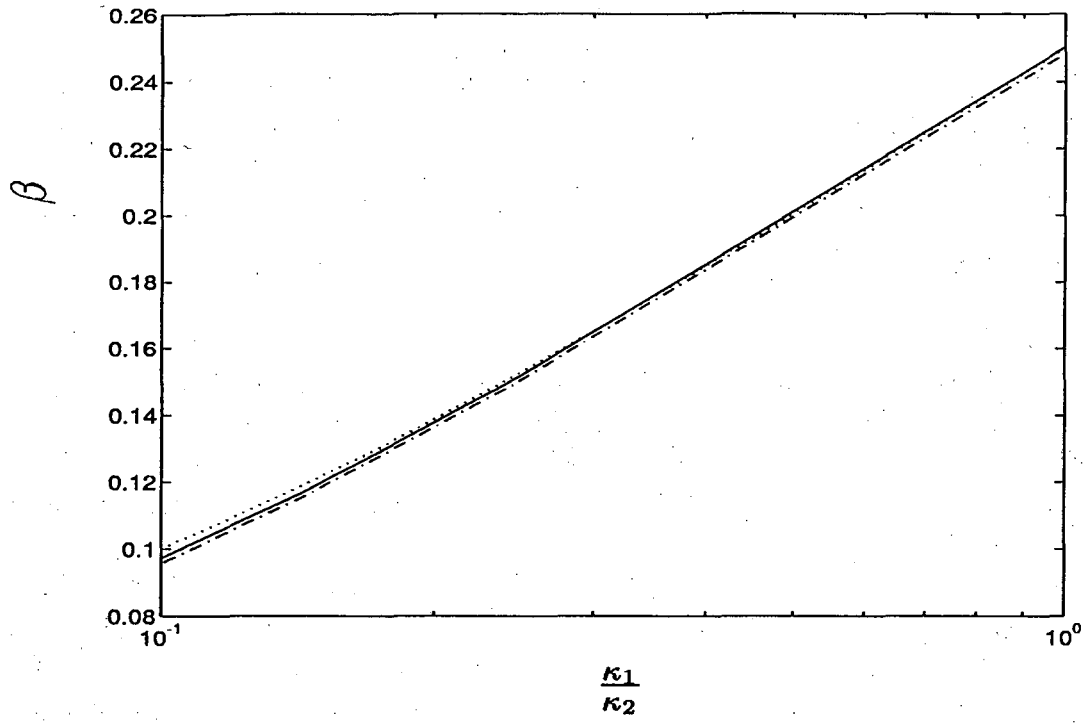

Figure 2. Dependence of β on (κ_1/κ_2)
Solid line – time evolution of x_r, dashed line – time evolution of h_{max}, both obtained from the solution of partial differential equation. Dotted line - β obtained from the ordinary differential equation.

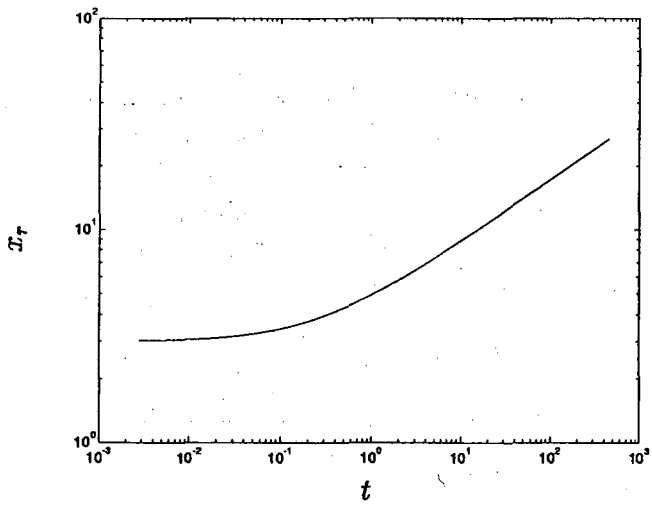

Figure 3. Time evolution of x_r.
(κ_1/κ_2=1/2)

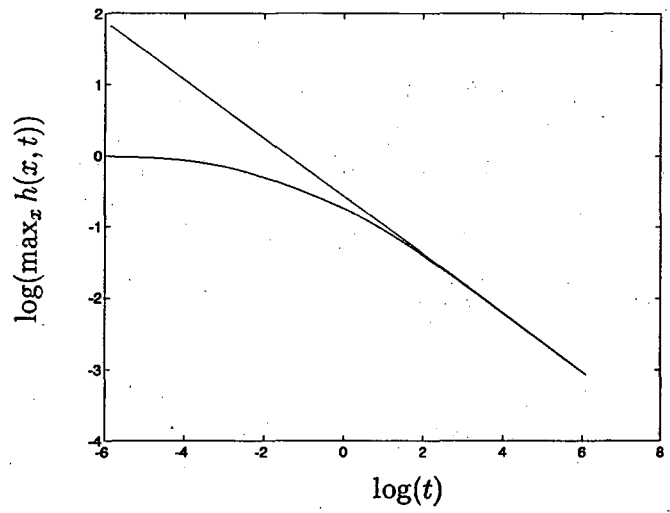

Figure 4.
Plot $log(max_x(h(x,t)))$ vs $log(t)$
(κ_1/κ_2=1/2)

Modeling Mass Transport Through Fractured Media Using the Statistical Continuum Method in Two and Three Dimensions

B. Parney and L. Smith. Department of Earth and Ocean Sciences, University of British Columbia. 6339, Stores Road, Vancouver B.C., Canada. V6T 1Z4.

Introduction

The statistical continuum method (SCM) provides a technique to model aqueous phase transport through a fractured rock mass at the field scale, while explicitly including the effects on transport of fracturing that is observed on the scale of a borehole or outcrop. The SCM approach models mass transport in two stages: (1) particles are tracked through a subdomain consisting of multiple discrete networks in order to capture the range of motion possible within a fracture system; and (2) particles are then moved in a random-walk through a larger continuum, obeying the range of motion "learned" within the subdomain. The use of discrete networks allows particle movements in the SCM continuum to honor the particle motion that occurs in the discrete subdomain, without the fundamental changes in the nature of the transport process necessary in most continuum approximations. The use of the continuum permits these movements to be extended into domains significantly larger or more complex than those that can be modeled by conventional discrete network simulations. The key element in the SCM method is the determination of the most appropriate methods for translating the motion of particles in the discrete subdomain into a set of statistical distributions that are then sampled in the continuum.

The SCM method in two dimensions

In the discrete subdomain, multiple network realizations are constructed from a set of parameters defining the fracture system within the region of interest. For each realization, the steady state flow field is calculated, and particles are moved by advection through the network. Fracture - matrix interactions have been neglected during this stage of concept development. The distance a particle travels between entering and exiting a fracture is referred to as the path-length. Each time a particle leaves a fracture the path-length, particle velocity, fracture set and orientation of the fracture are recorded. The mean, variance and skew are calculated for the length, velocity and orientation of the particle movements, and these parameters are sorted according to the direction of travel within each fracture set. Additional statistics calculated include the frequency of travel in each direction and the correlation coefficient between velocities of adjacent steps.

In the continuum domain, each step taken by a particle is generated by randomly sampling motion statistics calculated within the subdomain. Numerous models for statistical distributions used in the continuum have been tested, and several types of correlations have been applied including (1) histograms of velocity and path-length (2) Gaussian and Gamma distributions of velocity and path-length (3) correlation of velocities between adjacent steps and (4) correlation of the distance a particle travels in a single step to the velocity of travel.

To evaluate the effectiveness of the SCM approach, comparisons are made between

mass transport in a SCM model, and mass transport in an equivalent discrete network model. Mass transport through the discrete networks is measured by calculating spatial moments of particle distributions, and then averaging these moments over thousands of network realizations. The standard deviation of the moments for the network realizations is also calculated to quantify the range of moment values that occur between networks. Because the fracture network at a field site is equivalent to a single realization from a fracture system, the variability of the moments between realizations can be used to gauge how closely a moment obtained by averaging over multiple network realizations might relate to mass transfer at a field site. The discrete network model is based on the same fracture system used to generate the networks for the discrete subdomain, but the networks in the discrete subdomains are on the order of 10m x 10m, while the full-domain discrete networks used in model evaluation are on the order of 40m x 20m. The method has been tested for well-connected Poisson networks, Poisson networks near the percolation threshold, and a fracture system based on a fractal algorithm.

Solute transport, as described by the evolution of spatial moments through time, indicates that the SCM method is capable of reproducing mass movement through two-dimensional Poisson networks. The SCM approach in which both the path length and log of velocity are modeled with a three-parameter gamma distribution produces moment values closest to the average moments for the discrete network realizations. Most of the SCM statistical models that are tested produce moment values within one standard deviation of the average moments for the network realizations. Good performance has been observed for a wide range of fracture systems, although the three-parameter gamma model does not consistently produce the best results for all fracture systems.

SCM method in three dimensions

Particle movement in three-dimensional fracture networks requires an expansion of the motion statistics to capture the extended range of possible movement. In two dimensions a particle entering a fracture can travel in either direction, so that this motion is completely described by the direction chosen and the orientation of the fracture in the two-dimensional plane (θ). In order to capture particle motion in the third dimension, orientation statistics include an azimuthal angle (ϕ) in addition to the map-view angle (θ). Path-length in two dimensions is clearly defined as the distance between entry and exit points along a fracture. In three dimensions, particles may meander across fracture planes so that path-length is defined as the distance a particle travels between changes in direction, either within a fracture plane or upon leaving a fracture.

Particle tracking within the SCM continuum must also be expanded to include both the second directional angle and any additional correlation between motion statistics. As in the two dimensional modeling, the key element of the SCM method in three dimensions is the determination of the most appropriate method for translating the motion of particles in the discrete subdomain into a set of statistical distributions that are then sampled in the continuum. Several statistical distributions of velocity and path-length are tested, as are models including correlations between the velocity of travel and the path-length. SCM models including correlation of both velocity and path-length to ϕ are also examined.

Particle motion through discrete subdomains is generated using FRACMAN™ and MAFIC™, which have been modified to output all particle movements. Fractures are first generated using FRACMAN™, and then a finite element mesh is generated over the resulting fracture network. Prescribed head boundary conditions are chosen in order to apply a constant hydraulic gradient across the network. After a flow solution is calculated, particles are moved by advection from element to element within the mesh, at which point each of these motions is recorded. Unlike the two-dimensional model, in the discrete subdomain, it is not known a priori in which fracture set a particle is moving, or when a particle leaves a fracture. This necessitates an additional step in the subdomain model in which movements between elements are grouped into path-lengths, and assigned to fracture sets.

To evaluate the effectiveness of the SCM approach in three dimensions, the evolution of spatial moments through time for SCM models are compared with the evolution of moments through time for equivalent discrete network models. Fracture networks are created using four-sided, vertical fractures from two fracture sets, with differing mean strike and dip, and variation in both strike and dip within each fracture set. The aperture is constant across a single fracture plane, but varies from fracture to fracture.

The SCM method in three dimensions is capable of reproducing mass transport in three-dimensional discrete fracture networks, as evidenced by the match between the trends in spatial moments through time for the discrete network and the spatial moments for the SCM model. Results are similar to those in two-dimensions, as a number of SCM modeling approaches produce moment values within one standard deviation of the average of the network realizations, although no one model works best for all fracture systems.

GEOMETRICAL AND TRANSPORT PROPERTIES OF DISORDERED FRACTURE NETWORKS: ANALYTICAL RESULS

A. A. Rodríguez
PDVSA Intevep, S. A., Apartado. 76343, Caracas 1070A, Venezuela.
email address: adolfo@intevep.pdv.com
E. Medina
Centro de Física, Instituto Venezolano de Investigaciones Científicas, Apartado 21867, Caracas 1020A, Venezuela
email address: ernesto@ivic.ve

Abstract

We study the geometrical and transport properties of a 2D model[1] of disordered fracture networks which consists of a set of N lines located anywhere within a square region of area L^2. From the computational point of view, each line is represented by four numbers: a pair of numbers, (x,y), between 0 and L, which represent the coordinates of the center of the line, a number between 0 and π representing the orientation and a number l, between 0 and L, representing the length. For the purpose of the calculation of the transport properties, a fifth number s, representing the cross section of the fracture is needed. Figure 1 shows a typical system above the percolation threshold containing 2000 lines.

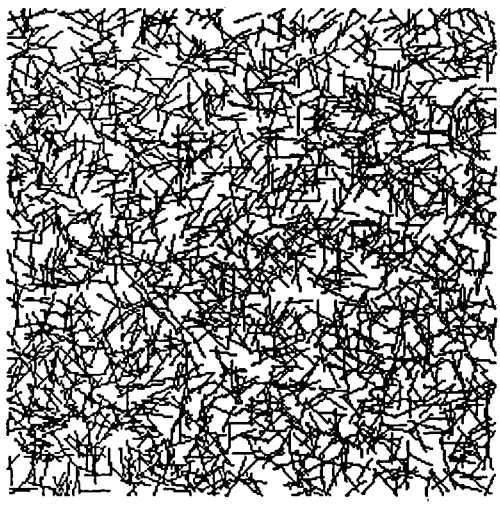

Figure 1. Typical two-dimensional system of 2000 lines with an areal density of $d=N/L^2=6$ (above the percolation threshold).

The transport properties of the fracture network described above, will depend on the distribution of local segment conductances G; $G = \sigma s/x$, where s is the cross section and x is the length of the segment, defined as the distance between two consecutive nodes over a given line, with the nodes defined as either the intersection between two lines or the end point of a line. We have shown that the distribution of segment lengths is given exactly by the following equation:

$$P(x)=\frac{(\rho l)^2}{(\rho l+1)l}e^{-\rho x}\left[1-\frac{x}{l}+2\rho l\right]+\frac{e^{-\rho l}}{(\rho l+1)}\delta(x-l) \tag{1}$$

Where the last term accounts for the isolated lines and $\rho = 2/\pi\, dl$ with $d=N/L^2$ the areal density of lines.

In figure 2 we show $P(x)/P(0)$ against x calculated numerically on systems of up to 500000 lines, the solid line represents the analytical estimate given by equation 1. The accuracy of the equation is very good in the whole range of segment lengths as it can be appreciated in the figure.

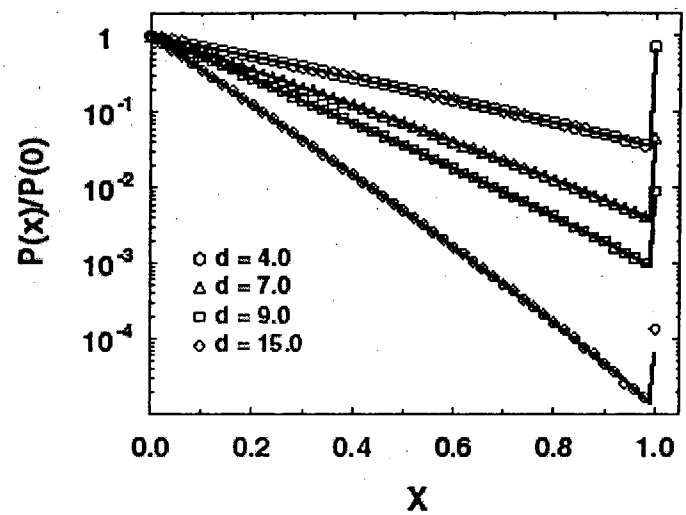

Figure 2. Comparison between the calculated distribution of segment lengths (symbols) and equation 2 (solid lines).

If only line intersections are taken as nodes, the distribution of segment lengths becomes:

$$P'(x)=\frac{(\rho l)^2}{\left(\rho l-1+e^{-\rho l}\right)}e^{-\rho x}\left[1-\frac{x}{l}\right]. \tag{2}$$

From this distribution of segment lengths it is possible to calculate the distribution of segment conductances according to the relation $|p(x)dx| = |p(g)dg|$. After straightforward calculations we find that, if both the line lengths and the cross sectional area are kept constant, the distribution of segment conductances is given by:

$$H(g)=\frac{(\rho l)}{\left(\rho l-1+e^{-\rho l}\right)}\frac{g}{g_0}\left(1-\frac{g_0}{g}\right)\exp\left(-\rho l\frac{g_0}{g}\right) \tag{3}$$

Here $g_0=\sigma s/l$, with σ a characteristic conductivity and s a typical fracture cross section.

Additionally we have shown that using a simple one-dimensional argument it is possible to approximate the average coordination number, z, through the following simple equation:

$$\bar{z} = 4\sum_{m=2}^{\infty} \frac{(\rho l)^2}{m!} e^{-\rho l} \frac{m-1}{m} = 4e^{-\rho l}\left[e^{\rho l} - 1 - Ei(\rho l) + ln(\rho l) + \gamma\right] \tag{4}$$

Where Ei(y) is the principal value of the Euler integral function and γ=0.577216.. This approximation is quite good for systems above the percolation threshold.

It is possible to map the network to a square lattice network with a probability occupation $p=z/z_{max}$, so that the effective conductance distribution is $P_{eff}(g)=pH(g)+(1-p)\delta(g)$. This final distribution can be used along Kirkpatrick's Effective Medium Theory[2] to obtain the macroscopic conductance of the network. In figure 3 we show the results obtained from effective medium theory (solid line) along with montecarlo calculations performed solving the exact equations (symbols). As it can be appreciated the approximation is quite good for high line densities.

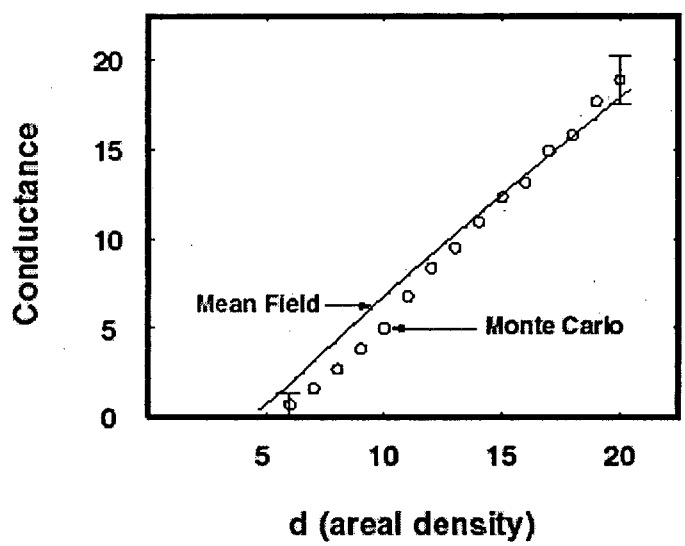

Figure 3. Comparison between the Mean Field approximation and the exact calculation of the effective conductivity of the system.

We have proven here that the macroscopic transport parameters of the fractured system can be satisfactorily estimated by using the Mean Field Theory. Also, the distribution of segment lengths seems to be the most important aspect in the simplified model presented here. The influence of the distribution of fracture lengths as well as cross sectional areas is under study at this time.

(1) Rodríguez, A.A. and E. Medina, Mod. Phys. Lett., **11**, 867, (1997)
(2) Kirkpatrick, S., Rev.Mod. Phys. **45**, 574 (1973).

Homogenization of Contaminant Transport in Fractured Porous Media

P. Royer, Laboratoire Sols, Solides, Structures, (UJF, INPG, CNRS), BP 53X, 38041 Grenoble cedex, France, Pascale.Royer@hmg.inpg.fr

C. Serres, Institut de Protection et de Sûreté Nucléaire, Département d'Evaluation de la Sûreté, BP 6 92265 Fontenay-aux-Roses, France, Christophe.Serres@ipsn.fr

1 Introduction

In the scope of performance assessment of a deep geological repository for nuclear wastes, numerical simulations, and therefore accurate mathematical models are of importance for a better understanding of underground contaminant migration. A common feature of the potential geological formations selected in France for nuclear wastes repository is the presence of discontinuities at several length scales. As a result, flow and transport models must account for the fractured nature of the host rock. The modelling strategy developed at IPSN (French Institute for Nuclear Safety and Protection) gives a great importance to continuum approaches, as it is more suitable for describing the large scale involved in the performance studies.

This work is aimed towards deriving the macroscopic governing equations of contaminant transport in a fractured porous medium. Such a medium is locally characterised by a representative elementary volume (REV) whose size is $O(l)$ and that consists of a porous matrix domain, Ω_m and a fracture domain, Ω_f, whose common boundary is denoted Γ (figure 1).

At the local scale, (i.e. at the REV scale), contaminant transport is governed by the following equations.

In the fractures (Ω_f):

$$\mu\Delta\vec{v}_f - \vec{\nabla}p_f = \vec{0}, \qquad \text{(Stokes equation)} \qquad (1)$$

$$\vec{\nabla}.\vec{v}_f = 0, \qquad \text{(mass balance equation)} \qquad (2)$$

$$\frac{\partial c_f}{\partial t} - \vec{\nabla}.(\tilde{D}_f\vec{\nabla}c_f - c_f\vec{v}_f) = 0, \qquad \text{(diffusion-convection equation)} \qquad (3)$$

where $\vec{v}_f$, p_f, c_f and $\tilde{D}_f$ are the velocity, pressure and concentration fields and the tensor of molecular diffusion in the fractures, respectively.

In the porous matrix (Ω_m):

$$\vec{v}_m = -\tilde{K}_m\vec{\nabla}p_m\ , \qquad \text{(Darcy's law)} \qquad (4)$$

$$\vec{\nabla}.\vec{v}_m = 0, \qquad \text{(mass balance equation)} \qquad (5)$$

$$\frac{\partial c_m}{\partial t} - \vec{\nabla}.(\tilde{D}_m \vec{\nabla} c_m - c_m \vec{v}_m) = 0, \qquad \text{(diffusion-advection equation)} \qquad (6)$$

where $\vec{v}_m$, p_m, c_m and $\tilde{D}_m$ are are the velocity, pressure and concentration fields and the tensor of dispersion in the matrix, respectively.

On the boundary (Γ):

$$\vec{v}_f.\vec{n} = \vec{v}_m.\vec{n} \qquad \text{(continuity of fluxes)} \qquad (7)$$

$$p_f = p_m \qquad \text{(continuity of pressures)} \qquad (8)$$

$$(\tilde{d}_f \vec{\nabla} c_f).\vec{n} = (\tilde{d}_m \vec{\nabla} c_m).\vec{n} \qquad \text{(continuity of diffusive fluxes)} \qquad (9)$$

$$c_f = c_m \qquad \text{(continuity of concentrations)} \qquad (10)$$

The essence of homogenization method is to determine an equivalent macroscopic behaviour by upscaling the local description. The purpose of the present study is to homogenize the local description (1-10), in order to determine the influence of the matrix-transport on the structure of the macroscopic transport equation.

The fundamental assumption behind homogenization theory is that the scales are separated:

$$l << L,$$

where l and L are the characteristic lengths at the heterogeneity scale and at the macroscopic scale, respectively. As this definition conjures up a geometrical separation of scales, we shall draw attention to the fact that this fundamental condition must also be checked regarding the phenomenon.

In this study, we use the method of homogenization for periodic structures, introduced by Bensoussan et al. (1978) and Sanchez-Palencia (1980). The key parameter of the model is the small parameter

$$\varepsilon = \frac{l}{L} << 1,$$

which is a measure of the separation of scales.

We also assume the medium to be periodic. This assumption is actually not a restriction: it allows determination of the macroscopic behaviour without any prerequisite on the form of the macroscopic equations. In the case of a periodic medium, the REV is merely the period.

In this study, we use the approach suggested in (Auriault, 1991), by which the problem is tackled in a physical rather than mathematical manner. Indeed, it offers the additional benefit that the conditions under which homogenization does apply are expressly stated. This formulation of the method is on the basis of definition and estimation of the non-dimensional numbers arising from

the local description under consideration. This fundamental step is called normalization and is aimed at specifying all cases that can be homogenized.

2 Normalization

The purpose of this section is to define the set of non-dimensional numbers that characterize the local description (1-9) and then to estimate them with respect to the small parameter ε.
From equations (1) and (3), we can define

$$F_f = \frac{\left|\mu\Delta\vec{v}_f\right|}{\vec{\nabla}p_f},\ N_f = \frac{\left|\frac{\partial c_f}{\partial t}\right|}{\left|\tilde{d}\vec{\nabla}c_f\right|},\ Pe_f = \frac{\left|c_f\vec{v}_f\right|}{\left|\tilde{d}\vec{\nabla}c_f\right|} \quad \text{(Peclet number in the fractures).}$$

Similarly, equations (4) and (6) introduce

$$Q_m = \frac{\left|\tilde{K}_m\vec{\nabla}p_m\right|}{\left|\vec{v}_m\right|},\ N_m = \frac{\left|\frac{\partial c_m}{\partial t}\right|}{\left|\tilde{d}\vec{\nabla}c_m\right|},\ Pe_m = \frac{\left|c_m\vec{v}_m\right|}{\left|\tilde{d}\vec{\nabla}c_m\right|} \quad \text{(Peclet number in the porous matrix).}$$

Finally, from the boundary conditions (7) and (9) we get the two following non-dimensional numbers:

$$\frac{\left|\vec{v}_m.\vec{n}\right|}{\left|\vec{v}_f.\vec{n}\right|},\ \frac{\left|(\tilde{d}_m\vec{\nabla}c_m).\vec{n}\right|}{\left|(\tilde{d}_f\vec{\nabla}c_f).\vec{n}\right|}.$$

For estimating these non-dimensional numbers, let us consider L as the reference characteristic length. This arbitrary choice does not affect the final result. Thus, the numbers to be estimated in powers of ε are the following:

$$F_f = \frac{\mu V_{f_c}}{L\delta P},\ N_f = \frac{L^2}{D_{f_c}T_f},\ Pe_f = \frac{V_{f_c}L}{D_{f_c}}, \qquad \text{(in the fractures)}$$

(V_{f_c} and D_{f_c} are characteristic values of the velocity and the molecular diffusion, respectively and δP is a characteristic macroscopic pressure drop).

$$Q_m = \frac{l_p^{\,2}}{L^2}\times\frac{V_{f_c}}{V_{m_c}}\times F_f^{-1},\ N_m = \frac{D_{f_c}}{D_{m_c}}\times N_f D_{f_c},\ Pe_m = \frac{V_{m_c}}{V_{f_c}}\times Pe_f, \qquad \text{(in the porous matrix)}$$

(l_p is the characteristic length at the pore scale).

$$\frac{V_{m_c}}{V_{f_c}}, \frac{D_{m_c}}{D_{f_c}}, \qquad \text{(on the boundary)}$$

The goals of the analysis are two-fold:

i) To define the conditions for which homogenization can be applied (homogenizable cases)
ii) To draw the cases for which the matrix-influence is maximum.

It can be shown that the physics does impose (Auriault and Adler, 1995): $F_f = O(\varepsilon^2)$, and that a maximum influence of the matrix-transport is characterised by (Auriault, 1983), (Auriault and Lewandowska, 1995):

$$\frac{V_{m_c}}{V_{f_c}} = O(\varepsilon), \ \frac{D_{m_c}}{D_{f_c}} = O(\varepsilon^2).$$

Now, the equations describing the flow and the transport in the porous matrix are meaningful if $l_p << l$. Let us assume that $\frac{l_p}{l} = O(\varepsilon)$.

Therefore, the non-dimensional numbers related to the boundary conditions are defined by the above estimations. As for the non-dimensional numbers related to the porous matrix, Q_m is defined and N_m and Pe_m are such that:

$$N_m = O(\varepsilon^{-2})N_f, \ Pe_m = O(\varepsilon^{-1})Pe_f.$$

Note that the fact that a physical situation is homogenizable and that the influence of matrix-transport is maximum is, in particular, characterised by the order of magnitude:

$$\frac{Pe_m}{Pe_f} = O(\varepsilon^{-1}).$$

Now, it turns out that the orders of magnitude of Pe_f and N_f are linked and that three distinct orders of magnitude for Pe_f can be considered:

i) $Pe_f = O(\varepsilon)$ (dominant diffusion)
ii) $Pe_f = O(1)$ (equivalent diffusion and convection)
iii) $Pe_f = O(\varepsilon^{-1})$ (dominant convection)

Any other order of magnitude for Pe_f will lead to a non-homogenizable physical situation, i.e, a physical situation for which no continuous macroscopic description is conceivable. We have homogenized the local description corresponding to case ii). The macroscopic description is presented in the next section.

3 Scaled-up Model in the Case of Equivalent Diffusion and Convection in the Fractures

This case is characterised by the following estimations:

$F_f = O(\varepsilon^2)$, $N_f = O(1)$, $Pe_f = O(1)$. (in the fractures)

$Q_m = O(\varepsilon)$, $N_m = O(\varepsilon^{-2})$, $Pe_m = O(\varepsilon^{-1})$. (in the porous matrix)

$\frac{V_{m_c}}{V_{f_c}} = O(\varepsilon)$, $\frac{D_{m_c}}{D_{f_c}} = O(\varepsilon^2)$ (on the boundary)

As a result, the non-dimensional local description is the following, in which all quantities are now non-dimensional quantities:

$$\varepsilon^2 \mu \Delta \vec{v}_f - \vec{\nabla} p_f = \vec{0} \quad \text{in } \Omega_f \tag{11}$$

$$\vec{\nabla}.\vec{v}_f = 0 \quad \text{in } \Omega_f \tag{12}$$

$$\frac{\partial c_f}{\partial t} - \vec{\nabla}.(\tilde{d}\vec{\nabla} c_f - c_f \vec{v}_f) = 0 \quad \text{in } \Omega_f \tag{13}$$

$$\vec{v}_m = -\varepsilon \tilde{K}_m \vec{\nabla} p_m \quad \text{in } \Omega_m \tag{14}$$

$$\vec{\nabla}.\vec{v}_m = 0 \quad \text{in } \Omega_m \tag{15}$$

$$\frac{\partial c_m}{\partial t} - \vec{\nabla}.(\varepsilon^2 \tilde{d}\vec{\nabla} c_m - \varepsilon c_m \vec{v}_m) = 0 \quad \text{in } \Omega_m \tag{16}$$

$$\vec{v}_f.\vec{n} = \varepsilon \vec{v}_m.\vec{n} \quad \text{on } \Gamma \tag{17}$$

$$p_f = p_m \quad \text{on } \Gamma \tag{18}$$

$$(\tilde{d}_f \vec{\nabla} c_f).\vec{n} = \varepsilon^2 (\tilde{d}_m \vec{\nabla} c_m).\vec{n} \quad \text{on } \Gamma \tag{19}$$

$$c_f = c_m \quad \text{on } \Gamma \tag{20}$$

Applying homogenization (Auriault, 1991) to this local description leads to the following macroscopic behaviour:

$$\vec{V}_f = -\tilde{K}_f \vec{\nabla} P, \tag{21}$$

$$\vec{\nabla}.\vec{V}_f = 0, \tag{22}$$

$$\vec{\nabla}.(\tilde{D}_f^* \vec{\nabla} C_f - C_f \vec{V}_f) = \frac{\partial C_f}{\partial t} - \underbrace{\int_{-\infty}^{t} \hat{H}(t-\tau) \frac{\partial^2 C_f}{\partial t^2} \, d\tau}_{\text{Coupling effect with the matrix-transport}} \tag{23}$$

$\tilde{K}_f$ and $\tilde{D}_f^*$ are the effective tensors of permeability and dispersion, respectively. They are symmetrical tensors and depend only upon the geometry of the periodic cell.

The influence of the porous matrix appears only in the transport equation (23) and, in particular, through the memory function $\hat{H}(t)$. The convolution product

$$\int_{-\infty}^{t} \hat{H}(t-\tau)\frac{\partial^2 C_f}{\partial t^2} \quad d\tau$$

shows that the behaviour, at a given time, depends on the history of the second time derivative of the concentration.

4 Conclusions

We have investigated the problem of contaminant transport in a fractured porous medium. An important conclusion drawn from this study is that the macroscopic description strongly depends upon the values of a set of specific physical parameters. Thus, we have defined three homogenizable physical situations for which the influence of matrix-transport is maximum.
In the present work, we have homogenized only one of these physical situations, which corresponds to equivalent diffusion and convection in the fractures. The macroscopic behaviour exhibits strong memory effects.
In the framework of performance assessment of a potential repository site, besides providing a model of solute transport in a fractured porous rock, as the analysis is focused at a particular scale, the present study also offers guidelines for the site characterisation.

References

Auriault J.L. (1983): Effective Macroscopic Description for Heat Conduction in Periodic Composites. Int. J. Heat Mass Trans., 26, 861-869.
Auriault J.L. (1991): Is an Equivalent Macroscopic Description Possible? Int. J. Engng. Sci., 2 (1), 45-64.
Auriault J.L., Adler P. (1995): Taylor Dispersion in Porous Media: Analysis by Multiple Scale Expansions, Adv. Water Res., 18 (4), 217-226.
Auriault J.L., Lewandowska J. (1995): Non-Gaussian Diffusion Modeling in Composite Porous Media by Homogenization: Tail Effects, T.I.P.M., 21, 47-70.
Bensoussan A., Lions J.L., Papanicolaou G. (1978): Asymptotic Analysis for Periodic structures, North-Holland Publishing Company, Amsterdam.
Sanchez-Palecia E. (1980): Non-Homogeneous Media and Vibration Theory, Springer-Verlag, Lecture Notes in Physics 127, Berlin.

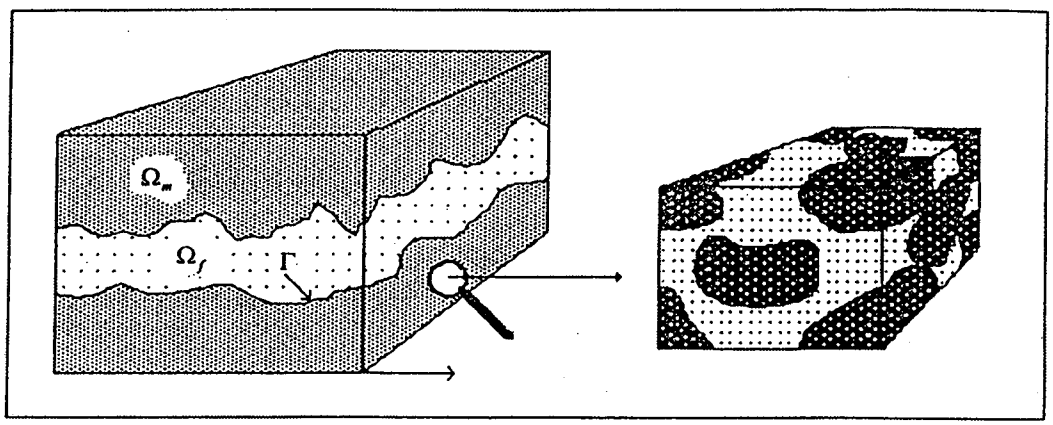

Figure 1: Periodic cell of the fractured porous medium.

Macroscopic Modelling of Gas Flow through a Fractured Porous Medium

P. Royer, J.L. Auriault, Laboratoire " Sols, Solides, Structures ", UJF, INPG, CNRS, Grenoble, France (Pascale.Royer@hmg.inpg.fr, Jean-Louis.Auriault@hmg.inpg.fr).

Summary: This work is concerned with modelling the seepage of gas through a rigid fractured medium. It summarises results obtained using the homogenization method for periodic structures. Thereby, unlike the phenomenological approaches, the macroscopic behaviour is deduced from the physics at the microscopic scales, without any prerequisite. Then, the result of the comparison of the homogenized model with the model of Warren and Root for a slightly compressible fluid flow is presented. Finally, a correction of pseudo steady state phenomenological models is proposed.

1 Introduction

A fractured porous medium is a dual porosity medium, i.e., it consists of two interacting porous systems whose permeabilities are very different. One of the two porous structures is associated with the fractures and the other one with the porous matrix. The internal disorder repetition may allow a large-scale continuous description. Two kinds of approaches may be distinguished: i) Directly macroscopic approaches ; ii) Upscaling methods.

The first investigations were on the basis of phenomenological approaches, i.e., directly macroscopic approaches (Barenblatt et al. 1960, Barenblatt 1963, Warren & Root 1963). The first model (Barenblatt et al. 1960) shows an important characteristic of dual porosity systems: the interporosity flow, i.e. the fluid exchange between both constitutive media. In these phenomenological models, a pseudo steady state flow is described. They are based on the conjecture that the interporosity flow occurs in response to the fracture-porous matrix difference in pressure.

On the other hand, homogenization techniques allow the determination of an equivalent macroscopic behaviour by upscaling the local description. By definition, this macroscopically equivalent medium behaves " in average " like the initial heterogeneous medium under a given excitation. The condition required for applying these methods is the separation of scales. Homogenization techniques have already proved to be efficient for modelling fluid flow in porous media. In particular, the homogenization method for periodic structures leads to precise descriptions since no macroscopic prerequisite is required. When looking for a macroscopic equivalent description of fluid flow in fractured porous media, three separated scales whose characteristic lengths are very different may be under consideration : the pore scale, the fracture scale and the macroscopic scale. An innovative three scale homogenization method for periodic structures was established in Auriault and Boutin (1992), Auriault and Boutin (1992), Royer and Auriault (1994), and Royer (1994). Pore-flow and fracture-flow are controlled by Stokes equations. This upscaling method allows the influence of the local effects, i.e. at the pore scale, to be conveyed to the macroscopic level.

The goals of this paper are two-fold: i) to present the model of gas flow in fractured porous media derived via homogenization; ii) to present the result of the comparison of the

homogenized model with the phenomenological models. Since there is no dual porosity phenomenological model for highly compressible fluid flow, this comparison is carried out for a slightly compressible fluid.

In section 2, the description obtained by the three scale homogenization approach is presented. Attention will be focused on the result itself. Section 3 relates specifically to comparing the homogenized model with the model of Warren and Root for a slightly compressible fluid. Finally, a correction of the interporosity flow term is proposed, which yields a more accurate description for transient regimes.

2 Homogenization Model of Gas Flow Through A Fractured Porous Medium

2.1 *General*

To fit the homogenization method for periodic structures to three scales problems, the medium is assumed to be doubly periodic. There is no loss of generality by introducing the assumption of periodicity (Auriault, 1991). No specific internal geometry is at issue for both periods, the work is aimed towards deriving a general macroscopic model. At the pore scale, consider the medium to be Ω-periodic and its characteristic length to be l. The solid and the pores occupy the domains Ω_s and Ω_p, respectively, and their common boundary is Γ (Fig. 1a). A second periodic structure exists at the fracture level, whose period is Ω' and whose characteristic length is l', such that $l' >> l$. The porous matrix and the fractures occupy the domains Ω'_{sp} and Ω'_f, respectively, and their common boundary is Γ' (Fig. 1b). In a given medium, l and l' are defined but the macroscopic characteristic length, l'', must be chosen such that $l'' >> l'$. Therefore, the dual porosity medium exhibits two separations of scales instead of one in the single porosity case: $l'/l'' << 1$ between the fracture scale and the macroscopic level, $l/l' << 1$ between the pore scale and the fracture scale.

If the first condition is not checked the homogenization cannot be applied because the macroscopic scale and the fracture scale are not separated. If the second one is not checked, it means that the medium is a two scale medium. Thus, it is assumed that both conditions of separation of scales are satisfied, so that the medium is a three scale medium and the homogenization theory can be applied.

The macroscopic behaviour of such a medium under fluid flow depends upon the relative order of magnitude between both scale ratios. The largest coupling effects between the pore-flow and the fracture-flow appear when the scales are equally separated (Auriault & Boutin 1992, Auriault & Boutin 1992, Royer & Auriault 1994, and Royer 1994), i.e., when $\frac{l}{l'} = O(\frac{l'}{l''}) = O(\varepsilon)$. This is the case under consideration hereafter for the investigation of gas flow in a rigid fractured medium.

2.2 *Local description*

In the pores (Ω_p) and in the fractures (Ω'_f), gas flow is governed by Navier-Stokes equations. For slow flows, inertial and transient terms of Navier-Stokes equations can be neglected (Auriault et al. 1990). For the sake of simplicity, assume the fluid to be linear. Thus, the gas state equation is a linear relationship between the fluid pressure and the fluid density. Let us assume the system to be initially at rest: fluid velocity is zero-valued and pressure and density are constant (P_0 and ρ_0, respectively). Thus, the problem is governed by the following set of equations with $k = p$ in the pores (Ω_p) and $k = f$ in the fractures (Ω'_f).

$$\mu\Delta\vec{v}_k + (\lambda+\mu)\vec{\nabla}(\vec{\nabla}.\vec{v}_k) - \vec{\nabla}P_k = \vec{0} \tag{1}$$

$$\frac{\partial\rho_k}{\partial t} + \vec{\nabla}.((\rho_0+\rho_k)\vec{v}_k) = 0 \tag{2}$$

$$\rho_k = AP_k \quad where\ A = \frac{\rho_0}{P_0}\ is\ a\ constant \tag{3}$$

$$\vec{v}_p = \vec{0} \quad on \quad \Gamma \tag{4}$$

$$\vec{v}_f.\vec{n}' = <\vec{v}_p>_\Omega.\vec{n}' = (\frac{1}{|\Omega|}\int_{\Omega_p}\vec{v}_p\ d\Omega).\vec{n}' \quad on\ \Gamma' \tag{5}$$

$$P_f = P_p \quad on\ \Gamma' \tag{6}$$

Fluid pressure and density are $P_0 + P_k$ and $\rho_0 + \rho_k$, respectively, where P_k and ρ_k are increments.

2.3 *Scaled-up model*

The derived macroscopic behaviour is:

$$\phi'\frac{\partial P_f}{\partial t} + \phi\frac{\partial < P_p >_{eff}}{\partial t} - \vec{\nabla}.[(P_0+P_f)\tilde{K}_f\vec{\nabla}P_f] = 0 \tag{7}$$

where $\phi' = \frac{|\Omega'_f|}{|\Omega'|}$ is the fracture porosity and $\phi = \frac{|\Omega_p|}{|\Omega|}$ is the pore porosity.

The term $\phi\frac{\partial < P_p >_{eff}}{\partial t}$ shows the fluid exchange between both porous systems. $< P_p >_{eff}$ is defined by $< P_p >_{eff} = \frac{1}{|\Omega'|}\int_{\Omega'_{sp}} P_p\ d\Omega$, where P_p is defined by the following boundary value problem over Ω'_{sp}:

$$\phi\frac{\partial P_p}{\partial t} - \vec{\nabla}.[(P_0+P_p)\tilde{K}_p\vec{\nabla}P_p] = 0$$

$$P_p = P_f \quad on\ \Gamma',$$

in which P_p is Ω'-periodic.

The macroscopic velocity is $\vec{V} = -\tilde{K}_f \vec{\nabla} P_f$ where $\tilde{K}_f$ is the fracture permeability and is determined from the geometry of Ω'_f. It turns out that P_p and P_f are such that $P_p = \mathrm{F}(P_f)$, where F is a non-linear time-dependent functional exhibiting memory effects.

The macroscopic behaviour is strongly influenced by the flow in the pores. It induces memory effects and strong non-linearities. This result highlights how the local effects may affect the macroscopic behaviour.

3 Comparison With The Model Of Warren And Root

To our knowledge, there is no rigorous phenomenological model for highly compressible fluid flow in fractured porous media. The existing models are derived for slightly compressible fluids. In these models, a pseudo steady state flow is described: it is assumed that the interporosity flow q, i.e. the flux of fluid from matrix to fractures, occurs in response to the fracture-pore difference in pressure:

$$q = sK_p(P_p - P_f) \tag{8}$$

where s is a characteristic coefficient of the fractured rock proportional to the specific surface of the block. One of these classical models, namely, the model of Warren and Root can be compared to the homogenized model for the flow of a slightly compressible fluid.

From this comparison, it turns out that the model of Warren and Root cannot be identified to the long time approximation of the linearised homogenized model (Auriault & Royer 1993), (Royer & Auriault 1994), (Royer 1994). This shows that the model of Warren and Root fails to reproduce transient regimes and is ascribed to the pseudo steady state approximation, i.e. to the form of the interporosity flow term. However, the result of this comparison suggests a way to improve the interporosity term in the classical models. In effect, by using the following correction:

$$q = sK_p(P_p - P_f - \theta \frac{\partial P_f}{\partial t}), \tag{9}$$

where θ is a constant, it can be shown that the model of Warren and Root can be identified with the long time approximation of the homogenized model (Auriault & Royer 1993), (Royer & Auriault 1994), (Royer 1994).

4 Conclusions

Through classical phenomenological approaches, transport phenomena in dual porosity media are directly modelled at the macroscopic scale. Thus, the influence of local heterogeneities on the

macroscopic behaviour cannot be perfectly disclosed. Furthermore, phenomena such as flow in the pores or storage capacity in the fractures are often simply discarded.

The homogenization method for periodic structures allows the derivation of the macroscopic behaviour from the complete microscopic description. Since there is no macroscopic prerequisite, the influence of the local effects is conveyed to the macroscopic level. Model (7) constitutes the first model of gas flow through a dual porosity medium that takes the strong compressibility of the fluid into account. Pseudo steady state phenomenological models are shown to be rough approximations for transient excitations in the context of slightly compressible fluid flow. Then, it is proved that adding a fracture pressure time derivative in the interporosity flow term overcomes, to some extent, the limitations of the pseudo steady state approximation.

References

Auriault, J.L. 1983. Effective macroscopic description for heat conduction in periodic composites. *Int. J. Heat Mass Transfer*, 26 (6):861-869.

Auriault, J.L. 1991. Heterogeneous medium - Is an equivalent macroscopic description possible? *Int.J. Eng. Sci.* 29(7): 785-795.

Auriault, J.L. & Boutin C. 1992. Deformable porous media with double porosity - Quasi-statics, I: Coupling Effects. *Transp. Por. Media*, 7: 63-82.

Auriault, J.L. & Boutin C. 1993. Deformable porous media with double porosity - Quasi-statics, II: Memory Effects. *Transp. Por. Media*, 10: 153-169.

Auriault, J.L. & Royer, P. 1993. Double conductivity media: A comparison betweenphenomenological and homogenization approaches. *Int. J. Heat Mass Transfer*, 36 (10):2613-2621.

Auriault, J.L., Strzelecki, T., Bauer, J. & He, S.1990. Porous deformable media saturated by a very compressible fluid: Quasi-statics. *Eur. J. Mech. A/ Solids*, 9(4): 373-392.

Barenblatt, G.I. 1963. On certain boundary value problems for the equations of seepage of liquid in fissured rocks. *PPM*, 27(2): 348-350.

Barenblatt, G.I., Zheltov, I.P. & Kochina, I.N. 1960.Basic concepts in the theory of seepage of homogeneous liquids in fissured rocks. *PPM*,24(5): 852-864.

Royer, P. 1994. Contribution de l'homogénéisation à l'étude de la filtration d'un gaz en milieu déformable à double porosité - Application à l'étude du système gaz-charbon. *PhD thesis, Université Joseph Fourier, Grenoble, France.*

Royer, P. & Auriault, J.L. 1994. Transient quasi-static flow through a rigid porous medium with double porosity. *Transp. Por. Media*, 17: 33-57.

Royer, P., Auriault, J.L. & Boutin, C. 1996. Macroscopic modeling of double-porosity reservoirs. *J. Pet. Sci. Eng.* 16: 187-202.Warren, J.R. & Root , P.J. 1963. The behavior of naturally fractured reservoirs. *Soc. Pet. Eng. J.* Sept: 245-255.

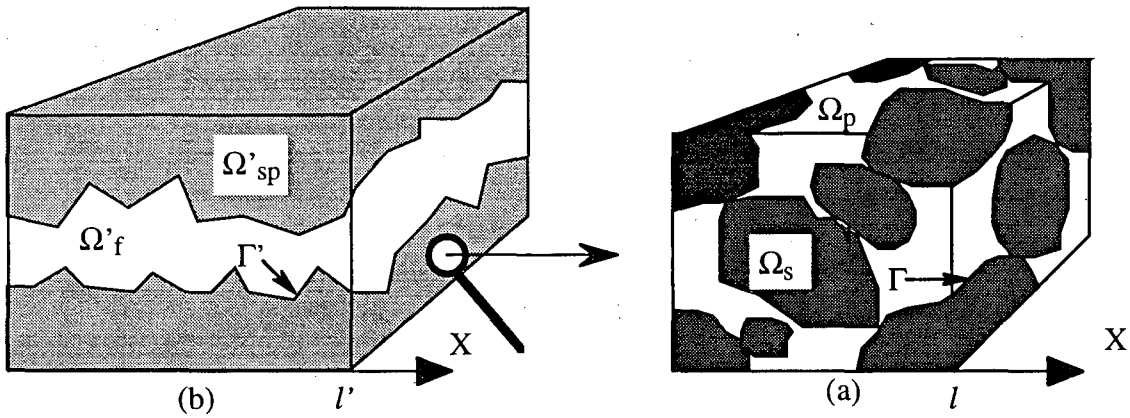

Figure 1: a) Fracture scale period; b) Pore scale period

Simulation of Strata-Bound Tight Gas Reservoirs: Discrete Irregular Stochastic Fracture Networks and Network Drainage, Including Dynamic Matrix Recharge

W. Neal Sams (WSAMS@FETC.DOE.GOV; 304-285-4068)
Mark L. McKoy (MMCKOY@FETC.DOE.GOV; 304-285-4426)
EG&G Technical Services of West Virginia, Inc.
P.O. Box 880, 3610 Collins Ferry Road
Morgantown, WV 26507-0880

Abstract

A set of computer codes has been developed to generate, simulate flow through, and plot the simulation results for tight fractured strata-bound dry gas reservoirs that contain irregular, discontinuous or clustered fracture networks.

The fracture network generator implements five 2-D Boolean models through a Monte Carlo process of sampling fitted distributions for various network attributes. These models produce a spectrum of patterns that vary from regular to random to clustered to *en echelon*. Clusters are either randomly located anisotropic swarms in which cluster overlap is permitted or parallel to semi-parallel swarms in which cluster overlap is not permitted. All five models may be used in any combination to generate a fracture pattern.

The user may specify the locations of individual fractures and individual clusters. And, with four models, the user may condition the network to known locations of fractures as observed along a borehole or sample line.

Individual fractures are treated as straight line segments; and all are perpendicular to bedding, extending from top to bottom of individual beds. Two models allow user-specified correlation of several fracture attributes.

While fractures can be placed in patterns that are regular to random to clustered, larger-scale spatial correlation is neglected. To at least some degree in all models, fractures may be moved to locations where user-specified termination frequencies or intersection frequencies are achieved. Thus local spatial correlation arises from these processes. Modeling fractures as sets and generating sets in chronological order accounts for hierarchial relations.

There are three methods for controlling connectivity: (1) fracture end-point shifting, (2) T-termination frequency control, and (3) intersection frequency control. The first method involves moving each fracture end-point toward or away from the center point to the first point of intersection found either with pre-existing fractures, or with subsequently generated fractures, or

[1]Research sponsored by the U.S. Department of Energy's Federal Energy Technology Center, under contract DE-AC21-95MC31346. Thomas H. Mroz, DOE project manager, 304-285-4071, TMROZ@FETC.DOE.GOV

both. Termination/intersection frequency control is implicit in the selection of the percentage of fracture length over which shifting is allowed.

The second method, T-termination frequency control, involves moving fractures to new locations or, preferentially, swapping fracture orientation until end-point shifting improves the match with user-specified percentages of fractures having zero, one, or two T-terminations. The program controls the percentage of fracture length over which end-point shifting occurs.

When it is more important to explicitly control the frequencies of intersections, as when modeling cross-fractures and late-formed fractures, the third method is used. It starts with a proposed fracture of maximum allowable length and counts all intersections with the proposed fracture. If an acceptable number of intersections is found, it truncates the proposed fracture at the optimal number of intersections needed to improve the match with a user-specified distribution of intersection frequencies. If too few intersections are found, it swaps the fracture's orientation or location and repeats the process until the desired number of intersections is found. To control the resulting fracture length distribution, maximum and minimum acceptable lengths are defined and varied to produce a fracture length distribution with lognormal statistics that match those specified by the user.

Both the second and third methods of connectivity control use a type of synthetic annealing in which the user specifies the frequency for swaps of location, the total number of swaps allowed, and the percentage of fractures generated in a set before synthetic annealing begins. These controls limit unintended parent-daughter clustering.

Work is currently in progress for multilayer network modeling. Multilayer modeling involves generating a fracture network for each layer and stacking the fractured layers. A user-specified percentage of fractures in each set extend into the overlying layer, where they are incorporated into the network of the overlying layer as it is generated. Which fractures extend into the overlying layer is determined by a correlation with fracture length, as specified by the user.

The models described above are implemented by a FORTRAN program called FRACGEN. FRACGEN reads an input file containing parameters and statistics for fracture network attributes. It produces several optional outputs, including: a screen plot, an output file consisting of fracture end-points and apertures, and copious diagnostics. Several ancillary programs for assistance with raw data analysis have been written in QBASIC and FORTRAN. Two of the three cluster models have an analytic technique for estimation of most clustering parameters. The other cluster model uses a computer program to determine clustering parameters via an optimized histogram matching.

Another FORTRAN program, called NFFLOW, simulates the flow of dry gas through the fractured reservoirs to one or more wells. The flow model is composed of two classes of objects: fracture planes and equivalent rock volumes (ERV). Fracture planes are idealized two-dimensional flow regions in which the volumetric flow rate is proportional to the pressure gradient and inversely proportional to the gas viscosity. The coefficient of proportionality relates to fracture aperture. In the absence of other data, the coefficient is assumed to vary as the cube

of the aperture. The flow coefficient need not be isotropic but can be reduced in the vertical direction to simulate restricted vertical flow. ERVs are idealized sources for gas recharging the fracture network. They are one-dimensional unsteady models that represent a linear flow into fracture segments. Darcy's Law describes flow within ERVs.

Fracture planes may penetrate one or more layers of the reservoir, but they are assumed to completely penetrate all layers that they enter. For purposes of representing fracture location, finding fracture intersections, and calculating ERVs, the portion of a fracture within each layer is treated as planar and vertical; however, the fracture is allowed to rotate from layer to layer. Also, the length of the fracture trace can vary from layer to layer. The fracture trace is given by the intersection of the fracture plane and a plane midway between the top and bottom of a layer. Intersections with other fracture traces within a layer determine the number and length of that fracture's segments within that layer. Intersection points become nodes in the flow simulation, and the mid-points of the segments become recharge points. Gas pressures at these two sets of points establish the pressure distribution within the fracture network.

Recharge of the network is modeled by flow from the ERVs located on either side of each fracture segment. The volume allocated to each ERV is based on the geometry of the fracture network and is that portion of the total rock volume that is estimated to drain into the specified fracture segment. ERVs are dimensioned so that the sum of all ERVs in a layer equals the total volume of the layer. Once the volume of an ERV is determined, a length and width of the flow path is computed using the length of the adjoining fracture segment. Flow rate from the ERV to the fracture becomes a function of the pressure gradient within the ERV and the gas pressure at the fracture segment midpoint. Pressure distribution within each ERV is obtained by numerical solution of a one-dimensional unsteady-flow partial differential equation. Each ERV is discretized using a geometric grid spacing. The longest flow path is divided into the maximum number of grid blocks specified by the user, and the smallest grid block produced by this procedure becomes the scale length for the smallest grid block in all the other ERVs. Thus the larger ERVs are divided into a greater number of grid blocks while the smaller ERVs are divided into a smaller number of grid blocks. Regardless of the size of the ERV, the smallest grid block (the one at the fracture face) is approximately the same size in all ERVs.

System equations are obtained by writing material balances at all nodes and recharge points. Because the gas density depends on pressure, the fracture-flow terms are nonlinear and are made linear by using a "real gas pseudopotential" formulation. This approach permits the use of pressure dependent terms for gas viscosity and fracture aperture without significantly increasing the model's complexity. However, the resulting system equations remain slightly nonlinear because of fracture recharge. Therefore, system equations are solved by a conventional Newton-Raphson technique, which produces linear equations that are solved by an over-relaxation method.

Flow within wells is treated similar to that within fractures. The simulator allows wells to be operated with either a time varying production rate or bottom-hole pressure. A well may be switched from rate mode to pressure mode as required. Output from the simulator consists of tabular production data and plots of gas pressure within the fracture network at specified times.

Multicontinuum Description of Flow and Transport in the Composite Heterogeneoues Media

Mark Shvidler and Kenzi Karasaki
Earth Science Division, Lawrence Berkeley National Laboratory, Berkeley , California 94720
e-mail :MShvidler@lbl.gov

The problem of rationally describing percolation transport in real, macroscopically essentially inhomogeneous media is of considerable interest in connection with the flow and transport theory and its technical applications. A phenomenological theory of the unsteady motion of a homogeneous fluid in heterogeneous composite systems (media with dual porosity, fractured porous media), which involves splitting the flow into a sequence of embedded continua and postulating the interaction mechanism is well studied. In accordance with this approach, the flow in each of the homogeneous subsystems of the heterogeneous composite or so called phase is characterized by its own pressure and flow-velocity fields, the relation between which takes the form of Darcy`s law. The rate of fluid transfer among the phases is assumed to be proportional to the difference of the phase pressures.

Another approach to the description of percolating transport in heterogeneous random systems including composite media involves the probabalistic treatment of the percolation parameters and flow and transport equations as well as the determination of the functionals from statistical solution or the analysis of the equations relating the unknown and given functionals.

Inhomogeneous systems of periodic structure are a convenient model for studying processes in highly inhomogeneous media. The theory of averaging the processes in periodic, as distinct from stochastic, structures is well established and constructive methods of analyzing many processes in periodic media have been developed.

The description in terms of average fields realized by the theory of homogenization leads to equations that relate these fields to the effective characteristic of the inhomogeneous medium. Under certain conditions the averaged equations can be treated as conservation laws, and their system as a mono-continuum model of the process. Obviously, this description gives sufficient information on the fields in the individual phases of the composite periodic system and the inter-phase transfer processes.

A more detailed description involves the determination of the conditionally averaged fields and the equations relating these fields. If it is possible to construct such equations and treat them as the equations of the process in a phase of the composite system, such description will be a multi-continuum one and the system can be modeled by superposing these continuums in accordance with the number of phases.

Irrespective of the method of realizing the multi-continuum description, it is necessary to solve the central problem of closing the systems of equations associated with the presence in them of terms responsible for inter-continuum transfers of mass, momentum, energy, etc.

We examine the problem of conditional averaging of a system of transport equations for a weakly compressible fluid in a periodic composite medium. The equations of the multi-

continuum model were obtained and the parameters regulating the interactions between the phase continua were calculated.

It has been shown that for those cases in which, for one and the same process, a multi-continuum description can be realized and the conservation laws of the multi-continuum model can be obtained, the closing transfer terms can be expressed in terms of the characteristic of the mono-continuum and the fields in the phase continua can be calculated. The information thus obtained makes it possible to evaluate and refine the phenomenological closing hypothesis. As an example we show that in case when heterogeneous system is locally isotropic and macro-isotropic, the hypothesis of the proportionality of the cross-flow between the phases to the phase pressure difference is the exact rule. On the other hand, for non-completely isotropic composite systems this relation is generally inadequate.

A Discrete-Fracture Boundary Integral Approach to Simulating Coupled Energy and Moisture Transport in a Fractured Porous Medium

S Stothoff (Stothoff Environmental Modeling, 1206 La Rue Street, Houston, TX 77019; 713-520-9484; email: stothoff@insync.net); G Ofoegbu (Center for Nuclear Waste Regulatory Analyses, 6220 Culebra Road, San Antonio, TX 78238; 210-522-6641; email: gofoegbu@swri.edu); R Green (Center for Nuclear Waste Regulatory Analyses, 6220 Culebra Road, San Antonio, TX, 78238; 210-522-5305; email: rgreen@swri.edu)

Background and Regulatory Concerns

The high-level nuclear waste geologic repository proposed for location at Yucca Mountain (YM), Nevada, is being designed for emplacement in a densely fractured welded tuff. Saturated hydraulic conductivities of the tuff at the repository horizon are roughly of the same order of magnitude as estimates of infiltration rates under current climatic conditions, and significantly lower than upper-bound estimates of infiltration under wetter and cooler climatic conditions. It is generally accepted by both the U.S. Department of Energy (DOE) and the Nuclear Regulatory Commission (NRC) that fractures may dominate the flow in the unsaturated zone. Appropriate modeling of the interaction of flowing fractures with drifts is of interest to the NRC, as this interaction affects waste-package degradation and determines release modes for radionuclides. Fracture-continuum methods, while computationally tractable, are theoretically weak for liquid flow at the drift scale as there are generally too few (flowing) fractures in the driftwall surface area to comfortably support a fracture-continuum Representative Elementary Volume (REV).

The theoretical appeal of discrete-fracture approaches has inspired renewed investigation of discrete-fracture modeling at the Center for Nuclear Waste Regulatory Analyses (CNWRA). Our experience has been that discrete-fracture modeling using standard domain (e.g., finite volume, finite element) methods is extremely computationally demanding due to the great contrast between fracture and matrix properties. An alternative approach to discrete-fracture simulations is by using a boundary-integral method, where the computational mesh is placed only on boundaries and fractures (discontinuities). Boundary integral methods have been used in saturated groundwater flow problems for some time (cf. Liggett and Liu, 1983). Rasmussen (1987) used a boundary-integral approach for saturated-flow simulations in three-dimensional fracture networks, although flow was restricted to the networks themselves (no matrix/fracture interaction was considered).

Boundary integral approaches are most effective when a Green's function can be determined for the problem (excluding discontinuities), all domain integrals can be brought to the boundary or discrete features, and nonlinearities are restricted to discrete features. If these requirements are met, the solution within the problem domain is exact (subject to the boundary discretization), even when a large range of scales is considered (e.g., mountain through drift scale at YM). As a practical matter, Laplacian-based problems with piecewise constant material properties are particularly suitable for the approach (e.g., saturated porous-medium flow). Time-dependent problems are most readily solved if they are amenable to a Laplace transform or feature a moving sharp interface with quasi-steady conditions elsewhere. Boundary integral approaches are not attractive when some portion of the governing equation cannot be distributed to the boundaries, so that domain integrals are required (e.g., the problem is highly heterogeneous).

Thermally forced redistribution of moisture, of particular interest at YM, is an application that may be amenable to discrete-fracture simulation using a boundary integral approach. Of particular interest are flow processes in a fracture network near the drift wall, as dripping would presumably be initiated from such a network unless diversion around the drift occurs. In the following development, a procedure is developed for simulating the thermally driven flux of liquid and vapor in a fracture network. A boundary integral technique is used to calculate the energy flux in the matrix and a standard finite volume approach is used to calculate mass and energy fluxes in the fractures. A problem refluxing in the boiling zone, was devised to test the methodology, in which it is assumed:

- An equilibrium state has been achieved
- Energy transport in the matrix is through conduction only
- Mass transport is confined to the fractures

The work is a first step to examine the potential of the approach. If the approach appears promising, these assumptions can be relaxed in future work.

Computational Approach

A finite volume approach is used in the fractures; the computational approach is familiar for water and gas transport in the fractures and will not be discussed in detail. The finite volume approach enables heterogeneity in the fractures to be incorporated on an element-by-element basis.

The Green's function, or direct boundary element approach, is followed herein for energy transport in the matrix, because of the generality of the approach and the ease of incorporating extensions to the basic formulation. An excellent derivation of the approach is presented by Liggett and Liu (1983), along with associated computer code. Summary discussions of the methodology are presented by Stothoff (1991).

The general boundary integral formulation for flow in the matrix provides values for u at particular points on the boundary or within the domain of interest, where u is a potential. The formulation below assumes that temperature is the potential of interest and material properties are piecewise constant, with a mesh along discontinuities. For simplicity of notation, conductivity is included into the potential, so that u and $q = -K_m \nabla T = -\nabla u$, where q is flux evaluated at a point in the domain. The formulation is:

$$\begin{aligned}\sum_i \alpha_i u_i &= \int_\sigma \left(G\frac{\partial u}{\partial n} - u\frac{\partial G}{\partial n} \right) d\sigma + \int_{\sigma_M} \left(G\Delta\frac{\partial u}{\partial n} - \Delta u \frac{\partial G}{\partial n} \right) d\sigma_M, \\ &= \int_\sigma \left(G\frac{\partial u}{\partial n} - u\frac{\partial G}{\partial n} \right) d\sigma + \int_{\sigma_M} \left(-Gq_s - \Delta u \frac{\partial G}{\partial n} \right) d\sigma_M,\end{aligned} \tag{1}$$

where G is the Green's function, q_s is the thermal flux entering the fracture, Δ is the jump operator (e.g., $\Delta u = u_1 - u_2$, where the subscripts represent sides 1 and 2 of the discontinuity), σ represents the domain boundary, σ_M represents discontinuities within the domain, n is the vector normal to the

boundary, and a_i is the fraction of the point in region i (the point may be partially within several domains). If the point is completely within the domain, $a = 1$. On a smooth boundary, $a = ½$. The free space Green's function for the Laplace equation in 2D is $G = \ln r/2\pi$, while in 3D, $G = 1/4\pi r$.

The boundary integral method requires that all terms within the integrals are known before u can be explicitly evaluated at any point. A well-specified problem does not provide all terms. In order to define the missing terms, a set of linear equations is formed by writing one integral equation for each unknown. If the representation of piecewise-linear u and piecewise-constant $\partial u/\partial n$ is chosen, equations along the boundary are written at nodes wherever there is an unspecified value of u and are written at element centroids wherever there is an unspecified value of $\partial u/\partial n$. Unknown jump values must also be determined during the solution process. Where jump values are unknown, the application of compatibility equations for continuity of the unknown or the gradient of the unknown provides the additional equations to complete a well-posed problem. For fractures, compatibility requires that energy is conserved during transfer across the fracture-matrix interface.

An energy balance equation for each fracture element explicitly accounts for diffusion between adjacent nodes, transfer between the matrix and fracture, and sources and sinks within the fracture. The sources and sinks might be externally applied (e.g., for testing purposes), but can also be formulated to capture advection and phase change effects. The energy balance equation for fracture node i can be stated

$$\sum_j C_{fij}\left(T_j - T_i\right) + \sum_k A_{fmk} q_{sk} + Q_{ci} = 0, \tag{2}$$

where C_{fij} is the conductance between fracture nodes i and j, A_{fmk}, is the area of the fracture exchanging with the matrix that is associated with the node, the summation over j represents the number of nodal connections exchanging with node i and the summation over j represents the number of nodal connections exchanging with node i, the summation over k represents the number of elements attached to node i, and Q_{ci}, represents sources and sinks.

The governing equations for the fractures are of reduced dimensionality relative to the matrix. For example, a two-dimensional problem yields one-dimensional fractures. Further, the fracture equations need not be solved using a boundary integral approach. Two discretization schemes were tried in preliminary conduction-only tests with applied sinks, a finite volume approach and a finite element approach. These schemes differ in that u was assumed piecewise constant between nodes in the finite volume approach while u was assumed piecewise linear between nodes in the finite element approach. In both cases, matrix/fracture linkage was evaluated at the element centroid. When the fracture conductivity was low, both methods provided acceptable results. As the matrix conductivity increases, the finite element approach begins to suffer from numerical oscillations, and the method is unusable for conditions mild relative to expected field conditions. On the other hand, the finite volume approach is unaffected by numerical stability even for unrealistically extreme conditions. The advantage of the finite volume approach is that fracture unknowns are defined for the same spatial location as matrix/fracture interaction occurs, while the finite element approach has nodal values that are indirectly felt by the matrix, leading to an underconstrained system.

Possible Extensions

The technique is equally appropriate for considering ambient conditions at YM. Again assuming that equilibrium conditions exist, the isothermal transport of liquid in both the matrix and discrete fractures can be addressed. Two approaches for handling matrix fluxes are available, treat each matrix block as having a spatially uniform conductivity (although the conductivity is dependent on the matrix saturation) or use the exponential representation of hydraulic conductivity (Gardner, 1958) and solve a quasi-linear problem (Pullan and Collins, 1987). In both cases, parameters characterizing the hydraulic conductivity for each block must be adjusted as the solution process iterates to convergence.

The problem of thermally driven redistribution is not restricted to the initial assumption set. It is feasible to consider quasi-steady moisture transport in the matrix, both in the liquid and gas phases that can interchange with the fractures, as well as considering the transient movement of the boiling isotherm. A transient boundary- and discontinuity-only formulation can be achieved if: (i) the boiling isotherm is treated as a sharp interface between a matrix gas zone and a matrix liquid zone, (ii) gas fluxes are limited to fractures in the matrix liquid zone, and (iii) gas properties are approximated as piecewise constant in the matrix gas zone. The formulation requires that pressure and temperature equilibrate quickly relative to the movement of the sharp interface.

Acknowledgments

This report was prepared to document work performed by the CNWRA for the NRC under Contract No. NRC-02-97-009. The activities reported here were performed on behalf of the NRC Office of Nuclear Material Safety and Safeguards, Division of Waste Management. The report is an independent product of the CNWRA and does not necessarily reflect the views or regulatory position of the NRC. The authors would like to acknowledge the suggestions and comments made by D. Hughson and B. Sagar that tremendously improved the quality of the presentation.

References

Gardner, W.R. 1958. Some steady-state solutions of the unsaturated moisture flow equation with application to evaporation from a water table. *Soil Science* 85: 228–232.

Liggett, J.A., and P.L-F. Liu. 1983. *The Boundary Integral Equation Method for Porous Media Flow.* London, England: George Allen & Unwin.

Pullan, A.J., and I.F. Collins. 1987. Two- and three-dimensional steady quasi-linear infiltration from buried and surface cavities using boundary element techniques. *Water Resources Research 23*(8): 1,633–1,644.

Rasmussen, T.C. 1987. Computer simulation model of steady fluid flow and solute transport through three-dimensional networks of variably saturated, discrete fractures. D.D. Evans and T.J. Nicholson, eds. *Geophysical Monograph 42: Flow and Transport Through Unsaturated Fractured Rock.* Washington, DC: American Geophysical Union.

Stothoff, S.A. 1991. *A Boundary Integral Technique for Modelling Two-Phase Flow in Porous Media.* Ph.D. thesis, Princeton University.

A Model of Microbial Growth in a Flowing Fracture

Bryan Travis
Earth & Environmental Sciences Division
Los Alamos National Laboratory
Los Alamos, NM 87545

bjt@vega.lanl.gov

Microbes are found in a great variety of environments, from the arctic ice to boiling springs. Microbes are ubiquitous in soils; they have been found at great depths, and are observed in fractured rock (Amy & Haldeman, 1997). Their potential role in facilitating or retarding transport in porous systems has only recently been investigated (e.g., Cunningham, Characklis, Abedeen & Crawford, 1991; Stoodley, DeBeer, and Lewandowski, 1994). One method of studying their possible impact in fractured systems is through modeling. A model is described here and applied to movement and growth of microbes in fractures and fracture networks. The model couples flow and transport of solutes, particulate matter and microbes with microbial metabolic activity. Microbial growth depends on electron acceptors and donors (e.g., oxygen and substrates) and nutrients in a multiplicative Monod kinetics formulation. By-products, e.g., carbon dioxide, are also tracked. Microbial kinetics is coupled to a flow and transport model, which includes advection, diffusion and dispersion. Sorption involves a number of interactions: sorption sub-models include an equilibrium reversible type, or a rate-dependent form. Both versions allow either linear or nonlinear behavior. Solutes can sorb to the rock matrix, and to colloidal material (which includes microbes), and colloidal particles can sorb to the matrix or experience filtration.

Microbes can be mobile or immobile - they will attach and detach from the matrix or fracture walls at rates that depend on the local food supply. Microbes are present in diverse species; there are trophic hierarchies in which some species (e.g., protozoa) feed on other species. Cooperation, competition and predation can all occur in microbial communities. Continued biofilm growth depends on diffusion of nutrients and electron acceptors/donors through the biomass film. Biofilms acquire complex structure; hydrodynamic flow can occur within the film, and the presence of a film can affect the primary flow in the fracture, both by changing the fracture aperture and by creating an interface whose texture and flow resistance may differ from that of the original fracture face. Structure of the biofilm can be related to a parameter G = maximum biomass growth rate divided by maximum substrate transport rate (Picioreanu, van Loosdrecht and Heijnen, 1998). Strong biofilm growth can lead to pore clogging. In this study, steady flow in uniform as well as in non-uniform aperture fractures is considered, with fracture flow governed by the viscous flow equations. Additionally, intermittent flow is considered. Comparison to experiment data is used to validate parts of the model.

Interesting nonlinear behavior has been observed in model simulations. Microbial growth, especially when competition and predation occur between species, can exhibit period doubling behavior as a function of spatial location relative to a growth origination point. In some cases, a dramatic on/off mode is seen, in which microbe population density is very low for a time, then quickly grows to a maximum level, remains there for an interval, and then reverts rapidly to the low population situation, switching indefinitely between these minimal and maximal states. Solutes can be retarded by diffusion into the biofilm and capture onto exopolymeric secretions of the microbial community, although enhanced transport is possible when solutes sorb to colloidal matter and mobile bacteria.

ESTIMATES OF FREQUENCY-DEPENDENT COMPRESSIBILITY FROM A QUASISTATIC DOUBLE-POROSITY MODEL

H. F. Wang,[1] J. G. Berryman,[2] and P. A. Berge[2]

1 Introduction

Gassmann's [1951] relationship between the drained and undrained bulk modulus of a porous medium is often used to relate the dry bulk modulus to the saturated bulk modulus for elastic waves, because the compressibility of air is considered so high that the dry rock behaves in a drained fashion and the frequency of elastic waves is considered so high that the saturated rock behaves in an undrained fashion. The bulk modulus calculated from ultrasonic velocities, however, often does not match the Gassmann prediction. Mavko and Jizba [1991] examined how local flow effects and unequilibrated pore pressures can lead to greater stiffnesses. Their conceptual model consists of a distribution of porosities obtained from the strain-versus-confining-pressure behavior. Stiff pores that close at higher confining pressures are considered to remain undrained (unrelaxed) while soft pores drain even for high-frequency stress changes. If the pore shape distribution is bimodal, then the rock approximately satisfies the assumptions of a double-porosity, poroelastic material. Berryman and Wang [1995] established linear constitutive equations and identified four different time scales of flow behavior: (1) totally drained (K), (2) soft pores are drained but stiff pores are undrained ($K[u^{(1)}]$), (3) soft and stiff pores are locally equilibrated, but undrained beyond the grain scale (K_u), and (4) both soft and stiff pores are undrained (K_{EB}). The relative magnitudes of the four associated bulk moduli (in parentheses above) will be examined for all four moduli and illustrated for several sandstones.

2 Constitutive Equations

Berryman and Wang [1995] expressed the constitutive equations for a double-porosity, poroelastic medium in matrix form:

$$\begin{pmatrix} \delta e \\ -\delta\zeta^{(1)} \\ -\delta\zeta^{(2)} \end{pmatrix} = \begin{pmatrix} a_{11} & a_{12} & a_{13} \\ a_{21} & a_{22} & a_{23} \\ a_{31} & a_{32} & a_{33} \end{pmatrix} \begin{pmatrix} -\delta p_c \\ -\delta p_f^{(1)} \\ -\delta p_f^{(2)} \end{pmatrix} \tag{1}$$

where e is volumetric strain, p_c is confining pressure (equal to the negative of the mean stress with the convention that extensional stresses are positive), $p_f^{(1)}$ is the pore pressure of the stiff component, $p_f^{(2)}$ is the pore pressure of the soft component, $\zeta^{(1)}$ is the increment of fluid content in the stiff component, and $\zeta^{(2)}$ is the increment of fluid content in the soft component. The coefficient matrix is symmetric. The coefficients a_{12} and a_{13} are *poroelastic expansion coefficients*, analogous to thermal expansion. The submatrix elements a_{22}, a_{33}, and a_{23} are *storage coefficients* of the matrix. The coefficient a_{11} is simply the compressibility of the drained (elastic) material.

[1]Department of Geology and Geophysics, University of Wisconsin-Madison, 1215 W. Dayton St., Madison, WI 53706; wang@geology.wisc.edu

[2]Lawrence Livermore National Laboratory, PO Box 808, Livermore, CA 94550; berryman1@llnl.gov, berge1@llnl.gov

The case of drained soft porosity and undrained stiff porosity is defined by $\delta p_f^{(2)} = 0$, while $\delta\zeta^{(1)} = 0$. The pore pressure buildup in the stiff porosity fraction is

$$B[u^{(1)}] \equiv \left.\frac{\partial \delta p_f^{(1)}}{\partial \delta p_c}\right|_{\delta\zeta^{(1)}=\delta p_f^{(2)}=0} = -\frac{a_{21}}{a_{22}}. \tag{2}$$

The effective unrelaxed bulk modulus is found to be

$$\frac{1}{K[u^{(1)}]} \equiv -\left.\frac{\partial \delta e}{\partial \delta p_c}\right|_{\delta\zeta^{(1)}=\delta p_f^{(2)}=0} = a_{11} - \frac{a_{21}^2}{a_{22}} = a_{11} + a_{21}B[u^{(1)}]. \tag{3}$$

Another compressibility similar to Eqn. 3 is one defined by no local flow at all. The pore pressure buildups in the stiff and soft pore fractions are, respectively,

$$B_{EB}^{(1)} \equiv \left.\frac{\partial \delta p_f^{(1)}}{\partial \delta p_c}\right|_{\delta\zeta^{(1)}=\delta\zeta^{(2)}=0} = \frac{a_{23}a_{13} - a_{12}a_{33}}{a_{22}a_{33} - a_{23}^2}, \tag{4}$$

$$B_{EB}^{(2)} \equiv \left.\frac{\partial \delta p_f^{(2)}}{\partial \delta p_c}\right|_{\delta\zeta^{(1)}=\delta\zeta^{(2)}=0} = \frac{a_{23}a_{12} - a_{13}a_{22}}{a_{22}a_{33} - a_{23}^2}. \tag{5}$$

The compressibility associated with the unequilibrated pore pressure buildups is

$$\frac{1}{K_u^{EB}} \equiv -\left.\frac{\partial \delta e}{\partial \delta p_c}\right|_{\delta\zeta^{(1)}=\delta\zeta^{(2)}=0} = a_{11} + a_{12}B_{EB}^{(1)} + a_{13}B_{EB}^{(2)}. \tag{6}$$

A final compressibility is the one associated with globally undrained conditions, but equilibration by local flow between the stiff and soft pores. The pore pressure buildup is

$$B \equiv \left.\frac{\partial \delta p_f}{\partial \delta p_c}\right|_{\delta\zeta^{(1)}+\delta\zeta^{(2)}=0} = -\frac{a_{21} + a_{31}}{a_{22} + 2a_{23} + a_{33}}, \tag{7}$$

where $\delta p_f \equiv \delta p_f^{(1)} = \delta p_f^{(2)}$. The long-time, globally undrained compressibility is

$$\frac{1}{K_u} \equiv -\left.\frac{\partial \delta e}{\partial \delta p_c}\right|_{\delta\zeta^{(1)}+\delta\zeta^{(2)}=0} = a_{11} + (a_{12} + a_{13})B. \tag{8}$$

Berryman and Wang [1995, 1998] used laboratory measurements of Coyner [1984] for various rocks to obtain the parameters necessary for the constitutive equations. The soft component parameters (including unjacketed solid compressibility and drained frame compressibility) were taken to be those measured at a confining pressure of 10 MPa, whereas the corresponding stiff component parameters were those measured at 25 MPa. The resulting four compressibilities, $1/K[u^{(1)}]$, $1/K_u^{EB}$, and $1/K_u$, together with $1/K$, are shown in Table 1 for three sandstones.

If it is assumed that the quasistatically *measured* value is the long-time, undrained limit for a double-porosity medium in which the pore pressures between the different subsets of pore shape have equilibrated, then $1/K_u$ in Table 1 would be the predicted value. Among the samples in Table 1, $1/K_u$ has been determined experimentally only for Berea sandstone [Hart and Wang, 1995]. The measured value $1/K_u = 0.063$ GPa^{-1} compares favorably with the value 0.076 GPa^{-1} in Table 1.

Time Scales	Compressibility	Weber	Berea	Navajo
long	$1/K$, GPa^{-1}	0.250	0.167	0.0769
intermediate	$1/K[u^{(1)}]$, GPa^{-1}	0.198	0.129	0.0638
short	$1/K_u$, GPa^{-1}	0.061	0.076	0.0541
very short	$1/K_u^{EB}$, GPa^{-1}	0.054	0.069	0.0518

Table 1: Compressibilities for different assumptions about pore pressure equilibration between soft and stiff pores, assuming that $K_f = 2.3$ GPa^{-1}. Values in the first row are drained frame compressibilities measured for 10 MPa confining pressure by Coyner [1984]. All other values are computed from formulas in the text.

3 Gassmann's Equation

A rigorous expression of the Gassmann relation for a single-porosity medium is [Brown and Korringa, 1975; Berge, 1998]

$$K_u - K = \frac{\alpha^2}{\frac{\alpha}{K_s} + \phi\left(\frac{1}{K_f} - \frac{1}{K_\phi}\right)}, \tag{9}$$

where K_u is the undrained bulk modulus, K is the drained bulk modulus, K_s is the unjacketed bulk modulus, K_f is the fluid bulk modulus, K_ϕ is the unjacketed pore bulk modulus, ϕ is the porosity, and $\alpha \equiv 1 - K/K_s$. Berge [1998] has shown that the assumption $K_\phi = K_s$ often fails for experimental values of $K_u - K$, even for monomineralic rocks, where in theory they are equal. A possible reason for the breakdown is that the pore structure of monomineralic rocks is not homogeneous, and the double-porosity poroelastic model may be more appropriate than the single-porosity poroelastic model.

Berge [1998] showed that K_ϕ may depend strongly on effective stress, with $K_\phi \to K_f$ at low stress and $K_\phi \to K_s$ at high stress. Stress dependence is routinely observed in laboratory measurements of B and K [e.g., Green and Wang, 1986; Fredrich et al., 1995; Hart and Wang, 1995]. At high confining pressures, K_ϕ values may represent the behavior of stiff pores in a double-porosity medium, whereas the K_ϕ values at low stresses may represent the response of the soft pores. In a single-porosity medium, K_ϕ is related to B and K by [Green and Wang, 1986; Berge, 1998]

$$\frac{1}{K_\phi} = \frac{1}{K_f} - \left(\frac{\alpha}{\phi K}\right)\left(\frac{1}{B} - 1\right). \tag{10}$$

In the double-porosity model, we can obtain two estimates of K_ϕ by considering first the case when soft pores are drained but stiff pores are undrained, and next the long-time, globally undrained case. In the first case, we can estimate K_ϕ using $B[u^{(1)}]$ in Eqn. 10, and we use B in the second case.

4 Discussion

The three compressibilities, $1/K[u^{(1)}]$, $1/K_u^{EB}$, and $1/K_u$, together with $1/K$, show that the equilibration of pore pressure affects the volumetric strain that results from the application of confining pressure. Achieving an approximation to the different boundary conditions in the definition of each compressibility depends on the permeabilities of the different subsets

of porosity. The frequency of an elastic wave relative to these permeabilities will determine which set of boundary conditions is most appropriate for a particular rock.

The unrelaxed compressibility of Mavko and Jizba, $1/K[u^{(1)}]$, represents a frequency for which flow from the soft porosity is globally drained. It is stiffer than the totally drained case $(1/K)$. The undrained case in which local flow equilibrates pore pressure between the soft and stiff porosity is represented by $1/K_u$, and it is lower except for the case of no local flow at all, which is represented by $1/K_u^{EB}$. The totally drained compressibility is largest, and the compressibility associated with no local flow at all is the smallest, and is associated with the highest frequency of elastic wave propagation. Pressure dependence of poroelastic parameters measured in the laboratory may be described using the double-porosity poroelasticity model.

Acknowledgments

Work by J. G. Berryman and P. A. Berge was performed under the auspices of the U. S. Department of Energy (DOE) by the Lawrence Livermore National Laboratory under contract no. W-7405-ENG-48 and supported specifically by the Geosciences Research Program of the DOE Office of Energy Research within the Office of Basic Energy Sciences (OBES), Division of Engineering and Geosciences. The work of H. F. Wang also was supported by OBES, under grant no. DE-FG02-98ER14852 to the University of Wisconsin.

References

Berge, P. A. (1998), Estimating pore compressibility in rocks, *Geophysics*, submitted.

Berryman, J. G., and Wang, H. F. (1995), The elastic coefficients of double-porosity models for fluid transport in jointed rock, *J. Geophys. Res.*, *100*, 24,611–24,627.

Berryman, J. G., and Wang, H. F. (1998), Double-porosity modeling in elastic wave propagation for reservoir characterization, UCRL-JC-131020, 17 pp.

Brown, R. J. S., and Korringa, J. (1975), On the dependence of the elastic properties of a porous rock on the compressibility of the pore fluid, *Geophysics*, *40*, 608–616.

Coyner, K. B. (1984), *Effects of Stress, Pore Pressure, and Pore Fluids on Bulk Strain, Velocity, and Permeability of Rocks*, Ph.D. thesis, MIT.

Fredrich, J. T., Martin, J. W., and Clayton, R. B. (1995), Induced pore pressure response during undrained deformation of tuff and sandstone, *Mech. of Mat.*, *20*, 95–104.

Gassmann, F. (1951), Über die elastizität poröser medien, *Veirteljahrsschrift der Naturforschenden Gesellschaft in Zürich*, *96*, 1–23.

Green, D. H., and Wang, H. F. (1986), Fluid pressure response to undrained compression in saturated sedimentary rock, *Geophysics*, *51*, 948–956.

Hart, D. J., and Wang, H. F. (1995), Laboratory measurements of a complete set of poroelastic moduli for Berea sandstone and Indiana limestone, *J. Geophys. Res.*, *100*, 17,741–17,751.

Mavko, G., and Jizba, D. (1991), Estimating grain-scale fluid effects on velocity dispersion in rocks, *Geophysics*, *56*, 1940–1949.

On the Effective Continuum Method for Modeling Multiphase Flow, Multicomponent Transport and Heat Transfer in Fractured Rock

Yu-Shu Wu
Lawence Berkeley National Laboratory
Berkeley, CA

Introduction

Flow and transport through fractured porous media occurs in many subsurface systems and has received considerable attention in recent years due to the importance in the areas of underground natural resource recovery, waste storage, and environmental remediation scheme. Among the methods of handling fracture/matrix flow and transport through geological media, the effective continuum method (ECM) has been widely used, and misused in some cases, because of its simplicity in terms of data requirements and computational efficiency.

This paper presents a rigorous, generalized effective continuum formulation, which has been implemented into the TOUGH2 code (Pruess, 1991) for modeling multiphase, multicomponent, non-isothermal flow and transport in fractured rocks. Also included in the paper are discussions of the conditions under which the ECM approach applies and the procedures for evaluating the effective parameters for both flow and transport simulations. Three application examples, one multiphase flow, one heat flow and one chemical transport problem, are given to demonstrate the usefulness of the ECM method.

Formulation

In concept, the effective continuum approach uses an "effective" porous medium to approximate a fractured/matrix system, and calculations for flow and transport are then simplified and performed by a single-porosity continuum approach with a set of "effective" parameters. The ECM relies on a critical assumption that there is approximate thermodynamic equilibrium (locally) between fracture and matrix at all times in the formation. It requires that temperatures, phase pressures, densities and viscosities, enthalpies, and component concentrations in fracture and matrix systems are the same locally at any location of the formation. Therefore, governing equations for component mass and energy conservation can be much simplified by adding the fluxes of mass and heat through fracture and matrix, respectively. This results in a set of partial differential equations in the ECM formulation for flow and transport in fractured media, which may be written in the same forms as those for a single continuum medium. For compositional transport equation of each of species κ:

$$\frac{\partial}{\partial t}\left\{\phi\sum_{\beta}\left(\rho_\beta S_\beta X_\beta^\kappa\right)+(1-\phi)\,\rho_s\,\rho_w\,X_w^\kappa\,K_d^\kappa\right\}+\lambda_\kappa\left\{\phi\sum_{\beta}\left(\rho_\beta S_\beta X_\beta^\kappa\right)+(1-\phi)\,\rho_s\,\rho_w\,X_w^\kappa\,K_d^\kappa\right\}$$
$$=-\sum_{\beta}\nabla\bullet\left(\rho_\beta\,X_\beta^\kappa\,\overset{\rho}{V}_\beta\right)+\sum_{\beta}\nabla\bullet\left(\rho_\beta\,\underline{D}^\kappa\bullet\nabla X_\beta^\kappa\right)+q^\kappa \qquad (1)$$

where β is an index for fluid phase [β = 1, ..., NP (total number of phases)]); κ is an index for components [κ = 1, 2, ..., NK (total number of components)]; and the rest of symbols are defined below. The left hand of side of Equation (1) consists of (a) an accumulation term of component mass summed over all dissolved phases and adsorption on rock solids, and (b) a first order decay term. The right hand of side of (1) is (a) an advection term contributed by all flowing phases; (b) diffusive and dispersive terms within all phases; and (c) a source/sink term. The energy conservation equation is

$$\frac{\partial}{\partial t}\left\{\sum_{\beta}\left(\phi\,\rho_{\beta}S_{\beta}U_{\beta}\right)+\left(1-\phi\right)\rho_{s}U_{s}\right\}=-\sum_{\beta}\nabla\bullet\left(h_{\beta}\rho_{\beta}\vec{v}_{\beta}\right)$$
$$+\sum_{\beta}\sum_{\kappa}\nabla\bullet\left(\rho_{\beta}h_{\beta}^{\kappa}\underline{D}^{\kappa}\bullet\nabla X_{\beta}^{\kappa}\right)+\nabla\bullet\left(K_{th}\nabla T\right)+q^{E} \tag{2}$$

Similarly, the left hand of side of Equation (2) is an energy accumulation term of summation over all phases and solids, and the right hand of side contains (a) a heat advection term contributed by all flowing phases; (b) diffusive and dispersive heat transfer term within all phases; (c) a heat conduction term; and (d) a source/sink term.

Equations (1) and (2) contain many "effective" parameters and constitutive correlations needed for the ECM approach, and are defined here. ϕ is effective porosity, defined as

$$\phi=\phi_{f}+\phi_{m} \tag{3}$$

with ϕ_f and ϕ_m being porosities of fracture and matrix continua, respectively; S_β is effective saturation of fluid β, defined as,

$$S_{\beta}=\frac{S_{\beta,f}\phi_{f}+S_{\beta,m}\phi_{m}}{\phi_{f}+\phi_{m}} \tag{4}$$

where $S_{\beta,f}$ and $S_{\beta,m}$ are saturation of fluid β, in fracture and matrix continua, respectively; X_β^κ is mass fraction of component κ in fluid β; K_d^κ is effective distribution coefficient of component κ between the water phase and rock solids of fracture and matrix, defined as,

$$K_{d}^{\kappa}=\frac{A_{s}K_{d}^{f}+(1-\phi_{m}-\phi_{f})K_{d}^{m}}{1-\phi} \tag{5}$$

where A_s is the ratio of fracture surface areas to a bulk rock (fracture + matrix) volume, representing total fracture surface areas per unit volume of rock; K_d^f and K_d^m are distribution coefficients of component κ between the water phase and rock solids of fracture and matrix continua, respectively; $\vec{v}_\beta$ is the effective Darcy velocity of fluid β, defined as,

$$\vec{v}_\beta = -\frac{k\,k_\beta}{\mu_\beta}\left(\nabla P_\beta - \rho_\beta \vec{g}\right) \tag{6}$$

where P_β, μ_β and $\vec{g}$ are pressure and viscosity of fluid β, and gravity vector, respectively; k is effective continuum permeability, defined as,

$$k = k_f + k_m \tag{7}$$

with k_f and k_m are absolute permeabilities of fracture and matrix continua, respectively; and the effective relative permeability to fluid phase β, k_β, is defined as,

$$k_\beta = \frac{k_f\, k_{\beta,f} + k_m\, k_{\beta,m}}{k_f + k_m} \tag{8}$$

$\underline{D}^\kappa$ is the combined fracture/matrix, diffusion-dispersion tensor accounting for both molecular diffusion and hydrodynamic dispersion for component κ, weighted by total porosity,

$$\underline{D}^\kappa = \frac{\phi_f\, \underline{D}_f^\kappa + \phi_m\, \underline{D}_m^\kappa}{\phi_f + \phi_m} \tag{9}$$

where the fracture diffusion-dispersion tensor is,

$$\underline{D}_f^\kappa = \left(\alpha_{T,f}\left|\vec{v}_{\beta,f}\right|\right)\delta_{ij} + \left(\alpha_{L,f} - \alpha_{T,f}\right)\vec{v}_{\beta,f}\,\vec{v}_{\beta,f} / \left|\vec{v}_{\beta,f}\right| + \left(\phi_f\, S_{\beta,f}\tau_f\, d_f\right)\delta_{ij} \tag{10}$$

and the matrix diffusion-dispersion tensor is,

$$\underline{D}_m^\kappa = \left(\alpha_{T,m}\left|\vec{v}_{\beta,m}\right|\right)\delta_{ij} + \left(\alpha_{L,m} - \alpha_{T,m}\right)\vec{v}_{\beta,m}\,\vec{v}_{\beta,m} / \left|\vec{v}_{\beta,m}\right| + \left(\phi_m\, S_{\beta,m}\tau_m\, d_m\right)\delta_{ij} \tag{11}$$

where $\alpha_{T,f}$, $\alpha_{L,f}$, $\alpha_{T,m}$ and $\alpha_{L,m}$ are the transverse and longitudinal dispersivities, respectively, for fracture and matrix continua; τ_f and τ_m is tortuosities of fracture and matrix continua, respectively; d_f and d_m is the molecular diffusion coefficients in phase β of fracture and matrix continua, respectively; $\vec{v}_{\beta,f}$ and $\vec{v}_{\beta,m}$ are Darcy's velocities of fluid β of fracture and matrix continua, respectively; and δ_{ij} is the Kroneker delta function. (δ_{ij}=1 for i = j, and δ_{ij}=0 for i $\neq$ j).

In (2), K_{th} is effective thermal conductivity, defined as,

$$K_{th} = \frac{\phi_f K_{th,f} + \phi_m K_{th,m}}{\phi_f + \phi_m} \tag{12}$$

where $K_{,th,f}$ and $K_{th,m}$ are the thermal conductivities of fracture and matrix continua, respectively.

In solving the governing equations (1) and (2) with the ECM approach, the primary variables selected in a numerical solution are normally fluid pressures, P_β, effective saturations, S_β, temperature, T, and mass fraction, X_β^κ. Once the primary variables are chosen, all the secondary variables must be evaluated using the primary variables, effective parameters and correlations to set up a set of solvable numerical equations. Many rock and fluid properties, such as porosities, absolute permeability, dispersitities, thermal conductivities, totuosities, and diffusion coefficients of fracture and matrix continua, fluid viscosities and densities, should be determined from site-characterization studies.

The numerical implementation of the ECM scheme for evaluating the effective constitutive relations is straightforward once we know fluid saturations in matrix and fracture, separately. This can be achieved by introducing a fracture/matrix combined (or composite) capillary pressure curve (using tabulated values, based on the individual fracture and matrix P_c curves from the input data for a given rock type), as discussed by Wu et al. (1996).

Verification and Application

The ECM formulation of Section 2 has been implemented into the TOUGH2 code, a multiphase, multicomponent, nonisothermal reservoir simulator (Pruess, 1991). It includes (a) the EOS3 and EOS4 modules for two-phase (water and gas), two components (water and air) and heat; (b) the EOS9 module for two-phase, isothermal flow by solving Richards' equation; and (c) the EOS1G module for single gas flow in a two-phase condition with aqueous phase as a passive phase (Wu et al., 1996a). In addition, a two-phase, three-component and non-isothermal version is implemented into a solute transport code, T2R3D (Wu and Pruess, 1998).

Because of computational efficiency and simplicity in data requirement with the ECM method, the implemented modules of the TOUGH2 code and the T2R3D code have found a wide range of applications in field characterization studies at the Yucca Mountain site, a potential underground repository for high-level radionuclide wastes (Wu et al., 1998). During these applications, several comparative and validation studies have also been carried out to investigate the accuracy and applicability of the ECM approach to field problems. These studies conclude that the ECM concept is adequate to modeling steady-state moisture and ambient heat flow, and transient gas flow in fractured unsaturated zones of Yucca Mountain, as long as there are strong fracture-matrix interactions in the system. However, the ECM approximation will introduce larger errors for the cases where a strong non-equilibrium condition exists between fracture and matrix systems, such as within fast flow pathways along high-permeability flow channels.

Summary

This paper presents a rigorous derivation of the generalized ECM formulation and defines a complete set of the effective ECM parameters for modeling multiphase flow, multicomponent transport, and heat transfer in fractured rocks. Also included are the discussions on implementation of the ECM formulation into a multidimensional, multiphase flow and transport reservoir simulators. In addition, three examples are provided for examining the ECM approach.

References

Pruess K. 1991. *TOUGH2—A General Purpose Numerical Simulator for Multiphase Fluid and Heat Flow.* Report LBL-29400, UC-251. Berkeley, California: Lawrence Berkeley National Laboratory.

Wu, Y. S and K. Pruess, *A 3-D Hydrodynamic Dispersion Model for Modeling Tracer Transport in Geothermal Reservoirs*, Proceedings of the Twenty-third Workshop, Geothermal Reservoir Engineering, Stanford University, CA, 139-146, 1998.

Wu, Y.S., Ritcey, A.C., Ahlers, C.F., Hinds, J.J., Mishra, A.K.. Haukwa, C., Liu, H.H., Sonnenthal, E.L., and Bodvarsson, G.S., *3-D UZ Site-Scale Model for Abstraction in TSPA-VA.* Yucca Mountain Project Level 4 Milestone Report SLX01LB3. Berkeley, California: Lawrence Berkeley National Laboratory, 1998.

Wu, Y. S., C. F. Ahlers, P. Fraser, A. Simmons, and K. Pruess, Software qualification of selected TOUGH2 modules, Report LBNL-39490, Lawrence Berkeley National Laboratory, Berkeley, CA, 1996.

SGILD Modeling and Inversion for Single Phase Flow

Ganquan Xie, Jianhua Li, and Paul Witherpon
Earth Sciences Division, Lawrence Berkeley National Laboratory

Abstract

In this paper, a Stochastic Global Integral and Local Differential (SGILD) equation modeling and inversion for single phase flow is presented. We derived new single phase flow integral equations and differential equations for statistical moments of the conductivity and head field. The new statistical moments integral equation on the boundary and local differential equations in domain will be used together to obtain mean head field and its moments in the modeling. The new moments global Jacobian volume integral equation and the local Jacobian differential equations in domain will be used together to update the mean hydraulic conductivity parameter and their moments in the inversion. A new parallel multiple hierarchy substructure direct algorithm or direct-iteration hybrid algorithm will be used to solve the sparse matrices and one smaller full matrix from domain to the boundary, in parallel. The SGILD modeling and imaging algorithm has many advantages over the conventional imaging approaches. The SGILD algorithm can be extended for a coupled stochastic seismic, electromagnetic, and flow modeling and inversion. Synthetic data tests show that SGILD imaging is fast, robust, and high resolution.

Introduction

Hydrology modeling and inversion are important for the prediction of nuclear waste, environment contamination, geothermal energy reservoirs and oil geophysical exploration. Many imaging works in the geophysical research areas are developed in the deterministic frame. Because the data is incomplete and contaminated by noise, it is reasonable to study inverse and forward problem in the probability frame and to use stochastic approaches.

In this paper, we developed a new parallel SGILD modeling and inversion using a stochastic global integral and local differential decomposition. The parameters and data are assumed to be random variables. We derived a new flow stochastic moments integral and differential equation system. A parallel SGILD algorithm is used to solve the equations. The second order correction term can be used to improve the resolution of the mean hydraulic conductivity imaging. The parameter covariance and standard deviations can be used to estimate the uncertainty and construct a confidence intervals for hydraulic conductivity.

The new SGILD inversion method consists of five parts (see Xie et al. 1997): (1) The domain is decomposed into subdomain SI and subdomain SII. (2) A new statistical moments global flow integral equation on the boundary and local differential equations in domain will be used together to obtain mean head field and moment fields in the modeling step. (3) The new moments global Jacobian volume integral equation in SI and the local Jacobian differential equations in SII will be used together to update the mean conductivity parameters and their moments from the random field data in the inversion step. (4) The subdomain SII can naturally be decomposed into 4^n smaller sub-cubic-domains; the sparse matrix in each sub-cubic-domain can be inverted separately, in parallel. (5) A new parallel multiple hierarchy substructure direct and direct-iteration hybrid algorithms will

This work was supported partially by the ER and BES of DOE. Authors would like to thank Dr. Sally Benson, Dr. Ernest Majer and Dr. Ki Ha Lee for their help and encouragement.

be used to solve the smaller full matrix in SI from domain to the boundary, recursively and in parallel.

The limitations of the conventional nonlinear inversion are: (1) the inaccurate reflection error of the absorption boundary condition enters the inversion domain as numerical noise, in particularly, the ill-posed property of the inversion will enhance the numerical noise that will cause divergence and low resolution; (2) the discrete integral equation in part II produces an ill-posed large full matrix which is difficult or impossible to invert and to store; (3) the CG iteration easily falls into a local minimum and gets a wrong or low resolution imaging.

The new SGILD parallel modeling and nonlinear inversion algorithm is designed to overcome the shortcomings of the conventional inversion. The advantages of the SGILD algorithm are:
(1) It reduces the numerical boundary noises and improves accuracy of the modeling and inversion; (2) It improves the ill-posed condition, and reduces computation time and storage requirements; (3) It is a high performance parallel multiple hierarchy algorithm with parallel efficiency of 90 %; (4) it minimized data communication between processors; (6) The moments of the parameters can be used to construct a confidence intervals of the parameters; (7) the SGILD parallel algorithm can be used to solve stochastic elliptic, parabolic, and hyperbolic modeling and inversion. A new SGILD flow head field, elastic wave, and electromagnetic field coupled geo-hydra modeling and inversion will be developed for prediction of oil, gas, coal, and geothermal energy reservoirs in geophysical exploration, atmosphere, and ocean sciences strategic simulation.

Stochastic flow equation for forward modeling

Flow equation

$$s(x)\frac{\partial h(x,t)}{\partial t} + \nabla \cdot F(x,t) = q(x,t),\ x \in \Omega, t > 0, \tag{1}$$

$$F(x,t) = -K(x)\nabla h(x,t),\ x \in \Omega,\ t > 0, \tag{2}$$

Initial condition

$$h(x,0) = H_0(x),\ x \in \Omega, \tag{3}$$

where F is flow flux, $s(x)$ is storage, $q(x,t)$ is source/sink function (due to recharge, pumping or injection; positive for source and negative for sink), $h(x,t) = \frac{p(x)}{\rho g} + z$ is hydraulic head ($p(x)$ is pressure, ρ fluid density, g gravitational acceleration factor, and z elevation), $K(x) = k(x)\frac{\rho g}{\mu}$ is hydraulic conductivity $k(x)$ is intrinsic or absolute permeability and μ is fluid viscosity).

Upon substituting the perturbation expansion ,$h = h_0 + h_1 + h_2 + \cdots$, into (1), we have the following forward moment Galerkin equations

$$\int_{\partial\Omega_e} < K > \frac{\partial h_0}{\partial n}\phi ds - \int_{\Omega_e} < K > \nabla h_0 \nabla \phi d\Omega - \frac{\partial}{\partial t}\int_{\Omega_e} S h_0 \phi d\Omega = \int_{\Omega_e} q\phi d\Omega, \tag{4}$$

$$FMG(< K >, C_{hk}, C_K, h_0, \phi) = \int_{\partial\Omega_e} < K > \frac{\partial C_{hk}(r,\Re)}{\partial n}\phi ds + \int_{\partial\Omega_e} C_K \frac{\partial h_0}{\partial n}\phi ds$$
$$-\int_{\Omega_e} < K > \nabla C_{hk}(r,\Re)\nabla\phi d\Omega - \int_{\Omega_e} C_K \nabla h_0 \nabla\phi d\Omega - \frac{\partial}{\partial t}\int_{\Omega_e} SC_{hk}\phi d\Omega = 0, \quad (5)$$

$FMG(< K >, C_h, C_{hk}, h_0, \phi) = 0$, and $FMG(< K >, < h_2 >, 1, \hat{C}_{hK}, \phi) = 0$. Where the Forward Moment Galerkin operation, *FMG*, is defined by (5), $< K >$ is the mean of the hydraulic conductivity, $< h_0 >= h_0$, $< h_1 >= 0$, covariance $C_K(r,\Re) =< K_s(r)K_s(\Re) >$, $C_h(r,\Re) =< h_1(r)h_1(\Re) >$, $C_{hK}(r,\Re) =< h_1(r)K_s(\Re) >$ which is cross covariance between head field and hydraulic conductivity, $\hat{C}_{hK} = \{C_{hK}\}|_{r=\Re}$, ϕ is a basic testing function, Ω_e is a compact set of the basic testing function ϕ.

Stochastic flow equations for nonlinear inversion

In this section, we describe the new stochastic acoustic volume integral equations and differential equations for nonlinear inversion.

$$h_d(r) = h_b(r) + \int_{V_s} (K - K_b)\nabla G_b(r', r) *_t \nabla h(r')dr', \quad (6)$$

Because measured data h_d, and hydaulic conductivity, K are assumed to be random variables, equation (6) becomes a stochastic first type nonlinear integral equation.
Substituting the expanding formulas,

$$\delta h_d(r) =< \delta h_d(r) > + \delta h_{d,s}(r),\ h =< h > + h_s,\ and\ \delta K = \delta K_0 + \delta K_1 + \delta K_2 + \ldots\ .$$

into (6), we have

$$< \delta h_d(r) >= \int_{V_s} \delta K_0 \nabla G_b(r', r) *_t \nabla < h > (r')dr', \quad (7)$$

$$IMI(< h >, C_{\delta h_d}, C_{\delta Kh}, C_h, \delta K_0) = C_{\delta h_d}$$
$$-\int_{V_s} C_{\delta Kh}\nabla G_b(r', r) *_t \nabla < h > (r')dr' \quad (8)$$
$$+\int_{V_s} \delta K_0 \nabla G_b(r', r) *_t \nabla C_h(r')dr' = 0,$$

$IMI(< h >, C_{\delta h_d \delta K}, C_{\delta K}, C_{\delta Kh}, \delta K_0) = 0$, and $IMI(< h >, 0, < \delta K_2 >, 1, \hat{C}_{\delta Kh}) = 0$. *IMI* means the inverse moment integral equation which is defined by (8), $< K_0 >= K_0$, $< K_1 >= 0$, $< h_s >= 0, C_{\delta h_d} =< \delta h_d(r)\delta h_d(\Re) >$, $C_{\delta Kh} =< \delta K_1(r)h_s(\Re) >, C_h =< h_s(r)h_s(\Re) >$, $C_{\delta h_d \delta K} =< \delta h_d(r)\delta K_1(\Re) >$, $C_{\delta K} =< \delta K_1(r)\delta K_1(\Re) >$, and $\hat{C}_{\delta Kh} = C_{\delta Kh}|_{\Re=r}$.

Because (6)-(8) are ill-posed integral equations, they can not be solved directly. We translate the inversion to the following posterior probability optimization.

$$P(K|h_d) = \max. \tag{9}$$

By Bayes theorem, the posterior probability optimization (9) can be translated into the following stochastic nonlinear regularizing optimization,

$$\|(h - h_d)\|_W^{\ 2} + \alpha_K R(K) = \min, \tag{10}$$

The α_K is a regularizing parameter which is depended on the confidence intervals of the random hydraulic conductivity and data set.

Parallel SGILD modeling and inversion algorithm

A new parallel stochastic global integral and local differential decomposition algorithm, SGILD, for the modeling and inversion is presented in this section. The SGILD algorithm is developed to overcome these limitations of the conventional nonlinear inversion. For simplicity, we used a rectangular mesh for modeling and inversion. The unknown head field and its moments are defined on the set of the nodes for modeling. The unknown conductivity parameters and their moments are defined on the set of the cells for inversion. The new SGILD modeling and inversion method consists of three steps: First, in Figure 1, the domain is decomposed into a subdomain SI with white cells □ and a subdomain SII with dark ■ cells. This decomposition is called a cells decomposition. The cells-decomposition induced a nodes-decomposition of the whole nodes of the domain, NSI and NSII. The subdomain NSI is the set of the boundary solid square nodes and internal solid bullet nodes •. The subdomain NSII is the set of the internal circle nodes o. Second, suppose that the mean conductivity K and the covariance are obtained by the previous iterative step, the discrete integral equation on the boundary nodes and the discrete Galerkin differential equations (4) and (5) on the internal nodes of domain will be coupled to construct a closed equation system for the discrete moments of head field. The nodes-decomposition and multi-level parallel direct or direct-iteration hybrid methods can be used for solving the modeling equations. Third, after obtaining the wave field and its moments, the global discrete Jacobian volume integral equations (7) and (8) with a strong regularizing on cells of SI and the local discrete Jacobian differential equations with a weaker regularizing on cells of SII will be coupled to construct a complete equation system for updating the conductivity. The cells-decomposition can be used for solving the equation system for updating parameters and their moments. The second step and third step are used to construct a loop of the parallel SGILD Gauss-Newton regularizing iteration. The new global integral and local differential parallel inversion has been tested in the multiple processor of the Special Parallel Processing (SPP) in the CRAY-A.NERSC.GOV and the Massively Parallel computer T3D. The parallel effective rate is 80% to 96%. The detailed description of the new parallel SGILD modeling and inversion algorithm is presented in our Lawrence Berkeley National Laboratory technology reports LBNL-42105 and 42106 and papers (Xie et al. 1998a). In the SGILD inversion, the strong Tikhonov regularizing method on SI and the weaker regularizing approach on SII will be combined to obtain a high resolution imaging. The SGILD modeling and inversion is very useful for large scale and multiple scope strategic simulations in the Earth, Ocean, and Atmosphere sciences.

Applications

The SGILD algorithm can be used for the hydraulic conductivity, electric conductivity, and seismic velocity imaging, A axis symmetry SGILD conductivity code is tested primarily using a synthetic data. The mean conductivity imaging and standard deviations are presented. In Figure 1, 18 point injection sources are located in the single hole. The 72 points receivers are located in the same hole. One and two months head response synthetic data with Gaussian noise, the maximum standard deviation of data is 5%.

The imaging of the mean conductivity is obtained (see Figure 1c). The total maximum standard deviation (TSTD) of the conductivity is 11.8%, The local standard deviation (LSTD) of the conductivity of the target in left side corner is 6%. The other local standard deviation of conductivity in right side is 18.6%, that is because the left side is near area of the data site in single hole. The 2D mesh is 148 x 128, 16 x 18 CPU minutes in MPP and 68 iterations are used to obtained these moments imaging. The optimization mean regularizing parameter is 0.687456E10-6. A acoustic, electromagnetic and flow head data coupled inversion is used to obtain conductivity imaging as shown in Figure 1b. It is obvious that the conductivity imaging from the coupled inversion has higher resolution than single inversion imaging in Figure 1c. other SGILD resistivity imaging from practical field data in the geothermal exploration is presented in Xie. t al. 1998d, The maximum standard deviation of the field data is 21%. A reasonable mean resistivity imaging is obtained. The maximum standard deviation of the resistivity is 31.8%, The local standard deviation of resistivity near the borehole area is 19%, which is less than standard deviation of the field data.

Conclusions

The primary tests show that the SGILD modeling and inversion is a high resolution, robust stable, and high performance parallel imaging algorithm. There are obvious improvements of resolution of imaging from the field data. Actually, most of the conventional deterministic inversion approaches were only used to obtain the zero order mean of the target parameters, but no the second order correction term and standard deviation term. The SGILD algorithm can be used to obtain the improved ensemble mean parameter with the second correction term, cross covariance between the parameter and field, and standard deviations of the parameters and field. These moments can be used to estimate the uncertainty and construct confidence intervals. The computational costs and storage of the stochastic modeling and inversion is 3~4 times the deterministic inversion. The big cost can not be accepted in the workstation. The high performance SGILD algorithm overcomes the limitations.

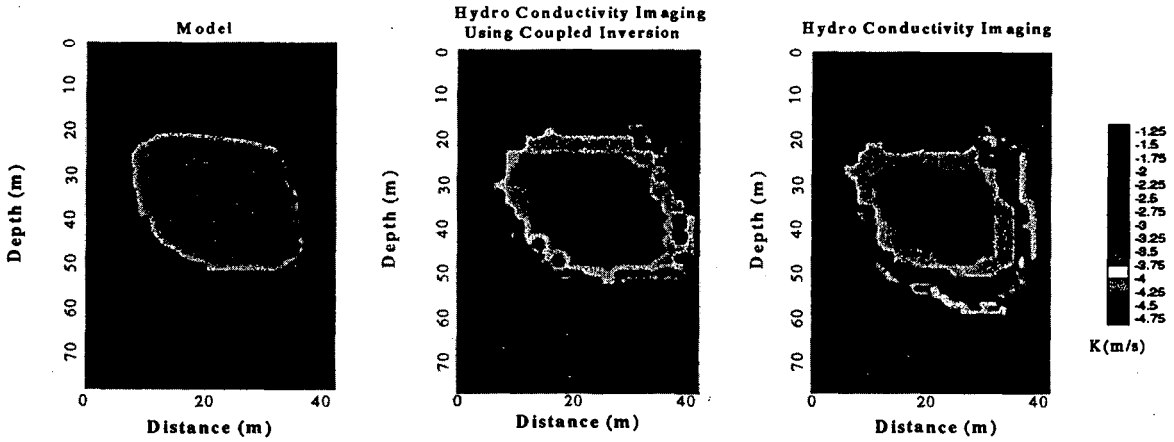

(a) (b) (c)

References

Ganquan Xie and Jianhua Li, 1998a, New 3D parallel GILD modeling and nonlinear inversion. Iterative Methods in Scientific Computation, IMACS Series book in Comput. and Applied Math., vol. 4, 135-140.

Ganquan Xie, Jianhua Li, Ernest Majer, and D. Zou, 1998b, New 3D parallel GILD electromagnetic modeling and nonlinear inversion using global integral and local differential equation. LBNL-42105.

Ganquan Xie, Jianhua Li, and Ernest Majer, 1998c, New SGILD modeling and inversion, LBNL-42252.

Ganquan Xie, Jianhua Li, and Ernest Majer, 1998d, New parallel SGILD modeling and nonlinear inversion for geophysical and hydrological coupled high resolution imaging. Proceedings of the 4th International SEG/Japan Symposium in Tokyo. 253-259.

Reactive chemical transport in fractured rock: Supergene copper enrichment

Tianfu Xu[1] (email: Tianfu_Xu@lbl.gov), Karsten Pruess[1] and George Brimhall[2]

[1] Earth Sciences Division, Lawrence Berkeley National Laboratory, University of California, Berkeley, CA 94720.
[2] Department of Geology and Geophysics, University of California at Berkeley.

1. Introduction

Supergene enrichment involves the oxidative weathering of sulfide minerals and acidification that causes mobilization of metals in the unsaturated zone, with subsequent formation of enriched deposits in the reducing conditions below the water table. Supergene copper enrichment mostly took place in geologic media with both fracture and matrix permeability [*Ague and Brimhall*, 1989] such as El Salvador, Chile. The method of "multiple interacting continua" [MINC; *Pruess and Narasimhan*, 1985] was employed to resolve "global" flow and transport of aqueous chemicals and oxygen gas in fractured rock systems, and its interaction with "local" exchange between fracture and matrix rock. We first consider the supergene copper enrichment in a one-dimensional unsaturated-saturated porous medium flow, and then present the case in a fractured rock system. Simulations were carried out using the TOUGHREACT multiphase reactive transport model [*Xu et al.*, 1998]. Results indicate that geochemical behavior and supergene enrichment patterns in fractured media are different from those in porous media. Physical heterogeneity (permeability contrast between fracture and matrix) results in heterogeneous distribution of secondary ore deposits. The chemical changes and secondary mineral assemblages predicted by our model are consistent with observations in supergene copper deposits in the Atacama Desert, Northern Chile [*Ague and Brimhall*, 1989]. The interaction between flow in fracture and matrix rock is effectively simulated using the MINC model. This problem has broad significance for geoscientific, engineering, and environmental applications.

2. One-dimensional porous medium

A schematic representation of the model system is shown in Figure 1. Oxygen is supplied to a protore containing pyrite and chalcopyrite (Table 1) as a dissolved species in infiltrating rainwaters, as well as by gaseous diffusion from the land surface boundary.

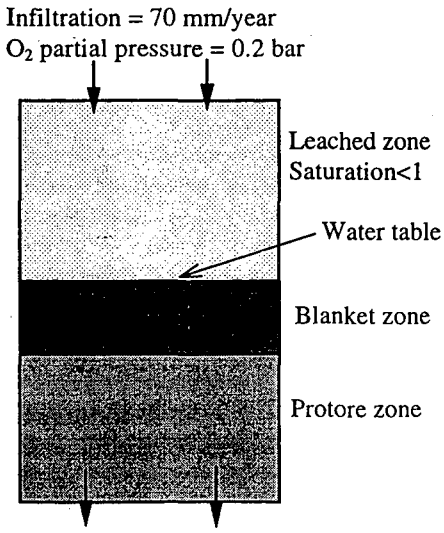

Figure 1. Schematic representation of a one-dimensional supergene copper enrichment system. A vertical column of 20 m thickness was used. The top 10 m represent the unsaturated zone, while the bottom 10 m represent the water saturated zone. A steady-state water flow regime is assumed throughout. A gaseous diffusion coefficient of 4.38×10^{-5} m^2s^{-1} and a tortuosity of 0.1 were used.

The column is initially filled entirely with a protore mineral assemblage as listed in Table 1. The dissolution of the protore minerals is kinetically controlled. The kinetic parameters used are listed in Table 1. Oxygen is treated as ideal gas, its interaction with the aqueous solution is assumed at local equilibrium. The precipitation of secondary minerals, Covellite, Chalcocite, Bornite, Goethite, Hematite, Kaolinite, Alunite, and Amorphous silica, during the simulation progress is modeled as instantaneous. A dilute oxidizing water in equilibrium with an oxygen partial pressure of 0.2 bar is initially placed in the unsaturated grid blocks, while a reducing water with a partial oxygen pressure of 1.0×10^{-70} bar is assumed for the remaining (saturated) grid blocks. The infiltration water composition is the same as the initial unsaturated water. A total of 52 aqueous species is considered.

Table 1. Chemical properties of protore mineral reactants. Volume fraction, rate constant and specific surface area are based on *Ague and Brimhall* [1989].

Mineral	Volume fraction (%)	Abundance (mol/dm^3 medium)	Rate constant ($mol/cm^2/s$)	Surface area (cm^2/dm^3 medium)
Pyrite	9.0	3.76	4.0×10^{-15}	586.7
Chalcopyrite	4.5	1.05	4.0×10^{-15}	586.7
Magnetite	4.5	1.01	2.0×10^{-15}	586.7
K-feldspar	18.0	1.65	3.1×10^{-16}	5866.7
Albite	9.0	0.9	3.1×10^{-16}	6981.3
Anorthite	9.0	0.89	1.5×10^{-16}	2992.0
Annite	4.5	0.29	2.4×10^{-18}	2933.3
Muscovite	9.0	0.64	2.4×10^{-18}	1760.0
Quartz	18.0	7.93	4.3×10^{-18}	6160.0
Anhydrite	4.5	0.98	1.5×10^{-16}	586.7
	Total=90			
	Void=10			

Results from the TOUGHREACT simulation are presented in Figure 2. In the unsaturated zone, pyrite and chalcopyrite are oxidized and dissolved (Figure 2a):

$$FeS_2\ (pyrite) + H_2O + 3.5O_2(aq) \rightarrow 2SO_4^{--} + Fe^{++} + 2H^+$$

$$CuFeS_2\ (chalcopyrite) + 4O_2(aq) \rightarrow 2SO_4^{--} + Fe^{++} + Cu^{++}$$

As aqueous phase oxygen is depleted through reaction with pyrite and chalcopyrite, it is replenished by dissolution from the gas phase, and by diffusive transport from the atmospheric boundary at the land surface. The pH decreases downward, and the total dissolved Cu and S concentrations increase due to pyrite and chalcopyrite oxidation. When the aqueous solution reaches the reducing saturated zone, the secondary copper bearing minerals chalcocite and covellite are precipitated (Figure 2b),

$$Cu^{++} + HS^- \rightarrow CuS\ (chalcocite) + H^+$$

$$2Cu^+ + HS^- \rightarrow Cu_2S\ (covellite) + H^+$$

forming the enrichment blanket immediately below the water table [*Ague and Brimhall*, 1989]. In addition, goethite precipitates in the unsaturated zone. At the same time magnetite, K-feldspar, albite, anorthite, annite and muscovite dissolve throughout the column due to decrease of pH. Further details are given in *Xu et al.* [1998].

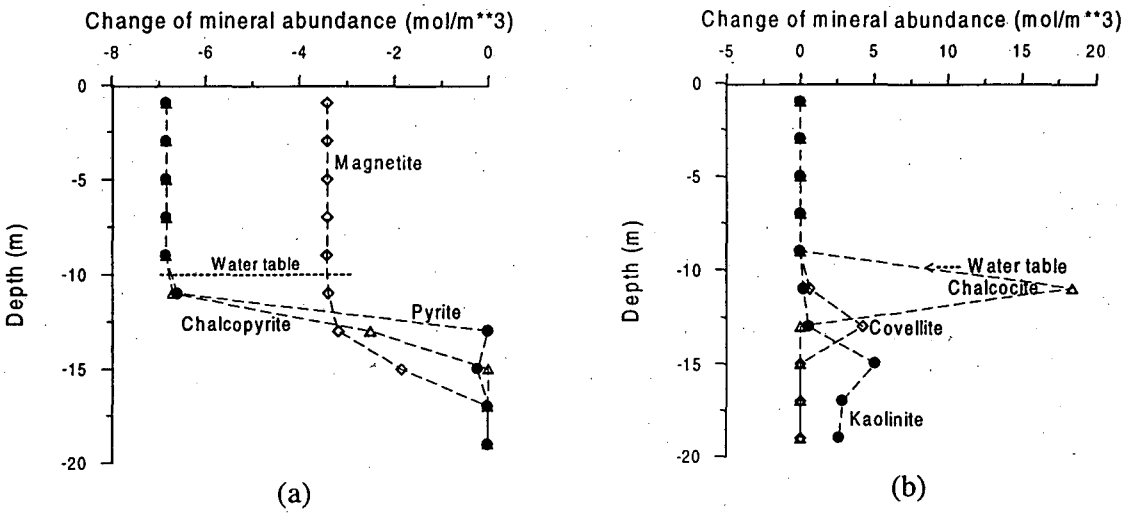

Figure 2. Change of mineral abundance (in moles per cubic meter medium) after 90 years. Negative values indicate dissolution, positive indicate precipitation.

3. Two-dimensional fractured rock

The MINC method [*Pruess and Narasimhan*, 1985] was employed for the fractured rock system. The resolution of fracture and matrix interaction is achieved by appropriate subgridding, as shown in Figure 3. The concept is based on the notion that changes in fluid pressures and chemical concentrations will propagate rapidly through the fracture system, while invading the tight matrix blocks only slowly. Therefore, changes in matrix conditions will (locally) be controlled by the distance from the fractures, and can then be modeled by means of one-dimensional strings of nested grid blocks.

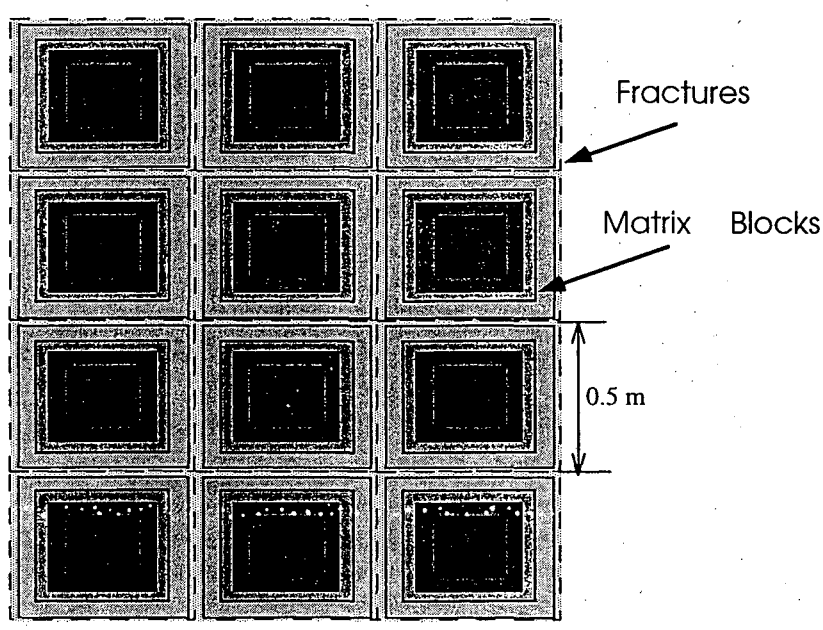

Figure 3. Subgridding in the method of "multiple interacting continua" (MINC). The figure represents an areal view of rock matrix columns that are separated by vertical fractures.

An idealized fractured porous medium with a set of equidistant, and vertical fracture zones was used (overview is given in Figure 3; for general, any fracture geometry can be considered by the MINC model). Because of symmetry only one column of matrix blocks, with a fracture spacing of 0.5 m and a depth of 20 m, needs to be modeled. The same rainwater infiltration rate as for the previous porous medium problem was used; all infiltration occurs in the fractures. Water pressure is held constant at 2 bar at the bottom and the water table is located at a depth of 10 m. The steady state water saturations obtained by ignoring chemical reactions are used as initial conditions for the calculation of reactive chemical transport. Parameters for the fracture and matrix are listed in Table 2. The other conditions are unchanged from the previous porous medium simulation.

Table 2 Parameters used for supergene copper enrichment in the fractured porous medium.

Parameter	Matrix	Fracture
Permeability (m^2)	10^{-16}	10^{-12}
Fracture domain volume fraction, v *		0.01
Porosity	0.08	0.5**
Relative permeability and capillary Pressure (van Genuchten, 1980):		
λ	0.457	0.457
S_{lr}	0.1	0.05
S_{ls}	1.0	1.0
P_0(pa)	2.17×10^5	6.2×10^3

* $v = V_f/(V_f + V_m)$ where V_f and V_m are fracture and matrix domain volumes.
** Fracture domain is defined to include 50% by volume of wall rock.

The tight rock matrix is almost water saturated, and oxygen access is impeded. Pyrite and chalcopyrite oxidative dissolution takes place mostly in close proximity to the unsaturated fracture zone (see Figure 4). Away from the fracture zones, dissolution rates decrease. Chalcocite precipitation occurs mainly in the matrix just above the water table, and also in the deep fracture far below the water table (see Figure 5a). A minor amount of covelite precipitates in the deep fracture (see Figure 5b). The pattern of precipitation is different from the previous porous medium system. In the saturated zone, most water flow is passed through the fracture. The flux is much higher than in the previous case, so much more aqueous oxygen is available in the fracture and the oxidizing zone is extended deeply.

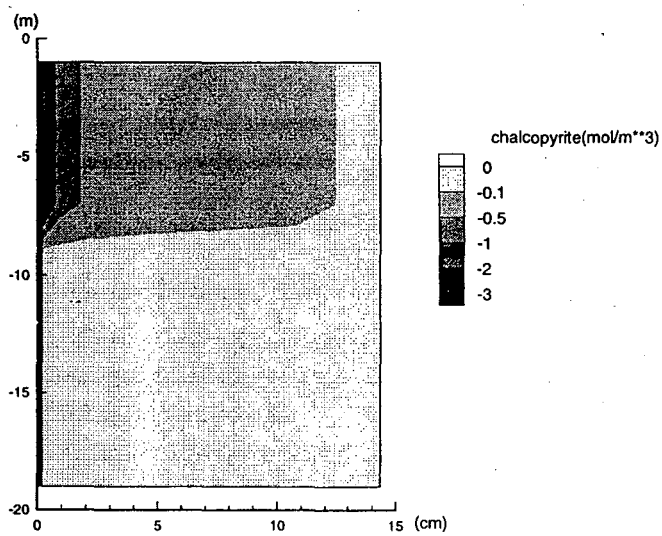

Figure 4. Change of chalcopyrite abundance (in moles per cubic meter medium) after 100 years.

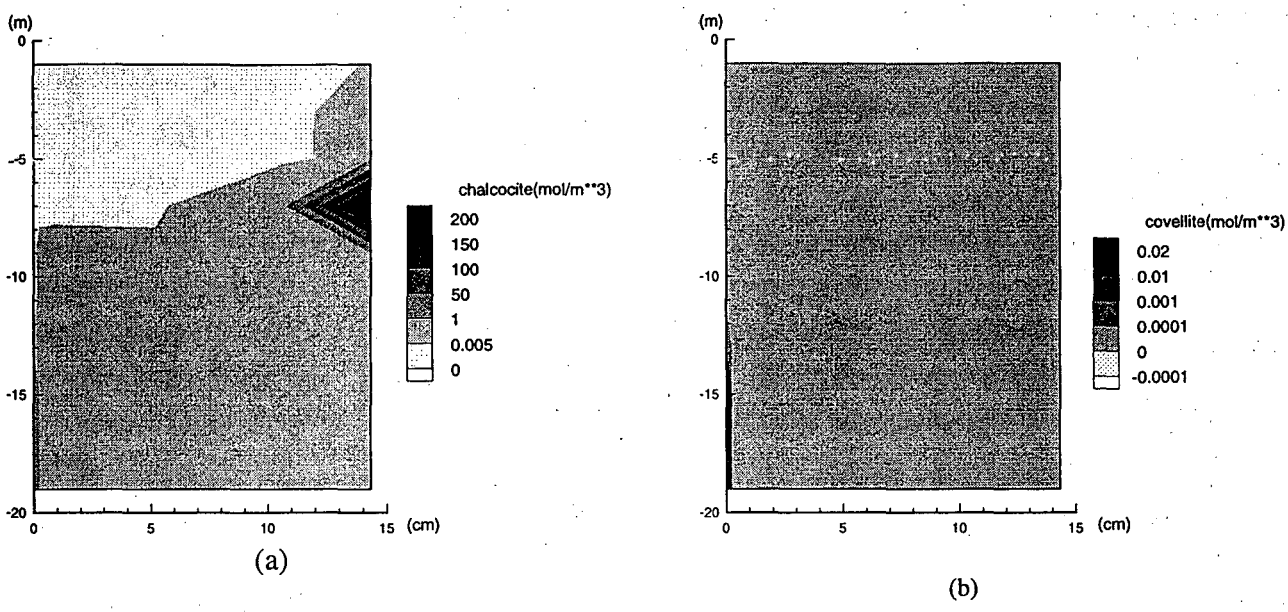

Figure 5. Change of chalcocite and covellite abundance after 100 years.

4. Conclusions

Pyrite and chalcopyrite oxidative dissolution takes place mostly in close proximity to the unsaturated fracture zone. Chalcocite precipitation occurs mainly in the matrix just above the water table, and also in the deep fracture far below the water table. Geochemical behavior and supergene enrichment patterns in fractured media are different from those in porous media. Physical heterogeneity (permeability contrast between fracture and matrix) results in this heterogeneous distribution of secondary ore deposits. The chemical changes and secondary mineral assemblages predicted by our model are consistent with observations in supergene copper deposits in the Atacama Desert, Northern Chile [*Ague and Brimhall*, 1989]. The resolution for fracture and matrix interaction is effectively simulated using the MINC model. This problem serves as a prototype for oxidative weathering processes with broad significance for geoscientific, engineering, and environmental applications.

Reference

Ague, J. J., and G. H. Brimhall, Geochemical modeling of steady state and chemical reaction during supergene enrichment of porphyry copper deposits, *Econ. Geol.*, 84, 506-528, 1989.

Pruess, K., and T. N. Narasimhan, A practical method for modeling fluid and heat flow in fractured porous media, *Society of Petroleum Engineers Journal*, 25(1), 14-26, February, 1985

Van Genuchten, M. T., A closed-form equation for predicting the hydraulic conductivity of unsaturated soils, *Soil Sci. Soc. Am. J.*, 44(5), 892-898, 1980.

Xu, T., K. Pruess and G. Brimhall, An improved equilibrium-kinetics speciation algorithm for redox reaction in variably saturated flow system, Lawrence Berkeley National Laboratory Report LBNL-41789 (also submitted to *Computer & Geosciences*), Berkeley, California, 1998.

Stochastic Analysis of Groundwater Flow in Fractured Porous Media: A Double-Permeability Approach

Dongxiao Zhang[1] and Alexander Y. Sun[1,2]
[1]Los Alamos National Laboratory
Geoanalysis Group (EES-5), MS C306, Los Alamos, NM 87545

[2]Department of Civil & Environmental Engineering
University of California, Berkeley

Preferential movement of fluid and solutes is believed to exist in most natural porous media. Over the years, a lot of efforts have been contributed to modeling flow in fractured media from either theoretical or practical aspects. Fluid flow and solute transport in fractured porous media may be described by either explicitly or implicitly accounting for the fractures. Because the specific geometry and other characteristics of the fracture system are generally unknown, it is difficult, if not impossible, to explicitly model fractures or matrix blocks at the microscopic level for any practical purpose. Therefore, various models are developed in attempt to capture the effects of microscopic processes through macroscopic model parameters and idealized model structures. Among these, the most popular one is the "dual-porosity/double-permeability" model or "double-permeability" model for brevity [e.g., *Barenblatt et al.*, 1960; *Warren and Root*, 1963; *Long et al.*, 1982; *Moench*, 1984]. In this approach, the fractured media are represented by two completely overlapping continua, one representing the fractures and the other representing the porous matrix. The two continua are coupled through a source/sink term accounting for the mass exchange between the two pore systems. Here, we emphasize the phrase "double-permeability" to differentiate the model we use from those dual-porosity models that allow flow to occur in the fractured media only.

In previous studies, the coupled equations for flow and mass transport in fractured rocks are established and solved numerically by many authors [e.g., *Gerke and van Genuchten*, 1993 a, b, 1996; *Zimmerman et al.*, 1990; *Pruess and Wang*, 1987]. Most of these studies, however, are limited to characterizing the deterministic behaviors of the fractured porous media. In recognizing the heterogeneity associated with most natural porous media, we believe that flow and transport in a "dual-porosity" system, similar as that in a "sole-porosity" system, are subject to a certain degree of uncertainty. The uncertainties mainly stem from inadequacy and inaccuracy of the available information on input model parameters, such as measurements of the permeability of the fractured system. In the present paper, we cast the "double-permeability" model in a stochastic framework and use it to study transient flow in saturated fractured media. Our starting points are the following system of governing equations for the double-permeability media,

$$w_f(\mathbf{x})S_f \frac{fh_f(\mathbf{x},t)}{ft} = \quad ?[w_f(\mathbf{x})K_f(\mathbf{x}) \quad h_f(x,t)] - Q_w(\mathbf{x},t)] \tag{1}$$

$$w_m(\mathbf{x})S_m \frac{fh_m(\mathbf{x},t)}{ft} = \quad ?[w_m(\mathbf{x})K_m(\mathbf{x}) \quad h_m(x,t)] + Q_w(\mathbf{x},t)] \tag{2}$$

where the subscripts f and m represent fractures and matrix blocks, respectively, w_p, p = f or m, represents the relative volume fraction of each pore system, S_p is the specific storativity, h_p is the total head and K_p is the hydraulic conductivity of each pore system. Equation (1) and (2) are coupled by a water transfer term, Q_w, which is proportional to the head difference between the pore systems. In our analysis, the model input parameters K_p, w_p as well as the first-order transfer coefficient in Q_w are regarded as statistically stationary random functions. As a result, equation (1) and (2) become stochastic partial differential equations (SPDE) which cannot be solved exactly. Instead, we seek to characterize the stochastic system through a cascade of moment equations. Using first-order perturbation analysis, we derive the first (mean) and second (covariance) moment equations for the stochastic system. The mean equations are similar to the original equations. The system of covariance equations, however, is more complicated and includes more than 10 coupled PDEs. In our numerical illustration, we solve the equations in two-dimensional domain using the finite-difference method.

To our knowledge, our stochastic analysis of flow in double-permeability media is the first of this kind. The analysis presented in this study can aid better interpretation of the preferential flow phenomena and enhance prediction results for field experiments.

Reference

1. Barenblatt, G. I., Iu. P. Zheltov, and I. N. Kochina, Basic concepts in the theory of seepage of homogeneous liquids in fissured rocks, J. Appl. Math. Mech., 24, 1286-1303, 1960.
2. Warren, J. E., and P. J. Root, The behavior of naturally fractured reservoirs, Soc. Petrol. Eng. J., 3, 245-255, 1963.
3. Long, J. C. S., J. S. Remer, C. R. Wilson, and P. A. Witherspoon, Porous media equivalents for networks of discontinuous fractures, Water Resour. Res., 18, 645-658, 1982.
4. Moench, A. F., Double-porosity models for a fissured groundwater reservoir with fracture skin, Water Resour. Res., 20, 831-846, 1984.
5. Gerke, H. H. and van Genuchten, M. T., A dual-porosity model for simulating the preferential movement of water and solutes in structured porous media, Water Resour. Res., 29, 305-319, 1993a.
6. Gerke, H. H. and van Genuchten, M. T., Evaluation of a first-order water transfer term for variably-saturated dual-porosity models, Water Resour. Res., 29, 1225-1238, 1993b.
7. Gerke, H. H. and van Genuchten, M. T., Macroscopic representation of structural geometry for simulating water and solute movement in dual-porosity media, Advan. Water Res., 19, 343-357, 1996.
8. Zimmerman, R. W., Chen, G., Hadgu, T. and Bodvarsson, G. S., A numerical dual-porosity model with semi-analytical treatment of fracture/matrix flow, Water Resour. Res., 29, 2127-2137, 1993.
9. Pruess, K., and J. S. Y. Wang, Numerical modeling of isothermal and non-isothermal flow in unsaturated fractured rock – A review, in Flow and Transport Through Unsaturated Fractured Rock, Geophys. Monogr. Ser., vol. 42, edited by D. D. Evans and T. J. Nicholson, pp. 11-22, AGU, Washington, D. C., 1987.

Lanczos Algorithm for the Simulation of Groundwater Flow in Fractured Porous Media Using Dual-Porosity Approach

Keni Zhang and Allan D. Woodbury
Department of Civil and Geological Engineering, University of Manitoba, Winnipeg, Canada R3T 2N2

W. Scott Dunbar
Department of Mining and Mineral Process Engineering, University of British Columbia, Vancouver, Canada V6T 1Z4

The use of spatial discretization procedures based upon the finite element techniques is a popular numerical approach for groundwater flow modeling. The computational effort for this technique strongly depends on both the number of unknowns and the number of time steps required to obtain an accurate and stable solution. In this paper we develop a modal decomposition technique based on the Lanczos algorithm to solve the equation of transient groundwater flow in fractured dual-porosity media. The Lanczos algorithm uses orthogonal matrix transformations to reduce the finite element equations to a much smaller tridiagonal system of first-order differential equations [Nour-Omid, 1987; Dunbar and Woodbury, 1989]. By using this method, problems with large meshes can be reduced into equivalent systems of much smaller size. Consequently, large savings in computer time can be realized, especially for the problems requiring many time steps. In addition, this paper shows how time-dependent boundary conditions or multiple sources and sinks can be solved using the Lanczos method. In order to verify the proposed numerical technique and show its efficiency, several examples are presented.

The partial differential equations describing groundwater flow in fractures of a dual porosity medium can be written as [Barenblatt *et al.*, 1960; Huyakorn *et al.*, 1983]

$$\frac{\partial}{\partial x_i}(T\frac{\partial h}{\partial x_j}) = S\frac{\partial h}{\partial t} - \Gamma - q \qquad \text{i, j=1,2,3} \qquad (1)$$

where h is the hydraulic head in the fracture, and T and S are the fracture transmissivity and storage coefficients of the formation. Γ is the volumetric rate of fluid transfer from porous matrix blocks to fractures per unit volume, and q is the volumetric rate of fluid flow via sinks or sources.

The term Γ represents the interaction between porous matrix and the fractures. In general, it is a function of both time and space. There are three popular alternative mathematical models for describing Γ. Detailed description of these models can be found in the works of Huyakorn *et al.* [1983].

For the dual-porosity parallel fracture model, Γ can be expressed as

$$\Gamma = (-\frac{2K'H}{a(a+b)})(\sum_{n=0}^{\infty}\int_0^t \frac{\partial h}{\partial \tau}e^{-\alpha_n(t-\tau)}d\tau \qquad (2)$$

where a, b are the half thickness of matrix block and fracture, H is the aquifer thickness, K′ is the hydraulic conductivity in the matrix, and α_n is a constant which can be determined by

$$\alpha_n = \pi^2(2n+1)^2 K'/(4S_s'a^2) \tag{3}$$

where S_s' is the specific storage of the rock matrix.

The numerical solutions of the flow governing equations are obtained by applying the standard Galerkin finite element method for spatial discretization. Their solution is complicated because strong contrasts in the material properties are likely to exist between the fractures and the porous matrix. In addition, a three dimensional model can easy involve hundreds of thousands of unknowns. Therefore, an efficient and robust numerical technique to solve the governing equation is necessary. Dunbar and Woodbury [1989] have shown that the Lanczos algorithm is well suited for solving large problems, particular when time duration are long.

Consider now the following flow equation obtained by substituting (2) into (1)

$$\frac{\partial}{\partial x_i}(T\frac{\partial h}{\partial x_j}) - S\frac{\partial h}{\partial t} + q - \beta\sum_{n=0}^{\infty} I_n = 0 \qquad \text{i, j=1, 2, 3} \tag{4}$$

where

$$I_n = \int_0^t \frac{\partial h}{\partial t} e^{-\alpha_n(t-\tau)} d\tau \tag{5}$$

and β for a parallel fracture model is

$$\beta = \frac{2K'H}{a(a+b)} \tag{6}$$

If the time step size is a constant Δt at time step k+1, the integral in (5) can be approximated by

$$\begin{aligned} I_n^{k+1} \approx & \frac{h^1 - h^0}{\Delta t}\int_0^{t_1} e^{-\alpha_n(t_{k+1}-\tau)} d\tau + \frac{h^2 - h^1}{\Delta t}\int_{t_1}^{t_2} e^{-\alpha_n(t_{k+1}-\tau)} d\tau + \ldots \\ & + \frac{h^{k+1} - h^k}{\Delta t}\int_{t_k}^{t_{k+1}} e^{-\alpha_n(t_{k+1}-\tau)} d\tau \end{aligned} \tag{7}$$

where the superscripts of h denote the groundwater heads at different time steps.

From (7), it is easy to show that the relation between I_n^k and I_n^{k+1} can be expressed as:

$$I_n^{k+1} = e^{-\alpha_n \Delta t} I_n^k + \frac{1 - e^{-\alpha_n \Delta t}}{\alpha_n \Delta t}(h^{k+1} - h^k) \tag{8}$$

Equation (8) is in a form of recursion. It can be rewritten as a function of groundwater head history.

$$I_n^{k+1} = b_n(h-h^k) + a_n(b_n(h^k - h^{k-1}) + a_n(..b_n(h^2 - h^1) + a_n(b_n(h^1 - h^0)))...) \qquad (9)$$

where

$$a_n = e^{-\alpha_n \Delta t},$$

$$b_n = \frac{1-e^{-\alpha_n \Delta t}}{\alpha_n \Delta t}$$

It is assumed here that the storage coefficient S is a constant for all the fractures. After substituting (9) into (4), solution of (4) by Galerkin finite element method leads to the following system of first-order differential equations

$$\mathbf{M}\dot{\mathbf{h}} + \mathbf{K}\mathbf{h} - \beta\frac{\mathbf{M}}{S}\sum_{n=0}^{\infty} b_n \mathbf{h} - \beta\frac{\mathbf{M}}{S}\sum_{n=0}^{\infty}(-b_n\mathbf{h}^k + a_n(b_n(\mathbf{h}^k - \mathbf{h}^{k-1}) + a_n(...a_n(b_n(\mathbf{h}^1 - \mathbf{h}^0))...))) = \mathbf{f} \qquad (10)$$

where **h** is a vector of hydraulic heads at nodes of a finite element mesh, **K** and **M** are conductivity matrix and capacity matrix respectively. Both of these matrices are symmetric and positive definite. The vector **f** includes the effects of source term as well as boundary conditions.

Following the Lanczos reduction method [Dunbar and Woodbury, 1989], a reduced system of equations is derived by letting **h**=**Qw** in (10).

$$\mathbf{T}\dot{\mathbf{w}} + \mathbf{w} - \beta\frac{\mathbf{T}}{S}\sum_{n=0}^{\infty} b_n \mathbf{w} - \beta\frac{\mathbf{T}}{S}\sum_{n=0}^{\infty}(-b_n\mathbf{w}^k + a_n(b_n(\mathbf{w}^k - \mathbf{w}^{k-1}) + a_n(...a_n(b_n(\mathbf{w}^1 - \mathbf{w}^0))...))) = \mathbf{g} \qquad (11)$$

where **T** is an m×m tridiagonal matrix, **w** is the solution vector of length m in the reduced Lanczos space. Note that m is much less than total number of original equations n. The system equations can then be solved by any time integration technique. The solution **h** is then found by the matrix-vector multiplication **h**=**Qw** at the desired time steps. The procedures for the determination of **Q** and **T** can be found in the work of Dunbar and Woodbury [1989].

At time k×Δt, the correction term of right hand side is

$$\mathbf{I}^k = \beta\frac{\mathbf{T}}{S}\sum_{n=0}^{\infty}\mathbf{I}_n^k \qquad (12)$$

and the correction term at time (k+1)×Δt is:

$$\mathbf{I}^{k+1} = \beta \frac{\mathbf{T}}{S} \sum_{n=0}^{\infty} a_n (\mathbf{I}_n^k + b_n \mathbf{w}^k) - \beta \frac{\mathbf{T}}{S} \sum_{n=0}^{\infty} b_n \mathbf{w}^k \tag{13}$$

Updating of the right hand side requires the storage of three extra array for $\mathbf{I}_n$, a_n and b_n with a length of the number of truncated terms for the infinite exponential series.

The right side vector of equation (11) also contains the effects of wells and boundary conditions. We divide it into several parts with each part having the same time history. At different time steps, each part is then updated by its own time history. Using the boundary condition data at the moment when all the data are non-zero chooses the starting Lanczos vector. In this way, time dependent boundary conditions or multi-well systems with different time histories can be implemented. Figure 1 shows the accuracy of Lanczos method for a multi-well system.

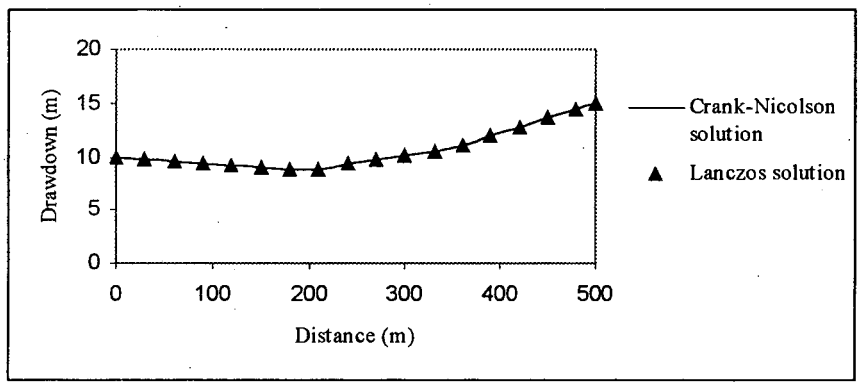

Figure 1. Comparison of the groundwater head solutions of the Lanczos method and classic Crank-Nicolson method for an 1-D problem with 2 pumping well located at 200m and 350m.

References

Barenblatt, G. I., I. P. Zheltov, and N. Kochina, Basic concepts in the theory of seepage of homogeneous liquids in fissured rocks, PMM, *Sov. Appl. Math. Mech.*, 24(5), 852-864, 1960.

Dunbar, W. S. and A. D. Woodbury, Application of the Lanczos algorithm to the solution of groundwater flow equation, *Water Resour. Res.*, 25(3), 551-558, 1989.

Huyakorn, P. S., B. H. Lester, and C. R. Faust, Finite element techniques for modeling groundwater flow in fractured aquifers, *Water Resour. Res.*, 19(4), 1019-1035, 1983

Nour-Omid, B., Lanczos method for heat conduction analysis, *Int. J. Numer. Methods Eng.*, 24, 251-262, 1979

The Reduced Degree of Freedom Procedures For Solving Coupled-Field Problems

George A. Zyvoloski and Peng-Hsiang Tseng

Geoanalysis Group, Los Alamos National Laboratory,
Los Alamos, New Mexico

Coupled-field problems play a dominant role in many engineering applications including porous media flow simulations. These problems involve the dynamic interactions of two or more physically distinct subsystems treated as a single system to account for the overall physical effects arising from the coupling. In the areas of flow and transport in porous media, the applications range from isothermal air-water flow in variably-saturated media to geothermal applications involving the simultaneous flow of air, water and heat to the flow of these processes in a dual-permeability media. To characterize the entire physical system requires not only an integrated understanding of all the coupling processes but also a realistic treatment of the solution procedures.

Several numerical solution methods have been developed to address the interacting mechanisms posed by the coupled equations [Lewis et al., 1984]. Among these methods, a so-called partitioned solution procedure has become increasingly popular for many practical applications due to its enhanced computational efficiency and program modularity [Park and Felippa, 1983]. In this approach, the time-integration process is carried out over each suitably decomposed subsystem treated as an isolated entity and recoupled subsequently by appropriate temporal extrapolation techniques. Although the partitioned solution method has been applied successfully to a variety of coupled problems, the numerical stability and accuracy may be affected by the partitioned treatment. The success of this scheme requires considerable investment in methodology issues to assure a stable and accurate solution. This difficulty has greatly restricted the generalization of this approach to some geoenvironmental applications which may require a solution of six coupled nonlinear equations. An alternative approach, first introduced by Zyvoloski et al. [1979] for the applications of nonlinear geothermal problems, circumvents this difficulty while preserves the computer memory savings and, to a certain degree, the computational efficiency. This approach reduces the degree of freedom at each computational node with some suitable simplifications during the Newton-Raphson iteration approximation and has the potential to be applied to a number of coupled-field problem-solvings especially when the number of state variables is large.

For most coupled processes, one or more of the processes usually changes slower than the other process. The basic idea behind the reduced degree of freedom method is to pre-factor one or several of those less active degrees of freedom into one or more primary degrees of freedom by an approximation of the Jacobian matrix. As such, the method has the flexibility to reduce a coupled system of n degrees of freedom per node to any positive number less than n depending upon the problem characteristics. In the following, the method was illustrated to reduce the problem from three unknowns per node to one unknown per node for the single continuum formulation of non-isothermal multiphase flow in a porous medium. For dual-permeability

approach, the same procedure was applied to reduce the system from six unknowns per node to two unknowns per node, i.e., one unknown for each of the two pore systems.

To model the flow of air, water, water vapor, and heat in a porous medium, three coupled equations which describe the conservations of mass of water, fluid-rock energy, and mass of noncondensible gas are used [Zyvoloski et al., 1997]. Under the assumption that the derivatives of the transmissibilities with respect to all three state variables are neglected, the submatrices of derivatives with respect to the two selected passive variables (in this case, saturation and temperature) become diagonal. The rest of the submatrices, the derivatives with respect to the dominant variable (i.e., pressure), are left in their original form. The solution process of solving three coupled equations can now be decoupled to solving one equation for the dominant variable plus a back substitution procedure for the two passive state variables. Experiences show that efficiency can be greatly improved when combine the decoupled system with a recoupling phase carried out by a successive over relaxation procedure [Zyvoloski, 1989].

For dual-permeability approach, equations which govern the flow and energy transport are described separately for each of the two subsystems (i.e., fractures and porous blocks) and coupled by means of a source-sink term to account for the exchange of mass and energy between the two interacting continua [Gerke and van Genuchten, 1993]. The number of unknowns per node has increased from three to six. In the derivations of the reduced system we assume one dominant variable in each of the two pore systems, the coupled system of equations can be rearranged such that the dominant variable in both the fracture and the matrix domains appears first. Following the same procedures as described above, the reduced degree of freedom method gives two enhanced pressure equations to solve plus a back substitution procedure for four passive variables.

Analysis show that solving the reduced system is numerically more efficient than that of the original system per one Newton-Raphson iteration. Simulation examples revealed that although the reduced degree of freedom method required generally more iterations than solving the original system, the increased number of iteration was only moderate hence the overall CPU time used was still less. In general, the reduced system allowed a larger average time step size and produced better mass and energy balance errors. In some cases tested, the reduced system requires even less iterations [Bullivant and Zyvoloski, 1990], the efficiency is thus greatly enhanced. In addition to the computational efficiency, the reduced degree of freedom method has the advantage of much less storage demand, which makes this method suitable to perform large real-world simulations in current personal computers or workstations. For instance, reduce a system from two coupled equations to one saves the computer storage to nearly 50% [Zyvoloski, 1989]. The reduced system of the current study requires approximately only one-third of the computer memory of the original system when the number of computational nodes is large.

REFERENCES

Bullivant, D., and G. A. Zyvoloski, An efficient scheme for the solution of linear system arising from coupled differential equations. Los Alamos National Laboratory Report LA-UR-90-3187, Los Alamos, NM, USA, 30 pp., 1990.

Gerke, H. H., and M. T. van Genuchten, A dual-porosity model for simulating the preferential movement of water and solutes in structured porous media. Wat. Resour. Res., 29, 305-319, 1993.

Lewis, R. W., P. Bettess, and E. Hinton, (eds), Numerical Methods in Coupled Systems, John Wiley & Sons Ltd., New York, NY, USA, 618 pp., 1984.

Park, K. C., and C. A. Felippa, Partitioned analysis of coupled systems. In Computational methods for Transient Analysis, eds T. Belytschko and T. J. R. Hughts, Elsevier Sci. Pub., Amsterdam, The Netherlands, pp. 157-219, 1983.

Zyvoloski, G. A., Efficient matrix procedures for the simulation of coupled processes. 1989 Eastern Multiconference, Computer Society of America, Tampa, FL, March 1989.

Zyvoloski, G. A., M. J. O'Sullivan, and D. E. Krol, Finite difference techniques for modeling geothermal reservoirs. Int. J. Numer. Methods Geomech., 3, 355-66, 1979.

Zyvoloski, G. A., B. A. Robinson, Z. V. Dash, and L. L. Trease, Summary of the models and methods for the FEHM application-a finite-element mass- and heat-transfer code. Los Alamos National Laboratory Report LA-13307-MS, Los Alamos, NM, USA, 64 pp., 1997.

☆ U.S. GOVERNMENT PRINTING OFFICE: 1999-783-830/19034

Earth Sciences Division
Ernest Orlando Lawrence Berkeley National Laboratory
University of California
1 Cyclotron Road, MS: 90-1116
Berkeley, CA 94720

Ernest Orlando Lawrence Berkeley National Laboratory is administered for the U.S. Department of Energy by the University of California under Contract No. DE-AC03-76SF00098.